JOURNAL OF POLYMER SCIENCE: PART A VOL. 3, PP. 1665–1674 (1965)

Polybenzothiazoles. I. Synthesis and Preliminary Stability Evaluation

PAUL M. HERGENROTHER, WOLFGANG WRASIDLO, and HAROLD H. LEVINE, *Whittaker Corporation, Narmco Research & Development Division, San Diego, California*

Synopsis

Completely aromatic polybenzothiazoles possessing superior oxidative and thermal stability have been prepared from aromatic bis(*o*-mercaptoamines) and aromatic dicarboxylic acids and benzothiazole forming derivatives thereof. The condensations were performed in *N,N*-diethylaniline and polyphosphoric acid. The former solvent gave meltable, low molecular weight prepolymers which were advanced to high molecular weight polybenzothiazoles by heating in the solid state. The course of the reaction was followed by removing samples periodically and determining the polymer melt temperature, inherent viscosity, specific extinction coefficient and observing changes in the infrared spectrum. In polyphosphoric acid, relatively high molecular weight polybenzothiazoles were obtained after a short reaction period. The polybenzothiazoles exhibited average TGA weight losses of 6% to 600°C. in static air. The maximum glass transition temperature obtained for poly-2,2′-(*m*-phenylene)-6,6′-bibenzothiazole was 910°C. Most of the polybenzothiazoles were soluble in concentrated sulfuric acid and 0.3% solutions exhibited inherent viscosities as high as 1.51.

INTRODUCTION

The acute need for high molecular weight polymers possessing hydrolytic, oxidative, and thermal stability provided the impetus for extensive high polymer synthetic efforts. The disclosure by Vogel and Marvel[1] on polybenzimidazoles demonstrated the potential possessed by a new family of polymers which can be broadly described as fully aromatic structures incorporating heterocyclic moieties. This paper is the first of a series dealing with polybenzothiazoles.

In recent years, a number of investigators have attempted to prepare polybenzothiazoles. Work by Rudner and Brumfield[2] failed to provide high molecular weight polybenzothiazoles; this appeared to be due to the unavailability of pure 3,3′-dimercaptobenzidine employed in their preparations. Investigations by Morten et al.[3] at the American Brake Shoe Company led to a patent for the preparation of benzothiazole polymers via the well known dye reaction in which toluidines were heated with sulfur. In 1961, Kiprianov and Mushkalo[4] attempted to obtain polybenzothiazole by the homopolymerization of 3-mercapto-4-aminobenzoic acid and its methyl ester but they encountered difficulties due to decomposition during the condensation.

In 1931, Lankelma and Knauf[5] employed *N,N*-dimethylaniline as a solvent for the preparation of benzothiazoles from substituted *o*-aminothiophenol hydrochloride and aromatic carboxylic acid derivatives. A variety of new bisbenzothiazoles were prepared in polyphosphoric acid (PPA) by Rai and Braunwarth[6] in 1961. PPA was also used to prepare high molecular weight polybenzimidazoles at the University of Tokyo by Iwakura, Uno, and Imai.[7]

This paper describes our research on the reaction of 3,3-′dimercaptobenzidine (DMB) with an aromatic dicarboxylic acid, or benzothiazole forming dicarboxylic acid derivatives. The reaction proceeds according to the general equation, (1):

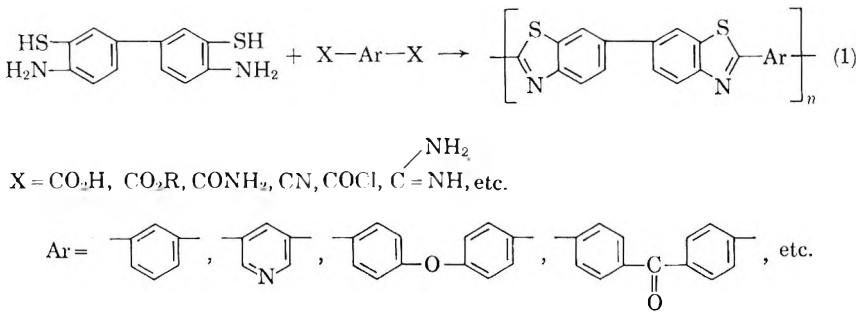

EXPERIMENTAL

3,3′-Dimercaptobenzidine was prepared[8] by thiocyanation of benzidine; after careful purification, condensations were carried out in *N,N*-diethylaniline (DEA) or polyphosphoric acid (PPA) with the dihydrochloride because the free base was highly sensitive to air oxidation. General reaction procedures for benzothiazole polymer formation in DEA and PPA are described below.

3,3′-Dimercaptobenzidine dihydrochloride was stirred in DEA under an argon atmosphere at elevated temperatures until a clear yellow solution resulted. A stoichiometric amount of an aromatic dicarboxylic acid derivative was added and the resulting reaction mixture stirred under reflux for a desired time. The cooled reaction mixture was poured into petroleum ether to precipitate a yellow prepolymer which was advanced to high molecular weight by heating in an argon atmosphere for 1 hr. at 400°C. under high vacuum.

In PPA, 3,3′-dimercaptobenzidine dihydrochloride was stirred under an argon atmosphere at elevated temperatures until a clear yellow solution was formed. A stoichiometric amount of an aromatic dicarboxylic acid or a benzothiazole-forming derivative was added and the reaction mixture stirred at the desired temperature for a certain time. In most cases, the reaction mixture gradually formed a blue to green fluorescent solution as polymer formation progressed. The polymer was isolated by pouring the

reaction mixture into a Waring Blendor containing hot water and was washed several times with sodium carbonate solution and distilled water.

The course of the reaction was followed by removing samples periodically and determining the polymer melt temperature (PMT), inherent viscosity (η_{inh}, 0.5% H_2SO_4 solution at 25°C.), specific extinction coefficient (K_{sp}, in H_2SO_4), and changes in the infrared spectrum.

RESULTS AND DISCUSSION

The reaction of 3,3′-dimercaptobenzidine dihydrochloride and diphenyl isophthalate in DEA, eq. (2), was studied most extensively.

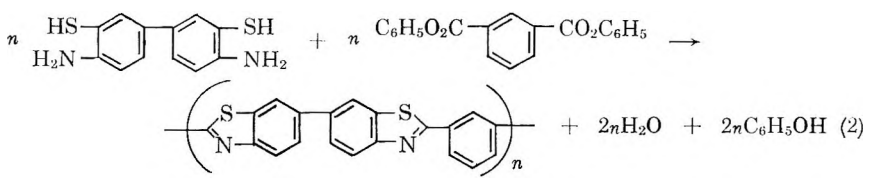

The plots of PMT, η_{inh}, and K_{sp} versus reaction time are given in Figure 1. As shown in Figure 1, the PMT increased to 300°C., η_{inh} to 0.07, and the K_{sp} to 38,000 after 33 hr. at reflux. It is significant to note that the η_{inh} was 0.05 after 5 hr. at 215°C. but increased to only 0.08 after an additional 33 hr. High molecular weight polybenzothiazoles could not be obtained directly in refluxing DEA presumably due to the limited reaction temperature and/or the limited solubility of the prepolymer which precipitated from solution as polymer formation progressed.

Water evolution was observed during the initial reaction period in refluxing DEA; phenol evolution was not detected by ferric chloride test on samples of the reaction mixture or condensate collected in a Dry Ice trap, until the isolated prepolymer was heated to about 240°C. These

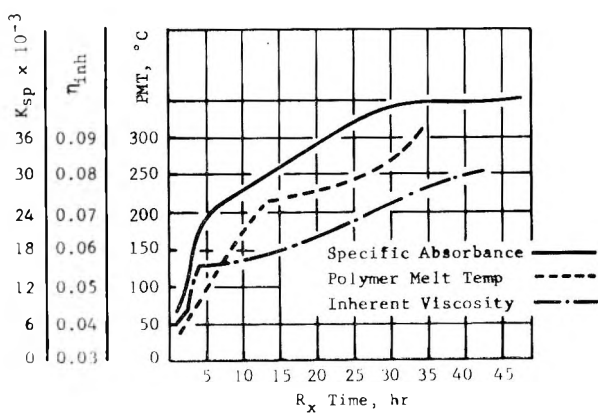

Fig. 1. Reaction of diphenyl isophthalate and 3,3′-dimercaptobenzidine dihydrochloride in *N,N*-diethylaniline at 215°C.

TABLE I
Benzothiazole Polymers from 3,3′-Dimercaptobenzidine Dihydrochloride

Carboxylic reactant	Medium	Temp., °C.	Time, hr.	Post-reaction polymerization conditions	Color	Max. η_{inh}[a]	Analysis[b] Found, %	Analysis[b] Total, %	TGA wt. loss, %[c] 538°C.	TGA wt. loss, %[c] 593°C.	T_v, °C.
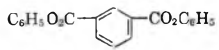	DEA	215	5	2 hr., 400°C./$h\nu$	Yellow	0.48	C, 68.46 H, 3.22 N, 5.43 S, 19.46	96.57	2.0	4.0	—
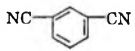	DEA	215	17	1 hr., 400°C./$h\nu$	Yellow	0.30	—	—	2.4	7.3	466
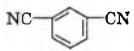	DEA	150	1	1 hr., 400°C./$h\nu$	Yellow	1.00	C, 69.77 H, 3.10 N, 8.30 S, 19.06	100.23	0.0	0.0	—
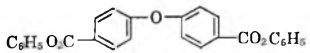	DEA	150	25	1 hr., 400°C./$h\nu$	Green	0.50	—	—	2.1	4.8	—
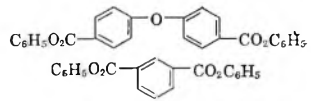	DEA	150	5	1 hr., 400°C./$h\nu$	Brown	Insol.	—	—	3.1	6.9	—
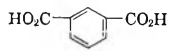	PPA	240	33	—	Yellow	0.47	C, 66.92 H, 2.96 N, 8.03 S, 18.15	96.06	2.9	8.3	527

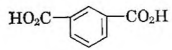	PPA	200	1	—	Yellow	1.51[e]	C, 68.82 H, 3.30 N, 7.86 S, 18.38	98.36	0.0	0.0	910
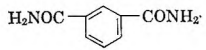	PPA	250	19	—	Yellow	0.49	—	—	0.0	1.0	—
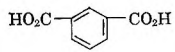	PPA	270	21	1 hr., 400°C./$h\nu$	Brown	0.41	—	—	3.2	6.4	—
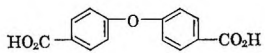	PPA	270	21	—	Light green	0.62	—	—	1.8	3.6	288
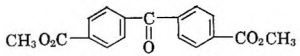	PPA	160	2	1 hr., 400°C /$h\nu$	Orange	0.36	—	—	3.9	8.8	—

[a] 0.5% H_2SO_4 solution.
[b] Polymer reported too resistant for complete combustion. Calcd. for $(C_{20}H_{10}N_2S_2)n$: C, 70.14%; H, 2.94%; N, 8.18%; S, 18.73%.
[c] ΔT = 3.2°C./min. in air.
[d] Extremely pure dimercaptobenzidine used.
[e] 0.3% H_2SO_4 solution.

observations and infrared evidence suggested the plausible reaction routes shown in eq. (3)

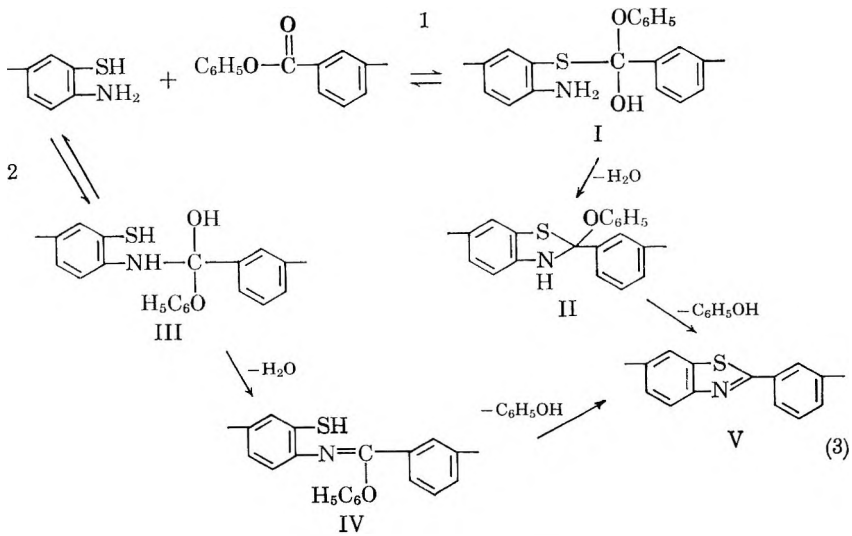

The difference in the nucleophilicity between the mercapto and amino groups tend to favor the first route as did infrared evidence which showed the presence of an N-H absorption at 3.05 μ and a strong absorption at 8.4 μ characteristic of an aryl ether, consistent with the structure of the phenoxybenzothiazolidine (II). It is apparent that this intermediate can also be formed by the cyclization of III but the nucleophilicity of the mercapto group tend to disfavor this possibility. Route 2 was suggested because the formation of the Schiff Base-type intermediate (IV) was the same as the one proposed for polybenzimidazole formation[9] which adds

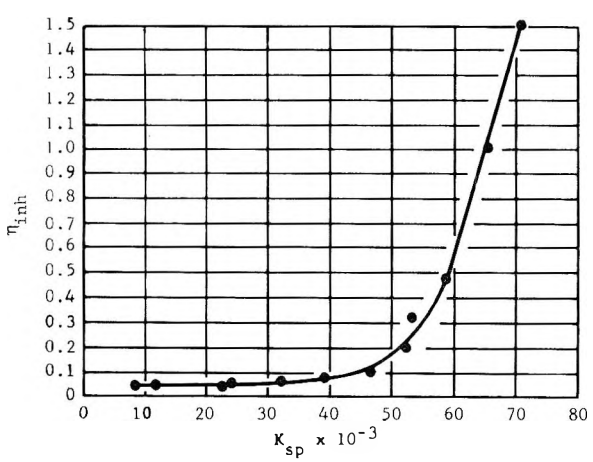

Fig. 2. Specific extinction coefficient (λ_{max} = 354–373 mμ) vs. inherent viscosity (0.5% H_2SO_4 solution) of poly-2,2′-(*m*-phenylene)-6,6′-bibenzothiazole.

resonance stabilization and could thereby enhance polybenzothiazole formation by this route. Infrared study failed to disclose mercaptan absorption but this could be due to the transitory nature of the intermediate (IV) and/or the intensity of the band being extremely weak.

Figure 2 illustrates the relationship between the specific extinction coefficient and inherent viscosity.

Meltable prepolymers have been obtained from isophthalic acid and its diesters, diamide, and dinitrile. All prepolymers began to solidify at 240°C. except those from the dinitrile which solidified completely at 210°C. indicating a lower reaction temperature and perhaps faster condensation reaction.

In PPA, relatively high molecular weight polymers were obtained after a short reaction period. The condensation of isophthalic acid and 3,3′-dimercaptobenzidine dihydrochloride in PPA at 225°C. gave a polymer after 0.5 hr. with an inherent viscosity of 0.29 while additional stirring for 33 hr. gave only an increase to 0.31. Increasing the temperature to 240°C. gave a polymer with an η_{inh} of 0.50. Preliminary work indicated a temperature of 240°C. was required to obtain a relatively high molecular weight polymer (η_{inh} = 0.50). However, additional work employing 3,3′-dimercaptobenzidine that had undergone extensive purification showed high molecular weight polymers (η_{inh} = 1.5) could be obtained at 200°C.

A number of benzothiazole polymers are listed in Table I along with reaction conditions and physical properties.

Thermal Stability

Thermogravimetric analysis (TGA) was performed on 0.5000 g. samples in static air at a constant heating rate of 3.2°C./min. The weight loss was automatically recorded, and after each analysis the cooled sample was reweighed as an additional check on the total weight loss.

Figure 3 shows thermograms obtained for poly-2,2′-(*m*-phenylene)-

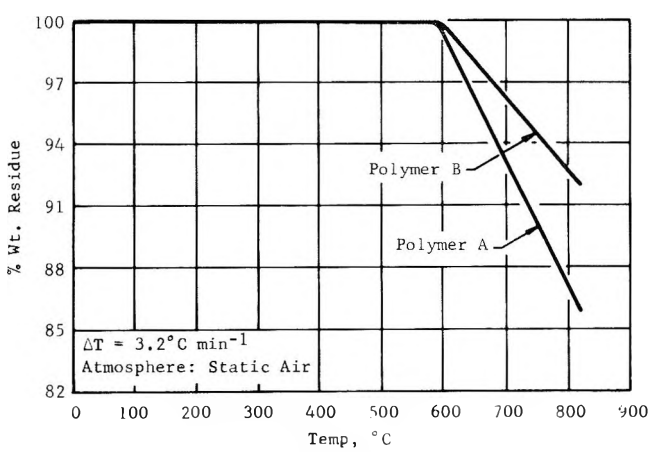

Fig. 3. Thermograms of poly-2,2′-(*m*-phenylene)-6,6′-bibenzothiazole.

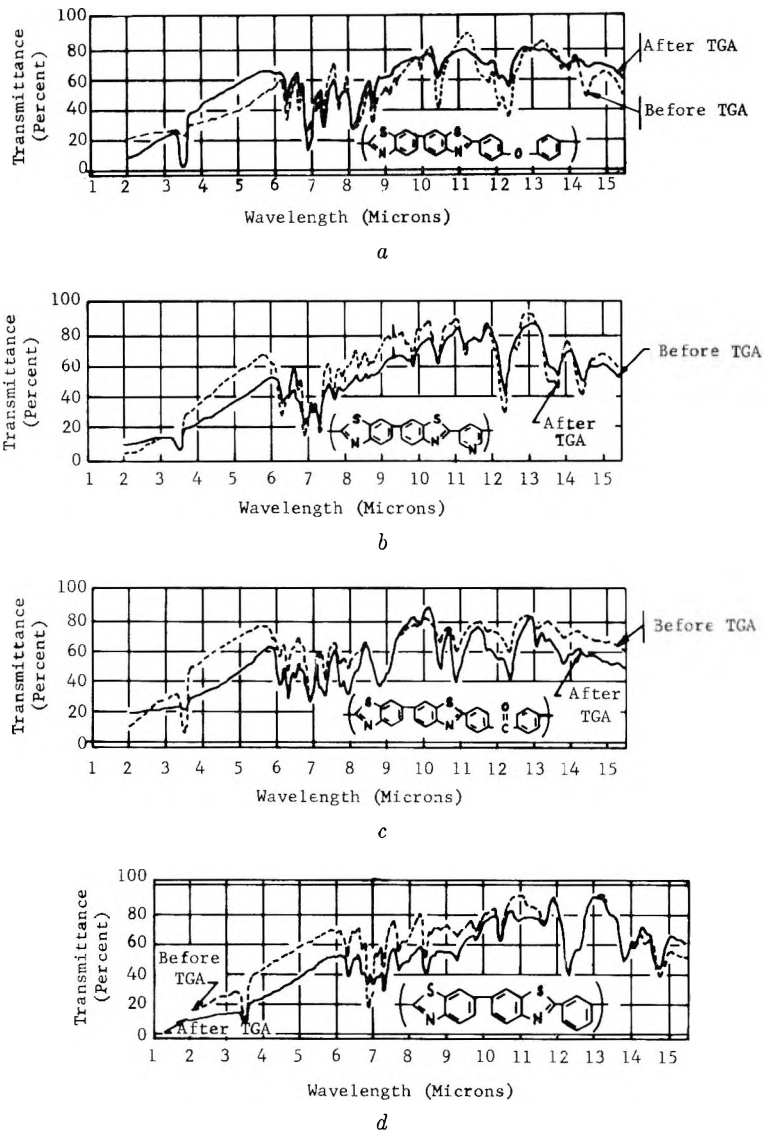

Fig. 4. Infrared spectra of polybenzothiazoles: (*a*) poly-2,2′-[*p,p*′-oxybis-(phenylene)]-6,6′-bibenzothiazole; (*b*) poly-2,2′-(3,5-pyridinediyl)-6,6′-bibenzothiazole; (*c*) poly-2,2′-(4,4′-benzophenone)-6,6′-bibenzothiazole; (*d*) poly-2,2′-(*m*-phenylene)-6,6′-bibenzothiazole.

6,6′-bibenzothiazole. Polymer A is the polymer (η_{inh} = 1.51, H_2SO_4) obtained from the reaction of 3,3′-dimercaptobenzidine and isophthalic acid in PPA. Polymer B is a polymer (η_{inh} = 1.00, H_2SO_4) of the same structure but obtained from the reaction of 3,3′-dimercaptobenzidine and isophthalonitrile in DEA followed by advancing the isolated prepolymer at 400°C. for 1 hr. under high vacuum. This is significant, since it showed

that low molecular weight prepolymers could be isolated and then subsequently condensed to high molecular weight thermally stable polymers.

To generalize, aromatic benzothiazole polymers are extremely thermally stable under oxidative conditions to about 600°C. The elemental analysis of Polymer A after TGA is given in Table II.

TABLE II
Elemental Analysis of Poly-2,2′-(*m*-phenylene)-6,6′-dibenzothiazole

	C, %	H, %	N, %	S, %	Total, %
Calcd for $(C_{20}H_{10}N_2S_2)_n$	70.14	2.94	8.18	18.73	100.00
Found:					
Before TGA	68.82	3.30	7.86	18.38	98.36
After TGA to 593°C.	68.92	3.02	8.07	18.57	98.58
After TGA to 816°C.	70.35	1.89	6.33	17.13	95.70

The analytical data before and after TGA to 593°C. are essentially identical. After TGA to 816°C., changes occurred in the elemental analysis, the largest change being in the hydrogen content which decreased 43% of its original value; this is presumably due to dehydrogenation which results in crosslinking of the polymer.

The elemental analysis and infrared investigation provided good evidence to show that the low weight losses were due to excellent oxidative and thermal stability and not masked by oxygen pickup forming oxidation products such as sulfoxide, sulfone, *N*-oxide, and carbonyl. The infrared spectra of representative polybenzothiazoles before and after TGA are shown in Figure 4.

Glass Transistion Temperature

The glass transition temperature (T_g) of various polybenzothiazoles was determined in an argon atmosphere at a constant heating rate of 3.2°C./min. by utilizing changes in the dielectric properties. The per cent change in power factor was plotted versus temperature, and the point where a drastic change in the power factor occurred was taken to be the T_g. As indicated in Table I, the T_g of poly-2,2′-(*m*-phenylene)-6,6′-bibenzothiazole obtained from the reaction of isophthalonitrile in DEA and isophthalic acid in PPA with 3,3′-dimercaptobenzidine dihydrochloride were 466 and 910°C., respectively. A polybenzothiazole containing diphenyl ether moieties had a T_g of 288°C.

CONCLUSIONS

Meltable and soluble prepolymers which have been isolated and advanced to high molecular weight have been prepared.

Polybenzothiazoles exhibit excellent intrinsic oxidative thermal stability.

Most of the polybenzothiazoles are completely soluble in sulfuric acid and therefore considered to be linear.

This research was supported by the United States Navy under Contract NOw 63-0420-c monitored by the Bureau of Naval Weapons, Washington 25, D. C.

References

1. Vogel, O. and C. S. Marvel, *J. Polymer Sci.*, **50**, 511 (1961).
2. Rudner, Brumfield, et al., ASD TDR 62-249, March 1963.
3. Morton, et al., U. S. Pat. 3,047,543 (1962).
4. Kiprianov and Mushkalo, *J. Gen. Chem.* (*USSR*), **32**, 4040 (1962).
5. Lankelma and Knauf, *J. Am. Chem. Soc.*, **53**, 309 (1931).
6. Rai and Braunwarth, *J. Org. Chem.*, **26**, 3434 (1961).
7. Iwakura, Y., K. Uno, and Y. Imai, private communication.
8. Houben-Weyl, *Methoden der Organischen Chemie*, E. Miller, Ed., George Thieme, Stuttgart, 1955, Vol. IX, p. 39.
9. Wrasidlo, W. and H. H. Levine, paper presented to Polymer Division, 145th Meeting, National American Chemical Society, New York, September 1963.

Résumé

Les polybenzothiazoles complètement aromatiques, possédant une stabilité à l'oxydation et thermique supérieure, ont été préparés à partir de bis-(*o*-mercaptoamines) aromatiques et d'acides dicarboxyliques aromatiques et de dérivés formant également des benzothiazoles. Les condensations ont été effectuées dans la *N,N*-diéthylaniline et dans l'acide polyphosphorique. Le premier solvant fournit des prépolymères fusibles de bas poids moléculaire, qui ont été transformés en polybenzothiazoles de haut poids moléculaire, par chauffage à l'état solide. Le cours de la réaction a été suivi en prenant régulièrement des échantillons et en déterminant la température de fusion du polymère, la viscosité inhérente, le coefficient spécifique d'extinction, et en observant les changements dans le spectre infar-rouge. Dans l'acide polyphosphorique, des polybenzothiazoles de poids moléculaire relativement élevés ont été obtenus, aprés une courte durée de réaction. Les polybenzothiazoles, présentent une perte de poids moyen TGA de 6% jusqu'à 600°C à l'air statique. La température de transition vitreuse la plus élevée a été obtenue pour le poly-2,2′-(*m*-phénylène)-6,6′-bibenzothiazol et s'élévait à 910°C. La plupart des benzothiazoles sont solubles dans l'acide sulfurique concentré et des solutions de 0.3% présentent de viscosités inhérentes aussi élevées que 1.51.

Zusammenfassung

Rein aromatische Benzothiazole mit überlegener oxidativer und thermischer Beständigkeit wurden aus aromatischen Bis(*o*-mercaptoaminen) und aromatischen Dicarbonsäuren und ihren Benzothiazol bildenden Derivaten dargestellt. Die Kondensation wurde in *N,N*-Diäthylanilin und Polyphosphosäure durchgeführt. Ersteres Lösungsmittel leiferte schmelzbare, neidermolekulare Präpolymere, welche durch Erhitzen im festen Zustand in hochmolekulare Polybenzothiazole umgewandelt wurden. Der Reaktionsverlauf wurde durch periodische Probenentnahme und Bestimmung der Schmelztemperatur, der Viskositätszahl und des spezifischen Extinktionskoeffizienten sowie durch Beobachtung der Änderung im Infrarotspektrum verfolgt. In Polyphosphorsäure wurden nach kurzer Reaktionsdauer verhältnismässig hochmolekulare Polybenzothiazole erhalten. Die Polybenzothiazole zeigten einen mittleren TGA-Gewichtsverlust von 6% bis zu Temperaturen von 600°C in unbewegter Luft. Die für Poly-2,2′-(*m*-phenylen)-6,6′-bibenzothiazol erhaltene maximale Glasumwandlungstemperatur betrug 910°C. Die meisten Polybenzothiazole waren in konzentrierter Schwefelsäure löslich, und 0,5%ige Lösungen besassen Viskositätszahlen bis zu 1,51.

Received June 24, 1964
Revised September 29, 1964
(Prod. No. 4528A)

JOURNAL OF POLYMER SCIENCE: PART A VOL. 3, PP. 1675–1683 (1965)

Analysis of Relaxation Constants in Polyurethanes

AJAIB SINGH and LEONARD WEISSBEIN, *Bound Brook Research Laboratories, American Cyanamid Company, Bound Brook, New Jersey*

Synopsis

A simple Maxwell model is shown to be inadequate in describing stress-relaxation behavior of polyurethanes at 120°C. These data fit better to a multi-Maxwell model. Various relaxation parameters contributing to the thermal degradation of polyurethanes have been resolved, and their significance is discussed.

INTRODUCTION

The stress relaxation in an elastomer at elevated temperatures provides a convenient means of following thermally induced changes in the network structure. It could also be used to gain insight into the processes, chemical or physical in nature, responsible for the observed stress decay. This method, first described by Tobolsky and his co-workers,[1,2] has since been used successfully[1–9] in studying the thermal degradation of various types of elastomers. In such cases, the isothermal stress decay observed in elastomers held at constant extension has usually been fitted to a Maxwell model, the behavior of which is described by the equation[1,2,10a]:

$$f(t) = f(0) \exp \{-t/\tau\} \tag{1}$$

or in terms of moduli

$$E_r(t) = E_r(0) \exp \{-t/\tau\} \tag{2}$$

where $f(0)$ and $f(t)$ are the tensile forces measured initially and after time t, respectively. $E_r(t)$ and $E_r(0)$ are the corresponding relaxation moduli. τ is a constant for the system under study and depends on the temperature.

In the thermal stress-relaxation work on polyurethanes published to date,[12,13] eq. (1) was used in interpreting the data. When applying this equation to the stress relaxation of elastomers undergoing thermal degradation, one assumes that the stress at any time, at constant extension, depends only on the number of originally effective chains which remain uncut. One can then relate the parameter τ to the specific rate constant of a single first-order scission reaction. According to eq. (1), data plots of the form $\log f(t)/f(0)$ versus time should be linear. However, we have observed that with polyurethanes such plots deviate markedly from linearity, suggesting the inadequacy of a simple Maxwell model in describing the

thermal stress-relaxation behavior of these systems. While this non-Maxwellian behavior is evident from the stress-relaxation data for polyurethanes reported in the literature,[12] this point has thus far not been considered. The nature of this deviation, especially the tendency of the plots of log $f(t)/f(0)$ or log $E_r(t)$ versus time to become linear at extended periods of time, suggests that these data might better fit a multicomponent, or more specifically, a multi-Maxwell model. A multicomponent model has been used to describe the chemical stress-relaxation data for natural rubber vulcanizates by Baxter[14] and for polysulfide rubbers by Beevers.[3] A theoretical analysis of Beevers' two-component equation was given later.[15] This paper represents the preliminary results of our attempts to apply such a model to the stress-relaxation data on polyurethanes.

RESULTS AND DISCUSSION

The polyurethane samples investigated were prepared by two different methods. All the samples save V were obtained by first capping the hydroxy-terminated polyethyleneopropylene adipate ($\bar{M}_n$ 2050) with 3,3′-bitolylene-4,4′-diisocyanate (TODI), and then curing the isocyanate-terminated prepolymer (P-A) thus obtained with a diol and/or a triol. Sample V was prepared by reacting monoallylglyceryl ether and polyethyleneopropylene adipate glycol with an equivalent (based on total OH) of TODI. The gummy polymer (P-B) obtained in this manner was cross-linked with a sulfur recipe. All the samples were thoroughly extracted with tetrahydrofuran and the solvent removed before subjecting the samples to the stress relaxation. All stress-relaxation measurements were made at a constant extension of 10.0% in a forced draft oven maintained at 120 ± 0.1°C. Figure 1 shows the typical plots of log $f(t)/f(0)$ versus time obtained for the various polyurethanes studied. A pronounced non-linearity is apparent in all the plots shown in Figure 1, indicating that a simple Maxwell model does not adequately describe the relaxation behavior of these polyurethanes. However, these plots do appear to become linear after extended periods of time, suggesting that the stress-relaxation data might better conform to a multi-Maxwell model expressed mathematically by:

$$E_r(t) = \sum_{i=1}^{m} E_{r_i}(0) \exp\{-t/\tau_i\} \tag{3}$$

$E_r(t)$ values used in the plots were calculated from $f(t)$ data by the formula

$$E_r(t) = \frac{3f(t) \times 980}{A_u}\left[\frac{\alpha}{\alpha^2 - (1/\alpha)}\right]$$

where $E_r(t)$ is the overall relaxation modulus at time t, $f(t)$ is force in grams at time t, A_u is the area of cross section of unstretched sample, and α is the elongation.[10b]

In applying the model of eq. (3) it is assumed that the observed decay

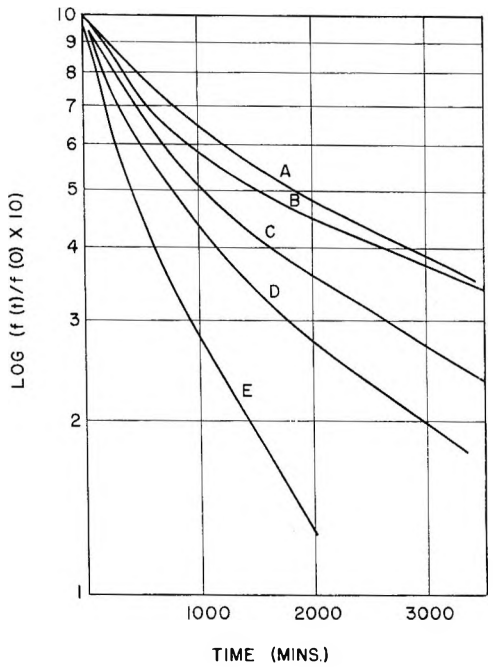

Fig. 1. Plots of log $f(t)/f(0)$ vs. time for various polyurethanes at 120°C. and 10% extension: (A) P-A cured with 1,2,6-hexanetriol; (B) P-B crosslinked with sulfur; (C) P-A cured with 100% TMP; (D) P-A cured with 50% TMP, 50% BDO; (E) P-A cured with 25% TMP, 75% BDO.

in modulus $E_r(t)$ is due to m concurrent degradative processes, each functioning as a Maxwellian element with its own modulus contribution E_{ri} and characteristic time constant τ_i. According to this model, the log $f(t)/f(0)$ versus time function should approach linearity in the relaxation time region where all but the slowest process have dissipated. This concept of a multi-Maxwell model seems reasonable in view of the ever-present possibility of inadvertently forming allophanates, urea, and biuret linkages in fabricating the urethane elastomer. The simultaneous cleavage of these various types of linkages would probably contribute to the observed stress-relaxation behavior. In addition to this possibility, such physical processes as viscous flow, stress crystallization, etc., might also contribute to the observed stress decay.

The stress-relaxation data obtained for the various polyurethanes were fit to eq. (3) by means of a unique graphical analytical procedure. This procedure was previously employed by Tobolsky[10c] in studying the viscoelastic behavior of polystyrene at temperatures well below the range in which significant chemical degradation would occur. It is illustrated in Figure 2 for the data obtained at 120°C. for prepolymer (P-A) cured with trimethylolpropane. Here, the straight-line portion of the plot of log $E_r(t)$ versus time is extrapolated to zero time. This straight line A repre-

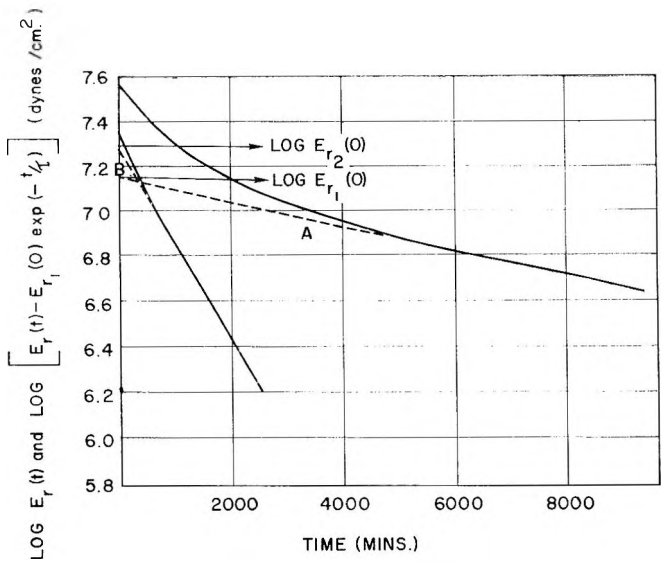

Fig. 2. Graphical technique for separating relaxation parameters (polyurethane I at 120°C.); $E_{r_1}(0) = 1.41 \times 10^7$ dyne/cm.^{2}, $\tau_1 = 8100$ min.; $E_{r_2}(0) = 1.95 \times 10^7$ dyne/cm.^{2}; $\tau_2 = 1160$ min.

sents the contribution to the modulus decay of the slowest Maxwellian process, i.e., the one with the longest relaxation time τ_1. The intercept of the line gives the magnitude of the initial modulus component $E_{r1}(0)$ established by the structural elements involved in this process. The value of τ_1 is obtained from the slope of the line A. A plot of log $[E_r(t) - E_{r1}(0) \exp \{-t/\tau_1\}]$ versus time also approaches a straight line. The values of τ_2 and $E_{r2}(0)$ of the next slowest process are calculated from the slope and inter-

TABLE I
Stress-Relaxation Constants For Polyurethanes at 120°C., Elongation 10%

	Polyurethane	τ_B, min.	τ_1, min.	τ_2, min.	$E_{r_1}(0)$, dyne/cm.^{2} $\times 10^7$	$E_{r_2}(0)$, dyne/cm.^{2} $\times 10^7$
I	P-A cured with trimethylolpropane	2550	8100	1160	1.41	1.95
II	P-A cured with 50% trimethylolpropane–50% butanediol	1060	5490	914	0.732	1.660
III	P-A cured with 25% trimethylolpropane–75% butanediol	690	1390	281	0.884	0.630
IV	P-A cured with 1,2,6-hexanetriol	3300	8820	1410	0.860	0.740
VA	Sulfur-vulcanized P-B, extracted	3150	8280	1087	1.46	0.560
VB	Sulfur-vulcanized P-B, unextracted	1020	2060	323	1.46	0.716

cept of this extrapolated line B. This procedure is repeated until the relaxation parameters of all the resolvable processes are evaluated. The data on the polyurethanes studied at 120°C. generally conform to a three-component model, although the fastest of these usually contributes very little to the over-all modulus decay. The relaxation parameters derived for the two major components of the polyurethane modulus decay curves are given in Table I.

Also given in Table I are the gross relaxation time constants τ_g for the various polyurethanes. τ_g represents the time required for the relaxation modulus to decay to $1/e$ or 36.8% of its initial value. This parameter, designated as τ or τ_{ch}, by Tobolsky et al.,[12,13] has been used by them to characterize the chemical decay of polyurethanes. They have later attempted to use τ_g values to derive the specific rate constants and activation energies for urethane cleavage.[13] The gross relaxation time constants published by Tobolsky and co-workers for stocks similar to IV are much smaller (by a factor of $^1/_5$ to $^1/_8$) than those found in this investigation. These differences may be due to the use of TODI in the sample preparations of this investigation in place of 2,4-toluene diisocyanate (TDI) used by the earlier workers. Furthermore, the samples prepared in this investigation were thoroughly extracted to remove chemical agents that could catalyze urethane breakdown, whereas no indication was given by the previous workers[12,13] that their samples were extracted prior to stress relaxation.

Of even greater significance than the observed differences in τ_g values, is the question that arises as to the fundamental significance of these values in cases where the stress-relaxation data deviate markedly from eq. (2). In such cases, a τ_g value may be used as a convenient empirical index of the overall thermal stability of a polyurethane system. However, if the deviations of the modulus data from eq. (2) stem from processes proceeding concurrently with the urethane cleavage process, the τ_g value cannot be used to derive a specific rate constant for thermal cleavage of urethane linkages.

In view of our assumption, in fitting the modulus decay data to eq. (3), that the resolvable components of the observed stress-decay curves represent different molecular processes, it was of interest to determine the effect on these components of a catalyst known to influence polyurethane network breakdown. To this end, small quantities of ferric acetylacetonate were added to the extraction solvent (tetrahydrofuran) in which polyurethane samples were swelled overnight at room temperature. The solvent was then removed by drying the samples under vacuum at 40°C. prior to stress-relaxing them. All the resolvable components of the modulus decay curves obtained with these samples are affected by the presence of this catalyst (see Table II). These results indicate that the degradation processes involved are chemical in nature, i.e., are due to the thermal cleavage of various types of chemical linkages. Work is now in progress to identify the components of the modulus decay curves with various chemical cleavage reactions.

TABLE II

Effect of Catalyst on the Relaxation Constants at Temperature of Relaxation 140°C., Elongation 10%

Polyurethane	Curative for P-A	Catalyst[a]	τ_0, min.	τ_1, min.	τ_2, min.	τ_3, min.	$E_{r1}(0)$, dyne/cm.^{2} 10^7	$E_{r2}(0)$, dyne/cm.^{2} 10^7	$E_{r3}(0)$, dyne/cm.^{2} 10^7
VI	75% TMP, 25% BDO	None	275	2260	371	75	0.75	1.33	1.62
VIA	"	Ferric acetyl acetonate	69	125	33	5	1.76	1.43	0.186
VIB	"	"	23	111	23	4	0.434	1.43	0.794

[a] Samples of VIA and VIB were swollen in 0.02 and 0.002% tetrahydrofuran solution of ferric acetyl acetonate. Samples of VI were swollen identically, but without ferric acetyl acetonate.

The relaxation constants (τ_1, τ_2, and τ_g) obtained for the extracted sulfur crosslinked polymer P-B are similar in magnitude to those obtained with extracted samples containing urethane crosslinks. (Compare results in Table I for samples I and IV with those of sample VA.) These results suggest that similar linkages are involved in the thermal degradation reactions of these systems. One can conclude, therefore, that the thermal degradation of VA does not involve the sulfur crosslinks.

It is apparent from Table I that the unextracted sulfur-cured system VB relaxed faster than its extracted counterpart VA. Apparently, some residual ingredients of the sulfur cure, removable on extraction, have a substantial adverse effect on the thermal stability of this system.

EXPERIMENTAL

The polyester used in preparing the prepolymer P-A, and the vulcanizable polymer P-B, was the commercially available hydroxy-terminated polyethylenepropylene adipate (90:10) with an $\bar{M}_n$ of 2050. 3,3′-Bitolylene-4,4′-diisocyanate (TODI) of 99.5% plus purity (Carwin Chemical Co.) was used without further purification.

1,4-Butanediol (Eastman Organic Chemical) was purified by distillation, b.p. 124°C./14 mm.

1,1,1-Trimethylolpropane (Celanese Chemical Company) was dried under vacuum (1 mm.) at 50°C. overnight before use.

1,2,6-Hexanetriol (Eastman Organic Chemical) was distilled under vacuum, b.p. 152–153°C./0.6 mm.

Glycerylmonoallyl ether, b.p. 84.5°C./1 mm. (Shell Oil Company) was dried under vacuum before use; water content less than 0.1%.

Preparation of Prepolymer P-A

The polyester (1 mole) was dehydrated by maintaining it at 140°C. under nitrogen at 10 mm. pressure for $1^1/_2$ hr. During this time a slow trickle of nitrogen was passed through the system. The temperature was then lowered to 80°C. and TODI (1.90 mole) was added with vigorous stirring. The temperature was allowed to increase to 120°C., and the reaction mixture was maintained at this temperature under a nitrogen blanket for $3^1/_2$ hr. The isocyanate content of the prepolymer thus obtained was found by titration to be 2.70%.

Casting of Sheets from Prepolymer P-A

Equivalent amounts (based on the isocyanate content of P-A) of diol and/or triol curatives and 0.5% *N*-ethylmorpholine catalyst (based on the weight of P-A) were blended into the prepolymer which had been preheated to 110°C. The resulting mixtures (which had gel times of 10–30 min. depending upon the curative) were pressure-molded into 75-mil sheets at 120°C. for 1 hr. These sheets were post-cured at 100°C. for 16 hr.

Preparation of Vulcanizable Polymer (P-B)

The polyester (1 mole) was dehydrated as in the preparation of P-A described above. Glycerylmonoallyl ether (1 mole) was added and the mixture brought to 70°C. TODI (2 mole) was then added with vigorous stirring. The reaction mixture was maintained at 105°C. under nitrogen for 72 hr. The resulting gummy polymer, P-B, had a Mooney value of 36.

To vulcanize P-B, the following recipe was milled into 100 parts of the polymer: stearic acid, 0.5 parts; MBTS, 3.0 parts; MBT, 1.0 parts; RCD-2098, 0.5 parts; sulfur, 1.0 parts; cadmium stearate, 0.5 parts.

The milled stock was then pressure-molded at 140°C. for 1 hr. to form 75-mil sheets which were post-cured as described above.

Extraction Procedure

The post-cured sheets were die-cut into strips to be used in the stress-relaxation measurements. These strips were swelled in baths containing large quantities of tetrahydrofuran. The baths were maintained at room temperature and mildly agitated during the extraction process. The strips were extracted in this manner for periods of 24–48 hr., during which time at least three changes of solvent were made.

Stress-Relaxation Apparatus

A six-channel autographic stress relaxometer was used in these studies. This instrument consisted of load-sensing elements, means of extending and maintaining the specimens at constant extension, and an air-circulating oven. The load-sensing elements were nonbonded resistance strain gages (Statham Instrument Corp. GI-48-675), each incorporated in a resistance bridge circuit. The outputs of these bridge circuits were fed to a six-channel L&N recorder. The sensitivity of this system was ±0.5% over a load range of 50–800 g. The extension device was controlled by a micrometer, with which the samples were extended to 10 ± 0.05%. The temperature in the oven could be controlled to within ±0.1°C. at 120°C.

The authors are indebted to Dr. G. Mino and to Professor A. V. Tobolsky for many helpful discussions. The experimental assistance of Mr. J. C. Mollica is also gratefully acknowledged.

References

1. Tobolsky, A. V., I. B. Prettyman, and J. H. Dillon, *J. Appl. Phys.*, 324, 380 (1944); *Rubber Chem. Technol.*, **17**, 551 (1944).

2. Andrews, R. D., A. V. Tobolsky, and E. E. Hauson, *J. Appl. Phys.*, **17**, 352 (1946).

3. Beevers, R. B., *J. Colloid Sci.*, **19**, 40 (1964).

4. Scanlan, J., *Trans. Faraday Soc.*, **57**, 839 (1961).

5. St. Pierre, L. E., and A. M. Bueche, *J. Phys. Chem.*, **63**, 1338 (1959).

6. Dunn, J. R., J. Scanlan, and W. F. Watson, *Trans. Faraday Soc.*, **27**, 730 (1958).

7. Berry, J. P., *Trans. Inst. Rubber Ind.*, **32**, 224 (1956).

8. Osthoff, R. C., A. M. Bueche, and W. T. Grubb, *J. Am. Chem. Soc.*, **76**, 4659 (1954).

9. Tobolsky, A. V., and A. Mercurio, *J. Polymer Sci.*, **36**, 467 (1959).
10. Tobolsky, A. V., *Properties and Structure of Polymers*, Wiley, New York, 1960 (a) pp. 223–265; (b) pp. 105–106; (c) pp. 16–193.
11. Offenbach, J. A., and A. V. Tobolsky, *J. Colloid Sci.*, **11**, 39 (1956).
12. Colodny, P. C., and A. V. Tobolsky, *J. Am. Chem. Soc.*, **79**, 4320 (1957).
13. Tobolsky, A. V., and E. Peterson, *J. Phys. Chem.*, **67**, 930 (1963); A. V. Tobolsky, H. Yu, and R. Thach, *J. Appl. Polymer Sci.*, **6**, S44 (1962).
14. Baxter, S., and H. A. Vodden, *Polymer*, **4**, 145 (1963).
15. Tobolsky, A. V., *J. Polymer Sci.*, **B2**, 823 (1964).

Résumé

On démontre qu'un modèle de Maxwell simple est incapable de décrire la relaxation de tension des polyurethanes à 120°C. Ces résultats conviennent mieux à un modèle de Maxwell complexe. Divers paramètres de relaxation, contribuant à la dégradation thermique des polyurèthanes, ont été résolus et on discute de leur signification.

Zusammenfassung

Das einfache Maxwell-Modell erweist sich zur Beschreibung des Spannungs-Relaxationsverhältnisses von Polyurethan bei 120°C als nicht geeignet. Ein Multi-Maxwell Modell wird den Ergebnissen besser gerecht. Verschiedene Relaxationsparameter, die sum thermischen Abbau von Polyurethan beitragen, wurden aufgelöst, und ihre Bedeutung wird diskutiert.

Received September 4, 1964
Revised October 19, 1964
(Prod. No. 4544A)

JOURNAL OF POLYMER SCIENCE: PART A VOL. 3, PP. 1685-1712 (1965)

Stress Relaxation of γ-Irradiated Fluorocarbon Elastomers*

T. YOSHIDA,† R. E. FLORIN, and L. A. WALL, *National Bureau of Standards, Washington, D. C.*

Synopsis

Poly(vinylidene fluoride), polytrifluoroethylene, and two rubbery copolymers with vinylidene fluoride were crosslinked by γ-irradiation in vacuum. Radiation-induced chain scissions in the copolymers were studied by observing the relaxation of stress at constant extension during further irradiation at 27°C., at 0.31–2.7 Mr./hr. in nitrogen and in air. From gel content, swelling, and elasticity, the values of G_c (crosslinking) and G_d (scission) were respectively; for CF_2CFH, $G_c = 2.2$ and $G_d = 0.4$; for CF_2CH_2, 2.0 and 0.3; for $CF_2CH_2 + C_3F_6$, 3.4 and 1.3; for $CF_2CH_2 + CF_2CFCl$, 1.8 and 1.4. The G_d values from stress relaxation were variable; the lowest were: for $CF_2CH_2 + C_3F_6$, 4.6 in nitrogen and 8.4 in air; for $CF_2CH_2 + CF_2CFCl$, 1.9 in nitrogen and 3.6 in air.

INTRODUCTION

Rubbery copolymers containing vinylidene fluoride crosslink readily under γ-irradiation,[1–5] but there appears to be no published information on the relative yields of crosslinks and scissions. Several methods are available to determine these yields.[6–8] If a strip of previously crosslinked elastomer is irradiated at constant extension, the study of stress f, as a function of time, offers a simple method of evaluating the yield of scissions unperturbed by any crosslinking that may occur.[9] For a scission rate k_d, in scissions/(monomer unit) (second), and uniformly distributed crosslinked chains of initial degree of polymerization between crosslinks P_0, the derived relation is

$$\ln (f/f_0) = -k_d P_0 t$$

In the present study, samples of the elastomers Viton A ($CF_2CH_2 + C_3F_6$) and Kel-F Elastomer 3700 ($CF_2CH_2 + CF_2CFCl$) were subjected to Co^{60} γ-irradiation, and the yields of crosslinks and chain scissions were determined from observations of gel content, gel swelling, elasticity, and

* Presented before the 144th National American Chemical Society Meeting, Los Angeles, California, April 1963. Based on work sponsored by the National Aeronautics and Space Administration.

† Guest worker at the National Bureau of Standards, 1962. Permanent address: The Furukawa Electric Co., Ltd., Tokyo, Japan.

stress relaxation. For comparison, yields of crosslinked units and chain scissions were also determined for the fluorine-containing homopolymers, polytrifluoroethylene and poly(vinylidene fluoride).

EXPERIMENTAL

Materials

Viton A is an elastomeric copolymer of vinylidene fluoride and hexafluoropropylene. From fluorine analysis, the composition of a low-molecular weight batch obtained from E. I. du Pont de Nemours and Co., was 82 mole-% vinylidene fluoride. It had an intrinsic viscosity of 1.62 dl./g. in a tetrahydrofuran–dimethyl-formamide (87:13, w/w) mixture at 29.2°C., and its number-average molecular weight was estimated as 330,000 with the aid of correlation charts.

Kel-F Elastomer 3700 is a copolymer of vinylidene fluoride and chlorotrifluoroethylene. The present batch from Minnesota Mining and Manufacturing Co., contained 70 mole-% vinylidene fluoride by chlorine analysis. Its intrinsic viscosity was 2.66 dl./g. in methyl ethyl ketone at 29.2°C., and the number–average molecular weight, estimated from viscosity correlation data, was 421,000.

The polytrifluoroethylene and poly(vinylidene fluoride) samples are described more fully elsewhere.[10]

Irradiation of Samples

Two Co^{60} γ-ray sources were used, of approximately 1500 curies and 50,000 curies strength, in a pool arrangement. Dose rates for different geometries were calibrated by commercial cobalt glass dosimeters (Bausch and Lomb Optical Company, Rochester, N. Y.) and also by ferrous sulfate dosimetry at the lowest dose rate used, 0.31 Mr./hr. For the preliminary irradiation, the dose rate was 1.9 Mr./hr. (1.9, 1.6, and 2.0 Mr./hr. at the ends and the middle (respectively, of a 14-cm. strip) and for the stress relaxation studies, 0.31, 0.80, and 2.7 Mr./hr. at the middle of the strip. For doses in rads, the conversion factors are 1 roentgen = 0.853 rads in Viton and 0.874 rads in Kel-F Elastomer. The irradiation temperature was 27°C.

For the preliminary crosslinking and radiation studies, the elastomers were molded into sheets and cut into strips approximately 0.2 by 0.6 by 14 cm., which were then placed in tubes, evacuated several hours at 1 μ or better, and irradiated in the source to the desired dose. Samples cut from these irradiated strips were used for the stress relaxation studies and also for measurements of specific gravity, elasticity, sol content, and swelling.

General Measurements

Extractions for sol determination of elastomers were done with acetone in a Soxhlet apparatus operated for 50 hr. The samples were then dried

in a vacuum at 10^{-3} mm. Hg for 75 hr. at 50°C. In sets of samples cut from different parts of the same strip, deviations from the strip average were as high as ±0.5% and seemed unrelated to the dose rate differences Swelling ratios were determined essentially according to ASTM D471-59T by immersing in ethyl acetate or other solvent for 40–50 hr. at 27°C., removing, rapidly blotting with filter paper, and weighing. This procedure was found to remove 80–90% of the sol content incidentally. Deviations in the weight gain ratio were below 0.03 for Viton but up to 0.3 for Kel-F Elastomer. The volume swelling ratio, $\mathbf{q}_m$, was computed by the formula

$$\mathbf{q}_m = 1 + [(w_2 - gw_1)/gw_1]\,(\rho/\rho')$$

where w_2 is the weight of swollen polymer, w_1 the weight of original polymer, g the gel fraction, ρ the density of polymer, and ρ' the density of solvent. Procedures for the homopolymers were different.[10]

Specific gravities of the whole polymer and gel residue were determined by hydrostatic weighing. To reduce errors due to surface tension, the sampling was immersed in ethanol momentarily before weighing.

Stress–strain diagrams were obtained on an Instron machine at 23°C. The jaw separation was 5.09 cm. The crosshead speed was 12.7 cm./min. for Viton A and 50.9 cm./min. for Kel-F Elastomer.

Tensile force at fixed extension was also measured, by using either the stress relaxation apparatus or improvised arrangements of clamps and weights.

Swollen Gel Elasticity

The principle of the method and earlier references are given by Smith.[5] The present procedure is a rough adaptation.

A rectangular prism, about 1 by 2 by 0.1–0.4 cm., of a sample of gel of known volume swelling ratio q_m was measured with vernier calipers and placed horizontally between glass surfaces. Force was applied by weights acting upon the upper member through a vertical glass pillar. The vertical displacement of a reference mark was read by a cathetometer to within 0.001 cm. The initial thickness, displacement, force, and cross-sectional area yielded values of the compression ratio α (here $\alpha < 1$) as a function of force per unit area, from which the effective crosslink density in the unswollen gel can be derived.[11] Because of the dimensions and slight surface irregularity, it was necessary to make measurements at relatively great compression, $\alpha = 0.80$–0.90. Shrinkage from loss of solvent was prevented in some instances by immersing the assembly in solvent. In other cases the unstressed length was interpolated from alternate measurements. The irradiated poly(vinylidene fluoride) and polytrifluoroethylene were studied by observing the elongation of thin, swollen strips under tensile stress.

Stress Relaxation Measurements

The stress relaxation apparatus is shown in Figure 1. (The apparatus was constructed by R. S. Pizer, Polymer Characterization Section, National Bureau of Standards.) Two strain gages, on opposite faces of a semielliptical spring, act as a stress transducer for the stretched sample. The strain gages form two arms of a bridge circuit, of which the unbalance is fed to a recorder.

The present method of mounting compensates for temperature differences between the region of the spring and the remainder of the bridge. Calibration of the present arrangement showed a deviation from linearity by amounts up to 20%. Trouble was experienced with gradual drifts and sudden shifts under load. As far as can be determined, the cementing of the gages to the spring is somewhat critical. A soft polyester cement produces a tendency toward gradual drift, while a hard epoxy cement produces a tendency toward sudden shifts. Good gage–spring combinations, after a break-in period of several weeks to achieve reproducibility, served satisfactorily for several months with minor recalibration.

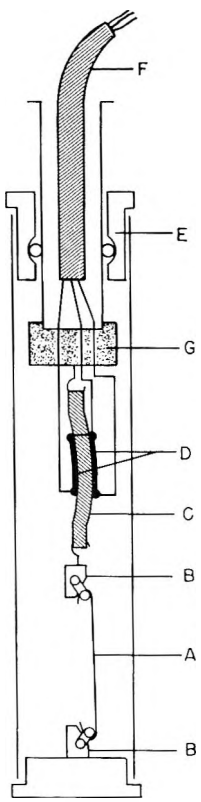

Fig. 1. Stress relaxation apparatus: (A) stretched polymer; (BB) clamps; (C) semielliptical spring; (DD) strain gages cemented to spring; (E) ball-bearing lock; (F) cable to resistance bridge and recorder; (G) terminal block.

Strips of elastomer were crosslinked by radiation before use. The sample dimensions for Viton A were 10 by 0.64 by 0.16 cm. and for Kel-F Elastomer 3700, 10 by 0.63 by 0.22 cm., the differences arising from shrinkage after molding. A sample was marked near the center, stretched to 200% elongation, and after a delay of 5–15 min., placed in the radiation source of calibrated intensity. The stress was recorded as a function of time. Atmospheres of air and flowing prepurified nitrogen were used. Corrections were applied for gage calibration, and a zero point drift of the order of 1–5% full scale, assumed to be continuous.

The present procedure compromises seriously one of the desired initial conditions for chemical stress relaxation, namely, that the initial stress shall be the equilibrium stress of the chemically crosslinked network. In the present study, it was decided to accept this disadvantage, since the usual expedients for preliminary relaxation seemed likely to alter the radiation chemistry. In particular, heat is known to increase the number of crosslinks in Viton A,[5] and solvents would be difficult to remove completely.

RESULTS AND DISCUSSION

Molecular Weights

Number-average molecular weights were estimated from intrinsic viscosity of Viton A in tetrahydrofuran–dimethyl-formamide (87/13 by weight) and of Kel-F Elastomer 3700 in methyl ethyl ketone, at 29.2°C., with the aid of correlation charts and data on whole polymer mentioned earlier.

Intrinsic viscosities in certain other solvents were also obtained (Table I). The benzene–methyl ethyl ketone solvent is an attempt to approxi-

TABLE I
Intrinsic Viscosities of Polymers[a]

Polymer	Solvent, weight-%	$[\eta]$, dl./g.
Viton A-HV	Tetrahydrofuran (THF) 87–dimethyl-formamide (DMF) 13	1.64
	Methyl ethyl ketone	1.48
	Ethyl acetate	1.40
	Benzene 68–methyl ethyl ketone 32	0.82
Viton A	The 87–DMF 13	0.86
	Ethyl acetate	0.80
Kel-F Elastomer 3700	Methyl ethyl ketone	2.66
	Ethyl acetate	2.80
	Benzene 81–methyl ethyl ketone 19	1.14
Polytrifluoroethylene[b]	Dimethylformamide	1.98
	THF 87–DMF 13	1.98

[a] At 29.2°C.
[b] Sol fraction from slow polymerization at room temperature.

mate a theta solvent. Incipient precipitation was observed at temperatures 5–10°C. below the temperature of the measurements.

Density

The density of the polymers undergoes very little change during irradiation (Table II), and there are no systematic differences between whole polymer and gel. If crosslinks are formed by a condensation eliminating HCl or HF, a steady increase in density could be expected; in fact, however, extracted Kel-F Elastomer has a density minimum at 8 Mr.

TABLE II
Specific Gravities of Irradiated Polymers

Polymer	Specific gravity various doses			
	0	4 Mr.	8 Mr.	16 Mr.
Viton A, whole	1.811	1.816	1.820	1.820
Viton A, extracted	—	1.821	1.815	1.814
Kel-F Elastomer, whole	1.827	1.827	1.828	1.836
Kel-F Elastomer, extracted	—	1.846	1.837	1.844

Stress–Strain Diagram

The stress–strain diagrams at high speed (Figs. 2 and 3) qualitatively resemble those of vulcanized rubbers. At low extension, the stress is least in the most highly crosslinked materials.

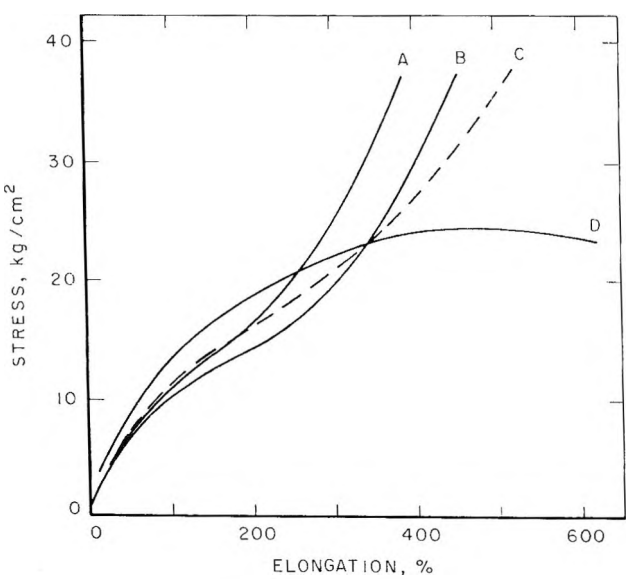

Fig. 2. Stress–strain diagram of Viton A samples at various crosslinking radiation doses of samples: (*A*) 16 Mr.; (*B*) 8 Mr.; (*C*) 4 Mr.; (*D*) none. Temperature 23°C., jaw separation 5.09 cm., crosshead speed 12.7 cm./min.

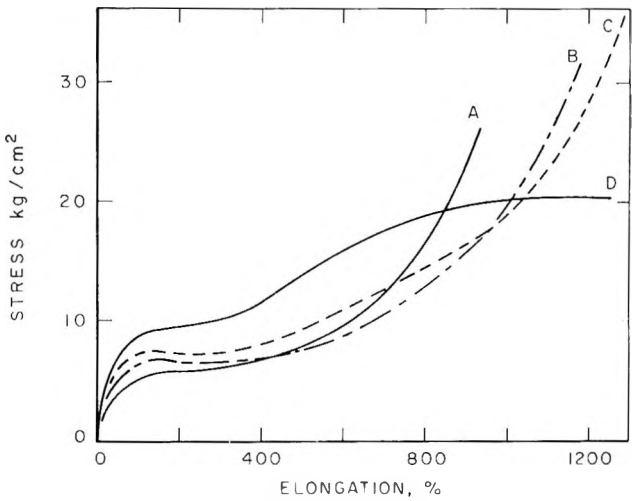

Fig. 3. Stress–strain diagram of Kel-F Elastomer 3700 samples at various crosslinking radiation doses of samples: (*A*) 16 Mr.; (*B*) 8; (*C*) 4; (*D*) none. Temperature 23°C., jaw separation 5.09 cm., crosshead speed 50.9 cm./min.

Sol Content

The variation of sol fraction s with dose is shown in Table III and in Figure 4 as a plot of $s + \sqrt{s}$ versus reciprocal dose.[7] Following Charlesby,

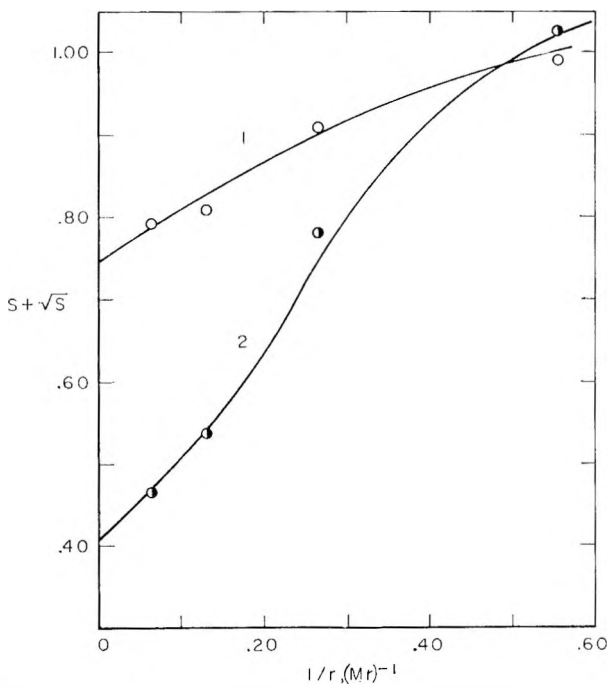

Fig. 4. Charlesby sol plot for irradiated elastomers: (*1*) Kel-F Elastomer 3700; (*2*) Viton A-HV.

TABLE III
Sol Content and Gel Swelling of Elastomers

Polymer	Dose, Mr.[a]	Sol fraction[b]	Weight gain, %[c]	Volume swelling ratio, q_m[d]
Viton A-HV	0.7	0.507	888	36.5
	1.7	0.397	695	21.25
	4	0.266	496	15.32
	8	0.149	388	10.54
	16	0.120	313	8.45
Kel-F Elastomer 3700	0.7	0.463	1770	64.6
	1.7	0.377	1652	51.8
	4	0.334	1332	42.6
	8	0.282	986	29.6
	16	0.271	816	22.7

[a] Co^{60} at 2 Mr./hr., 27°C.
[b] Soxhlet extraction with acetone, 70 hr.
[c] Ethyl acetate, 22°C., 42 hr.; whole polymer basis.
[d] Swollen volume/dry gel volume.

the sol content s should be related to the number of scissions per monomer unit p and the number of crosslinked units per monomer unit q by the equation

$$s + \sqrt{s} = p/q$$

provided that the polymer has a "most probable" initial molecular weight distribution and that the scissions and crosslinked units are formed at constant rates. Under these conditions

$$s + \sqrt{s} = (p_i + p_0 r)/q_0 r$$
$$= (p_0/q_0) + (p_i/q_0)\,(1/r)$$

where the subscript i refers to initial value and subscript zero to rate of accumulation per unit radiation dose, and r is the dose. A plot of $s + \sqrt{s}$ versus reciprocal dose should thus have an intercept $p_0/q_0 = G_d/G_c$, and a slope $p_i/q_0 \cong 1.11 \times 10^6/G_c M_{ni}$ for the present copolymers and megaroentgen dose units. If the initial molecular weight distribution differs from the "most probable," it will tend toward this distribution after sufficient random scissions and thus the given relation can be approached at high radiation doses. In Figure 4, the deviations at low dose (high $1/r$) may be an effect of molecular weight distribution or of a substantial change of G_d/G_c. The intercepts give the values $G_d/G_c = 0.40$ for Viton A and 0.76 for Kel-F Elastomer 3700. Utilizing slopes at moderately high doses from Figure 4 and the molecular weights stated for the materials, the computed G_c values are:

For Viton:

$$G_c = 1.11 \times 10^6/(0.74 \times 330{,}000) = 4.5$$

For Kel-F Elastomer:

$$G_c = 1.11 \times 10^6/(0.55 \times 421{,}000) = 4.8$$

These values are highly doubtful because of the variable slope and uncertain molecular weight distribution. Similar results, somewhat lower, can be obtained by the method of Shultz and Bovey,[12] in which logarithmic plots of per cent sol versus dose are compared by horizontal translation with a set of master curves derived for various values of G_d/G_c. Estimates of G_c derived from gel swelling and elasticity are probably more reliable.

Gel Elasticity of Elastomers

The number of moles of effective crosslinked chains per unit volume of the unswollen gel can be computed from the relationship[11]

$$F/A = RT\ (\nu_e/V_0)\ v_2^{1/3}\ [\alpha - (1/\alpha^2)] \tag{1}$$

where F/A = force per unit cross-sectional area of swollen unstretched sample (in dynes/square centimeter); R = gas constant (in ergs/mole-degree); (ν_e/V_0) = effective crosslinked chain density in unswollen gel (in moles/cubic centimeter); v_2 = volume fraction polymer in swollen polymer gel; and α = length, swollen, compressed/length, swollen, unstressed. By regarding the whole polymer as gel fraction, swollen by sol, the results can be used also to estimate effective crosslinked chain density and tensile stress in the unextracted whole polymer. Table IV lists the experimental values of ν_e/V_0 for the two elastomers. The polymers are not strictly comparable with those of Table III, since 5–12 months elapsed between the experiments. Lines 1, 2, and 3, and lines 4 and 6,

TABLE IV
Crosslinked Chain Concentration by Swollen Gel Elasticity

Polymer	Dose, Mr.	$10^5\nu_e/V_0$, moles/cm.^{3}[a]	Solvent	q[b]
Viton A	3.8	1.9	Ethyl acetate	17.50
				16.61[c]
Viton A	3.8	2.9	Acetone	2.77[d]
Viton A	15.2	8.4	Ethyl acetate	8.63
Viton A	15.2	7.8	Methyl ethyl ketone	9.31
Viton A	15.2	10.7	Mixed[e]	4.98
Viton A	15.2[f]	7.6	Ethyl acetate	7.25
Kel-F Elastomer	7.6	1.25	Ethyl acetate	32.6
Kel-F Elastomer	7.6	0.89	Ethyl acetate	36.8

[a] Moles of effective crosslinked chains per cubic centimeter dry gel.
[b] Volume/dry gel volume; swelling temperature usually 20–23°C.
[c] Swelling temperature 29°C.
[d] $q \ll q_m$.
[e] Benzene–methyl ethyl ketone, 68:32 (w/w).
[f] Heated 15 min., 125°C.

respectively, represent successive experiments on the same sample. The computed ν_e/V_0 is generally highest at the lowest swelling. The difference is serious for lines 1 and 3. The variation, in terms of $q^{1/3}$, is loosely comparable with reported variations of (F/A) $[\alpha - (1/\alpha^2)]$ as a function of α in the literature.[13] For lines 4 and 6, Table IV, the crosslink density is near 5×10^{-3} crosslinked units per monomer unit and the values of $q^{1/3}$ are 1.6 and 2.05, respectively; for a corresponding increase of α, decreases near 10% in (F/A) $[\alpha - (1/\alpha^2)]$ are reported. The ν_e/V values at low swelling, lines 3 and 6, may be the most reliable.

Although these values could be used directly in the calculation of radiation yields, it is preferable, because of their poor precision, to employ them as reference points to derive crosslinked chain densities from the gel swelling results.

Crosslinked Chain Densities from Gel Swelling

The complete swelling equation[11b] is:

$$-[\ln (1 - v_{2m}) + v_{2m} + \chi_1 v_{2m}^2] = V_1 (\nu_e/V_0)(v_{2m}^{1/3} - v_{2m}/2) \qquad (2)$$

Here v_{2m} is the volume fraction of solvent in the swollen gel, $q_m = v_{2m}^{-1}$ is the swelling volume ratio, χ_1 is the polymer–solvent interaction parameter, V_1 is the molar volume of the solvent, V_0 is the volume of the gel without solvent, and ν_e is the number of moles of effective crosslinked chains. A simpler approximation may be used if the swelling is greater than tenfold:

$$q_m^{5/3} = (V_0/\nu_e)\,(1/2 - \chi_1)/V_1 \qquad (3)$$

Each experimental swelling volume, from Table III and IV, yields a linear numerical relation between χ_1 and ν_e/V_0. By plotting these lines and also the experimental ν_e/V_0 of Table IV, a representative value of χ_1 can be selected from the data, and ν_e/V_0 can be estimated with the aid of this χ_1. The χ_1 values selected were: for Viton A, 0.30 ± 0.04 in ethyl acetate, 0.30 in methyl ethyl ketone, and 0.48 in benzene–methyl ethyl ketone; for Kel-F Elastomer, 0.26 ± 0.06 in ethyl acetate and 0.46 in benzene–methyl ethyl ketone.

G Values from Effective Crosslinked Chain Densities

The changes of elasticity and gel swelling with radiation dose involve two considerations: (*1*) the increase in the number of scissions and crosslinks in an irradiated polymer and (*2*) the relation of crosslinks and scissions to the elastic forces in a crosslinked network.

The theory of simultaneous crosslinking and chain scission has been discussed extensively.[6–8]

Although the processes can be described in principle for any initial molecular weight distribution, the description is especially simple if the polymer has initially a "most probable" molecular weight distribution.

If scissions occur at random, the distribution tends toward the "most probable" with increasing degradation.[7a] As an ideal case a hypothetical infinite polymer chain is imagined, into which scissions and crosslinked units are introduced at random, to the extent of p scissions and q crosslinked units per chain monomer unit. Before irradiation, the condition of the polymer can be represented by p_i cuts and, perhaps, in some cases by q_i crosslinked units per monomer unit. For an initial "most probable" distribution, $p_i \cong M_0/\bar{M}_n$, where M_0 is the monomer unit molecular weight and $\bar{M}_n$ the number-average molecular weight; in other cases p_i is merely an extrapolated number. Radiation introduces further cuts and crosslinked units at rates p_0 and q_0 per unit dose per monomer unit. At a dose r, the numbers of scissions and crosslinked units per monomer unit are $p = p_i + p_0 r$ and $q = q_i + q_0 r$, respectively; ordinarily, $q_i = 0$. The number-average molecular weight, if no crosslinking had occurred, would be $\bar{M}_n = M_0/(p_i + p_0 r)$, and the number-average molecular weight between crosslinked chains becomes $\bar{M}_c = M_0/(q_i + q_0 r)$. Considering the gel and sol separately, the random processes result in a selectivity[7b] such that

$$M_{cg} = M_c/(1 + s) \tag{4}$$

$$\bar{M}_{ng} = M_n\,(1 + \sqrt{s}) \tag{5}$$

where s is the sol fraction and the subscript g denotes the values in the gel fraction.

The equation of rubber elasticity

$$\begin{aligned} F/A_0 &= RT\,(\nu_e/V)\,[\alpha - (1/\alpha^2)] \\ &= RT\,(\rho/\bar{M}_c)\,[1 - 2(\bar{M}_c/\bar{M}_n)]\,[\alpha - (1/\alpha^2)] \\ &= RT\,(\rho/\bar{M}_c)\,[1 - 2(\bar{M}_n)]\,[\alpha - (1/\alpha^2)] \end{aligned} \tag{6}$$

can then be developed by substitution to yield the formula

$$\nu_e/V = (q/V^1)\,[1 - (2p/q)] \tag{7}$$

Here V^1 is the molar volume of monomer units and the other symbols are previously defined [eqs. (1)–(6)].

Under ordinary circumstances

$$q = q_0 r$$

$$p = p_i + p_0 r$$

$$q_0 \cong 10^{-6}\,G_c/M_0$$

$$p_0 \cong 10^{-6}\,G_d/M_0$$

and

$$\frac{d}{dr}\left(\frac{\nu_e}{V}\right) \cong 10^{-6}\rho\,(G_c - 2G_d) \tag{8}$$

where G_c and G_d are the G values of crosslinked units and scissions in molecules per 100 e.v. absorbed, M_0 is the monomer unit molecular weight, and r is in megaroentgens. The precise value of the factor shown as 10^{-6} varies somewhat with the energy absorption coefficients in the material and is approximately 0.90×10^{-6} for the present copolymers. For r in megarads the numerical factor is 1.04×10^{-6}. The above formulae [eqs. (7) and (8)] assume that the material is substantially all gel and rely upon a correction term $2\bar{M}_c/\bar{M}_n$, which is in dispute.[9b]

Equation (7) can apply only poorly to Viton A, which retains a substantial sol content at all radiation doses, and cannot be used at all for Kel-F Elastomer 3700, where the substitution of $G_d/G_c = 0.70$, determined from the sol plot, would lead to a decrease rather than the observed increase of ν_e/V (Table V). In the absence of a more reliable relation,

TABLE V
Effective Crosslinked Chain Concentration from Swelling Equation

Polymer	Dose, Mr.	$10^5\ \nu_e/V_0$, moles/cm.^{3}
Viton	0.7	0.50
	1.7	1.05
	3.8	2.65
	7.6	5.43
	15.2	8.15
	15.2[a]	10.5
Kel-F Elastomer	0.7	0.23
	1.7	0.33
	3.8	0.45
	7.6	0.95
	15.2	1.50

[a] Heated 15 min. at 125°C.

the values of M_n and M_c in the gel [eqs. (4) and (5)] can be substituted in eq. (7); the result is

$$\begin{aligned}(\nu_e/V)_g &= (\rho/\bar{M}_{cg})\ [1 - 2\ (\bar{M}_{cg}/\bar{M}_{ng})] \\ &= \rho\ \{(1 + s)/\bar{M}_c - [2/\bar{M}_n\ (1 + \sqrt{s})]\} \\ &= (\rho/M_c)\ \{q(1 + s) - [2p/(1 + \sqrt{s})]\}\end{aligned} \tag{9}$$

On substituting $p/q = s + \sqrt{s}$ and $q = q_i + q_0 r$, eq. (9) is reduced to:

$$(\nu_e/V)_g = (\rho/M_0)\ (q_i + q_0 r)\ (1 - \sqrt{s})^2 \tag{10}$$

A plot of $(\nu_e/V)_g\ (1 - \sqrt{s})^{-2}$ against dose should have a slope of $q_0\rho/M_0 = 10^{-6}\rho G_c$.

Figure 5 shows that such plots are not far from linear at doses greater than 4 Mr. The slopes of Figure 5 and the G_d/G_c values found from Figure 4 imply that for Viton A, $G_c = 3.45$, $G_d = 1.35$, and for Kel-F Elastomer, $G_c = 1.81$, $G_d = 1.37$.

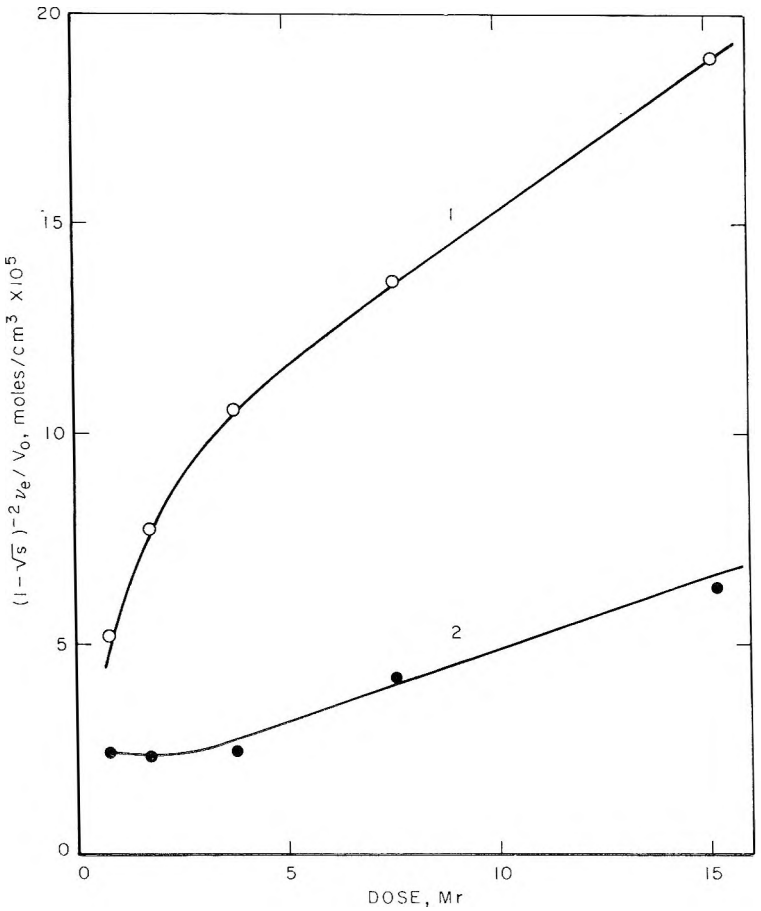

Fig. 5. Crosslink concentration function vs. dose, according to eq. (10), data of Tables III and V: (*1*) Viton A; (*2*) Kel-F Elastomer 3700.

It is disturbing that Figure 5, if extrapolated to neglect the lower doses, leads to a high initial crosslink density in Viton A.

$$\begin{aligned} q_i &= (\nu_e/V_0)\,(1-\sqrt{s})^{-2}\,(M_0/\rho) \\ &= 8 \times 10^{-5} \times 79.5/1.83 \\ &= 3.48 \times 10^{-3} \text{ crosslinked units/monomer unit} \end{aligned}$$

From the initial molecular weight, $p_i = 79.5/330{,}000 = 2.42 \times 10^{-4}$. The resulting ratio $p_i/q_i = 0.07$ corresponds to an almost totally gelled initial material, whereas both the originally received and the molded materials are completely soluble. Possibly an initial material of very broad molecular weight distribution could be represented by the indicated q_i and a much higher $p_i \leqslant 2q_i$. For Kel-F Elastomer 3700 this representation would be reasonable, as measurements are stated to yield high apparent ratios of $\bar{M}_w/\bar{M}_n$ and the value of intrinsic viscosity in Table I is unusually high for the given $\bar{M}_n$. With Viton A, the intrinsic viscosity

does not seem to indicate an abnormally broad distribution, and the apparent q_i is left unexplained. For comparison, the values of $G_c - 2G_d$ computed by eq. (8) are 3.3 for Viton A and 0.6 for Kel-F Elastomer. In view of the G_d/G_c ratios 0.40 and 0.76, this implies $Gc = 17.3$, $G_d = 6.9$ in Viton A, and this would give an infinite G_c in Kel-F Elastomer even if G_d/G_c were as low as 0.50. The values obtained from eq. (10) and Figure 5 are preferred.

Rubber Elasticity

The equilibrium stress of the extended elastomer should be a measure of the effective crosslinked chain concentration ν_e/V_0.

$$F/A_0 = RT(\nu_e/V_0)\ [\alpha - (1/\alpha^2)] \tag{6}$$

where F is the equilibrium tensile force. The force on the extended irradiated polymers appears to approach a steady-state value which changes little in 100 hr. The unirradiated polymers appear to do likewise, but tend to form beads ultimately and to slip at the clamp. These steady-state tensile forces, Table VI are considerably greater than those implied

TABLE VI
Steady-State Tensile Forces of Extended Elastomers[a]

Polymer	Dose, Mr.[b]	Elongation, %	F/A_0, kg./cm.^{2}	$10^5\nu_e/V_0$, moles/cm.^{3}
Viton A	0[c]	200	7.20	9.8
	4.0	55	4.23	14.5
	4.0	200	6.83	9.3
	4.0	585	11.36	9.3
	8.0	52	3.79	12.6
	8.0	200	7.46	10.2
	16.0	54	4.65	16.3
	16.0	200	10.60	14.4
Viton A, heated[d]	4.0	200	2.66	3.62
	8.0	50	1.28	4.79
	16.0	50	2.24	8.35
Kel-F Elastomer	0[c]	200	3.82	5.20
	4.0	200	2.78	3.78
	8.0	200	2.58	3.51
	16.0	200	1.92	2.61

[a] Measured at 25°C., 20–100 hr.; except as noted.
[b] Center of strip, doses higher than in Tables III–V.
[c] 25°C., 7–14 hr.
[d] Extended, heated 15 min. at 125°C., measured cold.

by the ν_e/V_0 of Table V. If the sample is heated to 120–130°C. while extended, the elastic force is more nearly comparable with results of Table V. The relatively high value of the steady-state tensile forces at 23°C. may be regarded as a purely viscoelastic phenomenon or as a con-

sequence of relatively durable virtual crosslinks, which may be entanglements, crystallites, or perhaps small regions of high local vinylidene fluoride concentration subject to large dipole attractions. Such assemblies would be easily broken up by the relatively polar solvents employed in swelling and extraction. At room temperature, the polar and chemical crosslinks could form a randomly mixed system, in which the numbers of crosslinked units and chain cuts go as $q = q_i + q_0r$ and $p = p_i + p_0r$, respectively, in the notation of eq. (7).

If we define a virtual sol fraction s^1, the root of $s^1 + \sqrt{s^1} = p/q$, the number of cuts and crosslinks in the continuous network is given by eq. (7). If the effect of dilution by the virtual sol fraction present [eq. (1)] is included, the tensile stress of the whole polymer will be given by:

$$F/A = (RT/V)\,(1 - s^1)^{-1/3}\,(1 - \sqrt{s^1})^2\,(q_i + q_0r) \qquad (11)$$

where $V = M/\rho$ is the molar volume of monomer units.

This form of variation accounts for the decreasing difference of the two ν_e/V with dose, and for the decrease in steady-state elasticity of Kel-F Elastomer while the chemical ν_e/V is growing.

Crosslinks and Scissions in Homopolymers

For the homopolymers CF_2CFH and CF_2CH_2, gel swelling, gel content, and crosslinked unit density, derived from gel elasticity by eq. (1), are given in Tables VII and VIII. The requisite physical constants are in Table IX. Plots of the sol function $s + \sqrt{s}$ against reciprocal dose are satisfactorily linear over a wide range, as discussed elsewhere.[10] The G_d/G_c values in Table X are extrapolated from the portion of the curves at moderate doses and are somewhat larger than values based on the highest doses. The sol values at the highest doses are subject to appreciable error arising from other causes of weight loss. The formation of crosslinks in the present polymers is presumably accompanied by loss of HF, which may not be completely released from hard polymers until

TABLE VII
Gel Content, Swelling, and Concentration of Crosslinked Chains from Gel Elasticity of Irradiated Polytrifluoroethylene

Dose, Mr.	Gel, %	q_m (acetone)[a]	q_m (DMF)	ν_e/V_0, moles/cm.^{3} × 10^{-4}[b]
1	0	—	—	—
9.8	56.15	15.43	—	—
18.5	64.18	6.27	—	—
38	83.95	3.04	—	—
86	93.00	2.79	6.19	1.3
124	95.80	2.63	4.85	2.4
203	96.80	2.21	2.74	—

[a] Total volume to gel volume, calculated with constants of Table IX.
[b] From elasticity of swollen gel.

TABLE VIII
Gel Content, Swelling, and Concentration of Crosslinked Chains from Gel Elasticity of Irradiated Poly(vinylidene Fluoride)

Dose, Mr.	Gel, %	q_m (in DMF)	ν_e/V_0, moles/cm.^{3} × 10^{-4}
1	Present	>21	—
9.8	84.44	26.37	0.12
18.5	90.27	13.42	0.38
38	95.55	8.70	1.00
86	96.16	5.60	2.00
124	96.76	4.68	—
203	97.62	3.74	—

TABLE IX
Constants of Polymers and Solvents

Material	Monomer or solvent mol. wt.	Density, g./cm.^{3}
$(CF_2CFH)_x$	82	2.03
$(CF_2CH_2)_x$	64	1.74
$(CH_3)_2CO$	58	0.792
$HCON(CH_3)_2$	73	0.9505

TABLE X
Radiation Yields and Solvent Interaction Parameters

	Polymer–solvent system		
	$(CF_2CFH)_x$–acetone	$(CF_2CFH)_x$–DMF	$(CF_2CH_2)_x$–DMF
G_d/G_c	0.16–0.21	—	0.18–0.21
G_c–$2G_d$	1.4	—	1.2
G_c	2.1–2.4	—	1.9–2.1
G_d	0.3–0.5	—	0.2–0.4
χ	0.62	0.38	0.33

extraction. For $G_c = 5$, about 2.5×10^{-4} equivalents of HF would be released per gram at 100 Mr, which in poly(vinylidene fluoride) amounts to a weight loss of 0.3%. Additional losses of HF during extraction, to form systems of conjugated double bonds, are indicated by the observed darkening of poly(vinyl fluoride) and poly(vinylidene fluoride) after extraction and drying. Losses from both causes can result in spurious high sol contents with a magnified effect on $s + \sqrt{s}$.

The swelling volumes of polyvinylidene fluoride, q_m (Table VIII) when treated by eq. (2), are highly consistent with the crosslink densities ν_e/V_0 obtained from gel elasticity; the constancy of χ (Table X) is excellent.

Results are less consistent with polytrifluoroethylene (Table VII and X). A χ_1 of 0.62 is obtained from swelling and elasticity at high radiation

doses. The χ value probably varies with crosslink density, but a χ_1 in the region of 0.50 is consistent with the observed erratic solubility of various batches of this polymer in acetone. The initial molecular weight

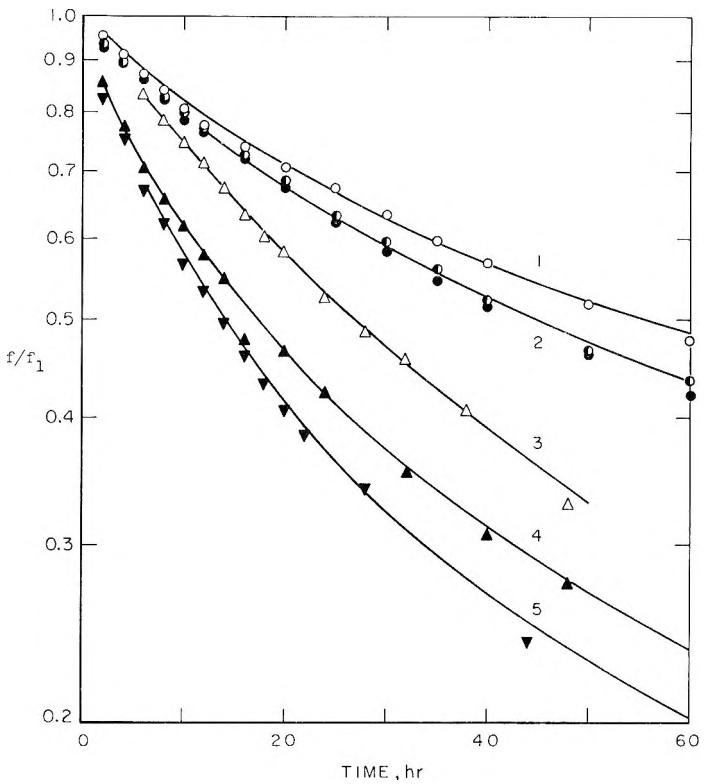

Fig. 6. Stress relaxation of Viton A at 0.31 Mr./hr.: (*1*) previous radiation dose 16 Mr., nitrogen atmosphere; (*2*) (◐) 8 Mr., nitrogen, and (●) 4 Mr., nitrogen; (*3*) 16 Mr., air atmosphere; (*4*) 8 Mr., air; (*5*) 4 Mr., air. Ordinates of curves *1* and *3* are 1.11 (f/f_1).

of the present batches is presumably low. The sol fraction plot, $s + \sqrt{s}$ versus $1/r$, furnishes a rough estimate of the initial molecular weight.

In Charlesby's notation [see eq. (7)]

$$s + \sqrt{s} = (p_0/q_0) + (p_i/q_0)\ (1/r)$$

where s is the sol fraction, r the dose, p_0 and q_0 the number of cuts and crosslinked units per monomer unit per megaroentgen, respectively, and p_i is the initial number of cuts per monomer unit in a sample. Taking $q_0 = 10^{-6}\ G_c M_1 = 2.1 \times 10^{-1} \times 82$ and the slope $p_i/q_0 = 14.4$ Mr., we obtain $p_i = 2.4 \times 10^{-3}$ and an initial $\overline{M}_n = M_1/p_i = 33{,}000$.

Presumably χ is sufficiently lower than 0.62 initially to permit solution of a low molecular weight polymer.

Stress Relaxation of Elastomers

In experiments conducted as described, without complete prior relaxation, the customary ratio of force to initial force and the customary plot of log $[f(t)/f(0)]$ against time are not simple measures of chain scission. Arguments will be developed to suggest that log $[f(t)/f_1(t)]$ is a reasonable measure, where $f_1(t)$ is the force sustained by an unirradiated sample at time t, and also that an appropriate molecular weight is that derived from the steady-state elasticity at long times. Figures 6–10 show the function $f(t)/f_1(t)$ on a logarithmic scale versus linear time for the several copolymers. Figure 11 shows that the force in the absence of radiation f_1, becomes nearly constant and differs little from this constant value over much of the time range of experimental interest. The time scale in Figure 11 is logarithmic for comparison with the theoretical linear variation of f_1 with log t.[14]

In the discussion of long-term rubber elasticity (Table VI) part of the elasticity was attributed to durable polar crosslinks. Besides the durable crosslinks there are entanglements which can be regarded formally as temporary crosslinks.[14] The effectiveness of a chain, in general, can be destroyed by thermal motion or by scission. If we consider the probabilities of scission and thermal relaxation to be independent, then we define: $\Phi(t)$ = probability of being cut at time t, $1 - \Phi(t)$ = probability

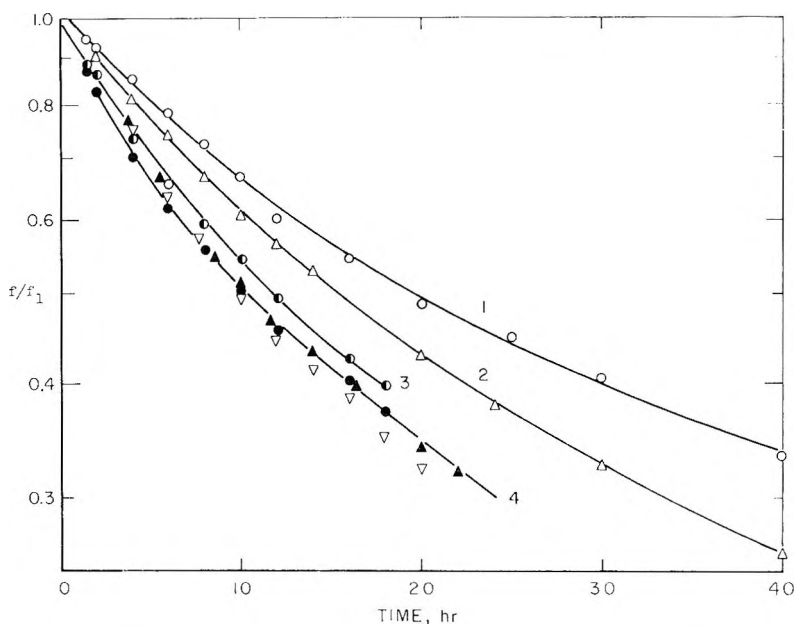

Fig. 7. Stress relaxation of Viton A at 0.8 Mr./hr.: (*1*) primary dose 16 Mr., N_2 atmosphere, ordinates $1.22f/f_1$; (*2*) primary dose 16 Mr., air atmosphere, ordinates $1.14f/f_1$; (*3*) primary dose 8 Mr., N_2, ordinates $1.11f/f_1$; (*4*) (●) primary dose 4 Mr., N_2, ordinates $1.11f/f_1$; (▲) primary dose 8 Mr., air, ordinates $1.00f/f_1$; (▽) primary dose 4 Mr., N_2, ordinates $1.11f/f_1$.

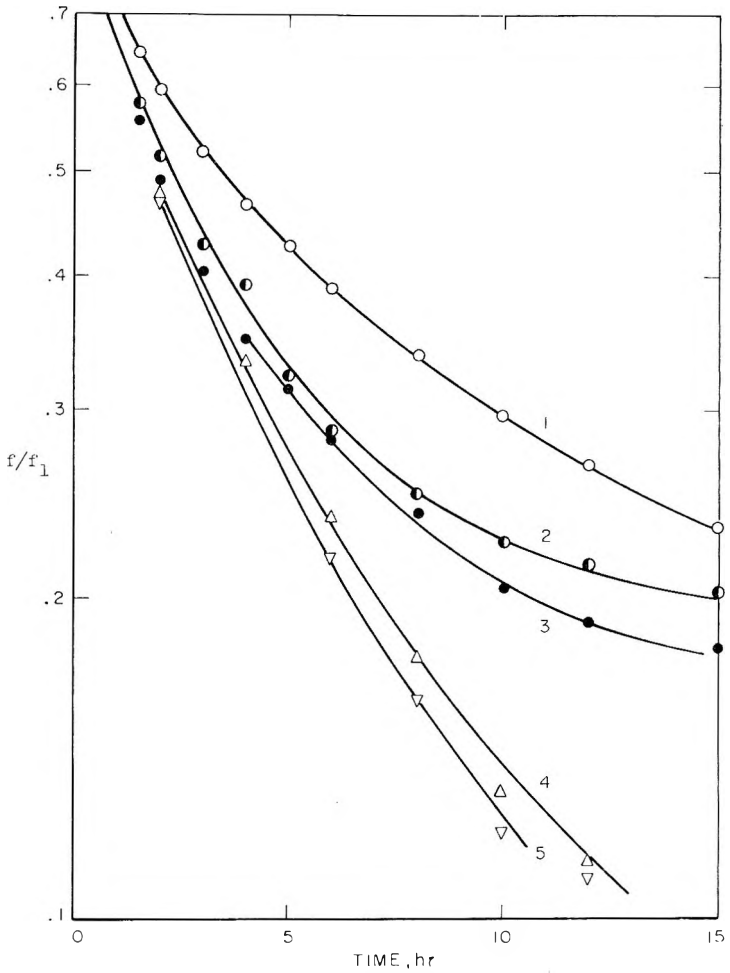

Fig. 8. Stress relaxation of Viton A at 2.7 Mr./hr.: (*1*) primary radiation dose 16 Mr., nitrogen atmosphere; (*2*) 8 Mr., nitrogen; (*3*) 4 Mr., nitrogen; (*4*) 8 Mr., air; (*5*) 4 Mr., air.

of being uncut, $\theta(t)$ = probability of being thermally relaxed at time t, $1 - \theta(t)$ = probability of being unrelaxed at time t. At time t some chains will be cut only, some relaxed only, some both cut and relaxed, and some untouched by either process. The chains supporting stress will be those in the last class.

Let $f(t)$ be the force at time t in a radiation field and $f_1(t)$ be the force at the same time, unirradiated. Then

$$f(t)/f(0) = [1 - \theta(t)]\,[1 - \Phi(t)] \tag{12}$$

$$f_1(t)/f(0) = 1 - \theta(t) \tag{13}$$

$$1 - \Phi(t) = \frac{f(t)}{f_1(t)} \tag{14}$$

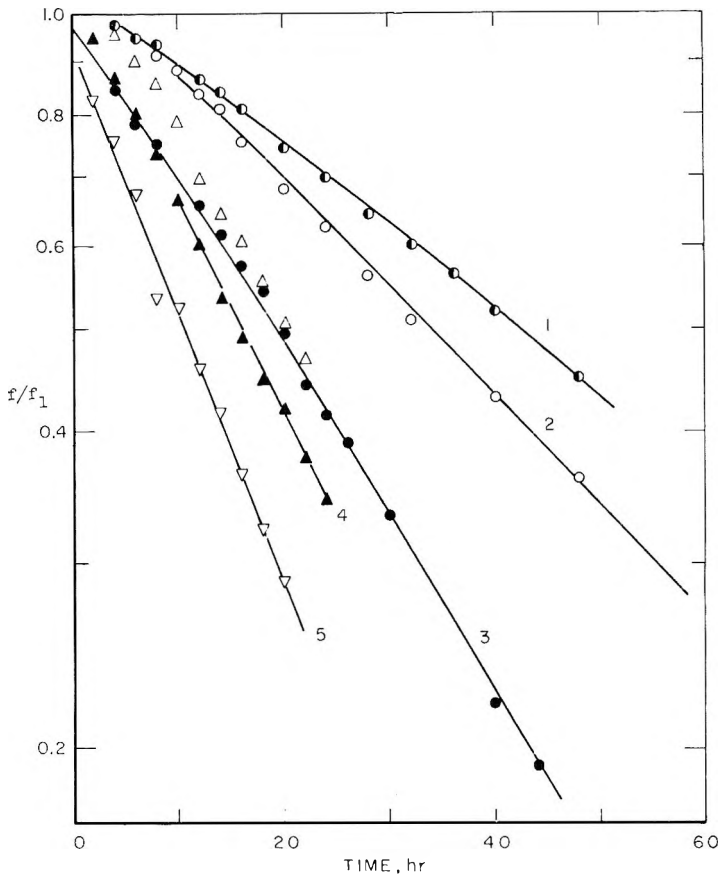

Fig. 9. Stress relaxation of Kel-F Elastomer 3700 at 0.31 Mr./hr.: (*1*) primary dose 8 Mr., nitrogen atmosphere; (*2*) 16 Mr., N_2; (*3*) (●) 4 Mr., N_2; (△) 16 Mr., air; (*4*) 8 Mr., air; (*5*) 4 Mr., air.

By eq. (4) the function $f(t)/f_1(t)$ gives the fraction of chains not cut by radiation, irrespective of temporary or permanent class. If there were no distinction in scission rates, this would also be the fraction of permanent chains remaining uncut.

By the basic equation

$$-dn/dt = K_d nP \tag{15}$$

where n = number of crosslinked chains, K_d = scission rate of units, molecules per unit time per molecule present, P = degree of polymerization between crosslinks, the rate of chain scission is proportional to the degree of polymerization P. The effective degree of polymerization varies considerably with the network considered, and may be designated P_t, P_d, and P_m for the temporary, durable, and mixed over-all systems, respectively. By the hypothesis of a mixed system and thermal relaxation at the crosslinks, the degree of polymerization of any surviving temporary chains at

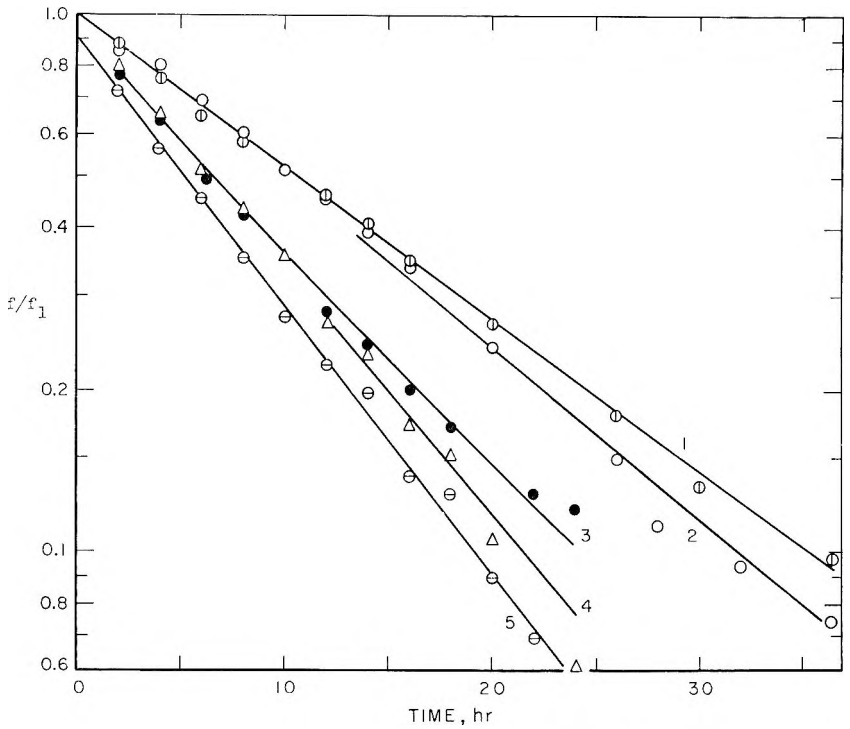

Fig. 10. Stress relaxation of Kel-F Elastomer 3700 at 0.8 Mr./hr.: (*1*) primary dose 8 Mr., nitrogen atmosphere, ordinates $1.18f/f_1$; (*2*) primary dose 16 Mr., nitrogen atmosphere; (*3*) primary dose 4 Mr., nitrogen atmosphere, (*4*) primary dose 16 Mr., air atmosphere; (*5*) primary dose 8 Mr., air atmosphere.

time t should be $P_t(t) = P_m(0) = 1/n_m(0)$. However, if all temporary chains could be removed, the degree of polymerization of the durable network would be

$$P_d(t) = P_d(0) = 1/n_d(0) = 1/n_1(\infty)$$

where $n_1(\infty)$ is the number of chains per monomer unit at infinite time in the absence of radiation. The number-average degree of polymerization of all chains surviving in the irradiated specimen at time t will be an average

$$\frac{n_t(t)P_t + n_d(t)P_d}{n_1(t) + n_d(t)}$$

which is equal to

$$\frac{\dfrac{n_t(t)}{n_m(0)} + \dfrac{n_d(t)}{n_1(\infty)}}{n_t(t) + n_d(t)}$$

At times when $n_t << n_d$, i.e., $f_1(t) - f_1(\infty) << f(t)$, the contribution from the temporary crosslinked chains will vanish and the effective degree

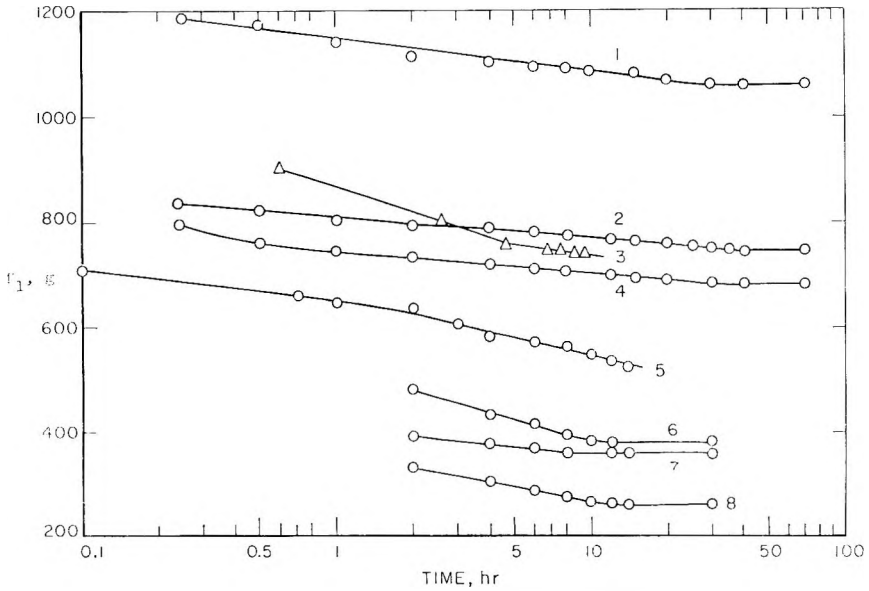

Fig. 11. Stress relaxation of elastomers in the absence of radiation at various crosslinking radiation doses: (*1*)–(*4*) Viton A, 16, 8, 0, and 4 Mr.; (*5*)–(*8*) Kel-F Elastomer 3700, 0, 4, 8, and 16 Mr. Elongation 200%, temperature 25 ± 2°C. f_1, force on test strip.

of polymerization will approximate P_d. In view of Figure 11, the deviation from P_d will be negligible at $t > 20$ hr. and small at much earlier times.

The plots of Figures 6–10, with f/f_1 on a logarithmic scale, should be nearly linear except initially, if the molecular weight between crosslinks $\bar{M}_c$ is uniform. The plots for Kel-F Elastomer (Figs. 9 and 10), appear to satisfy this requirement. Those for Viton A (Figs. 6–8), are obviously concave upward. It can be shown[15–17] that this curvature is to be expected for an initial "most probable" molecular weight distribution and a more nearly linear plot is often obtained from $f_1(t)/f(t)$ versus t. A few of the curves are redrawn in this fashion in Figure 12. The two treatments differ very little in the region $f(t)/f_1(t) > 0.6$.

The value of the scission yield, G_d, in scissions per 100 e.v., is obtained from the slope of either type of plot at low doses and the molecular weight between crosslinks of the initial sample. Taking the dose conversion factor 0.86 rads per roentgen for both polymers,

$$G_d = 1.11 \times 10^6 \, \bar{M}_c^{-1} \, I^{-1} \, m$$

where $\bar{M}_c$ is the initial molecular weight between crosslinks, I is the radiation field intensity in megaroentgens per hour, and m is the slope of the plot of f_1/f versus t or 2.303 times the slope of $\log f/f_1$ versus t per hour.

The choice of an appropriate $\bar{M}_c$ offers difficulties in a material con-

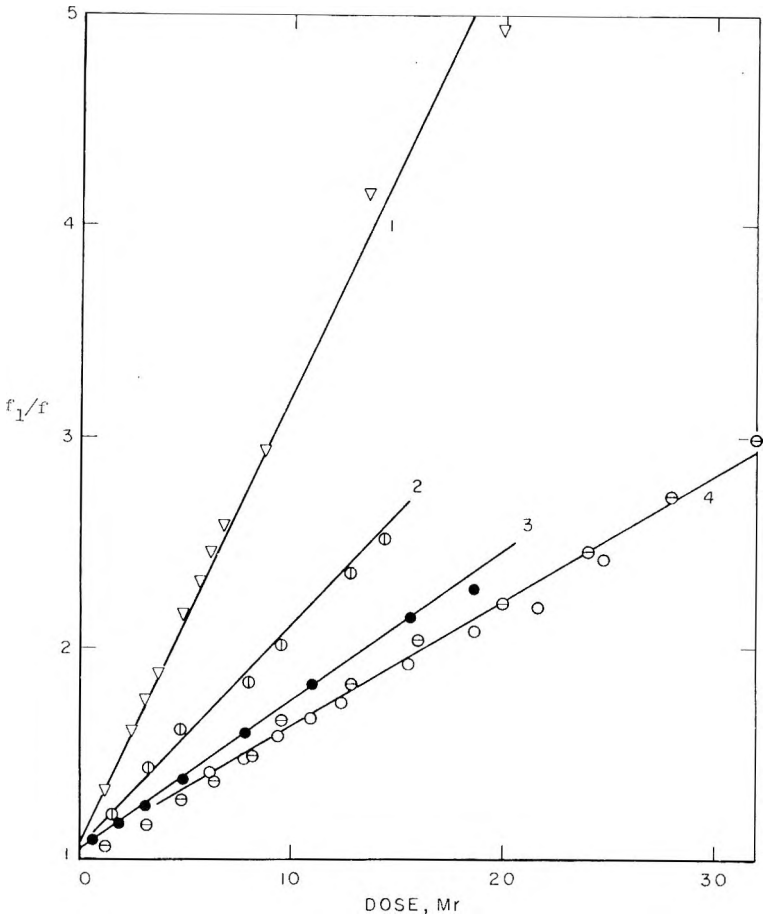

Fig. 12. Reciprocal stress plot for Viton A, preliminary doses, atmospheres, and dose rates as follows: (*1*) 4 Mr., air, 0.31 Mr./hr.; (*2*) 4 Mr., N_2, 0.8 Mr./hr.; (*3*) 4 Mr., N_2, 0.3 Mr./hr.; (*4*) (⊖) 16 Mr., N_2, 0.8 Mr./hr.; (◐) 16 Mr., N_2, 0.31 Mr./hr.

taining many scissions. Of the quantities in the usual equation of rubber elasticity,

$$F/A = RT\,(\nu_e/V)\,[\alpha - (1/\alpha^2)]$$
$$= RT\,(\rho/\bar{M}_c)\,[1 - (2\bar{M}_c/\bar{M}_n)]\,[\alpha - (1/\alpha^2)]$$

neither $\rho V/\nu_e$ (that is, $\bar{M}_e$) nor $\bar{M}_c$ is appropriate. If we imagine replicates of an arbitrary effective chain, containing some broken side branches, the frequency of scission of this type of chain will be equal to the volume rate of scissions multiplied by the volume of that part of the chain lying along the continuous route between crosslinks. This excludes material located on side branches as well as sol. The use of $V/\nu_e = \bar{M}_e/\rho$ thus gives too large an effective volume. Likewise $\bar{M}_c/\rho$ is too small, since cruciform structures containing two broken side chains, which are effectively one long chain,

will be counted as two short chains, and more generally the greater average circuit length in the scissioned polymer will be neglected. Since two cuts are required to make a molecule of sol and only one to make a dead-end chain, the proportion of dead-chain material will go rough as $\sqrt{s}$ and that of main-chain material as $1 - \sqrt{s}$. If we use eq. (10) as a relation between $\nu_e/V = \rho/M_e$ and (ν/V) total $= \rho/\bar{M}_c$, then:

$$1/M_c = 1/\bar{M}_e(1 - \sqrt{s})^2$$

$$1 - \sqrt{s} = (\bar{M}_c^{1/2}/\bar{M}_e)^{1/2}$$

$$\bar{M}_e\,(1 - \sqrt{s}) = (\bar{M}_c\bar{M}_e)^{1/2}$$

Table XI shows the values of $\bar{M}_e$, $\bar{M}_c$, and the geometric mean, computed from approximate G values, initial molecular weights, and initial apparent crosslinked chain densities of the unirradiated polymers. A zero virtual

TABLE XI
Molecular Weights between Crosslinks from Steady-State Elasticity

Polymer	Dose, Mr.	$\bar{M}_e = (\nu_e/\rho V)^{-1}$	$\bar{M}_c$ (computed)[a]	$(\bar{M}_c\bar{M}_e)^{1/2}$
Viton A	4	19,900	15,100	17,500
	8	18,500	13,000	15,400
	16	13,000	8,180	10,250
Kel-F Elastomer	4	36,800	27,300	31,600
	8	39,600	24,600	31,200
	16	53,500	26,400	37,500

[a] Assumed values: for Viton A, $\nu_e/V_0 = 9.3 \times 10^{-5}$ moles/cm.^{3} at zero dose, $\bar{M}_{ni} = 330{,}000$, $G_d = 1.41$, $G_c = 3.62$; for Kel-F Elastomer, $\nu_e/V_0 = 6.41 \times 10^{-5}$ moles/cm.^{3} at zero dose, $\bar{M}_{ni} = 421{,}000$, $G_d = 1.64$, $G_c = 2.17$.

TABLE XII
Apparent G_d from Stress Relaxation

Polymer	Atmosphere	Preparative dose, Mr.	G_d, scissions per 100 e.v. at given dose rate: At dose rate 0.31 Mr./hr.	At dose rate 0.8 Mr./hr.	At dose rate 2.7 Mr./hr.
Viton A	N_2	4	4.6	7.1	7.7
		8	5.2	7.3	7.0
		16	5.6	7.9	6.9
Viton A	Air	4	13.2	8.9	12.5
		8	12.5	8.4	15.2
		16	12.2	10.2	—
Kel-F Elastomer	N_2	4	4.1	4.1	—
		8	1.9	2.4	—
		16	2.1	2.4	—
Kel-F Elastomer	Air	4	6.2	4.8	—
		8	4.8	3.6	—
		16	3.7	—	—

sol is assumed for the initial material. The geometric mean values were used to derive the apparent G values for scission in Table XII.

The G_d values in nitrogen scatter greatly and all are appreciably higher than the values of 1.35 (Viton A) and 1.37 (Kel-F Elastomer) derived from the gel measurements on vacuum-irradiated polymer by eq. 10. The lowest values for Kel-F Elastomer are only 50% too high, but those for Viton A disagree by a factor of 3 or more. The agreement obviously could be improved by differences in treatment of data. The gel-based G_d would be raised indefinitely by using eq. (7) in place of eq. (10), and the stress relaxation G_d could be lowered to any desired extent by relying upon log slopes at sufficiently high dose. Possible material reasons for the discrepancy are the following: (*1*) the scission rate is genuinely high in the stretched polymer, (*2*) it is basically mistaken to associate the long-term steady-state elasticity with a network containing polar crosslinks, and (*3*) impurities in the nitrogen, especially oxygen and water, may raise the scission rate.

The first possibility is eliminated by the observation that stretched (α = 2.50) and unstretched regions of a strip of Viton A, exposed to the same dose of 4 Mr. in vacuum, exhibited the same sol contents and gel swelling volumes within 1 or 2%. Therefore, stretching has no large influence on scission rates.

Possibility (*2*) is very likely *a priori*. The observed stresses may be a complicated phenomenon, understandable only in terms of the phenomenological theory of viscoelasticity. The steady-state stress of the unirradiated specimen is involved as well as the temporary stresses, since the steady-state is approached within 10–20% after 1–2 hr. The problem is most easily avoided by the use of heat-relaxed specimens, at low enough elongation to avoid rupture.

Possibility (*3*) must also be considered, since leaks could have occurred, although the nitrogen was of "prepurified" quality and contained less than 0.05% oxygen by mass spectrometer analysis. Very small amounts in a flowing stream could provide sufficient oxygen for accelerated scission. Rapid diffusion into the interior of the sample is nevertheless unlikely. Small leaks could also have provided water as a reactant.

The results of stress relaxation in air (Figs. 5–12, Table XII) show a slight acceleration for Kel-F Elastomer and greater acceleration for Viton A. In the case of Kel-F Elastomer, the reported permeability to oxygen, 5.5×10^{-10} cm.^{3} (STP)/cm.^{2}-mm.-sec.-cm. Hg, is incompatible with any appreciable consumption of oxygen during scission.

The consumption of O_2 per unit volume in cubic centimeters (STP)/second is:

$$K = 6.2 \times 10^{-6} IG\rho$$

where I is the dose rate in megaroentgens per hour, G the G value for O_2 consumption, and ρ is the density. Solution of the diffusion equation for a consumption rate independent of concentration gives:

$$c = pS - (K/D)(L^2 - X^2)$$

and

$$c = 0$$

at

$$X^2 = L^2 - p(P/K)$$

where c is the concentration of o_2, p is the partial pressure of O_2, S is the solubility coefficient, K is the rate of consumption, D is the diffusion coefficient, $P = DS$ is the permeability, L is the half thickness, and X is the distance outward from the center of the strip. Substituting the half thickness of the Kel-F Elastomer strip at 200% elongation (0.061 cm.), the density 1.84 g./cm.^{3}, the partial pressure of oxygen in air (15.2 cm. Hg), and a typical dose rate of 1 Mr./hr, then if $G = 5$, $X/L = 0.998$ for exhaustion of oxygen, i.e., a negligible depth is penetrated.

If $X = 0$, i.e., some oxygen reaches the center, then $G = 0.02$, indicating that the consumption of oxygen is much less than the increase in scission rate.

Thus, unless the permeability of the stretched Kel-F Elastomer is much greater than the reported value, even a moderate effect of oxygen on scission may involve chain reactions.

To avoid a similar difficulty for Viton A in air, the permeability must be greater than 2×10^{-7} cm.^{3} STP/cm.^{2}-mm.-sec.-cm. Hg, assuming a G value of 10 and a dose rate of 1 Mr./hr. This would be rather higher than the permeability of natural rubber, recorded as 2×10^{-8} in the same units.[18]

Since the G values for scission in air (Table XII) do not vary systematically with dose rate, there is no evidence for diffusion controlled reaction in the range studied. Also, the form of the stress relaxation curves in air is similar to that in nitrogen for both elastomers, whereas a distorted form would be expected if the reaction rate varies greatly with depth.

TABLE XIII
Crosslink and Scission Yields

Polymer	G_c	G_d	G_d/G_c
$(CF_2CH_2)_x$	2.0	0.3	0.20
$(CF_2CH_2)_x(C_3F_6)_y$	3.4	1.3	0.40
$(CF_2CH_2)_x(CF_2CFCl)_y$	1.8	1.4	0.76

Although the evidence on reaction rates and permeabilities suggests the possibility of a chain mechanism for scissions in oxygen, it is not easy to propose plausible reaction steps involving oxygen and vinylidene fluoride copolymer units.

It is difficult to say whether the G_d values measured by gel swelling or those measured by stress relaxation are more reliable. The large ratio of

scissions to crosslinks requires sweeping assumptions in order to estimate both values by the gel swelling method, and the use of radiation crosslinked starting materials in the stress relaxation experiments introduced uncertainties regarding the effective molecular weight factor. Even the low G_d values from gel swelling are much larger than those of pure poly(vinylidene fluoride) (Table XIII). Part of the difference may depend upon physical state, since poly(vinylidene fluoride) is a glass. Since the ratios G_d/G_c are also higher in the copolymer, the transition from glass to rubber must facilitate scission more than crosslinking, unless there is an intrinsically high scission rate in the fluorocarbon comonomer units.

The authors wish to thank Dr. C. Sperati, E. I. du Pont de Nemours and Co. for data on intrinsic viscosity and osmotic pressure of Viton copolymers.

The authors wish to thank Dr. R. P. Bringer, Minnesota Mining and Manufacturing Co. for results of intrinsic viscosity and light scattering studies on Kel-F Elastomer 3700.

References

1. Dixon, S., D. R. Rexford, and J. S. Rugg, *Ind. Eng. Chem.*, **49**, 1687 (1957).
2. Jackson, W. W., and D. Hale, *Rubber Age*, **77**, 865 (1955).
3. Harrington, R., *Rubber Age*, **77**, 865 (1955).
4. Florin, R. E., L. A. Wall, *J. Res. Natl. Bur. Std.*, **65A**, 375 (1961).
5. Smith, J. F., and G. T. Perkins, *Rubber Plastics Age*, **1961**, 59.
6. Bovey, F. A., *The Effect of Ionizing Radiation on Natural and Synthetic High Polymers*, Interscience, New York, 1958.
7. Charlesby, A., *Atomic Radiation and Polymers*, Pergamon Press, New York, 1960, (a) p. 167; (b) pp. 146–148.
8. Chapiro, A., *Radiation Chemistry of Polymeric Systems*, Interscience, New York, 1962, Chap. 8, pp. 364–380.
9. Tobolsky, A. V., *Properties and Structure of Polymers*, Wiley, New York, 1960, (a) Chap. 5, pp. 223–265; (b) p. 95.
10. Straus, S., and L. A. Wall, paper presented at the 144th American Chemical Society Meeting, New York, September 1963.
11. Flory, P. J., *Principles of Polymer Chemistry*, Cornell University Press, Ithaca, N. Y., 1953, (a) p. 492; (b) p. 579.
12. Shultz, A. R., *J. Am. Chem. Soc.*, **80**, 1854 (1958).
13. Rabjohn, N., P. J. Flory, and M. C. Schaffer, *J. Polymer Sci.*, **4**, 225 (1949).
14. Furukawa, J., *Rubber Chem. Technol.*, **35**, 1016 (1962).
15. Yu, H., *J. Polymer Sci.*, **B2**, 631 (1964).
16. Bueche, A. M., *J. Chem. Phys.*, **21**, 614 (1953).
17. Berry, J. P., and W. F. Watson, *J. Polymer Sci.*, **18**, 201 (1955).
18. Barrer, R. M., *Diffusion in and through Solids*, Macmillan, New York, 1941, p. 417.

Résumé

La fluorure de polyvinylidène, le polytrifluoroéthylène, et deux copolymères caoutchouteux avec le fluorure de vinylidène, ont été pontés par irradiation gamma sous vide. La dégradation des chaînes dans les copolymères, induite par irradiation, a été étudiée en observant la relaxation de la tension à extension constante pendant une irradiation à 27°C, de 0.31 à 2.7 mégaröentgens par heure, dans l'azote et dans l'air. À partir de la teneur en gel, du gonflement et de l'élasticité, les valeurs de G_c (pontage) et G_d (dégradation) sont: pour CF_2CFH G_c = 2.2 et G_d = 0.4; pour CF_2CH_2, 2.0 et 0.3; pour

CF_2CH_2 + C_3F_6, 3.4 et 1.3; pour CF_2CH_2 + CF_2CFCL, 1.8 et 1.4. Les valeurs de G_d par relaxation de la tension sont variables; les plus bases sont: pour CF_2CH_2 + C_3F_6 4.6 dans l'azote et 8.4 dans l'air; pour le CF_2CH_2 + CF_2CFCl, 1.9 dans l'azote et 3.6 dans l'air.

Zusammenfassung

Polyvinylidenfluorid, Polytrifluoräthylen und zwei kautschukartige Copolymere mit Vinylidenfluorid wurden durch Gammabestrahlung in Vakuum vernetzt. Die strahlungsinduzierte Kettenspaltung in den Copolymeren wurde durch Beobachtung der Spannungsrelaxation bei konstanter Dehnung während weiterer Bestrahlung bei 27°C, bei 0,31 bis 2,7 Megaröntgen pro Stunde in Stickstoff und Luft untersucht. Die aus Gelgehalt, Quellung und Elastizitat erhaltenen Werte von G_c (Vernetzung) bzw. G_d (Spaltung) betrugen: für CF_2CFH, G_c = 2,2 und G_d = 0,4; für CF_2CH_2, 2,0; und 0,3; für CF_2CH_2 + C_3F_6, 3,4 und 1,3; für CF_2CH_2 + CF_2CFCl, 1,8 und 1,4. Die G_d-Werte aus der Spannungsrelaxation zeigten eine gewisse Variabilitat; die niedrigsten betrugen: für CF_2CH_2 + C_3F_6, 4,6 in Stickstoff und 8,4 in Luft; für CF_2CH_2 + CF_2CFCl, 1,9 in Stickstoff und 3,6 in Luft.

Received September 17, 1964
(Prod. No. 4551A)

JOURNAL OF POLYMER SCIENCE: PART A VOL. 3, PP. 1713–1724 (1965)

Mechanism of Fracture in Glassy Polymers. I. Fracture Surfaces in Polymethyl Methacrylate*

R. P. KAMBOUR, *General Electric Research Laboratory, Schenectady, New York*

Synopsis

The interference colors on poly(methyl methacrylate) fracture surfaces have been shown to arise from a layer of craze material. The order of interference can be determined in various ways for most areas on the fracture surface and craze layer thicknesses determined. Layer thickness is a function of fracture velocity; at zero velocity where the Griffith criterion may be applied with the least error an average surface layer thickness of 6800 A. is calculated. The plastic work of this amount of craze formation corresponds to 13–20% of the nominal Griffith energy.

Background

Nearly a decade ago, colors were first observed to exist on freshly produced fracture surfaces in glassy poly(methyl methacrylate) specimens. These colors have been extensively described in relation to fracture velocities and various fracture surface markings.[1] Fracture surface colors have also been observed sometimes on polystyrene and acrylonitrile–styrene copolymer specimens.[1] It has also been known for several years that the Griffith energy for crack propagation is roughly three orders of magnitude larger than that which could be assigned to the breakage of a monolayer of chemical bonds. Berry, in particular, has postulated that this discrepancy and the colors are associated, and more specifically that the large Griffith energy arises from the viscous work of aligning of polymer chains ahead of crack tip; subsequent crack growth leaves a thin, highly oriented layer of polymeric material on the fracture surface.[2] If the layer were of the right thickness and uniformity and had a sufficiently highly anisotropic refractive index, an optical interference phenomenon could result.

More recently, understanding of the crazing process has offered a somewhat different and more appealing hypothesis for the existence of the fracture surface colors. Crazes in glassy polymers were shown to be more or less filled with an oriented load-bearing polymeric material.[3–5] The elongation process appears to occur without macroscopic reduction in cross section through an interaction between a three-dimensional tensile stress system and a sort of strain hardening. This results in creation of a substantial void

* Presented in part at the Sixth Symposium of the Polymer and Fiber Microscopy Society, Camille Dreyfus Laboratory, Durham, N. C., April 1964.

content which is dispersed on a scale well below that of the wavelength of light, producing a craze refractive index roughly half way between that of air and that of bulk polymer.[6,7]

Since stresses beyond the tip of a crack have hydrostatic tensile components, a plastic response here might well be a crazing one. Subsequent splitting of the craze would leave an optically interfering layer on the fracture surface. The first experimental evidence that this might be occurring, at least qualitatively, came from the discovery that both crazes and fracture surfaces in glassy polymers cause a low-angle scattering of x-rays.[8]

Refractive Index of Poly(methyl Methacrylate) Fracture Surface Layers

Subsequent to the x-ray scattering discovery, a method was devised for measuring the refractive index of fracture surface layers.[9] The measurement is one of the critical angle for total reflection and is made possible by putting a suitable liquid of high refractive index in contact with the fracture surface. Such placement puts the surface layer in the same situation optically as the craze in bulk polymer: a thin planar layer expected to be of low refractive index sandwiched between regions of high refractive index. In the best of cases onset of total reflection still takes place over several degrees of arc. This is presumed to be due variously to deviations of the surfaces from planarity and orthogonality on a gross scale, to fracture surface roughness on a micro scale, and to layer thicknesses being small enough to cause some frustration of total reflection.

Surface layer indices have been measured for cleavage samples at two temperatures (25 and 60°C.) and for two molecular weights (3,000,000 and 110,000). Best results are obtained when the wedge is driven into the saw cut hard enough to produce a crack which runs rapidly at first but decelerates and stops close to the back edge of the sample; upon completion of the fracture one finds a characteristic saw tooth line where the crack stopped and just preceding this an area which appears quite smooth and monoplanar to the eye. In fact it has a roughness in the range of a few hundred angstroms (as determined from surface reflection interferometry). Measurements in these areas are least ambiguous. For both temperatures and molecular weights a surface layer refractive index of 1.32–1.34 is calculated. Since craze refractive indices in this material are the same, the cleavage surface layer appears quantitatively to be crazelike.

Attempts to measure critical angles on tensile fracture surfaces (i.e., high-speed fracture surfaces) have been unsuccessful. These surfaces have roughnesses in the range of 2000 A. and show no sudden onset of total reflection. Cleavage surfaces produced much below room temperature become quite complex, and above 60° the fracture surface layers become too susceptible to thermal collapse.

Aids in Establishing Surface Layer Thicknesses

In order to assess the contribution of the crazing response ahead of the crack tip to the fracture propagation energy it becomes necessary to measure

surface layer thicknesses. Such thicknesses could be estimated fairly accurately if, in addition to refractive index, the order of interference n for a surface showing any particular colors were known, since for this kind of interference[10]

$$(n + 1/2)\lambda = 2\mu d \cos \phi$$

where λ is the wavelength of light undergoing destructive interference, μ is the layer refractive index, d is the layer thickness, and ϕ is the angle of incidence. The constant $^1/_2$ is present because, in contrast to the more usual situation for producing interference (e.g., an air wedge between glass plates), the phase changes upon reflection from the air–craze interface and from the craze–bulk polymer interface are both zero. At optical thicknesses less than $^1/_4\lambda$, reinforcement should occur, in contrast to the black zero-order destructive interference arising in the more usual system. There would arise at greater thicknesses a $^1/_4\lambda$ destructive interference followed by the interferences of higher order. The $^1/_4\lambda$ interference is the closest phenomenon in this scheme to the conventional zero-order black interference.

It is useful to summarize here the characteristics of white light interference at constant incident angle to show how several of these can serve as bench marks in determining the order of interference in an area of interest. In a conventional interference wedge, as thickness increases, zero-order black fades out through a grey or grey-brown to a pale yellow to orange to red, usually rusty in appearance, which is commonly termed first-order red. This is followed by a brilliant and distinct second-order blue—by far the most distinct blue ever observed—then a bright second-order green, second yellow, and second red. The second-order red overlaps with third-order blue which gives the red a purple cast. Third-order green is again a strong, distinct color, sometimes hard to distinguish from second-order green, but third-order red is pastel. Higher order colors are increasingly pastel, and only red and green hues appear. When an interfering layer is varying in thickness from place to place in an irregular but not excessively abrupt manner then one can often use one or more of the above characteristics to establish order in one spot and then follow thickness changes over the surface to a place of particular interest. Because the higher order surface colors are rather weak and because color changes commonly occur over distances of a micron or less, a high resolution bright field reflection microscope with a well collimated light beam is required in following surface color changes. We have found a Zeiss GFL microscope with objectives up to 40× suitable in these regards.

Another technique which is sometimes useful with fracture surface layers is what could be termed the "hot scratch" treatment. Since these layers are unstable, application of heat tends to cause a thickness decrease. Because of the unique relationship for these interfering films between refractive index and thickness for a given film once formed, film collapse causes film index to rise toward that of the bulk. By combination of the interference equation with the Lorenz-Lorentz equation

$$p = [(\mu^2 - 1)/(\mu^2 + 2)](1/\rho)$$

where p is the specific polarizability of the polymer* and μ and ρ are taken to be the refractive index and density of the layer at any particular state of rarefaction, the following is obtained

$$(n + {}^1/_2)\lambda = 2d_0(1 + x)[(2p\rho_0 + 1 + x)/(x + 1 + p\rho_0)]^{1/2}$$

Here x is the degree of elongation of the craze material from the original bulk state, ρ_0 is the bulk density, and d_0 is the thickness of bulk material to

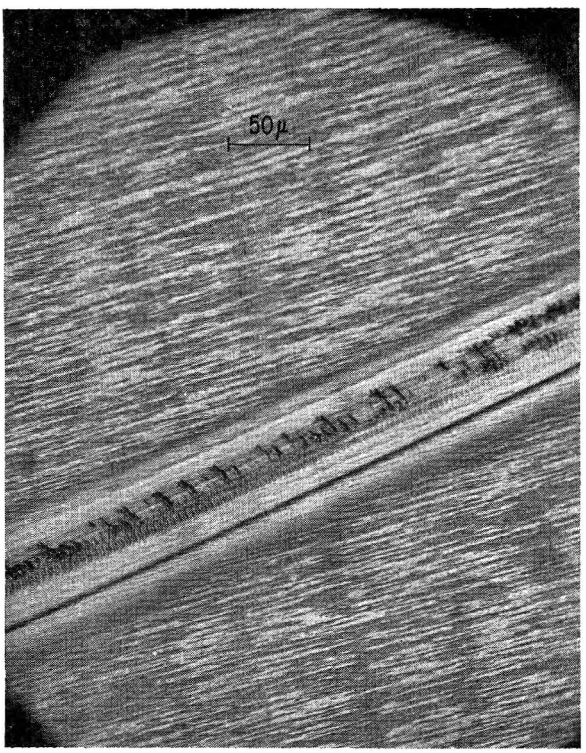

Fig. 1. Hot needle scratch on a Plexiglas II cleavage surface. The actual area of needle contact is bounded on one side by the narrow dark line. Beyond the succeeding light area (colorless) can be seen a diffuse dark band (second-order red) which is followed by the undisturbed surface (second-order red and third-order green). Green light.

undergo rarefaction. The quantity under the square root is just the refractive index as a function of elongation. A plot of the optical thickness $(n + {}^1/_2)\lambda$ against x shows that it increases in a linear fashion in spite of the decrease of μ with x. Therefore upon reversal of the process (e.g., thermal collapse of the craze), $(n + {}^1/_2)\lambda$ will show a decrease.

Consequently when a needle which has been heated to redness is drawn

* The weight fraction of air in dry craze material is essentially zero; thus p for the bulk polymer equals that for the film.

lightly over a fracture surface, a more or less annealed region can be seen between the actual area of contact and the unaffected surrounding area of surface color (Fig. 1). Close to the true scratch the surface is colorless, since collapse is complete or nearly so; next to the surrounding field a band of differing color is seen which is lower in order than the field. Thus if a particular field is suspected to be second- or third-order yellow rather than first-order, the hot scratch will produce a distinctly green border; if the color were first-order, no green could be produced in this manner.

The same kind of collapse in the surrounding field can be often caused by an indenter pushed into the material. Apparently plastic distortion of the substrate allows film collapse.

A final technique which is of some use is reflection interference microscopy. Most of the smoother areas on cleavage surfaces still show a biplanar structure. It is sometimes desirable to prove that in a particular field showing, for example, alternating second-order red areas interspersed with green areas that the latter are truly third-order green and not second- or fourth-order. The surface in question can be placed untreated on a Zeiss interference microscope and fringes produced on the surface which follow the changes in surface height. If such leads to calculated changes of only a few hundred angstroms, then the colors will truly be "adjacent" ones.

Newton's Rings on Fracture Surfaces

Perhaps the most useful observation about fracture surfaces is that under certain conditions these bear features which optically appear to be sets of more or less distorted Newton rings. With Plexiglas II (molecular weight $\sim 10^6$) these are the hyperbolic markings observed mostly on tensile fracture surfaces in intermediate speed areas (Fig. 2). These markings have been observed and studied for some time,[1,11] but to the author's knowledge their similarity to classical Newton's rings has not previously been pointed out. In any case the hyperbolic focus is usually a very small black spot thought to be $^1/_4\lambda$ interference. Complete destruction of all wavelengths is perhaps apparent to the eye because the spot is very small and the $^1/_4\lambda$ dependence is a small one. Beyond the black spot is a white or yellowish area surrounded by a nearly circular first-order red ring. This in turn is followed by a normal sequence of colors out to third or fourth-order, where the level of the hyperbola often becomes coincident with the surrounding fracture surface. The higher the color is the more distorted is the ring; away from the focus in the general fracture direction any one distorted color tends to cover a relatively broad range while in the opposite direction the rings are bunched up.

It can generally be observed both for cleavage and tensile fracture surfaces that layer optical thickness increases with fracture velocity. On tensile fracture surfaces this can be seen by simply observing general color progression with the naked eye. When such dependence becomes known quantitatively, it should become possible then to map velocity profiles in the hyperbola in a detailed way and arrive at a better understanding of its forma-

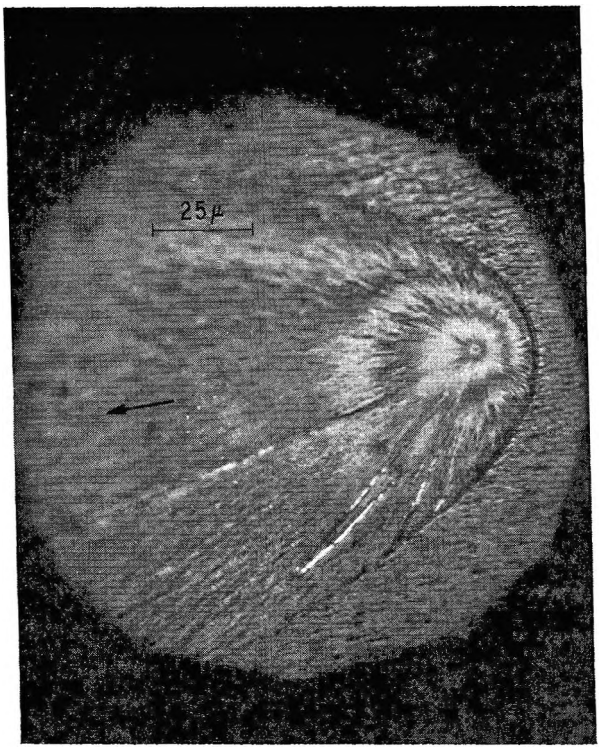

Fig. 2. Parabola including distorted set of Newton's rings on Plexiglas II tensile fracture surface. Green light. The black dot at the parabolic focus is thought to be $^1/_4\lambda$ destructive interference. The arrow indicates general fracture direction.

tion. At present it can only be observed that layer thickness in the hyperbola increases much more gradually in the direction of general crack propagation than it does in the counter direction.

Parenthetically, it has been observed that while the hyperbolic features are usually biplanar as previously noted,[11] some are monoplanar. The biplanarity is thus not an essential feature of their growth. Also hyperbolas are occasionally noted in Plexiglas II which have no black spots at their foci. These rather are the yellow-white which precedes the first-order red. Color progression is otherwise normal. The lack of the black spot would seem only to indicate a layer thickness at the focus slightly greater than the usual.

Surface Layer Thickness and Zero Crack Velocity

Since layer thickness is a function of crack velocity, it is of most importance to determine thickness at positions where the crack, under increasing stress, just begins to grow or where it has decelerated to a stop. It is at these points that the use of the Griffith criterion,[12] which is a thermodynamic one, is most nearly justified.

Experience here with both tensile and cleavage samples has shown that the zero-velocity position and layer thickness thereat are most easily deter-

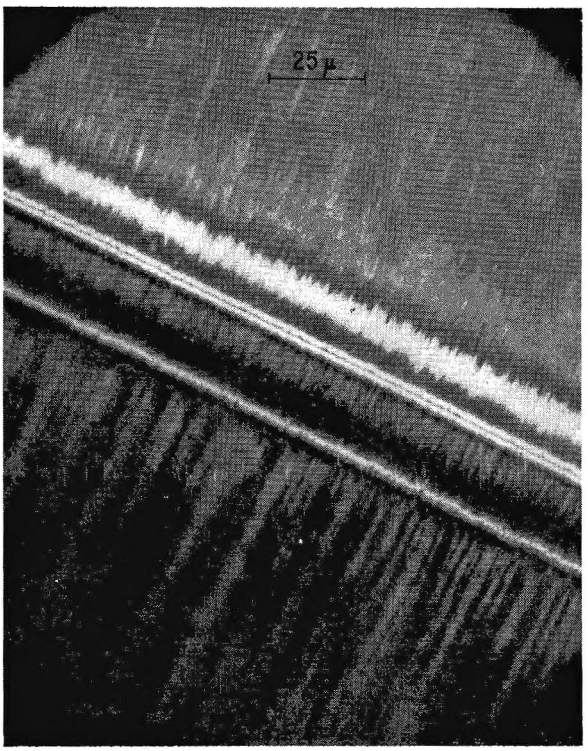

Fig. 3. Band of 25μ width at cleavage crack stop line. Green light. The band is defined by the narrow lines. The broad light line is not particularly characteristic of the crack stop position.

mined on the latter samples. The evolved procedure involves cutting a swallow-tailed groove (or other groove of varying depth) in a sample edge and then driving a sharp wedge into the saw cut. The crack can thus be started in a controlled manner and propagated to any desired length.[13] The back edge of the sample rests against a very blunt wedge the ridge of which lies in the expected plane of the crack. This arrangement is shown in Figure 1 of an earlier paper,[9] except that it has not been found necessary to use a disk-shaped specimen. The compressive stress developed in the crack plane keeps the crack from deviating from this plane. The actual device used is a portable vise to the movable jaw of which is attached the sharp wedge.

The procedure is to drive the wedge in until the crack begins to grow. Growth then decelerates and appears to stop. After waiting 5 or 10 min. to make sure it has stopped, the crack position at both edges of the specimen is marked by a razor blade. The crack is then propagated to a new position and the procedure repeated. In this way three or four suitable crack stopping points can be produced and marked in a single specimen.

Along the line on the fracture surface where the crack has stopped for a while before being repropagated a band of constant width ($\sim 25\mu$) is almost

always found (Fig. 3). Surface complexities which will be subsequently discussed often obscure the band to a greater or lesser extent, but where the surface is simple, layer optical thickness at any point in the band or on the surface surrounding the band can usually be determined. The aids previously described were most useful in the beginning, but as experience with this and other materials was accrued the eye became trained to know the order of a color often from its own hue alone. In Plexiglas II the optical thickness in the stop band is somewhat variable but the average is estimated purely by visual scanning to be third-order yellow. With a refractive index of 1.32 a layer thickness of 6800 A. is calculated. The layer on the surface preceding the band decreases in thickness upon approaching it and at the edge averages second-order red in color, i.e., 5500 A.

Cleavages have been performed at 0, 25, 45, 60, and 67°C. Layer thickness appears constant up to 60°C. At 67°C., even when the cleaved sample is immediately removed from the oven, a significant weakening of colors is observable due to thermal collapse.

Subsurface Crazing

In addition to the relatively simple color pattern due to the crazelike surface layer, there have often been observed on the fracture surface complicated sets of interference fringes. These can often be seen superimposed on the normal color of the field. An interference filter can be used to destroy the field color and make the faint fringes more visible (Fig. 4). These and even the uncomplicated surface colors themselves have been attributed sometimes to subsurface cracks.[1] This is reasonable, since crazes were not understood and also cracks do bifurcate markedly under the right conditions in certain materials. In Plexiglas II these fringes are best interpreted in terms of subsurface crazing. The evidence supporting this is simply that when a microindenter or probe is used to apply pressure to an area containing fringes, such pressure never produces either a permanent or a momentary shifting in the fringe patterns in the vicinity of the pressure point. Except for the damage to the surface from the point of the probe no other effects are ever observed. If the fringe set arose from a true crack lying slightly below the surface which acted as an air wedge, the lack of physical support over wide areas would allow for distortion of the wedge and fringe shift under the slightest pressure. The interference wedge must rather contain a pressure-bearing material. The only reasonable explanation thus is that these wedges arise from subsurface crazes.

Most of the subsurface crazes are probably offshoots from the fracture surface layer. Some, however, are probably completely separate entities. It is not uncommon to see two sets of fringes which cross one another. It is not known whether these arise from two subsurface crazes, one below the other, or to the intervening bulk polymer material between the main surface layer and the subsurface craze having a proper thickness and shape to act as a wedge itself.

Surface complexity (i.e., subsurface crazing plus the surface roughening which results) is a function of temperature, fracture velocity, and the stress situation. At 40°C. and above, complexity is not seen on cleavage surfaces. At 25°C. it is apparent on 5–30% or so of the surface, and below this temperature it increases markedly. At −80°C. the fracture surface is so complicated no color exists at all.[14] In regard to velocity, the situation has not been documented well at all; perhaps the most extensive observation is that on tensile fracture surfaces a so-called mirror area exists at intermediate

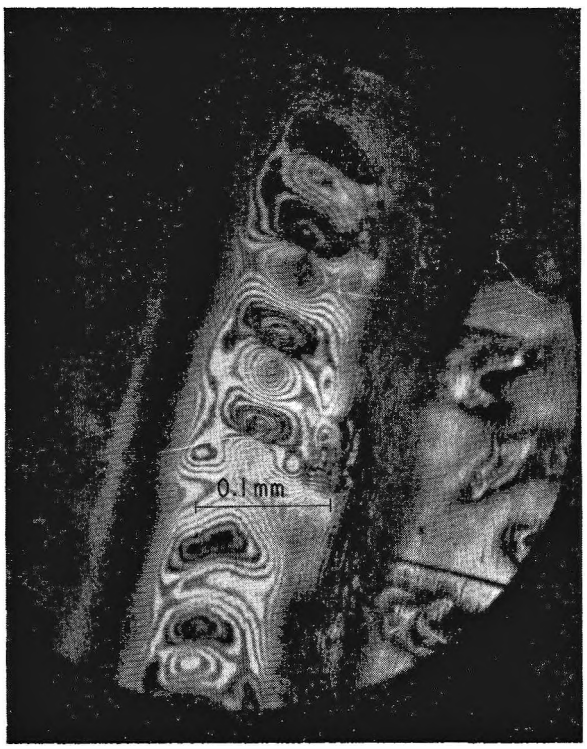

Fig. 4. Plexiglas II cleavage surface. Green light. Interference fringes from subsurface crazing.

velocities.[1] Subsurface crazing is at a minimum here and in the hyperbola-containing region bounding it on the high-speed side.

Although it is not possible to assess quantitatively the contribution of subsurface crazing to resistance to crack formation, it nonetheless can probably be substantial. In the first place, its retardation of crack propagation may be seen directly: where the surface is intermittently complex along the crack front it is usually noted that the front is held back somewhat at the areas of complexity and thus tends to assume a scalloped shape as in Figure 5. Secondly, the Griffith energy γ is essentially constant from 50 to 0°C. but increases markedly as temperature is further lowered;[14] part of this increase may be due to subsurface crazing. Certainly it must tend to use up

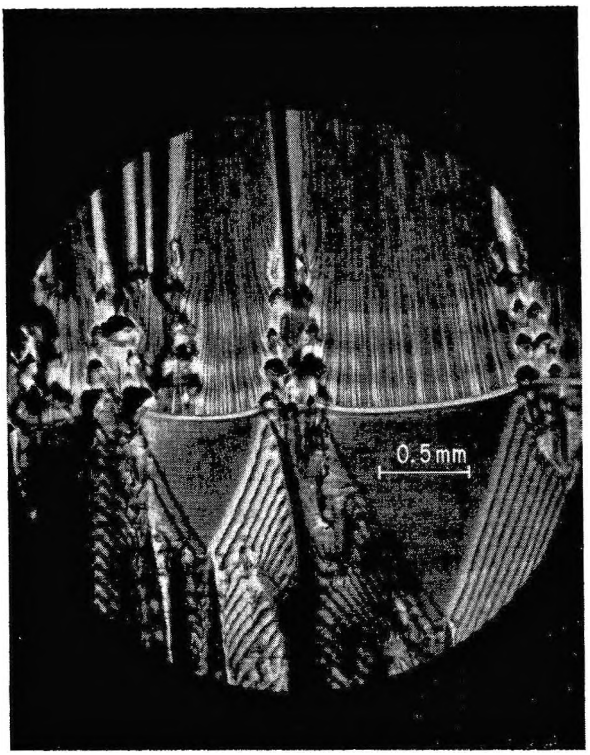

Fig. 5. Plexiglas II 0°C. cleavage surface. Alternating simple and complex areas. Cleavage stop band shows slight scalloped appearance being held back in complex areas. The complex areas appear complex in the figure largely because of surface roughness which is associated with the subsurface crazing observable at higher magnification. Green light.

strain energy and also to reduce the stress concentration upon the main craze.

Contribution of Crazing to the Crack Propagation Energy

There are three conceivable energy sinks in the fracture process: (*a*) bond breakage; (*b*) viscous work; and (*c*) true surface energy. Breakage of a monolayer of bonds—the ideal fracture mechanism—has been shown to equal a negligible fraction of the Griffith energy.[2] It is also to the point to reflect upon the consequences of assigning most of the crack propagation energy to bond breakage throughout the whole region undergoing crazing. Assuming for the moment that the Griffith energy as derived from experiment (1.40×10^5 ergs/cm.^{2})[13] is truly equal to the crack propagation energy and is concentrated instantaneously in the region undergoing crazing, then a simple calculation based on the known craze layer thickness of 6800 A. and a bond energy of 80 kcal./mole leads to the result that one bond for every two monomers in the chain would be broken if essentially all the energy went into this sink. Clearly, a major fraction of γ is not used in this way, since

after formation crazes can still exhibit very high strengths.[7] Nevertheless because the energy density in time and space could conceivably be so high, bond breakage on a minor scale throughout the craze cannot be ruled out.

The void content of crazes is dispersed on a scale far below the wavelength of light, which must result in a relatively high internal surface area. Calculations based on low-angle x-ray scattering results for one craze—that in polystyrene—indicate a maximum specific surface of approximately 200 $m.^2/cm.^3$ of craze.[8] Although surprisingly high, this value together with an assumed surface tension of 30 dynes/cm. yields only 3% of γ.

The final possibility—plastic work—seems the most promising. In view of the absence of knowledge about the mechanism of formation of crazes including the stress system, it can only be assumed that the plastic work involved is equal to that involved in cold drawing at an equivalent amount of material to the same degree of strain. The tensile yield stress σ_y at room temperature is not known; however it must lie between the fracture stress of 10,100 psi and the compressive yield stress of 15,200 psi measured here.* The material to be transformed develops 60% strain ($\epsilon = \Delta d/d_o$) in the crazing process.[7] Using these values plus a surface layer thickness ($d_o + \Delta d$) of 6800 A. we have

$$w = \sigma_y \epsilon d_o = 1.77 \times 10^4\text{–}2.67 \times 10^4 \text{ ergs/cm.}^2 \text{ of fracture surface.}$$

The best value of γ available is 1.40×10^5 ergs/cm.^{2},[2,13] so that w is between 13 and 20% of γ. The experimental quantity γ is itself in error on the high side; because the work is spread over a volume of material, the crack tip is substantially blunter than the ideal, which leads to a stress concentration and thus a crack propagation energy lower than the ideal. How much γ is in error on this account is unknown at present. Considering all the uncertainties, including the contribution from the craze breaking process and that from subsurface crazing, the extent of agreement between w and γ must be considered reasonably good.

Summary

From the determination of the fracture surface layer refractive index it has been shown that this layer is crazelike in nature. From the index and the colors of the layer its thickness may be determined conveniently and on a microscale. It has become apparent that glassy polymer fracture is doubly nonideal. Not only is plastic work involved but, as evidenced by changes in layer thickness, it varies with fracture velocity.

The plastic work entailed in the formation of craze material ahead of the crack tip appears to account for a substantial part of the Griffith energy and certainly more than has been accounted for in any other way. It must be borne in mind, however, that crack propagation involves craze formation

* See Robertson[15] for discussion of relationship between tensile and compressive yield stresses of glassy polymers.

and craze fracture; at present we have no understanding of the mechanism or energetics of the latter process. It is not inconceivable that significant amounts of plastic work are required for the craze fracture process.

The author wishes to thank Mr. R. H. Savage for help in the investigation of subsurface crazing and for many informative discussions.

References

1. Newman, S. B., and I. Wolock, in *Proceedings of the Symposium on Adhesion and Cohesion*, Elsevier, Amsterdam, 1962 (see references 1 to 7).
2. Berry, J. P., *J. Polymer Sci.*, **50**, 107 (1961).
3. Bessonov, M. I., and E. V. Kuvshinskiĭ, *Plasticheskie Massy*, **5**, 57 (1961).
4. Lebedev, G. A., and E. V. Kuvshinskiĭ, *Soviet Phys. Solid State* (Engl. Transl.), **3**, 1957 (1962).
5. Spurr, O. K., and W. D. Niegisch, *J. Appl. Polymer Sci.*, **6**, 585 (1962).
6. Kambour, R. P., *Nature*, **195**, 1299 (1962).
7. Kambour, R. P., *Polymer*, **5**, 107 (1964); *J. Polymer Sci.*, **A2**, 4159 (1964).
8. LeGrand, D. G., W. R. Haaf, and R. P. Kambour, to be published.
9. Kambour, R. P., *J. Polymer Sci.*, **A2**, 4165 (1964).
10. Rossi, B., *Optics*, Addison-Wesley, Reading, Mass., 1957, or any standard optics text.
11. Berry, J. P., *J. Appl. Phys.*, **33**, 1741 (1962).
12. Griffith, A. A., *Phil. Trans, Roy. Soc.*, **A221**, 163 (1921); *Proc. First Int. Congress Appl. Mech. (Delft)* (1924) p. 55.
13. Berry, J. P., *J. Appl. Phys.*, **34**, 62 (1963).
14. Berry, J. P., *J. Polymer Sci.*, **A1**, 993 (1963).
15. Robertson, R. E., *J. Appl. Polymer Sci.*, **7**, 443 (1963).

Résumé

Les couleurs d'interférence sur les surfaces de cassure du polyméthacrylate de méthyle proviennent d'une couche de matériel à structure inégale. Pour la plupart des surfaces, on peut déterminer l'ordre d'interférence de différentes façons sur la surface de cassure et sur l'épaisseur de la couche inégale. L'épaisseur de la couche est une fonction de la vitesse de cassure; à la vitesse zéro pour laquelle on peut appliquer le critére de Griffith avec la moindre erreur, on calcule une épaisseur de couche pour une surface moyene de 6.800 A. Le travail plastique correspondant à cette quantité de formation de structure inégale correspond à 13–20% de l'énergie nominale de Griffith.

Zusammenfassung

Die Interferenzfarben an Polymethylmethacrylat-Bruchoberflächen stammen von einer Schicht von Rissmaterial. Die Interferenzordnung kann auf verschiedene Weise für die meisten Bereiche der Bruchoberfläche und der Risschichtdicke bestimmt werden. Die Schichtdicke ist eine Funktion der Bruchgeschwindigkeit; bei der Geschwindigkeit null, wo das Griffith-Kriterium mit dem geringsten Fehler angewendet werden kann, wird eine mittlere Oberflächenschichtdicke von 6800A. berechnet. Die plastische Energie für diesen Betrag an Rissbildung entspricht 13–20% der nominellen Griffith-Energie.

Received September 11, 1964
Revised October 2, 1964
(Prod. No. 4554A)

JOURNAL OF POLYMER SCIENCE: PART A VOL. 3, PP. 1725–1728 (1965)

A Dye Partition Method for the Determination of Hydroxyl Endgroups in Polymers

PREMAMOY GHOSH, PRANAB K. SENGUPTA, and ANANDA PRAMANIK, *Department of Applied Chemistry, University College of Science and Technology, Calcutta, India*

Synopsis

A dye partition method for the determination of hydroxyl endgroups in poly(methyl methacrylate) samples prepared in aqueous media with the use of hydrogen peroxide as the photoinitiator has been described. The dried polymers were treated with chlorosulfonic acid under suitable conditions whereby the hydroxyl endgroups present in them were transformed to sulfate endgroups. Spectrophotometric analysis of sulfate endgroups in the treated polymers was carried out by the application of the dye-partition technique developed for the purpose, and thus a measure of hydroxyl endgroups in the original polymers was obtained. H_2O_2, in the concentration range of 0.004–0.1M, was found to incorporate an average of nearly 1 OH endgroup per polymer chain.

Recently two dye techniques, viz., the dye-partition technique[1] and the dye-interaction technique[2] have been developed for the analysis of ionic endgroups in polymers. The dye techniques are based on the principle of interaction between the ionic endgroups in polymers and suitable ionic dyes. Analysis of hydroxyl end6roups, ordinarily nonresponsive to the ionic dyes, has been possible by transforming them to anionic carboxyl groups by the phthalic anhydride–pyridine technique and then employing the dye-interaction technique in benzene solution.[3] This method is quite complicated, however, when anionic groups such as carboxyl groups are also present in the polymers. Purification of the polymer from the last traces of acidic impurities after phthalation is a tedious process, and even minute traces of residual or absorbed acidic impurities lead to errors in quantitative measurements.

A dye-partition method has been developed to minimize or to avoid these complications and difficulties. Hydroxyl endgroups are transformed to sulfate endgroups by treating the polymer with chlorosulfonic acid, and the sulfate endgroups are then determined spectrophotometrically by the dye-partition method.

EXPERIMENTAL

E. Merck hydrogen peroxide (30 vol.-%) was used as the source of hydroxyl radicals for the aqueous polymerization of methyl methacrylate

(MMA). Polymerization was usually carried out under nitrogen atmosphere in presence of sunlight.[3] The polymers obtained were filtered, washed thoroughly with water, and then dried in air at 45°C.

Transformation of Hydroxyl (~~OH) Endgroups to Sulfate (~~OSO_3^-) Endgroups

About 0.05–0.1 g. of the dried polymer was dissolved in 2–5 ml. pure pyridine in a hard glass test tube. The solution was cooled to 0–5°C. and about 0.5 ml. fresh, pure chlorosulfonic acid was slowly added to it. The test tube was then closed with an air-tight stopper and placed in a hot oil bath maintained at 85–90°C. for about 3 hr. Hydroxyl endgroups were transformed to sulfate endgroups during this treatment.

$$\sim\sim OH + ClSO_3H \rightarrow \sim\sim OSO_3H + HCl$$

The test tube was then taken out and cooled. A considerable part of the polymer was found to have separated out of the solution. The whole mass was poured into methanol in a beaker, and the polymer precipitated out completely. It was then washed several times with methanol and then purified by repeated precipitation with a methanol–petroleum ether mixture from its benzene solution.

Endgroup Analysis by the Dye-Partition Technique

The $ClSO_3H$-treated polymers were then tested for sulfate endgroups with aqueous methylene blue reagent according to the dye-partition method.[4] Quantitative analysis was carried out spectrophotometrically.[4]

RESULTS AND DISCUSSION

The results of endgroup analysis are given in Table I. H_2O_2 concentration was varied from 0.004 to 0.1*M*. All the H_2O_2–initiated polymers gave positive response to the dye-partition test only after treatment with chlorosulfonic acid, and the response was more intense with higher concentration of H_2O_2 used as the initiator. This evidently indicates the presence of OH endgroups in the polymers (transformed to sulfate endgroups on treatment with $ClSO_3H$). A thermal poly-MMA on identical treatment with $ClSO_3H$ gave in general a very faint response to the dye-partition test. Since the thermal polymer did not bear any hydroxyl endgroup, its faint response was presumably due to the incorporation of traces of sulfonate (~~SO_3^-) groups in the chain by the attack of $ClSO_3H$:

$$\sim\sim CHR\sim\sim + ClSO_3H \rightarrow \sim\sim \underset{\underset{SO_3H}{|}}{CR} \sim\sim + HCl$$

The trace amount of sulfonate groups thus introduced at some nonhydroxylic parts of the polymer chain and the sulfate endgroups obtained by the transformation of OH endgroups could be easily distinguished by the fact that the sulfonate groups are nonhydrolyzable while the sulfate

TABLE I
Determination of Hydroxyl Endgroups by Dye-Partition Method

Polymer	H_2O_2 concn., mole/l.	$[\eta]$ (benzene, 35 ± 1°C.)[a]	Dye-partition test with methylene blue reagent: Polymer solution in $CHCl_3$, %[b]	Dye-partition test with methylene blue reagent: Absorbance at 660 mμ	Average no. OH endgroups per chain
H_2O_2-initiated PMMA[c]	0.004	1.81	0.1	0.16	0.91
	0.01	1.35	0.1	0.23	0.98
	0.05	0.81	0.1	0.49	1.11
	0.08	0.69	0.1	0.52	0.91
	0.10	0.63	0.1	0.63	1.03
Thermal PMMA	—	2.2	0.1	0.02–0.04	—

[a] The equation[5] used for molecular weight (M_n) calculation is $M_n = 2.81 \times 10^5 [\eta]^{1.32}$.
[b] $ClSO_3H$-treated polymers.
[c] MMA = 0.094 mole/l.; N_2 atm., 30 ± 2°C.; sunlight.

groups are easily hydrolyzable.[4] The absorbance due to the thermal polymer could be taken as the blank reading and subtracted from the absorbance of the test samples before calculating for the sulfate endgroups.

It was observed that by aqueous photoinitiation with hydrogen peroxide (over the concentration range of 0.004–0.1M H_2O_2) an average of nearly one hydroxyl endgroup was incorporated per chain of poly-MMA (Table I). These results based on the dye-partition method are in close agreement with those obtained by the application of the dye-interaction method.[3] The advantages of the dye-partition method are that it is a more simple and specific method and far less complicated in the presence of weakly acidic carboxyl groups in the polymer and in the presence of minute traces of extraneous acidic impurities.

Thanks are due to C.S.I.R., India for awarding a fellowship to P. K. SenGupta.

References

1. Palit, S. R., *Makromol. Chem.*, **36**, 89 (1959); *ibid.*, **38**, 96 (1960).
2. Palit, S. R., and P. Ghosh, *Microchem. J., Symp. Ser.*, **2**, 663 (1961).
3. Ghosh, P., A. R. Mukherjee, and S. R. Palit, *J. Polymer Sci.*, **A2**, 2807 (1964).
4. Gosh, P., S. C. Chadha, A. R. Mukherjee, and S. R. Palit, *J. Polymer Sci.*, **A2**, 4433 (1964).
5. Baxendale, J. H., S. Bywater, and M. G. Evans, *J. Polymer Sci.*, **1**, 237 (1946).

Résumé

On décrit une méthode de partage de colorant pour déterminer des groupes hydroxyliques terminaux dans des échantillons de polyméthacrylate de méthyle, préparés en milieu aqueux en utilisant le peroxyde d'hydrogéne comme photoinitiateur. Les polymères sèchés sont traités à l'acide chlorosulfonique sous des conditions appropriées, de façon à transformer les groupes hydroxyliques terminaux présents en groupes sulfates. L'analyse spectrophotométrique des groupes sulfates terminaux dans les poly-

mères traités, a été effectuée en appliquant la technique de partage de colorant développée dans ce but et une mesure des groupes hydroxyliques terminaux dans les polymères originaux a été obtenue. On a trouvé que H_2O_2, dans le domaine de concentration allant de 0.004 M jusqu'à 0.1M, incorpore une moyenne d'environ un groupe terminal OH par chaîne de polymère.

Zusammenfassung

Es wurden eine Farbstoffverteilungsmethode zur Bestimmung der Hydroxylendgruppen in Polymethylmethacrylat beschrieben, die in wässrigen Medien mit Wasserstoffperoxyd als Photoinitiator dargestellt wurden. Die getrockneten Polymeren wurden unter geeigneten Bedingungen mit Chlorsulfonsäure behandelt, wobei die darin vorhandenen Hydroxylendgruppen in sulfatendgruppen umgewandelt wurden. Die spektrophotometrische Analyse der Sulfatendgruppen in den behandelten Polymeren wurde mit der für diesen Zweck entwickelten Farbstoffverteilungsmethode ausgeführt und so ein Mass für die Hydroxylendgruppen im ursprünglichen Polymeren erhalten. Es wurde gefunden, dass H_2O_2 im Konzentrationsbereich von 0,004M bis 0.1M zum Einbau von nahezu einer OH-Gruppe pro Polymerkette führt.

Received September 30, 1964
Revised November 24, 1964
(Prod. No. 4572A)

JOURNAL OF POLYMER SCIENCE: PART A VOL. 3, PP. 1729–1740 (1965)

Elemental Organic Compounds. Part XIV. Polymerization of Diene with Organotransition Metals

MINORU TSUTSUI* and JUNJI ARIYOSHI,
New York University, School of Engineering and Science, Department of Chemical Engineering, Research Division, New York, New York

Synopsis

The polymerization of 1,3-butadiene by using organotitanium catalysts, e.g. tetramethyltitanium (classified as a radical-type catalyst), gave rubberlike polybutadiene in low yield which was rich in the *trans*-1,4-stereoisomer, while the polymerization of 1,3-butadiene by use of organotitanium catalysts, e.g., tetravinyltitanium and tetraphenyltitanium (classified as a π-type catalyst) gave polybutadiene rich in the 1,2-configuration in high yield. Titanocene dichloride and bisbenzenechromium iodide were each used individually to catalyze the polymerization of 1,3-butadiene with methyl Grignard reagent. In both cases polybutadienes rich in the 1,4-configuration were obtained in quite low yield. These results were interpreted to be due to the lack of availability of 3*d* orbitals in the above-mentioned catalyst. Organic chromium, iron, cobalt, and nickel compounds were also investigated as catalysts for the polymerization of 1,3-butadiene. Viscous, low molecular weight products were obtained in all cases. When the chromium catalysts were used, a mixture of polymers, namely 1,2- and *trans*-1,4-polybutadiene, was obtained in high yield. On the other hand, low product yields were observed with the use of the other catalysts; however, *trans,trans,trans*-1,5,9-cyclododecatriene was found in each case. The configuration of polybutadiene was also dependent upon the number, odd or even, of organic groups on a transition metal atom.

INTRODUCTION

The configuration of polybutadiene is dependent upon the catalyst system, especially the type of organotransition metal compounds, and the reaction conditions.[1]

In our laboratory polymerizations of 1,3-butadiene have been conducted with the use of a catalyst system consisting of a stoichiometric mixture of the Grignard reagent and the transition metal halide in tetrahydrofuran solvent. (This catalyst system has been reasonably considered to react to form σ-bonded organotransition metals.[2,3] These compounds are considered to be the true catalyst of the polymerization of 1,3-butadienes. Magnesium halide is also formed from this reaction. This salt is not thought to participate in the catalysis.) The configuration, the molecular weight, and the yield of polybutadiene have depended significantly upon

* To whom all correspondence should be directed.

the nature of the organic group in the Grignard reagent and the transition metal halide. The mechanisms of the polymerizations involving radical and π-complexing mechanism[2,3] are discussed.

RESULTS AND DISCUSSION

The results of the polymerizations of 1,3-butadiene obtained by using a stoichiometric mixture of methyl-, ethyl-, vinyl-[4,5], and phenylmagnesium halides and titanium tetrachloride are shown in Table I.

The polymerization with the vinyl compound proceeded more vigorously than the others, and a rubberlike polymer was obtained in high yield. Absorbance ratio of vinyl group to *trans* double bond was 6.6.

A possible mechanism for this polymerization is described below, and the catalyst reaction is shown schematically in eq. (1). Tetravinyl-titanium (I) is formed at the first stage of the catalyst reaction of a stoichiometric mixture of vinylmagnesium chloride and titanium tetrachloride as previously reported.[3] It has never been isolated. The σ-bonded tetravinyl-titanium rearranges to give a π-bonded complex (II). Internal dimerization takes place within the complex to give a π-bonded 1,3-butadiene–titanium complex (III). [The complex (III) has not been isolated, but 4-vinylcyclohexene-1 has been obtained from catalyst reaction. This formation of this product is plausible from the proposed intermediate (III) through π-radical hybridization (II).[2,3]] Dimerization takes place through the coupling of carbons 2 and 4′, leaving radicals on carbons 1 and 3′. Another 1,3-butadiene molecule then may be attracted and form a π-complex with the titanium atom, and the radical on carbon 3′

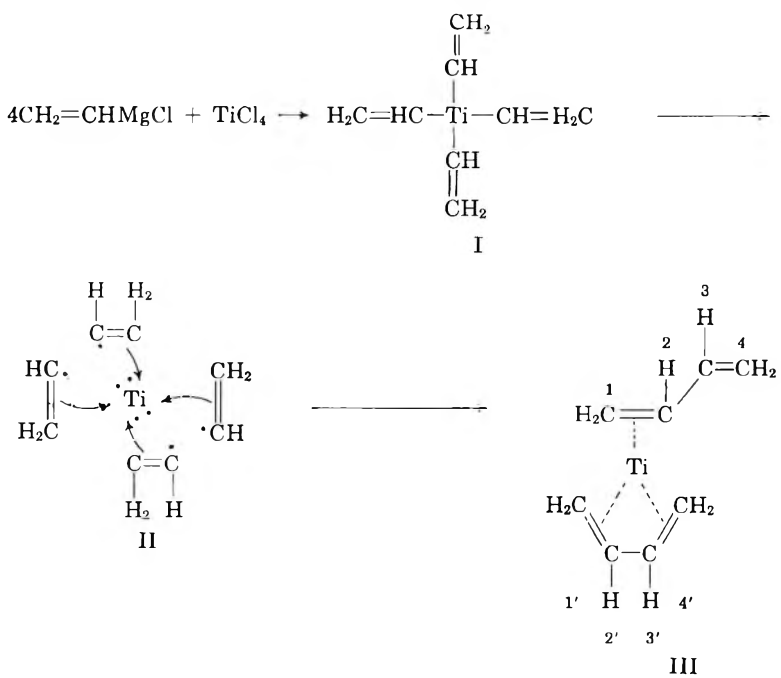

(1)

TABLE I
Configuration of Polybutadienes Prepared with Organotitanium Catalysts[a]

No.	Catalyst	Conversion, %	Polymer state	Absorbance ratio 1,2-/*trans*-1,4-[b]
1	$(CH_3)_4Ti$	25	Rubberlike	1.7
2	$(C_2H_5)_4Ti$	55	Semisolid	5.1
3	$(CH_2{=}CH)_4Ti$	90	Rubberlike	6.6
4	$(C_6H_5)_4Ti$	100	Viscous oil	5.4
5	$(C_5H_5)_2Ti(CH_3)_2$	3	Rubberlike	0.79

[a] Mole ratio of 1,3-butadiene to catalyst = 4.2:1; solvent THF; reaction time 24 hr.
[b] Absorbance ratio was calculated by baseline method at 10.3 and 11.0 μ.

of the dimer will attack the α-carbon atom on the 1,3-butadiene molecule. Thus a trimer is formed. Continuation of this process yields a polymer. To explain the formation of 1,2-stereoregular polymers the radical on carbon 1 may pick up hydrogen from the solvent. The coupling of carbons 1 and 1′ might also proceed, leaving radicals on carbons 2 and 2′.

The phenyltitanium compound showed the highest catalytic activity (the highest yield of polybutadiene), and the dimethyl-titanocene was the lowest in activity. The configuration of the polymers has some correlation with the catalytic activity of the organotitanium compounds, as shown in Table I,

The organotitanium compounds may be decomposed to organic radicals and active radical titanium atom, and these organic radicals may further couple to give dimers. An ethyl radical may lose β hydrogen to give an ethylene and a hydrogen radical,[6-9] as shown in Table II.

TABLE II
Initiation Mechanisms and Configurations of Polybutadiene Prepared with Organotitanium Catalysts

No.	Catalyst	Catalyst type[a]	Conversion, %	Polymer state	Absorbance ratio 1,2/*trans*-1,4-$\underline{\pi}$
1	$(CH_3)_4Ti \rightarrow CH_3\cdot$ or $CH_3{-}CH_3$	Radical	25	Rubberlike	1.7
2	$(C_2H_5)_4Ti \rightarrow CH_3CH_2\cdot$ + H or $CH_2{=}CH_2$	Radical + π	55	Semisolid	5.1
3	$(CH_2{=}CH)_4Ti \rightarrow CH_2{=}CH\cdot$ or $(CH_2{=}CH)_2$	Radical + $\underline{\pi}$	90	Rubberlike	6.6
4	$(C_6H_5)_4Ti \rightarrow (C_6H_5)\cdot$ or $C_6H_5{-}C_6H_5$	Radical + $\underline{\pi}$	100	Viscous oil	5.4
5	$(\pi\text{-}C_5H_5)_2Ti(CH_3)_2 \rightarrow CH_3\cdot$ or $CH_3{-}CH_3$	Radical	3	Rubberlike	0.79

[a] π: π-nature; $\underline{\pi}$: strong π-nature.

Organotransition metal catalysts may be classified into two groups, depending upon the nature of the products from their decomposition. One group yields mainly organic radicals, for example, methyl radicals from tetramethyltitanium. The other, which produces mainly 1,3-butadiene, has been previously described (vinyl radicals may couple to this right after the decomposition of the compound as previously mentioned). This second group is considered as the π-type catalyst. (These are of two types: strong or π-catalysts and weak π-catalysts.) The metalloethyl compound is considered a weak π-catalyst (no bar below the π) since its decomposition yields lower percentage of π-ligands, ethylene, than that obtained from the decomposition of vinyl compound.

As shown in Table II, polybutadienes obtained by using radical catalysts were richer in *trans*-1,4-polymer. It has been reported that the 1,3-butadiene polymerized by free radicals contains 80–82% of the 1,4-polybutadiene and only 18–20% of the 1,2-polybutadiene.[10] Thus polymerization of 1,3-butadiene by radical-type catalysts is generally expected to form 1,4-polybutadiene (*trans*-form throughout this experiment).

Polybutadiene obtained by using π-type catalysts was enriched in 1,2-polymer. Therefore the entire course of the polymerization of 1,3-butadiene with the use of π-type catalyst is considered to be carried out on the surface of the active metal atom. Consequently, polymerization of 1,3-butadiene with radical-type catalysts is considered to be carried out apart from the metal atom.

The polymerization of 1,3-butadiene with methyltitanium catalyst is considered to involve mainly a radical-type catalyst (methyl radical) and but to some extent also a π-type catalyst (active titanium metal atom), because an equimolar mixture of 1,2- and *trans*-1,4-polybutadiene was obtained as the product.

The dimethyltitanocene showed the lowest catalytic activity and was rich in *trans*-1,4-polybutadiene. These results may be explained by the low availability of the 3d orbital of the titanium atom in dimethyltitanocene, since the orbital is filled with π electrons of π-cyclopentadienes which may stay on titanium atom throughout the reaction. Therefore the polymerization of 1,3-butadiene on the active titanium atom (in the fashion of π-type catalyst) may be quite limited, and the radical-type polymerization with methyl radical formed from the decomposition of dimethyltitanocene may be predominant in this catalyst.

Organochromium compounds were also used as the catalyst of the polymerization of 1,3-butadiene as shown in Table III. The conversion of 1,3-butadiene to polymer with the use of chromium catalysts was generally higher but the molecular weight of the polymer was lower than those obtained with organotitanium catalysts.

The conversion of 1,3-butadiene to polymer was higher with radical and π-type catalyst (nos. 7, 8, and 9, Table III) than radical-type catalysts (nos. 6 and 10, Table III). This correlation is similar to the one found for the organotitanium catalysts. However in contrast to the organotitanium

catalysts, the ratio of *trans*-1,4 and 1,2-polybutadiene in the products was in all cases nearly 1:1. The reason for this difference in behavior may be due to whether the number of organic groups on the transition metal is odd or even. In tetravalent titanium compounds an even number of organic groups couple to form a nonradical compound. In trivalent chromium catalysts two of three organic radicals couple to form a nonradical compound, leaving uncoupled one of the three organic radicals, which may initiate the radical type polymerization of 1,3-butadiene.

The yield of polybutadiene with methylbisbenzenechromium as the catalyst was extremely low. This result may be rationalized as follows. Methylbisbenzenechromium may be cleaved in a homolytic fashion to form bisbenzenechromium and methyl radical. The availability of 3*d* orbitals of bisbenzenechromium (0) is zero, since 3*d* orbitals of the chromium

TABLE III
Polymerization of Butadiene with Organochromium Catalysts[a]

No.	Catalyst	Conversion, %	Polymer state	Absorbance ratio 1,2-/*trans*-1,4-
6	$(CH_3)_3Cr$	55	Viscous oil	1.1
7	$(C_2H_5)_3Cr$	100	Viscous oil	1.7
8	$(CH_2{=}CH)_3Cr$	60	Viscous oil	1.6
9	$(C_6H_5)_3Cr\cdot 3THF$[b]	100	Viscous oil	1.6
10	$(C_6H_6)_2CrCH_3$[c]	0	—	—

[a] Ratio of 1,3-butadiene to catalyst 4.2:1; solvent THF; reaction time 24 hr.
[b] Data of Herwig and Zeiss.[11]
[c] Data of Herwig and Zeiss[12] and Fischer and Hafner.[13]

atom are all filled with π-electrons of two benzene rings, and thus butadiene cannot be adsorbed on the active chromium atom. Even though this catalytic system may supply methyl radical, the yield of polybutadiene may be lower than in the case of dimethyltitanocene since only one molecule of methyl radical may be formed from the methylbisbenzenechromium and the concentration of methyl radical may be lower than that in the case of dimethyltitanocene.

Low molecular weight polymers are obtained from the chromium catalysts. The reasons can be considered as follows. The chromium radical formed by the decomposition of an organochromium compound shows a strong ability to dehydrogenate organic groups and forms chromium hydride and dehydrogenated organic groups.[9] The chromium hydride may be so unstable as to decompose to hydrogen radical and radical chromium. This hydrogen radical may terminate the polymerization reaction. The active chromium radical thus generated may promote the polymerization of 1,3-butadiene.

The polymerizations of 1,3-butadiene with vinyl derivatives of transition metals (iron, cobalt, and nickel) were also carried out as shown in Table IV.

TABLE IV
Polymerization of 1,3-Butadiene with Vinyl Derivatives of Transition Metals

No.	Catalyst $(CH_2{=}CH)_nM$	Conversion, %	Polymer state	Absorbance ratio, 1,2-/*trans*-1,4-	1,5,9-Cyclododecatriene
11	Ti^4	90	Rubberlike	6.6	—
12	Cr^3	60	Viscous oil	1.6	—
13	Fe^2	13[a]	Rubberlike	4.2	—
			Oil	1.1	Some
14	Co^2	30	Oil	3.7	Some
15	Ni^2	10	Oil	0.40	Some

[a] Data of Tsutsui and Ariyoshi[3] and Rochow, Hurd, and Lewis.[10]

Although organoiron catalyst[13] showed poor catalytic activity, a solid and oily material were obtained as the product. The solid product, which is rich in 1,2-polymer, is quite similar to that obtained with vinyltitanium catalyst. A small amount of *trans, trans, trans*-1,5,9-cyclododecatriene was obtained in experiments 13, 14, and 15 in which vinyliron, -cobalt, and -nickel were used as catalysts. This trimer of butadiene has already been synthesized by using a catalyst prepared on the basis of chromium compounds.[14] Recently Wilke and co-workers[15] reported the mechanism of formation of *trans, trans, trans*-1,5,9-cyclododecatriene using organonickel and organoaluminum compound. Their explanation of the mechanism seems to be similar to a catalysis at the atomic level, in which the polymerization of butadiene proceeded on a surface of transition metal atom. From these results, the degree of conversion, the state, and configuration of polymers seems due to the nature and number of organic groups and the dehydrogenation power of the metal. In addition, the stability of the bond between the carbon and metal atom and the nature of the metal atom are factors. For instance, polybutadienes obtained from the nickel catalyst are rich in *trans*-1,4 polymer. Polymerization in these cases seems to proceed more by a radical mechanism. Due to instability of the σ-bond between the carbon and nickel atom, organic radicals may be formed at a lower temperature than in the case of other metals. The radicals which may be stable at lower temperature may propagate radical polymerization before coupling of each radical.

EXPERIMENTAL

1. Tetravinyltitanium

A solution of 0.95 g. (0.005 mole) of titanium tetrachloride and 6.5 g. (0.12 mole) of butadiene in 50 ml. of freshly distilled tetrahydrofuran was stirred with a magnetic stirrer under nitrogen in a Schlenk tube at −80°C. while a solution of vinylmagnesium chloride in tetrahydrofuran 0.02 mole) was added in one portion. The dark brown solution turned black. The

temperature was raised to room temperature over 2 hr. and maintained at this temperature for an additional 18 hr. with stirring. Finally the reaction mixture changed to a viscous solution. After the addition of a small amount of phenyl α-naphthylamine, the reaction mixture was hydrolyzed with 50 ml. of ice water. A rubberlike material coagulated out from the reaction mixture, and was washed with cold water several times and dried under reduced pressure; 5.9 g. of product was obtained. This was dissolved in benzene and filtered to remove any insoluble material. The filtrate was added to a large amount of methanol which precipitated the rubberlike material. This procedure was repeated three times before the solvent was completely removed under reduced pressure. The infrared spectrum of the purified rubberlike product showed vinyl and *trans*-double bond absorption at 990 and 970 cm.$^{-1}$, respectively, and on this basis the reaction product was concluded to be a mixture of 1,2- and *trans*-1,4-polybutadienes.

2. Tetramethyltitanium

A solution of 0.95 g. (0.005 mole) of titanium tetrachloride and 6.5 g. (0.12 mole) of butadiene in 50 ml. of tetrahydrofuran was stirred under nitrogen in a Schlenk tube at −80°C. while a solution of methylmagnesium bromide in tetrahydrofuran (0.02 mole) was added in one portion. The reaction, hydrolysis with water, and purification of product were carried out in a similar fashion to that described for tetravinyl titanium. A 1.6-g. yield of rubberlike product was obtained. The infrared spectrum of the purified product showed vinyl and *trans*-double bond absorption, and on this basis the reaction product was concluded to be a mixture of 1,2- and *trans*-1,4-polybutadienes.

3. Tetraethyltitanium

A solution of 0.95 g. (0.005 mole) of titanium tetrachloride and 6.5 g. (0.12 mole) of 1,3-butadiene in 50 ml. of tetrahydrofuran was stirred under nitrogen in a Schlenk tube at −80°C. while a solution of ethylmagnesium bromide in tetrahydrofuran (0.02 mole) was added in one portion. The reaction and hydrolysis with distilled water were carried out in as described above. The hydrolyzed reaction mixture was extracted three times with 50 ml. of benzene and the combined benzene extracts washed with distilled water. The benzene solution was dried over sodium sulfate, and the solvent was completely removed under reduced pressure. A yield of 1.8 g. of light yellow semisolid material was obtained. The infrared spectrum of the product showed vinyl and *trans*-double bond absorption. From the evidence of the infrared spectrum, the product is most likely 1,2- and *trans*-1,4-polybutadienes.

4. Tetraphenyltitanium

A solution of 0.95 g. (0.005 mole) of titanium tetrachloride and 6.5 g. (0.12 mole) of 1,3-butadiene in 50 ml. of tetrahydrofuran was stirred under

nitrogen at −80°C. while a solution of phenylmagnesium bromide in tetrahydrofuran (0.02 mole) was added in one portion. The reaction and hydrolysis with water were carried out as described above. The hydrolyzed reaction mixture was extracted three times with 50 ml. of benzene. The combined benzene extract was washed with distilled water. The benzene solution was dried over sodium sulfate, and the solvent was completely removed under reduced pressure, yielding 8.09 g. of light-yellow viscous liquid material. The infrared spectrum of the product showed *vinyl*, *trans*-double bond, and biphenyl absorption. From the evidence of the infrared spectrum, the products are most likely 1,2- and *trans*-1,4-polybutadienes and biphenyl.

5. π-Dicyclopentadienyldimethyltitanium

A solution of 1.245 g. (0.005 mole) of dicyclopentadienyltitanium dichloride and 6.5 g. (0.12 mole) of 1,3-butadiene in 50 ml. of tetrahydrofuran was stirred under nitrogen at −80°C. while a solution of methylmagnesium bromide in tetrahydrofuran (0.01 mole) was added. The reaction and hydrolysis with water were carried out as described above. A small amount of yellow rubberlike precipitate was obtained. After drying, the yellow precipitate (0.3 g.) was dissolved in benzene, filtered to remove insoluble material, and precipitated in methanol. This procedure was repeated three times before the solvent was completely removed under reduced pressure. The infrared spectrum of the purified rubberlike product showed vinyl and *trans*-double bond absorption, and on this basis the reaction product was concluded to be a mixture of 1,2- and *trans*-1,4-polybutadienes.

6. Trimethylchromium

A suspension of 0.79 g. (0.005 mole) of chromium trichloride and 6.5 g. (0.12 mole) of butadiene in 50 ml. of tetrahydrofuran was stirred under nitrogen in a Schlenk tube at −80°C. while a solution of methylmagnesium bromide in tetrahydrofuran (0.015 mole) was added in one portion. The temperature was gradually raised to room temperature over 2 hr. and maintained at this temperature for an additional 3 days with stirring. After the addition of a small amount of α-naphthylamine, the reaction mixture was hydrolyzed with 50 ml. of ice water. The hydrolyzed reaction mixture was extracted three times with 50 ml. of benzene. The combined benzene extract was washed with distilled water. The benzene solution was dried over sodium sulfate, and the solvent was completely removed under reduced pressure, yielding 3.6 g. of yellow viscous liquid material. The infrared spectrum of the liquid product showed vinyl and *trans*-double bond absorption at 990 and 970 $cm.^{-1}$, and on this basis the reaction product was concluded to be a mixture of 1,2- and *trans*-1,4-polybutadienes.

7. Trivinylchromium

A suspension of 0.79 g. (0.005 mole) of chromium trichloride and 6.5 g. (0.12 mole) of butadiene in 50 ml. of tetrahydrofuran was stirred under

nitrogen in a Schlenk tube at −80°C. while a solution of vinylmagnesium chloride in tetrahydrofuran (0.015 mole) was added in one portion. The temperature was raised gradually to room temperature over 2 hr. and maintained at this temperature for an additional 24 hr. with stirring. Hydrolysis of the reaction mixture with distilled water and extraction with benzene were carried out in a similar fashion to that described above for tetravinyltitanium; 4.0 g. of viscous liquid material was obtained. The infrared spectrum of the liquid product showed vinyl and *trans*-double bond absorption, and on this basis the reaction product was concluded to be a mixture of 1,2- and *trans*-1,4-polybutadienes.

8. Triethylchromium

A suspension of 0.79 g. (0.005 mole) of chromium trichloride and 6.5 g. (0.12 mole) of butadiene in 50 ml. of tetrahydrofuran was stirred under nitrogen at −80°C. while a solution of ethylmagnesium bromide in tetrahydrofuran (0.015 mole) was added in one portion. The temperature was gradually raised to room temperature and maintained at this temperature for an additional 18 hr. Hydrolysis of reaction mixture with distilled water and extraction with benzene were carried out as described above. The product consisted of 7.0 g. of yellow viscous liquid material. The infrared spectrum of the liquid product showed vinyl and *trans*-double bond absorption, and on this basis the reaction product was concluded to be a mixture of 1,2- and *trans*-1,4-polybutadienes.

9. Triphenylchromium

A suspension of 0.79 g. (0.005 mole) of chromium trichloride and 6.5 g. (0.12 mole) of butadiene in 50 ml. of tetrahydrofuran was stirred under nitrogen at −80°C., and a solution of phenylmagnesium bromide in tetrahydrofuran (0.015 mole) was added in one portion. The reaction, hydrolysis with distilled water and benzene extraction were carried out as described above; 6.5 g. of yellow viscous liquid material was obtained. The infrared spectrum of liquid product showed vinyl and *trans*-double bond absorption, and on this basis the reaction product was concluded to be a mixture of 1,2- and *trans*-1,4-polybutadienes.

10. Bisbenzenemethylchromium

A solution of 1.68 g. (0.005 mole) of bisbenzene chromium iodide and 6.5 g. (0.12 mole) of butadiene in 50 ml. of tetrahydrofuran was stirred under nitrogen at −80°C., and a solution of methylmagnesium bromide in tetrahydrofuran (0.005 mole) was added at −80°C. The reaction and hydrolysis with distilled water were carried out as described above. Trace amounts of reaction product were obtained.

11. Black Chromium Complex

Preparation of Black Chromium π-Complex. A suspension of 0.79 g. (0.005 mole) of chromium trichloride in 50 ml. of tetrahydrofuran was

stirred under nitrogen in a Schlenk tube at −80°C. while solution of phenylmagnesium bromide in tetrahydrofuran (0.015 mole) was added in one portion. The temperature was gradually raised to room temperature, and maintained at this temperature for an additional 4 hr. The reaction mixture changed from dark brown color to dark red color. Then tetrahydrofuran was completely removed under high vacuum at room temperature to obtain the black material.

Reaction of Butadiene and Black Material. To the black material of chromium π-complex obtained above, 100 ml. of *n*-heptane and 9.75 g. (0.18 mole) of 1,3-butadiene were added under nitrogen at −50°C. and stirred with magnetic stirrer. The temperature was gradually raised to room temperature over 2 hr. and maintained at this temperature for an additional 3 days. After addition of a small amount of phenyl β-naphthylamine, the reaction mixture was hydrolyzed with 100 ml. of ice water. The *n*-heptane layer was concentrated and poured into a large amount of methanol. A small amount of white, rubberlike precipitate was obtained. The precipitate was dried under high vacuum. The infrared spectrum of the rubberlike product showed vinyl and *trans*-double bond absorption, and on this basis the reaction product was concluded to be a mixture of 1,2- and 1,4-*trans*-polybutadienes.

12. Divinyliron

A suspension of 0.63 g. (0.005 mole) of ferrous chloride and 6.5 g. (0.12 mole) of 1,3-butadiene in 50 ml. of tetrahydrofuran was stirred under nitrogen at −80°C. while a solution of vinylmagnesium chloride in tetrahydrofuran (0.01 mole) was added in one portion. The temperature was gradually raised to room temperature over 2 hr. and maintained at the same temperature for an additional 24 hr. with stirring. The hydrolysis and extraction of the product with benzene were carried out as described above. One part of the benzene solution of the product poured into large quantity of methanol to precipitate polybutadiene which was reprecipitated two times from same solvent for the purification of the polymer. The infrared spectrum of the rubberlike product showed vinyl and *trans*-double bond absorption, and on this basis the rubberlike product was concluded to be a mixture of 1,2- and *trans*-1,4-polybutadienes. After removal of benzene from another part of the benzene solution, a small amount of viscous liquid material was obtained. The oily product was concluded to be a mixture of *trans, trans, trans*,1,5,9-cyclododecatriene and 1,2- and *trans*-1,4-polybutadienes on the basis of the infrared spectra.

13. Divinylcobalt

A solution of 0.65 g. (0.005 mole) of cobaltous chloride and 6.5 g. (0.12 mole) of butadiene in 50 ml. of tetrahydrofuran was stirred under nitrogen at −80°C. while a solution of vinylmagnesium chloride in tetrahydrofuran (0.01 mole) was added in one portion. The reaction and hydrolysis of the reaction mixture were carried out as described above, yielding 1.8 g. of light

yellow oily material. This oily product was concluded to be a mixture of *trans, trans, trans*,-1,5,9-cyclododecatriene and 1,2- and *trans*-1,4-polybutadienes on the basis of the infrared spectra.

14. Divinylnickel

A suspension of 1.1 g. (0.005 mole) of nickelous bromide and 6.5 g. (0.12 mole) of butadiene in 50 ml. of tetrahydrofuran was stirred under nitrogen at −80°C. while a solution of vinylmagnesium chloride in tetrahydrofuran (0.01 mole) was added in one portion. The reaction, hydrolysis of reaction mixture and extraction of hydrolyzed reaction mixture by benzene were carried out as described above. The product was 0.5 g. of brownish-yellow oily material. This oily product was concluded to be a mixture of *trans, trans, trans*-1,5,9-cyclododecatriene and 1,2- and *trans*-1,4-polybutadiene on the basis of the infrared spectra.

This work was supported by the Petroleum Research Fund, administered by the American Chemical Society and the Arakawa Forest Chemical Industries, Ltd., Osaka, Japan.

References

1. Gaylord, N. G., and H. F. Mark, *Advances in Chemistry Series, No. 34*, American Chemical Society, Washington, D. C., 1962, p. 127.
2. Tsutsui, M., *Ann. N. Y. Acad. Sci.*, **93**, 133 (1961).
3. Tsutsui, M., and J. Ariyoshi, *Trans. N. Y. Acad. Sci.*, **26**, 431 (1964).
4. Normant, H., *Compt. Rend.*, **239**, 1510, 1811 (1954); *ibid.*, **240**, 314 (1955).
5. Ramsden, H. E., J. R. Leebrick, S. D. Rosenberg, E. H. Miller, J. J. Walburn, A. E. Balint, and R. Cserr, *J. Org. Chem.*, **22**, 1202 (1957).
6. Nystrom, R. F., and W. G. Brown, *J. Am. Chem. Soc.*, **69**, 1197 (1947).
7. Ziegler, K., *Angew. Chem.*, **64**, 323 (1952).
8. Ziegler, K., H. G. Gellert, and E. Bomtz, Brit. Pat. 778,098 (July 3, 1957).
9. Tsutsui, M., and H. Zeiss, *J. Am. Chem. Soc.*, **81**, 6090 (1959).
10. Rochow, E. L., D. T. Hurd, and R. N. Lewis, *The Chemistry of Organometallic Compounds*, Wiley, New York, 1957, p. 303.
11. Herwig, W., and H. Zeiss, *J. Am. Chem. Soc.*, **81**, 6798 (1959).
12. Herwig, W., and H. Zeiss, *Ann.*, **606**, 209 (1957).
13. Fischer, E. O., and W. Z. Hafner, *Z. Anorg. Chem.*, **286**, 146 (1956).
14. Burke, R. E., and A. A. Sekul (to Cities Service Research and Development Co.), U. S. Pat. 2,972,640 (1959).
15. Wilke, G., *Angew. Chem.*, **75**, 10 (1963).

Résumé

La polymérisation de 1,8-butadiène au moyen de catalyseurs organotitaniques, p.ex. le tétraméthyltitane (considéré comme catalyseur de type radicalaire), fournit un polybutadiène caoutchouteux, en faible rendement, riche en stéréoisomères *trans*-1,4- tandis que la polymérisation du 1,3-butadiène, au moyen de catalyseures organotitaniques de type π, p.ex. le tétravinyltitane et le tétraphényltitane, fournit du polybutadiène de configuration 1,2 avec un rendement élevé. Le dichlorure de titanocène et l'iodure de bisbenzènechrome ont été utilisés séparément pour catalyser la polymérisation du 1,3-butadiène avec le réactif méthylique de Grignard. Dans les deux cas, on a obtenu des polybutadiènes riches en configuration 1,4- avec des rendements plutôt faibles. On interprète ces résultats en les attribuant à la non-disponibilité des orbitales 3*d* dans les

catalyseurs mentionnés ci-dessus. On a encore étudié l'action catalytique des composés organochrome, organocobalt, organofer, et organonickel pour la polymérisation du 1,3-butadiène. Dans chacun des cas, des produits visqueux de bas poids moléculaire ont été obtenus. Avec le catalyseur organochrome, on obtient un mélange de polymère, principalement du 1,2- et du *trans*-1,4-polybutadiène, avec un rendement élevé. Par contre, avec les autres catalyseurs, les rendements sont faibles. Toutefois on a trouvé dans chaque cas du *trans, trans, trans*-1,5,9-cyclododécatriène. La configuration du polybutadiène dépend aussi du nombre, pair ou impair, de groupements organiques sur l'atome de métal de transition.

Zusammenfassung

Die Polymerisation von 1,3-Butadien mit Organotitankatalysatoren, z.B. Tetramethyltitan (als radikalischer Katalysator klassifiziert) lieferte in niedriger Ausbeute kautschukartiges Polybutadien reich an *trans*-1,4-Streeoisomeren, wahrend die Polymerisation von 1,3-Butadien mit Organotitankatalysatoren, z.B. Tetravinyltitan und Tetraphenyltitan (als π-Katalysatoren klassifiziert) in hoher Ausbeute Polybutadien reich an 1,2-Konfiguration lieferte. Titanocendichlorid und Bisbenzolchrom wurden jedes für sich zur Polymerisationskatalyse von 1,3-Butadien mit Methyl-Grignardreagens verwendet. In beiden Fällen wurden in ganz geringer Ausbeute Polybutadiene reich an 1,4-Konfiguration erhalten. Diese Ergebnisse wurden auf die mangelnde Zugänglichkeit von 3*d*-Orbitalen in den oben erwähnten Katalysatoren zurückgefükrt. Organochrom-, -eisen-, -kobalt- und -nickelvergindungen wurden ebenfalls als Katalysatoren für die Polymerisation von 1,3-Butadien untersucht. In allen Fällen wurden viskose, niedermolekulare Produkte erhalten. Mit dem Chromkatalysator entstand in hoher Ausbeute eine Mischung von Polymeren, nämlich 1,2- und *trans*-1,4-Polybutadien. Die anderen Katalysatoren lieferten niedrige Ausbeuten an Reaktionsprodukten; in jedem Fall wurde aber *trans, trans, trans*-1,5,9-Cyclododecatrien gefunden. Die Konfiguration von Polybutadien war auch von der Anzahl, ungerade oder gerade, organischer Gruppen an einem Übergangsmetallatom abhängig.

Received August 12, 1964
(Prod. No. 4537A)

JOURNAL OF POLYMER SCIENCE: PART A VOL. 3, PP. 1741-1763 (1965)

Morphology of Deformed Polypropylene. Quantitative Relations by Combined X-Ray, Optical, and Sonic Methods

ROBERT J. SAMUELS, *Hercules Research Center, Wilmington, Delaware*

Synopsis

The submicroscopic morphology of uniaxially deformed isotactic polypropylene films has been examined by x-ray diffraction, infrared dichroism, birefringence, sonic modulus, small-angle light scattering, density, and electron microscopic techniques. Several new theoretical relationships and techniques have been developed. These include (*1*) a two-phase sonic modulus theory which makes possible the determination of the amorphous orientation function and the intrinsic sonic moduli of the polymer, (*2*) a general relationship for the quantitative determination of the infrared transition moment angle and for the quantitative determination of the crystal orientation function from infrared dichroism measurements only, (*3*) the determination of the extension ratio of spherulites from the small-angle light-scattering patterns of deformed films, (*4*) a technique for the experimental determination of the intrinsic birefringence of the crystal and amorphous regions of isotactic polypropylene, (*5*) correlation of the polarizability difference determined from solid-state measurements with that determined from solution measurements, and (*6*) other techniques for the rapid determination of orientation functions. Morphological information about uniaxially deformed isotactic polypropylene films, obtained as a consequence of these developments, is reported.

INTRODUCTION

A number of theories and related techniques have been developed in recent years for investigating the submicroscopic structure of polycrystalline polymers. These include x-ray diffraction, birefringence, infrared dichroism, small-angle light scattering, and electron microscopy.[1] Though considerable success has been achieved with these systems in the elucidation of deformation mechanisms in polyethylene, the study of deformation mechanisms in isotactic polypropylene has been less successful.

The primary reason these methods have not been extended to the characterization of the deformation mechanisms in isotactic polypropylene has been a lack of the basic parameters required for application of the theoretical treatments. Thus, the infrared vibrational frequency assignments are not known with any assurance, and the intrinsic birefringence of the amorphous and crystalline regions of isotactic polypropylene have not been accessible to experimental determination. Similarly, small-angle light-scattering pictures from undeformed spherulitic samples can be interpreted quantitatively, but the patterns from deformed films have not been amenable to quantitative interpretation.

In the present study, these barriers to a comprehensive quantitative morphological study of isotactic polypropylene have been removed. New theoretical relationships, new techniques, and new insights into existing systems are set forth. These developments have made possible the quantitative study of the deformation of isotactic polypropylene films.

EXPERIMENTAL

Preparation of Films

Compression-Molded Unoriented Films. Profax 6523 was compression-molded into 5-mil films at 550°F. for 10 min., cooled to 400°F., and treated in the following manner: (*1*) quenched in a Dry Ice–cellosolve bath (−65°C.); (*2*) quenched in tap water (20°C.); (*3*) placed in hot tap water (55°C.); (*4*) press cooled.

Cast and Annealed Polypropylene Films. Profax 6320 was cast from the melt (ca. 280°C.) on a 20°C. roll at approximately 5 ft./min. The drawn films were produced by transferring cast film to a 110°C. roll and hot drawing over a 5-ft. gap to a room temperature roll. Sections of each of the films about 12 × 8 in. were annealed at fixed length for 15 min. at 110°C. and allowed to age for at least two months before being examined.

Density

Densities were measured in a 3A alcohol–water density gradient column at 23.2 ± 0.1°C.

X-Ray Diffraction

X-ray diffraction measurements were made with a Philips diffractometer equipped with a copper target, nickel filter, and a scintillation counter detector system. The measured intensities were corrected for polarization, absorption, background, and incoherent scattering. Calculations were made on a Bendix G15D computer.

Birefringence

Both birefringence and sonic velocity were measured on the same strips of 1–5-mil film. These strips were 1 mm. wide and 15–25 cm. long. The thickness at each point examined was measured with a Pratt and Whitney Electro-Limit Gage. The retardation of the sample was measured in a Zeiss polarizing microscope with the use of a Zeiss interference filter to produce $\lambda = 546$ mμ monochromatic light. Both quartz and calcite Ehringhaus compensators were used to measure the retardation.

Sonic Modulus

A KLH pulse propagation meter which produces longitudinal waves at a frequency of 10 kcycle/sec. was used for all sonic modulus measurements. The sample film strip was clamped at one end, passed over a pulley, and

kept taut by a 10-g. weight attached to the other end. In some instances the weight was replaced by a clamp attached to a strain gage, and a force of 10 g. was applied to the strip. An optical bench was used to support the test equipment. The transmitter and receiver were moved along the optical bench and the distance between the probes was read off a meter stick.

Small-Angle Light Scattering

A Spectra Physics Model 115 continuous wave He-Ne gas laser was used as the polarized, monochromatic (λ = 6328 A.) light source. The sample was the same as that used for sonic velocity and birefringence measurements. The sample was placed between the analyzer and the laser beam. The plane of polarization of the analyzer was perpendicular to that of the polarized laser beam (H_V) and the photographic film was set at an arbitrary distance behind the analyzer.

Infrared Absorption Measurements

Infrared dichroism and parallel-perpendicular ratio index measurements were made with a Beckman I.R. 7 infrared spectrophotometer.[2]

Electron Microscope Measurements

Photomicrographs of carbon replicas of the isotactic polypropylene film surfaces were taken in an RCA Model EMB-3 electron microscope.

DETERMINATION OF THE AMORPHOUS ORIENTATION FUNCTION

A prime barrier to the extension of present methods for the study of deformation mechanisms to isotactic polypropylene has been the lack of information about the amorphous orientation function of the polymer. A two-phase sonic modulus theory has been developed which makes this parameter accessible to experimental measurement. This theory requires the combined measurements of density, wide-angle x-ray diffraction, and sonic modulus.

Density

Isotactic polypropylene can be considered as a two-phase system consisting of crystalline and amorphous regions.[3] The crystalline region consists of type I (monoclinic) crystals,[4] type II (hexagonal) crystals,[5] or a mixture of both. The theoretical density of the type I crystal is 0.936 g./cm.^{3}; that of the type II crystal is 0.939 g./cm.^{3}.[6] The fraction of crystals (β) was calculated from the measured density by means of the equation of Danusso and Natta.[7] The amorphous density was assumed to be 0.858 g./cm.^{3},[7] and the crystal density, 0.936 g./cm.^{3}. The assumption that type I and type II crystals have the same density could lead to a

TABLE I
Sonic Modulus (E_u), Crystal Fraction (β), and Density of Unoriented Compression-Molded Isotactic Polypropylene Films

Sample	$E_u \times 10^{-10}$, dyne/cm.^{2}	Density, g./cm.^{3}	β
1	2.27	0.8875	0.410
2	2.48	0.8936	0.485
3	2.63	0.8980	0.540
4	3.01	0.9061	0.643

TABLE II
Sonic Modulus (E), Crystal Fraction (β), and Density of Cast and Annealed Polypropylene Films

Sample	Elongation, %	$E \times 10^{-10}$, dyne/cm.^{2}	Density, g./cm.^{3}	β
1	0	2.86	0.9034	0.608
2	50	3.09	0.9052	0.630
3	100	3.59	0.9056	0.636
4	200	5.07	0.9055	0.636
5	300	6.19	0.9060	0.643
6	400	6.55	0.9052	0.630

maximum error of less than 4% in the crystallinity. The experimentally determined sample densities are listed in Tables I and II.

Wide-Angle X-Ray Diffraction

Deformation of a polycrystalline polymer sample results in an orientation of both the crystalline and amorphous regions with respect to the deformation direction. The average orientation of the crystals can be described in terms of Herman's[8] defined orientation function, f. The average orientations of the b- and c-axis of the crystal were determined from azimuthal scans[9] of the (040) and (110) reflections, respectively (Table III). The orientation function for a given crystal axis varies from a value of +1 for

TABLE III
Birefringence (Δ_T) and Orientation Function (f) Data for Isotactic Polypropylene Films

Sample (cast and annealed)	Elongation, %	Birefringence $\Delta_T \times 10^3$	X-ray f_c	X-ray $-f_\beta$	Sonic modulus f_{am}
2	50	5.759	0.3472	0.2485	−0.0951
3	100	10.19	0.5790	0.2898	+0.0232
4	200	19.64	0.6805	0.3775	+0.2849
5	300	22.25	0.7728	0.4022	+0.3877
6	400	25.30	0.8016	0.3988	+0.4321

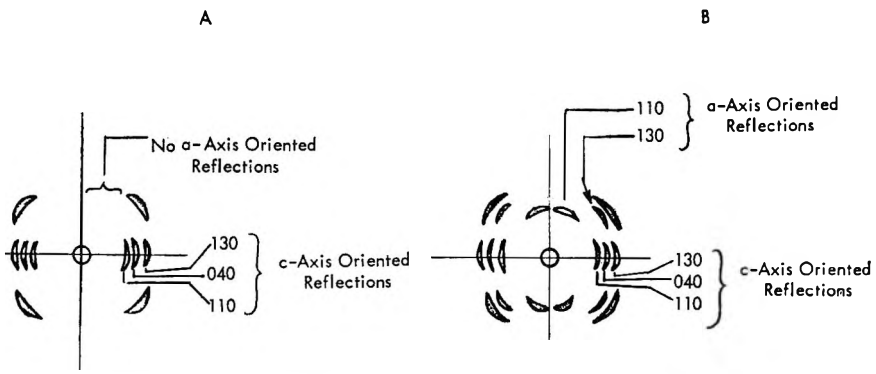

Fig. 1. X-ray diffraction diagrams of isotactic polypropylene fibers: (*A*) cold-drawn; (*B*) annealed or spun.

parallel orientation with respect to the stretch direction, through a value of zero for random orientation to a value of $-1/2$ if the axis is oriented perpendicular to the stretching direction.

For isotactic polypropylene the *c* axis of the crystal corresponds to the helical chain axis of the molecule. Generally, when a sample is deformed, the polymer chain axis orients in the direction of the deformation. Thus the *c*-axis of the crystal orients in the direction of the deformation in cold-drawn isotactic polypropylene. The resulting x-ray diffraction pattern for *c*-axis orientation is shown in Figure 1*A*.

Compostella et al.[10] found that melt-spun isotactic polypropylene exhibited two types of crystal orientation simultaneously. Most of the crystals exhibited the expected *c*-axis orientation but some of the crystals exhibited *a*-axis orientation. In *a*-axis orientation the polymer chain axis is nearly perpendicular to the stretching direction, and the *a*-axis of the crystal is oriented toward the stretch direction. This type of orientation appears in the x-ray diffraction pattern as shown in Figure 1*B*. Cold-drawn fibers annealed very close to the crystal melting temperature have yielded similar patterns in this laboratory. Thus *a*-axis orientation seems to be the high temperature form in oriented isotactic polypropylene.

The manner in which the crystal axes are orienting as the sample is deformed can be represented by an orientation function triangle diagram.[11] Figure 2 shows such a diagram for (*1*) the hot-drawn (110°C.) polypropylene films used throughout this study, (*2*) melt-spun isotactic polypropylene fibers, and (*3*) cold-drawn isotactic polypropylene reported by Stein.[12] In this diagram f_β and f_c are the orientation functions for the *b*- and *c*-axes of the crystal. The latter was calculated from the intensity distribution around the bimodal (110) azimuthal scan, assuming this to be representative of the average *c*-axis orientation as seen by birefringence, sonic modulus, and infrared measurements. The curve for the melt-spun fibers is highly bowed toward the $b_\perp$ axis, indicating a large amount of *a*-axis orientation. The cold-drawn polymer shows no such bow and

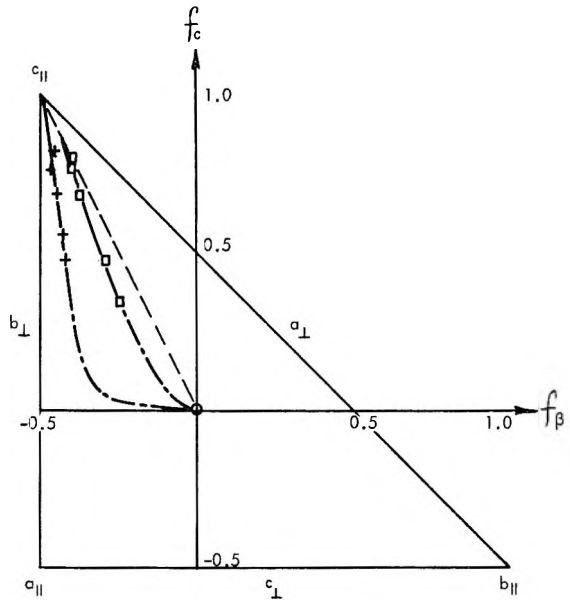

Fig. 2. Orientation function triangle diagram for the *b*- and *c*- axes of isotactic polypropylene: (□) hot-drawn film samples (110°C.); (+) melt-spun fibers; (- - -) cold-drawn polypropylene (data of Stein[12]); (–•–) extrapolation.

therefore has only *c*-axis orientation. The films used throughout this study were hot-drawn at a temperature between these extremes, and the resulting curve for these samples falls between the other two.

Sonic Modulus

The nature of the mechanism of sound propagation in oriented fibers has been examined by Ward[13] and Moseley.[14] Their independent treatments both reduce to the following expression for a single-phase polymer system:

$$1/E = 1/\rho C^2 = (1 - \overline{\cos^2 \theta})/E_t^0 \tag{1}$$

where ρ is the density of the polymer, C is the sonic velocity, E is the measured sonic modulus (Young's modulus), E_t^0 is the intrinsic lateral modulus, and θ is the angle between the molecular chain axis and the direction of sound propagation. The intrinsic lateral modulus is defined as the transverse Young's modulus for a perfectly oriented fiber.[13] It is a function of the intermolecular forces in the fully oriented fiber.

Ruland has demonstrated[3] that isotactic polypropylene cannot be described as a single-phase system but is best represented by a two-phase system of crystalline and noncrystalline regions. To extend the sonic modulus equation to a two-phase system, a mixing equation involving bulk compressibilities has been used. This equation has been found to represent validly the behavior of bulk isotropic samples of suspensions of

solids in liquids[15] and of polyethylene over a range of temperatures and crystallinities:[16]

$$K = \beta K_c + (1 - \beta)K_{am} \tag{2}$$

where K is the bulk compressibility of the mixture, K_c is the bulk compressibility of the crystalline region, K_{am} is the bulk compressibility of the amorphous region, β is the fraction of crystalline polymer, and $(1 - \beta)$ is the fraction of amorphous polymer. Combining eqs. (1) and (2) (see Appendix I for derivation) leads to a relation between the measured sonic modulus, E_u, of an unoriented sample and the fraction of crystalline and amorphous phases present.

$$3/2E_u = (\beta/E_{t,c}^0) + [(1 - \beta)/E_{t,am}^0] \tag{3}$$

where $E_{t,c}^0$ is the intrinsic lateral (transverse) modulus of the crystal and $E_{t,am}^0$ is the intrinsic lateral modulus of the amorphous region. The variation of the sonic modulus with β is given in Table I for unoriented films.

The intrinsic lateral modulus of the crystal, $E_{t,c}^0$, is the intermolecular Young's modulus of the chains. If the polymer chains are in a folded single crystal with the chain axes all aligned along a vertical axis, Z, and in a given crystallographic plane, such as the (110) for polyethylene, the intrinsic lateral modulus may be visualized as the force per molecule required to separate the planes of molecules [(110) faces] a given distance by applying the force in the direction perpendicular to the Z-axis and normal to and away from the crystal face. The intrinsic sonic modulus of the isotactic polypropylene crystal, calculated from the experimental values of E_u and β determined at room temperature, is $E_{t,c}^0 = 3.96 \pm 0.09 \times 10^{10}$ dyne/cm.^{2}. Sakurada et al.,[17] using stress–x-ray diffraction methods, obtained a value of $E_{t,c}^0$ of 2.8×10^{10}–3.1×10^{10} dyne/cm.^{2} for isotactic polypropylene. Using similar methods, investigators[18,19] have obtained experimental values of $E_{t,c}^0$ for polyethylene ranging from 2.2×10^{10}–4.2×10^{10} dyne/cm.^{2}. Thus, the agreement between the sonic modulus and stress–x-ray diffraction values for $E_{t,c}^0$ of isotactic polypropylene is at least as good as the agreement obtained by different investigators, each using the same stress–x-ray diffraction method, on polyethylene.

The intrinsic sonic modulus of the amorphous region is defined as the transverse Young's modulus the amorphous chains would have in a perfectly oriented fiber. The lateral forces between amorphous chains in this system would be expected to be lower than those in the crystal lattice. The calculated intrinsic lateral modulus of the amorphous region of isotactic polypropylene is $E_{t,am}^0 = 1.06 \pm 0.01 \times 10^{10}$ dyne/cm.^{2}, which is, as predicted, lower than the value of the intrinsic lateral modulus obtained for the crystal.

For an oriented polymer, the sonic modulus equation becomes (see Appendix I):

$$3/2(\Delta E^{-1}) = (\beta f_c/E_{t,c}^0) + [(1 - \beta)f_{am}/E_{t,am}^0] \tag{4}$$

where

$$(\Delta E^{-1}) = (E_u)^{-1} - (E_{or})^{-1}$$

E_{or} is the measured sonic modulus of the oriented sample. For a given fraction of crystals the difference in the sonic moduli of an oriented and unoriented film depends on the orientation function of each of the components. The dependence of E_{or} on elongation is illustrated in Table II. Since the intrinsic lateral moduli are now established, eq. (4) permits calculation of the amorphous orientation function, f_{am}, for any oriented isotactic polypropylene sample from experimental values of the sonic modulus (E_{or}), density (β), and the crystal orientation function (f_c) determined by x-ray diffraction. Values of f_{am} determined for the oriented isotactic polypropylene samples are listed in Table III.

SUPPORTING EVIDENCE FROM BIREFRINGENCE FOR THE SONIC MODULUS THEORY

Birefringence theory can be used to test the validity of the amorphous orientation functions determined by the sonic modulus theory above. The birefringence equation for a uniaxially oriented system[20] may be written in the form:

$$\Delta_T/\beta f_c = \Delta_c^0 + \Delta_{am}^0 \{[(1 - \beta)/\beta](f_{am}/f_c)\} \tag{5}$$

where Δ_T is the measured birefringence (see Table III), Δ_c^0 and Δ_{am}^0 are the intrinsic birefringences of the crystalline and amorphous regions, respectively, and the other symbols have the same meanings as previously defined. A plot of $\Delta_T/\beta f_c$ against $[(1 - \beta)/\beta](f_{am}/f_c)$ for the five oriented samples studied gives the predicted straight-line behavior (see Fig. 3). Each point on this plot is a combination of a birefringence, a density, an

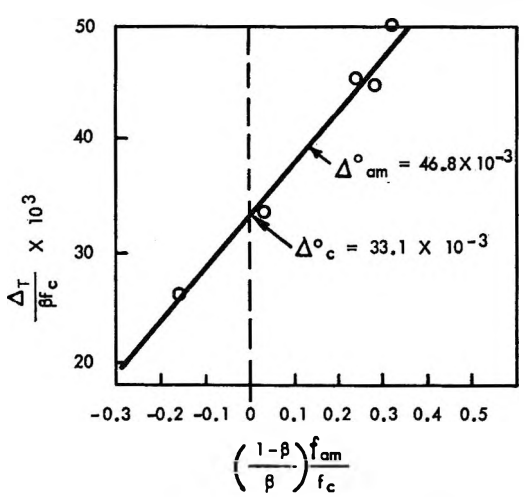

Fig. 3. Determination of intrinsic birefringence.

x-ray diffraction, and a sonic modulus measurement. The ratio, f_{am}/f_c, should be very sensitive to errors in f_{am}.

The intrinsic birefringence of the crystalline ($\Delta_c^0 = 33.1 \times 10^{-3}$) and amorphous ($\Delta_{am}^0 = 46.8 \times 10^{-3}$) regions of isotactic polypropylene have been calculated from the intercept and slope of the line in Figure 3. This is the first time the intrinsic birefringences of the amorphous and crystalline regions of a polycrystalline polymer have been obtained from measurements made directly on the polymer. The Δ_c^0 value generally accepted for polyethylene was obtained on single crystals of low molecular weight (C_{36}) paraffin homologs.[21] Theoretical attempts at calculation of Δ_c^0 have had to assume additivity of bond polarizabilities and to ignore internal field effects known to be important in the crystal.[22]

The intrinsic birefringence of the crystal is found to be smaller than that of the amorphous region of isotactic polypropylene. The smaller value of Δ_c^0 is due to the ordered lattice arrangement of neighboring molecules in the crystal. A bond within the molecule experiences not only the electromagnetic field of the incident light but also the polarization field of the surrounding molecules. This internal field is more anisotropic in the ordered lattice of the crystal than in the disordered amorphous phase. Consequently, there are different effective polarizabilities in the two phases. Stein[23] has recently derived a theory which satisfactorily accounts for internal field effects in the polyethylene crystal. He concluded that, due to internal field effects, the intrinsic birefringence of the crystal will be lower than that of the amorphous material. Our experimental results with isotactic polypropylene are consistent with Stein's theoretical treatment.

The principal polarizability difference per monomer unit $(a_{\parallel} - a_{\perp})_{mer}$ can be calculated for isotactic polypropylene from the expression:[20]

$$(a_{\parallel} - a_{\perp})_{mer} = \Delta_{am}^0/(2/9)\pi[(\bar{n}^2 + 2)^2/\bar{n}]N_{mer}$$
$$= +4.49 \times 10^{-25} \text{ cm.}^3 \qquad (6)$$

where $\Delta_{am}^0 = 46.8 \times 10^{-3}$, $\bar{n}$ is the average refractive index of the polymer $= 1.51$, and N_{mer} = (amorphous density/molecular weight mer unit) $\times$ Avogadro's number.

The intrinsic birefringence of the amorphous region is used to minimize internal field effects. The value of $+4.49 \times 10^{-25}$ cm.^{3} is in very good agreement with the value of $+3.5 \times 10^{-25}$ cm.^{3} for isotactic polypropylene determined by Tsvetkov[24] from measurements of flow birefringence in dilute solution. This agreement between measurements in the solid state and in dilute solution is quite striking, especially since the $(a_{\parallel} - a_{\perp})$ values for polymers are known to range from -35 to $+21$ ($\times 10^{-25}$) cm.^{3}

The contributions of the crystalline and amorphous regions to the total birefringence of the film samples are shown in Figure 4. The negative amorphous contribution at low elongations indicates that the amorphous chains are oriented toward the perpendicular to the direction of stretch. Similar results were obtained by Stein et al.[12] from low-density poly-

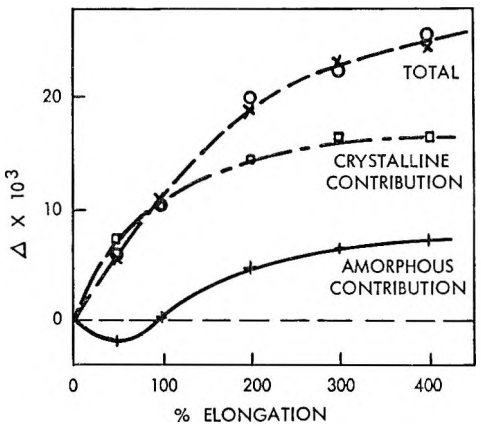

Fig. 4. Crystalline and amorphous contributions to the birefringence of deformed isotactic polypropylene films: (O) $\Delta = \Delta_T$ (experimental); (×) $\Delta = \Delta_T$ (calculated); (□) $\Delta = \beta\Delta_c$ (calculated); (+) $\Delta = (1-\beta)\,\Delta_{am}$ (calculated).

ethylene. Low-density polyethylene is about 60% crystalline and structurally similar to polypropylene; therefore, the similar behavior of their crystalline and amorphous regions is not surprising.

The coupling of sonic modulus and birefringence measurements leads to a rapid method for determining the orientation functions f_c and f_{am} of a polymer sample. Once $E_{t,c}^0$, $E_{t,am}^0$, Δ_c^0, and Δ_{am}^0 have been determined for the polymer, measurement of the sonic modulus, the birefringence, and the density are sufficient to obtain f_c and f_{am}, by solution of the equations:

$$\Delta_T = \beta\Delta_c^0 f_c + (1 - \beta)\Delta_{am}^0 f_{am}$$

$$3/2(\Delta E^{-1}) = (\beta f_c/E_{t,c}^0) + [(1 - \beta)f_{am}/E_{t,am}^0]$$

QUANTITATIVE DETERMINATION OF TRANSITION MOMENT ANGLES AND FURTHER SUPPORT FOR THE SONIC MODULUS THEORY FROM INFRARED MEASUREMENTS

Infrared Dichroism

The infrared dichroic ratio D of a uniaxially oriented polymer is a function of two characteristic orientation angles, θ and α. θ is the angle the polymer chain axis makes with the reference direction (e.g., stretch direction), and α is the angle the transition moment makes with the polymer chain axis. To the polymer morphologist interested in determining the chain orientation angle, θ, the dependence of the dichroic ratio on α becomes a hindrance. The angle α is seldom known; when it is known, the relation between the measured dichroic ratio and the chain orientation angle can be derived geometrically. Thus, Stein[20,11] was able to derive the relation between D and θ for polyethylene because α was known for the two infrared frequencies he used. Since the α's for those frequencies were

directed along the crystal axes his geometric analysis involved only one orientation function for each frequency. If α had not been directed along a crystal axis, the geometric analysis would have involved more than one orientation function for each frequency.[1]

The general equations relating θ and α to the dichroic ratio of a uniaxially oriented fiber have been derived by Fraser.[25] He showed that if all of the molecular chain axes of an oriented fiber were perfectly aligned parallel to the reference direction the dichroic ratio would be a function of the transition moment angle, α, only:

$$D_0 = 2 \cot^2 \alpha \tag{7}$$

where D_0 is the dichroic ratio for perfectly aligned chains and α is the transition moment angle. Under normal conditions, when the molecular chain axis is oriented at an average angle θ to the reference direction, the equation takes the form:

$$f = (D - 1)(D_0 + 2)/[(D + 2)(D_0 - 1)] = (3\,\overline{\cos^2 \theta} - 1)/2 \tag{8}$$

where D is the measured dichroic ratio and D_0 and θ are defined above. The form of f derived by Fraser is the same as Herman's orientation function. Thus, for an infrared band which absorbs in the crystalline region only, Fraser's f is identical to the crystal orientation function, f_c, determined from x-ray diffraction by Wilchinsky's method.[26] Therefore, a plot of f_c (from x-ray diffraction) against $(D - 1)/(D + 2)$ (from infrared measurements) should be linear with zero intercept. From the slope of the

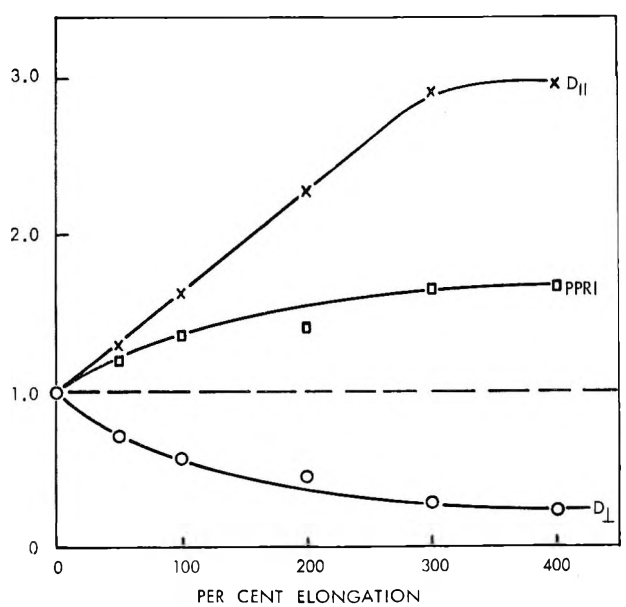

Fig. 5. Relation between the elongation of isotactic polypropylene films and $D_{\parallel}$, $D_{\perp}$ and, PPRI: (O) 1220 cm.$^{-1}$ band; (×) 1256 cm.$^{-1}$ band; (□) PPRI.

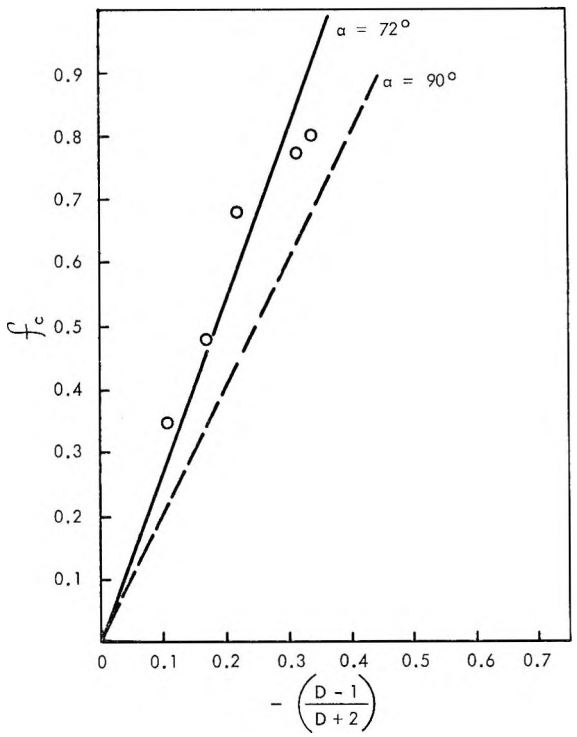

Fig. 6. Determination of the transition moment angle α for the 1220 cm.$^{-1}$ band in isotactic polypropylene.

line, $(D_0 + 2)/(D_0 - 1)$, the transition moment angle, α, can be calculated by using eq. (7).

The infrared dichroic ratios of the oriented polypropylene samples, determined for the 1220 cm.$^{-1}$ perpendicular (σ) crystal band and the parallel (π) 1256 cm.$^{-1}$ mixed (amorphous and crystalline) band are given in Figure 5.

It is generally agreed that the 1220 cm.$^{-1}$ band is due to absorption by the crystalline phase only, although there is no general agreement as to the assignment of the vibrational modes of the chain characterized by this band. There is agreement in the vibrational mode assignment only to the extent that various authors[27–32] characterize the band as represented by the motions of one, two, or a mixture of the three bonds CH_2, CH, C—CH_3. Isotactic polypropylene has a helical conformation in the crystalline phase,[4] and each of these bonds makes an angle of about 72° with the helical axis.

In Figure 6 the crystal orientation function f_c (from x-ray diffraction, Table III) is plotted against the infrared 1220 cm.$^{-1}$ (σ) band dichroic ratio according to eq. (8). The experimental points fit a calculated line drawn for $\alpha = 72°$ quite reasonably. This indicates the transition moment is directed along one of the bonds mentioned above. The dashed line in Figure 6 has been calculated for $\alpha = 90°$ (i.e., where the transition

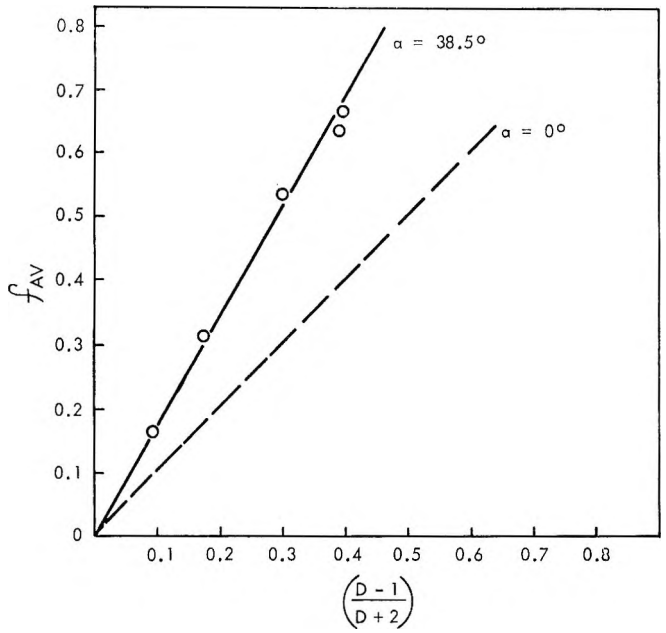

Fig. 7. Relation between the average orientation function and the infrared dichroism of the 1256 cm.$^{-1}$ band in isotactic polypropylene.

moment of the σ band is perpendicular to the helical axis of the chain). An assignment of $\alpha = 90°$ for the 1220 cm.$^{-1}$ band is not reasonable in light of the experimental data.

Since the 1256 cm.$^{-1}$ band results from absorption in both the crystalline and amorphous regions, its infrared dichroism would be expected to correlate with some average orientation function. Such an average can be expressed as the average orientation of each phase weighted by the amount of each phase present:

$$f_{av} = \beta f_c + (1 - \beta) f_{am} \tag{9}$$

where the fraction of crystals β, is determined from density, f_c is derived from x-ray diffraction, and f_{am} is determined from sonic modulus. Figure 7 is a plot of f_{av} against $(D - 1)/(D + 2)$ for the 1256 cm.$^{-1}$ (π) band of the oriented isotactic polypropylene samples. A good linear plot with a zero intercept is obtained as predicted. No structural significance can be given to the value of α. The good fit obtained by using the f_{am} values obtained from sonic modulus measurements further supports the validity of the sonic modulus, two-phase theory.

The above method of relating orientation functions to infrared dichroism is a general one. If absorption takes place only in the crystalline phase, the value of α can be determined quantitatively for any crystal by using Wilchinsky's method for determining f_c. This method can thus have considerable utility in structure analysis. Conversely, once α has been

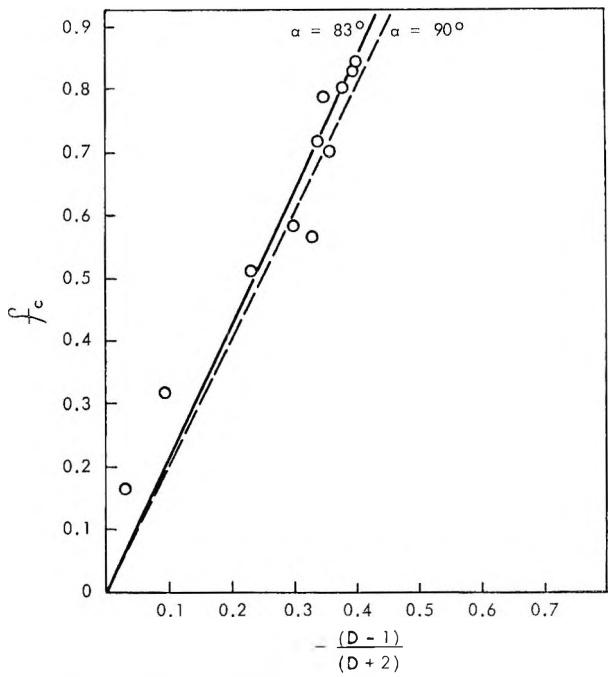

Fig. 8. Determination of the transition moment angle α, for the 730 cm.$^{-1}$ band in low-density polyethylene (data of Norris and Stein[24]).

determined quantitatively by this method, infrared dichroism alone can be used to determine the crystal orientation function, f_c, of oriented polymers.

An example of the general utility of this method to other polymers is illustrated in Figure 8, which represents the data of Norris and Stein[20] for low-density polyethylene. Polyethylene has a planar zigzag conformation in the crystal lattice. The 730 cm.$^{-1}$ (σ) band absorbs only in the crystalline region and has been assigned as a CH_2 rocking mode. The α for this motion would be expected to be 90° to the backbone axis. From Figure 8, $\alpha \cong 83°$ seems to be more reasonable. The observed difference in α between theory and experiment may be due to experimental difficulties in separating the 730–720 cm.$^{-1}$ doublet into its components, orientation effects of the amorphous region in the 720 cm.$^{-1}$ band affecting the resolution of the 730 cm.$^{-1}$ band, or possible coupling effects from bending and stretching modes.

Parallel–Perpendicular Ratio Index

The parallel–perpendicular ratio index (PPRI), defined as the ratio of the intensity of the parallel mixed (1256 cm.$^{-1}$) band to that of the perpendicular crystal (1220 cm.$^{-1}$) band of a film relative to the same ratio of a standard unoriented film, is a measure of the orientation of the polymer chain axis relative to the surface of the film.[2] When a film is stretched

uniaxially, the chain axes orient in the direction of stretch and consequently parallel to the film surface. To eliminate the effects of axial orientation and measure only the planar orientation (where the chain axes are randomly oriented around the normal to the film surface), the polymer film is rotated about the normal to the film surface during measurement. For this reason the PPRI method cannot distinguish between planar and uniaxial orientation. When the chains are all oriented in the plane of the film PPRI = 2. If the chains are randomly oriented with respect to the plane of the film PPRI = 1. Thus for a uniaxial system, in which the chain axes are orienting in the direction of stretch, the PPRI value would be expected to increase toward a limiting value of 2 with elongation, $D_{\parallel}$ (the infrared dichroism of the 1256 cm.$^{-1}$ parallel band) would increase with elongation, and $D_{\perp}$ (the infrared dichroism of the 1220 cm.$^{-1}$ perpendicular band) would decrease with elongation. Figure 5 is a plot of $D_{\parallel}$, $D_{\perp}$, and PPRI as a function of the elongation of the film. The observed behavior of these parameters is qualitatively consistent with uniaxial orientation.

The PPRI as defined above would be expected to be related to the average orientation function defined by eq. (9). Figure 9 is a plot of the PPRI of the film samples against f_{av}. The solid line is not theoretical but is simply a straight line drawn through the two theoretical limiting points, i.e., PPRI = 1, f_{av} = 0 for random orientation and PPRI = 2, f_{av} = 1.0 for completely planar or uniaxial orientation. The PPRI is found to be a linear function of the average orientation function as well as consistent with the limiting conditions of the PPRI theory. This provides the first experimental verification of the PPRI theory. The internal consistency of these results adds further support to the validity of f_{am} determined from the sonic modulus measurements.

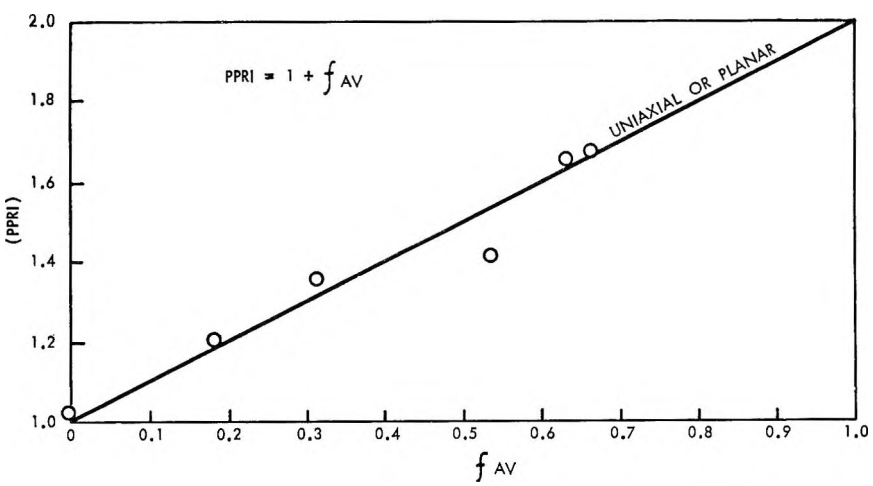

Fig. 9. Relation between the PPRI and the average orientation of isotactic polypropylene films.

DETERMINATION OF THE MECHANISM OF SPHERULITE DEFORMATION

At present, three methods are available for the examination of spherulites which are too small to be observed with the light microscope. These methods are electron microscopy, wide-angle x-ray diffraction, and small-angle light scattering. Electron micrographs of the cast films showed the presence of spherulites with a diameter of 1–2 μ. These spherulites were deforming from a spherical to a fibrillar form with increasing extension of the films. Wide-angle x-ray diffraction and small-angle light-scattering techniques were used to further elucidate the mechanism of spherulite deformation in the films.

Wide-Angle X-Ray Diffraction

Wilchinsky[33] has calculated values of the crystal orientation function at various extension ratios, λ, for two kinds of spherulite deformation in a fiber. One (expressed as f_λ), he assumed to have uniform deformation within the spherulite; in the other (f_λ'), he included the enhanced orientation of the inner regions of the spherulite when it is deformed. Both were derived for simple elongation at constant volume. In both, the spherulite was assumed to increase in length by an extension ratio λ while it decreased $\lambda^{-1/2}$ in the other two orthogonal directions. Equating λ of the spherulite with λ of the deformed sample implies an affine deformation. The two models differed in the nature of the crystallite displacement within the affinely deformed spherulite.

Our experimental values of the crystal orientation function fall between Wilchinsky's two theoretical curves (Fig. 10), thus indicating that an affine deformation of the spherulites has occurred. The exact nature of the

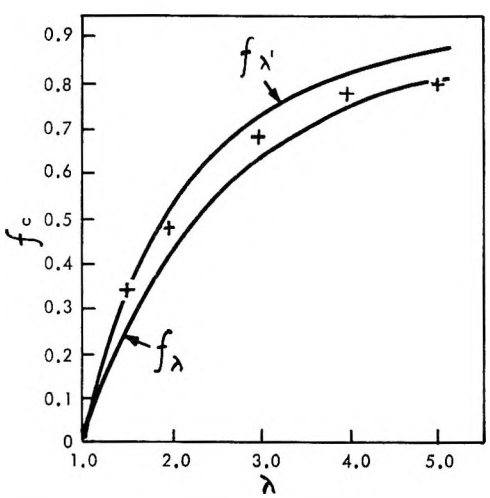

Fig. 10. Relation between the predicted and experimental crystal orientation functions and the extension ratio of the sample: (——) predicted; (+) experimental.

crystallite displacement mechanism (uniform or enhanced orientation) within the spherulite is uncertain.

Small-Angle Light Scattering (SALS)

Stein[34] and his co-workers have developed a theory for the SALS of undistorted spherulites. The theory predicts that the H_V scattering

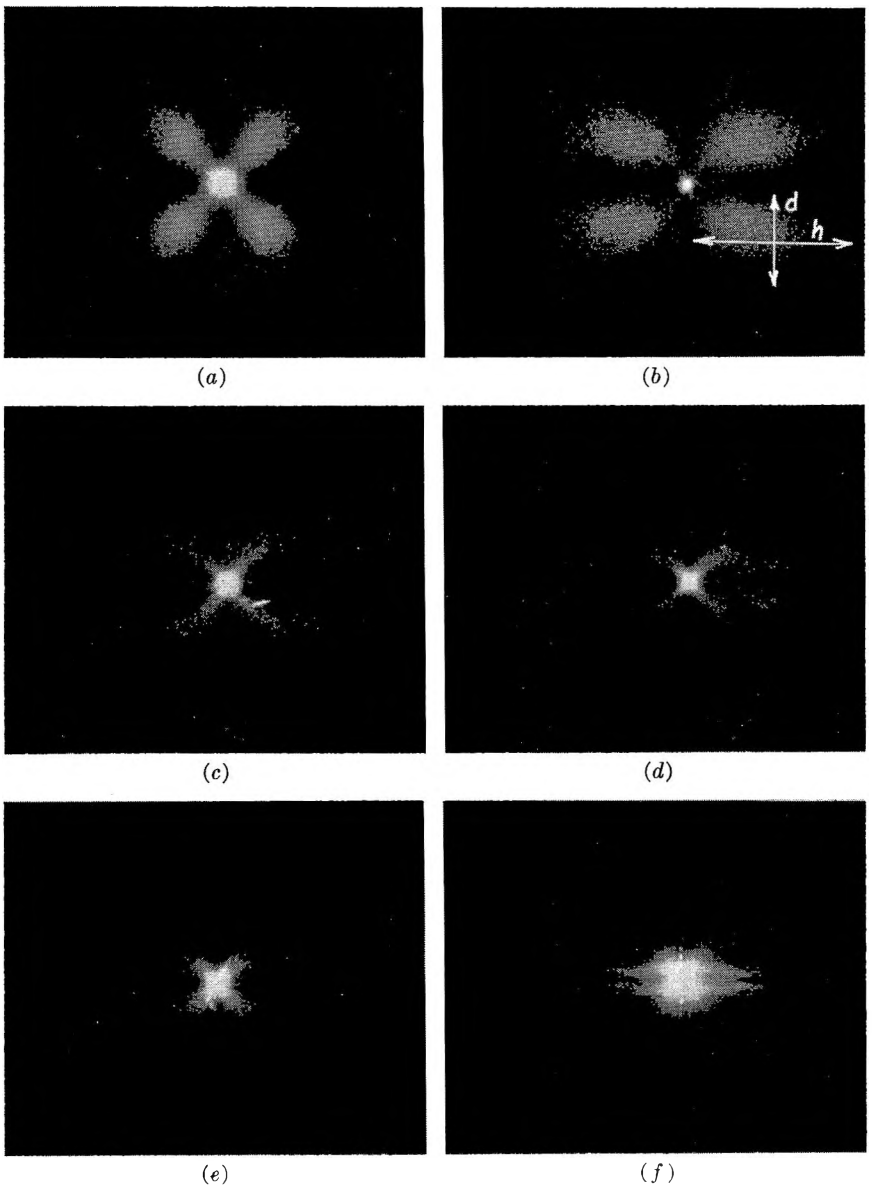

Fig. 11. Change in the H_V SALS pattern of isotactic polypropylene film with elongation: (*a*) 0%; (*b*) 50%; (*c*) 100%; (*d*) 200%; (*e*) 300%; (*f*) 400%. The polarization direction and the film stretch direction are vertical.

pattern of an unoriented sample arises solely from the anisotropy of the spherulite. The resulting H_V pattern appears as a four-leaf clover (see Fig. 11*a*), with the leaves oriented at 45° to the plane of the analyzer and polarizer. The size of the spherulite is calculated from (*1*) the measured distance of the center of one of the lobes from the center of the pattern and (*2*) the known sample-to-film distance. Spherulites on the order of two microns in diameter were calculated from the SALS pattern of the unoriented isotactic polypropylene cast film. This is in good agreement with the electron microscope observations. The only previously reported observation of polypropylene spherulites by the SALS technique was by Powers.[35]

When a sample is stretched uniaxially, the shape of the H_V SALS lobe changes from circular to ellipsoidal. The change in the lobe scattering envelope takes the form of an extension of the lobe perpendicular to the polarization direction and a shrinkage of the lobe parallel to the polarization direction. This is illustrated in Figure 11*b*, in which the extension is along the major axis of the ellipse, *h*, and the shrinkage is along the minor axis of the ellipse, *d*. Stein[84] has demonstrated that, as the lobe of the H_V SALS pattern goes through a deformation from a circular to an elliptical to an extended elliptical (rodlike) form, there is a very similar transition in the shape of the spherulite observed under the electron microscope. Thus the shape of the H_V SALS lobe reflects the continuous transition from a spherulitic to a fibrous structure occurring in the sample when it is deformed.

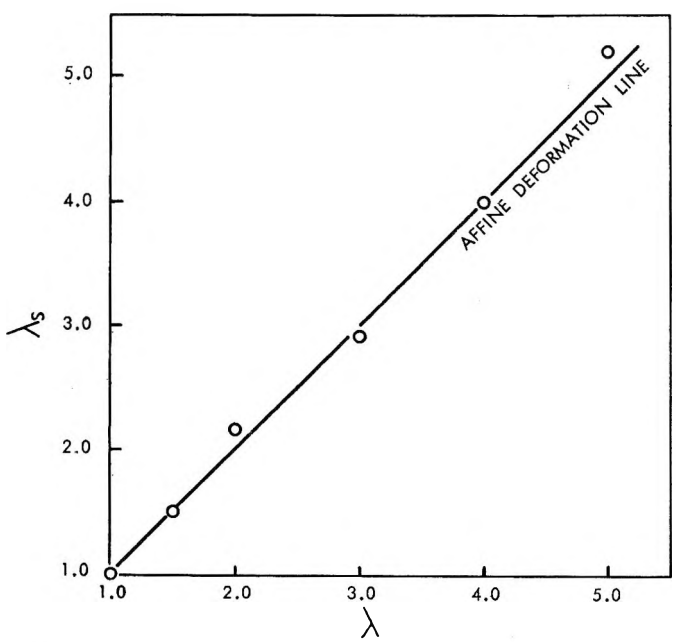

Fig. 12. Relation between λ_s from SALS and the sample extension ratio λ.

If any change in the shape of the spherulite is assumed to lead to an equivalent change in the shape of the H_V SALS lobe, the following equation relating the shape of the H_V SALS lobe to the average extension ratio of the spherulites producing that lobe, λ_s, can be derived (see Appendix II):

$$\lambda_s = (h/d)^{2/3} \tag{10}$$

The extension ratio, λ_s, for the spherulite can be equated to the extension ratio of the uniaxially deformed film, λ, if an affine deformation of the spherulites has occurred. Figure 12 is a plot of λ_s, obtained from the SALS patterns in Figure 11, against the sample extension ratio, λ. The experimental points fit the predicted line for an affine deformation of the spherulites. Thus, both the SALS measurements and the wide-angle x-ray diffraction analysis have shown that the spherulites deform affinely with the sample when it is elongated at 110°C.

CONCLUSIONS

This study of uniaxially oriented isotactic polypropylene films has used seven independent physical methods to characterize the submicroscopic morphology of the films. Several new theoretical relationships were developed and verified by the application of independent techniques and theories. The following conclusions have resulted from the new theories and techniques developed in this study.

(*1*) From the two-phase sonic modulus theory: (*a*) The measured sonic modulus varies with the crystallinity and degree of orientation of the sample. (*b*) The amorphous orientation function and the intrinsic lateral modulus of the crystalline and amorphous regions can be determined from combined sonic modulus, density, and x-ray diffraction measurements. (*c*) The intrinsic birefringence of the crystalline and amorphous regions can be determined experimentally by coupling the results of (*b*) with birefringence measurements. (*d*) The crystalline and amorphous orientation functions can be determined quickly and quantitatively by combined sonic modulus, density, and birefringence measurements. (*e*) The principal polarizability per monomer unit can be obtained from measurements on polymer film. The value obtained from polypropylene films agrees with the value reported from dilute solution measurements.

(*2*) From the combined infrared and x-ray diffraction theories: (*a*) The infrared transition moment angle of a "crystal only" absorbing frequency can be determined quantitatively from a combination of x-ray diffraction and infrared dichroism measurements. (*b*) The crystal orientation function of a uniaxially oriented polymer can be determined quantitatively directly from infrared dichroism measurements. (*c*) The transition moment angle for the 1220 cm.$^{-1}$ band is 72° in isotactic polypropylene. (*d*) The transition moment angle for the 730 cm.$^{-1}$ band is 83° in polyethylene.

(*3*) From the small-angle light-scattering approach: The small-angle light-scattering technique can be used to describe quantitatively the deformation of spherulites in a uniaxially deformed film.

(*4*) Other combinations of the seven techniques could have been used to confirm these findings.

When isotactic polypropylene films are elongated uniaxially at 110°C., many measurable changes occur at the submicroscopic level. The spherulites are deformed from a spherulitic to a fibrillar character while the crystalline and amorphous regions orient to relieve the imposed stress. The final oriented film is a consequence of these submicroscopic mechanisms. The following conclusions can be made about the morphological characteristics of the uniaxially oriented films studied: (*1*) the cast film contained spherulites 2μ in diameter; (*2*) the spherulites deformed affinely with the sample; (*3*) some *a*-axis orientation was present in the films; (*4*) the amount of *a*-axis orientation increases with draw temperature and decreases with extension; (*5*) The chain axis of the crystals tend to align themselves in the stretch direction as the sample is deformed; (*6*) The amorphous chains are oriented perpendicular to the stretch direction at low elongations and orient toward the stretch direction as elongation continues.

APPENDIX I

Derivation of the Two-Phase Sonic Modulus Equations

For a single-phase system, both Ward[13] and Moseley[14] derived the following expression:

$$1/E = 1/\rho C^2 = (1 - \overline{\cos^2 \theta})/E_l^0 \tag{1}$$

where ρ is the density of the polymer, C is the sonic velocity, E is the measured sonic modulus (Young's modulus), E_l^0 is the intrinsic lateral modulus, and θ is the angle between the molecular chain axis and the direction of sound propagation.

For a homogeneous ideal mixture, both the density and bulk compressibility are additive properties. If isotactic polypropylene is considered an ideal mixture of amorphous and crystalline phases, then the mixing equation takes the form:

$$K = \beta K_c + (1 - \beta)K_{am} \tag{2}$$

where K is the bulk compressibility of the mixture, K_c is the bulk compressibility of the crystal regions, K_{am} is the bulk compressibility of the amorphous regions, β is the fraction of crystalline material, and $(1 - \beta)$ is the fraction of noncrystalline material. An equation of this form has been found to be valid for isotropic suspensions of solids in liquids[15] and for polyethylene over a range of crystallinities and temperatures.[16] The bulk compressibility K is related to the bulk modulus B, Young's modulus E, and Poisson's ratio ν, by the expression:[36]

$$K = 1/B = 3(1 - 2\nu)/E \tag{A-1}$$

Waterman[37] found that $\nu = 0.33$ for isotactic polypropylene at room temperature. For this specific case, then

$$K = 1/B = 1/E = 1/(\rho C^2) \tag{A-2}$$

Combining eqs. (1), (2), and (A-2) leads to the expression:

$$1/E_{or} = (\beta/E_{t,c}^0)(1 - \overline{\cos^2 \theta_c}) + [(1 - \beta)/E_{t,am}^0](1 - \overline{\cos^2 \theta_{am}}) \tag{A-3}$$

where the subscripts (c, am) stand for the crystalline and amorphous regions, respectively and E_{or} is the measured sonic modulus of the oriented sample.

For an unoriented sample $\overline{\cos^2 \theta} = {}^1/_3$, and eq. (A-3) reduces to:

$$3/2E_u = (\beta/E_{t,c}^0) + [(1 - \beta)/E_{t,am}^0] \tag{3}$$

where E_u is the measured sonic modulus of the unoriented sample. The orientation function f is defined by:[8,38]

$$f \equiv (3\,\overline{\cos^2 x} - 1)/2$$

where x represents the angle between the polymer chain axis and a specified reference direction in the sample. Applying this definition to each phase separately and substituting in eq. (A-3) gives:

$$3/2E_{or} = (\beta/E_{t,c}^0)(1 - f_c) + [(1 - \beta)/E_{t,am}^0](1 - f_{am}) \tag{A-4}$$

where f_c and f_{am} are defined orientation functions for the crystal and amorphous phases, respectively, and x is referred to the direction of sound propagation.

Combining eq. (A-4) with eq. (3) gives the following expression for the sonic modulus of oriented isotactic polypropylene at room temperature:

$$3/2(\Delta E^{-1}) = (\beta f_c/E_{t,c}^0) + [(1 - \beta)f_{am}/E_{t,am}^0] \tag{4}$$

where

$$(\Delta E^{-1}) = (E_u^{-1} - E_{or}^{-1})$$

APPENDIX II

Derivation of the Relation Between the Deformation and the Extension Ratio, λ_s, of a Spherulite

The unstretched spherulite has a volume $V_U = (\pi/6)d_0^3$, where d_0 is the diameter of the sphere.

The deformed spherulite is a prolate spheroid, $V_D = (\pi/6)d^2h$, where h is the length of the major axis and d the length of the minor axes. In the unstretched state, $V_U = V_D$, and therefore:

$$d_0^3 = d^2h$$

Now during extension $d_0 \rightarrow (\lambda_s d_0)$ in the stretch direction and therefore $\lambda_s d_0 = h$; here λ_s is the extension ratio of the spherulite; also $d_0 \rightarrow \lambda_s^{-1/2} d_0$

in the width (minor axis) direction for simple extension at constant volume, and obviously then $d = \lambda_s^{-1/2} d_0$.

To take our pictures, the film holder was placed at an arbitrary position for each picture, and hence the sample-to-film distances varied. For this reason a ratio of (h/d) was required to cancel out effects of sample-to-film variations. On substitution of the above expressions for h and d one obtains:

$$(h/d) = \lambda_s d_0 / d_0 \lambda_s^{-1/2} = \lambda_s^{3/2}$$

or the extension ratio of the spherulite:

$$\lambda_s = (h/d)^{2/3} \tag{10}$$

The author acknowledges the assistance of Mr. E. P. Moore, Jr. who prepared the films, Mr. J. A. Gailey who obtained the infrared data, Mrs. M. D. Chris and Mr. R. J. Gardecki who obtained the x-ray diffraction data, and Mr. C. E. Green who wrote the program for and ran the computer analysis of the x-ray diffraction data.

References

1. Stein, R. S., in *Newer Methods of Polymer Characterization*, B. Ke, Ed., Interscience, New York, 1964, Chap. 4.
2. Gailey, J., *Anal. Chem.*, **33**, 1831 (1961).
3. Ruland, W., *Acta Cryst.*, **14**, 1180 (1961).
4. Natta, G., *Nuovo Cimento (Suppl.)* [10], **15**, 40 (1960).
5. Keith, H. D., F. J. Padden, Jr., N. M. Walter, and H. W. Wyckoff, *J. Appl. Phys.*, **30**, 1485 (1959).
6. Gailey, J., and R. Ralston, *SPE Trans.*, **4**, 29 (1964).
7. Danusso, F., G. Moraglio, and G. Natta, *Ind. Plast. Modernes*, **10**, 40 (1958).
8. Hermans, J. J., P. H. Hermans, D. Vermaas, and A. Weidinger, *Rec. Trav. Chim.*, **65**, 427 (1946).
9. Wilchinsky, Z. W., *J. Appl. Phys.*, **31**, 1969 (1960).
10. Compostella, M., A. Coen, and F. Bertinotti, *Angew. Chem.*, **74**, 618 (19M2).
11. Stein, R. S., *J. Polymer Sci.*, **31**, 327 (1958).
12. Hoshino, S., J. Powers, D. G. LeGrand, H. Kawai, and R. S. Stein, *J. Polymer Sci.*, **58**, 185 (1962).
13. Ward, I. M., *Textile Res. J.*, **34**, 806 (1964).
14. Moseley, W. W., Jr., *J. Appl. Polymer Sci.*, **3**, 266 (1960).
15. Urick, R. J., *J. Appl. Phys.*, **18**, 983 (1947).
16. Waterman, H. A., *Kolloid-Z.*, **192**, 9 (1963).
17. Sakurada, I., T. Ito, K. Nakamae, *Kobunshi Kagaku*, **21**, 197 (1964).
18. Sakurada, I., T. Ito, and K. Nakamae, *J. Japan. Soc. Test. Mat.*, **11**, 683 (1962).
19. Horio, M., paper presented at Symposium at Polytechnic Institute of Brooklyn, Sept. 7, 1963.
20. Stein, R. S., and F. H. Norris, *J. Polymer Sci.*, **21**, 381 (1956).
21. Bunn, C. W., and R. de Daubeny, *Trans. Faraday Soc.*, **50**, 1173 (1954).
22. Keedy, D. A., J. Powers, and R. S. Stein, *J. Appl. Phys.*, **31**, 1911 (1960).
23. Stein, R. S., private communication.
24. Tsvetkov, V. N., in *Newer Methods of Polymer Characterization*, B. Ke., Ed., Interscience, New York, 1964, Chap. 14.
25. Fraser, R. D. B., in *Analytical Methods of Protein Chemistry*, Vol. 2, Alexander and Block, Eds., Pergamon Press, London, 1960, Chap. 9.
26. Wilchinsky, Z. W., *J. Appl. Phys.*, **30**, 792 (1959).
27. Krimm, S., *Fortschr. Hochpolymer.-Forsch.*, **2**, 51 (1960).

28. McDonald, M. P., and I. M. Ward, *Polymer*, **2**, 341 (1961).
29. Liang, C., in *Newer Methods of Polymer Characterization*, B. Ke., Ed., Interscience, New York, 1964, Chap. 2.
30. Miyazawa, T., and Y. Ideguchi, *Bull. Chem. Soc. Japan*, **36**, 1125 (1963).
31. Snyder, R. G., and J. H. Schachtschneider, *Spectrochim. Acta*, **20**, 853 (1964); *J. Polymer Sci.*, **C7**, 85 (1964).
32. Miyazawa, T., *J. Polymer Sci.*, **C7**, 59 (1964).
33. Wilchinsky, Z. W., *Polymer*, **5**, 271 (1964).
34. Stein, R. S., M. B. Rhodes, P. R. Wilson, and S. N. Stidham, *Pure Appl. Chem.*, **4**, 219 (1962).
35. Powers, J., Ph.D. Thesis, Univ. of Mass., Amherst, Mass., 1961.
36. *Encyclopaedic Dictionary of Physics*, Vol. 2, J. Thewlis, ed., Pergamon Press, London, 1961, p. 21.
37. Waterman, H. A., *Kolloid-Z.*, **192** 1 (1963).
38. Samuels, R. J., *Norelco Reptr.*, **10**, 101 (1963).

Résumé

On a examiné la morphologie submicroscopique des films de polypropylène isotactique déformé uniaxialement, par des measures de diffraction aux rayons-X, de dichroisme infra-rouge, de biréfringence, du module mesuré par la vitesse du son, de diffusion lumineuse aux petits angles, de densité et par des techniques de microscopie électronique. Ainsi on a développé plusieurs nouvelles relations théoriques ainsi que plusieurs techniques. Ceci comprend: (*1*) une théorie du module à deux phases measuré par la vitesse du son, qui permet la détermination de la fonction d'orientation en phase amorphe et des modules intrinsèques du polymère mesurés par la vitesse du son; (*2*) une relation générale pour la détermination quantitative de l'angle du moment de transition à l'infra-rouge et pour la détermination quantitative de la fonction d'orientation des cristaux uniquement par des mesures de dichroisme infra-rouge; (*3*) la détermination du rapport d'extension des sphérulites par les diagrammes de diffusion lumineuse aux petits angles des films déformés; (*4*) une technique pour la détermination expérimental de la biréfringence intrinsèque des régions cristallines et amorphes du polypropylène isotactique; (*5*) une corrélation entre la différence de polarisabilité, déterminée par des measures en phase solide et celle déterminée par des mesures en solution; (*6*) d'autres techniques pour la détermination rapide des fonctions d'orientation. Faisant suite à ces développements, on donne des informations morphologiques au sujet des films déformés uniaxialement de polypropylène isotactique.

Zusammenfassung

Die submikroskopische Morphologie einaxial deformierter isotaktischer polypropylenfilme wurde durch Röntgenbeugung, Infrarotdichroismus, Doppelbrechung, Schallmodul, Kleinwinkel-Lichtstreuung, Dichte und elektronenmikroskopische Verfahren untersucht. Neue theoretische Beziehungen und Verfahren wurden entwickelt. Dazu gehören (*1*) eine Zweiphasen-Schallmodultheorie, welche die Bestimmung der amorphen Orientierungsfunktion und des spezifischen Schallmoduls des Polymeren ermöglicht, (*2*) eine allgemeine Beziehung zur quantitativen Bestimmung des Infrarot-Übergangsmomentwinkels und für die quantitative Bestimmung der Kristallorientierungsfunktion nur aus der Messung des Infrarotdichroismus, (*3*) die Bestimmung des Ausdehnungsverhältnisses der Sphärolithe aus dem Kleinwinkellichtstreuungsdiagramm deformierter Filme, (*4*) ein Verfahren zur experimentellen Bestimmung der Doppelbrechung der kristallinen und amorphen Bereiche von kristallinem und isotaktischem Polypropylen, (*5*) Korrelation zwieshen aus Messungen im festen Zustand bestimmten Polarisierbarkeitsunterschieden und denjenigen aus Lösungsmessungen und (*6*) andere Verfahren zur raschen Bestimmung von Orientierungsfunktionen. Die durch diese Enwicklungen erhaltenen morphologischen Informationen über den einaxial deformierten isotaktischen Polypropylenfilm werden mitgeteilt.

Received October 13, 1964
Revised November 25, 1964
(Prod. No. 4582A)

JOURNAL OF POLYMER SCIENCE: PART A VOL. 3, PP. 1765–1773 (1965)

Etude de la Polymérisation des Oléfines Catalysée par les Oxydes Métalliques. II. Influence des Impuretés sur la Cinétique de Polymérisation du Propylène par le Système Catalytique Phillips

ALAIN GUYOT, JEAN-CLAUDE DANIEL, MARC DURRIEU, *C.N.R.S. Institut de Recherches sur la Catalyse, Lyon-Villeurbanne, France, et* MARIUS PTACK, *Laboratoire de Biophysique, Muséum d'Histoire Naturelle, Paris, France*

Synopsis

A study was made of the influence of oxygenated impurities probably present in propylene on the polymerization kinetics and on the paramagnetic properties of the Phillips catalysts which contain about 2.5% chromium. Only a fraction of chromium atoms are active centers, which could be the pentavalent atoms.

Dans toutes les polymérisations, il est toujours nécessaire de'apporter un soin particulier à la purification des monomères et solvants, car ils peuvent contenir des impuretés en quantités faibles mais suffisantes pour inhiber l'action des catalyseurs employés. Toutefois, lorsque la purification n'est pas parfaite, une partie du catalyseur sert souvent à détruire les dernières traces: ceci est particulièrement vrai dans le cas des systèmes Ziegler-Natta; alors les centres catalytiques sont portés par le composé du métal de transition et une très faible quantité de cocatalyseur organométallique est suffisante pour activer ces centres; mais on utilise toujours un large excès de cocatalyseur et celui-ci est partiellement consommé par des réactions qui éliminent les dernières traces d'impuretés. En revanche, dans les polymérisations d'oléfines catalysées par les systèmes catalytiques Phillips, oxyde de chrome déposé sur gel de silice–alumine, aucun constituant ne joue normalement ce rôle protecteur, de sorte que les traitements de purification revêtent une importance critique; d'ailleurs, dans la pratique industrielle de ce procédé on tend de plus en plus à rajouter une certaine quantité de trialkyl-aluminium uniquement dans un but de purification ultime.

Il est déjà bien connu que l'oxygène, le gaz carbonique et l'eau sont des poisons des catalyseurs Phillips.[1] Boreskov et coll[2] ont déjà étudié l'influence de l'eau sur l'activité des catalyseurs: il est probable que l'un des effets du traitement d'activation des catalyseurs consiste à éliminer l'eau adsorbée ou même chimisorbée sur le support silicate d'aluminium.

Plus récemment Kazansky et Petcherskaya[3] ont montré que l'eau et l'oxygène modifiaient le signal EPR des catalyseurs, en élargissant le pic dû aux ions Cr^{5+}.

Avec du propylène et du propane commerciaux débrarrassés de ces impuretés, nous avons rencontré de sérieuses difficultés dans nos essais de polymérisation. Nous avons été amenés à effectuer un traitement de purification supplémentaire. L'analyse détaillée des réactifs avant et après traitement montre une légère modification du diagramme de spectrographie de masse correspondant à des produits dont la masse moléculaire est comprise entre 55 et 60. Nous présentons ici quelques résultats relatifs à l'étude cinétique des polymérisations en l'absence et en présence de quelques produits oxygènés probablement présents dans les réactifs. Nous étudions aussi l'effet de ces impuretés sur les spectres EPR des catalyseurs.

METHODES EXPERIMENTALES

Polymerisation

Les techniques de préparation des catalyseurs, l'appareillage de polymérisation et la méthode expérimentale d'étude cinétique ont été décrites dans la première partie de cette étude.[4] Le catalyseur utilisé ici contient 2,19% de chrome, dont le degré moyen d'oxydation est de 4,99 ± 0,01. Il est conditionné en ampoules scellées sous vide et utilisé sous cette forme.

Le propane et le propylène sont des produits purifiés commerciaux. Ils contiennent normalement un peu d'éthane et éventuellement des traces d'éthylène. Les résultats des essais de polymérisation dépendent cependant des bouteilles de gaz utilisées, à tel point que dans certains cas, le rendement en polymère est nul. Pour obtenir des résultats reproductibles, quelle que soit la provenance des réactifs, nous avons été amenés à leur faire subir un traitement supplémentaire de purification. Ce traitement consiste à faire circuler lentement les gaz au travers d'une colonne remplie de tamis moléculaire (Union Carbide type 5A) avant de les recueillir par piégeage dans des containers en acier inoxydable soigneusement séchés et vidés au préalable.

L'analyse chromatographique du propane et du propylène, avant et après ce traitement ne révèle aucune différence de composition. La spectrographie de masse montre que certaines impuretés oxygénées sont totalement ou partiellement éliminées. Leur masse moléculaire est comprise entre 55 et 60; leur proportion initiale varie entre 5/10.000 (propyléne) et 1/1.000 (propane). Ces impuretés peuvant être le sulfoxyde de carbone COS (60), l'alcool allylique (58) ou l'aldehyde propionique (58).

Des expériences de polymérisation ont été effectuées tout d'abord avec les réactifs purifiés, et ensuite avec ces mêmes réactifs mais en présence d'alcool allylique ou d'aldehyde propionique. Il suffit de quantités très faibles (50 mg) de ces composés oxygénés pour empoisonner totalement des quantités de l'ordre de quelques grammes de catalyseur. C'st pourquoi nous les avons utilisés en solutions diluées dans le cyclohexane. Celui-ci

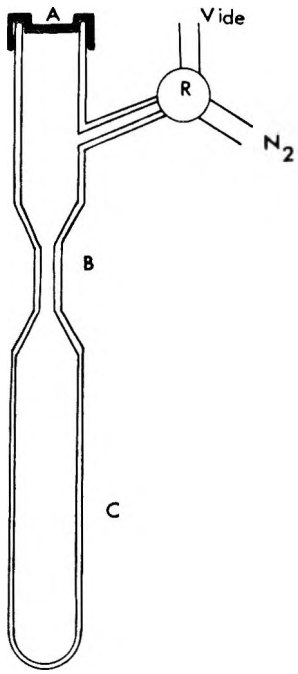

Fig. 1. Appareillage pour le remplissage d'ampoules avec une solution d'inhibiteur.

est pratiquement purifié par chauffage à reflux et distillation, successivement en présence de sodium métallique et de triethyl-aluminium. Il est placé dans un container tubulaire en verre serré entre des plaques métalliques par l'intermédiaire de joints toriques en Viton A; une des plaques est munie d'une vanne pour permetre le raccordement à l'appareil de distillation et la seconde plaque porte une rondelle de caoutchouc Viton A susceptible d'être traversée par une aiguille de seringue. Avant emploi, le container est chauffé à 180°C., monté évacué sous 10^{-3} mm de mercure, et pesé. Après introduction du cyclohexane on pèse à nouveau et au moyen d'une seringue hypodermique de précesion Hamilton, on introduit une quantité connue d'aldehyde ou d'alcool. Des volumes convenables de solution ainsi préparée sont transférés ensuite dans des ampoules en verre mince qui seront scellées puis placées dans l'autoclave de polymérisation en même temps que les ampoules de catalyseur. La figure 1 représente le dispositif de remplissage des ampoules. Cet appareillage en verre pyrex se compose de l'ampoule C soudée à une partie supérieure qui comporte une capsule de caoutchouc A et une tubulure latérale fermée par un robinet à trois voies R. L'appareil est tout d'abord purgé et évacué à chaud; la solution est introduite dans l'ampoule C au moyen d'une seringue hypodermique de précision dont l'aiguille traverse la capsule A. On scelle en B et l'ampoule C remplie est détachée. Il est ainsi possible d'introduire dans l'autoclave des quantités d'alcool ou d'aldehyde de l'ordre du milligramme.

Resonance Paramagnétique Électronique

Au moyen de l'appareil représenté sur la figure 2, le catalyseur est placé dans des ampoules en quartz et traité avec les composés oxygénés précédents. Une ampoule scellée, en verre fragile, contenant le catalyseur est placée dans un logement horizontal. Les robinets R_2 étant fermés, l'appareil est purgé et finalement rempli d'azote purifié au moyen du robinet R_1. La manoeuvre du marteau magnétique M permet de briser l'ampoule

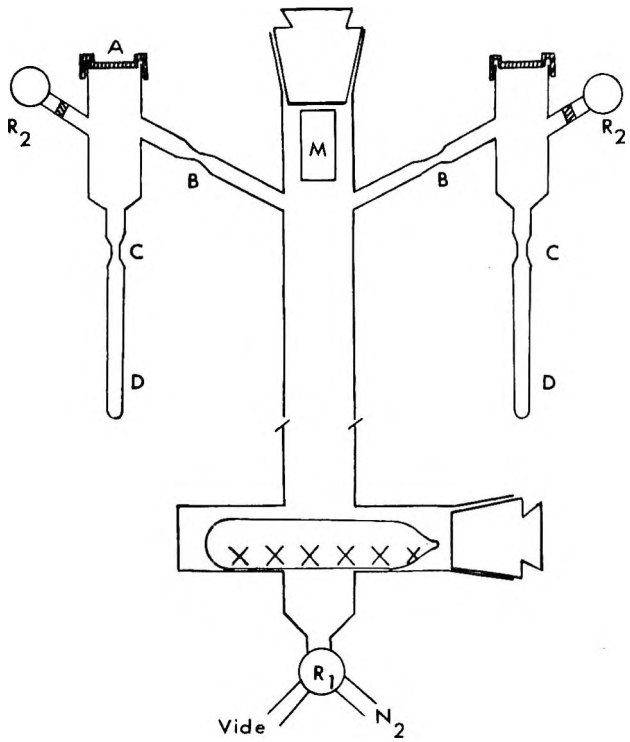

Fig. 2. Appareillage pour la manipulation et le traitement de catalyseur en vue de son étude par résonance électronique paramagnétique.

de catalyseur. Celui-ci est ensuite transféré et réparti dans les ampoules D en quartz par un courant d'azote arrivant par R_1 et ressortant après passage au traverse d'un verre fritté par les robinets R_2. Après avoir scellé en B, les ampoules D et les parties de l'appareillage qui les surmontent, sont détachées. Le réactif approprié est introduit par une seringue hypodermique au travers de la capsule A. Le catalyseur, initialementorangé prend rapidement une couleur verte dont la teinte dépend peu du réactif utilisé. Après un certain temps on fait le vide par R_2 de façon à éliminer le réactif qui n'est pas adsorbé. On scelle en C et l'ampoule D contenant le catalyseur teinté est placée dans la cavité d'un spectromètre Varian 4502-02.

RESULTATS ET DISCUSSION

Dans notre précédent article[4] nous avons montré que la réaction de polymérisation du propylène par le système catalytique oxyde de chrome-silicate d'aluminium admettait l'ordre 1 par rapport au monomère. On a donc, si M est la concentration en monomère:

$$-dM/dt = k_1 M$$

En portant ce facteur de proportionnalité k_1 en fonction du poids de catalyseur, nous avions obtenu la courbe *1* de la figure 3, qui présente une partie linéaire et se raccorde avec l'origine des coordonnées par un arc de courbe. Normalement en catalyse hétérogène l'activité catalytique est proportionnelle à la masse de catalyseur; nous avions attribué l'écart observé à l'action d'impuretés contenues dans les réactifs.

En opérant avec le même catalyseur, mais après purification des réactifs par passage sur tamis moléculaire, nous avons obtenu la courbe *2* de la figure 3, qui est une droite passant par l'origine et dont la pente est nettement supérieure à celle de la partie linéaire de la courbe *1*. Des effets analogues ont été observés avec des catalyseurs possédant des activités

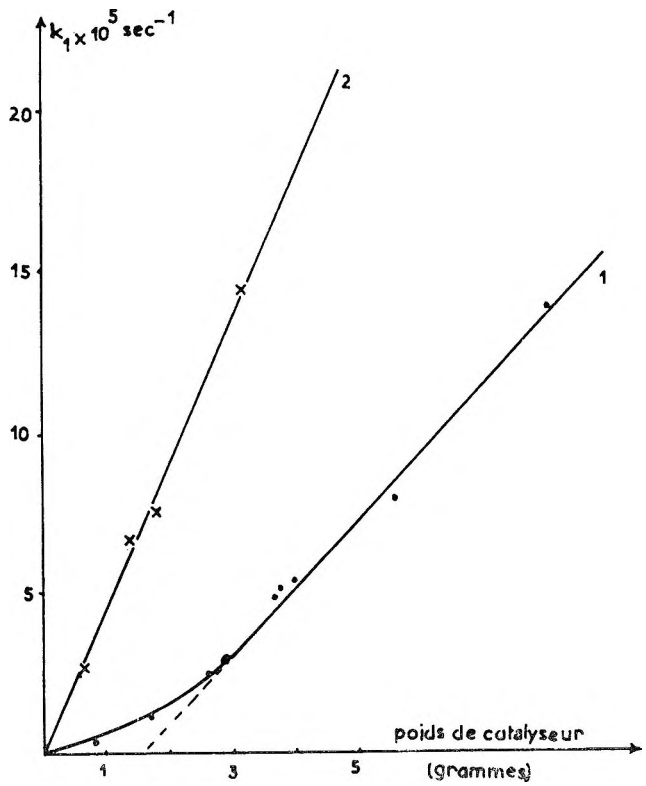

Fig. 3. Activité catalytique en fonction du poids de catalyseur: (*1*) réactifsnon purifiés; (*2*) réactifs purifiés.

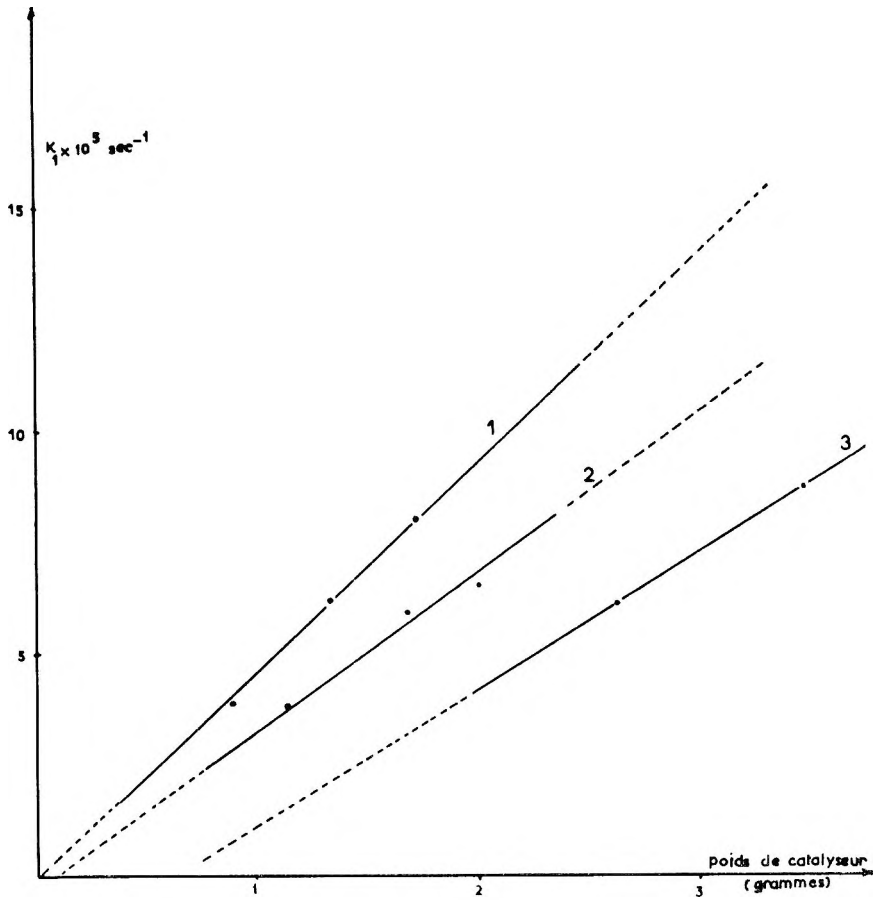

Fig. 4. Activité catalytique en fonction du poids de catalyseur: (*1*) sans inhibiteur; (*2*) en présence de 1 mg d'alcool allylique; (*3*) en présence de 3 mg d'alcool allylique.

différentes; l'écart de pente est d'autant plus important que le catalyseur est moins actif. Il est difficile de donner une interprétation quantitative de ces phénomènes. Le catalyseur possède un certain nombre de sites d'activités différentes: certains seulement sont actifs vis à vis de la polymérisation. Ils adsorbent irréversiblement et rapidement les impuretés, mais celles-ci peuvent aussi s'adsorber sur d'autres sites. Il y a de plus compétition entre le monomère et les impuretés pour l'occupation des sites actifs, de sorte que même lorsque ceux-ci sont en petit nombre (faibles quantités de catalyseur) la polymérisation peut avoir lieu en présence d'impuretés. Les adsorptions initiales de monomère et d'impuretés doivent être pratiquement instantanées puisque dans tous les cas, la réaction admet l'ordre 1 par rapport au monomère tout au long de l'expérience.

Nous avons observé que des quantités d'alcool allylique ou d'aldehyde propionique de l'ordre de 3 mg étaient largement suffisantes pour inhiber totalement l'activité d'un gramme de catalyseur. Ceci implique, en admet-

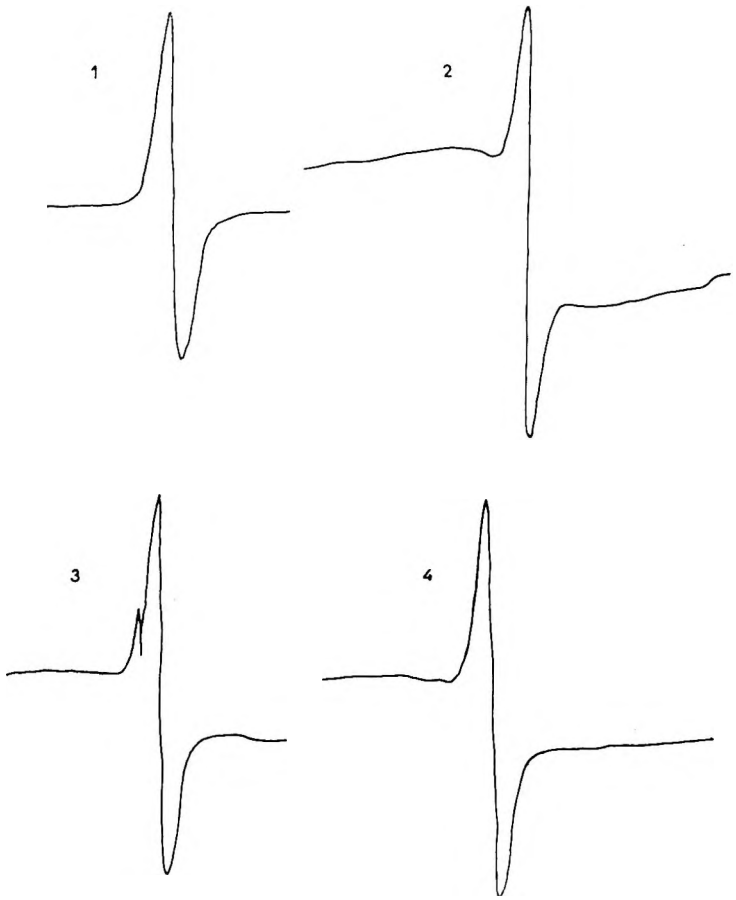

Fig. 5. Signaux de résonance paramagnétique électronique: (*1*) catalyseur non traité; (*2*) catalyseur traité par l'aldehyde propionique; (*3*) catalyseur traité par 44 mg d'alcool allylique; (*4*) catalyseur traité par 78 mg d'alcool allylique.

tant qu'une molécule d'impureté peut empoisonner un site actif, que le nombre des sites actifs par gramme de catalyseur est inférieur à 3×10^{19}. Les catalyseurs utilisés contiennent environ 2,5% de chrome, soit 3×10^{20} atomes de chrome par gramme. Si l'on admet que les sites de polymérisation impliquent essentiellement les atoms de chrome, alors la proportion de ces atomes effectivement utilisés est inférieure à 10%, et peut-être moindre encore, dans la mesure où les impuretés peuvent être adsorbées sur des sites superficiels inactifs.

Ces résultats sont confirmés par une nouvelle série d'expériences au cours desquelles nous avons introduit dans l'autoclave des quantités déterminées d'alcool allylique en solution dans le cyclohexane. Sur la figure 4, nous avons porté les facteurs de proportionnalité observés en fonction des poids de catalyseur. En l'absence d'additif, ou en présence de cyclohexane pur, les points expérimentaux se placent sur la droite *1* qui passe par l'origine.

Les droites *2* et *3* correspondent à des expériences effectuées en présence de solutions contenant respectivement 1 et 3 mg d'alcool allylique. L'effet inhibiteur de ce produit se traduit par des modifications de la pente et de l'abcisse à l'origine. En extrapolant les résultats pour des quantités plus importantes d'impuretés, on peut estimer que 1 mg d'impuretés détruit les centres actifs portés par 1–1,5 g de catalyseur. On peut conclure de nouveau que la proportion des atomes de chrome qui constituent ces centres actifs est inférieure à 10%.

Cette conclusion pourrait être en accord avec l'hypothèse suggérée d'abord par Cossee et van Reijen[5] et reprise plus explicitement par Bukanaeva, Petcherskaya, Kazansky et Dzis'ko,[6] selon laquelle l'activité catalytique est due à des ions Cr^{5+} qui ne représentent que 3–4%[6] du chrome total. Kazansky et Petcherskaya[3] ont déjà montré que l'oxygène et l'eau modifiant le signal de résonance paramagnétique électronique caractéristique des ions Cr^{+5}; l'intensité du signal n'est pas changée mais le pic est sensiblement élargi lorsque le catalyseur est traité par l'oxygène ou l'eau. Ceci implique que l'electron libre du Cr^{+5} entre dans une liaison de coordination avec le molécule inhibitrice. Nous avons effectué des expériences analogues avec l'alcool allylique et l'aldehyde propionique. Les spectres observés sont représentés sur la figure 5. Les courbes *1*, *2*, *3*, et *4* correspondent respectivement au catalyseur non traité, traité par l'aldehyde propionique et traité avec deux quantités différentes (44 et 77 mg) d'alcool allylique. La modification des spectres est évidente, mais porte à la fois sur le signal étroit du Cr^{5+}, dont la dissymétrie est augmentée, et sur le signal large qui devient très important; ce dernier phénomène traduit simplement la réduction du chrome de la valence VI à la valence III.

Nos expériences montrent donc que les centres actifs sont en nombre relativement restreint; ils ne représentent qu'une faible proportion des atomes de chrome, qui pourrait effectivement correspondre à celle du chrome pentavalent.

Ces observations sont limitées aux catalyseurs contenant 2,5% de chrome environ, de même que la proportion d'atomes de chrome pentavalent indiquée par les auteurs russes. Lorsque la teneur en chrome est inférieure, la proportion active est probablement plus forte; en effet, des études magnétochimiques effectuées sur des catalyseurs analogues, ont montré que l'oxyde de chrome n'était pas réparti sur le support de façon uniforme;[7] au contraire, il serait plutôt réparti en "paquets" dont les dimensions augmentent avec la teneur en chrome du catalyseur. La proportion des atomes de chrome superficiels est donc fonction de la teneur en chrome et il en est évidemment de même de la proportion des atomes actifs. Tout récemment d'ailleurs, Clark, Finch et Ashe,[8] en étudiant l'adsorption de l'éthylène à basse température sur des catalyseurs à faible teneur en chrome, ont pu calculer un nombre maximum de sites actifs. Ces nombres représentent des proportions d'atomes de chrome actifs respectivement égales à 78 et 57% pour des teneurs en chrome de 0,1 et 0,25%.

References

1. Phillips Pétroléum Co., Brevet Belge 530,617 (1954).
2. Boreskov, G. K., V. A. Dzis'ko, et T. Y. Tiulikova, *Dokl. Akad. Nauk SSSR*, **136**, 125 (1961).
3. Kazansky, V. B., et Yu. N. Petcherskaya, *Kinetika i Kataliz*, **4**, 244 (1963).
4. Guyot, A., et J. C. Daniel, *J. Polymer Sci.*, **A1**, 2989 (1963).
5. Cossee, P., et L. L. van Reijen, *Actes IIe Congrès International de Catalyse*, Ed. Technip, Paris, 1960, p. 1679.
6. Bukanaeva, F. M., Yu. N. Petcherskaya, V. B. Kazansky, et V. A. Dzis'ko, *Kinetika i Kataliz*, **3**, 358 (1962).
7. Mihail, R., P. Cortoleanu et A. G. Ionesco, *J. Chim. Phys.*, **56**, 568 (1959).
8. Clark, A., J. N. Finch et B. H. Ashe, *Proceedings of the Third International Congress of Catalysis, Amsterdam*, **1964**, Preprint I66.

Résumé

Cette étude porte sur l'influence d'impuretés oxygénées, probablement présentés dans le propylène, sur la cinétique de polymérisation, et sur les propriétés paramagnétiques des catalyseurs Phillips, contenant environ 2,5% de chrome. Une fraction seulement des atomes de chrome constituent les centres actifs, qui pourraient correspondre aux atomes de chrome pentavalent.

Zusamenfassung

Wir beschreiben den Einfluss der im Propylen wahrscheinlich vorhandeners sauerstoffhaltigen Verunreinigungen, auf die Kinetik der Polymerisation und die paramagnetischen Eigenschaften der Phillips Katalysatoren mit einem Gehalt von ungefäkr 2,5% in Chromium. Nur eine Fraktion der Cr Atome bilden die aktiven Plätze, die Cr^{5+} Atome sein mögen.

Received August 7, 1964
Revised December 11, 1964
(Prod. No. 4589A)

JOURNAL OF POLYMER SCIENCE: PART A VOL. 3, PP. 1775–1784 (1965)

A Study on a Three-Component Polymer Formation

A. RAVVE, J. T. KHAMIS, and L. X. MALLAVARAPU,
Corporate R&D Laboratories, Continental Can Company, Chicago, Illinois

Synopsis

Solution terpolymerization studies, with addition of a mixture of monomers and initiator at a constant rate to the solvent, are reported. The monomers represented are styrene, 2-ethylhexyl acrylate, and glycidyl acrylate, with polymerization initiated either by di-*tert*-butyl peroxide or dicumyl peroxide. Data are presented regarding polymer composition with respect to the three monomers, rates of conversion to polymer, and effect of changes in monomer and initiator composition. Also included are results of polymer fractionation studies utilizing molecular weight determination of the fractions by high-speed membrane osmometry. The steady-state equation, which is commonly used in the kinetic treatment of solution or bulk polymerizations carried to low conversions, was applied to this continuous feed system even up to high conversions. Furthermore, with the proper choice of initiator, narrower molecular weight distributions were obtained.

INTRODUCTION

Copolymerization of binary systems via free radical initiation has been investigated quite thoroughly. Ternary systems, on the other hand, have received less attention. The theoretical basis for the relationships between monomers in terpolymer formation were expressed by Alfrey and Goldfinger.[1] A general study of terpolymers from relationships in copolymerization azeotropic data was conducted by Slocombe.[2] Recently, a more simplified relationship was developed by Ham.[3]

In this work, a three-component system consisting of styrene, 2-ethylhexyl acrylate, and glycidyl acrylate was studied experimentally with respect to composition of terpolymers formed, molecular weight distributions, and rates of conversion.

RESULTS AND DISCUSSION

Reactivity ratios for this three-component system, determined by Khamis,[4] are: styrene, $r_{12} = 0.91$, $r_{13} = 0.73$; 2-ethylhexyl acrylate, $r_{21} = 0.29$, $r_{23} = 0.98$; glycidyl acrylate, $r_{31} = 0.25$, $r_{32} = 1.08$.

By setting the level of each of the three monomers at 0.3 moles and substituting the r values into the Alfrey-Goldfinger equation,[1] we find that the ratio of styrene/ethylhexyl acrylate is 2.98/1.31 and that the ratio of styrene/glycidyl acrylate equals 2.98/1.17.

From these values one can determine the composition of the initial terpolymer to be as follows:

$$\left[\text{(Styrene)}_{0.365}\text{—(Ethylhexyl acrylate)}_{0.18}\text{—(Glycidyl acrylate)}_{0.161}\right]_n$$

The actual composition of the initial terpolymer was determined experimentally by carrying out a polymerization on a ternary mixture of the monomers comprising 0.3 mole each. This was conducted in the usual manner by initiating with a peroxide initiator and then quenching the reaction with methanol upon reaching 1–2% conversion. The product, polymer I, was analyzed and found to contain 2.81% oxirane oxygen and 15.31% total oxygen. From this the actual composition of the initial terpolymer turned out to be:

$$\left[\text{(Styrene)}_{0.365}\text{—(Ethylhexyl acrylate)}_{0.18}\text{—(Glycidyl acrylate)}_{0.175}\right]^n$$

This is in fair agreement with the composition calculated from the Alfrey-Goldfinger equation.[1] Whether the small differences can be ascribed to the penultimate effect[3] is not certain. According to Ham,[3] in the cases of "purest" growing chains, close agreement will be found for the expression:

$$r_{13}r_{21}r_{32} = r_{12}r_{31}r_{23}$$

By substituting the r values we find:

$$(0.73)(0.29)(1.08) = (0.91)(0.25)(0.98)$$

or

$$0.229 = 0.223$$

Generally, a solution polymerization conducted by a free radical mechanism can be carried out in two ways. One way is to place all three, solvent, initiator, and monomer(s) into the reactor at once and then apply heat. In such a system the concentration of the initiator in the early stages of the reaction only changes a few per cent. As a result, the polymerization can be assumed to have a steady-state character and various dependencies can be investigated quantitatively. At higher temperatures, the square root dependence of rates upon initiator concentration has to be modified, and new kinetic relationship must be written for the nonstationary state which corresponds to a high rate of initiator decomposition. A differential equation for such a relationship was written by Burnett:[5]

$$-d[\mathrm{M}]/dt = k_p(k_i[\mathrm{I}_0]/k_t)^{1/2}[\mathrm{M}] \tan \{(k_ik_t[\mathrm{I}_0])^{1/2}t\}$$

and studied by Magat,[6] who showed it to be applicable to polymerizations in precipitating media.

The second type of free radical-initiated solution polymerization reaction is conducted by feeding either the monomer or the initiator or both continuously into the reaction mixture during the course of the reaction. The above described nonstationary state would apply to such polymerization

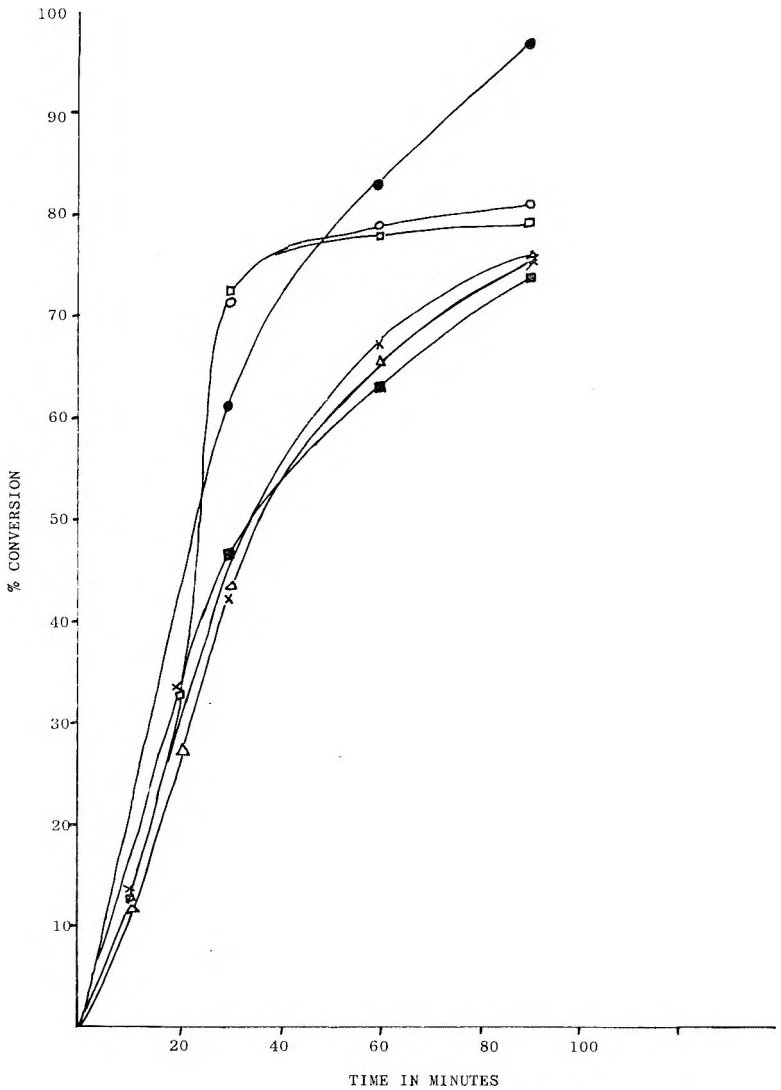

Fig. 1. Per cent conversion versus time in minutes for: (○) polymer II; (□) polymer III (△) polymer IV; (×) polymer V; (●) 2-Ethylhexyl acrylate; (■) styrene.

conditions when the initiator is being decomposed rapidly. Such conditions, at elevated temperatures were studied by Coupek, Kolinsky, and Lim,[7] where the initiator was fed at a constant rate into the reaction mixture at temperatures high enough for rapid consumption. Hoffmann, Schreiber, and Rosen[8] have shown that by conducting the reaction in a system of continuous feed polymerization, where either the monomer or the initiator is added at constant rate to the polymerization solution, narrow molecular weight distributions result for many monomers, provided the molecular weights do not exceed 100,000 and the conversions are kept below 50%.

This study was limited to a continuous feed process, but the additions of both initiator and monomers were carried out simultaneously as one mixture. Such polymerization procedures were described for homopolymers by Riddle.[9] All additions were carried out by us over a 1.5-hr. period at constant rate. The solvent used in these polymerizations was xylene, due to its relatively low chain transferring properties. The quantity of xylene in all reactions comprised 25% of the final mixture. The temperature used throughout was 138°C., controlled to ±2°C.

The initiator content of all polymerizations was kept at 2% based on weight of the monomer mixture, two different initiators being used: (*1*) dicumyl peroxide, with the half life of 0.7 hr. at 138°C.[10] and (*2*) *tert*-butyl peroxide, with a half life of 3 hr. at 138°C.[10]

Polymer II was formed from an equimolar mixture (0.3 mole each) of the three monomers and initiated with dicumyl peroxide. During the preparation, three aliquots were withdrawn from the reaction mixture at 0.5, 1.0, and 1.5 hr. interval and analyzed for total oxygen and oxirane oxygen of the polymer. The results shown in Table I allowed us to calculate the average composition of these terpolymers as the reaction was proceeding. From the aliquots were also determined the rates of conversion under these conditions. These are shown in Table II and Figure 1, together with the data for the remaining polymers prepared.

TABLE I
Composition of Polymer II Aliquots

Time, hr.	Oxirane oxygen, %	Total oxygen, %
0.5	3.32	16.68
1.0	3.22	18.18
1.5	3.22	18.08

Thus the compositions of the polymers in the aliquots from the preparation of polymer II are as follows:

First aliquot (0.5 hr.):

$$+\text{(Styrene)}_{0.334}\text{—(Ethylhexyl acrylate)}_{0.21}\text{—(Glycidyl acrylate)}_{0.21}+_n$$

Second aliquot (1.0 hr.):

$$+\text{(Styrene)}_{0.243}\text{—(Ethylhexyl acrylate)}_{0.226}\text{—(Glycidyl acrylate}_{0.20}+_n$$

Third aliquot (1.5 hr.):

$$+\text{(Styrene)}_{0.248}\text{—(Ethylhexyl acrylate)}_{0.262}\text{—(Glycidyl acrylate)}_{0.20}+_n$$

The differences in the compositions of the polymers in the first, second, and third aliquots are small, with the second and third aliquots being so close in composition that it could be assumed that these differences are only experimental errors.

Polymer III was then prepared from a similar equimolar mixture of monomers in the same manner as polymer II, but with *tert*-butyl peroxide as initiator.

Polymers IV and V were also prepared in the same manner, but with a 4.1:1.625:1 molar mixture of monomers. Dicumyl peroxide was used as the initiator in the preparation of polymer IV, while *tert*-butyl peroxide was used for the initiation in the preparation of polymer V. Again, aliquots were withdrawn at regular intervals and their polymer content determined in order to gain information on the rates of conversion.

As comparison, homopolymerization was then conducted on each monomer individually, again under the same conditions. Here *tert*-butyl peroxide was used as the initiator. Glycidyl acrylate homopolymer is insoluble in xylene, and, therefore, its polymerization was carried out in cyclohexanone, keeping other conditions the same. The conversion rates of the homopolymers are included in Table II, with the rest of the polymers.

TABLE II
Conversion Rates of the Polymers Prepared

	Conversion, %				
	10 min.	20 min.	30 min.	60 min.	90 min.
Ethylhexyl acrylate			61.0	83.0	97.0
Styrene			46.5	63.0	74.0
Glycidyl acrylate			—	—	93.0
Polymer II			71.6	79.0	81.3
Polymer III	12.7	32.2	72.2	77.5	79.3
Polymer IV	11.7	27.3	43.5	65.5	76.0
Polymer V	12.7	32.6	42.0	67.0	75.4

From Table II it appears that the rate is not dependent upon initiator efficiency, but is influenced by the reactivity of the individual monomers. Specifically, both polymers II and III were prepared from equimolar mixtures of the three monomers. On the other hand, polymers IV and V were prepared from a mixture of monomers in which styrene was the major component, actually comprising half the weight of the monomers, whereas 2-ethylhexyl acrylate was present in much lower concentration. As a result, mixtures giving rise to polymers II and III polymerized much like 2-ethylhexyl acrylate, and mixtures IV and V behaved essentially like styrene. There also appears to be a suggestion of autocatalytic acceleration, as seen from Figure 1, occurring somewhere between the periods of 10 and 30 min. In addition, there can be seen, of course, the manifestation of the Trommsdorff-Norrish[11,12] effect occurring somewhere beyond this time period.

Polymers II, III, IV, and V were then fractionated by fractional precipitation technique and the number-average molecular weights determined on each fraction obtained as well as on the whole polymers. The results are presented in Table III. All the polymers used for the molecular weight dis-

tribution studies were from samples obtained after the addition of monomers was completed (1.5 hr.). For comparison, however, part of polymer V was further maintained at 138°C. with stirring under a nitrogen atmosphere for an additional hour, with the result that conversion appears to become quantitative. The molecular weight and the distribution were then determined on this material as well.

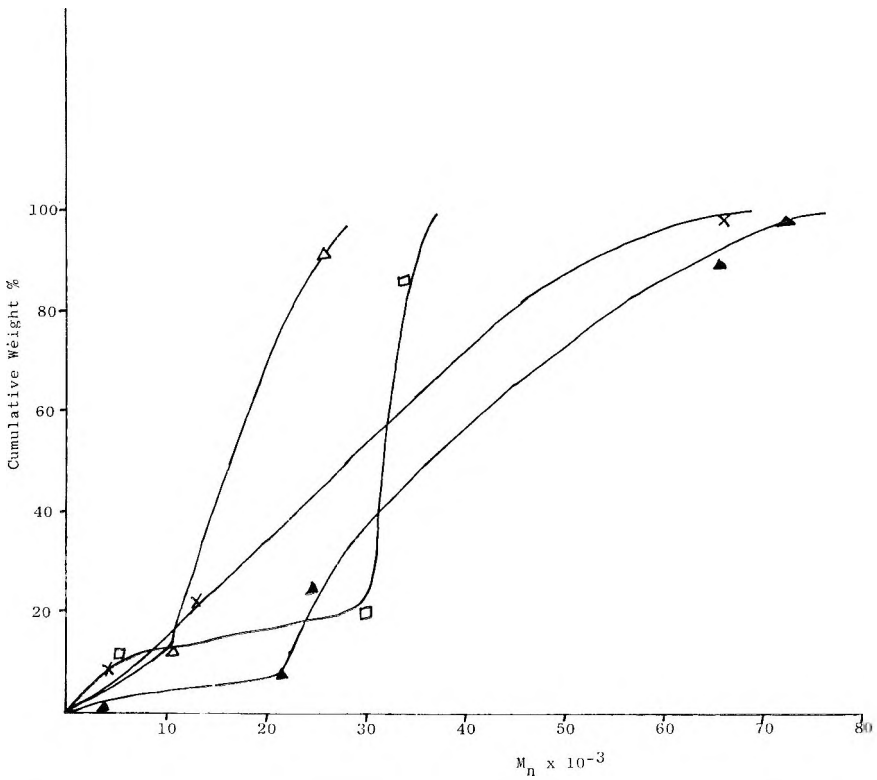

Fig. 2. Cumulative weight per cent versus number-average molecular weight for: (□) polymer III; (Δ) polymer IV; (×) polymer V before further heating; (▲) polymer V after further heating.

The cumulative molecular weight distributions are shown in Figure 2.

The data suggest that relatively narrow molecular weight distributions can be obtained with the more efficient initiator. The distribution of polymer II was too narrow to permit fractionation by the method used.

The data presented in Table II for polymers III, IV, and V were analyzed by use of the usual equation[13] for polymerization under steady-state conditions, viz.

$$-d[\mathrm{M}]/dt = k_p[\mathrm{M}][\mathrm{I}_0]^{1/2}$$

to determine whether meaningful results could be obtained. The results are presented in Table IV.

TABLE III
Molecular Weights of the Polymers and Their Fractions[a]

Fraction	Polymer II		Polymer III		Polymer IV		Polymer V[b]	
	%	$\bar{M}_n$	%	$\bar{M}_n$	%	$\bar{M}_n$	%	$\bar{M}_n$
Whole polymer	100.0	27,300	100.0	22,160	100.0	23,830	100.0	27,500
Fraction 1	100.0	27,300	66.0	34,230	79.0	25,970	78.0	66,000
Fraction 2	—	—	8.85	30,110	12.0	10,690	12.0	17,500
Fraction 3	—	—	11.3	5,920	—	—	8.9	3,000–5,000

[a] All molecular weights shown are believed to be determined within ±10%.
[b] Polymer V after further heating: 8.5%, $\bar{M}_n$ = 72,000; 64.5% $\bar{M}_n$ = 65,420; 17.85%, $\bar{M}_n$ = 24,700; 4.35%, $\bar{M}_n$ = 21,600; 3.2% $\bar{M}_n$ = 3420.

TABLE IV
Data in Table II Calculated by Using the Steady-State Equation[a]

Time t, min.	Polymer	$[M_0]$	$[M_t]$	[M]	[M] − [M]	$[I_0]^{1/2}$[b]	$k_p \times 10^3$[c]	$[M_t]/[I_0]$[b]
10	III	0.333	0.333	0.0423	0.0423	0.0771	2.74	556
	IV	0.3505	0.3505	0.0410	0.0410	0.0496	3.92	105
	V	0.3505	0.3505	0.0445	0.0445	0.1731	2.93	615
20	III	0.666	0.6243	0.1717	0.214	0.108	4.25	535
	IV	0.701	0.660	0.150	0.191	0.0729	5.20	100
	V	0.701	0.6565	0.1835	0.228	0.105	4.45	593
30	III	1.000	0.786	0.508	0.722	0.130	8.30	465
	IV	1.052	0.861	0.267	0.458	0.0802	6.45	87.3
	V	1.052	0.824	0.215	0.443	0.127	3.51	507
60	III	2.000	1.278	0.828	1.55	0.145	2.49	600
	IV	2.104	1.646	0.922	1.38	0.0897	3.47	83.5
	V	2.104	1.661	1.017	1.46	0.169	2.01	579
90	III	3.000	1.450	0.830	2.38	0.186	1.71	418
	IV	3.150	1.770	1.015	2.395	0.0921	3.44	60.0
	V	3.150	1.690	0.910	2.370	0.197	1.52	431

[a] Subscripts zero and t refer to total amounts added till time t, and present at time t, respectively, both for monomers (M) and initiator (I).
[b] Initiator concentration is corrected for amount depleted at time t.
[c] This is apparent k_p calculated for the mixture of monomers at time t.

From the calculations, the values obtained indicate that the apparent k_p does not vary by a magnitude of several hundred, as might be expected if the steady-state condition was not met.[13]

The steady-state equation is commonly used in bulk or solution polymerizations, provided the conversions are not too high, and the initiator concentration remains constant. In many "conventional" polymerizations, the initiator is used up at a much faster rate than the monomers; furthermore the conversion does not proceed beyond a limiting fraction at infinite time.[14]

From the data in Table IV, the monomer:initiator ratio throughout the entire addition period does not seem to vary to any great extent, and thus might not affect seriously the valid use of the steady-state equation. Further evidence pointing in this direction may be seen from Figure 2. Over a wide span of time, after an initial spurt, the number of moles of monomers converted per unit time is seen to be quite steady, which is to be expected unless a drastic change in the ratio of monomer/initiator concentration occurs. The linearity of the plot gives further meaning to the ratio $[M_t]/[I^0]$ in Table IV, strengthening the indication that the variations are within limits where steady state conditions exist. This condition, we believe, gives rise to a relatively narrow molecular weight distribution at the end of 90 min. as shown with polymers II and IV in Table III. Also, during the period of further heating after completion of addition of monomers, it is interesting to note that the molecular weight distribution of polymer V broadens; the system now behaves as a conventional polymerization system, and during the time it takes to go to complete conversion, approximately one quarter of the monomers are converted to polymer with different molecular weights.

Thus it appears to us that in spite of the fact that these reactions were conducted at elevated temperatures it may not be necessary to use the equation developed by Burnett,[5] when both initiator and monomer are added as a combined mixture This will be particularly true for less rigorous treatment of the kinetic data.

EXPERIMENTAL

Monomers

The monomers used were obtained from commercial sources and purified by distillation prior to use: styrene, n_D^{20} 1.5460; 2-Ethylhexyl acrylate, n_D^{20} 1.4349; glycidyl acrylate, n_D^{20} 1.4469.

Continuous Feed Polymerization Procedure

All continuous feed polymerization procedures were carried out in three-necked flasks, equipped with mechanical stirrers, reflux condensers, dropping funnel, nitrogen atmosphere, a thermowell for a thermocouple, and a heating mantle connected to an electronic controller. A 66-g. portion of xylene was placed into the flask and the temperature raised to 138°C.; 200 g. of monomer mixture containing 4 g. of initiator was then added dropwise at an even rate over a period of 1.5 hr. The reaction mixture was then cooled rapidly. Aliquots were removed from the flask at regular intervals with the aid of a pipet, 1–2 ml. being withdrawn at each time.

The aliquots were cooled, weighed, quenched with methanol and then solvent, and monomers removed by vacuum at 50–60°C.

Fractionation

Polymer fractionation was conducted by dissolving the polymer studied in methyl ethyl ketone to form a 10–15% solution. To this solution was then added petroleum ether until a light haze formed. The solution was then cooled for 24 hr. at −40°C. to precipitate the first fraction. The supernatant liquid was then carefully decanted and fraction I collected. To the liquid portion was then added sufficient amount of methanol to form again a light haze (at room temperature). This solution was again stored at −40°C. for 24 hr. to precipitate fraction II. The supernatant liquid was again decanted to collect the second fraction. If a new cloud developed, storage and cooling were repeated to obtain the subsequent fraction. Otherwise, the solvents were removed under vacuum in a rotatory evaporator to yield the final fraction.

Molecular weight determinations were carried out with a high-speed membrane osmometer with the use of S&S, UO very dense, gel cellophane membranes at 37°C.

Analysis for oxirane oxygen was carried out by titration with HBr in acetic acid.[15]

References

1. Alfrey, T., Jr., and G. Goldfinger, *J. Chem. Phys.*, **12**, 322 (1944).
2. Slocombe, R. J., *J. Polymer Sci.*, **26**, 9 (1957).
3. Ham, G. E., *J. Polymer Sci.*, **A2**, 2735 (1964).
4. Khamis, J. T., unpublished data.
5. Burnett, G. M., *Trans. Faraday Soc.*, **46**, 772 (1950).
6. Magat, M., *J. Polymer Sci.*, **16**, 491 (1955).
7. Coupek, J., M. Kolinsky, and D. Lim, *J. Polymer Sci.*, **C4**, 1261 (1964).
8. Hoffmann, R. F., S. Schreiber, and G. Rosen, *Ind. Eng. Chem.*, **56**, 51 (1964).
9. Riddle, E. H., *Monomeric Acrylic Esters*, Reinhold, New York, 1954.
10. Mapstone, G. E., *Chem. Proc.*, **26**, 347 (Dec. 16, 1963).
11. Norrish, R. G. W., and E. F. Brookman, *Proc. Roy. Soc. (London)*, **A171**, 147 (1939).
12. Trommsdorff, E., H. Kohle, and P. Lagally, *Makromol. Chem.*, **1**, 169 (1948).
13. Flory, P. J., *Principles of Polymer Chemistry*, Cornell Univ. Press, Ithaca, N. Y., 1953, Chap. 4.
14. Tobolsky, A. V., *J. Am. Chem. Soc.*, **80**, 5927 (1958).
15. Durbetaki, A. J., *Anal. Chem.*, **28**, 2000 (1956).

Résumé

On étudie la terpolymérisation en solution, en ajoutant à vitesse constante au solvant, un mélange de monomères et d'initiateurs. Les monomères sont le styrène, l'acrylate de 2-éthyl-hexyl et l'acrylate de glycidyle. La polymérisation est initiée soit par le peroxyde de di-*t*-butyle, soit par le peroxyde de dicumyle. On présente des résultats concernant la composition du polymère en fonction des trois monomères, concernant la vitesse de conversion en polymère et l'influence des variations dans la composition en monomère et en initiateur. On donne également les résultats du fractionnement du polymère, et on détermine le poids moléculaire des fractions par osomométrie à vitesse élevée. L'équation de stationnarité habituellement utilisée dans la cinétique des polymérisations en solution on en bloc à faibles taux de conversion, a été appliquée à ce système d'apport continu, même jusqu'à des taux de conversion élevés. De plus, en

employant l'initiateur approprié, on a obtenu des distributions plus étroites des poids moléculaires.

Zusammenfassung

Es wird über Lösungsterpolymerisationsuntersuchungen bei Zusatz der Monomer-Startermischung zum Lösungsmittel mit konstanter Geschwindigkeit berichtet. Als Monomere werden Styrol, 2-Äthylhexylacrylat und Glycidylacrylat bei Polymerisationsanregung entweder mit Di-*t*-butylperoxyd oder Dicumylperoxyd verwendet. Daten über die Polymerzusammensetzung aus den drei Monomeren, über die Umsatzgeschwindigkeit zum Polymeren und über den Einfluss einer Änderung der Monomer- und Starterzusammensetzung werden angegeben. Weiters wird über Ergebnisse der Polymerfraktionierung und Molekulargewichtsbestimmung an den Fraktionen durch Schnellmembranosomometrie berichtet. Die Beziehung für den stationären Zustand, die allgemein bei der kinetischen Behandlung von Polymerisationen in Lösung oder in Substanz bei neidrigem Umsatz verwendet wird, werden auf dieses kontinuierliche System sogar bis zu hohen Umsätzen angewendet. Bei geeigneter Wahl des Starters wurde eine engere Molekulargewichtsverteilung erhalten.

Received September 25, 1964
(Prod. No. 4559A)

JOURNAL OF POLYMER SCIENCE: PART A VOL. 3, PP. 1785–1792 (1965)

Dynamic Mechanical Properties of Poly(*n*-butyl Methacrylate) near Its Glass Transition Temperature

H. H. MEYER, P.-M. F. MANGIN, and JOHN D. FERRY, *Department of Chemistry, University of Wisconsin, Madison, Wisconsin*

Synopsis

The storage and loss shear compliances (J', J'') of poly(*n*-butyl methacrylate) (number-average molecular weight 320,000) were measured at frequencies between 0.08 and 1.0 cycle/sec. in the temperature range of 18–33°C., encompassing the glass transition. Data were obtained both at voluminal equilibrium and as a function of time during the slow isothermal contraction which follows a quench to a temperature near the transition. The latter data were supplemented by dilatometric measurements on similar samples to determine the magnitude of the volume contraction. Correlation of the dependences of J' and J'' on temperature and on elapsed time (at constant frequency) indicated that the relaxation mechanisms are controlled primarily by free volume. The method of reduced variables was successfully applied to the dependence of J' on temperature and elapsed time using shift factors $a_{T,t}$ calculated from the modified Doolittle equation and the magnitudes of volume contraction measured dilatometrically. The dependence of J'' on both temperature and elapsed time was more complicated, indicating a change in the shape of the retardation spectrum with free volume. The behavior is qualitatively very similar to that of poly(vinyl acetate), previously studied, except that the magnitudes of J' are considerably larger and the thermal expansion coefficient of the free volume is smaller.

I. INTRODUCTION

In a recent study of poly(vinyl acetate),[1] the dynamic viscoelastic properties in shear were measured in the glass transition temperature range as a function of temperature and time. By correlating the dependence on temperature after attainment of voluminal equilibrium with the isothermal time dependence during approach to equilibrium after quenching, it was concluded that the relaxation times are primarily governed by the free volume. In the present paper, similar but less extensive measurements are reported for poly(*n*-butyl methacrylate).

II. MATERIAL AND METHOD

The poly(*n*-butyl methacrylate) was generously furnished by Dr. John G. Brodnyan of the Rohm and Haas Company (sample PF 873). It had been polymerized in toluene solution to 28% conversion and precipitated with methanol, then reprecipitated from benzene solution with methanol

and dried *in vacuo* at 40°C. The number-average molecular weight was 320,000. Samples were molded and cut as described previously.[1]

The prism-shaped samples were mounted and installed in the torsion pendulum for measurements of the frequency and damping of free oscillations, from which the storage shear modulus and loss tangent were calculated. All procedures were the same as described for poly(vinyl acetate),[1] except that the samples were annealed at 40°C. instead of 45°C. before quenching to the temperature of measurement. Two types of experiments were made: (*1*) dynamic measurements at various temperatures and frequencies after attainment of voluminal equilibrium, achieved always in the torsion pendulum rather than in a separate thermostat, requiring as much as one week at the lowest temperature of 18°C.; (*2*) dynamic measurements repeated several times over a range of frequencies at constant temperature during approach to voluminal equilibrium while the sample was slowly contracting. The magnitude of the contraction was determined in parallel dilatometric experiments by use of methods described in detail elsewhere.[1,2] Precautions were taken for keeping the samples under negligible tensile stress during the torsion pendulum measurements, and corrections were made for small dimensional changes of the samples with temperature and time, as previously described.[1]

III. RESULTS AND DISCUSSION

Dilatometric Measurements

The results of the dilatometric measurements of isothermal contraction following quench from 40.0°C. are presented in Figure 1, where the relative difference between the volume v at an elapsed time t (in minutes) after the quench and the equilibrium volume v_∞ is plotted against log $(t - t_i)$; t_i, a rather arbitrary constant associated with the approach to thermal equi-

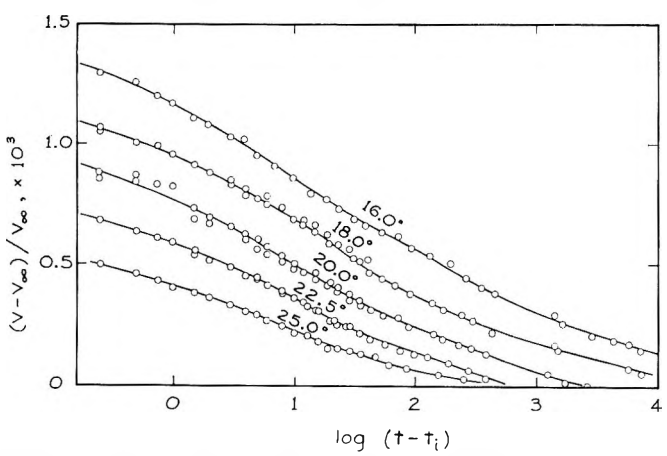

Fig. 1. Isothermal volume contraction of samples in dilatometer at temperatures indicated; t in minutes, with $t_i = 1$.

librium following Kovacs,[3] is taken as 1 min. As usual,[2,3] v_∞ was obtained directly at temperatures high enough so that voluminal equilibrium was reached within the experimental time scale, and at lower temperatures by a suitable extrapolation against T.

The negative slopes of these curves at $\log (t - t_i) = 2.0$ are given in Table I and will be used for derived calculations below. (Here and in subsequent calculations t is sufficiently long that t_i is negligible by comparison.) Similar measurements by Kovacs[4] on another sample of poly(n-butyl methacrylate) show essential agreement. The data of Figure 1 are used below for calculating the volume changes with time needed for interpretation of the time-dependent mechanical properties in shear.

TABLE I
Correlation Derivatives for Effects of Temperature and Elapsed Time

Temp., °C.	$-(\partial f/\partial \log t) \times 10^4$	$(\partial \log t/\partial T)_{J',\infty}$	$(\partial \log t/\partial T)_{J'',\infty}$	$(\partial \log t/\partial T)_f$
16.0	2.7	—	—	1.0
18.0	2.4	1.0	0.5	1.1
20.0	2.1	1.2	0.8	1.2
22.0	1.9[a]	2.9	1.5	1.4

[a] At 22.5°C.

Dynamic Shear Measurements at Voluminal Equilibrium

The storage shear modulus and loss tangent were determined after attainment of voluminal equilibrium at eight temperatures in the range of 18–33°C. in the frequency range from 0.08 to 1 cycle/sec., and from these were calculated the storage and loss compliances, J' and J''. The individual data are not reproduced here, but values of J' and J'' interpolated for three radian frequencies are plotted in Figure 2. The slopes of these curves will be used in calculating the correlation derivatives described below.

The individual data were reduced to a reference temperature of 27.0°C. by shift factors a_T calculated from the WLF equation,

$$\log a_T = -c_1(T - T_0)/(c_2 + T - T_0) \tag{1}$$

taking $c_1 = 17.0$, $c_2 = 96.6$, and $T_0 = 300.2$°K. These values are identical with those used by Child and Ferry[5] for another sample of poly(n-butyl methacrylate) (FF-2) in applying reduced variables to dynamic data at higher frequencies and at higher temperatures (44–135°C.). They correspond to a fractional free volume $f_{27} = 0.026$ and a thermal expansion coefficient of the free volume $\alpha_f = 2.6 \times 10^{-4}$ deg^{-1}. The data are plotted with reduced variables in Figure 3. A good composite curve is obtained for J', but the level of J'' drops with decreasing temperature, indicating a change in the shape of the retardation spectrum as was also apparent in the relaxation spectrum of poly(vinyl acetate).[1] Such a change could affect the shape of J' much less, escaping notice. The dashed lines in Figure 3

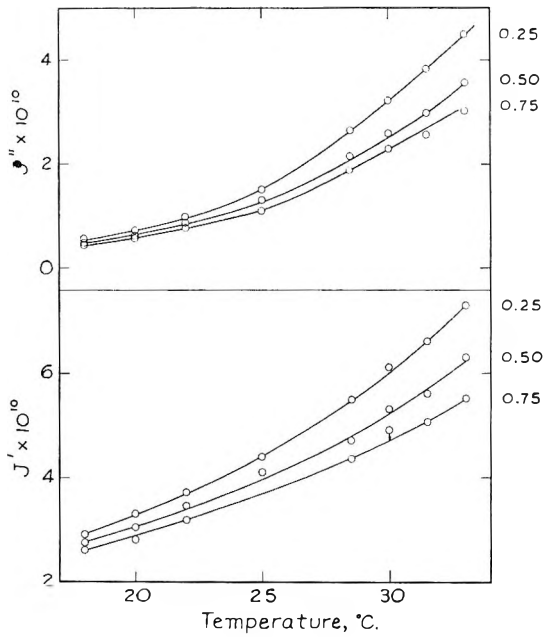

Fig. 2. Storage (J') and loss (J'') compliances, interpolated at three values of radian frequency indicated at right margin, plotted against temperature (at voluminal equilibrium).

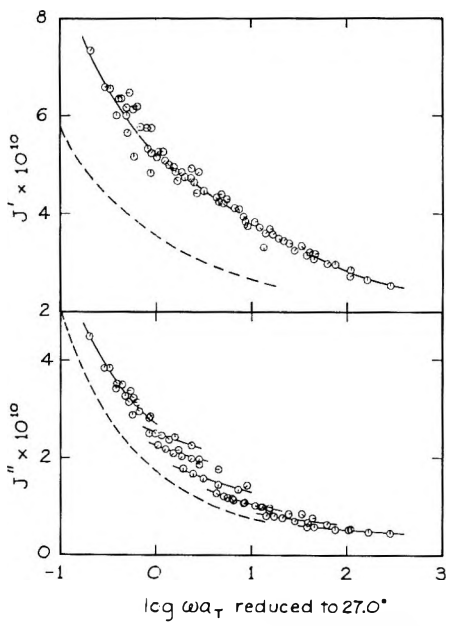

Fig. 3. Storage (J') and loss (J'') compliances reduced to 27°C. by shift factors calculated from eq. (1), (⊖) measurements at 18.0°C., successive 45° rotations clockwise correspond to 20.0, 22.0, 22.5, 25.0, 27.0, 28.5, 30.0, 31.5, and 33.0°C.; (- -) data reduced from transducer measurements at higher temperatures[5] on another sample of poly(*n*-butyl methacrylate).

represent the compliances of poly(n-butyl methacrylate) FF-2 similarly reduced from measurements in 1956 by use of the Fitzgerald transducer in the temperature range 50–60°C. and at frequencies of 60–250 cycles/sec. The differences may be partly due to a greater contribution from the β mechanism to J' at 27°C. than at 50°C., as would be expected from the earlier analysis of α and β contributions,[5] but if J' were dominated by the β mechanism it would not be expected to be reducible by the shift factors used in Figure 3 which are appropriate to the α mechanism. The recent work of Koppelmann[6] has cast doubt on the assumption of additivity of α and β contributions. In any case, the two sources of data are similar in magnitude and closely similar in shape.

Dynamic Shear Measurements During Isothermal Contraction

Measurements of the storage and loss compliance as functions of frequency at various elapsed times after quench from 40.0°C. to 16, 20, and

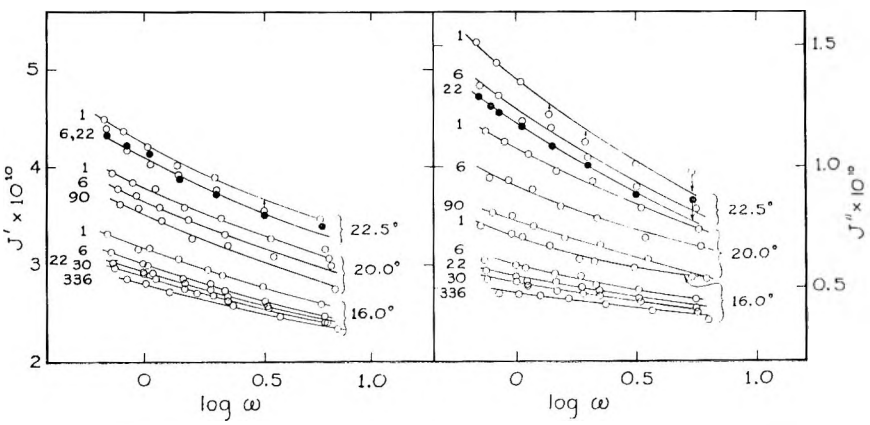

Fig. 4. Storage (J') and loss (J'') compliances plotted against frequency at various temperatures (indicated at right) and elapsed time in hours (indicated at left).

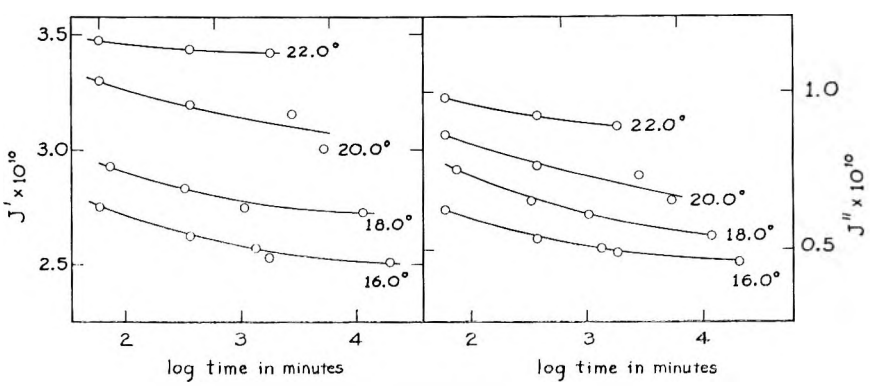

Fig. 5. Storage (J') and loss (J'') compliances at 0.5 radians/sec. plotted against elapsed time during isothermal contraction at temperatures indicated.

22.5°C. are plotted in Figure 4. This shows, at each temperature, the progressive shift with elapsed time toward lower frequencies, caused by the prolongation of relaxation times as the free volume gradually collapses.

By interpolating from Figure 4 at a frequency of 0.5 radians/sec. at 16 and 20°C. and adding some less extensive data obtained at 18 and 22°C., the change in J' and J'' with elapsed time can be represented at these temperatures of measurement as shown in Figure 5.

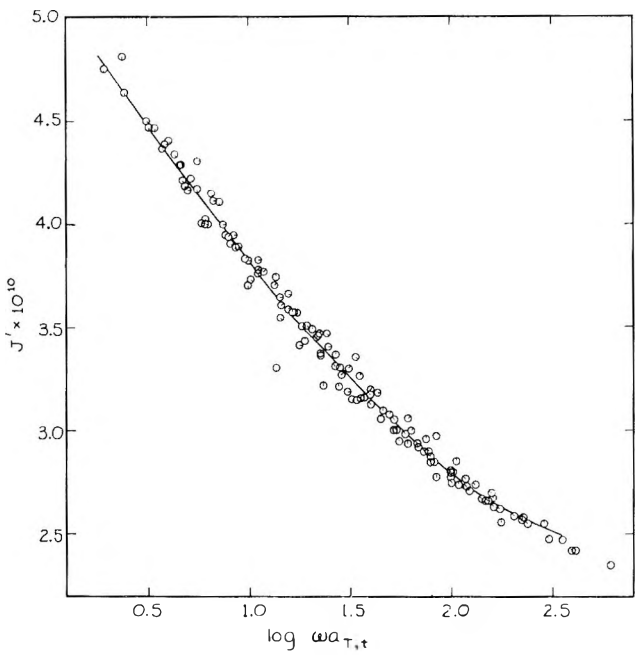

Fig. 6. Storage compliance from data of Fig. 5, reduced to 27°C. and voluminal equilibrium by shift factors $a_{T,t}$ calculated from free volume as described in text. Solid curve same as in Fig. 3; (⊖) measurements at 16.0°C.; successive 45° rotations clockwise correspond to 18.0, 20.0, 22.0, 22.5, and 25°C.

The slopes of the curves of Figures 1, 2, and 5 can be used to test the hypothesis that the temperature dependence of J' and J'' is due to changes in relaxation times which are controlled by free volume alone.[1] Thus, we define a correlation derivative

$$(\partial \log t/\partial T)_{J',\infty} = -(\partial J'/\partial T)_\infty/(\partial J'/\partial \log t)_T \qquad (2)$$

which compares the effects of temperature and elapsed time on J'. This relation is analogous to eq. (3) of ref. 1. The slope $(\partial J'/\partial T)_\infty$ is taken from Figure 2 at 0.5 radian/sec.; the slope $(\partial J'/\partial \log t)_T$ is taken from Figure 5 at several temperatures at $t = 100$ min. The resulting values of the derivative $(\partial \log t/\partial T)_{J',\infty}$ are given in Table I together with those for the corresponding derivative $(\partial \log t/\partial T)_{J'',\infty}$. If both temperature and

time effects are controlled by free volume, these derivatives should both be equal to

$$(\partial \log t/\partial T)_f = -(\partial f/\partial T)_{t=\infty}/(\partial f/\partial \log t)_T \quad (3)$$

Here the value of $\partial f/\partial T$ is taken as $\alpha_f = 2.6 \times 10^{-4}$ deg.$^{-1}$, and $(\partial f/\partial \log t)$ is taken as the slope of Figure 1 at an elapsed time of 100 min., assuming that only the free volume is collapsing during the isothermal contraction. The three correlation derivatives, compared in Table I, show fair agreement, indicating that the free volume dominates the relaxation rates.

The same conclusion is reached by reducing the data for J' in Figure 4 for both temperature and elapsed time, calculating the frequency shift factor $a_{T,t}$ from the modified Doolittle equation[1]

$$\log a_{T,t} = (1/2.303)(1/f_{T,t} - 1/f_{27,\infty}). \quad (4)$$

Here the fractional free volume $f_{27,\infty}$ is taken as 0.026 and $f_{T,t}$ is obtained as

$$f_{T,t} = f_{27,\infty} + \alpha_f(T - 300.2) + [(v_t - v_\infty)/v_\infty]_T \quad (5)$$

the last term being interpolated from Figure 1. Rather good superposition is obtained for all points at different temperatures and elapsed times, as shown in Figure 6. For J'', of course, no single composite curve is obtained.

It may be remarked that the highest values of G' obtained in these measurements (about 0.4×10^{10} dyne/cm.^{2}) are considerably smaller than those obtained for poly(vinyl acetate) (1.4×10^{10} dyne/cm.^{2}), reflecting the lower rigidity of poly(*n*-butyl methacrylate) in the glassy state, which in turn is undoubtedly associated with the presence of longer side groups. Thus the time-dependent phenomena described here are occurring in a somewhat softer matrix than in poly(vinyl acetate), yet the general features of the behavior are very similar.

This work was supported in part by the U. S. Army Research Office (Durham), and in part by the National Science Foundation. We are much indebted to Dr. A. Kovacs for valuable discussions, and to Miss Monona Rossol for help with the calculations.

References

1. Kovacs, A. J., R. A. Stratton, and J. D. Ferry, *J. Phys. Chem.*, **67**, 152 (1963).
2. Kovacs, A. J., *J. Polymer Sci.*, **30**, 131 (1958).
3. Kovacs, A. J., *Phenomènes de Relaxation et de Fluage en Rhéologie Non-Lineaire*, Editions du Centre National de la Recherche Scientifique, Paris, 1961, p. 191.
4. Kovacs, A. J., private communication.
5. Child, W. C., Jr., and J. D. Ferry, *J. Colloid Sci.*, **12**, 327 (1957).
6. Koppelmann, J., *Proceedings Second International Conference on Physics of Non-Crystalline Solids*, North Holland, Amsterdam, 1965, in press.

Résumé

La partie réelle et la partie imaginaire de l'inverse du module (J', J'') du polyméthacrylate de *n*-butyle (poids moléculaire moyen en nombre 320.000) ont été mesurées à des fréquences situées entre 0.08 et 1.0 cycle/sec dans un domaine de température allant de 18 à 33°C, aux environs de la transition vitreuse. On a obtenu des résultats à l'équilibre de volume et en fonction du temps pendant la contraction lente isothermique, qui

fait suite à un refroidissement jusqu'à une température située près de celle de transition. Les derniers résultats ont été complétés par des mesures dilatométriques sur des échantillons semblables en vue de déterminer l'importance de la contraction de volume. La corrélation de la dépendance de J' et J'' vis-à-vis de la température et le temps écoulé (à une fréquence constante) montrent que les mécanismes de relaxation sont contrôlés en premier lieu par le volume libre. La méthode des variables réduites a été appliquée avec succès à la dépendance de J' vis-à-vis de la température et du temps écoulé en utilisant les facteurs $a_{T,t}$ calculés à partir de l'équation modifiée de Doolittle et les grandeurs de la contraction de volume ont été mesurées par dilatométrie. La dépendance de J'' vis-à-vis de la température et du temps écoulé est plus compliquée, ce qui indique un changement dans le modèle du spectre avec le volume libre. Le comportement est qualitativement très semblable à celui de l'acétate de polyvinyle, étudié antérieurement, sauf que les grandeurs de J' sont considérablement plus grandes et que le coefficient d'expansion thermique du volume libre est plus petit.

Zusammenfassung

Real- und Imaginärteil der komplexen Nachgiebigkeit (J', J'') von Poly-*n*-butylmethacrylat (Zahlenmittel-Molekulargewicht 320.000) wurden bei Frequenzen zwischen 0,08 und 1,0 Hz im Temperaturbereich von 18 bis 33°C, was die Glasumwandlung einschliesst, gemessen. Ergebnisse wurden sowohl beim Volumsgleichgewicht als auch als Funktion der Zeit während der langsamen isothermen Kontraktion, welche auf eine Abschreckung auf eine Temperatur in der Nähe der Umwandlung folgt, erhalten. Diese Daten wurden durch dilatometrische Messungen an ähnlichen Proben zur Bestimmung der Grösse der Volumskontraktion ergänzt. Die Korrelation der Abhängigkeit von J' und J'' von der Temperatur und dem Zeitintervall (bei konstanter Frequenz) zeigte, dass der Relaxationsmechanismus primär durch das freie Volumen bestimmt wird. Die Methode der reduzierten Variablen wurde mit aus der modifizierten Doolittlegleichung und der dilatometrisch gemessenen Grösse der Volumskontraktion berechneten Verschiebungsfaktoren $a_{T,t}$ erfolgreich auf die Abhängigkeit von J' von der Temperatur und dem Zeitintervall angewendet. Die Abhängigkeit von J'' von Temperatur und Zeitintervall war komplizierter, was für eine Änderung der Gestalt des Verzögerungsspektrums mit dem freien Volumen spricht. Das Verhalten ist qualitativ demjenigen des früher untersuchten Polyvinylacetat sehr ähnlich, nur dass J' beträchtlich grösser und der thermische Expansionskoeffizient beträchtlich kleiner ist.

Received September 28, 1964
Revised November 16, 1964
(Prod. No. 4563A)

JOURNAL OF POLYMER SCIENCE: PART A VOL. 3, PP. 1793–1800 (1965)

Copolymerization of Allylureas with Lauryl Methacrylate

K. I. BEYNON and E. J. HAYWARD, *Shell Research Ltd., Thornton Research Centre, Chester, England*

Synopsis

Monomer reactivity ratios have been measured for the copolymerization of lauryl methacrylate and allylureas at 100°C., benzoyl peroxide being used as catalyst: lauryl methacrylate–monoallylurea, $r_1 = 29.9 \pm 1.2$, $r_2 = -0.22 \pm 0.06$; lauryl methacrylate–*N,N*-diallylurea, $r_1 = 27.4 \pm 0.8$, $r_2 = 0.014 \pm 0.05$; lauryl methacrylate–*N,N'*-diallylurea; $r_1 = 14.5 \pm 0.7$, $r_2 = -0.12 \pm 0.04$. The reactivity ratio r_1 is of lauryl methacrylate relative to the allylurea molecule as a whole and the monomer reactivity ratio r_2 is of the allylurea molecule relative to lauryl methacrylate. The values of the monomer reactivity ratios of lauryl methacrylate relative to a single allyl group in each of the allylureas have been calculated. It appears that the allyl groups in all of these molecules have similar reactivity for copolymerization with lauryl methacrylate. The monomer reactivity ratios provide evidence for cyclic propagation reactions in the copolymerization involving *N,N*-diallylurea.

INTRODUCTION

We have previously reported the copolymerization of lauryl methacrylate with phosphorus compounds containing one or two allyl groups.[1,2] These studies have now been extended to the copolymerization of lauryl methacrylate with monoallylurea (I), *N,N*-diallylurea (II), and *N,N'*-diallylurea (III).

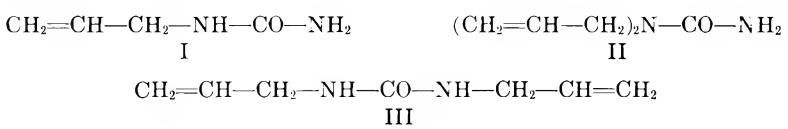

We have previously discussed[1] the form of the copolymer composition equation that should be used when one of the monomers (1) is monofunctional and the other monomer (2) is bifunctional, the two groups in monomer 2 being equivalent. The normal copolymer composition equation [eq. (1)] can be used for this system.

$$dm_1/dm_2 = M_1 (r_1M_1 + M_2)/M_2(r_2M_2 + M_1) \quad (1)$$

In eq. (1), m_1 and m_2 are the numbers of moles of the two monomers, 1 and 2, respectively, entering the polymer and M_1 and M_2 the moles of each of these monomers in the monomer mixture; r_1 is the monomer reactivity

ratio of monomer 1 relative to the molecule of 2 as a whole, and r_2 is the monomer reactivity ratio of the molecule of 2 as a whole relative to monomer 1. The equation can be used whether both functional groups in monomer 2 are involved in the polymerization or not.

The copolymer composition equation may be used in a different form [eq. (2)],

$$dm_1/dm_2 = M_1 (R_1M_1 + 2M_2)/2M_2(2R_2M_2 + M_1) \quad (2)$$

which is equally valid, but in which R_1 is the monomer reactivity ratio of monomer 1 relative to the single functional group in monomer 2 and R_2 is the monomer reactivity ratio of a single functional group of monomer 2 relative to monomer 1. If eq. (2) is used it is important that both of the functional groups in monomer 2 are involved in the propagation reaction. From eqs. (1) and (2) it is evident that eqs. (3) and (4) are valid for those systems in which both of the functional groups of monomer 2 are involved in the propagation reaction.

$$R_1 = 2r_1 \quad (3)$$

$$2R_2 = r_2 \quad (4)$$

In the present work the integrated form[6] of eq. (1) has been used to describe the copolymer composition, and eqs. (3) and (4) have been applied to the copolymerization of lauryl methacrylate and allylureas to give evidence of cyclic reactions during propagation.

EXPERIMENTAL

Monomers

The preparation and analysis of the lauryl methacrylate has been described previously.[1]

Monoallyl urea was purchased from Polymer Consultants Ltd. and was used without further purification.

N,N-Diallylurea was prepared by reaction between diallylamine hydrochloride and potassium cyanate.[3] Recrystallization from benzene gave colorless crystals, m.p. 65–66°C.

N,N'-Diallylurea was prepared by heating allyl isocyanate with water.[4] Allyl isocyanate was prepared by the reaction of potassium cyanate and allyl bromide in *N,N*-dimethylformamide solution.[5] The diallylurea was recrystallized twice from water as colorless crystals, m.p. 99–100°C.

Polymerization Procedure

The monomers (total amount about 0.06 mole) and redistilled, dried dioxane (20 ml.) were weighed into a cylindrical tube of 50 ml. capacity. The tube was purged with nitrogen and closed with a hypodermic cap. It was agitated in a thermostat at 100°C., and a solution of benzoyl peroxide (0.73 g. in 25 ml. of dioxane, 0.12 mmole/ml.) was added when the

TABLE I
Copolymerization of Lauryl Methacrylate (LMA) and Monoallylurea at 100°C.[a]

LMA initially, $(M_1)_0$, moles	Urea initially, $(M_2)_0$, moles	Reaction time, min.	Yield of polymer, g.	Nitrogen, %
0.05399	0.00599	8	2.881	0.05
0.05360	0.00599	35	7.640	0.06
0.04850	0.01199	7	1.197	0.09
0.04791	0.01199	3	0.779	0.08
0.04194	0.01798	20	3.884	0.16
0.03589	0.02397	21	3.745	0.21
0.02993	0.02996	20	3.369	0.29
0.02405	0.03596	32	3.488	0.46
0.01920	0.04205	30	2.820	0.65
0.01213	0.04804	35	1.653	1.12

[a] 0.12 mmole of initiator (1 ml. solution) was used in each experiment.

TABLE II
Copolymerization of Lauryl Methacrylate (LMA) and *N,N*-Diallylurea at 100°C.[a]

LMA initially $(M_1)_0$, moles	Urea initially $(M_2)_0$, moles	Reaction time, min.	Yield of polymer, g.	Nitrogen, %
0.04800	0.01200	10	2.933	0.12
0.04202	0.01802	10	3.113	0.20
0.04194	0.01800	10	3.086	0.19
0.03610	0.02400	15	4.023	0.33
0.03010	0.03000	15	3.225	0.50
0.02400	0.03600	23	3.000	0.79
0.01801	0.04200	22	2.401	1.23
0.01209	0.04800	97	1.663	2.10

[a] 0.12 mmole of initiator (1 ml. solution) was used in each experiment.

TABLE III
Monomer Reactivity Ratios for the Copolymerization of Lauryl Methacrylate and *N,N'*-Diallylurea at 100°C.

LMA initially, $(M_1)_0$, moles	Urea initially, $(M_2)_0$, moles	Initiator solution, ml.[a]	Reaction time, min.	Yield of polymer, g.	Nitrogen, %
0.05561	0.006522	1.0	15	3.129	0.085
0.05376	0.006805	1.0	15	3.522	0.11
0.05215	0.01012	1.0	15	2.645	0.185
0.04104	0.02009	3.5	120	6.907	0.465
0.03568	0.02844	3.5	180	4.525	0.72
0.03493	0.02606	3.5	120	4.756	0.64
0.02965	0.03092	3.5	240	3.596	0.82
0.02758	0.03287	1.0	120	1.182	0.64
0.02659	0.03053	4.0	360	3.800	0.92
0.02387	0.03763	1.0	90	0.468	0.72
0.01690	0.04357	1.0	120	0.3613	1.265

[a] 1 ml. = 0.12 mmole initiator.

monomers had dissolved. The polymerization was stopped after the required reaction time by pouring the contents of the tube into methanol. The polymers were purified by repeated precipitation from benzene or chloroform solution by the addition of methanol. The nitrogen contents of the polymers were measured by the Kjeldahl method. Nitrogen analysis of polymers by this method can give low results and a correction factor is normally applied. However, we were unable to prepare homopolymers of the nitrogen-containing monomers which were sufficiently pure for measurement for the nitrogen contents, and a correction factor was not applied to the analytical results.

The experimental conditions and the analyses of the polymers are given in Tables I–III.

Calculation of the Monomer Reactivity Ratios

The conversion exceeded 20% in most of the polymerizations and the integrated form[6] of the copolymer composition equation was used. The intersection method was used to calculate the reactivity ratios (Figs. 1–3). The determination of reactivity ratios by the intersection method is fully discussed by Alfrey, Bohrer, and Mark,[7] and their procedure was used. Intersections of lines of similar slope were neglected whether these were in the region of most of the other intersections or not. Only intersections

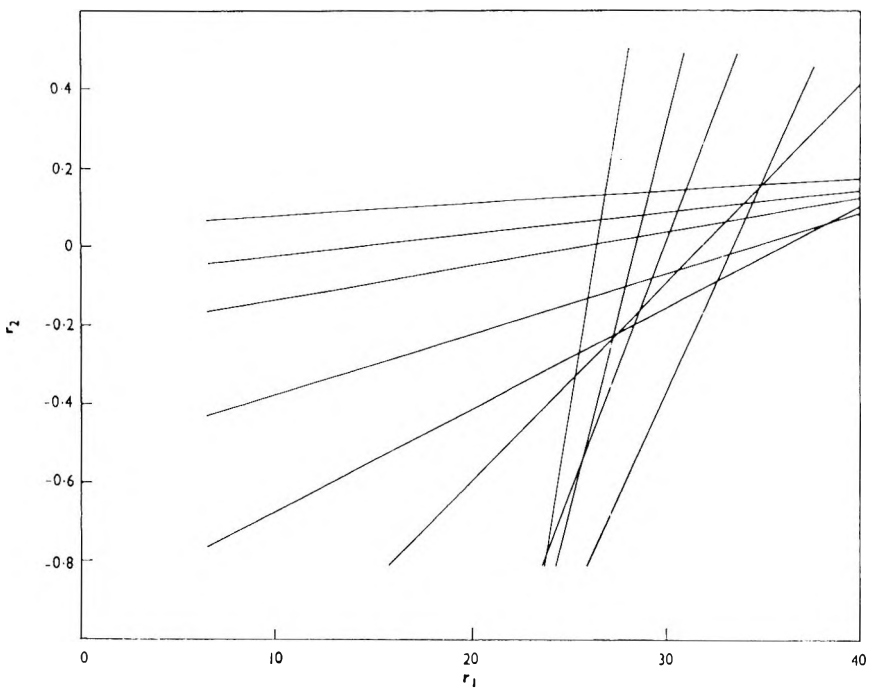

Fig. 1. Determination of r_1 and r_2 for copolymerization of lauryl methacrylate and monoallylurea.

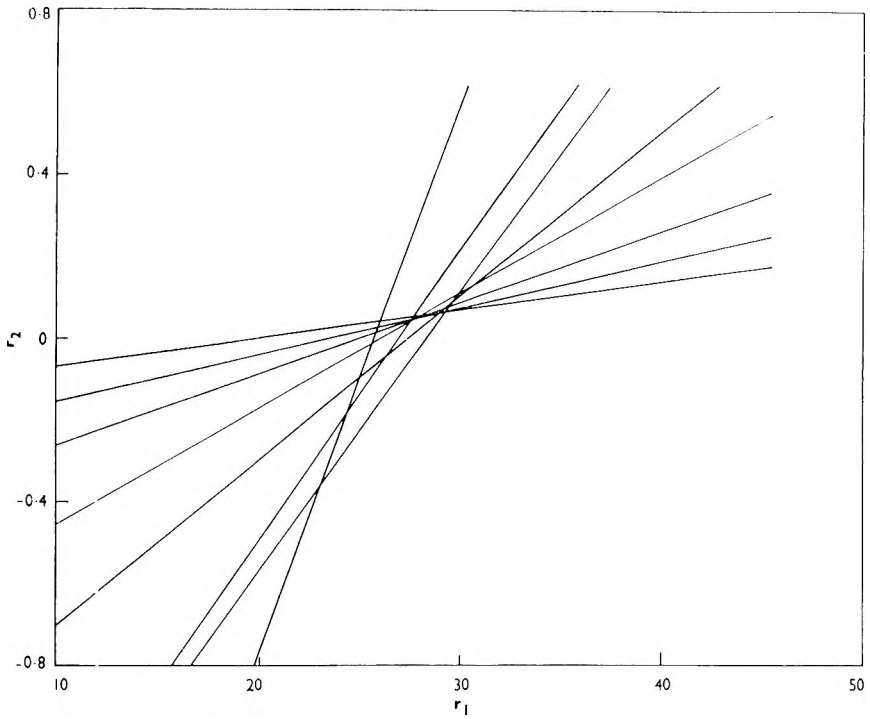

Fig. 2. Determination of r_1 and r_2 for copolymerization of lauryl methacrylate and N,N-diallylurea.

between lines of very different slopes were used in the subsequent calculations. The best values of r_1 and r_2 and the corresponding standard deviations were then found statistically.

Infrared Analysis of the Copolymers

Infrared spectrometric analysis of the copolymers of N,N-diallylurea and lauryl methacrylate gave no evidence for the existence of double bonds of any kind. The infrared spectra of the copolymers of N,N'-diallylurea and lauryl methacrylate indicated the presence of a small concentration of double bonds.

DISCUSSION

The values of the monomer reactivity ratios (Table IV) show that these allylureas are not very reactive in copolymerizations with lauryl methacrylate. The copolymers that are formed contain a considerably higher proportion of lauryl methacrylate than the corresponding monomer mixture.

The values of r_1 given in Table IV are the reactivity ratios for lauryl methacrylate relative to the allylurea molecules. The reactivity ratios (R_1) of lauryl methacrylate relative to the allyl groups in the allylureas may

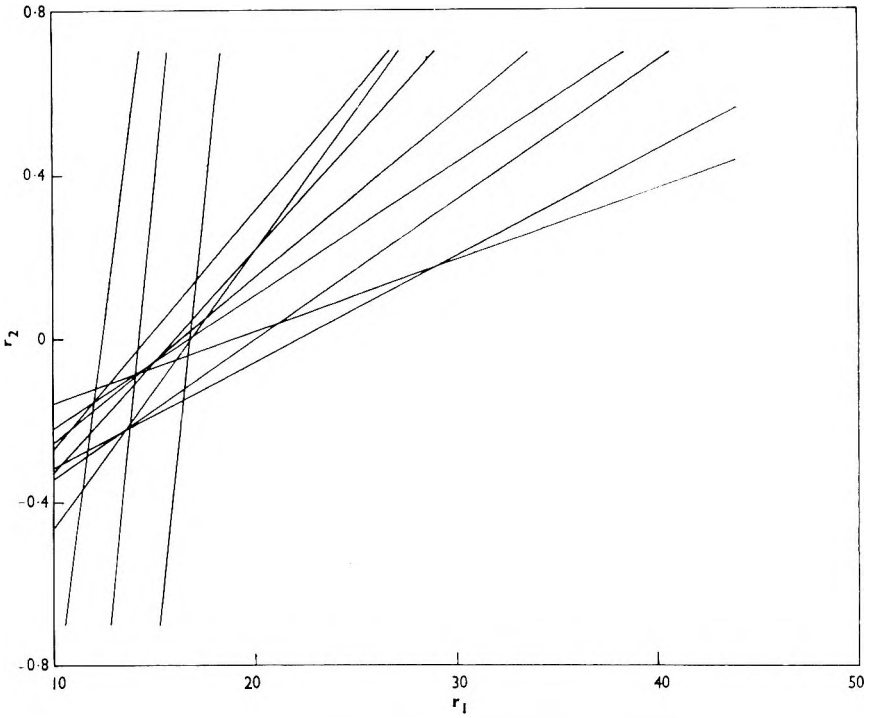

Fig. 3. Determination of r_1 and r_2 for copolymerization of lauryl methacrylate and N,N-'diallylurea.

be calculated [eqs. (3) and (4)]: lauryl methacrylate monoallylurea, ($R_1 = r_1$), $R_1 = 29.9$; lauryl methacrylate N,N'-diallylurea, ($R_1 = 2r_1$); $R_1 = 29.0$.

The allyl groups in monoallylurea and N,N-diallylurea are thus of similar reactivity in respect to copolymerization with lauryl methacrylate.

TABLE IV
Monomer Reactivity Ratios for the Copolymerization of Lauryl Methacrylate and Allylureas at 100°C.

Monomer 1	r_1	95% confidence limits of mean value of r_1	Monomer 2	r_2	95% confidence limits of mean value of r_2
Lauryl methacrylate	29.9	1.2	Monoallylurea	−0.22	0.06
Lauryl methacrylate	27.4	0.8	N,N-Diallylurea	0.014	0.05
Lauryl methacrylate	14.5	0.7	N,N'-Diallylurea	−0.12	0.04

If the value of R_1 is calculated for the copolymerization of lauryl methacrylate with N,N-diallylurea, a value of 54.8 is obtained (when it is assumed that $R_1 = 2r_2$); this value indicates that the allyl groups in N,N-diallylurea are far less reactive than the allyl groups in the other monomers. However, this is not necessarily correct, for it is possible that N,N-diallylurea polymerizes by a cyclic mechanism

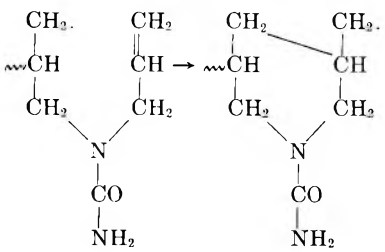

and such cyclization reactions have been postulated for the polymerization of diallylphenylphosphine oxide.[8] If this cyclization reaction were faster than the propagation reaction, then N,N-diallylurea would behave in copolymerization as though it were a monofunctional monomer, and eqs. (3) and (4) would not apply to this system. The reactivity ratio R_1 for lauryl methacrylate relative to the allyl group in N,N-diallylurea should then be 27.4 ($R_1 = r_1$), and the allyl groups in all three ureas would have similar reactivities for copolymerization with lauryl methacrylate.

The cyclic propagation is most unlikely to occur in the polymerization of N,N'-diallylurea with lauryl methacrylate because an eight-membered ring would result. The value of r_1 for this system would be expected to be half the value of r_1 for the lauryl methacrylate monoallylurea copolymerization, and this is found in practice.

We consider that the values of the monomer reactivity ratios r_1 for these copolymerizations provide good evidence for the cyclic propagation of N,N-diallylurea. Cyclic propagation reactions have been proposed in the past but in many cases the only evidence to support the proposition was the absence of double bonds in the polymer and the absence of crosslinking, as judged from the solubility of the polymer. The reactivity ratios, as discussed here can provide good evidence for cyclic propagation reactions in many copolymerizations involving bifunctional monomers.

The values of the monomer reactivity ratios r_2 are very close to zero, but two of the values are significantly negative. This should not be possible but probably arises because of the penultimate group effect, and suggests that the reactivity ratios should be calculated by the more refined method given by Ham.[9] This has not been possible in the present work because the method can only be applied to the results of experiments with low conversions, and in most of the experiments in the present work the yields of polymer exceeded 20%.

References

1. Beynon, K. I., *J. Polymer Sci.*, **A1**, 3343 (1963).
2. Beynon, K. I., *J. Polymer Sci.*, **A1**, 3357 (1963).
3. Milionis, J. P., and P. Adams, U. S. Pat. 2,734,083 February 1956.
4. Cahours, A., and A. W. Hofmann, *Ann.*, **102**, 300 (1857).
5. Schaefer and Drechsel, U. S. Pat. 2,640,068.
6. Mayo, F. R., and C. Walling, *Chem. Rev.*, **46**, 191 (1950).
7. Alfrey, T., J. J. Bohrer, and H. Mark, *Copolymerization*, Interscience, New York, 1952.
8. Berlin, K. D., and G. B. Butler, *J. Am. Chem. Soc.*, **82**, 2712 (1960).
9. Ham, G. E., *J. Polymer Sci.*, **14**, 87 (1954); *ibid.*, **24**, 349 (1957); *ibid.*, **45**, 169, 177, 183 (1960).

Résumé

On a mesuré les rapports de réactivités des monomères pour la copolymérisation du méthacrylate de lauryle et des urées allyliques à 100°C, en présence de peroxyde de benzoyle comme catalyseurs: méthacrylate de lauryle–monoallylurée; $r_1 = 29.9 \pm 1.2$, $r_2 = 0.22 \pm 0.06$; méthacrylate de lauryle–*N,N*-diallylurée: $r_1 = 27.4 \pm 0.8$; $r_2 = 0.014 \pm 0.05$; méthacrylate de lauryle–*N,N'*-diallylurée: $r_1 = 14.5 \pm 0.7$; $r_2 = 0.12 \pm 0.04$. Le rapport de réactivité r_1 étant la relation entre la constante de vitesse du méthacrylate de lauryle et de la molécule d'allylurée, prise en sa globalité. De même r_2 est le rapport entre les constantes de vitesse de la molécule d'allylurée et du méthacrylate de lauryle. Les valeurs des rapports de réactivité du méthacrylate de lauryle, relativement à une fonction allylique séparée dans chacune des urées allyliques, ont été calculées. Il semble que dans chacune de ces molécules, les fonctions allyliques possèdent une réactivité comparable concernant la copolymérisation avec le méthacrylate de lauryle. Les rapports de réactivités des monomères mettent en évidence une propagation cyclique dans la copolymérisation avec des urées *N,N*-diallyliques.

Zusammenfassung

Monomerreaktivitätsverhältnisse wurden für die Copolymerisation von Laurylmethacrylat und Allylharnstoffen bei 100°C mit Benzoylperoxyd als Katalysator gemessen: Laurylmethacrylat-Monoallylharnstoff; $r_1 = 29{,}9 \pm 1{,}2$; $r_2 = -0{,}22 \pm 0{,}06$; Laurylmethacrylat–*N,N*-Diallylharnstoff; $r_1 = 27{,}4 \pm 0{,}8$; $r_2 = 0{,}013 \pm 0{,}05$; Laurylmethacrylat–*N,N'*-Diallylharnstoff; $r_1 = 14{,}5 \pm 0{,}7$; $r_2 = -0{,}12 \pm 0{,}04$. Das Reaktivitätsverhältnis r_1 bezieht sich auf Laurylmethacrylat relativ zum Allylharnstoffmolekül als Ganzem und das Monomerreaktivitätsverhältnis r_2 bezieht sich auf das Allylharnstoffmolekül relativ zu Laurylmethacrylat. Die Werte des Monomerreaktivitätsverhältnisses von Laurylmethacrylat relativ zu einer einzelnen Allylgruppe in jedem der Allylharnstoffe wurde berechnet. Es scheint, dass die Allylgruppe bei allen diesen Molekülen eine ähnliche Reaktivität bei der Copolymerisation mit Laurylmethacrylat besitzt. Die Monomerreaktivitätsverhältnisse lassen das Auftreten zyklischer Wachstumsreaktionen bei der Copoylymerisation von *N,N*-Diallylharsntoff erkennen.

Received July 14, 1964
(Prod. No. 4534A)

JOURNAL OF POLYMER SCIENCE: PART A VOL. 3, PP. 1801–1805 (1965)

Free Radical Chain Transfer to Allyl Monomers at Low Polymerization Temperatures

T. L. DAWSON and R. D. LUNDBERG, *Research and Development Department, Union Carbide Corporation, Plastics Division, South Charleston, West Virginia*

Synopsis

Alkylboron–oxygen, an active, low-temperature free radical initiator, has been employed to investigate the effects of very low polymerization temperatures on the free radical homopolymerization and copolymerization of allyl monomers. Unlike some polymerizations which have been reported to undergo dramatic changes in polymerization rates at very low polymerization temperatures, the allyl systems behaved in a like manner at high and low temperatures. Similar, low values of reduced viscosities were obtained for homopolymers of allyl monomers prepared over a 300°C. temperature range. An almost identical effect of allyl chloride concentration on the molecular weight of ethyl acrylate/allyl chloride copolymers was also observed for copolymerizations performed over a 100°C. temperature range. For solution homopolymerizations and copolymerizations the activation energy for free radical abstraction from the allyl monomer is, therefore, nearly equal to the activation energy for addition of that radical to the allyl double bond, even at temperatures down to the melting points of the monomers.

Introduction

In a recent publication by Brown and James,[1] it was reported that the activation energies for the addition of ethyl radicals to the double bond of allyl alcohol and for the abstraction of an allylic hydrogen atom are equal, within experimental error, for reactions occurring in the gas phase from 50 to 142°C. These results, in conjunction with reports of dramatic increases in polymerization rates at low polymerization temperatures[2] and the establishment of alkylboron–oxygen as an active, low-temperature free radical initiator,[3] prompted us to perform the related low-temperature studies.

Only very low yields of allyl homopolymers are obtained with low initiator concentrations both at ambient and low polymerization temperatures. Copolymerization studies with a highly reactive comonomer were, therefore, utilized to increase the yields of high polymer. This technique proved adequate to demonstrate that allyl polymerization occurs at low polymerization temperatures and to study the relative effect of very low polymerization temperatures on the free radical propagation and chain transfer reactions. The facile, low-temperature free radical polymerizability of ethyl acrylate in conjunction with its low freezing point and high

reactivity toward free radicals led to its choice as the reactive monomer to be copolymerized with allyl chloride. Allyl chloride was employed as the allyl component because of the ease of copolymer composition analysis from chlorine content.

Experimental

All monomers and solvent were purified by fractional distillation and stored at −20°C. prior to use. To obtain quantitative results with the alkylboron–oxygen initiator, the control of oxygen content in catalytic concentrations is required. High vacuum techniques were, therefore, employed throughout.

Monomers, solvent, and tributylboron (TBB) were degassed thoroughly prior to their distillation *in vacuo* into the polymerization flasks. The volumes of the liquids were measured by distillation from graduated tubes or by employing a cathetometer to measure the vertical distance on a tube of known inside diameter. After melting and mixing the liquid components thoroughly, a small measured quantity of oxygen was then added by condensation of the oxygen from the manifold into the polymerization tube cooled in liquid nitrogen. From the known volume of the manifold, the measured pressure drop in the manifold, and the temperature, the exact weight of condensed oxygen was controlled and measured. After adding the oxygen the contents were again melted, mixed thoroughly, and then warmed to the desired polymerization temperature.

The possibility of postpolymerization was minimized both by polymerizing the ethyl acrylate to greater than 90% conversion and also by mixing a precooled acetone solution of a free radical inhibitor, monomethyl ether of hydroquinone, into the cold polymerizations prior to their precipitation. Subsequently the polymers were repeatedly precipitated into water from acetone to remove the remaining monomer. Water was employed as the precipitant to insure that even the lowest molecular weight fraction be recovered. The samples were dried *in vacuo* and then analyzed for monomer composition by chlorine analyses. Only relative values of molecular weights were required for interpretation of the results. The molecular weights were, therefore, estimated from reduced viscosity measurements at 30°C. in benzene at 0.2% concentration by using the approximation $\eta_{red} \cong [\eta] \cong 10^{-4}M^{0.7}$.

Results and Discussion

In these studies the allyl chloride participated as both comonomer and chain transfer agent and the ethyl acrylate was polymerized to high conversion. Accurate chain transfer constants could not, therefore, be calculated from these data. The existence of nonsteady-state free radical concentrations, in the highly viscous media which were produced, also required that comparative data be obtained for a less reactive chain transfer agent at similar compositions.

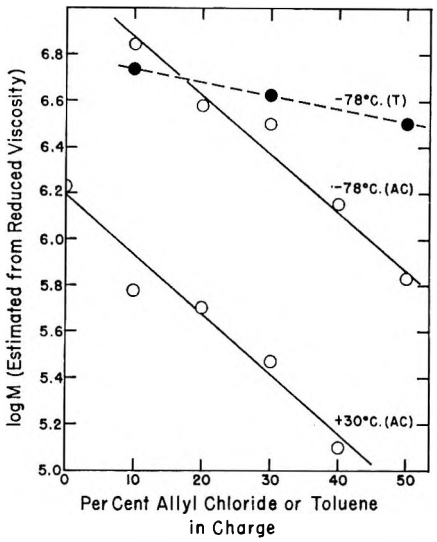

Fig. 1. Effect of allyl chloride (AC) at +30°C. and −78°C. and of toluene (T) a −78°C. on the molecular weight of poly(ethyl acrylate) and ethyl acrylate/allyl chloride copolymers: [TBB] is 0.061M, and [O_2] is 0.024–0.029M.

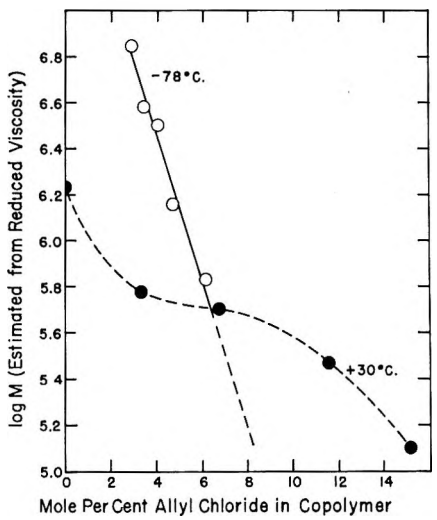

Fig. 2. Variation of molecular weight of ethyl acrylate/allyl chloride copolymers prepared at −78°C. and +30°C. with mole per cent allyl chloride contained in the copolymer: [TBB] is 0.061M, and [O_2] is 0.024–0.029M.

In Figure 1, it is shown that at −78°C. the presence of toluene does not decrease the molecular weight of the resultant polymer nearly as much as does the allyl chloride. Chain transfer to the allyl chloride is, therefore, reflected measurably in the high conversion data. In Figure 1, it is also illustrated that the rate of decrease of log M with increasing allyl chloride content in the charge is, within experimental error, the same at +30 and

−78°C. As expected, copolymers of consistently higher molecular weight were obtained at the lower polymerization temperature from charges identical to those employed at the higher polymerization temperature. The same rate of change of log M with allyl chloride content for polymers of similar molecular weight demonstrates, however, that chain transfer to allyl chloride, relative to propagation, is as pronounced at −78°C. as at +30°C.

The same data, plotted in Figure 2, illustrate that, while significant quantities of allyl chloride are copolymerized at both temperatures, allyl chloride enters the copolymer more readily at the higher polymerization temperature. At the lower polymerization temperature a larger value for the reactivity ratio for ethyl acrylate relative to the reactivity ratio for the allyl chloride is, therefore, indicated. This figure illustrates further that, from a practical point of view, copolymers of low allyl chloride content were of higher molecular weight when prepared at the low polymerization temperature. Extrapolation of the low temperature data indicates, however, that the reverse would be true for copolymers containing higher allyl chloride contents.

The conclusions obtained from the copolymerization studies were supported by the results of studies of free radical homopolymerizations of allyl chloride from its melting point, −136°C. to +100°C. and allyl alcohol from its melting point, −129°C. to +175°C. In all cases homopolymers with similar, low reduced viscosities were obtained.

These similar, low values of reduced viscosities of polymers obtained from homopolymerizations of allyl monomers performed over a 300°C. temperature range and the almost identical effect of allyl chloride concentration on the molecular weights of ethyl acrylate/allyl chloride copolymers prepared over a 100°C. temperature range extend the results of Brown and James for gas-phase free radical reactions of allyl alcohol at 50–142°C. For solution homopolymerizations and copolymerizations of these monomers the activation energy for free radical abstraction from the allyl monomer is, therefore, very nearly equal to the activation energy for addition of that radical to the allyl double bond, even at temperatures down to the melting points of the monomers.

The authors wish to thank Mr. P. E. Peters for assistance in the experimental work.

References

1. Brown, A. C. R., and D. G. L. James, *Can. J. Chem.*, **40**, 796 (1962).
2. Semenov, N. N., *J. Polymer Sci.*, **55**, 563 (1961).
3. Zutty, N. L., and F. J. Welch, *J. Polymer Sci.*, **43**, 445 (1960).

Résumé

L'alcoyl bore-oxygène, initiateur radicalaire actif en pouvant être utilisé à basse température, a été employé pour étudier l'influence des températures de polymérisation très basses sur l'homo- et la co-polymérisation radicalaires de monomères allyliques. Contrairement à certaines polymérisations, qui subissent des changements profonds dans la vitesse de polymérisation à très basse température, les système allyliques se comportent

de la même façon à haute et basse température. De même, on a obtenu des valeurs faibles pour les viscosités réduites des homopolymères allyliques, préparés dans un domaine de température de 300°C. Une influence presqu'identique de la concentration en chlorure d'allyle sur les poids moléculaires des copolymères acrylate d'éthyle/chlorure d'allyle a également été observée pour des copolymérisations effectuées dans un domaine de température de 100°C. Pour les homo- et copolymérisations en solution, l'énergie d'activation pour l'arrachement d'un radical du monomère allylique est dès lors à peu près égale à l'énergie d'activation d'addition de ce radical à la double liaison allylique, même à des températures inférieures aux points de fusion des monomères.

Zusammenfassung

Alkylbor-Säuerstoff, ein aktiver, radikalischer Tieftemperaturstarter, wurde zur Untersuchung des Einflusses sehr niedriger Polymerisationstemperaturen auf die radikalische Homo- und Copolymerisation von Allylmonomeren verwendet. Im Gegensatz zu anderen Polymerisation, für welche über eine dramatische Änderung der Polymerisationsgeschwindigkeit bei sehr niedrigen Polymerisationstemperaturen berichtet wurde, verhalten sich die Allylsysteme bei hohen und niedrigen Temperaturen gleichartig. Ähnliche niedrige Werte für die reduzierte Viskosität wurden für Homopolymere von Allylmonomeren bei Darstellung in einem Temperaturbereich von 300°C erhalten. Ein fast identischer Einfluss der Allylchloridkonzentration auf das Molekulargewicht von Äthylacrylat/Allylchlorid-Copolymeren wurde bei Copolymerisation in einem Temperaturbereich von 100°C beobachtet. Die Aktivierungsenergie für die radikalische Übertragung von Allylmonomeren ist daher bei Lösungshomo- und -copolymerisation nahezu der Aktivierungsenergie für die Addition des Radikals an die Alkyldoppelbindung sogar bei Temperaturen bis hinunter zum Schmelzpunkt der Monomeren gleich.

Received October 12, 1964
(Prod. No. 4560A)

JOURNAL OF POLYMER SCIENCE: PART A VOL. 3, PP. 1807–1823 (1965)

Dye-Sensitized Photopolymerization. V. Polymerization of Acrylamide in Deaerated Systems

CATHERINE S. HSIA CHEN, *Chemical Department, Central Research Division, American Cyanamid Company, Stamford, Connecticut*

Synopsis

The photopolymerizations of acrylamide sensitized by thiazine dyes and eosin Y in deaerated aqueous and ethylene glycol systems were investigated. The removal of most of the dissolved oxygen resulted in higher rates and higher quantum yields of polymerization. Linear per cent polymerization–time relationships were obtained. The induction period was eliminated or reduced, depending on the structure of the dye. The rate of polymerization and the molecular weight of the polymers were proportional to the 1.5 power of the monomer concentration in water and to the first power in ethylene glycol. The presence of an appropriate reducing agent was essential. In the absence of an added reducing agent, no polymerization took place in ethylene glycol and in aqueous solutions of pH ≤ 7. At pH >7, when hydroxyl or other anions were present as the reducing species, polymerizations took place at lower rates than in systems where a reducing agent was added. The polymerization was dependent on the nature of the buffer as well as the pH of the solution. The effectiveness of the reducing agent was also pH-dependent. In aqueous polymerization, no enhancement in rate was observed when an appropriate combination of a cationic and an anionic dye was used as the sensitizer. The initiation mechanisms were probably different for deaerated systems and for systems under ambient atmospheric conditions. In anaerobic polymerizations, where oxygen was completely removed, enhanced rates were observed when both methylene blue and triethanolamine were used as the sensitizer. In the absence of triethanolamine polymerization took place at pH >7 but only very slowly.

INTRODUCTION

In dye-sensitized photopolymerizations, it had been reported by Oster and co-workers that, when a photoreducible dye and a weak reducing agent were used as the sensitizer, an appropriate amount of oxygen was essential for the initiation of polymerization.[1–3] Subsequently, Shepp and co-workers reported that a reducing agent was not necessary if oxygen was carefully excluded from the system.[4] In the present series of investigations the polymerizations reported so far were carried out under ambient atmospheric conditions and in the presence of a reducing agent.[5–8] This communication describes the effect of air (oxygen) on the dye-sensitized photopolymerizations. In connection with it, the effects of the reducing agent and the pH of the solution are also discussed.

EXPERIMENTAL

The light source and experimental procedures were the same as described in the first paper of this series.[5] All polymerizations were carried out at 25 ± 0.2°C. Complete removal of oxygen from the solution was accomplished by the standard thrice freeze-thaw procedure. Most of the results reported in this communication were obtained with solutions which were deaerated by a helium purge for 30–40 min. General procedures for oxygen removal are given below.

Freeze-Thaw Procedure

This procedure enabled complete removal of oxygen from the solution. Cylindrical cells, comparable in dimensions to those described previously,[5] with an optical glass top window and a side arm were used. While in the dark the respective solutions of the monomer and the sensitizer were pipetted into a cell. A total volume of 10 ml. (+0.1 ml.) was employed. The cell was then attached to a high vacuum line through the side arm and the solution was degassed by three cycles of freezing and thawing. The degassed solution, while under a vacuum of 1×10^{-5} mm. Hg, was irradiated through the top window under the same conditions as described previously.[5]

Helium Purge Procedure

Cylindrical open cells used previously[5–8] were employed. While in the dark, a steady stream of helium gas (Matheson) was flushed through the solution (10 ml. + 0.1 ml.) to be polymerized for 30–40 min., and the flushing was maintained during irradiation. Both aqueous and ethylene glycol systems were investigated. For polymerization at different pH's, standard buffer solutions (Fisher) were used in place of distilled water. It was determined polarographically that the removal of dissolved oxygen in the above manner reached a steady state after 2 min. In aqueous solutions, the level of the dissolved oxygen at the steady state and after 30 min. flushing was $6.6 \times 10^{-5}M$ (2.1 ppm) from the original $2.51 \times 10^{-4}M$ (8 ppm). In ethylene glycol solutions the dissolved oxygen was reduced to $2.23 \times 10^{-4}M$ (6.4 ppm) from the original $5.15 \times 10^{-4}M$ (14.8 ppm).

RESULTS AND DISCUSSION

Polymerization in Deaerated Systems

Aqueous Polymerization

Polymerization Rates. Typical per cent polymerization and molecular weight versus time relationships under various experimental conditions are shown in Figures 1 and 2. In contrast to the corresponding polymerizations under ambient atmospheric conditions,[5] the initial polymerization was linear with time, showed no induction period, and proceeded at considerably greater speed. Both Figures 1 and 2 show the polymerization before the

complete fading of the dye. The polymerizarion slowed down after a certain period of time. The rates of polymerization were taken as the slopes of the initial straight-line portions of the plots.

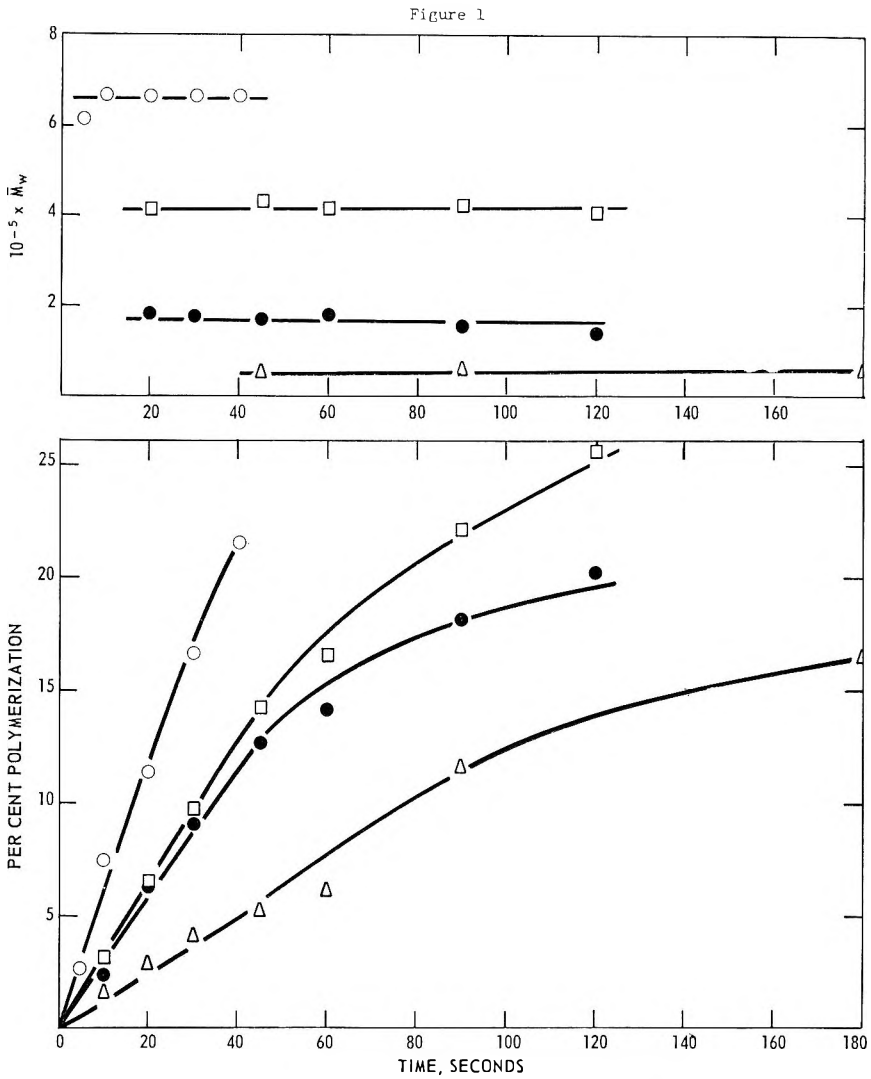

Fig. 1 Polymerization of deaerated aqueous acrylamide at different concentrations; [methylene blue] = $7.0 \times 10^{-4} M$ [triethanolamine] = $2.0 \times 10^{-2} M$. (○) 7 molar; (□) 4 molar; (●) 2 molar; (Δ) 1 molar.

The molecular weights (top, Fig. 1) seemed to remain essentially constant with time or with the per cent polymerization and were in the similar range to those obtained in the corresponding systems under ambient atmospheric conditions.[5] These results again indicate that the molecular weights are controlled by a chain transfer process as discussed previously.

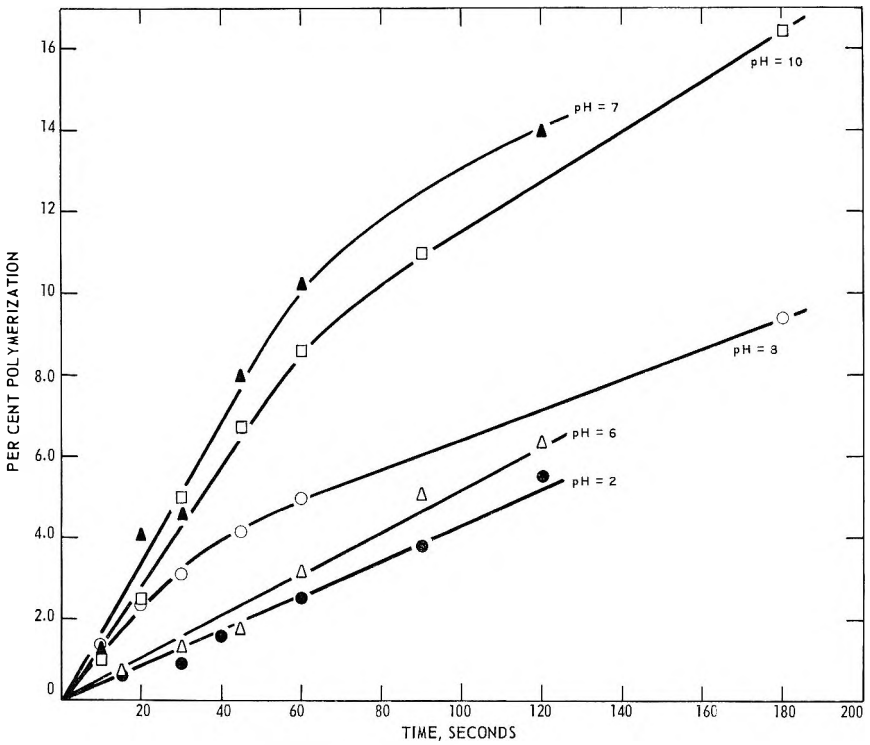

Fig. 2. Deaerated polymerization of $1M$ acrylamide in different buffer solutions; [methylene blue] = $7.0 \times 10^{-5}M$; [triethanolamine] = $2.0 \times 10^{-2}M$.

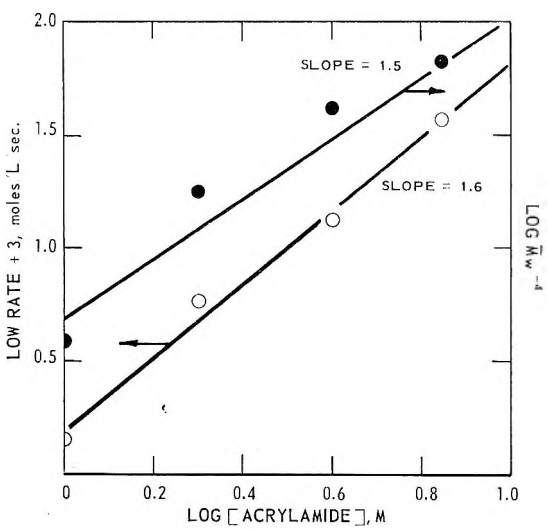

Fig. 3. Dependence of (●) rate and (○) $\bar{M}_w$ on the monomer concentration; [methylene blue] = $7.0 \times 10^{-5}M$; [triethanolamine] = $2.0 \times 10^{-2}M$.

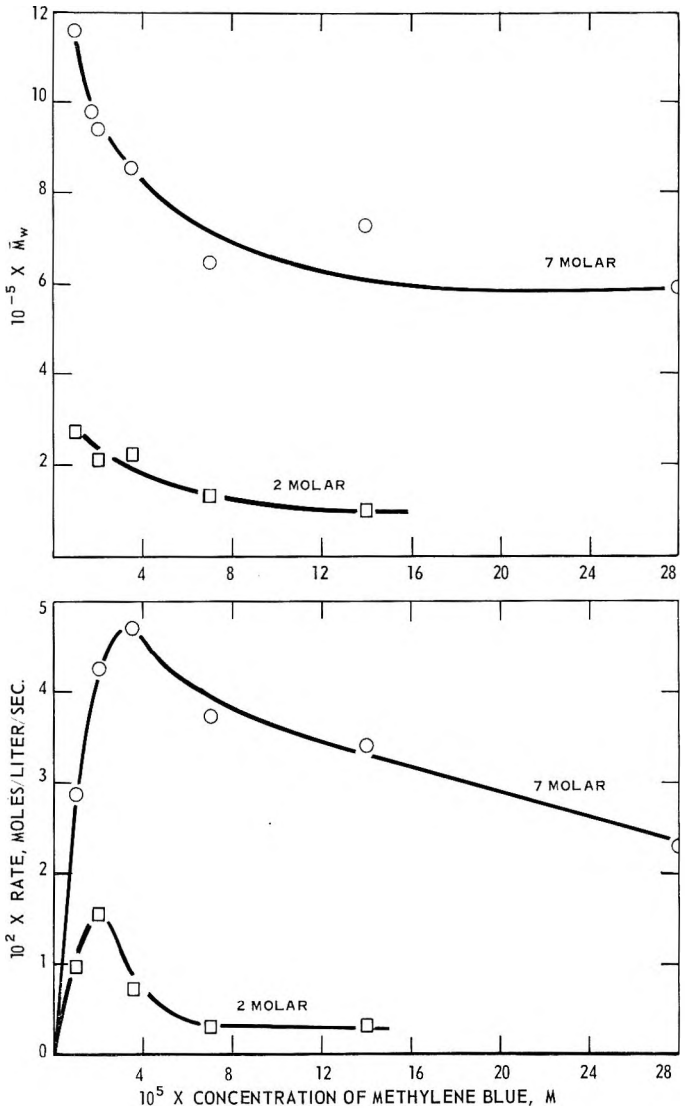

Fig. 4. Effect of dye concentration on polymerization of aqueous acrylamide; [triethanolamine] = $2.0 \times 10^{-2}M$, pH = 10.9–11.

Effect of Monomer Concentration. The results for polymerizations at different acrylamide concentrations are represented in Figure 1. The dependencies of the rate and the molecular weight on the concentration of acrylamide are depicted in Figure 3. The following relationships were derived:

$$\text{Rate} \propto [\text{Acrylamide}]^{1.6}$$

$$M_w \propto [\text{Acrylamide}]^{1.5}$$

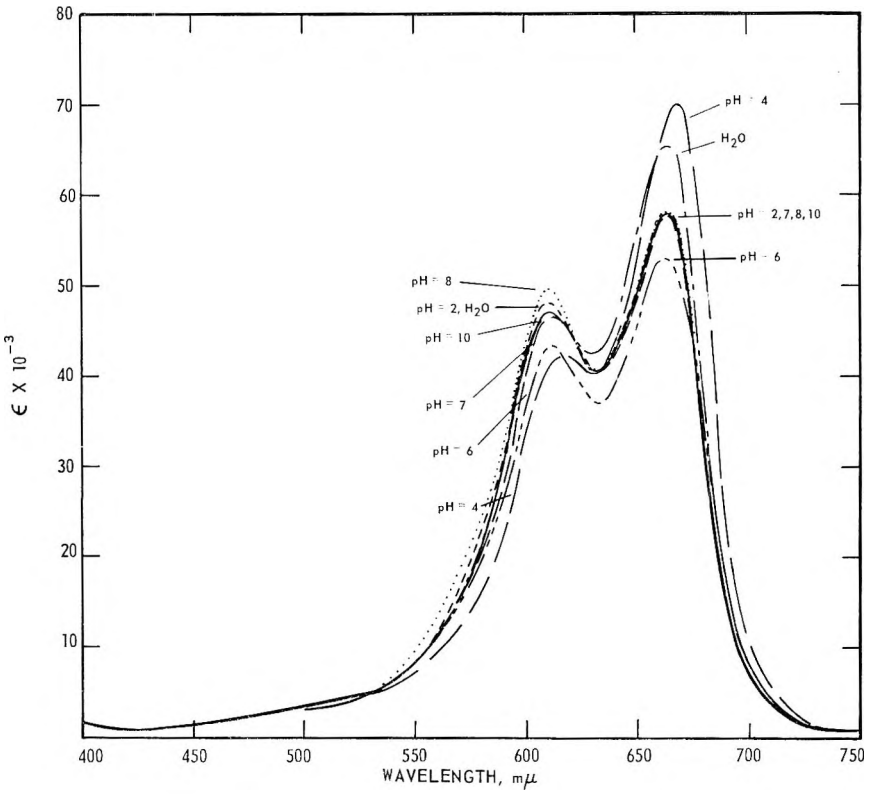

Fig. 5. Absorption spectra of methylene blue in different buffer solutions; [methylene blue] = $7.0 \times 10^{-5}M$.

In essence, both the rate and the molecular weight are proportional to the 1.5 power of the acrylamide concentration.

Effect of Dye Concentration. The effect of the concentration of methylene blue on polymerization has been investigated in two series of experiments with the use of $2M$ and $7M$ acrylamide, respectively. The ambient pH of the solutions was 10.9–11. The results of the polymerizations with $1 \times 10^{-5}M$–$28 \times 10^{-5}M$ methylene blue are depicted in Figure 4. As discussed previously[5] for the corresponding systems in air, the rate passed through a maximum, and the molecular weight decreased with the increase of methylene blue concentration.

Polymerizations in Different Buffer Solutions. The spectra of $7.0 \times 10^{-5}M$ methylene blue in different buffer solutions are depicted in Figure 5. The polymerizations of $1M$ acrylamide in different pH buffers in the presence of $7.0 \times 10^{-5}M$ methylene blue and $2.0 \times 10^{-2}M$ triethanolamine are represented in Figure 2. Other related data are summarized in Table I.

The behavior of methylene blue (and other basic dyes) in different solutions and at different temperatures has been described in the literature.[9,10] The present results (Fig. 5 and Table I) show that although the positions of

TABLE I

Polymerization of 1M Acrylamide in Different Buffer Solutions at [Methylene blue] = $7.0 \times 10^{-5}M$; [Triethanolamine] = $2.0 \times 10^{-2}M$

Buffer	pH at 25° C.	α-peak (λ_{max} = 665 mμ) $\epsilon \times 10^{-4}$	β-peak (λ_{max} = 610 mμ) $\epsilon \times 10^{-4}$	Ratio $\epsilon\alpha/\epsilon\beta$	Rate $\times 10^4$, mole/l./sec.	$[\eta]_{1N\,NaCl}^{30}$, dl./g.	$M_w \times 10^{-4}$
Potassium chloride–hydrochloric acid, 0.05M	2	5.76	4.89	1.178	3.71	0.63	5.77
Potassium biphthalate, 0.05M	4	7.00	4.14	1.691	No polymerization	—	—
Monopotassium phosphate–sodium hydroxide, 0.05M	6	5.29	4.33	1.222	5.67	0.52	4.32
Monopotassium phosphate–sodium hydroxide, 0.05M	7	5.77	4.84	1.192	17.35	0.58	4.71
Monopotassium phosphate–sodium hydroxide, 0.05M	8	5.80	4.96	1.169	10.34	0.49	3.95
Potassium carbonate–potassium borate–potassium hydroxide, 0.05M	10	5.84	4.71	1.240	14.67	0.48	3.82
None, distilled H_2O	5	6.57 (pH 5)	4.69 (pH 5)	1.401	14.10 (pH 11)	0.48	3.82

the peaks were not affected appreciably by the nature of the buffer, the height and the ratio of the two peaks, as well as the total energy absorption, varied somewhat for the different buffers. However, there was no apparent relationship between the pH and the absorption when different types of buffers were employed. When the same types of buffer solutions were employed (mono-sodium phosphate–sodium hydroxide buffer, pH = 6, 7, 8) the total absorption increased while the α/β peak ratio decreased with the pH. These effects are more pronounced during the change from pH 6 to pH 7 than from pH 7 to pH 8. The highest absorptions and the α/β peak ratios are observed with the pH 4 buffer and the unbuffered solution (pH 5 in distilled water and pH 10.9–11 in $2.0 \times 10^{-2}M$ triethanolamine) and in that order.

The polymerization results (Fig. 2 and Table I) showed that the highest rate was obtained with pH 7, and that polymerization was more favored in alkaline than in acidic solution. In addition, polymerization did not take place at all in pH 4 buffer. However, there was no definite relationship between the rate of polymerization and the pH value of the solution. The nature of the buffer appeared to be a more important factor in determining the rate than did the pH value itself. For an example, in the pH 4 buffer no polymer was formed, while polymerization took place in buffers of pH units above and below this value. It was thought, at first, that the formalin present in the standard pH 4 buffer as a preserve might be the retarding compound. However, upon further experimentation no polymerization took place in freshly prepared 0.05M potassium biphthalate solution also. This indicated that potassium biphthalate itself is the retarder. The nature and

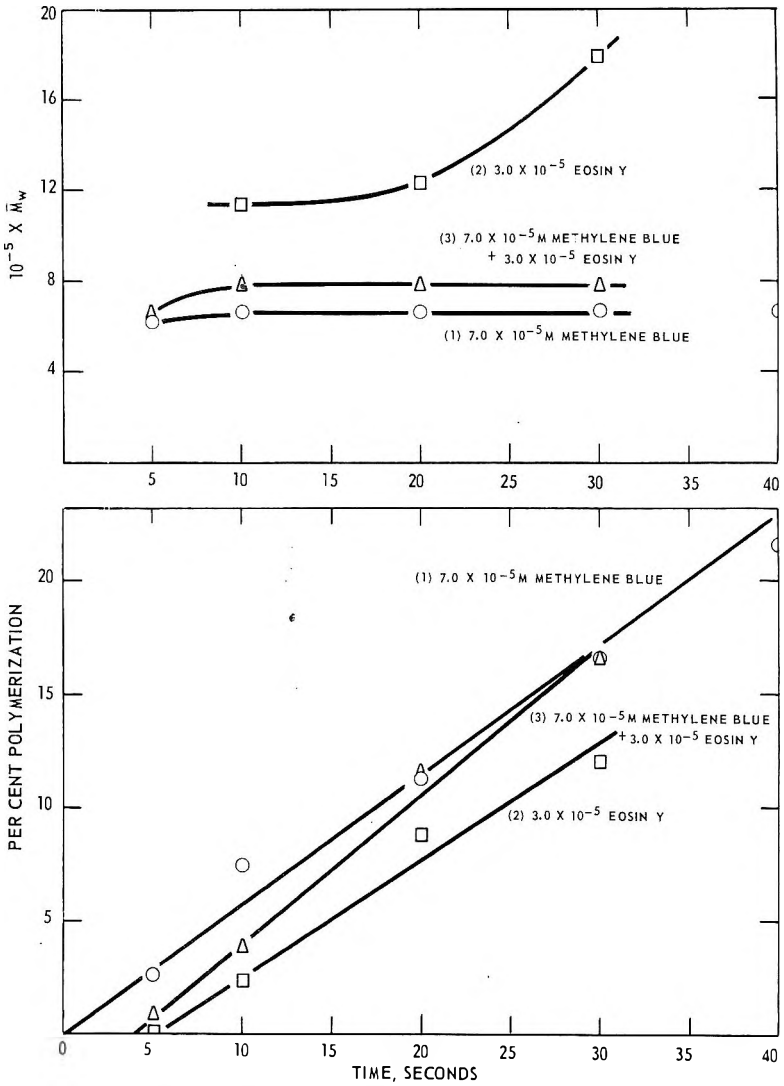

Fig. 6. Effects of combination of a cationic and anionic dye on the polymerization in water; [acrylamide] = 7.0M [triethanolamine] = 2.0 $\times$ $10^{-2}M$.

the pH of the buffer should have a far greater effect on the primary initiation than on the propagation of polymerization step, for the initiation involves oxidation–reduction of acid–base salts while the propagation involves only the addition of acrylamide which is a neutral monomer and unhydrolyzed under the experimental conditions.

Since in the present investigation the α/β peak ratio depends on the nature of the buffer solution, therefore, it also shows no definite relationship to the rate of polymerization, as was the case reported previously for the polymerization in unbuffered solutions at different dye concentrations.[5]

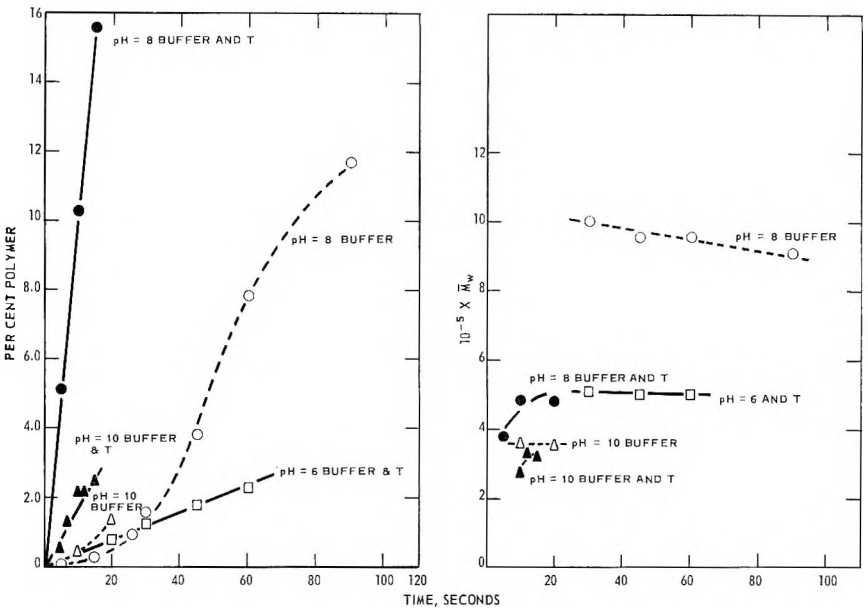

Fig. 7. Polymerization of $7M$ acrylamide, deaerated; [methylene blue] $= 7.0 \times 10^{-5}M$; $T = 2.0 \times 10^{-2}M$ triethanolamine.

Combination of a Cationic and an Anionic Dye. In Figure 6 are shown a comparison of rates of polymerization and molecular weights of the polymers for polymerizations of $7M$ acrylamide sensitized by a mixture of $2.0 \times 10^{-2}M$ triethanolamine and (*1*) $7.0 \times 10^{-5}M$ methylene blue, (*2*) $3.0 \times 10^{-5}M$ eosin Y, and (*3*) a mixture of $7.0 \times 10^{-5}M$ methylene blue and $3.0 \times 10^{-5}M$ eosin Y, respectively. While the relationships pertaining to per cent polymerization versus time were linear, in the two latter cases where eosin Y was present induction periods were observed. Both the rate and the molecular weights for the polymerization carried out with the use of the dye mixture as the sensitizer fell between those for either dye alone (see Fig. 6). These results differed significantly from those obtained under ambient atmospheric conditions,[6] where enhancement of polymerization was observed. This contrast in polymerization behaviors between the two cases suggests that the initiation mechanisms are different under atmospheric conditions and in deaerated systems.

Effect of Reducing Agent in the Absence of an Added Reducing Agent. When $7M$ acrylamide in different buffer solutions in the presence of $7.0 \times 10^{-5}M$ methylene blue was irradiated, no polymerization and no fading of the dye took place after 30 min. in buffer solutions of pH 2, pH 5 (ambient pH in distilled H_2O), pH 6, and pH 7. However, both polymerization and fading of methylene blue were observed in buffer solutions of pH 8 and pH 10. The data on the polymerization rates (up to complete fading of the dye) and the molecular weights of polymers are represented by dotted curve in Figure 7.

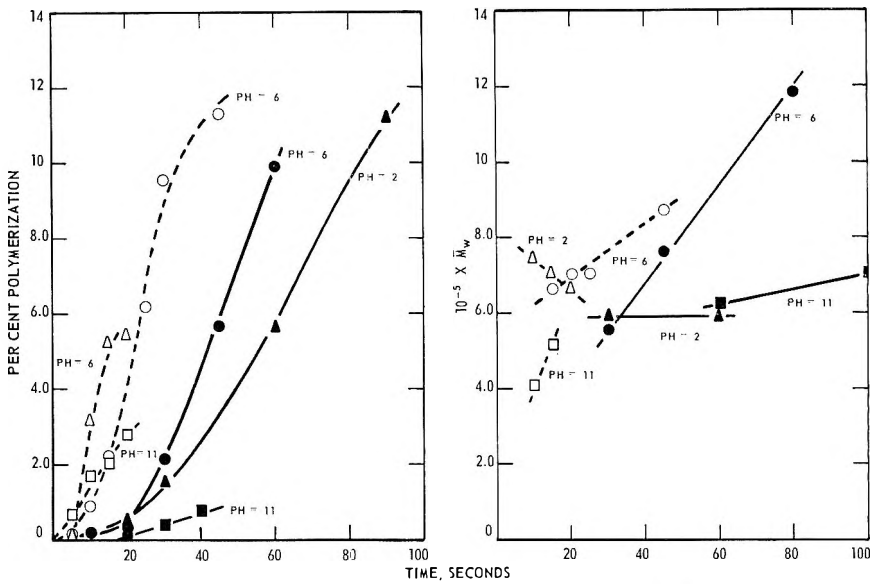

Fig. 8. Polymerization of $7M$ acrylamide sensitized by $7.0 \times 10^{-5}M$ methylene blue and $2.0 \times 10^{-2}M$ tetrasodium ethylenediamine tetraacetate: (——) in air; (- - -) deaerated.

These observations agreed with the results reported by Shepp et al.[4] for the thionine–acrylamide system, where they showed that at a suitable pH (8.4) both polymerization and fading of the dye took place essentially in the absence of oxygen without any added reducing agent. However, in contrast to the present results, they mentioned that with methylene blue, polymerization of acrylamide took place without fading of the dye.

Effect of Reducing Agent in the Presence of Triethanolamine. For comparison, $7M$ acrylamide in pH 8, pH 10, and pH 6 buffers in the presence of $2.0 \times 10^{-2}M$ triethanolamine and $7.0 \times 10^{-5}M$ methylene blue were investigated. The polymerization results are represented by the solid curves in Figure 7. By comparing the corresponding solid curves with the dotted curves, it is seen that polymerization rates are higher and the molecular weights of the polymers are lower in the presence of triethanolamine. These effects are clearly shown in the case of pH 8 buffer and to a lesser extent in the case of pH 10 buffer. Furthermore, in pH 6 buffer both polymerization and fading of the dye took place, contrasting with the results obtained in the absence of triethanolamine. There was, however, again no definite relationship between the rate of polymerization and the pH of the solution. In addition, different kinetic characteristics were observed. In the presence of triethanolamine the relationship between the per cent polymerization and time was linear without any induction period, while in the absence of a reducing agent it was S-shaped.

Effect of Reducing Agent in the Presence of Tetrasodium Ethylenediamine Tetraacetate. The results for polymerization of $7M$ acrylamide sensi-

tized by $7.0 \times 10^{-5}M$ methylene blue and $2.0 \times 10^{-2}M$ tetrasodium ethylenediamine tetraacetate in pH 2 and pH 6 buffers and at ambient pH (pH 11), both deaerated and under atmospheric conditions, are shown in Figure 8. Both the rates of polymerization and the molecular weights of the polymers were higher in deaerated systems. Again there appeared to be no definite relationship between the pH of the solution and the polymerization. Furthermore, the order of rate of polymerization relative to the pH was different in systems deaerated by flushing with helium and under ambient atmospheric conditions.

The above results regarding the effect of a reducing agent can be summarized as follows: (*1*) In the absence of a reducing agent, polymerization takes place only at pH >7. (*2*) an added reducing agent favors the polymerization. At lower pHs (pH <7) tetrasodium ethylenediamine tetraacetate is a more efficient reducing agent than triethanolamine, while at higher pH (pH >7) the reverse is true. As expected, triethanolamine is also a better chain transfer agent than tetrasodium ethylenediamine tetraacetate. (*3*) The nature of the buffer ($5 \times 10^{-2}M$) plays an important role in determining the rate of polymerization.

The results summarized above suggest that a reducing agent is necessary for dye sensitization even in deaerated systems. In the absence of an added reducing agent, the hydroxyl ions (OH^- at pH >7) act as the reducing agent in the formation of radicals for initiation. For similar thionine-acrylamide systems, Shepp, Chaberek, and MacNeil[4] proposed the following scheme

$$D \xrightarrow{\text{light}} D^*$$

$$D^* + OH^- \rightarrow SD^{\cdot} + OH^{\cdot}$$

where D and D* are dye and excited dye molecules, respectively, and $SD^{\cdot}$ is the semiquinone dye radical.

The present investigation further suggests that, depending on the nature of the buffer ions, the reducing agent can be an anion from the buffer solution (B^-) rather than the hydroxyl ion. Thus the following scheme applies:

$$D^* + B^- \rightarrow SD^{\cdot} + B^{\cdot}$$

When a more powerful reducing agent ($\ddot{R}$), e.g., tetrasodium ethylenediamine tetraacetate or triethanolamine, is added, the initiation is favored, and the following scheme applies:

$$D^* + \ddot{R} \rightarrow SD^{\cdot} + \dot{R}$$

Polymerization in Ethylene Glycol

Polymerization Kinetics and the Effect of Acrylamide Concentration on the Polymerization. By employing 7.0×10^{-5} M methylene blue as the sensitizer, it was found that polymerization does not take place in the absence of an added reducing agent. In the presence of $2.0 \times 10^{-2}M$

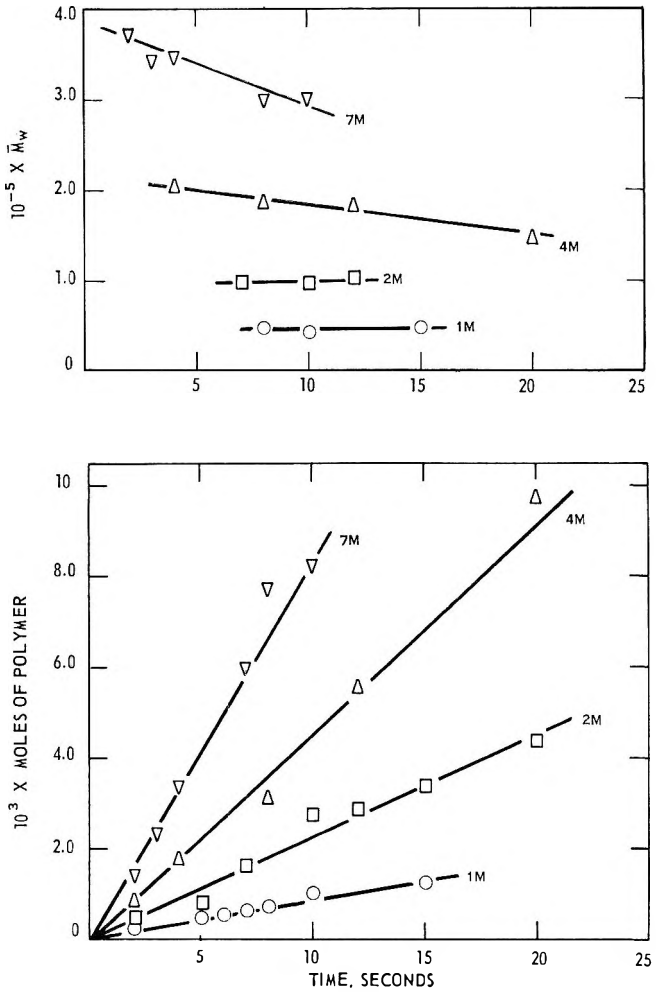

Fig. 9. Polymerization of acrylamide in ethylene glycol at different concentrations; [methylene blue] = $7.0 \times 10^{-5}M$ [triethanolamine] = $2.0 \times 10^{-5}M$.

triethanolamine, linear conversion versus time relationships were obtained. Typical results are shown in Figure 9. The polymerization rates were ascertained by the slopes of the straight lines. The molecular weight (Fig. 9) remained essentially constant with time or per cent polymerization, and, as mentioned previously,[8] they were controlled by a chain transfer process with ethylene glycol. In more concentrated acrylamide solutions (4 and $7M$ in Fig. 9), the molecular weight decreases somewhat with time or per cent polymerization; this could be attributed to monomer depression as the polymerization progressed.

Based on the results depicted in Figure 9 for the polymerization of 1, 2, 4, and $7M$ acrylamide, the following relationships were derived:

$$\text{Rate} \propto [\text{acrylamide}]^{1.2}$$
$$M_w \propto [\text{acrylamide}]^{0.98}$$

In essence, both the polymerization rate and the molecular weight of the polymers are directly proportional to the acrylamide concentration. These results differ from those obtained for similar polymerizations in air, where

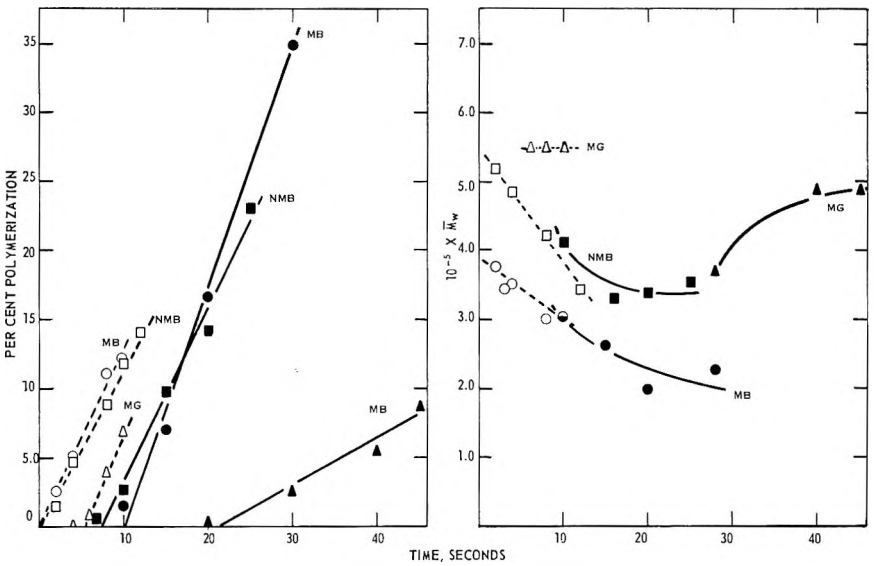

Figure 10

Fig. 10. Comparison of polymerizations of $7M$ acrylamide in ethylene glycol sensitized by different thiazine dyes at [triethanolamine] $= 2.0 \times 10^{-2}M$ [dye] $= 7.0 \times 10^{-5}M$: (——) in air; (- - -) in deaerated systems.

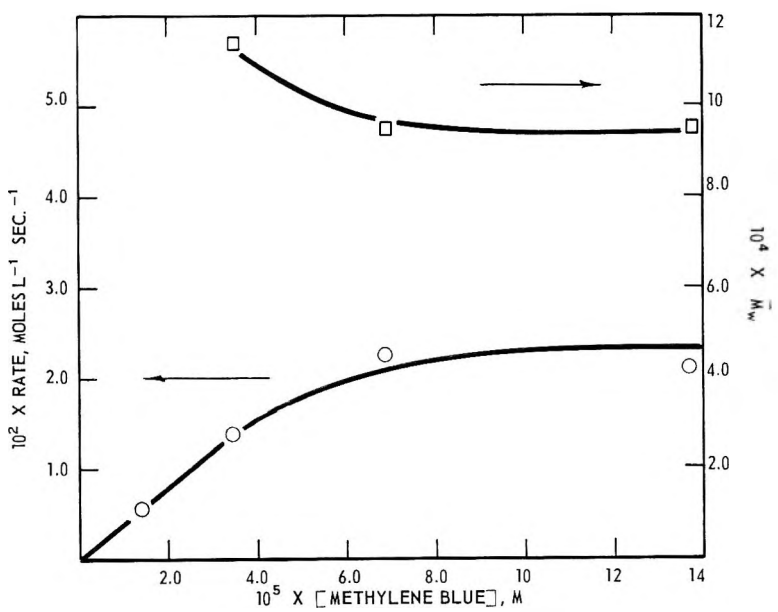

Fig. 11. Polymerization of $2M$ acrylamide at different methylene blue concentrations; [triethanolamine] $= 2.0 \times 10^{-2}M$.

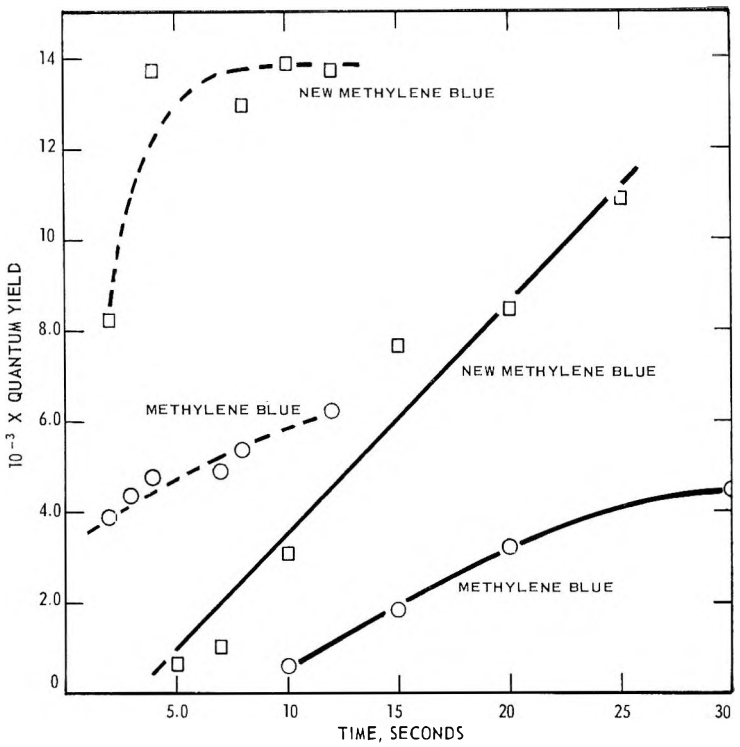

Fig. 12. Comparison of quantum yields for the polymerizations in ethylene glycol at [acrylamide] = $7M$; [triethanolamine] = $2.0 \times 10^{-2}M$ [dye] = $7.0 \times 10^{-5}M$: (——) in air; (- - -) deaerated.

the rate is proportional to the second power of the acrylamide concentration and molecular weight increases with the acrylamide concentration up to $4M$ and gradually thereafter.[8]

Effect of Dye Structure. The polymerizations of $7M$ acrylamide in the presence of $7.0 \times 10^{-5}M$ methylene blue, new methylene blue, and methylene green, respectively, as the sensitizer and in the presence of $2.0 \times 10^{-2}M$ triethanolamine are shown in Figure 10. As was reported previously for the ethylene glycol systems in air,[7] the conversion–time relationships are linear; however, in the present deaerated systems no induction period was observed with methylene blue and new methylene blue N. For convenient comparison, the corresponding polymerizations in air are given in Figure 10 also. Again the results show that the polymerizations are favored in the deaerated systems.

Effect of Dye Concentration. The results for the polymerizations of $2M$ acrylamide in ethylene glycol at methylene blue dye concentrations of 1.38×10^{-5}, 3.44×10^{-5}, 6.88×10^{-5}, and $13.76 \times 10^{-5}M$ are depicted in Figure 11. The change of rates of polymerization and of molecular weights of the polymers as a function of the dye concentration are similar to what have been described previously for the systems in air.[8]

Quantum Yields. A comparison of quantum yields for the polymerizations in ethylene glycol in air and in corresponding deaerated systems with the use of $7.0 \times 10^{-5}M$ methylene blue and new methylene blue N, respectively, in the presence of triethanolamine as sensitizers is shown in Figure 12. Significantly higher quantum yields were obtained in deaerated systems. This is attributed primarily to the elimination of the induction periods in the deaerated systems.

Anaerobic Polymerizations

For comparison with the polymerizations of the above deaerated systems (reduced oxygen) and with systems under ambient atmospheric conditions, some representative results for polymerizations in the absence of oxygen are presented here. The results for $4M$ aqueous acrylamide are given in Table II. In the absence of a reducing agent, no polymerization took place after 180 sec. at pH 5 (ambient pH of the solution) and only a minute amount of polymers was formed in pH 8 buffer. However, in the presence of triethanolamine as the reducing agent, fast polymerization proceeded which was accompanied by the fading of methylene blue. This finding is contrary to what Oster had proposed, that oxygen was essential for the initiation.[1-3]

TABLE II
Anaerobic Polymerization of Aqueous Acrylamide at
[Acrylamide] = $4M$; [Methylene blue] = $7.0 \times 10^{-5}M$

pH of solution	Reducing agent	Irradiation time, sec.	Fading of the dye	Polymerization, %
5 (Ambient)	None	180	None	0
pH 8 buffer	None	180	None	0.31
pH 10.9–11	$2.0 \times 10^{-2}M$ triethanolamine	0[a]	None	0
"	"	70	Completely faded at 60 sec.	21.96

[a] The solution was degassed by three freeze-thaw cycles in the dark. This experiment showed that no polymerization took place during this process.

CONCLUSIONS

It has become evident, based on the above results and discussion, that dye-sensitized photopolymerizations are favored by the removal of oxygen. Higher rates and quantum yields of polymerization are obtained and the polymerization kinetics are altered. Both in aqueous and in ethylene glycol systems, in the essential absence of oxygen, the conversion–time relationship is linear. When dyes with structures like methylene blue and new methylene blue N (methyl substituted methylene blue) are used as the sensitizers there is no induction period for the polymerization. However, when structurally different dyes like methylene green (nitro-substituted methylene blue) or eosin Y are used as the sensitizers, there is an induction period

which is considerably shorter than that for the corresponding polymerization in air.

The above results also suggest that the presence of an appropriate reducing agent is essential. In the absence of an added reducing agent, no polymerization takes place in ethylene glycol and in aqueous systems at pH $\leqslant 7$. At pH >7, when the OH^- ions serve as the reducing agent, polymerizations take place at lower rates compared to systems where a reducing agent is added. Furthermore, the conversion–time relationship is S-shaped instead of linear.

The polymerization is dependent on the nature of the buffer as well as the pH of the solution. Certain buffers, e.g., pH 4 potassium biphthalate buffer, can serve as a retarder for the polymerization. In addition, the effectiveness of the reducing agent is pH-dependent, as is evidenced by the fact that tetrasodium ethylenediamine is more efficient as a reducing agent than triethanolamine at pH <7, while the reverse is true at pH >7.

The strikingly different results obtained for polymerizations sensitized by a combination of a cationic and an anionic dye under ambient atmospheric conditions previously reported[6] and in the present deaerated systems suggest that the initiation mechanism might be different in the two systems.

An important conclusion derived from the anaerobic investigation is that oxygen is not necessary for the initiation. Since it is detrimental to the polymerization, removal of oxygen is desirable.

References

1. Oster, G., *Nature*, **173**, 300 (1954).
2. Oster, G. K., G. Oster, and A. Prati, *J. Am. Chem. Soc.*, **79**, 595 (1957).
3. Oster, G., U. S. Pats. 2,850,445 (1958); 2,857,045 (1959); 3,019,104 (1962); 3,097,096 (1963).
4. Shepp, A., S. Chaberek, and R. MacNeil, *J. Phys. Chem.*, **66**, 2563 (1962).
5. Chen, C. S. H., *J. Polymer Sci.*, **A3**, 1107 (1965).
6. Chen, C. S. H., *J. Polymer Sci.*, **A3**, 1127 (1965).
7. Chen, C. S. H., *J. Polymer Sci.*, **A3**, 1137 (1965).
8. Chen, C. S. H., *J. Polymer Sci.*, **A3**, 1155 (1965).
9. Lewis, G. N., O. Goldschmid, T. T. Magel, and J. Bigeleisen, *J. Am. Chem. Soc.*, **65**, 1150 (1943).
10. Michaelis, L., and S. Granick, *J. Am. Chem. Soc.*, **67**, 1212 (1945).

Résumé

On a étudié la photopolymérisation de l'acrylamide sensibilisée par des colorants thiaziniques et par l'éosine, Y, en milieu aqueux exempt d'air et dans l'éthylène glycol. L'elimination de la majeure partie de l'oxygène dissous produit une augmentation des vitesses et des rendements de polymérisation. On a obtenu des relations linéaires entre le pourcentage de polymérisation et le temps. La période d'induction est soit éliminée soit réduite suivant la structure du colorant utilisé. La vitesse de polymérisation et le poids moléculaire des polymères sont proportionnels à la puissance 1.5 de la concentration en monomère en milieu aqueux et à sa puissance 1 dans l'éthylène glycol. La présence d'un agent réducteur adéquat est essentielle. En absence de réducteur, il n'y a aucune polymérisation ni dans l'éthylène glycol ni en solution aqueuse de pH < 7. A pH >7, les anions hydroxyles jouent le rôle d'espèce réductrice, la polymérisation se

produit à vitesse plus faible que dans un système où un agent réducteur a été ajouté. La polymérisation dépend à la fois de la nature du tampon et du pH de la solution. L'efficacité de l'agent réducteur dépend également du pH. Lors de la polymérisation en solution aqueuse, on n'observe aucune augmentation de vitesse en utilisant une combinaison appropriée d'un colorant cationique et anionique. Les mécanismes d'initiation sont probablement différents pour les systèmes en milieu anaérobique et pour les systèmes dans les conditions atmosphériques normales. Dans les polymérisations où l'oxygène a été complètement éliminé, on a observé une augmentation de vitesse avec le bleu de méthylène et la triéthanolamine comme système sensibilisateur. En absence de triéthanolamine, il y a une polymérisation très lente à pH >7.

Zusammenfassung

Die durch Thiazinfarbstoffe und Eosin Y in entlüfteten wässrigen und Äthylen glycolsystemen sensibilisierte Photopolymerisation von Acrylamid wurde untersucht. Die Entfernung des Hauptteiles des gelösten Sauerstoffs führte zu höheren Polymerisationsgeschwindigkeiten und höheren Quantenausbeuten. Es wurde eine lineare Abhängigkeit des Polymerisationsumsatzes von der Dauer erhalten. Die Induktionsperiode wurde je nach der Struktur des Farbstoffs entweder beseitigt oder herabgesetzt. Die Polymerisationsgeschwindigkeit und das Molekulargewicht des Polymeren war in Wasser der 1,5. Potenz der Monomerkonzentration und in Äthylenglycol der ersten Potenz proportional. Die Anwendung eines geeigneten Reduktionsmittels war wesentlich. Ohne Zusatz eines Reduktionsmittels fand in Äthylenglycol und in wässrigen Lösungen von pH $\leqslant$ 7 keine Polymerisation statt. Bei pH >7 und Anwesenheit von Hydroxyl- oder anderen Anionen war die Polymerisationsgeschwindigkeit niedriger als in Systemen, denen ein Reduktionsmittel zugesetzt wurde. Die Polymerisation zeigte sich sowohl von der Natur des Puffers als auch vom pH der Lösung abhängig. Die Wirksamkeit des Reduktionsmittels war ebenfalls pH-abhängig. Bei Polymerisation in wässrigen Systemen wurde bei Zusatz einer geeignete Kombination eines kationischen und eines anionischen Farbstoffes als Sensibilisator keine Erhöhung der Geschwindigkeit beobachtet. Bei entlüfteten Systemen und bei Systemen mit freiem Luftzutritt bestand wahrscheinlich ein verschiedener Startmechanismus. Bei anaerober Polymerisation mit völligem Sauerstoffausschluss wurden bei gemeinsamer Verwendung von Methylenblau und Äthanolamin als Sensibilisator erhöhte Geschwindigkeiten beobachtet. In Abwesenheit von Triäthanolamin fand bei pH >7 zwar Polymerisation statt, sie war jedoch sehr langsam.

Received October 14, 1964
(Prod. No. 4561A)

JOURNAL OF POLYMER SCIENCE: PART A VOL. 3, PP. 1825–1832 (1965)

Hydrodynamic Behavior of Fully Acetylated Guaran. Test of the Eizner-Ptitsyn Theory for the Semirigid Macromolecule

SHELDON F. KURATH, CHARLES A. SCHMITT, and JOHN J. BACHHUBER, *The Institute of Paper Chemistry, Appleton, Wisconsin*

Synopsis

Previous results on the hydrodynamic and configurational properties of fully acetylated guaran in acetonitrile have been reexamined in light of the recent Eizner-Ptitsyn theory for the intrinsic viscosity of the semirigid macromolecule. Numerical values for the hydrodynamic function arising in the theory were calculated by numerical summation on an electronic computer and are tabulated. The theory is found to remove some of the inconsistencies inherent in earlier hydrodynamic theories and leads to reasonable values of the persistence length and monomeric friction coefficient of guaran acetate. The persistence length calculated from viscosity data was 57.8 A., only slightly lower than the limiting value of 64 A. obtained from light scattering. The ratio of monomeric friction coefficient to solvent viscosity was $\zeta/\eta_0 = 6\pi r_0 = 57.3$ A., from which a value of $r_0 = 3.04$ A. was obtained for the hydrodynamic radius of the monomer unit.

INTRODUCTION

The configuration and hydrodynamic properties of the fully acetylated galactomannan, guaran triacetate[1] (GTA), have been examined in acetonitrile over a range in degree of polymerization from 171 to 12,400. The GTA molecule exhibits a transition from partial to nondraining hydrodynamic behavior while excluded volume effects have been shown to be negligible. Reliable estimates of the polymolecularity of GTA fractions are available so that suitable tests of current hydrodynamic theories are possible.

Recently, Eizner and Ptitsyn[2] have treated the intrinsic viscosity of semirigid macromolecules in light of the intrinsic viscosity equation of Peterlin,[3,4] and the "wormlike" chain of Kratky and Porod.[5] The hydrodynamic behavior of GTA is such that the conditions under which the theory may be applied are fully satisfied. It is the purpose of the present work to test the Eizner-Ptitsyn theory and to comment on the applicability of the theories of Kirkwood and Riseman,[6] Kurata and Yamakawa,[7] and of Hearst.[8]

THE EIZNER-PTITSYN THEORY

According to the theory of Eizner and Ptitsyn, the intrinsic viscosity of the semirigid molecule is given by,

$$[\eta] = \frac{2^{3/2}\Phi_0(b^3/M_0)N^{\chi}(N/\lambda)}{[45(2\pi/3)^{1/2}/32(3 - 2^{1/2})](b/\lambda r_0) + (1/\lambda^{3/2})\varphi(\lambda,N)N^{1/2}} \quad (1)$$

where $[\eta]$ is the intrinsic viscosity in milliliters per gram, Φ_0 is the Flory coefficient whose limiting value is 2.86×10^{23} mole^{-1} at high molecular weight,[2] N is the degree of polymerization, r_0 is the hydrodynamic radius of the monomer unit, M_0 its molecular weight, and $\lambda = a/b$. The persistence length of the Kratky-Porod wormlike chain is a and b is the length of the monomer unit. The hydrodynamic radius is related to the monomeric friction coefficient ζ by $r_0 = \zeta/6\pi\eta_0$, where η_0 is the solvent viscosity. The function $\chi(N/\lambda)$ is a geometric factor and $\varphi(N,\lambda)$ is a complicated hydrodynamic function.

The Flory coefficient is defined by[9]

$$\Phi = [\eta]M/(6\bar{S}^2)^{3/2} \quad (2)$$

where $(\bar{S}^{-2})$ is the mean-square radius of gyration of a polymer molecule with molecular weight M. According to the Eizner-Ptitsyn theory, the Flory coefficient is given by

$$\Phi = \frac{\Phi_0}{\{\varphi_{(\lambda,N)} + [45(2\pi/3)^{1/2}/32(3 - 2^{1/2})](b/r_0)(\lambda/N)^{1/2}\}\chi^{1/2}(N/\lambda)} \quad (3)$$

CALCULATION OF GEOMETRIC AND HYDRODYNAMIC FUNCTIONS

The geometric function is given by

$$\chi(Z) = 1 - (3/Z^3)[Z^2 - 2(Z - 1 + e^{-Z})] \quad (4)$$

where $Z = N/\lambda$. The corresponding hydrodynamic function is given by,

$$\varphi_{(\lambda,N)} = \frac{15(\pi/3)^{1/2}}{4(3 - 2^{1/4})} \cdot \frac{1}{\lambda^{1/2}N^{5/2}}$$
$$\times \left\{ \sum_{k=1}^{N-1} \frac{(k^2 + k - Nk - 2N)\psi(x)}{[x - 1 + \exp\{-x\}]^{1/2}} + \sum_{k=1}^{(N/2)-1} \frac{[(N^2/2) - 2k^2 + N]\psi(x)}{[x - 1 + \exp\{-x\}]^{1/2}} \right\} \quad (5)$$

where

$$\psi(x) = 0.4270 + 0.5730$$
$$\times \{[45x^2 + 156x + 214 - 54(4 + x)e^{-x} + 2e^{-3x}]/27(x - 1 + e^{-x})^2\} \quad (6)$$

and $x = k/\lambda$.

The geometric and hydrodynamic functions have been calculated by Eizner and Ptitsyn and are presented in graphical form by these authors.[2]

Unfortunately, the numerical results of their calculations are not given, so that their graphs cannot be easily reproduced.

The geometric function is relatively easy to calculate. The hydrodynamic function, on the other hand, must be calculated on an electronic computer. We have, therefore, recalculated values of the hydrodynamic

TABLE I
The Function $\varphi(\lambda,N)$ from the Eizner-Ptitsyn Theory for the Intrinsic Viscosity of Semirigid Molecules[a]

N	$\lambda = 1$	$\lambda = 5$	$\lambda = 10$	$\lambda = 15$	$\lambda = 20$	$\lambda = 30$	$\lambda = 50$	$\lambda = 100$
10	—	—	0.349	0.460	0.550	0.695	0.920	1.324
16	0.158	0.690	1.056	1.323	1.544	1.910	2.484	3.532
26	0.372	0.962	1.431	1.781	2.071	2.554	3.315	4.704
40	0.508	1.067	1.566	1.944	2.261	2.786	3.613	5.125
64	0.620	1.101	1.581	1.959	2.277	2.807	3.641	5.165
100	0.700	1.095	1.525	1.878	2.181	2.689	3.491	4.954
160	0.766	1.075	1.435	1.746	2.018	2.484	3.227	4.584
250	0.814	1.056	1.349	1.611	1.846	2.258	2.928	4.164
400	0.854	1.039	1.270	1.480	1.674	2.020	2.601	3.697
640		1.026	1.206		1.526	1.808	2.293	
1,000	—	1.018	1.159	—	1.413	1.639	2.036	
1,600	—	1.012	1.121	—	1.318	1.496	1.811	
2,500	—	1.008	1.093	—	1.248	1.389	1.639	
4,000	—	1.005	1.071	—	1.192	1.301	1.496	
6,400	—	1.003	1.055	—	1.148	1.233	1.386	
10,000	—	1.002	1.043	—	1.117		1.304	

[a] Values calculated from eqs. (5) and (6).

function from eqs. (5) and (6) by numerical summation on an IBM 1620 computer. Fortran II programming was used to avoid truncation errors. The results of the calculations are given in Table I where values of the hydrodynamic function are given for selected values of N and λ.

EXPERIMENTAL RESULTS

Intrinsic Viscosity and Light Scattering

The intrinsic viscosity and light-scattering results given in Table II have been reported previously.[1] The intrinsic viscosities are the result of measurements conducted in a capillary viscometer of the Ubbelohde type. Corrections for non-Newtonian flow have been applied where necessary. Values for the weight-average degree of polymerization were calculated from light-scattering molecular weights obtained in a Brice-Phoenix light-scattering photometer. The values are based on an average monomer molecular weight of 432.

The polymolecularity of the GTA fractions has been estimated from osmotic pressure and ultracentrifuge measurements. The results are expressed in terms of the Zimm-Schulz[10] parameter h and the number-

TABLE II
Experimental Results and Calculated Hydrodynamic Parameters for Guaran Triacetate in Acetonitrile at 25°C.

Fraction	$\bar{N}_w$	$[\eta]$, ml./g.	h	q_0	$\bar{S}^2 \times 10^{-4}$, A.^{2} [a]	$\Phi \times 10^{-23}$, mole^{-1}
2A	12,400	945	4.00	1.35	147	2.61
2B	11,200	912	4.00	1.35	133	2.66
3	7,640	703	3.03	1.44	94.2	2.49
4	6,200	678	5.10	1.28	71.3	2.62
2C	4,770	560	4.00	1.35	56.4	2.50
5	1,970	387	12.4	1.13	20.7	2 69
6	764	179	33.3	1.04	7.47	2.05
7	532	116	45.7	1.03	5.07	1.64
8	171	44	11.1	1.14	1.54	1.32

[a] Calculated from eq. (11) for a persistence length of a = 57.8 A.

average and z-average degrees of polymerization may be calculated from the relation

$$h/\bar{N}_n = (h + 1)/\bar{N}_w = (h + 2)/\bar{N}_z \tag{7}$$

where $\bar{N}_n$, $\bar{N}_w$, and $\bar{N}_z$ are, respectively, the number-, weight-, and z-average degrees of polymerization.

Molecular Parameters from Intrinsic Viscosity

In treating intrinsic viscosity data, Eizner and Ptitsyn rearrange eq. (1) to yield,

$$2^{3/2}\Phi_0 \frac{b^3}{M_0} \frac{N}{[\eta]} \chi\left(\frac{N}{\lambda}\right) = \left(\frac{2\pi}{3}\right)^{1/2} \frac{45}{32(3 - 2^{1/2})} \frac{b}{\lambda r_0} + \frac{1}{\lambda^{3/2}} \varphi\left(\frac{\lambda}{N}\right) N^{1/2} \tag{8}$$

which is of the form, $Y = A + BX$. A plot of $Y = 2^{3/2}\Phi_0(b^3/M_0)(N/[\eta])\chi(N/\lambda)$ versus $X = \varphi(\lambda,N)N^{1/2}$ should be a straight line, providing an appropriate value of λ is used. An initial value of λ_i was assumed, and trial values of χ and φ were determined as a function of the known weight-average degree of polymerization. Values of the geometric and hydrodynamic functions were obtained from plots of $\chi(Z)$ versus Z and $\varphi(\lambda,N)$ versus N, respectively. A final value of λ_f was then calculated from a least-squares treatment of the data according to eq. (8). The procedure was repeated several times, and a correct value of λ was determined from the intersection of the curve relating λ_i to λ_f with the straight line, $\lambda_i = \lambda_f$.

The final results are shown in Figure 1 for the correct value of λ = 11.2 based on a value of 5.15 A. for the length b of the monomer unit. The intrinsic viscosity is correlated with the weight-average degree of polymerization, since this average is closer to the viscosity-average molecular weight and the correlation is less sensitive to fractionation efficiency than one based on the number-average.[11] The straight line as determined by the method of least squares is given by $Y = 0.194 + 0.0266X$. The

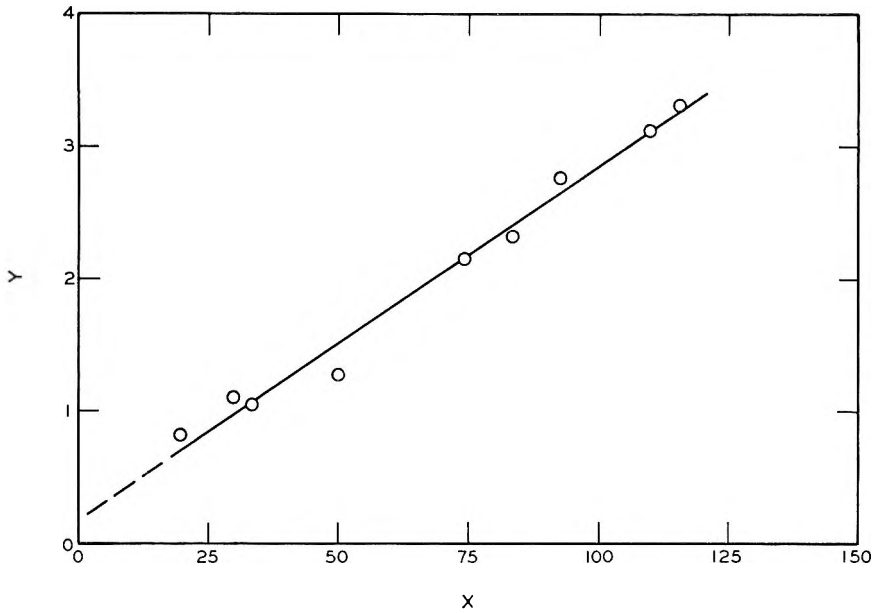

Fig. 1. Intrinsic viscosity data for guaran triacetate in acetonitrile treated according to the Eizner-Ptitsyn theory for the semirigid macromolecule. Points and curve based on $\lambda = 11.2$.

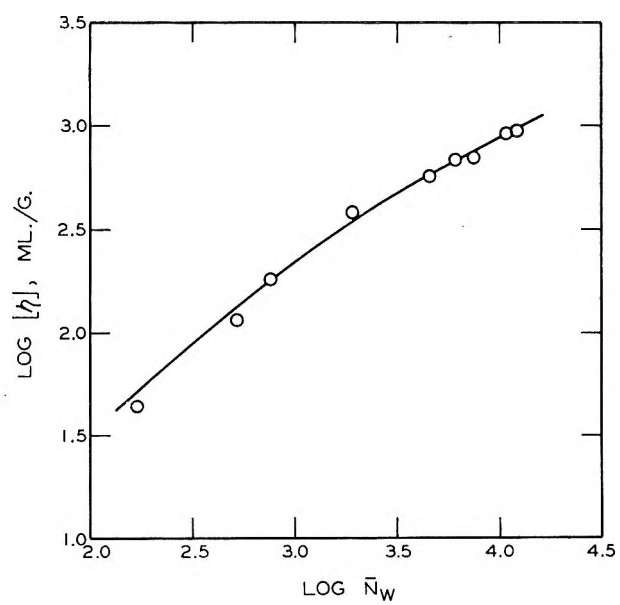

Fig. 2. Intrinsic viscosity as a function of weight-average degree of polymerization for guaran triacetate in acetonitrile: (O) experimental data; (——) theoretical Eizner-Ptitsyn curve calculated from eq. (1).

persistence length a obtained from λ is 57.8 A., which is only slightly lower than the limiting value of 64 A. obtained from light scattering.[1] A value of 3.04 A. is obtained for the radius of the monomer unit r_0, and the ratio $\zeta/\eta_0 = 6\pi r_0$ is 57.3 A.

Since all important parameters are known, eq. (1) may be used to calculate the dependence of intrinsic viscosity on degree of polymerization as shown in Figure 2. The circles represent experimental data and the solid line represents the intrinsic viscosity calculated from eq. (1). It is apparent that the agreement between theory and experiment is excellent.

The Flory Coefficient

The Eizner-Ptitsyn theory can also be used to predict the dependence of the Flory coefficient on degree of polymerization according to eq. (3). The Flory coefficient may also be calculated from experimental data by using the relation[12]

$$\Phi = q_0[\eta]\bar{M}_w/(6\overline{S_z^2})^{3/2} \tag{9}$$

where $\bar{M}_w$ is the weight-average molecular weight, $\overline{S_z^2}$ is the z-average mean-square radius of gyration, and q_0 is a factor to correct for sample polymolecularity. For a distribution of the Zimm-Schulz type, q_0 is given by[12]

$$q_0 = (h + 2)^{3/2}\Gamma(h + 2)/(h + 1)^2\Gamma(h + 1.5). \tag{10}$$

Since the persistence length of the GTA molecule is known from hydrodynamic measurements, the radius of gyration may be calculated[13] from

$$(\overline{S_z^2}) = a^2[(\bar{N}_z b/3a) - 1 + (2a/\bar{N}_w b)(1 - (a/\bar{N}_n b))]. \tag{11}$$

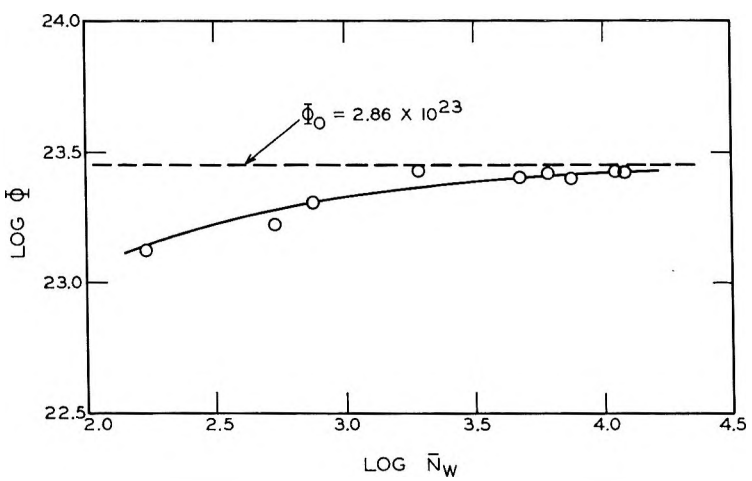

Fig. 3. The Flory coefficient as a function of weight-average degree of polymerization for guaran triacetate in acetonitrile: (O) experimental data; (——) theoretical Eizner-Ptitsyn curve calculated from eq. (3).

Values of the Flory coefficient calculated from experimental data are given in Table II. It should be noted from the magnitude of q_0 that appreciable heterogeneity corrections are required.

The dependence of the Flory coefficient on degree of polymerization is shown in Figure 3. The circles represent values calculated on the basis of eqs. (9), (10), and (11) and experimental data, while the solid line represents the theoretical curve calculated from eq. (3). Here again the agreement between theory and experiment is good.

DISCUSSION

A number of hydrodynamic theories dealing with the intrinsic viscosity of high polymers have been tested in the course of the present investigation. The excluded volume theory of Kurata and Yamakawa[7] has been used by Koleske and Kurath[1] in their analysis of the hydrodynamic behavior of GTA. In their work, excluded volume effects were shown to be unimportant, so that the theoretical equations of the Kurata-Yamakawa theory reduce to those of Kirkwood and Riseman.[6] More recently, Hearst[8] has modified the theory of Zimm[14] to determine the effect of partial draining on the viscosity of flexible macromolecules.

All of these theories were considered in the present investigation and while they predict the qualitative behavior of the dependence of intrinsic viscosity and Flory coefficient on degree of polymerization, they fail in a quantitative sense. For example, at high degrees of polymerization where $[\eta] \sim \bar{N}_w^{1/2}$, the Kirkwood-Riseman theory leads to a value of 23.3 A. for the effective bond length.[1] This requires, however, that the viscosity function, $xF(x)$, in the theory reach its asymptotic limit of 1.259, and this in turn requires that the ratio ζ/η_0 be assigned an unusually large value of the order of 500 A.

Reasonable values of ζ/η_0 can be obtained from the Kirkwood-Riseman theory by following the calculational procedure of Marrinan and Hermans.[15] From light-scattering measurements the radius of gyration of GTA can be represented by $S = 1.13\ M^{0.462}$ and if the revised values[7] for $xF(x)$ are represented by $xF(x) = 0.666x/(1 + 0.52x)$ the Marrinan-Hermans procedure leads to a value of 18.8 A. for ζ/η_0. This is, unfortunately, incompatible with the value of 23.3 A. obtained for the effective bond lengths at high molecular weights. A similar situation arises when the Marrinan-Hermans procedure is applied to the Hearst extension of the Zimm theory.

The Eizner-Ptitsyn theory appears to be free from this difficulty and leads to a reasonable value for the hydrodynamic radius of a monomer unit and the persistence length.

We are indebted to Dr. Julia Stapinski for translating the work of Eizner and Ptitsyn from the original Russian.

References

1. Koleske, J. V., and S. F. Kurath, *J. Polymer Sci.*, **A2**, 4123 (1964).
2. Eizner, Yu. E., and O. B. Ptitsyn, *Vysokomol. Soedin.*, **4**, 1725 (1962).
3. Peterlin, A., *J. Polymer Sci.*, **5**, 473 (1950).
4. Peterlin, A., *J. Chem. Phys.*, **33**, 1799 (1960).
5. Kratky, O., and G. Porod, *Rec. Trav. Chim.*, **68**, 1106 (1949).
6. Kirkwood, J. G., and J. Riseman, *J. Chem. Phys.*, **16**, 565 (1948).
7. Kurata, M., and H. Yamakawa, *J. Chem. Phys.*, **29**, 311 (1958).
8. Hearst, J. E., *J. Chem. Phys.*, **37**, 2547 (1962).
9. Flory, P. J., and T. G Fox, Jr., *J. Am. Chem. Soc.*, **73**, 1904 (1951).
10. Schulz, G. V., *Z. Physik. Chem.*, **B43**, 25 (1939).
11. Flory, P. J., *Principles of Polymer Chemistry*, Cornell Univ. Press, Ithaca, N. Y., 1953, p. 314.
12. Krigbaum, W. R., and L. H. Sperling, *J. Phys. Chem.*, **64**, 99 (1960).
13. Hunt, M. L., S. Newman, H. A. Scheraga, and P. J. Flory, *J. Phys. Chem.*, **60**, 1278 (1956).
14. Zimm, B. H., *J. Chem. Phys.*, **24**, 269 (1956).
15. Marrinan, H. J., and J. J. Hermans, *J. Phys. Chem.*, **65**, 385 (1961).

Résumé

Des résultats antérieurs sur les propriétés hydrodynamiques et configurationnelles du guarane peracétylé dans l'acétonitrile ont été réexaminés du point de vue de la théorie de Eizner-Ptitsyn relative à la viscosité intrinsèque des macromolécules semirigides. Des valeurs numériques pour la fonction hydrodynamique de la théorie ont été calculées par sommation numérique à l'aide d'une machine à calculer électronique et ont été mises en tableau. La théorie ulève certaines incohérences inhérentes aux théories hydrodynamiques antérieures et donne des valeurs raisonnables de la longueur de persistance et du coefficient de friction monomérique de l'acétate de guarane. La longueur de persistance calculée à partir des résultats viscosimétriques est de 57.8 A, (légèrement inférieure à la valeur limite de 64 A. obtenue par diffusion lumineuse. Le rapport entre le coefficient de friction monomérique et la viscosité du solvant est $\zeta/\eta_0 = 6\pi r_0 = 57.3$ A., dont on déduit une valeur $r_0 = 3.04$ A. pour le rayon hydrodynamique de l'unité monomérique.

Zusammenfassung

Frühere Ergebnisse über die hydrodynamischen und Konfigurationseigenschaften von voll acetyliertem Guaran in Acetonitril wurde im Lichte der neuen Theorie von Eizner-Ptitsyn für die Viskositätszahl halbstarrer Makromoleküle überprüft. Numerische Werte für die in der Theorie auftretende hydrodynamische Funktion wurden durch numerische Summation auf einem elektronischen Computer berechnet und tabelliert. Die Theorie kann einige bei früheren hydrodynamischen Theorien auftretende Unstimmigkeiten beseitigen und führt zu vernünftigen Werten für die Persistenzlänge und den Monomerreibungskoeffizienten von Guaranacetat. Die aus Viskositätsdaten berechnete Persistenziange war mit 57,8 A, nur wenig niedriger als der aus der Lichtstreuung erhaltene Grenzwert von 64 A. Das Verhältnis von Monomerreibungskoeffizienten zur Lösungsmittelviskosität $\zeta/\eta = 6\pi r_0 = 57,3$ A., woraus für den hydrodynamischen Radius des Monomerbausteins ein Wert $r_0 = 3,04$ A. erhalten wurde.

Received September 3, 1964
Revised November 12, 1964
(Prod. No. 4562A)

JOURNAL OF POLYMER SCIENCE: PART A VOL. 3, PP. 1833–1843 (1965)

Macroreticular Redox Polymers. I. Hydroquinone–Quinone Redox Polymers

KENNETH A. KUN, *Research Laboratories, Rohm & Haas Co., Philadelphia, Pennsylvania*

Synopsis

Redox polymers based upon the hydroquinone–quinone redox system are prepared by the addition of hydroquinone and hydroquinone derivatives to preformed polystyrene matrices. Conventional gel and macroreticular styrene–divinylbenzene copolymers were chloromethylated with chloromethyl ether by using a Friedel-Crafts catalyst and the reaction products were treated, by a second Friedel-Crafts reaction, with hydroquinone, benzoquinone, or alkyl homologs of these materials or with the dimethyl ether or the diacetoxy derivatives of hydroquinone to give polymeric vinylbenzylhydroquinones. Macroreticular redox polymers show greater reactivity and better stability than resins having redox systems on conventional gel-type matrices. These redox polymers convert iron III to iron II, cerium IV to cerium III, iodine to iodide, and remove dissolved oxygen and peroxides from aqueous and organic liquids when the resins are in the reduced form. When in the oxidized form, the resins are reduced with titanium III, sodium sulfite, sodium bisulfite, sodium dithionite, sulfur dioxide, and sodium borohydride.

INTRODUCTION

A number of synthetic procedures exist for the preparation of high molecular weight polymers having functional groups that may be oxidized and reduced reversibly.[1] These methods involve either the polymerization of monomers containing redox systems or the addition of redox systems to preformed matrices. Synthesis of specific monomers for specific redox polymers has the advantages that the composition and structure of the products are known with increased certainty and that the products are readily characterized. Preparation and polymerization of monomers, however, are limited by relatively low yields of products and the structural properties of the polymers are limited by the polymerization methods available for monomers containing redox groups. Addition of redox systems to preformed matrices, by contrast, allows flexibility in the physical properties of polymers that cannot be readily obtained by other synthetic methods. Oxidation–reduction or redox polymers have been prepared by the addition of redox systems to polymeric matrices by irreversible chemical bonding,[2–15] by the sorption of redox systems on polyelectrolytes,[16–23] and by precipitating redox systems on inert matrices.[24,25]

Though a large variety of redox systems can be readily placed on insoluble matrices by sorption and precipitation techniques, the adducts are not irreversibly bound to the matrices. By use of solvents for the precipitates or by displacement from the polyelectrolytes, adducts containing redox systems can be readily removed from the resin matrices. Thus, redox systems that can be leached from the redox polymers results both in the loss of redox capacity and the contamination of the solutions in contact with the resin. Redox systems bound to polymeric structures by irreversible chemical reactions, however, prevent the loss of redox activity by solvolysis or leaching. Examples of this type of bound redox systems are described in the literature. Sansoni prepared redox polymers by the addition of triphenylmethane dyes, ferrocene, and *p*-phenylenediamine to polystyrene using a poly(styrene diazonium salt) intermediate.[2,3] Rao, Mukerjee, and Palit,[4] using the poly(styrene diazonium intermediate), added the hydroquinone redox system to polystyrene, while Gregor, Dolar, and Hoeschele[5] used this intermediate to prepare polythiolstyrene which contains the sulfhydryl–disulfide redox system. Polyvinylbenzylmercaptan, a homolog of polythiolstyrene, was obtained by Parrish[8] and Trostyanskaya and Tevlina[9] by treating chloromethylated polystyrene with either sodium sulfide or thiourea followed by saponification. Etienne and Izoret[10] and Izoret[11,12] added the anthraquinone redox system to preformed matrices by forming the acetal of 2-formylanthraquinone with poly(vinyl alcohol), esters from anthraquinonyl-2-carboxylic acid or anthraquinonyl-2-sulfonic acid with poly(vinyl alcohol), and ethers from 2-chloromethyl- or 2-hydroxymethylanthraquinone.

A preliminary investigation of crosslinked redox polymers was made where the polymeric matrices are of the conventional gel type and various macroreticular type structures. By using the polymerization technique described by Meitzner and Oline,[26] i.e., a suspension polymerization with styrene and divinylbenzene in the presence of a substance that is a good solvent for the monomers and a poor swelling agent for the copolymer, crosslinked resins are produced that contain a significant nongel porosity in addition to the normal gel porosity. Chemical and physical characteristics of gel and macroreticular ion exchange resins are compared in the literature[27–29] and, therefore, will not be discussed here. By combining a convenient, high-yield synthesis procedure with the stability and increased reactivity of a macroreticular structure, redox polymers are obtained that approach the reactivity of commercial ion-exchange resins.

DISCUSSION AND RESULTS

Synthesis of Redox Polymers

The copolymers used for the preformed matrices were of both the conventional gel-type and the macroreticular structure. Synthesis of styrene–divinylbenzene gel-type beads are described by D'Alelio,[30] while a polymerization technique to produce macroreticular beads is described by

Meitzner and Oline.[26] Chloromethylation of the resulting poly(styrene–divinylbenzene) beads by means of the procedure of McBurney[31] yields the corresponding poly(vinylbenzyl chlorides), I. The chloromethylated poly(styrene–divinylbenzene) copolymers (I) are used as the reactive preformed matrices for the synthesis of gel-type and macroreticular redox polymers.

By using the standard alkylation conditions for a Friedel-Crafts reaction, hydroquinone, benzoquinone, 1,4-dimethoxybenzene, and 1,4-diacetoxybenzene may be placed on the chloromethylated polystyrene resins. The preparative steps are summarized in eq. (1). Addition of an ethylene dichloride solution of 1,4-diacetoxybenzene (hydroquinone diacetate) or 1,4-dimethoxybenzene (hydroquinone dimethyl ether) to crosslinked chloromethylated polystyrene suspended in ethylene dichloride gives the corresponding polyvinylbenzyl derivative (II) after refluxing the mixture in the presence of anhydrous zinc chloride. The addition reaction can be easily followed by the evolution of hydrogen chloride. Acid cleavage of the methoxyl groups of polyvinylbenzyldimethoxybenzene (IIa) with 47% aqueous hydriodic acid or hydrolysis of acetoxyl groups of IIb, polyvinylbenzyldiacetoxybenzene, gives the desired polyvinylbenzylhydroquinone (III). The resulting polymer can be oxidized to polyvinylbenzylbenzoquinone (IV), which in turn, may be reduced to III again.

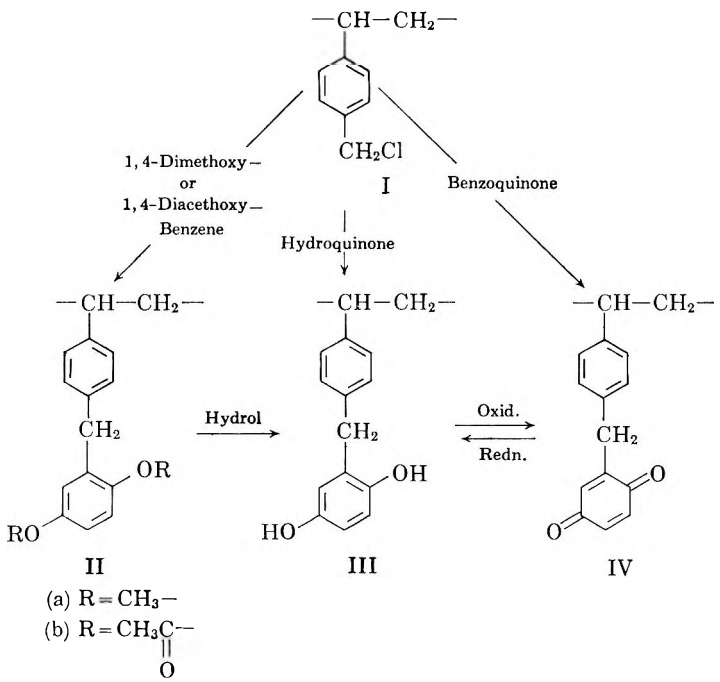

(1)

Benzoquinone addition to the chloromethylated beads gives resins having redox properties similar to the dimethoxy- or the diacetoxybenzene adducts with the protecting groups removed. This reaction, however, also gives

highly colored side products which require extensive hot alcoholic extractions for complete removal. Reaction yields, based on the chloride content of the resins, are approximately 90% for the protected hydroquinone adducts and about 65% for the benzoquinone adducts. Modifications in reaction conditions were made with reaction times from 2 to 18 hr., quinone to chloromethylated polystyrene concentrations varied from 1.10 to 3.30 based on moles of reactive "unit" groups in the polymer, and the mode of addition of quinone varied from a single addition at the start of the reaction to a series of benzoquinone additions throughout the course of the reaction. Results of the reaction condition modifications indicate the reaction time may be cut to approximately 4 hr. Large excesses of benzoquinone did not appreciably increase the redox capacity of the resins, but a series of benzoquinone additions during the reaction increases the concentration of redox groups found on the resin. The highly colored side products were still present in all the reaction mixtures.

Preliminary work at the start of this study showed that the reaction of hydroquinone with chloromethylated poly(styrene–divinylbenzene) beads gave a product with redox properties. The redox capacities obtained, however, were very low compared to the values obtained from cleaved dimethoxybenzene, hydrolyzed diacetoxybenzene or the benzoquinone adducts, i.e., capacities less than 0.5 meq./g. (dry) were obtained when hydroquinone is used with ethylene dichloride. Replacing ethylene dichloride, a poor solvent for hydroquinone, with dioxane, a good solvent for hydroquinone, materials having redox capacities of approximately 4–5 meq./g. of dry resin were obtained. The possibility of free hydroquinone trapped in the polymeric matrix was eliminated by extractions of the resin with hot ethanol in a Soxhlet extractor for 48 hr. Hydroquinone additions, in dioxane, were run without the Friedel-Crafts catalyst in analogy to the condensation of *tert*-butyl chloride with phenol.* The uncatalyzed reaction did yield a resin having a redox capacity though it was only about one-tenth the capacity of the catalyzed control material.

Direct addition of hydroquinone to chloromethylated poly(styrene–divinylbenzene) beads is successful if a good solvent for hydroquinone is used and if the solvent–hydroquinone system is compatible with the anhydrous zinc chloride catalyst. Reaction time was reduced to 5 hr., at reflux temperature, without a decrease in the redox capacity of the product. Checking the reproducibility of the reaction under identical conditions gave virtually identical materials with an average redox capacity of 5.13 meq./g. of dry resin with ceric ion. A dimethoxybenzene adduct with the methoxyl groups cleaved by hydriodic acid, that was used as a control, had a redox capacity of 3.85 meq./g. of dry resin with ceric ion and a capacity of 3.3 meq./g. of resin with an aqueous iodine solution.

Oxidation of a hydroquinone to the quinone can cause dimerization. Di- and polyquinones have been prepared by the oxidation of the corresponding hydroquinones.[32] Oxidation of 1,4-dimethoxy-2-substituted

* This analogy was suggested by Dr. David Curtin.

benzenes with chromic oxide yields diquinones,[33] and diquinones are also produced in the oxidation of 2-methoxy-6-*n*-propylhydroquinone.[34] Hydroquinone dimethyl ether and the dimethyl ethers of 2-methyl- and 2,5-dimethylhydroquinone were oxidized with excess ceric sulfate to yield dimeric quinones.[35] Dimers could not be isolated from the oxidation of 2,3,4-trimethyl- and 2,3,4,6-tetramethylhydroquinone dimethyl ethers.[35] This type of dimerization can be completely suppressed by three alkyl substituents on the hydroquinone ring, but it still persists when two groups are present.

Evaluation of redox polymers, in most cases, have been in neutral or acidic solutions. This is due to the fact that the oxidized form of the hydroquinone redox resin—the quinone form—is unstable under basic conditions. In many of the more desirable fields of application for redox polymers there are increased rates of reactivity at pH levels greater than seven, e.g., in oxygen removal from water or the formation of hydrogen peroxide. Quinone stability, however, increases in basic solutions as the ring hydrogens are replaced with other substituents; the fully substituted quinones are quite stable.[36,37]

The direct synthesis of methylated polyvinylhydroquinones requires the use of monomers obtained by tedious synthetic routes.[36,37] Therefore, as part of this study the addition reactions with methyl-substituted dimethoxybenzene, benzoquinone, and hydroquinone to chloromethylated polystyrene copolymers were run. By using the reaction conditions for the addition of dimethoxybenzene, dimethoxytoluene was added to the chloromethylated polystyrene beads. Cleavage of the protecting ether groups with hydriodic acid gave a material having a good redox capacity. Similarly, by using the conditions of the benzoquinone reaction, the 2,5-dimethylbenzoquinone and 2,3,5-trimethylbenzoquinone addition products were formed. Though the methylated benzoquinone resins showed redox properties, the rate of attainment of the maximum redox capacities were not as good as the unsubstituted benzoquinone analog. Treatment of 2,5-dimethylhydroquinone, in dioxane, with the chloromethylated polystyrene copolymers, also yields a redox polymer having good redox capacities. Thus, hydroquinone–quinone redox polymers may be readily obtained by using quinones and protected or unprotected hydroquinones in a Friedel-Crafts reaction with chloromethylated poly(styrene–divinylbenzene) copolymers.

Matrices for the Redox Resins

Four different physical structures of the poly(styrene–divinylbenzene) copolymers were used as matrices for the hydroquinone–quinone redox system. Three were macroreticular, while the fourth was a conventional gel-type matrix. The copolymers, in bead form, varied in crosslinker content, porosity, and surface area. Crosslinker concentrations varied from 3 to 20% divinylbenzene, surface areas of the resins ranged from negligible for the gel resin up to 65 $m.^2/g.$ for the macroreticular resins,

and porosities were negligible for the gel resin to 0.45 cc. of pores/cc. of dry resin. Table I gives the chemical composition and the physical structure of the copolymer used as matrices for the redox systems.

TABLE I
Composition and Physical Properties of Bead Matrices

	Compositions, %		Porosity, %	Surface area, m.²/g.
	Styrene	Divinylbenzene		
Matrix 1	97	3	None	None
Matrix 2	80	20	45	50
Matrix 3	80	20	30	65
Matrix 4	97	3	25	20

Redox Properties of the Resins

The hydroquinone or reduced form of the resins can reduce molecular oxygen, iodine to iodide, cerium IV to cerium III, and iron III to iron II, while the quinone or oxidized form can oxidize titanium II to titanium III and iodide to iodine. The oxidized form of the resin can also be reduced with sulfurous acid, sodium bisulfite, sodium sulfite, and sodium borohydride. Both columnar and batchwise reductions, with the hydroquinone form of the redox resins, indicated that the macroreticular structures were more reactive than the conventional gel structure. Figures 1 and 2 indicate the comparative rates of reaction and the breakthrough curves, respectively, of some hydroquinone–quinone redox resins, however, de-

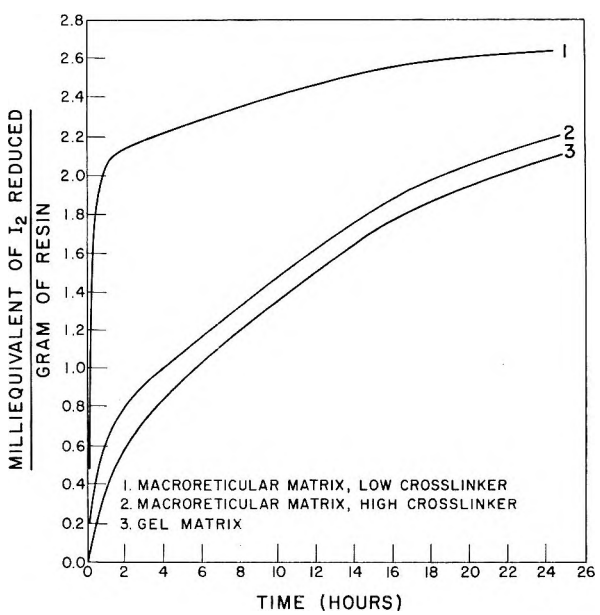

Fig. 1. Comparative rates of reaction of some hydroquinone–quinone redox resins.

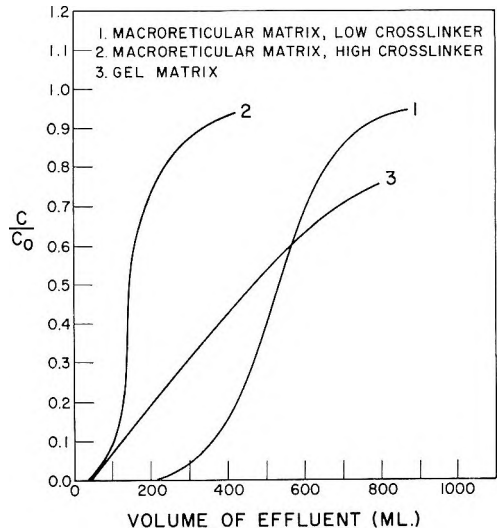

Fig. 2. Break-through curves of aqueous iodine with some redox resins (using 10 ml. of resin).

tailed discussions of the test methods, redox capacities, reaction rates, and equilibria of these materials will be presented in a forthcoming publication.

Applications

Areas of utility for redox polymers have been the subject of many discussions (summarized by Cassidy and Kun[1]); however, the lack of easily prepared materials hampered investigations into fields of application.

One area of interest is the removal of oxygen from water and organic

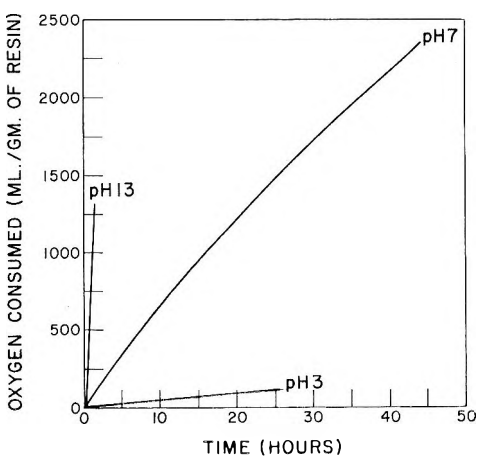

Fig. 3. Rate of oxygen removal from water by using a macroreticular hydroquinone redox polymer.

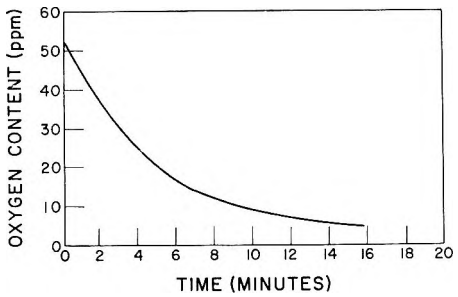

Fig. 4. Oxygen removal from ethyl acrylate with a macroreticular redox polymer.

liquids. The corrosive effect of dissolved oxygen in boiler water requires the removal of oxygen to near-zero levels. Manecke[38,39] and Abrams and Brestlin[40] used redox polymers for oxygen removal from water. Redox polymers on matrix 4 were evaluated by use of the Warburg technique for oxygen uptake. Figure 3 shows the rate of removal of oxygen, dissolved in water, under acidic, neutral, and basic conditions. The rate of oxygen consumption increases with an increase in pH. At a pH of 13, 13,000 cc. of oxygen was removed per gram of dry resin in 1 hr., while at a pH of 2.9 only 110 cc. oxygen/g./hr. was removed.

Oxygen may also be removed from organic liquids by redox polymers. By using a standard polarographic method for the determination of oxygen in acrylic monomers, oxygen was removed from methyl and ethyl acrylate. Figure 4 shows the rate of oxygen removal from ethyl acrylate with the macroreticular redox polymers having matrix 4. These initial results seem to indicate the oxygen content of monomers may be reduced to less than 5 ppm in approximately 15 min. A more detailed discussion of the applications of redox polymers will be the subject of a forthcoming publication.

EXPERIMENTAL

Preparation of Crosslinked Polyvinylbenzyl-2′,5′-dimethoxybenzene

To a one-liter three-necked round-bottomed flask, fitted with a stirrer, reflux condenser, and thermometer, are added 152.6 g. (1.0 mole based on a chloromethylstyryl unit) of chloromethylated poly(styrene–divinylbenzene), 200 ml. of ethylene dichloride, and 152.0 g. (1.1 mole) of *p*-dimethoxybenzene. The mixture is stirred for several minutes and 2.7 g. (0.02 mole) of zinc chloride (freshly fused powder) added. With continuous stirring, heating at reflux temperature, 90°C., is continued for 16 hr. At the beginning of the heating period, the beads take on a dark brown color and retain this color throughout the entire reflux period. Hydrogen chloride is evolved. At the end of the reflux period, the ethylene dichloride is distilled from the mixture. Unreacted dimethoxybenzene codistills with the ethylene dichloride. As ethylene dichloride is removed, water is added to the reaction flask; the volume of liquid in the distillation flask

being kept constant. The distillation is continued until only water is found in the distillate. On cooling, the beads are filtered and may be dried or carried directly to the next step.

Acid Cleavage of the Dimethoxybenzene Adduct to give Polyvinylbenzylhydroquinone

To the beads from the above reaction is added 350 g. of 47% hydriodic acid. This mixture is stirred and heated at reflux temperature, 110°C., for 16 hr. The beads are drained of acid, washed with deionized water until the washings are neutral to pH paper, and then dried to constant weight. This reaction gave 196.6 g. of crosslinked polyvinylbenzylhydroquinone redox polymer.

Preparation of Polyvinylbenzylbenzoquinone

To a one-liter three-necked round-bottomed flask, fitted with a stirrer, reflux condenser, and thermometer, are added 50 g. of chloromethylated poly(styrene–divinylbenzene) (0.33 mole based on a chloromethyl styryl unit) and 80 g. (0.74 mole) of *p*-benzoquinone in 325 ml. of ethylene dichloride. The mixture is stirred for several minutes at room temperature, and then 1 g. of zinc chloride (0.007 mole) is added. With continuous stirring, the reaction mixture is refluxed for 8 hr. at 92°C. At the end of the reflux period the ethylene dichloride solution is drained from the resin. The beads are washed with ethylene dichloride and then with water. To insure the removal of unreacted *p*-benzoquinone and the remaining ethylene dichloride, a steam distillation is employed to remove all residual volatile impurities from the beads. The filtered beads are extracted with methanol in a Soxhlet extractor until the washing are colorless. The product, crosslinked polyvinylbenzylbenzoquinone, is isolated by filtration and dried to constant weight.

The reduced form of this resin may be obtained by washing the beads with 10% aqueous solution of sodium bisulfite to give crosslinked polyvinylbenzylhydroquinone. This reaction gave 82.5 g. of material.

Preparation of Polyvinylbenzylhydroquinone

To a 500-ml. three-necked round-bottomed flask, fitted with a stirrer, reflux condenser, and thermometer, are added 100 g. of chloromethylated poly(styrene–divinylbenzene) (0.66 mole based on a chloromethylstyryl unit) and 100 g. (0.95 mole) of hydroquinone in 600 ml. of dioxane. The mixture is stirred for several minutes; then 4 g. (0.03 mole) of freshly fused zinc chloride is added. With continuous stirring, the reaction mixture is refluxed for 5 hr. At the end of the reflux period, the mixture is cooled to 75°C. and the warm dioxane solution drained from the beads. The resin is washed twice with hot ethanol and then drained while keeping the ethanol above 50°C. or extracted with methanol in a Soxhlet extractor for 16 hr to remove the last traces of unreacted hydroquinone. The

product, polyvinylbenzylhydroquinone, is isolated by filtration and dried to constant weight.

Preparation of Poly(vinylbenzylhydroquinone diacetate)

Hydroquinone diacetate may be reacted with the chloromethylated polystyrene copolymers by the same procedure used for the addition of 1,4-dimethoxybenzene. The acetate groups will be hydrolyzed during the steam distillation to remove the ethylene dichloride to yield the same material obtained by the direct addition of hydroquinone or the product obtained by the hydriodic acid cleavage of the dimethoxybenzene adduct.

References

1. Cassidy, H. G., and K. A. Kun, *Oxidation-Reduction Polymers*, Interscience, New York, 1965.
2. Sansoni, B., German Pat. 1,005,734, 1957.
3. Sansoni, B., and O. Sigmund, *Angew. Chem.*, **73**, 299 (1961).
4. Rao, M. L. B., B. Mukerjee, and S. R. Palit, *Chem. Ind. (London)*, **1961**, 145.
5. Gregor, H. P., D. Dolar, and G. K. Hoeschele, *J. Am. Chem. Soc.*, **77**, 3675 (1955).
6. Okawawara, M., Y. Oiji, and E. Imoto, *Kogyo Kagaku Zasshi*, **65**, 1658 (1962).
7. Lloyd, W. G., and T. E. Durocher, *J. Appl. Polymer Sci.*, **7**, 2025 (1963).
8. Parrish, J. R., *Chem. Ind. (London)*, **1956**, 137.
9. Trostyanskaya, E. B., and A. S. Tevlina, *Zhur. Anal. Khim.*, **15**, 461 (1960).
10. Etienne, A., and G. Izoret, *Compt. Rend.*, **252**, 2111 (1961).
11. Izoret, G., *Ann. Chim. (Paris)*, **7**, 151 (1962).
12. Izoret, G., *Compt. Rend.*, **254**, 671 (1962).
13. Lindsey, A. S., Brit. Pat. 891,467, 1962.
14. Lindsey, A. S., and S. E. Hunt, Brit. Pat. 949,302, 1964.
15. Manecke, G., in *Methods in Organic Chemistry*, Praxis I, Teil I, Houben-Weil, Ed., Thieme Verlag, Stuttgart, 1958, pp. 605–617.
16. Mills, G. F., and B. N. Dickinson, *Ind. Eng. Chem.*, **41**, 2842 (1949).
17. Sansoni, B., *Naturwiss.*, **39**, 281 (1952).
18. Sansoni, B., *Naturwiss.*, **41**, 212 (1954).
19. Sansoni, B., and K. Dorfner, *Angew. Chem.*, **71**, 160 (1959).
20. Dalibor, H., *Chem. Ber.*, **91**, 1955 (1958).
21. Grubhofer, N., *Naturwiss.*, **42**, 557 (1955).
22. Meditsch, J. deO., *Rev. Quim. Ind. (Rio de Janeiro)*, **26**, 142 (1957).
23. Erdey, L., J. Inczedy, and I. Markovits, *Talanta*, **4**, 25 (1960).
24. Cassidy, H. G., M. Ezrin, and I. H. Updegraff, *J. Am. Chem. Soc.*, **75**, 1615 (1953).
25. Cerrai, E., and C. Testa, *Anal. Chim. Acta*, **28**, 205 (1963).
26. Meitzner, E. F., and J. A. Oline, Union S. Africa Pat. Appl. 59/2393.
27. Kunin, R., E. F. Meitzner, and N. Bortnick, *J. Am. Chem. Soc.*, **84**, 305 (1962).
28. Kunin, R., E. Meitzner, J. A. Oline, S. Fisher, and N. Frisch, *Ind. Eng. Chem. Prod. Res. Dev.*, **1**, 140 (1962).
29. Kun, K. A., and R. Kunin, *J. Polymer Sci.*, **B2**, 587 (1964).
30. D'Alelio, G. F., U. S. Pat. 2,366,007, 1944.
31. McBurney, C. H., U. S. Pat. 2,629,710, 1953.
32. Erdtman, H., M. Coranath, and G. Schultz, *Acta Chem. Scand.*, **8**, 1442 (1954).
33. Pasternak, M., W. Alanlary, R. Luzzati, and A. Tardent, *Helv. Chim. Acta*, **31**, 525 (1948).
34. Dean, F. M., A. M. Osman, and A. Robertson, *J. Chem. Soc.*, **1955**, 11.

35. Giza, Y.-H. C., K. A. Kun, and H. G. Cassidy, *J. Org. Chem.*, **27**, 679 (1962).
36. Kun, K. A., and H. G. Cassidy, *J. Polymer Sci.*, **56**, 83 (1962).
37. Manecke, G., and G. Bourwieg, *Chem. Ber.*, **95**, 1413 (1962).
38. Manecke, G., *Z. Electrochem.*, **67**, 613 (1955).
39. Manecke, G., *Angew. Chem.*, **68**, 582 (1956).
40. Abrams, I. M., and T. P. Brestlin, paper presented at the International Water Conference of the Engineer's Society of Western Pa., 22nd Annual Meeting, Pittsburgh, Oct. 25, 1961.

Résumé

On a préparé des polymères redox basés sur le système redox hydroquinone–quinone par l'addition d'hydroquinone et de ses dérivés à des matrices préformées de polystyrène. Un gel conventionnel et des copolymères macroréticulés de styrène–divinylbenzène ont été chlorométhylés avec l'éther chlorométhylique au moyen d'un catalyseur de Friedel-Crafts et les produits de réaction ont été traités par une seconde réaction de Friedel-Crafts, avec l'hydroquinone, la benzoquinone ou les homologues alcoylés de ces composés, ou avec le diméthyléther ou les dérivés diacétones de l'hydroquinone, pour donner des vinylbenzylhydroquinones polymérisées. Les polymères redox macroréticulés sont plus réactionnels et plus stables que les résines possédant un système redox sur des matrices du type gel conventionnel. Ces polymères redox transforment le fer III en fer II, le cérium IV en cérium III, l'iode en iodure, et enlèvent l'oxygène dissous et les peroxydes des liquides aqueux et organiques, lorsque ces résines sont sous la forme réduite. Sous la forme oxydée, les résines sont réduites par le titane III, le sulfite de sodium, le bisulfite de sodium, le dithionite de sodium, l'anhydride sulfureux et le borohydrure de sodium.

Zusammenfassung

Redoxpolymere auf Grundlage des Hydrochinon-Chinonredoxystems werden durch Addition von Hydrochinon und Hydrochinonderivaten an eine vorgebildete Polystyrolmatrix dargestellt. Konventionelle Gel- und Makronetzstyrol–Divinylbenzolkopolymere wurden mit Chlormethyläther und einem Friedel-Crafts-Katalysator chlormethyliert und die Reaktionsprodukte in einer zweiten Friedel-Crafts-Reaktion mit Hydrochinon, Benzochinon oder Alkylhomologen dieser Stoffe oder mit Dimethyläther oder Diacetoxyderivaten des Hydrochinons unter Bildung polymerer Vinylbenzylhydrochinone behandelt. Makronetz-Redoxpolymere zeigen grössere Reaktivität und bessere Stabilität als Harze mit Redoxystemen auf konventionellen Matrizen vom Geltyp. Diese Redoxpolymeren wandeln in ihrer reduzierten Form Eisen III in Eisem II, CerIV in CerIII, Jod in Jodid um und entfernen gelösten Sauerstoff und Peroxyde aus wässrigen und organischen Flüssigkeiten. In der oxydierten Form werden die Harze durch Titan III, Natriumsulfit, Natriumbisulfit, Natriumdithionit, Schwefeldioxyd und Natriumforhydrid reduziert.

Received September 17, 1964
Revised November 12, 1964
(Prod. No. 4564A)

JOURNAL OF POLYMER SCIENCE: PART A VOL. 3, PP. 1845–1857 (1965)

Stress Crazing of Transparent Plastics. Computed Stresses at a Nonvoid Craze Mark

ALAN C. KNIGHT, *Plastics Department, Experimental Station, E. I. du Pont de Nemours & Company, Inc., Wilmington, Delaware*

Synopsis

The mechanism of the stress crazing of transparent plastics is discussed in terms of a model suggested by recent publications in which the interior of the craze mark contains tenacious, elongated fibrils connecting the parallel faces. Internal and external stress distributions have been computed for a two-dimensional model of equilibrium crazes. Three shape parameters are used; the length of a uniform section, the thickness of the uniform section, and the length of a tapered tip section. The configuration of the tapered tip is determined in the model by the requirement that stresses remain finite. Stabilization of the craze is attributed to reduction of stress intensity by an increase in the ratio of tip length to thickness as the craze propagates. Two conditions are noted where craze stability is not predicted. Qualitative agreement was found between the model and growth kinetics reported in the literature, but the simple equilibrium model does not provide a basis for explaining the effects of stress level and temperature on the size of craze marks. The occurrence of crazing rather than general elongation is explained in this model by the stress intensification which occurs when the fibrils of the craze material are elongated.

Introduction

Investigation of the stress crazing of transparent plastics has shown that craze marks in polystyrene, polymethyl methacrylate, and poly(bisphenol-A carbonate) contain material which can support tensile stresses.[1–3] Such craze marks or crazes must be clearly distinguished from cracks containing no internal material. True fractures arising from combinations of stress and environment have been studied extensively in plastics and are the subject of a recent review.[4] A criterion has been described[5] for distinguishing between cracks and crazes. The mechanism of crazing has been the subject of recent discussions.[6]

The presence of tenacious material in the craze mark has suggested the computation of stresses in its vicinity to find, for example, the force supported by the internal material as well as to indicate the mechanism by which a growing craze mark becomes stabilized and stops growing.

A computation is presented here of the stresses at the boundary of a craze mark as defined by a simple yet fairly realistic model. The major assumptions which have been made are: (*1*) stresses remain finite so that strains in the material surrounding the craze mark are small (equations of elasticity for infinitesimal displacements have been used); (*2*) the

shape of a craze mark is well represented as a large section of uniform thickness with tapering edges; (*3*) no qualitative errors are introduced by representing the craze mark as uniform with respect to one coordinate direction; (*4*) all stresses at the craze surface are perpendicular to the long axis of the craze.

Basis for the Use of Normal Stresses

The assumption of normal stresses requires some discussion. Although it seems likely to be correct over most of the craze mark, it is most certainly incorrect for a small region of the tip. This statement is to be justified by consideration of the reduced density of the material in the interior of the craze. Studies of refractive index of the craze material[2] and penetration by solvents into crazes in polycarbonate[2] and poly(methylmethacrylate)[7] have demonstrated the existence of voids in the craze material.

It has seemed reasonable to assume that the material in the interior of the craze mark has been elongated in the direction of stress with resultant orientation. Such orientation results in weakness in the perpendicular direction so that oriented polystyrene, for example, can be readily split into fibers.[8] The voids in the craze material are thus explained as spacings between oriented fibrils. The assumption of fibrils passing from face to face of the craze mark seems needed in order to explain not only voids but the high strength observed of crazed specimens. The strength of fibers is increased as their diameter decreases. Observations have been reported for polystyrene of breaking strength increasing from 5400 psi for fibers 0.015 in. in diameter to 35,000 psi at 0.0025 in. in diameter.[9] These fibers, of course, are large compared with the fibrils postulated in crazes.

If the material in the craze consists of oriented fibrils extending from face to face in the direction of applied stress, it can support large normal stresses, but it cannot support stresses which are not parallel to the direction of the fibrils. This justifies the assumption of normal stresses except at the end of the growing craze mark where the fibrils become separated from each other. At this point, nonnormal stresses are not only allowed, but required, in order to overcome the weakened forces still holding the fibrils together. These nonnormal stresses, however, have been neglected in the treatment reported here.

Computation of External Stress Distribution

Consider a craze mark with the dimensions and coordinate framework indicated in Figure 1. This shows a cross section of a craze which is increasing in length in the y direction along the $x = 0$ plane. The medium is considered infinite and the cross section assumed to remain the same for all values of the third coordinate. Symmetry is assumed with respect to both the x and y axes. The applied stress is parallel to the x axis in accordance with experimental observations of the direction of crazes.[1,2,10,11]

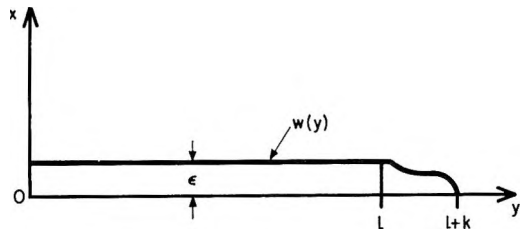

Fig. 1. Coordinate system and parameters of the craze model which is analyzed.

The total length of the craze mark is $2(l + k)$. The portion from $|y| = 0$ to $|y| = l$ is a section of constant thickness, while the portion where $l \leq |y| \leq l + k$ is the tip with a shape to be defined more exactly at a later stage. The quantity 2ϵ represents, not the total thickness of the craze mark, but the thickness after elongation of the interior resin less the original thickness of the material which was elongated during the crazing process. In other words, 2ϵ is the increase in thickness of the layer which becomes the craze mark. It is the displacement which material immediately adjacent to the craze mark must undergo.

It has been shown[12] that the unidirectional stress required to maintain an equilibrium opening of a given shape in an elastic material is

$$\sigma_x(y) = -(2/\pi) \int_0^\infty \bar{P}(\xi) \cos(\xi y) d\xi \tag{1}$$

where

$$\bar{P}(\xi) = [\xi E/2(1 - \sigma^2)] \int_0^C w(y) \cos(\xi y) dy \tag{2}$$

and $w(y)$ is an even function which describes the shape of the opening in the range $-C$ to C, there being no opening where $|y| > C$.

In these equations, y is the coordinate described in Figure 1, E is Young's modulus, and σ is Poisson's ratio. The equations were derived under the assumption of plane strain, that is, that displacements perpendicular to the x, y plane are zero, and that derivatives of the displacements with respect to the perpendicular direction are also zero. The medium is assumed to be of infinite extent.

The boundary of the craze mark, $w(y)$, was taken to be (see Fig. 1):

$$\begin{aligned} w(y) &= \epsilon & 0 \leq |y| \leq l \\ w(y) &= f(y) & l \leq |y| \leq l + k \end{aligned} \tag{3}$$

where $f(y)$ is a function which decreases from ϵ at $y = l$ to zero at $y = l + k$. This function is represented by the power series

$$f(y) = \epsilon[1 + \sum_n a_n(y - l)^n] \tag{4}$$

subject to the condition

$$1 + \sum_n a_n k^n = 0 \tag{5}$$

Putting eqs. (3) and (4) into eq. (2), noting that C is equivalent to $l + k$, gives

$$\bar{P}(\xi) = \frac{\xi E \epsilon}{2(1 - \sigma^2)} \left\{ \frac{1}{\xi} \sin [\xi(l + k)] + \sum_n a_n I_n \right\} \tag{6}$$

where

$$I_n = \int_l^{l+k} (y - l)^n \cos (\xi y) dy \tag{7}$$

Integrating by parts, it is found that

$$I_n = \cos [\xi(k + l)] \sum_{m=1,2,3,\ldots}^{m \leq \frac{n+1}{2}} (-1)^{m+1} \frac{k^{n-2m+1}}{\xi^{2m}} \prod_{j=0}^{2m-2} (n - j)$$

$$+ \sin [\xi(k + l)] \left[\frac{k^n}{\xi} + \sum_{m=2,3,\ldots}^{m \leq \frac{n+2}{2}} (-1)^{m+1} \frac{k^{n-2m+2}}{\xi^{2m-1}} \prod_{j=0}^{2m-3} (n - j) \right] + J_n \tag{8}$$

where

$$J_n = (-1)^{\frac{n+2}{2}} \frac{n!}{\xi^{n+1}} \sin (\xi l) \qquad n = 0, 2, 4, \ldots$$

$$J_n = (-1)^{\frac{n+1}{2}} \frac{n!}{\xi^{n+1}} \cos (\xi l) \qquad n = 1, 3, 5, \ldots$$

Separating from I_n the term $(k^n/\xi) \sin [\xi(k + l)]$, eq. (6) can be written:

$$\bar{P}(\xi) = \frac{\xi E \epsilon}{2(1 - \sigma^2)} \left(1 + \sum_n a_n k^n \right) \frac{1}{\xi} \sin [\xi(k + l)]$$

$$+ \frac{\xi E \epsilon}{2(1 - \sigma^2)} \sum_n a_n \left\{ I_n - \frac{k^n}{\xi} \sin [\xi(k + l)] \right\} \tag{9}$$

The first term is zero from eq. (5). Combining this with eq. (1) gives:

$$\sigma_x(y) = \frac{-E \epsilon}{\pi(1 - \sigma^2)} \sum_n a_n \mathbf{K}_n \tag{10}$$

where

$$\mathbf{K}_n = \int_0^\infty \xi \{ I_n - (k^n/\xi) \sin [\xi(k + l)] \} \cos (\xi y) d\xi$$

The integrals where $n \leq 3$ are evaluated to be:

$$\mathbf{K}_1 = \frac{1}{2} \ln \frac{l + y}{k + l + y} + \frac{1}{2} \ln \left| \frac{l - y}{k + l - y} \right| \tag{11}$$

$$\mathbf{K}_2 = (l + y) \ln \frac{k + l + y}{l + y} + (l - y) \ln \left| \frac{k + l - y}{l - y} \right| - 2k \tag{12}$$

$$\mathbf{K}_3 = \frac{3}{2}(l + y)^2 \ln \frac{l + y}{k + l + y} + \frac{3}{2}(l - y)^2 \ln \left| \frac{l - y}{k + l - y} \right| + \frac{3k}{2}(2l - k) \tag{13}$$

When n is 4, or larger, the indefinite integrals can be obtained, but they do not have finite limits as $\xi \rightarrow \infty$. It seems probable that certain combinations of higher terms can be found which will give finite results, but it is clear from these results that there are many tip shapes which cannot be maintained by finite unidirectional stresses. I interpret this as indicating that these shapes can only be maintained by stresses with components which are not parallel to the x axis.

Tip Shape Required for Finite Stress

The individual integrals, $\mathbf{K}_1$, $\mathbf{K}_2$, and $\mathbf{K}_3$, have poles at $y = l + k$, the end of the opening. This is due to a discontinuity at that point in the derivative, $w'(y)$, of the displacement at the boundary. In physical terms, this result indicates that openings whose boundaries contain abrupt changes in direction cannot be maintained in equilibrium by finite unidirectional forces.

It is possible by adjustment of the constants, a_n, in eq. (4) to make $w'(y)$ continuous at $y = l$ and $y = l + k$ as well as at all other points. When this is done and if n is limited to the values 1, 2, and 3, eq. (4) becomes:

$$f(y) = \epsilon[1 - (3/k^2)(y - l)^2 + (2/k^3)(y - l)^3] \tag{14}$$

Then, from eqs. (10), (12), and (13)

$$\sigma_x(y) = [-E\epsilon/\pi(1 - \sigma^2)]F(y, l, k) \tag{15}$$

where

$$F(y,l,k) = \frac{3}{k^2}(2l + k) - \frac{3}{k^3}(l + y)(k + l + y) \ln \left| \frac{k + l + y}{l + y} \right| - \frac{3}{k^3}(l - y)(k + l - y) \ln \left| \frac{k + l - y}{l - y} \right| \tag{16}$$

This function is everywhere finite.

Stress Distribution Result

For application to craze marks, the principle of superposability of stresses is used to combine the stress field of eq. (15) with the homogeneous applied tensile stress which is constant over all the material and assigned the value T. Then, the distribution of stress along the craze mark is the sum of the two stresses, or

$$S_x(y) = T - [E\epsilon/\pi(1 - \sigma^2)]F(y,l,k) \tag{17}$$

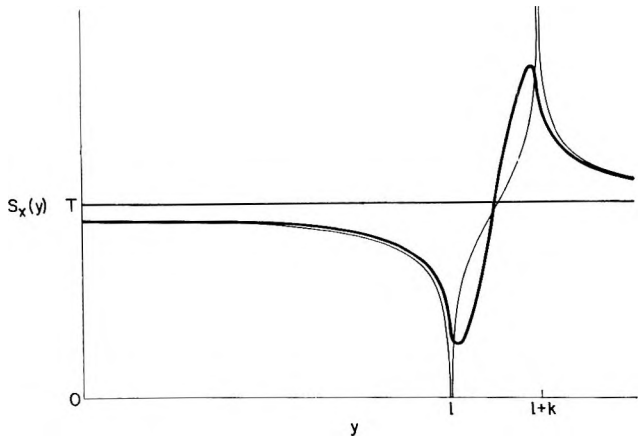

Fig. 2. Computed results for the stress distribution along a craze mark for two tip shapes. The heavy line shows the stress for the tip shape with continuous first derivative. The light line is computed with all parameters the same, but with a linear tip shape that makes $w'(y)$ discontinuous at $y = l$ and $y = l + k$. T is the average applied stress.

The numerical value of $F(y,l,k)$ is not changed much by changing the shape of the tip except right at the tip and particularly at any points where $w'(y)$ has a discontinuity. This is illustrated in Figure 2. The heavy line shows the stress distribution for a configuration in which the shape of the tip is described by eq. (14). To show the effect of changing the shape of the tip, a second (lighter) line is plotted which represents the stress distribution obtained with all other parameters the same, but with the tip described by a linear function [eq. (18)].

$$f(y) = \epsilon\{1 - [(y - l)/k]\} \quad l \leq |y| \leq l + k \tag{18}$$

This function makes the first derivative of the displacement discontinuous at $y = l$ and $y = l + k$ with resulting poles in the stress distribution. The close correspondence of the stresses at points away from the immediate neighborhood of the poles provides good demonstration of the insensitivity of the stress distribution to the detailed shape of the tip. In all that follows, the shape of the tip will be described by eq. (14).

Maximum and Minimum Stresses

In eq. (16) the following substitutions are made:

$$y = kz$$

$$l = k\lambda$$

then

$$F(y,l,k) = (3/k)G(z,\lambda) \tag{19}$$

where

$$G(z,\lambda) = 2\lambda + 1 - (\lambda + z)(1 + \lambda + z) \ln \left| \frac{1 + \lambda + z}{\lambda + z} \right| - (\lambda - z)(1 + \lambda - z) \ln \left| \frac{1 + \lambda - z}{\lambda - z} \right|$$

$G(z,3)$, like $F(y,l,k)$, has a maximum and a minimum with respect to the coordinate y or z. The values of these stationary points have been computed numerically with the results shown in Table I.

TABLE I
Approach of Stationary Stresses to Constancy as Craze Length Increases

λ	$3G_{min}$ (λ)	z at minimum	$3G_{max}$ (λ)	z at maximum
0	−1.438	0.922	3	0
0.1	−1.485	1.021	2.515	0.161
0.3	−1.549	1.219	2.240	0.375
1.0	−1.653	1.918	1.995	1.082
3.0	−1.732	3.917	1.876	3.083
10.0	−1.776	10.917	1.824	10.083
30.0	−1.791	30.917	1.808	30.083
100.0	−1.80	100.92	1.801	100.083
300.0	−1.80	300.92	1.793	300.083

The values of the maximum and minimum are seen to change very slowly with λ and approach a constant value. Putting these constant values into eq. (19) and then eq. (17) gives the eqs. (21) and (22) for the maximum and minimum stresses. Table I indicates that these provide an excellent degree of approximation when the length of the craze is more than ten times the length of the tip.

$$S_{max} = T + [1.80E/\pi(1 - \sigma^2)](\epsilon/k) \tag{21}$$

$$S_{min} = T - [1.80E/\pi(1 - \sigma^2)](\epsilon/k) \tag{22}$$

Internal Stress Distribution

The fibrils inside the craze mark are subject to higher stresses than the boundary stresses of the continuous exterior since the fibrils must carry the load for the adjacent void regions. The increase in stress is determined by the amount of elongation of individual fibers. Thus, the relation between internal stress and external stress at each point is

$$S_{int}(y) = S_{ext}(y)(1 + \chi) \tag{23}$$

where χ is the longitudinal strain, or elongation, at the point y. Assuming that the widening of the tip is due entirely to increasing elongation of the

same layer of material, the elongation in the tip can be derived from eq. (14) so that

$$\chi = \chi_m \left[1 - \frac{3}{k^2}(y - l)^2 + \frac{2}{k^3}(y - l)^3 \right]$$

$$l \leq |y| \leq l + k \qquad (24)$$

where χ_m is the elongation in the main body of the craze. Expressions for the internal stress follow immediately from eqs. (17), (23), and (24). They are

$$S_{\text{int}}(y) = \left\{ 1 + \chi_m \left[1 - \frac{3}{k^2}(y - l)^2 + \frac{2}{k^3}(y - l)^3 \right] \right\} \times \left\{ T - \frac{E\epsilon}{\pi(1 - \sigma^2)} F(y,l,k) \right\}$$

$$l \leq |y| \leq l + k$$

$$S_{\text{int}}(y) = (1 + \chi_m) \left\{ T - \frac{E\epsilon}{\pi(1 - \sigma^2)} F(y,l,k) \right\}$$

$$0 \leq |y| \leq l \qquad (25)$$

The intensification of stress inside the craze mark seems important because it provides an explanation of why the material inside the craze continues to elongate in spite of strain hardening. If there were no such concentration of stress in the interior, the material outside the craze would elongate. Crazing would then not be observed, but only general elongation. A possible criterion for whether a material will craze or not is thus suggested. Crazing seems to require separation of material into fibers by relatively low crosswise stresses at a low degree of elongation.

Comparison of Results with Experiment

Having developed the quantitative consequences of the crazing model under consideration, it is now necessary to compare the results with experiment. As a first step, the growth kinetics of crazes will be examined. This involves the use of equilibrium results to interpret a non-equilibrium situation and requires a kinematic assumption. This assumption is that the rates of the processes involved are increased as the actual stress shows an increasing excess over the equilibrium stress.

The following specific nomenclature will be used. The point of the craze in this nomenclature is the geometric point where $y = l + k$. The tip of the craze is the region where the thickness of the craze is changing from zero to the constant thickness observed over the main body of the craze. This is the region shown in Figure 1 where $l \leq y \leq l + k$. The base (of the tip) is the point $y = l$ where the thickness becomes constant. The craze mark in this terminology can be said to increase in thickness from point to base over the entire length of the tip and to have a constant thickness in its main portion.

Studies of large crazes substantiate[1] the geometric description used here. Examples have been given of very fine crazes which show the same kind of pattern.[2,13] Descriptions of observations have often emphasized growth in the longitudinal direction with statements or implications that transverse growth does not occur. On the other hand, the following explicit statement should be noted.[2]

"Growth of craze material occurs mainly but not solely at the craze tip. Thickening of the craze occurs behind the craze tip although usually at a rate which appears roughly to be inversely related to the distance from the craze tip."

In the discussion that follows, it has been considered that longitudinal growth is the primary process with the thickness remaining essentially constant behind the base of the tip. Widening, if it occurs, would be thought of as a secondary process. This point of view is not inconsistent with the statement quoted if the word "tip" in the quotation is equated with the word "point" as used here. The primary process of craze growth can then be divided into the stages of initiation, propagation at constant thickness, and termination.

The Initiation Process

With few exceptions, craze marks have been observed to be initiated at the surface of the specimen.[1,2,7,11,14] In one investigation,[14] crazes in the interior of the specimen were observed to occur in groups of two or more, associated, in most instances, with a visible particle of foreign matter. Initiation of crazes has been demonstrated, in the presence of active liquids, at deliberately introduced flaws.[15]

The initiation of crazes must be considered to be experimentally linked with stress concentrations due to inhomogeneities or surface defects. It has even been shown that coatings can prevent surface-initiated stress crazing, presumably by filling stress-raising cracks.[11]

An induction period has been observed before growth of craze marks begins.[1] After the induction period, a very rapid growth occurs.[1,7,11] In one case, it was observed that sharp cracking sounds were associated with the appearance of crazing, so rapid is the initial growth phase.[11] This suggests the possibility that the onset of crazing might be detected in opaque materials by amplifying the sounds generated. The occurrence of crazing in opaque materials has been demonstrated by increased retention of pigments at the intersection of the craze with the surface.[16] The very rapid initial growth of crazes may be the reason that the existence of a minimum craze length has been postulated.[14] The initial growth rate was perhaps too fast to allow observation of crazes shorter than the minimum.

The thickness of the craze mark is to be considered determined during the initiation step by factors which include the size of the defect and the overall stress level. As the propagation period begins, I will consider the thickness parameter ϵ to have been determined during the rapid release of elastic energy which accompanies initiation.

Propagation and Termination

Consideration of the rate of craze growth during the propagation step is complicated by the existence of apparently contradictory observations. It has been reported on the one hand that the lineal growth rate decreases with time and approaches zero.[1,17] On the other hand, a linear dependence on time and stress has been reported.[11] It appears, nevertheless, that both types of behavior can be accounted for in the framework of the present model.

Assume that in the growing craze mark, the stress distribution is similar to that found for the equilibrium shape. In the growing craze, however, there is an excess of stress which is constantly being relieved by the yielding of the material inside the craze mark.

The rate of yielding will be greater as the excess stress is larger. Near the point, where the stress is a maximum, initial elongation takes place. Elongation continues throughout the length of the moving tip, but ceases beyond the base of the tip.

The maximum stress is given by eq. (21) which can be rewritten in the form of eq. (26) to distinguish between variables and constants.

$$S_{max} = T + (b/k) \tag{26}$$

where

$$b = [1.80E\epsilon/\pi(1 - \sigma^2)]$$

The stress decreases from the point to the base, as is shown in Figure 2. Since the stress decreases, the excess stress also decreases from point to base.

At least initially the rate of elongation at the base is slower than at the point because the excess stress is lower. The result is that the point propagates more rapidly than the base, and the tip becomes longer. Since the length of the tip, k, is becoming larger the maximum stress becomes smaller according to eq. (26). As the excess stress decreases, the rate of elongation decreases and growth of the craze slows down.

The rate of movement of the base is not reduced, however, as k increases, because the stress at the base is a minimum with a value that increases as k becomes longer [see eq. (22)]. The rate of increase of k is thus reduced as the craze propagates. There will be two cases, depending on the relative values of the applied stress T and the other parameters. In one case, k will increase until it reaches its equilibrium value and the craze will stop growing because there is no longer any excess stress. In the other case, k will reach a steady-state value, and growth may continue. This occurs when the rate of propagation at the base becomes equal to the rate of propagation at the point before the equilibrium value of k is reached.

The dependence of growth rate on applied stress has been described for a case in which a steady-state growth of crazes in polystyrene seems to have been reached.[11] The experimental data in the range of applied

stress of 2500–3250 psi was summarized by the observational equation

$$D - D_0 = K(\sigma - \sigma_0)(t - t_0) \tag{27}$$

where D = depth of penetration of crazing front in inches, σ = applied stress in psi, t = time in hours, $D_0 = -0.015$ in., $K = 0.851 \times 10^{-7}$ in./hr./psi, $\sigma_0 = 1670$ psi, and $t_0 = -400$ hr. Negative values of constants resulted from the effects of the induction period and the very rapid initial growth period which are not otherwise represented by eq. (27). Setting the growth rate equal to $(D - D_0)/(t - t_0)$ and assuming that this is proportional to the excess strain, we obtain

$$S_{\text{exc}} \sim \sigma - \sigma_0$$

or in the previous nomenclature,

$$S_{\text{exc}} \sim T - T_0 \tag{28}$$

On comparison of eq. (29) with eq. (22) we may write

$$S_{\text{exc}} \sim S_{\text{min}} = T - [1.80E/\pi(1 - \sigma^2)](\epsilon/k) \tag{29}$$

The agreement of form suggests that the rate of steady-state growth of a craze is limited by the minimum stress, that is, by the rate of propagation of the base of the craze. In these circumstances, the ratio ϵ/k can be computed from the experimental value of T_0, since

$$T_0 = [1.80E/\pi(1 - \sigma^2)](\epsilon/k) \tag{30}$$

For values of E = 450,000 psi[18] and $\sigma = 0.3$, eq. (3) gives $k = 170\epsilon$ for steady-state propagation of a craze mark in polystyrene. At 100% elongation, ϵ is 1/4 the thickness, so the tip length at steady-state propagation would be about 42 times the craze thickness.

It is of interest to compare the above results with the measured shape of small wedge-shaped craze marks in poly(methyl methacrylate).[7]

A craze mark examined after 1 hr. of application of a stress of 7100 psi had not yet developed a uniform portion. The cross section was wedge-shaped, about 300 μ long and 1 μ thick at the thickest portion. Since such crazes were still growing, it may be concluded that in an equilibrium craze at these conditions, the length of the tip must be greater than 300 times the thickness. This enables limits to be estimated for the critical stress at the point.

We postulate the existence of a critical stress S_c, which must be exceeded in order that the point continues to move. Thus, for a growing craze, $S_{\text{max}} > S_c$.

Now, from eq. (21) and the data above

$$S_{\text{max}} = 7100 + [1.80E/\pi(1 - \sigma^2)][1/(300)(4)]$$

The divisor four is obtained by assuming 100% elongation in computing ϵ from the observed thickness. For E = 450,000 psi[18] and $\sigma = 0.3$, $S_{\text{max}} = 7336$ psi. On these assumptions, the critical stress S_c must lie, therefore, in the range of 7100–7336 psi for poly(methyl methacrylate)

at 20°C. If this is correct, a craze mark in poly(methyl methacrylate) cannot be stable when the applied stress is above about 7400 psi. (It should be noted that the measurements on which this conclusion is based were made on slightly plasticized resin.)

Effect of Stress Level on Size of Craze

For an equilibrium craze mark $S_{max} \leq S_c$ and

$$S_c \geq T + [1.80E/\pi(1 - \sigma^2)](/\epsilon k)$$

Solving for k/ϵ yields:

$$k/\epsilon \geq [1.80T/\pi(1 - \sigma^2)(S_c - T)] \qquad (T < S_c)$$

k/ϵ becomes larger as T increases. The observed decrease[1] in craze size as the applied stress increases must, therefore, depend entirely upon a decrease in ϵ, or a reduction of the relative rate of movement between base and point.

It is reasonable to suppose that ϵ will be small at large stresses because smaller defects will come into play during initiation, but a detailed consideration of this point is outside the scope of computations reported here. Similarly, more detailed consideration of the relative movement of point and base requires a nonequilibrium model which takes into account time-dependent elasticity.

Conclusions

It may be concluded that the two-dimensional equilibrium model which assumes fibrillar material within the craze mark is in reasonable agreement with observations. The stress distribution calculated shows that craze marks can become stable when the ratio of tip length to thickness becomes sufficiently large. Stability of a craze can fail for two reasons; because the applied stress exceeds a critical stress, or because the rate of propagation of the base becomes equal to the rate of propagation of the point.

This model does not provide a basis for explaining the decrease in craze size with increasing stress or temperature. Such an explanation will depend on consideration of the initiator mechanism, nonequilibrium viscoelastic response, or upon an alternate equilibrium model.

References

1. Spurr, O. K., Jr., and W. D. Niegisch, *J. Appl. Polymer Sci.*, **6**, 585 (1962).
2. Kambour, R. P., *Polymer*, **5**, 143 (1964).
3. Kambour, R. P., *J. Polymer Sci.*, **A2**, 4159 (1964).
4. Howard, J. B., in *Engineering Design for Plastics*, Reinhold, New York, 1964, Chap. 11, pp. 742–794; cf. *SPE J.*, **15**, 397 (1959).
5. Kambour, R. P., *Nature*, **195**, 1299 (1962).
6. Stuart, H. A., and G. Markowski, *Werkstoffe Korrosion*, **14**, 825 (1963); H. A. Stuart, D. Jeschke, and G. Markowski, *Materialprüfung*, **7**, 77, 236 (1964).
7. Bessonov, M. I., and E. V. Kuvshinskiĭ, *Fizika Tverdogo Tela*, **1**, 1441 (1959); English translation: *Soviet Phys. Solid State*, **1**, 1321 (1960).

8. Cheatham, R. G., and A. G. H. Dietz, *Trans. ASME*, **74**, 31 (1952).
9. Bailey, J., *India Rubber World*, **118**, 225 (1948).
10. Maxwell, B., and L. F. Rahm, *Ind. Eng. Chem.*, **41**, 1988 (1949).
11. Sauer, J. A., and C. C. Hsiao, *Trans. ASME*, **75**, 895 (1953).
12. Sneddon, I. N., *Fourier Transforms*, McGraw-Hill, New York, 1951, p. 426.
13. Russell, E. W., *Nature*, **165**, 91 (1950).
14. Newman, S. B., and I. Wolock, *J. Res. Natl. Bur. Standards*, **58**, 339 (1957).
15. Sternstein, S. S., and K. J. Sims, *Am. Chem. Soc. Polymer Preprints*, **5**, No. 2, 422 (1964); presented at the 148th National Meeting of the American Chemical Society, Chicago, 1964.
16. Ziegler, E. E., *SPE J.*, **10**, No. 4, 12 (1954).
17. Regel, V. R., *Soviet Phys. Tech. Phys.*. **1**, 353 (1956).
18. *Modern Plastics Encyclopedia*, **39**, insert; *Modern Plastics*, 1962.

Résumé

On discute le mécanisme de formation de crevasses dans les plastiques transparents, d'après un modèle suggéré récemment (1,2) dans lequel l'intérieur de la crevasse contient des fibrilles, adhérentes et allongées, reliant entr'elles les faces parallèles. On a évaulé les distributions des tensions internes et externes pour un modèle bidimensionnel de crevasses à l'équilibre. On a employé trois paramètres dimensionnels: la longueur d'une section uniforme, l'épaisseur de la section uniforme et la longueur de la section du bout pointu. La configuration du bout pointu est déterminée dans le modèle à condition que les forces restent constantes. La stabilisation de la crevasse est attribuée à la réduction de l'intensité de la force par une augmentation du rapport entre la longueur du bout et l'épaisseur lorsque la crevasse se propage. On a noté deux conditions lorsque la stabilité de la crevasse n'est pas prévue. Un accord qualitatif a été trouvé entre le modèle et la cinétique du développement rapporté dans la littérature, mais le simple modèle ne prévoit pas une base pour l'explication des effets du niveau de la force et de la température, sur la grandeurs de la crevasse. L'apparition de crevasse plutôt que l'élongation en général est expliquée dans ce modèle par l'augmentation de la force qui a lieu lorsque les fibrilles des crevasses sont allongées.

Zusammenfassung

Der Mechanismus der Spannungs-Rissbildung in transparenten Kunststoffen wird an Hand eines durch neuere Veröffentlichungen (1,2) nahegelegten Modells diskutiert, bei welchem das Innere der Risspur zähe elongierte Fibrillen enthält, welche die parallelen Flächen verbinden. Die innere und äussere Spannungsverteilung wurde für ein zweidimensionales Modell von Gleichgewichtsrissen berechnet. Drei Gestaltsparameter werden verwendet; die Länge eines einheitlichen Abschnitts, die Dicke des einheitlichen Abschnitts und die Länge eines zugespitzten Endabschnitts. Die Konfiguration des zugespitzten Endes wird im Modell durch die Bedingung bestimmt, dass die Spannungen endlich bleiben. Die Stabilisierung des Risses wird auf einen Rückgang der Spannungsintensität durch eine Zunahme des Verhältnisses von Spitzenlänge zu -dicke bei wachsendem Riss zurückgeführt. Zwei Bedingungen werden festgestellt, unter welchen keine Risstabilität vorhergesagt wird. Zwischen dem Modell und der in der Literatur angegebenen Wachstumskinetik bestand qualitativ Ubereinstimmung, das einfache Gleichgewichtsmodell kann jedoch keine Erklärung für den Einfluss des Spannungsniveaus und der Temperatur auf die Grösse der Risspur liefern. Das Auftreten einer Rissbildung an Stelle einer allgemeinen Dehnung wird bei diesem Modell durch die bei der Dehnung der Fibrillen des Rissmaterials auftretenden Spannungintesivierung erklärt.

Received November 6, 1964
(Prod. No. 4568A)

JOURNAL OF POLYMER SCIENCE: PART A VOL. 3, PP. 1859–1868 (1965)

Investigation of the Elastic Properties of the Particle Network in Gelled Solutions of Hydrocolloids. I. Carboxymethyl Cellulose

JAN HERMANS, JR.,* *FMC Corporation, American Viscose Division, Research and Development, Marcus Hook, Pennsylvania*

Synopsis

In order to obtain information on the structure of the particle network existing in gelled solutions of carboxymethyl cellulose, the elastic modulus was determined of series of dilutions of three samples of different molecular weight. It was found that these results could be accounted for reasonably well with the assumptions (*1*) that the crosslinking of molecules can be described as a reversible bimolecular aggregation between surface sites, (*2*) that the network formed may be described by Flory's theory of gelation and (*3*) that the network is deformed according to the theory of rubber elasticity.

INTRODUCTION

Solutions of many water-soluble colloids are gels at sufficiently high concentrations. The most characteristic property of a gel is its behavior as a solid as long as shear stresses applied to the gel are below some finite value, i.e., the yield stress, but as a viscous liquid at shear stresses larger than the yield stress. This behavior is shown by solutions of polyelectrolytes of which the molecules are random coils and by suspensions of asymmetric rigid particles such as clays and cellulose microcrystals.

Such solutions are gels only at concentrations larger than some well defined value, which is called the gel point. The properties of such gels are qualitatively explained by assuming the existence of many noncovalent crosslinks between different molecules. These form a network extending throughout the solution which has properties of a solid, albeit a soft one.[1–5]

Such networks may be formed also in polymerizing mixtures containing polyfunctional units which react to form three-dimensional polymers. In this case, the state of the system is determined by the degree of reaction (rather than by the concentration), and the gel point is a well defined value of the degree of reaction. The appearance of infinite networks in three-dimensional polymerizations has been analyzed theoretically by Flory[6,7a] and by Stockmayer.[8] Subsequently, Bardwell and Winkler[9] successfully used Flory's description of the infinite networks to analyze the gels they

* Present address: Department of Biochemistry, University of North Carolina, Chapel Hill, North Carolina.

obtained in three-dimensional polymers. These networks were characterized by the measurement of their elastic modulus which is related in a simple way to the structure of the network by equations familiar from the theory of rubber elasticity.

In this work the same approach has been applied to the study of gels formed by the reversible aggregation of water-soluble particles. The present paper is concerned with gels of carboxymethyl cellulose in which the aggregating particles are randomly coiled macromolecules. It is of interest to mention here that Eliassaf and Silberberg made measurements similar to those reported here, on gels of poly(methacrylic acid), without, however, providing a quantitative analysis.[10]

EXPERIMENTAL

Materials

Three samples of carboxymethyl cellulose (CMC) from Hercules were used, coded 7L, 7MSP, and 7HOP. By potentiometric titration these samples were found to have degrees of substitution of 0.93, 1.06, and 0.79, respectively. They had intrinsic viscosities in 0.1*M* NaCl of 214, 442, and 1430 ml./g., respectively, from which one derives values of the molecular weight of 46,000, 100,000, and 370,000.[11] These samples were used without further treatment.

Solutions

Solutions in water of these samples were made up at various concentrations and were left overnight in the cold to become homogeneous. No salt was added to the solutions, since it was found in a single trial that addition of NaCl did not affect the modulus very much.

Measurements

For the measurement of the shear modulus use was made of a Couette type viscometer (Rao flow birefringence viscometer, Rao Instruments, Brooklyn, N. Y.). Depending on the consistency of the gel this instrument was used in one of the following ways.

For gels which can support shear stresses larger than 50 dyne/cm.^{2}, the inner cylinder was mounted in sapphire bearings, and the shearing force was obtained by hanging weights from a string running over a pulley, pulling horizontally on one of the arms attached to the inner cylinder, while the displacement of the inner cylinder was measured with the aid of a differential transformer-type transducer of which the core is attached to the other arm.

For less strong gels, a hollow inner cylinder was used to decrease friction; this was further reduced by holding the inner cylinder in position with a brass spring. The usefulness of this arrangement is limited to gels with a modulus greater than a value of about 2×10^3 dyne/cm.^{2}, determined by the stiffness of the spring.

For even weaker gels, a point is reached where the resistance to displacement of the inner cylinder due to the presence of the gel is insignificant with respect to the resistance offered by the brass spring. This difficulty was overcome by suspending the inner cylinder from a thin wire. In the same range of moduli it became necessary to use a transducer exerting a negligible force on the core. Such a transducer was designed for us by Mr. F. Alexander, of this laboratory. It is a concentric cylinder condenser, which is completely shielded between the electrodes with an additional grounded cylinder. Its capacity may be varied in the useful range 0.6–1.0 $\mu\mu$F. by placing an insulated metal plate at a distance varying from 0.03 to 0.14 in. from its face. These low capacities were measured accurately with a Marconi Instruments TF 1342 low capacitance bridge, the metal plate being a 2 × 2 in. aluminum vane attached to one inner cylinder arm. The small forces which could only be applied when studying these soft gels were obtained by sending a direct current of up to 200 ma. through the primary winding of the differential transformer transducer.

The various transducers used were all calibrated. It was found that these calibrations could readily be reproduced.

Finally, the modulus of solutions of concentrations near 20% were measured in a viscometer according to the method of Mooney[12,15] when the other instrument could no longer be filled with the gel because of its high viscosity.

RESULTS

When a CMC gel is strained as described, the shear σ varies at a decreasing rate (which is never too great to be measured) over a period of about 10 min. Thereafter, the shear does not change appreciably over a considerable length of time, provided the stress τ is low enough. When the stress is removed, all the shear is recovered in about 10 min. However, there is for each gel a value of the shear stress above which the shear cannot be completely recovered by removing the stress.

It is to be noted that the observation of a fully recoverable deformation resolves an important problem which poses itself because of the demonstrated reversibility of the formation of the crosslinks. Namely, it is to be expected that the latter "wander," i.e., are continuously formed in new and broken in old places. It is well known that this phenomenon will lead to a gradual relaxation of any applied stress or to the occurrence of flow if a constant stress is applied.[14,15] However, if the part of the shear due to the wandering of the crosslinks is very small compared with the reversible part of the shear, the latter can safely be taken to represent the recoverable shear to be observed in the hypothetical case in which the crosslinks are held frozen.[14,15]

The flow due to the wandering of the crosslinks is generally distinguished from plastic flow, and it is supposed that, in order to obtain plastic flow, a stress must be applied which is great enough to break so many links between molecules that an infinite network is no longer present. In many

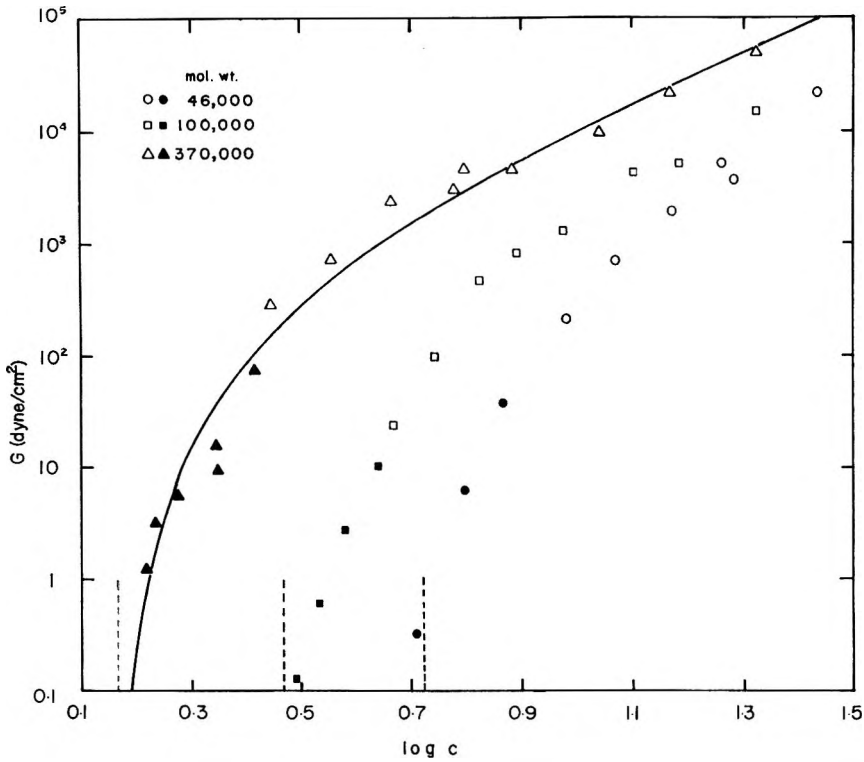

Fig. 1. Experimental values of the shear modulus of three samples of carboxymethyl cellulose at various concentrations (expressed in g./100 ml.): (○,□,△) data obtained with the bearing-type suspension and magnetic displacement indicator; (●,■,▲) data obtained with the frictionless suspension and electrostatic displacement indicator. The curve drawn is theoretical and is equivalent to the curve shown in Figure 2.

cases plastic flow begins at a fairly well defined stress, the yield stress, whose value can, furthermore, be obtained by extrapolation of data of the stress as a function of the shear rate to zero shear rate.[16]

At stresses lower than the yield stress, the number of crosslinks should diminish with the stress. However, for CMC gels in the elastic region, the recoverable shear is found to be proportional to the shear stress, the ratio

$$G = \tau/\sigma = d\tau/d\sigma$$

being the modulus of elasticity. Consequently, it appears that this decrease of the number of crosslinks under stress is important only near the yield stress.

With many of the CMC gels investigated a recoverable shear as large as two or three could be attained, the modulus being constant up to this value. This constancy is, of course, required if the theory of rubber elasticity is to be applied to these gels.[7b,17,18] The calculated moduli have been plotted as a function of the concentration (log-log plot) in Figure 1. Values of the modulus lower than 0.5 dyne/cm.^{2} cannot be considered very reliable. These results are discussed below.

DISCUSSION

The aim of this discussion is to give a quantitative analysis of the data obtained on the basis of a model of macromolecules linked together to form an infinite network, to which we referred in the introduction. In so doing, two independent problems arise. It must be asked in the first place how many links between molecules are present in any solution, and in the second place what will be the elastic modulus of a network containing a known number of particles which are bonded by a known number of links. We shall treat these problems in turn.

The solution is assumed to contain per unit of volume a number N_0 of identical macromolecules carrying f identical groups, each capable of reacting with one group on another molecule.* A fraction α of these groups has reacted to form intermolecular links, and it is assumed that the reacted groups are distributed at random over the particles, while the probability that any one group has reacted is independent of the number of groups on the same molecule which have reacted. We shall, furthermore, assume that $f \gg 1$ and introduce appropriate approximations.

Relation of α to the Concentration

In irreversible three-dimensional polymerizations, the degree of reaction α is readily determined by chemical analysis.[9] In gels whose formation is due to noncovalent interaction between macromolecules, this is not the case. Since the formation of the links between molecules is a dimerization equilibrium, it may be assumed that the concentration of reacted groups is equal to a constant multiplied by the square of the concentration of the groups which have not reacted, i.e.,

$$\alpha f N_0 = K' \, [(1-\alpha) \, f N_0]^2 \tag{1}$$

where K' is independent of the molecular weight, i.e., of f. When $\alpha \ll 1$ (as we shall see below to be the case in these gels), this becomes

$$\alpha = K' f N_0 = Kc \tag{2}$$

where c is the concentration and K again independent of the molecular weight.

The use of these equations may be justified by a consideration of the

* The assumption that the molecules are identical is made because we do not know the molecular weight distribution of the samples studied. The assumption to be made about the variation of the number of intermolecular bonds with the concentration is not affected by the type of molecular weight distribution. Those to be made about the elasticity of the particle network do depend on the distribution of the lengths of the primary molecules. A theory of networks formed from a polydisperse system of primary molecules has been derived by Flory.[7a]

It should, furthermore, be mentioned that in Flory's theory, whether for mono- or for polydisperse systems, the effect, both of links occurring between different parts of the same primary molecule and of links occurring within finite aggregates of molecules (i.e., those not belonging to the infinite network) is ignored.[8] The effect of this approximation on the results obtained here is uncertain.

lattice model of polymer solutions.[7c,19,20] For this model the number of polymer–polymer contacts is

$$n_{22} = z\,(xn_2)^2/2(n_1 + xn_2) \tag{3}$$

where z is the lattice coordination number, n_1 and n_2 are the number of solvent and polymer molecules respectively; x, the ratio of the molar volumes of solute and solvent, is proportional to the molecular weight of the polymer, and hence to f. Since n_{22}/xn_2 is proportional to α and $xn_2/(n_1 + xn_2)$ to the concentration, eq. (3) is equivalent to eq. (1). (It ought not to be assumed that all polymer–polymer contacts are crosslinks capable of withstanding a finite force. Rather, it must be assumed that only a small constant fraction of these contacts are crosslinks.)

Elastic Modulus

Knowing α, the degree of reaction of the groups, it is asked to know the properties of the infinite network which may be present. The approach used here was worked out by Flory[6,7a] and by Stockmayer.[8] Results from Flory's work pertinent to the present problem are the following.[7a]

It is found that only a part of the molecules is indeed linked to form the infinite structures which are typical of the gel. It can be shown that for large f the fraction of the molecules forming part of the gel is related to α by

$$\left.\begin{aligned} W_g &\sim 1 - \exp\{-\alpha W_g/\alpha_c\} \\ \text{where} \qquad & \\ \alpha_c &= 1/f \end{aligned}\right\} \tag{4}$$

Clearly $W_g \geqslant 0$ only when $\alpha \geqslant \alpha_c$, and hence α_c is the degree of reaction of the functional groups at which gel appears, i.e., the gel point. Combining this result with eq. (2), we have, for polymer samples differing only in molecular weight, that the gel point occurs at a concentration c_c inversely proportional to the length of the chain:

$$c_c = 1/Kf \tag{5}$$

It follows, then, that gelation occurs when, on the average, one group on each particle has reacted, that is, when there is one intermolecular bond for every two molecules. Since with these colloidal gels an extremely rigid system results when the number of reacted groups per molecule exceeds more than a few, it follows that in cases of practical interest α is of the same order of magnitude as α_c and that $\alpha \ll 1$. [This is, in fact, a necessary condition for eq. (4) to be a good approximation.]

A knowledge of W_g is necessary in order to calculate other properties of the gel, but insufficient. The elastic modulus of an assembly of infinite branched chains is zero unless the chains are crosslinked. Since the chains are composed of randomly coiled molecules, the theory of rubber elasticity[16,17,18] tells us that the shear modulus G is given by

$$G = N_c kT \tag{6}$$

Here N_c is the number of chains between crosslinks per unit of volume (or very nearly the number of crosslinks per unit of volume), and kT has its usual meaning. We are, therefore, seeking the number of crosslinks in a system of linear particles when the number of links between particles is known. For infinite aggregates containing no cyclic chains, i.e., no crosslinks, there is one interparticle link for each particle, and the degree of reaction of the reactive groups is

$$\alpha_0 = 2/f \tag{7}$$

i.e.,

$$\alpha_0 = 2\alpha_c \tag{8}$$

by eq. (1). An increase of α of the gel, α_g, over this value will result in a structure with a modulus of elasticity greater than zero, and, clearly, N_c is given by

$$\begin{aligned} N_c &= {}^1/_2\,(\alpha_g - 2\alpha_c) f W_g N_0 \\ &= {}^1/_2\,(\alpha_g/\alpha_c - 2) W_g N_0 \end{aligned} \tag{9}$$

f being equal to $1/\alpha_c$.

Finally, the degree of reaction of the active groups in the gel α_g may be obtained by subtracting the number of reacted groups in the finite aggregates, the sol fraction, from the total number of reacted groups and dividing the difference by the total number of reactive groups in the gel. A different approach, used by Flory,[7a] gives the same result:

$$\alpha_g = \alpha(1 + W_s) = \alpha(2 - W_g)$$

W_s being the fraction of the molecules in the sol fraction.

It is seen that the modulus can be written as a known function of α and of the concentration:

$$G = {}^1/_2\, kT\, (\alpha_g/\alpha_c - 2)\, W_g N_0$$

But since the parameter α is proportional to the concentration [eq. (1)], we may eliminate N_0 and write

$$G = (RT/2fMK)(\alpha_g/\alpha_c - 2)(\alpha/\alpha_c)\, W_g = (RT/2fMK)\, F(\alpha) \tag{11}$$

Thus, the modulus G and the concentration c are proportional to, respectively, the known function $F(\alpha)$ and to α itself, and a plot of log $F(\alpha)$ versus log α is, except for adjustable vertical and horizontal displacements, the theoretical curve of log G versus log c. This curve is shown in Figure 2. At the gel point ($\alpha/\alpha_c = 1$) the modulus is zero; hence log G goes to $-\infty$ asymptotically.

For large α/α_c, on the other hand, the dashed line with a slope of two is the asymptote. This is so, because we have assumed that the linking of the molecules is a bimolecular association equilibrium, in which the number of links per molecule is proportional to the concentration [eqs. (1) and (2)] and the concentration of intermolecular links is proportional to the square of the concentration of the molecules. Only N_0 links are needed to link

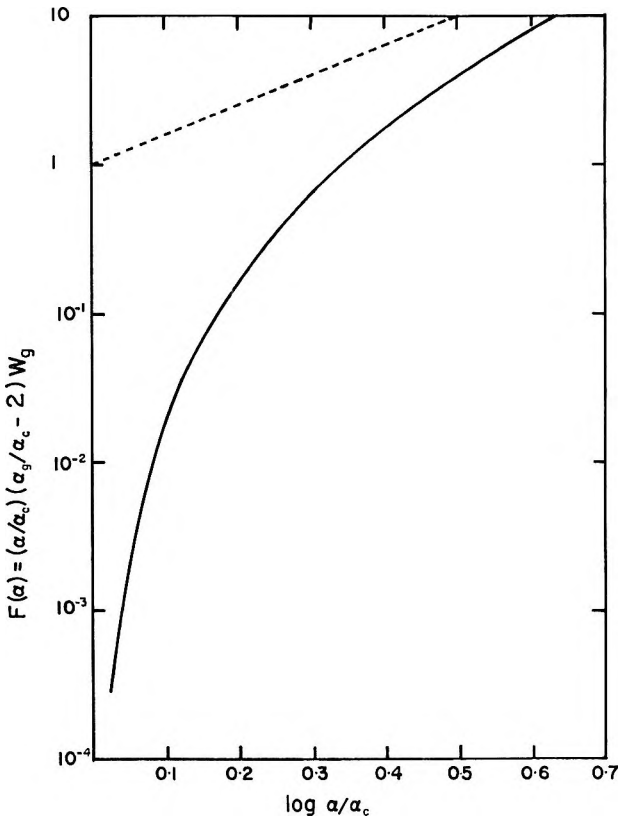

Fig. 2. Graphical representation of log $F(\alpha)$ as a function of log α/α_c, equivalent to a curve of log G as a function of log c for a monodisperse polymer. The dashed line with a slope of two is asymptotic to the curve at high α/α_c.

all the molecules together to an uncrosslinked network, and at sufficiently high concentrations this number is insignificant compared with the total concentration of links. The latter can, therefore, be put equal to the total concentration of active crosslinks, N_c which will vary as c^2.

Comparison with Experimental Data

We have fitted the curve of Figure 2 to the three sets of experimental data of Figure 1. For the sample of highest molecular weight the curve has been drawn. The gel point (where $\alpha/\alpha_c = 1$) has been indicated by a dashed line for all three samples. Quite obviously, the curve is a very reasonable approximation of the experimental data.

In particular, one will note that at high concentration, the modulus of all three samples becomes proportional to c^2. This justifies our assumption about the linking of the molecules, independently of the assumption that the network may be described by Flory's theory of gelation. It is interesting to note that at high concentrations the experimental data for the three samples do not coincide, as one would expect for materials differing

only in molecular weight. However, these differences may well correspond to the differences in degree of substitution between the samples.

The gel point of the three samples as indicated in Figure 1 varies in reasonable agreement with eq. (5), the differences in the values of log c_c being only slightly lower than the differences in the logarithm of the molecular weight.

The most stringent test of the applicability of the theory is made, however, when it is asked that the values of the modulus be in accord with the theory of rubber elasticity. It will be seen that the two proportionality constants in eqs. (2) and (11) contain only one unknown, the equilibrium constant K. This comes about from the fact that at the gel point there are precisely half as many intermolecular links as there are molecules. The number of molecules is known from the concentration c_c and the molecular weight, and hence from eq. (2) the number of intermolecular links is known, not only at the gel point, but at any concentration. Since the number of intermolecular linkages determines the number of crosslinks and this again the modulus by eq. (6), the modulus is fully determined once the gel point is known.

In order to verify this relationship, one may proceed as follows. On the asymptote $\log G = 2 \log c +$ constant, all links are counted as crosslinks. Hence the value of G on this asymptote at the gelpoint is equal to $kTN_0/2 = RTc/2M$. When the molecular weight of sample 7HOP is calculated in this way, one obtains 740,000, a value twice as large as the value derived from the intrinsic viscosity. This discrepancy is acceptable, and could be accounted for if G were equal to $N_ckT/2$ instead of N_ckT, there being some uncertainty regarding the proportionality constant in this relationship.[7b,18] More serious is the discrepancy between the molecular weights obtained in this manner for the other two samples (1.3×10^6 and 7×10^5) and the molecular weights from the intrinsic viscosities (10^5 and 4.6×10^4). It is possible that the discrepancies noted are due to the polydispersity of the samples.

From these results it is apparent that the simple hypothesis that the crosslinking reaction may be described as an equilibrium between surface sites is a good approximation and that the theory of Flory gives a reasonable description of the networks formed in gelled solutions of randomly coiled hydrocolloids. Further experimentation on sharp molecular weight fractions would appear desirable, however. It would furthermore appear feasible to use the quantitative information on the particle network obtained in this manner to analyze the stress relaxation and plastic flow shown by such gels at higher shear stresses, phenomena which have so far been described only in a qualitative manner.

Finally, these results encouraged the author to investigate the elastic behavior of gels containing rigid particles. Such results are described in Part II[21] of this study.

The author records with pleasure the advice received from Dr. Robert Simha in the execution of this work and the experimental aid given by Mr. R. VanScoy and Mr. A. G. Lankitus.

References

1. Goodeve, C. F., *Trans. Faraday Soc.*, **35**, 342 (1939).
2. Verwey, E. J. W., and J. Th. C. Overbeek, *Theory of the Stability of Lyophobic Colloids*, Elsevier, Amsterdam, 1948, p. 10.
3. Hermans, J. J., in *Flow Properties of Disperse Systems*, North Holland, Amsterdam, 1953, p. 61.
4. Ward, A. G., and P. R. Saunders, in *Rheology*, Vol. II, F. R. Eirich, Ed., Academic Press, New York, 1958, p. 313.
5. Ferry, J. D., *Adv. Protein Chem.*, **4**, 1 (1948).
6. Flory, P. J., *J. Am. Chem. Soc.*, **63**, 3083, 3091 (1941).
7. Flory, P. J., *Principles of Polymer Chemistry*, Cornell Univ. Press, Ithaca, N. Y., 1953, (a) Chap. 9; (b) Chap. 11; (c) Chap. 12.
8. Stockmayer, W. H., *J. Chem. Phys.*, **11**, 45 (1943); *ibid.*, **12**, 125 (1944).
9. Bardwell, J., and C. A. Winkler, *Can. J. Res.*, **27**, 116, 128, 139 (1949).
10. Eliassaf, J., and A. Silberberg, *Polymer*, **3**, 555 (1962).
11. Sitaramaiah, G., and D. A. I. Goring, *J. Polymer Sci.*, **58**, 1107 (1962).
12. Mooney, M., and R. H. Ewart, *Physics*, **5**, 350 (1934).
13. Philippoff, W. P., and F. H. Gaskins, *J. Polymer Sci.*, **21**, 205 (1956).
14. Tobolsky. A. V., *Properties and Structure of Polymers*, Wiley, New York, 1960, pp. 206, 223.
15. Ferry, J. D., *Viscoelastic Properties of Polymers*, Wiley, New York, 1961, p. 405.
16. Alfrey, T., *Mechanical Behavior of High Polymers*, Interscience, New York, 1948, p. 34.
17. Kuhn, W., *Kolloid-Z.*, **76**, 258 (1936).
18. Treloar, L. R. G., *The Physics of Rubber Elasticity*, Clarendon Press, Oxford, 1958.
19. Huggins, M. L., *J. Phys. Chem.*, **46**, 151 (1942).
20. Flory, P. J., *J. Chem. Phys.*, **10**, 51 (1942).
21. Hermans, J., *J. Appl. Polymer Sci.*, **9**, 1973 (1965).

Résumé

Afin d'obtenir des informations sur la structure du réseau existant dans des gels de carboxyméthyl-cellulose, le module d'élasticité a été déterminé pour une série de dilutions de trois échantillons de poids moléculaires différents. On a trouvé que ces résultats pourraient être assez bien expliqués par les suppositions suivantes: (*1*) que le pontage des molécules peut être décrit comme une aggrégation bimoléculaire réversible entre les sites en surface, (*2*) que le réseau formé peut être décrit par la théorie de Flory concernant la formation de gel, et (*3*) que le réseau est déformé en accord avec la théorie de l'élasticité du caoutchouc.

Zusammenfassung

Um die Struktur des in gelierten Lösungen von Carboxymethylzellulsose vorhandenen Partikelnetzwerks kennen zu lernen, wurde der Elastizitätsmodul von Verdünnungsreihen dreier Proben mit verschiedenem Molekulargewicht bestimmt. Die Ergebnisse können befriedigend mit der Annahme erklärt werden, dass (*1*) die Vernetzung der Moleküle als reversible bimolekulare Aggregierung von Oberflächenplätzen beschrieben werden kann, (*2*) das gebildete Netzwerk durch die Gelbildungstheorie von Flory beschrieben werden kann und (*3*) die Netzwerkdeformation der Theorie der Kautschukelastizität entspricht.

Received March 6, 1964
Revised July 28, 1964
(Prod. No. 4573A)

JOURNAL OF POLYMER SCIENCE: PART A VOL. 3, PP. 1869–1875 (1965)

Entropy and Heat of Fusion of Polymers

I. KIRSHENBAUM, *Chemicals Research Division, Esso Research and Engineering Company, Linden, New Jersey*

Synopsis

Methods are presented for estimating the entropy and heat of fusion of polyolefins, polyamides, polyesters, etc. Although the formulas are approximate, good agreement is obtained with experimental values, where available. For example, the calculated entropies for polypropylene, polyoxymethylene, nylon 66, polyester 210, and poly(ethylene terephthalate) are 5.4, 3.4, 11.2, 8.3, and 5.9 e.u./mole of repeating unit, respectively, as compared to the experimental values of 5.4, 3.5(3.9), 11, 7, and 5.8(5.4), respectively. Application of the formulas to the polyamides support the calorimetric and DTA estimates of the heats of fusion which are significantly greater (by 25–75%) than those determined by the diluent method. Thus, the calculations also indicate that the heats of fusion of the polyamides are higher than those of similar polyesters.

Although the heat and entropy of a crystalline polymer can be determined readily by a number of techniques, in two specific cases the different methods do not give data that agree.[1–4] This is especially true in the case of polyamides, where the calorimetric values are about 50% greater than those determined by the diluent method. General acceptance of the diluent data has led to the conclusion that the heats of fusion of polyesters are higher than those of similar polyamides. There are, moreover, wide discrepancies in the literature for the experimental values of the heat of fusion of polypropylene, with recent values varying between 650 and 2600 cal./mole.[1] This paper outlines a simple method for estimating the heat and entropy of fusion of a polymer from available properties and applies the formulas to a large number of polymers including polypropylene, polyamides, polyesters, etc. The method gives results in agreement with experimental where the experimental data are unequivocal and gives a way of choosing between data when a conflict exists.

The heat of fusion can be calculated from the entropy of fusion by the well-known relationship $\Delta H_u = T_m \Delta S_u$, where T_m is the crystalline melting point and ΔH_u and ΔS_u are the heat and entropy of fusion (per mole of repeating unit), respectively, of a 100% crystalline polymer. The entropy of fusion may be considered as consisting of two contributions:[5]

$$\Delta S_u = \Delta S_{\text{exp}} + (\Delta S_c)_v \tag{1}$$

where ΔS_{exp} represents the change in entropy associated with the increase in volume and $(\Delta S_c)_v$ represents the change in entropy due to the increase

in the number of conformations a macromolecule can assume on passing from the solid to the liquid state. Starkweather and Boyd[6] have considered a contribution to ΔS_u of long-range disorder in the liquid, but this effect can be assumed negligible for polymers. The assumption is also made that ΔS_{exp} and $(\Delta S_c)_v$ can be treated separately and that $(\Delta S_c)_v$ is concerned solely with rotational contributions to the entropy of fusion.

The term ΔS_{exp} can be calculated from the relationship[6-8]

$$\Delta S_{\text{exp}} = (\partial P/\partial T)_v \Delta V_m \tag{2}$$

where ΔV_m is the volume change on melting. The value for $(\partial P/\partial T)_v$ can be obtained from the compressibility β and from the coefficient of thermal expansion α. The compressibility, in turn can be calculated from Young's modulus E and Poisson's ratio σ.[9] Thus

$$\Delta S_{\text{exp}} = (\alpha/\beta)\Delta V_m = (\alpha E \Delta V_m/3)[1/(1 - 2\sigma)] \tag{3}$$

Although the various parameters should be determined for "100% crystalline" material at the melting point, room temperature data can often be used without introducing a too large an error in the calculated overall entropy of fusion of the polymer. The error is invariably negative, i.e., a lower value is calculated for ΔS_{exp}. Thus in the case of high-density polyethylene, eq. (3) gives $\Delta S_{\text{exp}} = 0.34$ e.u. per CH_2 when room temperature values are used for the parameters, as compared to the 0.46 e.u. estimated by Quinn and Mandelkern[10] for data at the melting point.

Since all of the data needed for eq. (3) are not readily available for new polymers, there are two approximations that can be used to estimate ΔS_{exp} for semicrystalline polymers. For crystalline solids, Poisson's ratio approaches 0.33, and where this is true

$$\Delta S_{\text{exp}} \simeq E \Delta V_m \tag{4}$$

Moreover, for most crystalline polymers studied, the ratio $\Delta S_{\text{exp}}/\Delta V_m$ falls within a comparatively narrow range of 0.12–0.26, averaging 0.18 e.u./cc. per repeating unit. This suggests that where no other data are available, ΔS_{exp} may be estimated from

$$\Delta S_{\text{exp}} \simeq 0.18 \Delta V_m \tag{5}$$

Values for ΔS_{exp} for a number of different polymers, as calculated by the various formulas, are shown in Table I. In no case, where the test could be made, were the calculated values more than 0.2–0.6 e.u. different than those reported in the literature.

The molecules in the solid crystalline polymer may be considered essentially frozen in one conformation. This, of course, is no longer true on melting, and the contribution to $(\Delta S_c)_v$ is determined by the magnitude of the energy difference between the *gauche* and *trans* conformations for chains such as polyethylene. Although to a first approximation, the conformational entropy gain per skeletal bond in a polyethylene or polypropylene molecule might be taken as $R \ln 3$, this value is too large because

TABLE I
ΔS_{exp} for Various Polymers

Polymer	ΔV_m, cc./mole	ΔS_{exp}, cal./mole deg. Eq. (3)	Eq. (2)[8]	Eq. (5)	Literature values
Polyethylene	3.1[6]	0.34	0.42	0.55	0.5[6,10]
Polypropylene	9.6[11]	0.6	1.3	1.7	—
Poly-4-methyl-1-pentene	9.8	1.2	—	1.8	—
Poly-1-butene	8.4[8]	—	1.7	1.5	—
Isotactic polystyrene	12.7[12]	—	2.1	2.3, 2.0	—
	11.4[8]				
Polyoxymethylene	3.5[a]	0.6	—	0.6	0.8[6]
Poly(ethylene oxide)	5.3[8]	—	1.3	0.95	1.6[13]
Poly(ethylene terephthalate)	11.5[8]	—	2.0	2.1	—

[a] Calculated from data in ref. 6.

of restricted internal rotation.[14] This restriction, discussed by Taylor[15] as the "pentane effect," lowers the entropy in a hydrocarbon molecule by about 0.4 e.u. for each —CH_2— linkage having a rotational potential function with three minimum. Applying the "pentane interference effect" to the carbon chain of the polymer backbone, the change in conformational entropy of fusion per skeletal C—C bond becomes (R ln 3) − 0.4 or 1.8 cal./deg. Generalizing for a polymer with various atoms comprising the skeletal chain:

$$(\Delta S_c)_v = 1.8n + \sum_0^m R \ln N_c \tag{6}$$

where n is the number of C—C linkages in the skeletal chain per repeating unit, m is the number of other bonds (e.g., C—H, O=C—N) in the skeletal chain per repeating unit, and N_c is the number of stable conformations these bonds can assume with respect to the preceding bond.

The amount of information available on potential barriers to internal rotation for polymers of interest is meager. It appears, however, that one can assume three conformations (corrected for the "pentane interference effect") for each skeletal carbon–carbon bond in polymers such as polyethylene, polypropylene, and probably poly-4-methyl-1-pentene. The same appears to be true for the C—C bonds in polyamides, polyesters, etc. Steric hindrance becomes quite important in a molecule such as isotactic polystyrene, where rotation about the skeletal bond is highly restricted by the branch phenyl groups. The value of N_c has been taken as 2, assuming that the melting point of 240°C. is sufficiently high to overcome much of the energy difference between the two conformations.

In a polyamide, the CO—NH bond has some double-bond character,[16] and it has been estimated that the barrier for rotation about the C—H bond in amides may be 15 kcal. or higher.[3] Consequently N_c for this bond has been taken to be unity. The following bonds found in polyamides,

polyesters, and polyurethanes rotate readily and have been assumed to have N_c values of 2:NH—CH_2, CO—CH_2, O—CH_2, and —C(=O)—O. The addition of a phenyl group to a chain increases rigidity, reflected in a higher melting point and higher glass transition temperature. An enhanced effect is produced when the aromatic ring is linked directly to a carbonyl group, i.e., (O)C—C_6H_4—C(O)—, as in aromatic esters. This effect, due to conjugation, does not appear to act as a serious barrier to rotation, and a value of $N_c = 2$ can be used in calculating $(\Delta S_c)_v$ in aromatic polyesters. On the basis of the above considerations, $(\Delta S_c)_v$ has been calculated for the polymers listed in Table II. Calculated values for ΔS_u are also given in Table II and, where possible, are compared to experimental values reported in the literature.

TABLE II
Entropy Changes on Fusion

Polymer	$(\Delta S_c)_v$, e.u.	ΔS_u, e.u.	
		Calc.	Experimental
Polyethylene	1.8	2.13	2.27[3,10]
Polypropylene	3.6	5.1	5.4[1]
Poly-4-methyl-1-pentene	3.6	4.8	—
Isotactic polystyrene	2.8	4.8	4.2,[4] 3.9[17]
Poly-1-butene	3.6	5.3	3.8,[18] 8[19]
Polyoxymethylene	2.8	3.4	3.9,[20] 3.5,[21] 2.0[6]
Poly(ethylene oxide)	4.6	5.9	5.8,[4] 5.4[22]

It is readily apparent that the agreement between the calculated and experimental ΔS_u values is at least as good as the agreement between experimental values from different laboratories. The value of $(\Delta S_c)_v$ = 1.8 e.u. for polyethylene is in good agreement with the value of 1.84 e.u. estimated by Quinn and Mandelkern[10] from the experimental heat of fusion. The value of $(\Delta S_c)_v$ = 3.6 e.u. for poly-4-methyl-1-pentene would be too low if there were an entropy contribution arising from an increase in side chain mobility on melting. However, dynamic mechanical measurements and NMR indicate the onset of side-chain motion in the crystalline polymer at about 40°C.[23–25] The value for $(\Delta S_c)_v$ would be too high if the three conformations were less readily available for each bond than in polypropylene. The value for ΔS_u of 4.8 e.u. for poly-4-methyl-1-pentene corresponds to a heat of fusion about 2400 cal./mole repeating unit. A value of ΔS_u = 5.1 e.u. for polypropylene corresponds to a heat of fusion of about 2260 cal./mole of repeating unit. This value is in good agreement with the experimental values of 2500 ± 300,[1] 2225,[19] and 2600[26] cal./mole.

In light of this agreement between calculated and experimental values for ΔS_u and ΔH_u, the various equations were used to calculate the entropy and heat of fusion for various polyamides. The data are shown in Table

III and are compared to the conflicting experimental data reported in the literature.

TABLE III
Entropy and Heat of Fusion of Polyamides

Polyamide	ΔS_u (calc.), e.u.	ΔH_u (calc.), kcal./mole	ΔH_u (experimental), kcal./mole: Calorimetry[3,6]	DTA[20,27]	Copolymer or diluent eq.[2,28,29]
6	11.3	5.5	5.6	5.2	4.3
6, 6	20.9	11.2	11.0	10.6	9.7, 8
6, 10	28.1	14.0	13.5	13.0, 13.5	7.5
10, 10	35.3	17.2	—	—	8.3
10, 9	33.5	16.3	—	—	8.3

The calculated values for ΔH_u (in kilocalories/mole repeating unit) agree well with and support the calorimetric and DTA values for the heats of fusion for polyamides, all of which are significantly greater (by 25–75%) than those determined by the diluent method.

Application of various equations to the polyesters gave values for ΔS_u and ΔH_u which agreed well with the observed values for both aliphatic and aromatic polyesters. Comparative data are shown in Table IV.

TABLE IV
Entropy and Heat of Fusion of Polyesters

Polyester	T_m, °C.	ΔH_u, kcal./mole: Calc.	Obs.[a]	ΔS_u (calc.), e.u.[b]
2, T[c]	267	5.9	5.8, 5.4	11.2
4, T	232	7.5	7.6	14.8
6, T	161	8.0	8.3	18.4
10, T	138	10.5	10.4, 11.6	25.6
2, 10	76	8.3	7.0	23.8
9, 9	65	11.7	10.3	34.6
10, 9	69	12.1	10.0	36.4
10, 10	80	13.5	12.0	38.2
10, 6	80	10.9	10.2	31.0

[a] Data of refs. 2, 4, and 30–33.
[b] ΔS_{exp} taken as unity.
[c] 2,T = poly(ethylene terephthalate).

The aromatic polyesters have high melting points, primarily because of their low entropies of fusion. The aliphatic polyesters, in contrast, have extremely low melting points primarily due to their low heat of fusion, as shown by the comparison with polyamides in Table V. The data in this table are the heat and entropy of usion per chain atom (i.e., C, N, etc.) for several polyesters and polyamides.

TABLE V
Comparison of Polyesters and Polyamides

Polymer		ΔH_u per chain unit (calc.), kcal.	ΔS_u per chain unit (calc.), e.u.
Polyester	2, 10	590	1.5
	10, 6	605	1.7
	10, 10	610	1.7
Nylon	10, 10	780	1.6
	6, 10	720	1.6
	6, 6	800	1.5
	2, 10	780	1.5

It should be noted that with use of either the calculated ΔH_u data or the ΔH_u data obtained calorimetrically (or by DTA) for the polyamides (Tables III and V) the heats of fusion for the polyamides are higher than for those for similar polyesters. This is contrary to the conclusion that has been drawn when weight is given to the ΔH_u for polyamides derived from melting point depression data. Thus the ΔH_u for the polyamides and polyesters correlated with molecular cohesion data and hydrogen bonding does appear to contribute to the heat of fusion of these polymers.

References

1. Kirshenbaum, I., Z. W. Wilchinsky, and B. Groten, *J. Appl. Polymer Sci.*, **8**, 2723 (1964).
2. Evans, R. D., H. R. Mighton, and P. J. Flory, *J. Am. Chem. Soc.*, **72**, 2018 (1950).
3. Dole, M., and B. Wunderlich, *Makromol. Chem.*, **34**, 29 (1959).
4. Nielsen, L. E., *Mechanical Properties of Polymers*, Reinhold, New York, 1962.
5. Tobolsky, A. V., *Properties and Structure of Polymers*, Wiley, New York, 1960.
6. Starkweather, H. W., and B. H. Boyd, *J. Phys. Chem.*, **64**, 410 (1960).
7. Mandelkern, L., *Chem. Rev.*, **56**, 903 (1956).
8. Allen, G., *J. Appl. Chem.*, **14**, 1 (1964).
9. Alfrey, T., Jr., *Mechanical Behavior of High Polymers*, Interscience, New York, 1948.
10. Quinn, F. A., and L. Mandelkern, *J. Am. Chem. Soc.*, **80**, 3178 (1958).
11. Fortune, L. R., and G. N. Malcom, *J. Phys. Chem.*, **64**, 934 (1960).
12. Natta, G., F. Danusso, and G. Moraglio, *Makromol. Chem.*, **28**, 166 (1958).
13. Malcom, G. N., and G. L. D. Ritchie, *J. Phys. Chem.*, **66**, 852 (1962).
14. Pitzer, K. S., *J. Chem. Phys.*, **8**, 711 (1940).
15. Taylor, W. J., *J. Chem. Phys.*, **16**, 257 (1948).
16. Bunn, C. W., *J. Polymer Sci.*, **26**, 323 (1958).
17. Dedeurwaerder, R., and J. F. M. Oth, *J. Chim. Phys.*, **56**, 940 (1959).
18. Danusso, F., and G. Gianotti, *Makromol. Chem.*, **61**, 139 (1963).
19. Passaglia, E., and H. K. Kevorkian, *J. Appl. Phys.*, **34**, 90 (1963).
20. Inoue, M., *J. Polymer Sci.*, **A1**, 2697 (1963).
21. Inoue, M., *J. Polymer Sci.*, **51**, S18 (1961).
22. Mandelkern, L., *J. Appl. Phys.*, **26**, 443 (1955).
23. Kirshenbaum, I., R. B. Isaacson, and W. C. Feist, *J. Polymer Sci.*, **B2**, 897 (1964).
24. Woodward, A. E., A. Odajim, and J. A. Sauer, *J. Phys. Chem.*, **65**, 1384 (1961).
25. Chan, K. S., G. Rånby, H. Brumberger, and A. Odajima, *J. Polymer Sci.*, **61**, S29 (1962).

26. Danusso, F., G. Moraglio, and P. Flores, *Atti Accad. Nazl. Lincei, Rend. Classe Sci. Fis. Mat. Nat.*, **25**, 529 (1958).
27. Ke, B., and A. W. Sisko, *J. Polymer Sci.*, **50**, 87 (1961).
28. Geschele, G. B., and L. Crescentini, *J. Appl. Polymer Sci.*, **7**, 1349 (1963).
29. Rybnikar, F., *Chem. Listy*, **52**, 1042 (1948).
30. Smith, C. W., and M. Dole, *J. Polymer Sci.*, **20**, 37 (1956).
31. Flory, P. J., H. D. Bedon, and E. H. Keefer, *J. Polymer Sci.*, **28**, 151 (1958).
32. Mandelkern, L., R. R. Garrett, and P. J. Flory, *J. Am. Chem. Soc.*, **74**, 3949 (1952).
33. Wunderlich, B., and M. Dole, *J. Polymer Sci.*, **32**, 125 (1958).

Résumé

On présente des méthodes pour estimer l'entropie et la chaleur de fusion de polyoléfines, de polyamides, de polyesters etc. Bien que les formules soient approximatives, on obtient une bonne concordance avec les valeurs expérimentales. Par exemple, les entropies calculées pour le polypropylène, le polyoxyméthylène, le nylon 6,6, le polyester 2.10 et le téréphtalate de polyéthylène sont 5.4, 3.4, 11.2, 8.2 et 5.9 comparées aux valeurs expérimentales 5.4, 3.5(3.9), 11.7 et 5.8(5.4). L'application des formules aux polyamides confirmens les estimations calorimétriques et DTA des chaleurs de fusion, qui sont sensiblement plus grandes (de 25 à 75%) que celles déterminées par la méthode de dilution. Donc, les calculs indiquent aussi que les chaleurs de fusion des polyamides sont plus grandes que celles des polyesters similaires.

Zusammenfassung

Methoden zur Bestimmung der Schmelzentropie und -wärme von Polyolefinen, Polyamiden, Polyestern usw. werden angegeben. Obwohl es sich nur um Näherungsgleichungen handelt, wird gute Übereinstimmung mit den Versuchswerten erhalten, wo solche zugänglich sind. Die berechneten Entropiewerte z. B. betragen für Polypropylen, Polyoxymethylen, Nylon-66, Polyester-2,10 und Polyäthylenterepthalat 5,4, 3,4, 11,2, 8,3 und 5,9 im Vergleich zu den experimentellen Werten von 5,4, 3,5(3,9), 11,7 und 5,8(5,4). Anwendung der Gleichungen auf die Polyamide liefert eine Stütze für die kalorimetrische und DTA-Bestimmung der Schmelzwärme, welche merklich grösser (um 25–75%) als die nach der Verdünnungsmethode bestimmten sind. Die Berechnungen zeigen damit auch, dass die Schmelzwärme der Polymaide höner als diejenige von ähnlichen Polyestern ist.

Received September 4, 1964
Revised November 16, 1964
(Prod. No. 4576A)

JOURNAL OF POLYMER SCIENCE: PART A VOL. 3, PP. 1877-1883 (1965)

Polyamides via the Ritter Reaction

FLOYD L. RAMP, *B.F. Goodrich Research Center, Brecksville, Ohio*

Synopsis

A new series of polyamides has been prepared by the condensation of dinitriles with bis(acetoxymethyl)durene in sulfuric acid.

DISCUSSION

The condensation of a nitrile with a tertiary alcohol or olefin derived from such an alcohol has been extensively studied by Ritter and co-workers. The reaction involves the attack of nitrile on the carbonium ion produced by the action of sulfuric acid and yields after hydrolysis an amide.[1-3]

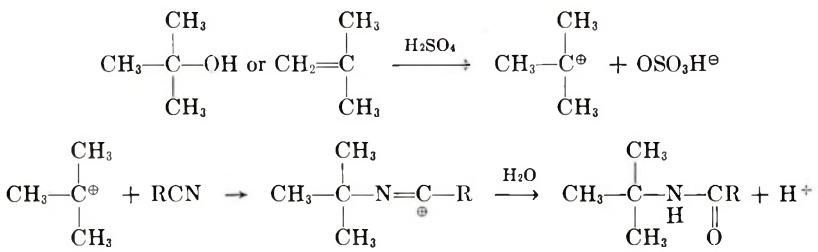

Tertiary alcohols give very high yields, but moderate to very poor yields are obtained with secondary or primary alcohols. The high yields available from suitable reactants prompted investigation of this reaction for the production of polyamides. The related reaction where formaldehyde is the source of carbonium ions has been extensively studied.[4-7] Polyamides obtained from formaldehyde are highly branched as a result of side reactions, and they are readily cleaved by 98% formic acid at room temperature.

The choice of a suitable diene or diol for polymer production requires several considerations. One of the simplest ditertiary olefins is bimethallyl, but Meyers and Ritter obtained 2,5,5-trimethyl-3-isopropylidene-1-pyrroline (28% yield from acetonitrile and bimethallyl).[8] The proximity of the double bonds no doubt accounts for the cyclization. Increased separation of the double bonds should eliminate this difficulty. However, the longer chain coupled with the requirement of a tertiary carbon at the site of reaction would probably depress the melting point of the polyamide below a useful range.

Since the initiation of this work, it has been shown that allyl and benzyl alcohols also condense well with nitriles.[9-12] Sirupy phosphoric acid gave

the highest yield of amide. The use of small amounts of sulfuric acid in acetic acid gave a mixture of ester and amide. As will be noted later, higher concentrations of sulfuric acid give excellent yields of amide in the presence of acetic acid.

1,4-Butenediol was condensed with adiponitrile, but no water-insoluble product was obtained. Benzyl alcohol resinifies readily in strong acid due to condensation polymerization with ring alkylation.[13] Even though the amide has been shown to form in good yield, this side reaction could give crosslinking in a polymeric system. Introduction of a negative group on the ring, e.g., *p*-cyano, protects the ring from alkylation, but the electron-withdrawing influence of the nitrile causes such a benzyl alcohol to behave as a typical primary alcohol;[14] hence, polymerization of *p*-cyanobenzyl alcohol in sulfuric to a high polymer is not to be expected. *p*-Nitrobenzyl alcohol was inert to nitriles in concentrated sulfuric acid.

One compound was found to be eminently suited for this condensation reaction. Bis(acetoxymethyl)durene (I) reacts readily with nitriles in strong sulfuric acid giving high polymers (II). The diacetate was chosen because it is soluble in solvents inert to concentrated sulfuric acid. This permits better dispersion of the durene derivative than can be achieved by addition of the diol directly to the acid media. In the latter case, localized decomposition and poor dispersion of the diol in the reaction media leads to lower yield and molecular weights. The diol is not readily soluble in solvents inert to sulfuric acid.

Condensation of bis(acetoxymethyl)durene with acetonitrile yielded III, bis(acetamidomethyl) durene. The structure of III was established by elemental analysis, and infrared and NMR (in sulfuric acid) spectra. Hydrolysis of III with constant-boiling hydrobromic acid gave bis(bromomethyl) durene, which in turn was identified by conversion to bis(acetoxymethyl) durene. Hydrolysis of the polyamide II was also effected in the same manner. Bis(bromomethyl)durene was isolated as a sublimate which collected in the condenser.

Dark polymers are formed in lower yields in very strong sulfuric acid. Hydride transfer such as that observed by Deno et. al.[15] is probably the cause of the side reactions under these conditions. Thus, the effective concentration of sulfuric acid for polymerization is in the broad range be-

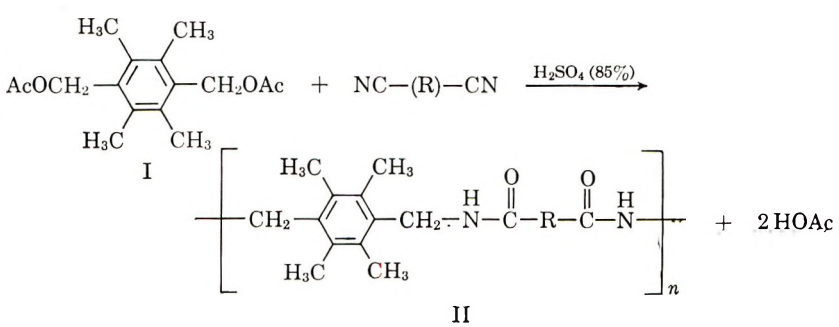

tween that producing ester from acetic acid (~ 15%) and that yielding hydride transfer (97%). The yields of polyamide are in most instances essentially quantitative.

An attempt was made to extend the reaction to other bis(acetoxymethyl) alkylated benzenes. Bis(acetoxymethyl)mesitylene and bis(acetoxymethyl) pseudo-cumene were readily prepared. Condensation of these compounds with adiponitrile in sulfuric acid gave low yields of product of low molecular weight. No other tetraalkylated bis(acetoxymethyl) compounds were prepared.

The reaction is applicable to both aliphatic and aromatic dinitriles. One exception observed was with β,β'-thiodipropionitrile. This dinitrile gave a viscous mass when the reaction mixture was poured on ice. The precipitate dissolved completely after a few hours. This cleavage of the polyamide does not occur when formaldehyde is used with the sulfide in place of bis(acetoxymethyl)durene. The intermediate present in sulfuric acid would be expected to show sulfonium ion character.

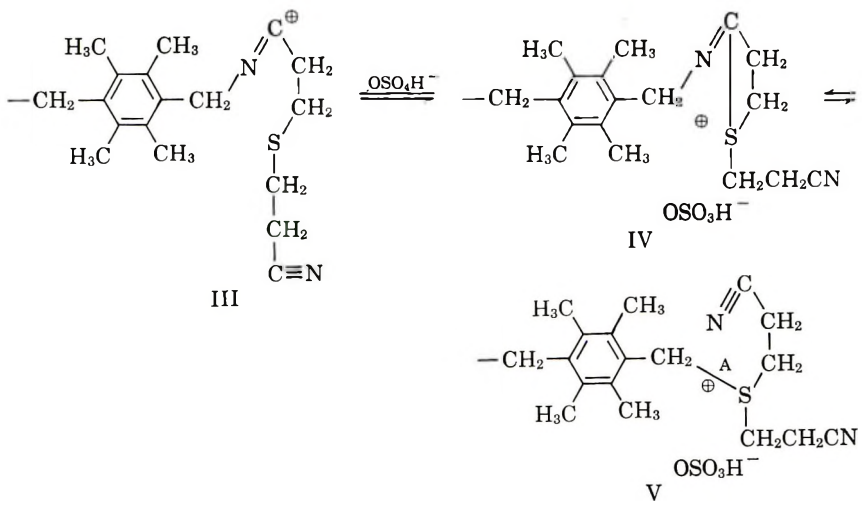

The ready reversibility of sulfonium salt formation[16] with some cleavage of bond A in V could account for the degradation of the polymer initially precipitated by addition of the sulfuric acid solution to water. This requires a greater contribution from structure V in polymers from bis(acetoxymethyl) durene than in polymers from formaldehyde. The ability of the benzylic carbon to accept electrons from sulfur should not be appreciably influenced by a similar structure at the other end of the durene molecule. However, a nitrogen atom attached directly to the methylene of a formaldehyde polymer could be expected to decrease the ability of the methylene to accept electrons from sulfur. Hence, the degradation of the polymer has been ascribed to contributions from structure V. Low molecular weights obtained from β,β'-dioxypropionitrile may result from a similar type of cleavage.

TABLE I

Nitrile	Yield, %	DSV[h]	Formula	Calculated C, %	Calculated H, %	Found C, %	Found H, %	T_1, T_2, °C.[a]
Pimelonitrile	—	0.764[b]	$C_{19}H_{28}N_2O_2$			—	—	T_2 300
Isosebaconitrile	97	0.54[c]	$C_{22}H_{34}N_2O_2$					T_1 211
Glutaronitrile	100	[d]	$C_{17}H_{24}N_2O_2$	71.4	8.38	70.73	8.44	T_1 192
								T_2 >300
Adiponitrile (50)–Azelaonitrile (50)	94	0.863[e]	$C_{37}H_{61}N_4O_4$					T_2 >300
2,2-Di(*p*-cyanophenyl) propane	89	—	$C_{29}H_{32}N_2O_2$					T_2 >300
Sebaconitrile	99	0.27[e]	$C_{22}H_{34}N_2O_2$	73.8	9.32	73.05	9.69	—
Terephthalonitrile[e]	98	—	$C_{20}H_{22}N_2O_2$					T_2 >300
Bis(cyanomethyl)durene	86	Insol.	$C_{24}H_{34}N_2O_2$					T_2 >300
β,β-Oxydipropionitrile	95	0.1[e]	$C_{18}H_{26}N_2O_2$	67.9	8.2	67.19	8.3	T_1 191
								T_2 246
Isophthalonitrile	80	Insol.	$C_{20}H_{22}N_2O_2$			—	—	T_2 >300
Adiponitrile	99	[f]	$C_{18}H_{26}N_2O_2$[g]					T_2 >300

[a] Dynamic extrusion values T_1, roughly the second-order transition temperature, and T_2, the melt flow temperature, were estimated using a dynamic extrusion rheometer. In the operation of this instrument the (granular) polymer sample is placed in a chamber under a plunger comprising a load of 3263 lb./in.^{2}. The sample is gradually heated to effect its ultimate extrusion through a 0.0625-in. diameter orifice. Plunger advance and temperature increase are measured. A plot of these values provides a curve from which T_1 and T_2 can be obtained.

[b] 1% in 98% formic acid, 25°C.

[c] 1% in *m*-cresol, 25°C.

[d] Insoluble in *m*-cresol, gelled in 98% formic acid after two days at room temperature.

[e] Sulfuric acid (88%) was added to a nitrobenzene suspension of the reactants.

[f] Soluble in *m*-cresol at 50°C. but not at 25°C.

[g] ANAL. Calc. for $C_{18}H_{26}N_2O_2$: N, 9.28%; O, 10.6%. Found: N, 9.67%; O, 11.22%.

[h] DSV = dilute solution viscosity, i.e., the natural logarithm of relative viscosity at concentration specified divided by the concentration in g./cc.

The reaction is best carried out by addition of a chloroform solution of the reactants to sulfuric acid diluted with water, formic, or acetic acid. Complicating reactions were anticipated with the use of formic acid. Some carbon monoxide is always liberated from the reaction mixture. The reaction of carbon monoxide with carbonium ions in sulfuric acid media has been studied extensively.[17] Hence, the nitrile and carbon monoxide might be expected to compete for the carbonium ions present. The latter reaction results in chain termination.

$$R^{\oplus} + N{\equiv}CR' \xrightleftharpoons{H_2SO_4} R{-}N{=}\overset{\oplus}{C}R'$$

$$R^{\oplus} + CO \xrightleftharpoons{H_2SO_4} R\overset{O}{\overset{\|}{C}}{}^{\oplus} \rightleftharpoons R\overset{O}{\overset{\|}{C}}OH$$

The reversibility of the former reaction has been well established.

Both the formation of glycolic acid from carbon monoxide and formaldehyde under acidic conditions[18] and the decomposition of the acid in sulfuric acid to give trioxymethylene and carbon monoxide have been reported.[19] High pressures of carbon monoxide are required for glycolic acid synthesis, but atmospheric pressure is adequate to give reaction with olefins which yield tertiary carbonium ions.

In the polymerizations with bis(acetoxymethyl)durene, formic acid appeared to be equivalent with acetic acid or water as a diluent for the sulfuric acid. Hence, the carbon monoxide does not effectively compete with nitrile for carbonium ions under the conditions used.

As with most condensation polymerizations, the molecular weight is a function of monomer purity and reactant ratio. Since the polymers did not show adequate thermal stability at fusion temperature, extensive purification to achieve high molecular weight was not attempted. No nitrile endgroups could be detected by infrared. If one assumes nitrile endgroups, this would indicate a molecular weight greater than 5000. The molecular weight of a polymer obtained from adiponitrile DSV = 0.5 cc./g. in *m*-cresol at 50°C.) was determined with a Mechrolab membrane osmometer #502. The number-average molecular weight obtained in *m*-cresol at 110°C. with the use of SS-08 membranes was 7300. Typical data are shown in Table I.

These polyamides, in contrast with the products from formaldehyde,

TABLE II
Influence of Formic Acid (98%) on the Polyamide from Pimelonitrile–Bis(acetoxymethyl)durene (0.04% solution)

Time, hr.	DSV
0	0.764
2	0.777
4	0.799
6	0.822
18	1.152

are stable to 98% formic acid at room temperature. Some increase in molecular weight was noted after several hours (Table II). All pressed films were very brittle, but, in contrast with polymers from formaldehyde, remained soluble in *m*-cresol.

The facile solvolysis of tertiary chloride in strong sulfuric acid has been reported by Corey and Hertler.[20] Bis(chloromethyl)durene undergoes a similar solvolysis readily. However, substitution of the chloride for the acetate in condensation with nitriles results in low yields. The reaction of nitriles with tertiary alcohols and hydrogen chloride has been studied by Zil'berman and Sladkov.[21] The synthesis of *N*-substituted amides from halides and nitriles has been reported but only in low yield and in the presence of excess aluminum chloride.[22]

An attempt was made to achieve solvolysis of both halogens of bis(chloromethyl)durene giving bis(acetoxymethyl)durene for subsequent condensation with a dinitrile. Under the conditions used (50 ml. HOAc, 100 ml. concentrated H_2SO_4, 50°C. for 4 hr.) only 55% of the theoretical amount of hydrogen chloride was liberated. This solvolysis was not studied further.

EXPERIMENTAL

Preparation of Bis(acetoxymethyl)durene

The procedure of Rhoad and Flory[23] was used, except that sodium acetate was used in place of silver acetate. The reaction mixture was heated under reflux for 3 hr. and filtered. The product crystallized from the hot acetic acid. The yield was ~90% and could be improved by reuse of the acetic acid for a second preparation.

General Procedure for Preparation of Polyamide

A solution of dinitrile (0.05 mole) and bis(acetoxymethyl)durene (0.05 mole) in 125 ml. of chloroform was added slowly to a stirred solution prepared from 60 ml. of concentrated sulfuric acid and 20 ml. of water. The acid was maintained at 20–30°C. during the addition. The mixture darkened, and the acid phase became quite viscous. The mixture was stirred for a total of 24 hr., then the chloroform was removed under vacuum. The acid solution was poured into 300 g. of cracked ice. The white polymer which precipitated was stirred in the aqueous acid media for 2 hr. then collected on a filter and washed with water until neutral. The use of more concentrated acid gave a black reaction mixture whose color was not discharged when added to cracked ice. The use of more dilute sulfuric acid resulted in lower yields. Acetic acid, formic acid, or nitrobenzene could be used in place of water to dilute the sulfuric acid.

References

1. Ritter, J. J., and P. P. Minceri, *J. Am. Chem. Soc.*, **70**, 4048 (1948).
2. Ritter, J. J., and F. X. Murphy, *J. Am. Chem. Soc.*, **74**, 763 (1952).
3. Ritter, J. J., and E. J. Tillmanns, *J. Org. Chem.*, **22**, 839 (1957).
4. Mowry, D. T., and E. L. Ringwald, *J. Am. Chem. Soc.*, **72**, 4439 (1950).

5. Magat, E. E., L. B. Chandler, B. F. Faris, J. E. Reith, and L. F. Salisbury, *J. Am. Chem. Soc.*, **73**, 1031 (1951).
6. Magat, E. E., B. F. Faris, J. E. Reith, and L. F. Salisbury, *J. Am. Chem. Soc.*, **73**, 1028 (1951).
7. Magat, E. E., and L. F. Salisbury, *J. Am. Chem. Soc.*, **73**, 1037 (1951).
8. Meyers, A. I., and J. J. Ritter, *J. Org. Chem.*, **23**, 1918 (1958).
9. Christal, H., and A. Laurent, *Bull. Soc. Chim. France*, **1958**, 920.
10. Mousseron, M., H. Christal, and A. Laurent, *Compt. Rend.*, **248**, 1904 (1959).
11. Christal, H., and A. Laurent, *Bull. Soc. Chim. France*, **1960**, 418, 599.
12. Parris, C. L., and C. M. Christenson, *J. Org. Chem.*, **25**, 331 (1960).
13. Cannizzaro, C., *Ann.*, **92**, 114 (1854).
14. Newman, M., and M. C. Deno, *J. Am. Chem. Soc.*, **73**, 3644 (1951).
15. Deno, N. C., P. T. Groves, J. J. Jaruzelski, and M. N. Lugasch, *J. Am. Chem. Soc.*, **82**, 4719 (1960).
16. Ray, F. E., and I. Levine, *J. Org. Chem.*, **2**, 267 (1937).
17. Koch, H., and W. Haaf, *Ann.*, **618**, 251 (1958).
18. Loder, D. J. (du Pont), U. S. Pat. 2,152,852, April 4, 1939.
19. Heintz, W., *Ann.*, **138**, 43 (1866).
20. Corey, E. J., and W. R. Hertler, *J. Am. Chem. Soc.*, **82**, 1657 (1960).
21. Zil'berman, E. N., and A. M. Sladkov, *Zh. Obschch. Khim.*, **31**, 245 (1961).
22. Cannon, G. W., K. K. Grebber, and Y.-K. Hsu, *J. Org. Chem.*, **18**, 516 (1953).
23. Rhoad, M. J., and P. J. Flory, *J. Am. Chem. Soc.*, **72**, 2218 (1950).

Résumé

Une nouvelle série de polyamides a été préparée par condensation des dinitriles à l'aide de bis(acétoxyméthyle)durène dans l'acide sulfurique.

Zusammenfassung

Eine neue Reihe von Polyamiden wurde durch Kondensation von Dinitrilen mit Bis(acetoxymethyl)durol in Schwefelsäure dargestellt.

Received January 16, 1964
Revised November 17, 1964
(Prod. No. 4578A)

JOURNAL OF POLYMER SCIENCE: PART A VOL. 3, PP. 1885–1894 (1965)

Proton Magnetic Resonance Spectra of Variously Treated Nylon 66*

R. E. GLICK and R. C. PHILLIPS, *Department of Chemistry and The Institute of Molecular Biophysics, The Florida State University, Tallahassee, Florida*

Synopsis

A proton NMR study on variously treated nylon 66 has been made to gain additional information on hydrogen bonding in solids. The nylon sample was found to be 48% amorphous based on the deuterium exchange of amide protons. The broad line NMR spectra of all samples consisted of a superposition of a broad and narrow component at all temperatures studied. Dried nylon and dried deuterated nylon afforded identical NMR spectra. This identity was interpreted as indicating a possible electrostatic rather than overlap description of hydrogen bonds in amorphous regions. Additives, such as water, deuterium oxide, methanol, and deuterium methoxide, lowered the temperature at which the narrow-component line width was further reduced. Such effect was consistent with other studies that indicated such additives were associated with hydrogen bonds in amorphous regions of the polymer. This effect appeared to saturate at a concentration of additive equal to that for the amide functions in the amorphous regions. Contrary to our previous studies, little difference in spectra were found for proteo and the corresponding deutero additives.

Introduction

Poly(hexamethylene adipamide) (nylon 66) and other nylons appear to be useful substances for studies of certain aspects of amide–carbonyl hydrogen bonding. An x-ray structural examination[1] on nylon 66 reveals that the crystalline regions, comprising some 50% of the solid,[2] have an extended planar *trans* chain configuration linked by interchain hydrogen bonds. The amorphous regions are as such less characterized, but appear to contain interchain hydrogen bonds. The amorphous regions absorb potential hydrogen bonding agents, water, etc.[3] that can interact with the amide and/or carbonyl groups,[4] while the crystalline regions do not appear to absorb these substances. In an attempt to obtain additional information on hydrogen bonding in such solids, proton nuclear magnetic resonance (NMR) studies on specially treated nylon 66 have been undertaken.

NMR studies on nylon 66 have been reported by several authors.[5–12] The NMR method provides information on molecular reorientations found in each region of the polymer, crystalline and amorphous, that, depending

* This work was supported in part by Public Health Service Research Grant GM 11337-03 and in part by a contract between the Division of Biology and Medicine, U. S. Atomic Energy Commission and the Florida State University.

upon the transition region, can be interpreted as arising from the breaking of pertinent hydrogen bonds. Thermodynamic and structural information can be inferred from the variation with temperature of the signal width δH, as δH decreases whenever reorientation frequencies are of the order of 10^3–10^5 cycle/sec. Relaxation time measurements would be preferred for thermodynamic purposes and a further derived quantity, the signal second moment, ΔH_2^2, for structural studies. Although an increased understanding of molecular structure can be gained by examining ΔH_2^2, the mixed state nature of nylon renders difficult such analysis.[13]

Experimental

Proton resonance spectra of nylon 66 were taken at a fixed frequency of 24.3 Mcycle/sec. with a Varian Model V4500 EPR spectrometer, modified for wide-line NMR, and equipped with a Model V4340 variable temperature probe accessory (slightly modified) and a Model V2100A 12-in. electromagnet. The Varian sample holder, (#961257), was so modified that the sample could be enclosed. This holder, with a 10 mm. outside diameter, allowed a 0.3-g. sample to be contained within the insert.

A suitable power level, below saturation, was determined by the measurement at room temperature and at 160°C. of ΔH_2^2 for an untreated nylon sample containing an equilibrium amount of water, and ΔH_2^2 was calculated for each temperature. The signal, possessing common features at all temperatures studied, consisted of a broad and narrow component. Adjustments were made in the time constant, amplifier gain, modulation sweep, scanning rate, and recorder speed so that each component could be resolved.

The broad component of the spectrum was scanned at approximately 4 gauss/min. The scanning rate for the narrow component was in the range 1.60–0.36 gauss/min., depending upon the width and intensity of the spectrum. Modulation amplitudes were set in the range of 0.50–2.00 gauss to resolve the broad component and 0.03–0.30 gauss for the narrow component. The scanning rate was calibrated by the side band technique. The sample temperature, determined by a calibrated copper–constantan thermocouple, was varied by allowing dry, heated or cooled, nitrogen gas to flow through the insert.

The nylon was supplied by the Textile Fibers Department, E. I. du Pont de Nemours and Company, as chunks which ranged in size from 4 mm.^{2} by 1 mm. to 0.25 mm.^{2} by 1 mm. The nylon possessed the same physical properties[6,7] as our previous samples.

Proton resonance spectra were taken on nylon (*1*) soaked with several different liquids known to form hydrogen bonds, (*2*) exhaustively dried samples, and (*3*) a sample that was exhaustively dried, soaked in D_2O, then exhaustively dried again. All samples used were first dried to a constant weight. This drying took approximately one month, although the largest portion of the moisture had been removed after five days. The drying was

accomplished in an abderhalden heated to approximately 115°C., magnesium perchlorate being used as an absorbent.

Several dried samples were placed in tubes containing a large excess of each of the solute liquids. These tubes were immersed in liquid nitrogen, evacuated, and then sealed. The tubes were then heated at 115°C. for 15–20 days and allowed to stand at room temperature for at least 15 days. Two samples treated in this way, one with D_2O and the other with H_2O, were opened and evacuated until the desired concentrations were obtained. One sample that had been treated in this way with D_2O was exhaustively dried.

The samples used were: (1) dried, soaked in D_2O, and dried; (2) dried; (3) sample (1) containing 5.4×10^{-3} mole D_2O/g. dried nylon; (4) sample (2) containing 5.6×10^{-3} mole H_2O/g.; (5) sample (1) containing 1.4×10^{-3} mole D_2O/g.; (6) sample (2) containing 1.6×10^{-3} mole H_2O/g.; (7) sample (1) containing 4.1×10^{-3} mole CH_3OD/g.; and (8) sample (2) containing 3.7×10^{-3} mole CH_3OH/g. The above quantities have been corrected to account for the exchange of solvent deuterons for protons within the nylon. This correction was taken from samples that had been dried, soaked in D_2O, and dried again. The increase in weight of these samples was 0.41% (average of three determinations). This is equivalent to a 48% amorphous content for the sample.

The D_2O used in preparing the samples was 99.7% pure. Distilled water was used in preparing the H_2O-soaked samples. The two methanol-soaked samples were prepared from purified methanol and synthesized deuterium methoxide. Purified methanol was treated with magnesium turnings to remove any water present, refluxed, and distilled from the mixture at a constant temperature of 64.0°C. Deuterium methoxide was prepared by titration of $NaOCH_3$ with an equivalent quantity of D_3PO_4 in an excess of D_2O. The CH_3OD was then refluxed and distilled from this mixture at a constant temperature of 64.0°C. High-resolution NMR was used to determine the relative intensities of both the CH_3 and HO peaks. The CH_3-OD contained an HO peak that corresponded to less than 1% of the protons present in the compound. The line widths, δH, of the spectra are the distances in gauss between the maxima and minima of the derivative of the absorption curve.

Results

The proton resonance spectra of the dried nylon Dr(H_2O), dried deuterated nylon, Dr(D_2O), and liquid-treated samples consisted of a superposition of a narrow component upon a broad component at all temperatures studied. Below a transition temperature, the intensity of the narrow component increased with respect to that of the broad component as the temperature was increased. The narrow-component line width, δH, remained more or less constant. At and above the transition temperature, the narrow-component intensity increased further, and a marked decrease in δH occurred.

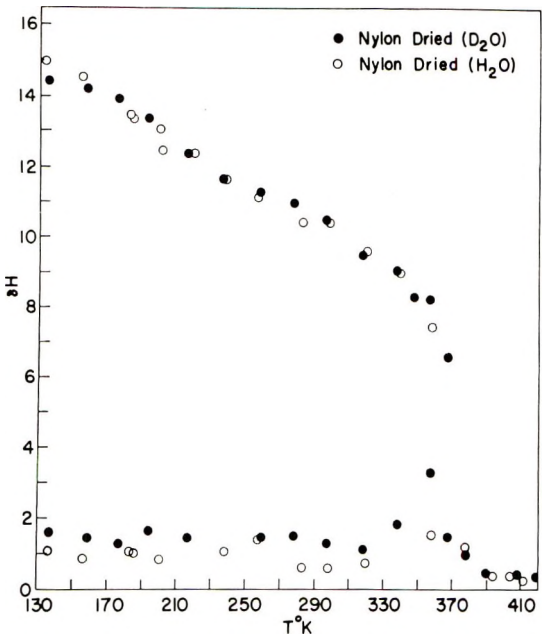

Fig. 1. Variation of NMR line width with temperature for (O) dried nylon and (●) deuterated nylon.

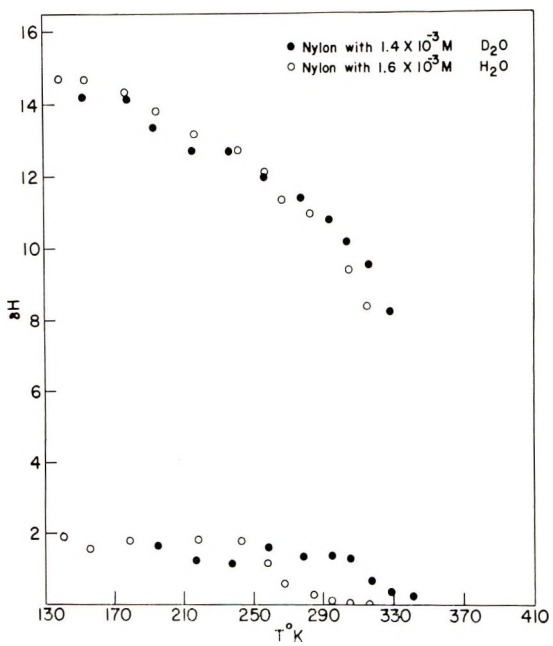

Fig. 2. Variation of NMR line width with temperature for dried nylon containing (●) 1.4×10^{-3} mole H_2O and (O) 1.6×10^{-3} mole D_2O per gram of nylon.

The spectral intensities of the narrow components were approximately equal for all the samples in the low temperature range. At temperatures where the narrow component increased in intensity and narrowed, there was a marked difference in relative intensities between the various liquid-soaked samples. The approximate order of increasing narrow-component intensity was as follows (in moles per gram dry nylon): 1.4×10^{-3} D_2O $\simeq 5.4 \times 10^{-3} D_2O < 1.6 \times 10^{-3} H_2O < 5.6 \times 10^{-3}$ $H_2O < 4.1 \times 10^{-3}$ $CH_3OD < 3.7 \times 10^{-3}$ CH_3OH.

Figures 1–4 are plots of temperature versus δH for the broad and narrow components of the individual samples. In Figure 1 are given the curves for $Dr(D_2O)$ and $Dr(H_2O)$. In general the broad component could not easily be resolved above 370°K.

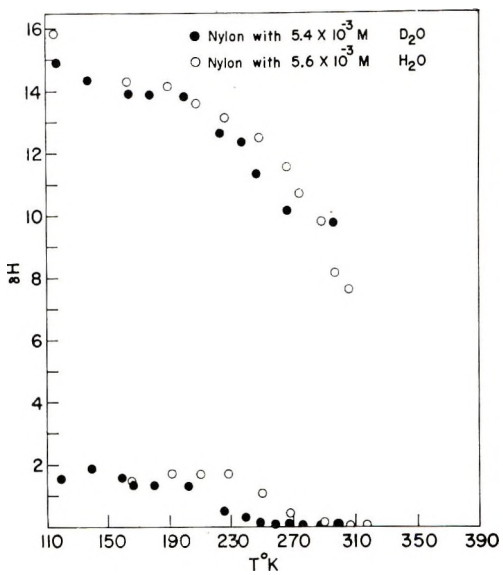

Fig. 3. Variation of NMR line width with temperature for dried nylon containing (O) 5.6×10^{-3} mole H_2O and (●) 5.4×10^{-3} mole D_2O per gram of nylon.

The narrow-component curves for these samples exhibit a rapid narrowing from 370 to 395°K.; δH dropped from an average of 1.2 to 0.3 gauss. The "wild" point at 3.25 gauss in the narrow-component curve for $Dr(D_2O)$ probably has a relatively larger line width because of the difficulty in resolving the spectra at this temperature, the intensity of the broad component being equal to the intensity of the narrow component; under this condition artificial broadening of the narrow component probably occurred.

The line width curves in Figure 2 are for 1.4×10^{-3} mole D_2O and 1.6×10^{-3} mole H_2O. These curves exhibit a gradual narrowing of the broad component with a slightly sharper narrowing in the 305–330°K. range for 1.4×10^{-3} mole D_2O and in the 260–320°K. range for 1.6×10^{-3} mole H_2O. The narrow components of these curves exhibit rapid narrowing in

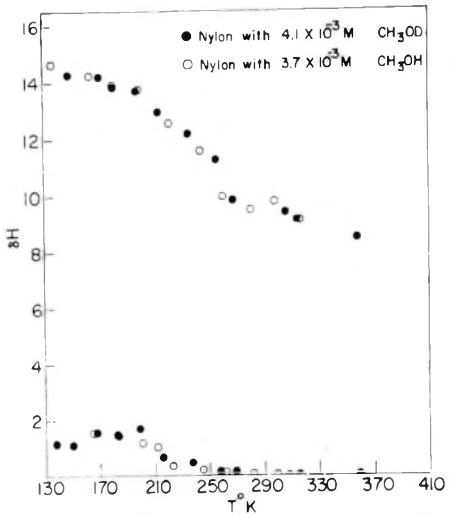

Fig. 4. Variation of NMR line width with temperature for dried nylon containing (○) 3.7×10^{-3} mole $HOCH_3$ and (●) 4.1×10^{-3} mole $DOCH_3$ per gram of nylon.

the 305–330°K. range for 1.4×10^{-3} mole D_2O and in the 250–285°K. range for 1.6×10^{-3} mole H_2O.

The line width curves in Figure 3 are for 5.4×10^{-3} mole D_2O and 5.6×10^{-3} mole H_2O samples. These curves exhibit a gradual narrowing of the broad component at low temperatures, with a more pronounced narrowing in the 225–305°K. range for 5.4×10^{-3} mole D_2O and in the 240–305°K. range for 5.6×10^{-3} mole H_2O.

The line width curves in Figure 4 are for 4.1×10^{-3} mole CH_3OD and 3.7×10^{-3} mole CH_3OH samples. The broad-component line widths gradually decrease to about 9.5–10.0 gauss; then the curves begin to level off at about 260°K. The line widths become hard to resolve in the leveling-off region, so that no attempt is made to interpret the very gradual slope in this region, but sufficient resolution was obtained to determine that this region does exist. The narrow components of these curves exhibit rapid narrowing in the 200–240°K. range for 4.1×10^{-3} mole CH_3OD and in the 195–240°K. range for 3.7×10^{-3} mole CH_3OH.

Discussion

The proton NMR spectra of the various nylon samples can be conveniently interpreted by a separate analysis of each component. At the lowest temperature, the broad component predominated. The second moment, 26 gauss^2, was found to be consistent with that calculated[14] for fixed CH_2-protons in a polycrystalline long-chain aliphatic solid. The line width of the broad component slowly decreased as the temperature increased until 330–370°K., when the width rapidly reduced to a minimum value. The initial slow decrease was interpreted as a low activation energy process that might possibly be reorientation of chain methylene

groups. The rapid decrease indicated that a more effective reorientation, presumed to require the breaking of hydrogen bonds, had occurred.

The narrow-component width remained approximately constant as the temperature increased until, depending on the sample treatment, the component width reduced rapidly. The original width of the narrow component can be ascribed to chain reorientation in regions of lower density, amorphous regions, while the final reduction can be related again to reorientations that became possible when interchain hydrogen bonds were no longer of importance with respect to the time scale of this experiment. These interpretations were consistent with previous morphological examinations of nylon versus dielectric relaxation[15–17] and dynamic mechanical[18,19] as well as NMR relaxation studies.[11]

The line width variation obtained for Dr(H_2O) agreed with that computed from NMR transverse relaxation measurements (T_2) of McCall and Anderson.[11] By using the equation relating T_2 to γH, a value of 7.5 gauss for the line width at 360°K. was obtained as compared to our experimental value of 7.4 gauss at the same temperature. T_2 measurements predict line widths of 1.25 and 1.07 gauss at 403 and 410°K., respectively, as compared to our experimentally determined values of 0.38 and 0.27 gauss at 404.8 and 412.4°K. The disparity between experiments might partly be due to the large absolute errors inherent in measuring the line widths of the narrowest components. Differences in line width, i.e., those indicating transitions, are easily determined.

The narrow or amorphous component was observed for all samples at all temperatures studied, as predicted by McCall and Anderson from their dielectric relaxation[15] and NMR relaxation studies.[11] A narrow component had been reported in dried nylon 66[10–12] at high temperatures, i.e., 370–420°K., but was not reported by Glick,[6] Woodward,[7] Gupta,[8] and Jones[9] in their studies. As Jones attributes the narrow component to improperly dried material, our results should be examined with respect to those for Dr(D_2O) and Dr(H_2O) given by Jones,[9] as well as Glick,[6] Woodward,[7] and Gupta.[8] Our spectra resembled fairly closely those obtained by these investigators when we employed sweep modulation amplitudes between 1.1 and 2.2 gauss. Using modulation amplitudes in the range 0.25–0.80 gauss, the narrow component was found at all temperatures studied and indicated that these two effects had not been separated. Saturation, as well as overmodulation effects, also complicated our earlier studies,[6–8] leaving these earlier works open to question.

It was of interest to compare the NMR line width behavior of Dr(D_2O) with that for Dr(H_2O). An examination of the data presented in Figure 1 clearly indicated the NMR identity of the two substances. These samples, in contrast to those with additives, were believed to be easily characterizable. The question as to whether all water had been removed could be answered by the dried deuterium oxide treated samples, since a proton NMR signal from a possible water component would be absent. Nor was there any likelihood of temperature-dependent complications that might

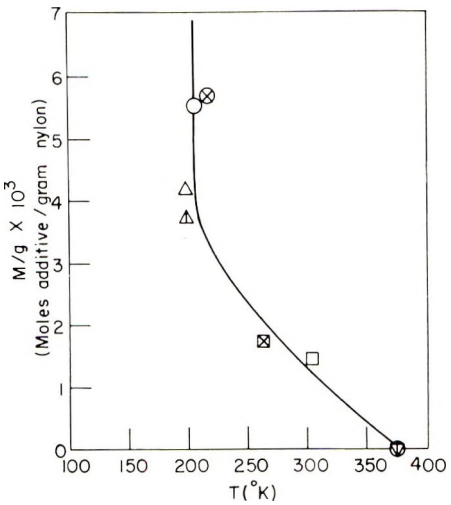

Fig. 5. Plot of moles of additive vs. temperature of onset of narrow component NMR line width transition: (⦶) dried nylon; (▽) dried deuterated nylon; (□) 4.4 × 10^{-3} mole H_2O; (⊠) 1.6 × 10^{-3} mole D_2O; (△) 4.1 × 10^{-3} mole $DOCH_3$; (⟁) 3.7 × 10^{-3} mole $HOCH_2$; (⊗) 5.6 × 10^{-3} mole H_2O; (O) 5.4 × 10^{-3} mole D_2O.

be possible in the liquid-treated samples. That these spectra were identical tended to indicate that intermolecular interactions in the amorphous regions were, to the precision of this measurement (estimated as ±5°K.), isotope-independent. Such lack of isotope dependence, at least in the amorphous regions, could be interpreted as requiring a predominant electrostatic rather than an overlap description for the hydrogen-bond interaction.[20]

It has been concluded from infrared and other studies[3,4] that the additives were associated with hydrogen bonds in the amorphous regions. Further evidence appeared to be provided by this study. As has been noted, the major transition in the crystalline regions was most probably due to the breaking of hydrogen bonds. The effect of additives on this transition was much less pronounced and less regular than that found for the narrow or amorphous component of the dried sample. The transition temperature for line narrowing attributed to reorientation in the amorphous regions decreased with increasing amounts of additive. This effect, however, appeared to saturate at about 4 × 10^{-3} mole of additive per gram of dry nylon (Fig. 5). This saturation concentration was that expected from the determination of exchangeable hydrogens. Thus, a one-to-one relationship existed between the apparent number of amide groups in the amorphous regions and uptake of solvating agent.

Outside of superficial details—the apparent primary solvation of the hydrogen-bonded elements in the amorphous regions and the accompanying saturation effect—an interpretation of the exact nature of the interaction between the additive and the polymer cannot be provided by this study.[17,21] Clearly, the predominant effect of the additive was the reduction in temperature of the narrow-component transition without significantly altering

the broad component. The least complicated spectra in this connection were those obtained with deuterium oxide as the additive, since proton-containing additives contributed NMR signals. Even with this complication, the water and deuterium oxide samples behaved similarly. Contrary, therefore, to earlier studies, there appeared to be little, if any, difference between spectra obtained with samples containing proton additives and those with appropriately substituted deuterium additives.[6-8]

References

1. Bunn, C. W., and E. V. Garner, *Proc. Roy. Soc. (London)*, **A189**, 39 (1947).
2. Hermans, P. H., and A. Weindinger, *J. Polymer Sci.*, **4**, 718 (1949); H. W. Starkweather, Jr. and R. E. Maynihan, *ibid.*, **22**, 236 (1956).
3. Starkweather, H. W., Jr., G. E. Moore, J. E. Hansen, T. M. Roder, and R. E. Brooks, *J. Polymer Sci.*, **21**, 189 (1956).
4. Glatt, L., and J. W. Ellis, *J. Chem. Phys.*, **16**, 551 (1948).
5. Slichter, W. P., *J. Appl. Phys.*, **26**, 1099 (1955); *J. Polymer Sci.*, **35**, 77 (1958); *SPE J.*, **15**, 303 (1959).
6. Glick, R. E., R. P. Gupta, J. A. Sauer, and A. E. Woodward, *J. Polymer Sci.*, **42**, 271 (1960).
7. Woodward, A. E., R. E. Glick, J. A. Sauer, and R. P. Gupta, *J. Polymer Sci.*, **45** 367 (1960).
8. Gupta, R. P., *J. Phys. Chem.*, **65**, 1128 (1961).
9. Jones, D. W., *Polymer.*, **2**, 203 (1961); *J. Polymer Sci.*, **54**, 271 (1962).
10. Shaw, D. J., and B. A. Dunell, *Can. J. Chem.*, **39**, 1154 (1961).
11. McCall, D. W., and E. W. Anderson, *Polymer*, **4**, 93 (1963).
12. Statton, W. O., *J. Polymer Sci.*, **C3**, 3 (1963).
13. Abragam, A., *The Principles of Nuclear Magnetism*, Oxford, 1961 (general reference).
14. Andrews, E. R., *J. Chem. Phys.*, **18**, 607 (1950); W. P. Slichter, *J. Appl. Phys.*, **26**, 1099 (1955).
15. McCall, D. W., and E. W. Anderson, *J. Chem. Phys.*, **32**, 237 (1960).
16. Schmieder, K., and K. Wolf, *Kolloid-Z.*, **134**, 149 (1953).
17. Boyd, R. H., *J. Chem. Phys.*, **30**, 1276 (1959).
18. Deeley, C. W., A. E. Woodward, and J. A. Sauer, *J. Appl. Phys.*, **28**, 1124 (1957).
19. Woodward, A. E., J. M. Crissman, and J. A. Sauer, *J. Polymer Sci.*, **44**, 23 (1960).
20. Orgel, L., *Rev. Mod. Phys.*, **31**, 100 (1959).
21. Curtis, A. J., *J. Res. Natl. Bur. Std.*, **65A**, 185 (1961).

Résumé

On a effectué une étude des protons par NMR du Nylon 66 traité de différentes façons pour obtenir des informations sur les liaisons hydrogènes dans les solides. On a trouvé que l'échantillon de nylon était amorphe pour 48%, en se basant sur l'échange des protons des fonctions amides avec le deutérieum. Le spectre NMR en phase solide provient d'une superposition d'une bande large et étroite à toutes les températures étudiées. Du nylon sèché et du nylon deutéré séché donnent des spectres NMR identiques. Cette identité a été interprètée comme provenant d'une influence électrostatique plutôt que d'un recouvrement des liaisons hydrogène dans les régions amorphes. Les additifs, l'eau, l'oxyde de deutérium, le méthanol et le méthylate de deutérium abaissent la température à laquelle la largeur de la bande étroite est réduite. Un tel effet correspond avec d'autres études, qui indiquent que ces additifs s'associent avec les liaisons-hydrogène dans les régions amorphes du polymère. Cet effet semble atteindre la saturation à une concentration d'additif égale à celle des fonctions amides dans les régions amorphes.

Contrairement à nos études antérieures, on n'a trouvé qu'une légère différence dans les spectres des additifs correspondants protonés et deutérés.

Zusammenfassung

Eine-Proton-NMR-Untersuchung von verschieden behandeltem Nylon-66 wurde zur Gewinnung zusätzlicher Information über die Wasserstoffbindung in Festkörpern ausgeführt. Die Nylonprobe war nach ihrem Verhalten beim Deuteriumaustausch der Amidprotonen zu 48% amorph. Das Breitlinien-NMR-Spektrum aller Proben bestand bei allen verwendeten Temperaturen aus einer Überlagerung einer breiten und einer engen Komponente. Getrocknetes Nylon und getrocknetes Deutero-Nylon lieferten identische NMR-Spektren. Diese Identität wurde als Hinweis auf die Möglichkeit einer elektrostatischen Beschreibung anstelle einer Überlappung der Wasserstoffbindung in amorphen Bereichen gedeutet. Additive, Wasser, Deuteriumoxyd, Methanol und Deuteriummethoxyd erniedrigten die Temperatur, bei welcher eine weitere Verengung der Linienbreite der engen Komponente eintrat. Eine solcher Effekt ist mit anderen Untersuchungen, die auf eine Wasserstoffbrückenassoziation solcher Additive in amorphen Bereichen des Polymeren hinweisen, konsistent. Der Effekt scheint bei einer Additivkonzentration entsprechend derjenigen der Amidfunktion in den amorphen Bereichen eine Sättigung zu erreichen. Im Gegensatz zu unseren früheren Untersuchungen trat in den Spektren nur ein geringer Unterschied bei Wasserstoff- und den entsprechenden Deuterioadditiven auf.

Received June 4, 1964
Revised December 7, 1964
(Prod. No. 4586A)

JOURNAL OF POLYMER SCIENCE: PART A VOL. 3, PP. 1895–1909 (1965)

Characterization of Emulsion Polyethylene

JAMES E. KURZ, *Central Research Department, Monsanto Company, St. Louis, Missouri*

Synopsis

Polyethylene which was made by emulsion polymerization was characterized by means of osmometry, light scattering, and viscometry. The samples have unusually high weight- and number-average molecular weights. Low molecular weight polymer which is usually present in commercial polyethylenes was not detected. The data indicate a compact, highly ramified molecular structure. The light-scattering data suggest each latex particle is made up of essentially one giant molecule which swells but does not dissolve in organic solvents at 100°C. Swelling factors calculated from viscosity and light-scattering data indicate low degrees of crosslinking. A clear distinction cannot be made between a highly long-chain branched structure and the crosslinked structure of microgels. Of the low-density polyethylene, 1–2 wt.-% is made up of molecules which have a comparable structure. In contrast, the greatest portion of the experimental samples is composed of the high molecular weight, highly ramified molecules.

INTRODUCTION

In a series of papers,[1–3] it was demonstrated that low-density polyethylenes, in general, are characterized by broad molecular weight distributions and have molecules with varying degrees of branching. Subsequent light-scattering studies[4–8] revealed the presence of a small number of large particles in low-density polyethylenes.

These particles were identified in more recent studies. Bryant and co-workers[9] found crosslinked networks in Fawcett-type polyethylene. For a particular sample, the volume fraction of crosslinked networks is about 1.5%. The average diameter of the particles is about 10 μ, which corresponds to a molecular weight of 10^{14}.

Spherical particles which range in size from 300 to 800 A. were found in low-density polyethylene by electron microscope investigations.[10,11] These particles were concentrated and roughly fractionated by filtration of solutions of the polyethylene sample through Millipore filters. These particles behave as entities in the bulk polymer, do not join in the folded structure of a single crystal of polyethylene, and do not uncoil in solution. The authors believe the particles are highly branched molecules with molecular weights of several million, and are formed in small numbers by a long-chain branching mechanism[1,3] in the high-pressure polymerization of ethylene to high conversions.

The subject of this study is the characterization of samples made by the

emulsion polymerization of ethylene. These samples have unusually high number- and weight-average molecular weights. Light scattering and viscosity data indicate that the molecules of these samples are highly ramified, with possible crosslinking, and have a compact, spherical shape. In contrast to low-density polyethylene, which has only a few per cent of such molecules, the greatest portion of the experimental samples is composed of these high molecular weight, highly ramified molecules.

EXPERIMENTAL

Samples

The experimental samples labeled A, B, C, and D in the tables and figures were made by a laboratory free-radical, emulsion polymerization of ethylene. The polymer was coagulated by freezing the latex and recovered by filtration. The samples were washed exhaustively with water and methanol to remove the emulsifier. Residual emulsifier was removed by dissolving the polymer in stabilized xylene at 100°C. and precipitating in methanol, followed by drying. The procedure was repeated three times to assure the removal of all emulsifier.

Samples of commercially available high-density polyethylene (HDPE) and of commercially available low-density polyethylene (LDPE), are included for the sake of comparison.

All samples were dried at 60°C. in a vacuum oven before use.

Chain Branching

An estimate of chain branching was made by infrared absorption measurements.[12,13] A Beckman IR-4 spectrometer was used. The samples were held at 150°C. in a heated cell.

Density

The densities of compression-molded samples were determined by the displacement technique. A silicone fluid was used as the medium of known density.

Melt Index

The ASTM D1238-52T standard method was used.

Viscometry

Cannon-Fenske viscometers were used to measure the relative viscosities of xylene solutions of the samples at 105°C. The solutions were made with 0.1 g. polymer/100 ml. solvent at room temperature. The concentration is 0.092 g./100 ml. at 105°C. after correcting for the change in density of the xylene. The efflux times of the solvent always exceeded 100 sec. The data are presented as the reduced specific viscosity (RSV), η_{sp}/c.

Osmometry

Osmotic pressure measurements were made with Stabin osmometers[14] with the use of reagent grade xylene (mixed isomers) at 105°C. The solutions were stabilized with 0.1% di-*tert*-butyl-*p*-cresol (Ionol).

Type PT 600 dry cellophane membranes were swollen in water for several hours and conditioned to xylene by the gradual exchange of the solvents: water, ethanol, acetone, and xylene. These membranes required 40–50 hr. to reach equilibrium in the Stabin osmometers.

The osmotic pressure of the solutions of HDPE and LDPE gradually decreased with time, indicating diffusion of low molecular weight polymer through the membranes. The molecular weights were derived by observing the decrease in osmotic pressure with time for one week for each solution, plotting Δh versus time, and extrapolating the linear portion of the curve to zero time to obtain the corrected Δh value. Although this procedure does not compensate entirely for the diffusion, the molecular weights

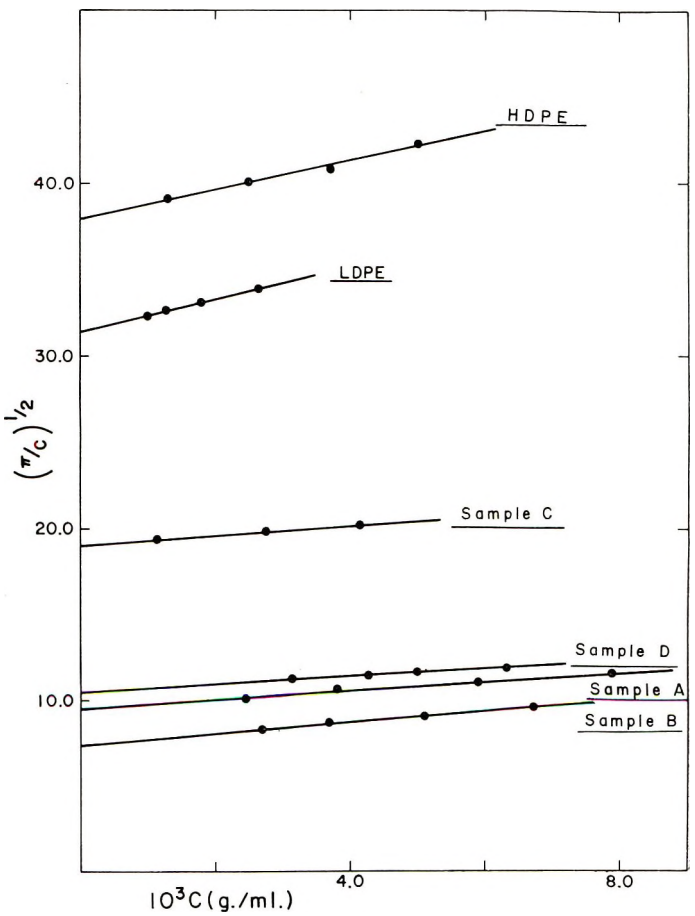

Fig. 1. Osmotic pressure data.

obtained establish upper limits to the true values. Diffusion of low molecular weight polymer was not observed with any of the experimental samples made by the emulsion polymerization process.

The values of Δh were measured to 0.01 cm. with a desk cathetometer. The data are presented in Figure 1 according to the equation:

$$(\pi/c)^{1/2} = (\pi/c)_0^{1/2}[1 + 1/2\Gamma_2 c] \quad (1)$$

where π is the osmotic pressure and $(\pi/c)_0 = RT/\bar{M}_n$. The second virial coefficient A_2 is given by $\Gamma_2/\bar{M}_n$. The concentration c is in grams per milliliter, 0.787 g./ml. being taken as the density of xylene at 105°C.

Light Scattering

A S.O.F.I.C.A. photogoniodiffusometer was used to measure the light-scattering intensities, I_θ, over the angular range of 30–150°. Unpolarized light of 546 mμ wavelength was used. The instrument was calibrated with benzene, the value[15] $I_{90} = 15.7 \times 10^{-6}$ cm.$^{-1}$ at 20°C. and 546 mμ being used. The instrument alignment and uniformity of each cell were checked with dust-free CCl_4. The products of the galvanometer readings and the factor, $\sin\theta/(1 + \cos^2\theta)$, were constant to within 2.0% over the angular range 30–150°.

The measurements were made at 105°C. with the use of distilled tetralin as the solvent. Master solutions of each sample were prepared and filtered under nitrogen pressure through filters with medium and fine porosity fritted glass disks. Aliquots of the master solution were diluted to give the desired concentrations. Finally, each solution was filtered through an ultrafine porosity fritted glass disk filter directly into a dust-free cell.

The filtration procedure usually progressed without the removal of polymer, except that 1–2% gel was filtered from the master solution of LDPE. The most concentrated solutions of samples A and B exhibited a slight blue haze which was not eliminated by filtration through the ultrafine filter (0.9–1.4 μ pore diameter). The haze shows that the very large, swollen molecules are sufficiently compact to pass the filters. The solutions of sample D tended to clog the fine porosity filter (4–5.5 μ pore diameter) and would not pass the ultrafine filter.

Bryant and co-workers[9] demonstrated that light-scattering intensity data in the angular range 0–30° are required for very high molecular weight polyethylene particles. These data cannot be obtained with the S.O.F.I.C.A. instrument. Therefore, measurements with the solutions of any sample which would not pass an ultrafine filter were not carried out.

Depolarization measurements were made on all solutions. The correction was negligible for all samples except LDPE in tetralin at 105°C., for which the Cabannes factor is 1.07. The intercept of the Zimm plot was multiplied by this correction factor.

The Brice-Phoenix differential refractometer[16] was calibrated at 28°C. with aqueous sucrose solutions. The cell was electrically heated to 105°C. and held within 1°C. by an on-off relay. The values of dn/dc in Table I

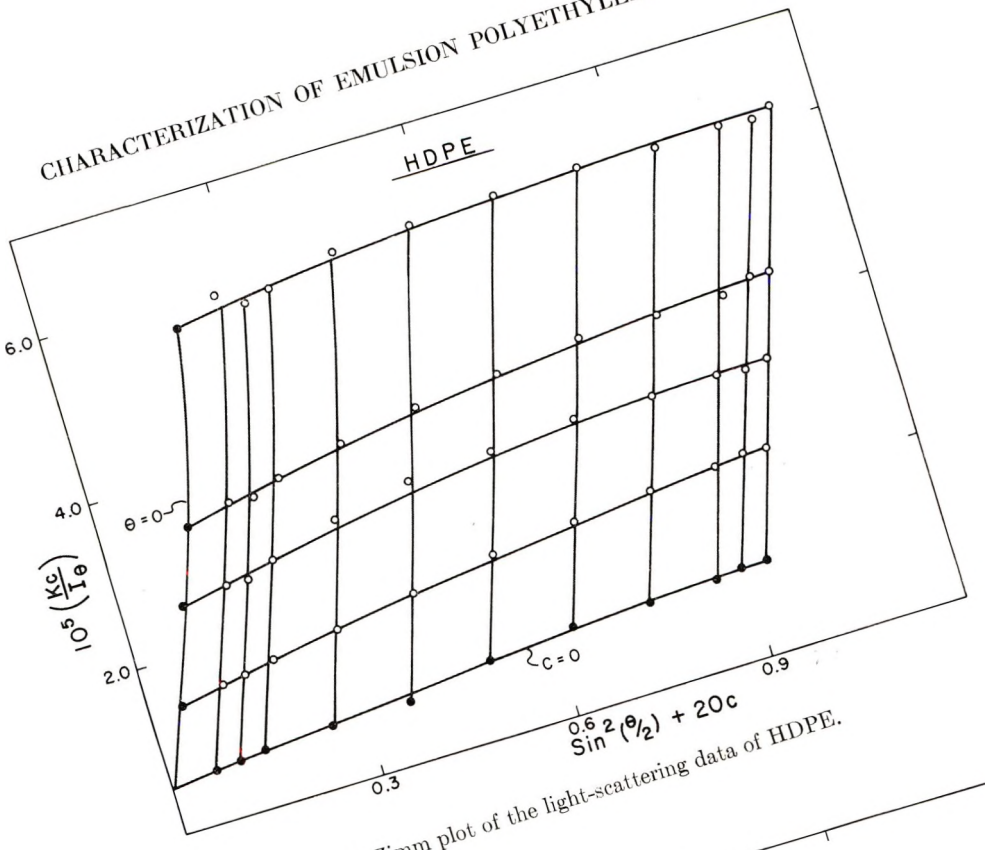

Fig. 2. Zimm plot of the light-scattering data of HDPE.

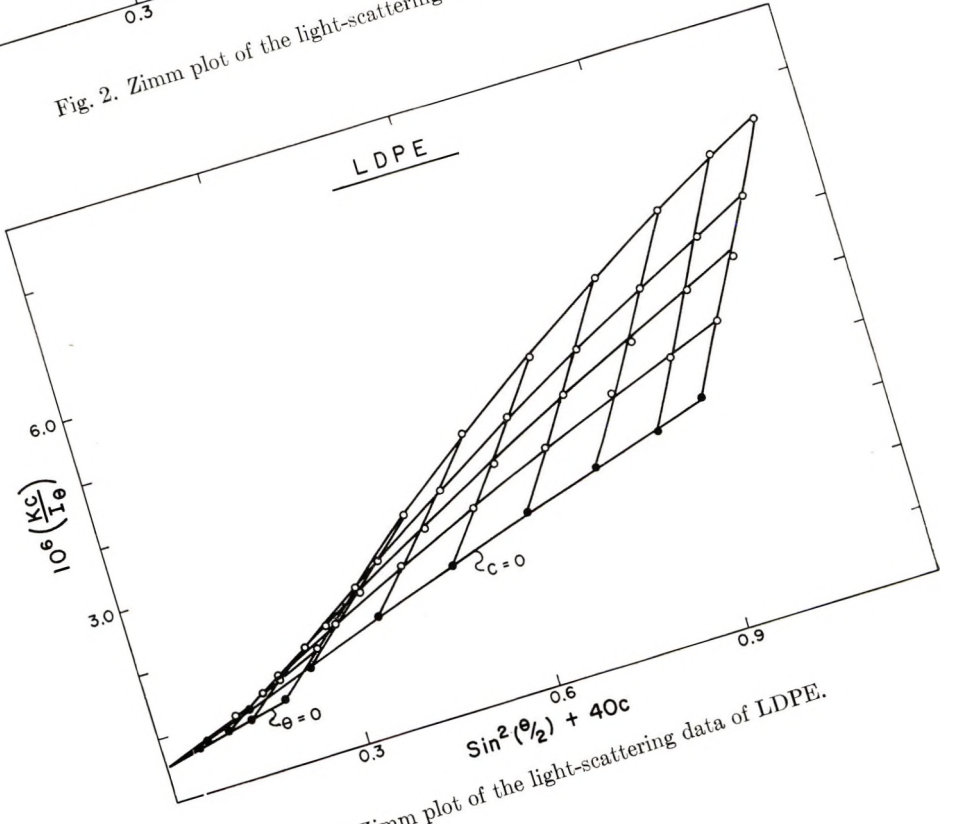

Fig. 3. Zimm plot of the light-scattering data of LDPE.

TABLE I
Summary of the dn/dc Data (λ = 546 mμ)

Sample	Solvent	Temperature, °C.	dn/dc
A	Tetralin	105	0.078
A	*o*-Dichlorobenzene	120	0.078
B	Tetralin	105	0.078
C	Tetralin	105	0.072
HDPE	Tetralin	105	0.083
LDPE	Tetralin	105	0.078
Polystyrene	Toluene	28	0.111

are in satisfactory agreement with the results recently reported by Drott and Mendelson[17] on samples of low-density polyethylene.

The light-scattering data are presented in Figures 2–5 according to the procedure described by Zimm.[18] The dissymmetry $[z]$, is the ratio I_{45}/I_{135} in the limit c = 0.

Since low-angle intensities cannot be obtained with the S.O.F.I.C.A. instrument, the exact curvature of the Zimm plots of samples A and B in the angular range 0–30° is unknown. An accurate extrapolation of the angular data to $\theta = 0$ is not possible. Following Moore and Peck,[10] a preliminary plot of log (Kc/I_θ) versus $\sin^2(\theta/2)$ was used to determine the intercept. This plot appeared to be linear at the three lowest angles enabling a linear extrapolation of the data to $\theta = 0$. There is not theoretical justification for this procedure, but it does provide a rough estimate of the molecular weight and dimensions.

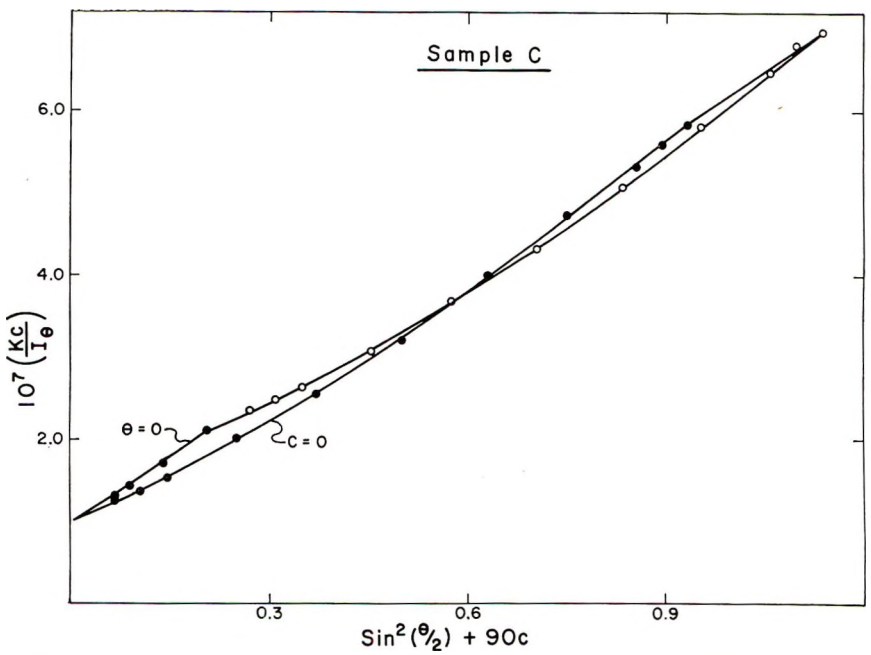

Fig. 4. Zimm plot of the light-scattering data of Sample C.

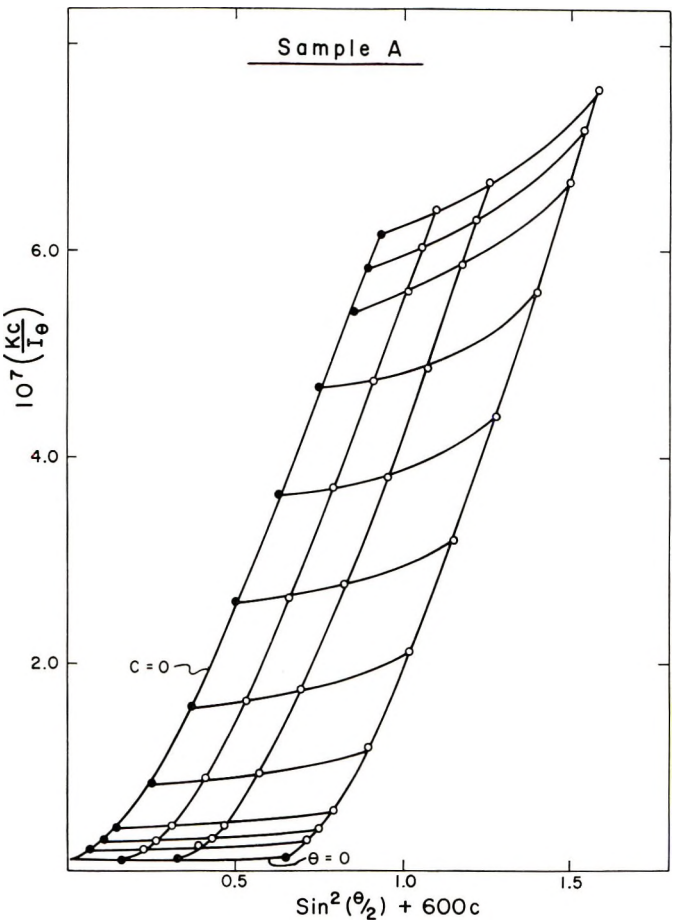

Fig. 5. Zimm plot of the light-scattering data of Sample A.

To simplify the appearance of Figure 4, only the outermost curves of the Zimm plot are shown. The Zimm plots of sample B in tetralin and sample A in *o*-dichlorobenzene are identical in appearance to that of sample A in tetralin and are not shown.

Particle Size Determination

An estimate of the average particle diameter of each latex was obtained from the ratio I_{45}/I_{135} by using the tables of Pangonis and Heller.[19] The measurements were made with 546 mμ unpolarized light taking $m = 1.15$.

RESULTS AND DISCUSSION

Osmometry

The results of the osmotic pressure measurements are in Table II. The number-average molecular weights of the experimental samples range

from 8.85×10^4 to 5.9×10^5, and diffusion of low molecular weight polymer was not observed. The number-average molecular weights of the commercial samples are an order of magnitude lower, and diffusion was observed. The molecular weights of the experimental polymers not only are substantially higher than those of the commercial polyethylenes, but low molecular weight polymer, which is found in both the low and high density samples cannot be detected in the experimental samples.

TABLE II
Characterization Results

Sample	10^{-4} $\bar{M}_n$	10^4 A_2	$\bar{M}_w/\bar{M}_n$	Density, g./cc.	CH_3/-100 CH_2	Melt index	η_{sp}/c
A	36.0	1.6	280	0.936	1.25	0.35	1.98
B	59.0	1.6	250	0.935	1.0	0.85	1.75
C	8.85	3.6	113	0.930	1.65	21.0	1.15
D	29.4	1.6	—	0.929	1.45	2.7	1.31
HDPE	2.2	21	8.3	0.960	0.75	0.3	2.48
LDPE	3.25	18.5	53	0.916	2.6	0.25	1.21

The second virial coefficients of the experimental polymers are much lower than expected for linear polyethylene. For example, a fraction of linear polyethylene with $\bar{M}_n = 1.8 \times 10^5$ in xylene at 105°C. has an $A_2 = 11.9 \times 10^{-4}$.[20] The values of A_2 of the experimental polymers are considerably lower than this value. Although A_2 decreases somewhat with increasing molecular weight, the low values of A_2 indicate considerable long-chain branching in the molecules.

The very large $\bar{M}_w/\bar{M}_n$ ratios indicate extreme polydispersity which has been observed in low-density polyethylene.[6–8]

Branching and Flow Behavior

The densities and CH_3/100 CH_2 ratios of the experimental polymers are intermediate between those of the low-density and high-density samples. The CH_3/100 CH_2 ratios, which are a measure of total branching, are lower than generally observed in low-density polyethylene. The low values of A_2, which indicate long-chain branching, and the CH_3/100 CH_2 ratios of the experimental polymers when considered together are consistent with a long-chain branched structure.

The reduced specific viscosities appear to be insensitive to molecular weight. This observation is consistent with the ramified structure of the polymer molecules proposed above.

The melt indices of the experimental polymers are equal to or larger than those of the lower molecular weight commercial polymers. A single melt index measurement on each sample is insufficient for a discussion of the structure of the molecules of these polymers. Melt flow data at several shear rates or with several molecular weight fractions of each

sample are required. Nevertheless, the following observations are worth noting. The weight-average molecular weights of the experimental samples are from 1 to 3 orders of magnitude higher than those of the commercial polymers. Furthermore, the number-average molecular weights of the experimental samples are high, and low molecular weight polymer, which is found in the commercial samples, was not detected in the emulsion-prepared polymers. In spite of these great molecular weight differences, the melt indices of the experimental samples are equal to or higher than either of the commercial samples. The long-chain branched structure proposed above and indicated by the light-scattering data which follows may very well be the most important factor contributing to the good melt flow at high molecular weights.

The broad molecular weight distributions indicated by the $\bar{M}_w/\bar{M}_n$ ratios of the experimental samples may be another factor contributing to the good melt flow.

Fractionation of Sample D

Since light-scattering measurements were not made with sample D, an attempt was made to characterize this sample by an elution fractionation procedure which is adequately described in the literature.[21] A mixed solvent system of xylene and cellosolve at 127°C. was used, and a charge of 1.18 g. polymer was deposited on the sand column. The results are found in Table III.

The reduced specific viscosities indicate some fractionation of the sample. The RSV of fractions 3 and 4 indicate little fractionation occurred after the first 20% of the initial charge was eluted. A molecular weight of 4×10^6 was obtained by light scattering for fraction 2, but there was an insufficient amount of fraction 1 for a measurement. Tetralin solutions of fractions 3 and 4 plugged the ultrafine filters, and light-scattering measurements were not made. The first four fractions account for 43% of the initial charge. The remainder could not be eluted from the column even by prolonged washing with hot xylene.

TABLE III
Fractionation of Sample D

Fraction	Solvent ratio (xylene/cellosolve)	Weight of each fraction, g.	η_{sp}/c	$\bar{M}_w$
1	60/40	0.06	0.43	—
2	64/36	0.18	1.10	4×10^6
3	70/30	0.20	2.09	—
4	100/0	0.07	2.15	—
5	Remained on the column	0.67	—	—
Whole polymer		1.18	1.31	—

Only 20% of the sample was actually fractionated and had measurable molecular weights. The remaining 80% of the sample is too limited in solubility for a fractionation and is too high in molecular weight for a light-scattering measurement. This behavior suggests a highly ramified or a crosslinked structure which alters the solubility to an extent that fractionation is no longer practical.

Light Scattering

The size of the latex particle in an emulsion polymerization limits the molecular weight of the polymer. The average molecular weight of the latex particles, $\langle M_p \rangle$, which is the highest possible molecular weight for a given sample, can be calculated from the particle diameter in Table IV and the density assuming that the particles are hard spheres. The values of $\langle M_p \rangle$ are 3.5×10^8 for sample A, 4×10^8 for sample B, and 6.3×10^7 for sample C. The corresponding values of $\bar{M}_w$ in Table IV are 1×10^8, 1.5×10^8, and 1.0×10^7 for samples A, B, and C, respectively.

TABLE IV
Results of the Light-Scattering Measurements

Sample	Latex particle diameter, mμ	$10^{-6}\ \bar{M}_w$	$10^4\ A_2$	$[z]$	$10^5\overline{\langle s^2 \rangle_z}^{1/2}$	$10^{18}(s^2/M)$
A	106	100	0	13.7	1.76	3.1
B	112	150	0	14.3	1.76	2.1
C	60.0	10	0.2	3.52	0.920	8.5
D	124	—	—	—	—	—
A[a]		160	0	8.9	1.58	1.6
HDPE	—	0.182	20	1.54	0.545	163
LDPE	—	1.70	0.4	3.25	1.22	88

[a] *o*-Dichlorobenzene, 120°C.

The agreement between the values of $\bar{M}_w$ and $\langle M_p \rangle$ for sample A and sample B is good, considering the approximate nature of $\bar{M}_w$ as discussed in the experimental section. This result implies that the average number of polymer molecules per latex particle is near one on the basis of the light-scattering data.

A plot of the angular data of sample C in the limit $c = 0$ has much less curvature than the corresponding plot of sample A (Figs. 4 and 5). The precision of $\bar{M}_w$ for sample C is estimated to be 10–20%. Since the $\langle M_p \rangle$ of the sample C latex is about six times larger than $\bar{M}_w$, the average number of polymer molecules per latex particle must be greater than one.

The light scattering and osmotic pressure results are consistent. Light-scattering molecular weights are weighted in favor of the large molecules. Small amounts of low molecular weight polymer are not detected in the presence of many very high molecular weight molecules. On the other hand, measurements of osmotic pressure are insensitive to molecular

weights higher than 1×10^6. The high values of $\bar{M}_n$ and the agreement of $\bar{M}_w$ with $\langle M_p \rangle$ show that samples A and B are composed mostly of high molecular weight polymer. The lower $\bar{M}_w$ and $\langle M_p \rangle$ show that sample C has significant numbers of comparatively low and high molecular weight long-chain branched molecules.

The shape of the Zimm plots is sensitive to the composition of the samples. The samples which have a majority of molecules of one type have regular plots. HDPE, which has no long-chain branched molecules, and sample A, which has predominantly long-chain branched molecules, have undistorted Zimm plots (Figs. 2 and 5). LDPE, which has a few large particles,[4-11] has a Zimm plot that is distorted only at the lower angles (Fig. 3). Sample C, which is a mixture of substantial numbers of both low and high molecular weight, long-chain branched molecules, has a Zimm plot (Fig. 4) that seems to be a compromise. This comparison of Zimm plots provides a confirmation of the conclusions of the previous paragraphs.

The ratio of the mean square radius of gyration to the molecular weight provides a measure of the spatial extension of the molecules of a given sample. A change in polarity of the solvent alters this ratio without changing the molecular weight. For example, the values of $\bar{M}_w$ of sample A in tetralin at 105°C. and *o*-dichlorobenzene at 120°C. agree within error, whereas the ratio, s^2/M, and the dissymmetry of sample A in the more polar solvent are lower as expected. By using this ratio, it is possible to compare the spatial extension of the molecules of various samples. The results in Table IV show that the molecules of samples A and B are the most compact, and that the spatial extension of the molecules increases in the order sample A = sample B < sample C < LDPE < HDPE. The molecules of the experimental samples are much more compact than those of HDPE suggesting that they are swollen spheres.

The experimental data can be compared with the curves of theoretical models of the monodisperse random coil[22] and the sphere[23,24] by plotting the particle scattering function $P(\theta)^{-1}$ versus $\mu^2\langle s^2 \rangle_z$.

$$P(\theta)^{-1} = (Kc/I_\theta)_{c=0}/(Kc/I)_{\substack{c=0\\ \theta=0}}$$
$$\mu = (4\pi\eta_0/\lambda_0) \sin(\theta/2) \tag{2}$$

where λ_0 is the wavelength of the incident light and η_0 is the refractive index of the medium. The curve of the sphere is plotted as $P(\theta)^{-1}$ versus $(\mu D/2)^2$, where the diameter, D, is obtained from $D^2 = (20/3)\langle s^2 \rangle_z$.

One expects the data of a polydisperse polymer to lie below the curve of the monodisperse random coil, whereas long-chain branching produces an upward curvature.[25] The effects of long-chain branching and polydispersity are apparent on comparing the experimental and theoretical curves in Figure 6. The data of HDPE and LDPE fall below the monodisperse random coil curve indicating the effect of polydispersity. The data of sample C lie just above the theoretical curve. Since sample C is

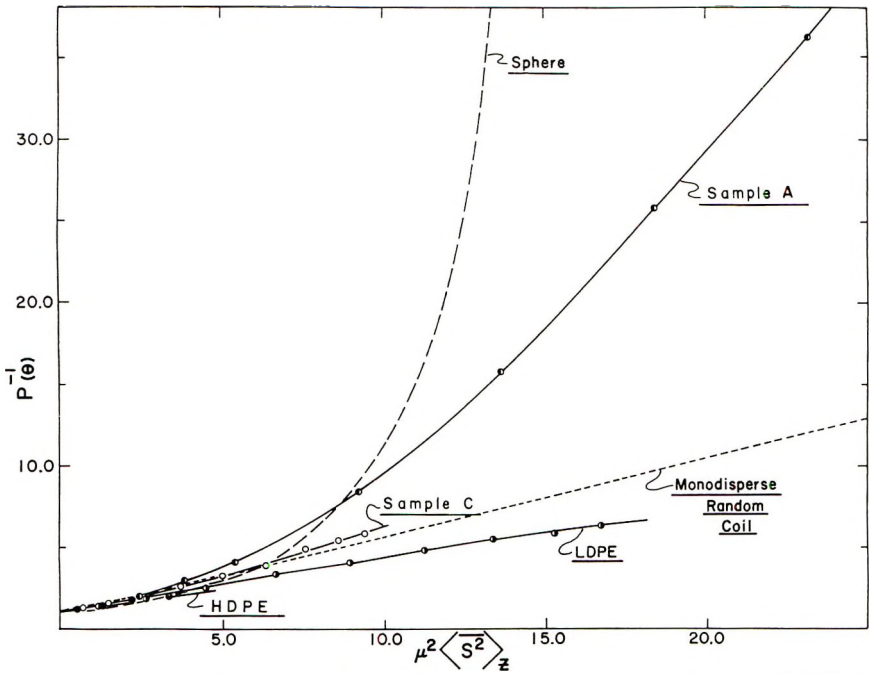

Fig. 6. Variation of the reciprocal particle scattering function, $P(\theta)^{-1}$, with $\mu^2 \langle\overline{s^2}\rangle_z$ for each of the experimental samples, a monodisperse random coil, and a sphere.

polydisperse, the effect of long-chain branching is evident, but the molecules of sample C in solution do not conform to a sphere. The data of sample A are situated midway between the two theoretical curves. If sample A were monodisperse, a closer coincidence of the data and the curve of the sphere probably would be obtained. This observation suggests that sample A is composed of a large number of compact spherical molecules which in fact could be the latex particles swollen by solvent.

Swelling Factors

The solution viscosities of microgels are not related to the molecular weights of the polymers, which are a function of particle size, but appear to depend upon the degree of crosslinking of the particles.[26–28] The latex particle diameter and $\overline{M}_w$ of sample B are larger than those of sample A (Table IV), but the reduced specific viscosity of sample B is smaller. The calculation of swelling factors illustrates the difference.

Following Shashoua and Beaman,[28] one assumes that the Einstein equation is applicable to swollen spheres as well as to hard spheres. It is also assumed that the latex particles of the experimental polymers only swell in organic solvents without breaking up into smaller polymer molecules. The swelling factor S is the ratio of the volume of a swollen sphere to that of the same hard, dry sphere. It is calculated from the specific viscosity according to:

$$\eta_{sp} = 2.5\psi_2 S \tag{4}$$

where ψ_2 is the volume fraction of the hard spheres in suspension. The swelling factor is obtained from light-scattering data as follows:

$$D_s^3 = SD_h^3 \tag{5}$$

The diameter of the swollen sphere, D_s, is calculated from the radius of gyration, and the latex particle diameter is used as the diameter of the hard sphere, D_h. The results are in Table V.

TABLE V
Swelling Factors from Light Scattering and Viscosity

	From light scattering			From viscosity	
Sample	Swollen particle diameter, mμ	Latex particle diameter, mμ	S	η_{sp}	S
A	455	106	79	0.182	73
B	456	112	68	0.161	64
C	238	60	62	0.106	42
D	—	—	—	0.120	48

The light-scattering swelling factors of the samples A and B are in good agreement with those calculated from viscosity data. The difference in the swelling effect of xylene and tetralin at 105°C.[29] is negligible considering the assumptions made in the calculation. The good agreement is additional evidence that the latex particles of the experimental polymers only swell in organic solvents without breaking up into smaller molecules. The swelling factors of both sources show that the molecules of sample B are more compact than those of sample A.

The poorer agreement between the swelling factors of sample C is consistent with previous conclusions. The latex particles of sample C are made up of several molecules of polymer, and the light-scattering evidence indicates that these long-chain branched molecules do not conform to the spherical model in solution.

The swelling factors are a factor of 2–5 times larger than those observed for microgels with varying degrees of crosslinking.[28,30] There cannot be a high density of crosslinks in the molecules of the experimental samples. These samples, therefore, certainly have a compact, long-chain branched structure with possibly a low degree of crosslinking.

CONCLUSIONS

The samples which were made by the emulsion polymerization of ethylene are composed of unusually high molecular weight, compact molecules. The molecules have a highly ramified structure with possible crosslinking and are spherical in shape. Light-scattering evidence suggests that two of the samples are made up of microgel particles, but the

rather large swelling factors indicate a low degree of crosslinking. A clear distinction cannot be made between a highly long-chain branched structure and the crosslinked structure of microgels.

The molecules of the experimental samples are much smaller than the crosslinked networks observed by Bryant and co-workers.[9] However, the molecular structure of the samples is comparable to that of the ramified molecules found in low-density polyethylene by Peck and Moore.[11] The content of these spherical molecules in low density polyethylene is only 1–2%. In contrast, the experimental polyethylenes described in this paper are composed of the high molecular weight, spherical molecules, and the physical properties of these polymers should correspond accordingly. The good melt flow at high molecular weights has already been observed.

The author wishes to thank R. Gnarra and B. Chinman for assistance in the experimental work, and Dr. A. S. Kenyon and Dr. J. D. Calfee for helpful discussions and suggestions.

The samples were prepared by Dr. O. D. Deex and Dr. H. J. Hileman.

References

1. Roedel, M. J., *J. Am. Chem. Soc.*, **75**, 6110 (1953).
2. Billmeyer, F. W., Jr., *J. Am. Chem. Soc.*, **75**, 6118 (1953).
3. Beasley, J. K., *J. Am. Chem. Soc.*, **75**, 6123 (1953).
4. Moore, L. D., Jr., *J. Polymer Sci.*, **20**, 137 (1956).
5. Muus, L. T., and F. W. Billmeyer, Jr., *J. Am. Chem. Soc.*, **79**, 5079 (1957).
6. Kobayashi, T., A. Chitale, and H. P. Frank, *J. Polymer Sci.*, **24**, 156 (1957).
7. Trementozzi, Q. A., *J. Polymer Sci.*, **23**, 887 (1957).
8. Nicolas, L., *J. Polymer Sci.*, **29**, 191 (1958).
9. Bryant, W. M. D., F. W. Billmeyer, Jr., L. T. Muus, J. T. Atkins, and J. E. Eldridge, *J. Am. Chem. Soc.*, **81**, 3219 (1959).
10. Moore, L. D., Jr., and V. G. Peck, *J. Polymer Sci.*, **36**, 141 (1959).
11. Peck, V. G., and L. D. Moore, Jr., *J. Polymer Sci.*, **C3**, 9 (1963).
12. Slowinski, E. J., H. Walter, and R. L. Miller, *J. Polymer Sci.*, **19**, 353 (1956).
13. Cross, L. H., R. B. Richards, and H. A. Willis, *Discussions Faraday Soc.*, **9**, 235 (1950).
14. Stabin, J. B., and E. H. Immergut, *J. Polymer Sci.*, **14**, 209 (1954).
15. Kratohvil, J. P., Gj. Dezelic, M. Kerker, and E. Matijevic, *J. Polymer Sci.*, **57**, 59 (1962).
16. Brice, B. A., and R. Speiser, *J. Opt. Soc. Am.*, **36**, 363 (1946).
17. Drott, E. E., and R. A. Mendelson, *J. Polymer Sci.*, **B2**, 187 (1964).
18. Zimm, B. H., *J. Chem. Phys.*, **16**, 1099 (1948).
19. Pangonis, W. J., and W. Heller, *Angular Scattering Functions for Spherical Particles*, Wayne State Univ. Press, Detroit, Michigan, 1960.
20. Krigbaum, W. R., and Q. A. Trementozzi, *J. Polymer Sci.*, **28**, 295 (1958).
21. Kenyon, A. S., and I. O. Salyer, *J. Polymer Sci.*, **43**, 427 (1960).
22. Debye, P., *J. Phys. Chem.*, **51**, 18 (1947).
23. Rayleigh, J. W. S., *Proc. Roy. Soc. (London)*, **A90**, 219 (1914).
24. Oster, G., *Chem. Rev.*, **43**, 337 (1948).
25. Benoit, H., *J. Polymer Sci.*, **11**, 507 (1953).
26. Baker, W. O., *Ind. Eng. Chem.*, **41**, 511 (1949).
27. Cragg, L. H., and J. A. Manson, *J. Polymer Sci.*, **9**, 265 (1952).
28. Shashoua, V. E., and R. G. Beaman, *J. Polymer Sci.*, **33**, 101 (1958).
29. de la Cuesta, M. O., and F. W. Billmeyer, Jr., *J. Polymer Sci.*, **A1**, 1721 (1963).
30. Sieglaff, C. L., *Polymer*, **4**, 281 (1963).

Résumé

Le polyéthylène obtenu par polymérisation en émulsion a été caractérisé par des mesures d'osmose, de diffusion lumineuse, et de viscosité. Les échantillons possèdent des poids moléculaires moyens en poids et en nombre inhabituels. On n'a pas détecté de polymère de faible poids moléculaire, habituellement présent dans les polyéthylènes commerciaux. Les résultats montrent une structure moléculaire compacte, fortement ramifiée. Les résultats de la diffusion lumineuse suggèrent que chaque particule de latex se compose essentiellement d'une molécule géante qui gonfle mais ne se dissout pas dans les solvants organiques jusqu'à 100°C. Les facteurs de gonflement obtenus à partir des résultats de la viscosité et de la diffusion lumineuse indiquent un faible degré de pontage. On ne peut pas faire de distinction claire entre une structure à longue chaîne fortement ramifiée et la structure pontée des microgels. Le polyéthylène de faible densité se compose, à raison de un à deux pourcent en poids, de molécules possédant une structure comparable. Au contraire, la plus grande partie des échantillons expérimentaux se compose de molécules de poids moléculaire élevé et fortement ramifiées.

Zusammenfassung

Durch Emulsionspolymerisation erzeugtes Polyäthylen wurde mittels Osmometrie, Lichtstreuung, und Viskosimetrie charakterisiert. Die Proben besitzen ungewöhnlich hohe Gewichts- und Zahlenmittelwerte des Molekulargewichts. Niedermolekulares Polymeres wie es gewöhnlich in handelsüblichem Polyäthylen enthalten ist, konnte nicht gefunden werden. Die Daten sprechen für eine kompakte, hochgradig verzweigte Molekülstruktur. Die Lichtstreuungsdaten zeigen, dass jedes Latexpartikel im wesentlichen aus einem Riesenmolekül besteht, welches in organischen Lösungsmitteln bei 100°C zwar quillt, aber sich nicht löst. Die aus Viskositäts- und Lichtstreuungsdaten berechneten Quellungsfaktoren weisen auf einen niedrigen Vernetzungsgrad hin. Eine klare Unterscheidung zwischen einer Struktur mit hochgradiger Langkettenverzweigung und der vernetzten Struktur eines Mikrogels ist nicht möglich. Nur ein oder zwei Gewichtsprozent von Polyäthylen neiderer Dichte sind aus Molekülen mit vergleichbarer Struktur aufgebaut. Im Gegensatz dazu besteht der grösste Teil der Proben aus hochmolekularen, hochgradig verzweigten Molekülen.

Received December 24, 1964
(Prod. No. 4593A)

JOURNAL OF POLYMER SCIENCE: PART A VOL. 3, PP. 1911-1939 (1965)

Use of a Capillary Extrusion Rheometer to Measure Curing of Thermosetting Plastics and Rubbers

I. O. SALYER, *Dayton Laboratory, Monsanto Research Corporation, Dayton, Ohio*, and J. W. HEYD, R. M. BRODBECK, L. W. HARTZEL, and L. E. BROWN, *Mound Laboratory, Monsanto Research Corporation, Miamisburg, Ohio*

Synopsis

By use of a modified, small-bore, capillary extrusion rheometer (MCER) with an Instron tensile testing machine, the flow and set-up properties of thermosetting plastics and rubbers were characterized. The majority of the experiments were performed with diallyl phthalate, where the rate of curing was also followed by infrared determination of the reduction in unsaturation as the polymerization-curing proceeded. Phenol–formaldehyde was also characterized. Finally, the curing of ethylene–propylene and ethylene–vinyl acetate copolymer rubbers with peroxide was studied and correlated with the type of peroxide used. The MCER data are shown to be of practical use for predicting the time–temperature–pressure relationships for processing thermosetting plastics and rubbers. Moreover, the history of the curing, as obtained by analysis of the continuously extruded strand, is also of theoretical interest for studying reaction kinetics and for evaluating the effectiveness of various curing systems. It is predicted the MCER will be widely used for studying the curing of thermosetting plastics and rubbers.

I. INTRODUCTION

A small-bore ($^3/_8$ in.) capillary extrusion rheometer (MCER), for use with an Instron tensile tester, was developed in the Dayton Laboratories of Monsanto Chemical Company in 1954 by Salyer and Steingiser.[1] This instrument was subsequently applied by Merz and Colwell[2,3] to study further the flow of thermoplastic polymers, including polystyrene, polyethylene, poly(vinyl chloride), and vinyl chloride–vinyl acetate copolymers. Because the MCER can measure apparent viscosity over the entire range of shear stress and shear rates encountered in extrusion, injection molding, and other melt processing of the thermoplastics, it has gained acceptance throughout the plastics industry. A commercial model of the MCER is now available as a standard accessory for the Instron tensile tester.

In current work the authors have further modified the rheometer and extended the application of the instrument to characterizing the flow and set-up properties of thermosetting plastics and rubbers. The majority of the experiments were performed using diallyl phthalate; the rate of curing was also followed by infrared determination of the reduction in unsatura-

tion as the polymerization proceeded. A second thermosetting polymer, phenol–formaldehyde, was also analyzed. Finally, the curing of ethylene–propylene and ethylene–vinyl acetate copolymer rubbers with peroxide was studied, and the results were correlated with the type of peroxide used.

II. EQUIPMENT

The Monsanto capillary extrusion rheometer, MCER (Fig. 1), shown schematically in Figure 2, contains an insulated, electrically heated steel cylinder supported on a steel framework. The cylinder is insulated by two transite disks (*1*), a cylinder of high temperature insulating wool (*3*), and an outer jacket of asbestos tubing (*2*). Four narrow-banded cylindrical heaters (*4*), manufactured by the Watlow Electric Manufacturing Company, supply heat to the steel cylinder. A thin aluminum sleeve (*5*), inserted between the steel cylinder and the heaters, improves heat transfer and alleviates thermal gradients. To prevent burn-out of the heaters, a $^1/_2$-in. dead air space separated the heaters and the asbestos tubing insulation. The tempered steel cylinder (*6*) is $8^1/_8$ in. long, 2 in. in diam-

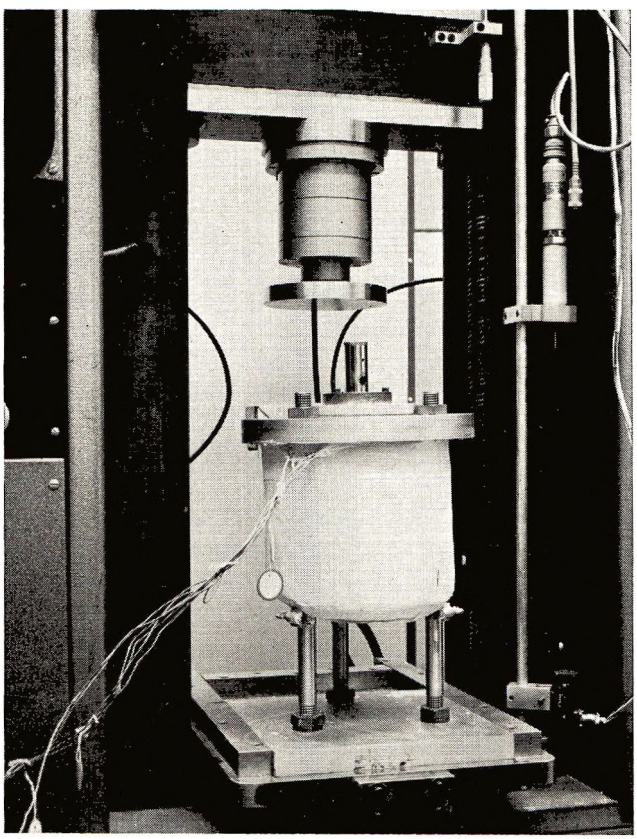

Fig. 1. Monsanto capillary extrusion rheometer in position in Instron testing machine.

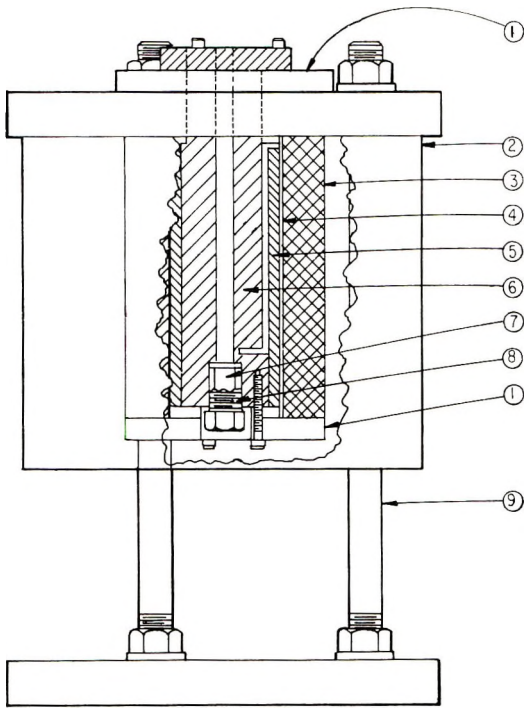

Fig. 2. Schematic cross section of Monsanto capillary extrusion rheometer.

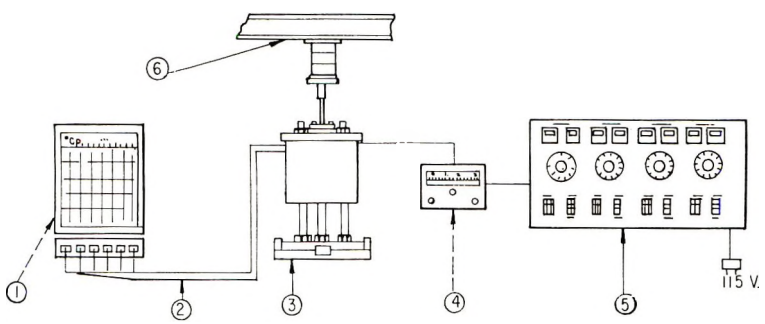

Fig. 3. Temperature control system for Monsanto capillary extrusion rheometer.

eter, and has a hard chromium-plated bore, 0.3760 in. in diameter. A threaded beryllium–copper orifice retainer (*8*) provides for interchange of orifices (*7*), as well as ease of maintenance and cleaning. Three steel rods (*9*), $^3/_4$ in. in diameter, support the assembly.

Each of the four heaters has two heating coils. The No. 1 coils of each are in parallel and controlled by one Variac. The saturable core reactor West temperature controller is included in this circuit and supplies equal, adjustable current to all four heaters. The No. 2 coil of the top heater is controlled by its own Variac, as is the No. 2 coil of the bottom heater.

The No. 2 coils of the two inner heaters are wired in parallel and controlled by a separate Variac.

The temperature-control equipment (Fig. 3) consists of a Variac Control Panel manufactured by the Standard Electric Time Company (*5*), a West Gardsman indicating pyrometer-type controller, manufactured by the West Instrument Corporation (*4*), a Speedomax temperature recorder (*1*), and seven thermocouples (*2*).

The Speedomax temperature recorder indicates the temperature of six thermocouple junctions, one placed in the orifice, one near the bottom of the steel cylinder, and four placed in the steel cylinder wall at the intervals between the heaters. A separate thermocouple at the interval between the bottom heater and the one above it is connected to the West Gardsman.

All a.c. current to the four Variacs is regulated by a Sola transformer to eliminate heat fluctuations due to line voltage changes. The Variacs controlling the No. 2 coils are adjusted to compensate for end cooling to keep the temperature profile of the inner tube constant. The temperature is then controlled by heat supplied by the bottom coils of the three heaters and controlled via the saturable core reactor and the West Gardsman pyrometer.

A standard Instron testing machine, fitted with a CD compressive load cell, supplies the required extrusion pressure. Time–force curves were obtained from the instrument's recording unit.

III. EXPERIMENTAL

The preforms to be extruded from the rheometer were pressed in a pellet die (Fig. 4) at 7 tons total pressure on a Wabash Hydraulic Press.

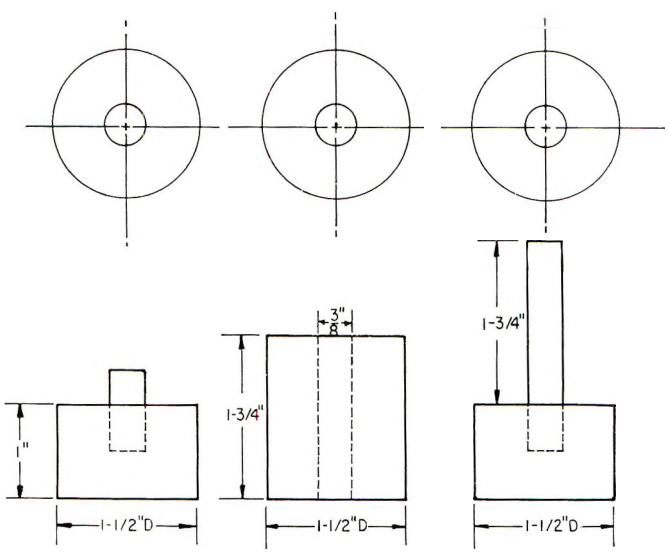

Fig. 4. Pellet preform die.

The sample weight was either 1.0 or 1.5 g., depending on whether the material to be extruded was unfilled or asbestos-filled diallyl phthalate (DAP). When 1.5 g. of asbestos-filled DAP was used, a preform 0.370 in. in diameter and approximately 0.52 in. long was obtained.

The crosshead speed of the Instron, using a CD compression cell, was set at 1.0 in./min. The rheometer was then heated by means of the temperature control circuit in Figure 3. To prevent a time lag between introduction of the sample in the rheometer and application of the pressure, the crosshead was lowered so that the compression cell would contact the driving piston when the preforms and the driving piston were in place.

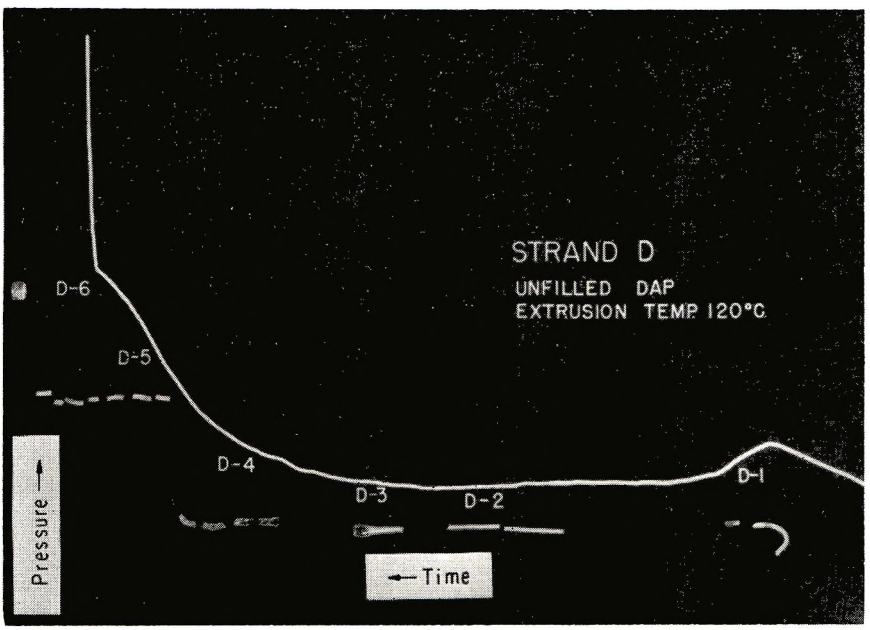

Fig. 5. Extrusion pressure vs. time of curing at 120°C. of unfilled DAP with portions of the extruded strand.

When the rheometer had attained thermal equilibrium, three preforms were simultaneously placed in the heated cylinder using a modified cork borer and a brass rod. The Instron's recording unit was activated, the driving piston introduced, and the pressure applied. During the extrusion the strand was guided away from the rheometer base (without pulling) to obtain a reasonably straight and uniform strand. With an orifice in the rheometer simulating the contours of a transfer molding nozzle, the application of pressure was terminated when a load of over 400 lb. was indicated on the recording unit of the testing machine (greater than 4000 psi pressure in the rheometer). The strand was then broken off at the orifice and the orifice was removed. The material remaining in the orifice and the cylinder was collected for weighing. The cylinder and orifice were then thoroughly cleaned by use of a copper brush.

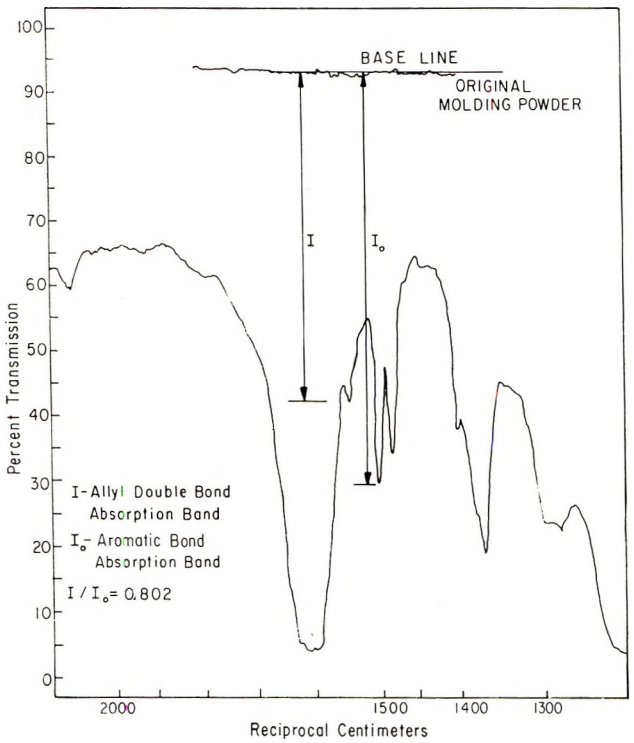

Fig. 6. Infrared absorption spectrum of DAP molding powder.

The time–force curves obtained during extrusion recorded the phase changes of a thermosetting molding compound as it proceeded from the solid preform through a viscous liquid form to the crosslinked thermoset solid. During early investigation of the physical properties of the extruded strands, some question arose as to whether crosslinking proceeded at a uniform rate. The time–force curves indicated that it did; the physical properties indicated that such was not necessarily the case. For this reason, five strands of unfilled DAP (designated A, B, C, D, E) were extruded from the rheometer (at 120°C.) to study the crosslinking of the material. This investigation included determining the sol/gel ratio, the swelling index, the molecular weight, and the transmittance of the infrared absorption band of the allyl double bond.

Sample selection, in each case, was based on the time–force curves obtained during extrusion, as shown in Figure 5 for strand D. Samples were designated by numbers to indicate extrusion time. For example, sample D-1 was the first portion of strand D to be extruded.

In a method described by Spurr et al.,[4] the infrared absorption band of the allyl group (1645 cm.$^{-1}$) is compared with the absorption band due to the aromatic double bond (1598 cm.$^{-1}$). During polymerization, the intensity of the allyl group band decreased, while the intensity of the aromatic band remained essentially constant. Thus, a measure of the

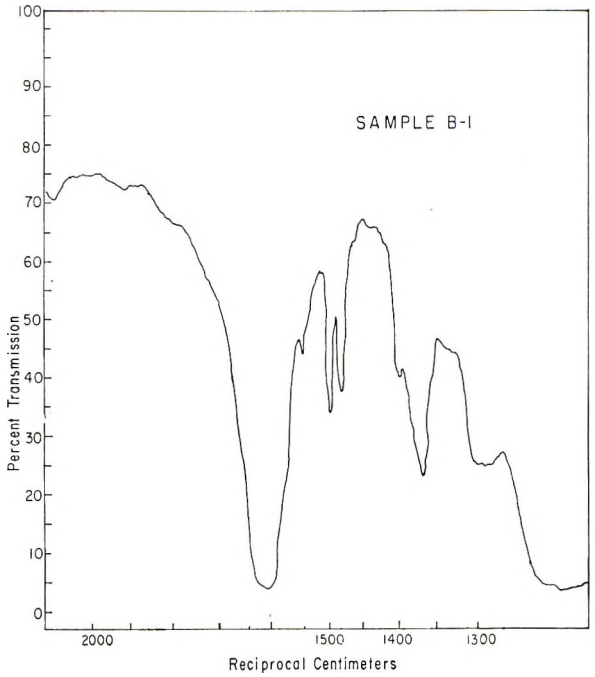

Fig. 7. Infrared absorption spectrum of partially cured DAP molding powder.

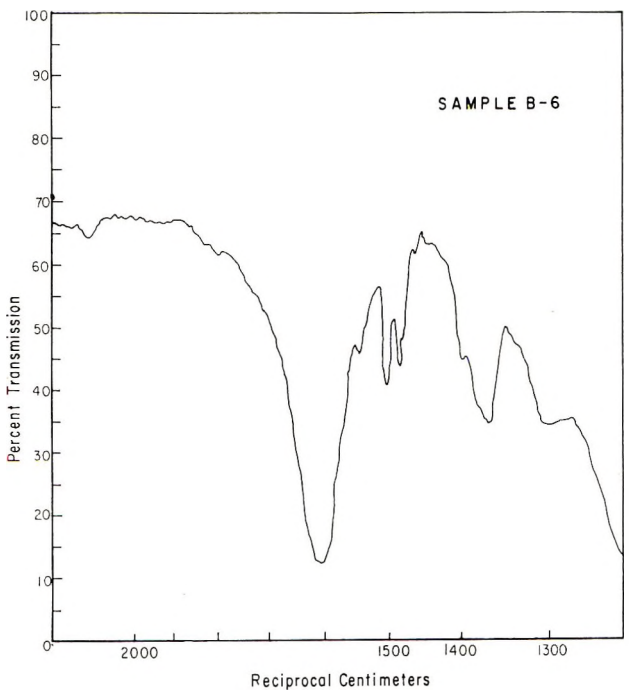

Fig. 8. Infrared spectrum of partially cured DAP molding powder.

difference in the absorption peaks at 1645 and 1598 cm.$^{-1}$ in an infrared spectrum can give a crude approximation of the degree of crosslinking

For the infrared determinations of the allyl double bond, strands A, B, and a portion of the original molding powder were used. Initially, the samples were ground to a powder in a mortar and pestle for 5 min. Potassium bromide pellets were then prepared by mixing 0.40 g. KBr with 0.0035 g. of sample in a mortar and pestle for 4 min., and then by placing the powdered mixture in a pellet die under 15,000 psi for 3 min. The infrared spectrum of the pellets was determined on a Perkin-Elmer 221 spectrophotometer. Typical absorption spectra for molding powder, the earliest material extruded from the rheometer (B1), and the unextruded material left in the rheometer at the end of the run (B6) are presented in Figures 6, 7, and 8, respectively.

The data were evaluated by comparing the absorption band at 1645 cm.$^{-1}$ (allyl double bond I) with the absorption band at 1598 cm.$^{-1}$ (aromatic double bond I_0) for the original molding powder with the extruded samples from strands A and B. These data are recorded in Table I, along with time of extrusion and pressure necessary to effect extrusion. It will be observed from the data that as curing time increases (sample dwell time at elevated temperature), there is an increase in the ratio I/I_0, indicating a gradual disappearance of the allyl double bonds. There is also a general increase in the pressure necessary to extrude the sample (increase in viscosity with crosslinking).

The swelling index, sol–gel ratio, and per cent soluble and insoluble was determined on samples taken from strand E. To determine the swelling index, a weighed sample from the strand was placed in 20 ml. of chloroform

TABLE I
Infrared Absorption Data on Partially Cured DAP Molding Powder

Sample	I_0	I	I/I_0	Time, min.	Extrusion pressure, psi
MP-1	59.0	47.0	0.797	0.0	
MP-1	56.5	45.3	0.802	0.0	
MP-2	63.2	50.7	0.802	0.0	
A-1	58.7	46.8	0.797	0.68	96.0
A-2	65.3	52.0	0.796	1.54	133.3
A-3	63.4	52.0	0.820	1.74	269.3
A-4	60.6	49.3	0.814	1.94	666.7
A-5	59.8	49.7	0.831	2.09	986.7
A-6	63.6	51.9	0.816	2.18	1200.0
A-7	62.2	53.5	0.860	∞	2560.0
B-1	59.0	48.7	0.825	0.65	261.3
B-2	60.1	49.4	0.822	1.05	77.3
B-3	57.3	48.5	0.846	1.40	213.3
B-4	56.4	46.3	0.821	1.55	480.0
B-5	55.5	46.8	0.843	1.95	1120.0
B-6	52.4	46.9	0.895	∞	2640.0

for a period of 5 days. At the end of this time a small portion of the gel was removed from the solution and weighed. The gel sample was then dried in a vacuum oven for 24 hr. and reweighed. The swelling index was determined by dividing the weight of the gel before removal of the solvent by the weight of gel after removal of the solvent. These data are presented in Table II.

TABLE II
Swelling Index of Cured DAP Molding Powder

Sample	Gel wt., g.	Gel. wt. after evap., g.	Swelling index	Time, min.	Extrusion pressure, psi
E-1	0	—	—	0.53	154.7
E-2	0	—	—	1.10	120.0
E-3	1.278	0.083	15.40	1.35	154.7
E-4	0.220	0.017	12.94	1.60	664
E-4′	0.385	0.034	11.30	1.60	664
E-5	0.465	0.042	11.07	1.75	1026.7
E-6	0.393	0.043	9.14	∞	2640.0

The sol/gel ratio was determined by filtering the chloroform solution from the swelling index ratio determination. The filtrate was then evaporated and the dissolved material weighed (solute weight). The sol/gel ratio was then calculated:

Total sample weight − solute weight = gel weight

$$\text{Sol/gel ratio} = \text{solute weight/gel weight}$$

The per cent soluble and insoluble material was also calculated. These data appear in Table III.

Three samples from selected portions of strand A were dissolved in chloroform, filtered to remove insoluble material, and the solutions transferred to 50-ml. volumetric flasks. The average molecular weights (M_n) of the soluble resin were determined in a vapor-pressure osmometer manufactured by Mechrolab Inc. This instrument measures the resistivity differential (ΔR) of two matched thermistors, one immersed in a drop of resin

TABLE III
Sol/Gel Ratio of DAP Molding Powder

Sample	Sample wt., g.	Solute wt. after evap., g.	Gel. wt. (total), g.	Sol/gel	Solubles, %	Insolubles, %
E-1	0.3871	0.3871	0	∞	100	0.0
E-2	0.4064	0.4064	0	∞	100	0.0
E-3	0.6396	0.5948	0.0448	13.27	92.99	7.0
E-4	0.5488	0.2416	0.3072	0.786	44.02	55.98
E-5	0.1566	0.0678	0.0888	0.764	43.29	56.70
E-6	0.4467	0.0563	0.3904	0.126	12.60	87.40

solution, the other immersed in a drop of pure solvent. By means of a calibration curve, the molarity of the resin solution is determined. The molecular weight of the soluble resin was then calculated using the formula,

$$\text{M.W.} = \text{grams}/0.05 \times \text{molarity}$$

The sample weight was determined by evaporating the solvent from a 5-ml. aliquot of the sample solution. These data appear in Table IV.

TABLE IV
Molecular Weight of Partially Cured DAP Molding Powder by Vapor Pressure Osmometry

Sample	ΔR (av.), ohms	Molarity	Sample wt., g.	Molecular wt.
A-3	0.98	0.00160	0.3020	3770
A-5	0.53	0.00050	0.0785	3140
A-7	0.37	0.00012	0.014	2330
Dapon 35	0.54	0.00052	0.422	16,230

IV. RESULTS AND DISCUSSION

A. Thermosetting Diallyl Phthalate (DAP)

The data obtained from the infrared spectra of the samples (plotted in Fig. 9 and presented in Table I) indicated that the crosslinking increased as time and pressure increased. This is especially true of the last point of each curve. This point represents that portion of the strand that re-

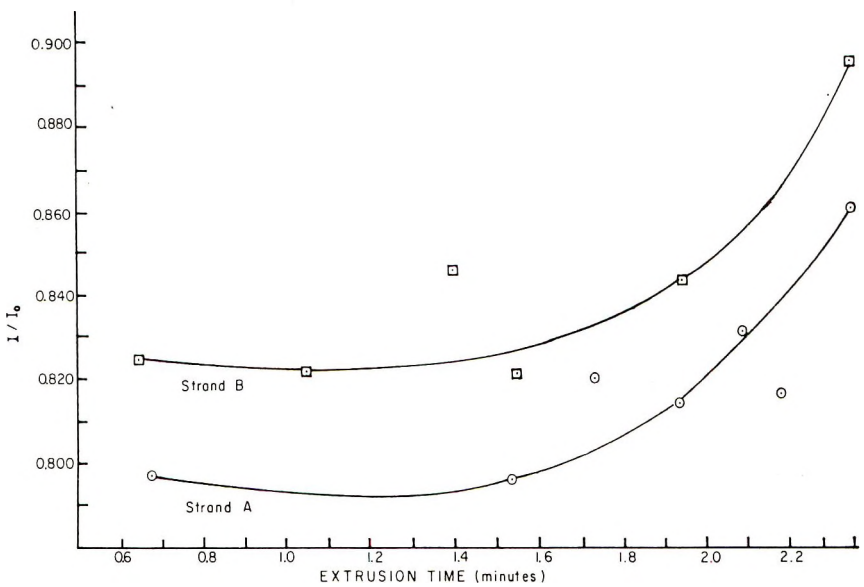

Fig. 9. Crosslinking rate of DAP molding powder via infrared determination.

mained in the orifice and cylinder after extrusion. Since it remained at the extrusion temperature for a longer time, the degree of crosslinking shows a marked increase.

The swelling index decreased with increasing time and pressure (Fig. 10), indicating that crosslinking increased, since the swelling index is a measure

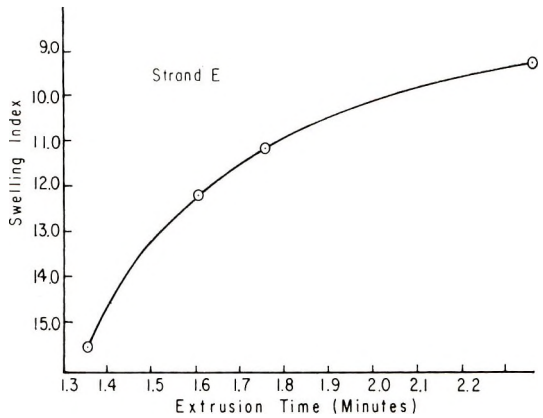

Fig. 10. Swelling index of DAP molding powder vs. extrusion time.

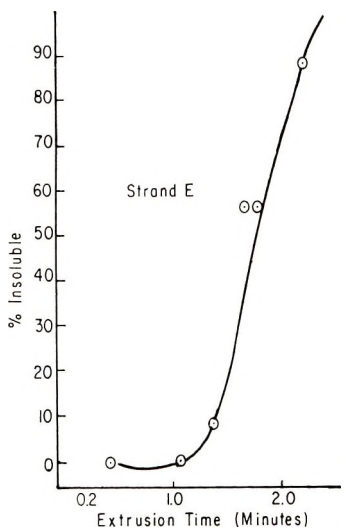

Fig. 11. Per cent insolubles of DAP molding powder vs. extrusion time.

of the solvent present in a portion of the gel. The more crosslinking in the DAP, the less solvent there will be in the voids of the gel.

The sol/gel ratio, and the per cent of solubles and insolubles, (Fig. 11 and Table III) also indicate increased crosslinking with increasing time. The longer the extrusion time of the sample, the higher the percentage of insoluble material, and the lower the sol/gel ratio.

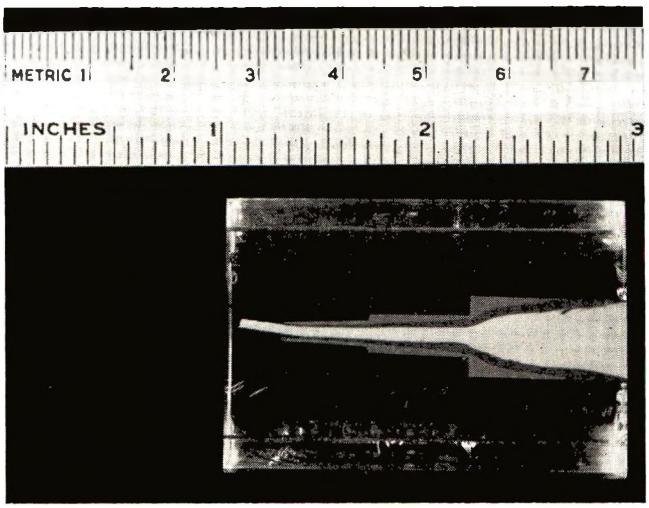

Fig. 12. Cross section of orifice slug of DAP molding powders.

All portions of the strand (after 1.10 min. extrusion time) contained a mixture of low and crosslinked high molecular weight material. This is indicated by the fact that even in the portion of the strand that remains in the rheometer, there is some soluble material. Also, the solvent ($CHCl_3$) dissolved only the lower molecular weight chains, as indicated by the molecular weight data in Table IV. The higher molecular weight crosslinked chains remain undissolved, in the form of a gel.

In order to study the flow of material through the orifice, an extrusion was made at 145°C. of asbestos-filled preforms of three different colors: red, ivory, and gray. The slugs remaining in the rheometer cylinder, with the material in the orifice attached, were cast in clear plastic, cross-sectioned, and polished. A black-and-white reproduction of such a cross section is shown in Figure 12. The preforms were stacked with the gray on the bottom, the red in the center, and the ivory on top. The colors are, reading from the outside in, gray, red, and ivory. The largest diameter is the slug remaining in the rheometer cylinder proper. The next two smaller diameters are the material remaining in the orifice, while the smallest diameter is the last material to be extruded from the orifice.

A number of tentative conclusions can be drawn from this cross section. The flow appears to be laminar, but the material flowing through the. orifice is not homogeneous. The first material to contact the hot metal stuck to the surface and cured at a faster rate than the bulk of the material, which decreased the effective diameter of the orifice. Since all three colors are visible in the cross section, the buildup of material throughout the extrusion cycle was continuous. Note the extrusion of red, semi-cured plastic in the ivory plastic within the rheometer slug; this is probably due to the increased pressure during the latter part of the extrusion cycle pulling the red layer into the ivory plastic. Strands usually exhibited a rough

outer layer of material. This roughness of the strand was probably caused by material pulled from the static layer by the extruding plastic. For example, in the three-color extruded strand mentioned above, the first material extruded was gray; only gray roughness could appear on the gray portion of the strand. However, the first portion of red material extruded was nearly completely covered with a rough coat of gray, and as extrusion progressed the strand appeared red, and with rough, gray flecks. Later the roughness was largely red with only very small flecks of gray. The first ivory plastic to extrude had a relatively thick, continuous, but rough coat of red; this became discontinuous and finally merely a red roughness in an ivory strand as extrusion proceeded. However, the last of the ivory plastic to extrude had a nearly continuous coating of red, indicating that moving plastic was now highly crosslinked and that all of the unextruded plastic was beginning to weld into a single, thermoset mass. The fact that higher crosslinked material was formed on the exterior of the strand might explain some of the anomalies found in the experimental data (Tables I–IV).

B. Applications of MCER Data in Diallyl Phthalate

The time–pressure curves obtained during extrusion may prove to be valuable in determining the difference in molding characteristics of various thermosetting materials. However, the fact that this method is only an approximate one must be kept in mind. The four most valuable parameters that can be determined from the rheometer curves are the time preceding plastic flow T_1, the plastic flow time T_2, the total extrusion time T_3, and the average flow pressure P_f (Fig. 13). Various methods of determining these parameters have been investigated; however, no one method was found to be entirely satisfactory.

For a general discussion of the application of the rheometer, the following procedure was used. The time preceding plastic flow T_1 is the time elapsed from the charging of the rheometer to the beginning of extrusion; T_1 ends shortly after the small initial pressure increases. The plastic flow time T_2 is the time elapsed from the beginning of extrusion until the termination of fluid flow. This is indicated by the sharp pressure increase near the end of the rheometer curve. The total extrusion time T_3 is the time elapsed

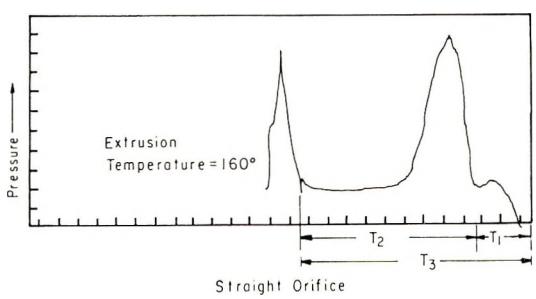

Fig. 13. Extrusion pressure vs. curing time of DAP molding powder, cylindrical orifice.

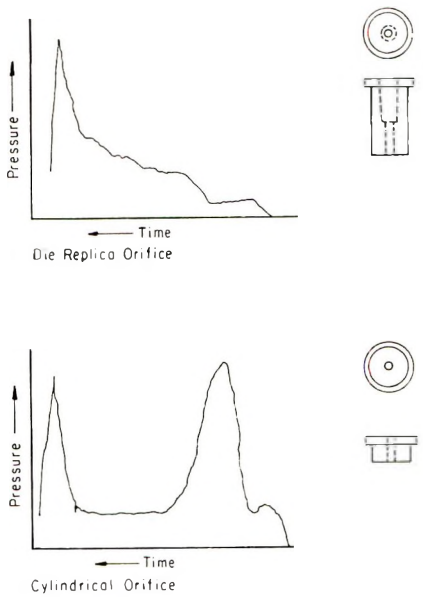

Fig. 14. Extrusion pressure vs. curing time of DAP molding powder with different orifices at 160°C.

from the charging of the rheometer until the extrusion pressure rises sharply at the end of T_2.

A planimeter was employed to determine the average flow pressure P_f during the time of plastic flow T_2. The end of T_2 was determined by the intercept of the pressure axis and a straight line nearly coincident with the initial portion of the final, steeply rising part of the curve.

As noted previously, the orifice design affects the shape of the rheometer curve (Fig. 14). Extrusion through a straight orifice requires a large initial pressure before viscous flow is attained; this is indicated on the curve by the first large pressure peak. Therefore, to obtain a maximum viscous flow time, an orifice that gives a "funneling" effect, similar to the die-replica orifice, should be used. In this respect, the rheometer could be used to test the feasibility of molding, using orifices which would simulate sprues with special configurations such as used in any specific applications.

The first practical application of the extrusion rheometer consisted of a series of tests including both commercially produced DAP molding compounds as well as experimental Mound Laboratory materials, especially formulated and processed to obtain specific curing characteristics.

The objective of this work was to define a DAP formulation and prepolymer processing condition which would yield predictable and desirable flow and curing characteristics, such as found in one sample of a commercial molding material. The extrusion rheometer was used as an analytical instrument to define the flow/time/temperature curing properties of the materials. These data were checked against the results obtained in actual

transfer molding of larger pieces. An example of the data obtained from a series of such experiments appears in Table V. The Mound Laboratory B-86 formulation contained 0.025 pph Dapon 35 (hydroquinone) inhibitor; samples PB-2, PB-3, PB-6, and B100 did not contain an inhibitor. The third number appearing in the sample designation (e.g., B86-1-70) indicates the maximum surface temperature of the mill roll to compound the batch before the test.

TABLE V
Extrusion Pressure vs. Time for Commercial and Experimental DAP Molding Powders (Cylindrical Orifice at 145°C.)

Material	Extruded, %	P_f, psi	T_1, sec.	T_2, sec.	T_3, sec.
Commercial 1	70.7	634	16.6	42.6	59.2
Commercial 2	78.7	668	14.8	34.2	49.0
Mound B86-3	63.3	520	15.0	22.5	37.5
Mound B86-1-70	76.8	487	15.7	37.2	52.9
Mound B86-1-80	76.2	418	16.6	42.2	58.8
Mound B86-1-90	69.1	464	17.7	31.0	48.7
Mound PB-2	55.0	728	16.8	15.8	32.6
Mound PB-3	60.6	464	17.2	22.2	39.4
Mound PB-7	46.0	3322	20.8	24.5	45.3
Mound B-100	55.6	890	16.2	27.6	43.8

The values of the per cent extruded and T_2 were similar for the samples of commercial material and Mound Laboratory B86 formulation, while the values for the PB samples were lower. These data led to the conclusion that an inhibitor was probably used in the formulation of commercial materials, since the Mound formulations without inhibitor (PB) showed marked differences in the plastic flow time and per cent extruded, while the Mound formulations (B-86) with an inhibitor exhibited similar flow properties to the commercial materials. Because of the varying flow properties of the B-86 materials milled at different temperatures it was concluded that mixing, milling time, and temperature affect the flow properties of the finished molding powder. Further, extrusion of materials milled at different surface temperatures established an optimum mill roll temperature of 80–85°C. for this particular formulation. Additional extrusions with different formulations led to the standardization of a molding powder containing clean, short-fiber asbestos, *tert*-butyl perbenzoate catalyst, hydroquinone inhibitor, and calcium stearate lubricant. This molding powder formulation gave flow curves similar to the commercial materials and had excellent molding qualities.

Several general conclusions that can be applied to the prediction of molding characteristics can be drawn from the data. The plastic flow time T_2 should be a measure of the relative times between introduction of a preform into the pot and seal-off of the gate in a molding operation. The average flow pressure P_f is a measure of the plasticity of the material during

extrusion, and the pressure required to fill the die. Also, the time to flow T_1 is significant, since the flow characteristics may be influenced by the time between the introduction of samples and the first application of pressure. It would appear that a maximum time in the plastic state would be desirable if the cure rate were rapid enough at later times to insure adequate curing in a short molding cycle, that is, if T_2 should be a relatively large fraction of T_3.

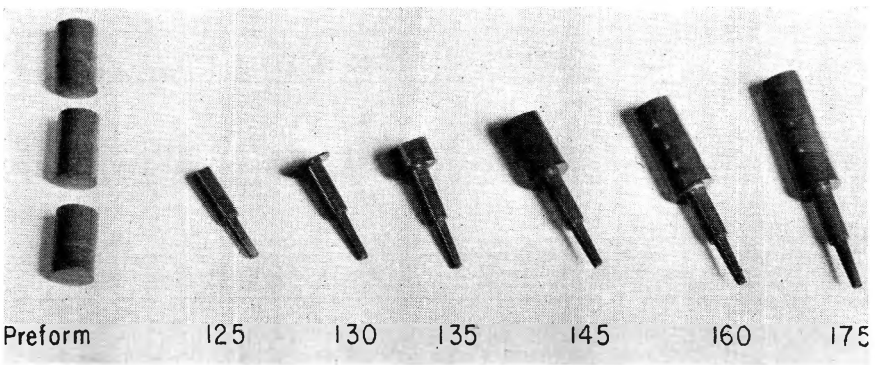

Fig. 15. Orifice slugs of DAP molding powders obtained at different extrusion temperatures (°C.).

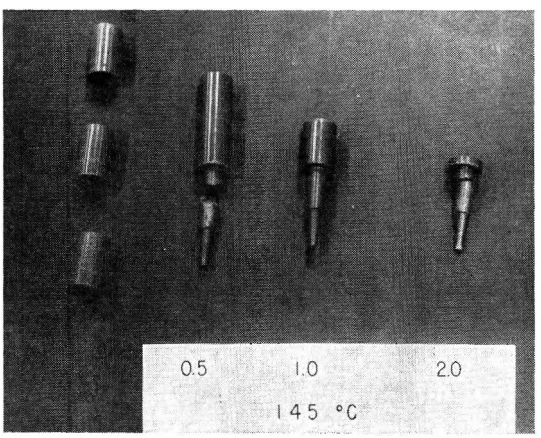

Fig. 16. Orifice slugs of DAP molding powder obtained at different crosshead speeds (in./min.).

The extrusion temperature had a definite effect on the total per cent of material extruded. Figure 15 shows the slugs that remained in the rheometer after extrusion.

The speed of the Instron crosshead also had an effect on extrusion (Fig. 16). Therefore, by evaluating the quantity of plastic extruded at different die temperatures and/or crosshead speeds, an optimum set of conditions that would give the most efficient molding could be determined.

C. Extrusion Curing of Thermosetting Phenol–Formaldehyde Molding Powder

The experimental apparatus and procedure were similar to those used in the study of the curing of diallyl phthalate, except that a Baldwin Mechanical Tate-Emery tensile machine was used instead of an Instron. A cylindrical orifice (0.083 × 0.315 in.) was employed in this work. Preforms were prepared from commercial phenol–formaldehyde resin, Resinox 10900

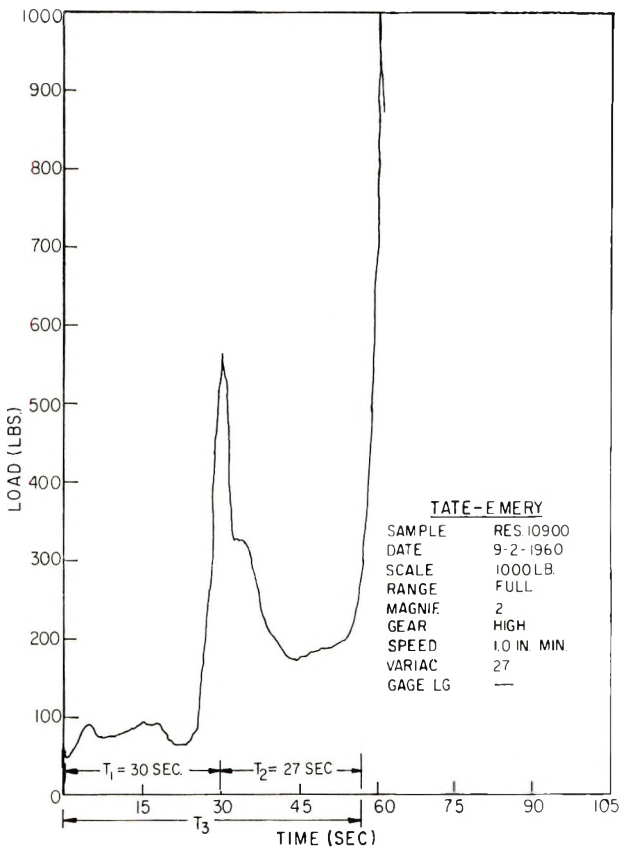

Fig. 17. Extrusion pressure vs. time of curing of Resinox 10900.

Natural (Monsanto Company), by using the rheometer in the tensile machine at room temperature as a tableting press. The pressed preforms were removed from the rheometer, and the apparatus was heated to a temperature of 150°C. The pellets were then quickly loaded into the cylinder of the rheometer (5 sec.), and the extruder piston was driven by the crosshead of the tensile machine at a speed of 1 in./min. The extrusion pressure was recorded continuously throughout the experiment on the stress-strain recorder of the tensile machine.

The extruded strand went through the same variations in size, surface roughness, and appearance as previously noted for DAP. Tunneling-through was also noted as the reaction neared completion.

The curve of pressure as a function of time, shown in Figure 17, can be divided into three sections: T_1, a time for heat-up and compression of the preform; T_2, a period of fluid flow at relatively low pressure; and T_3, the period of time from the beginning until the onset of rapid crosslinking at progressively higher and more erratic extrusion pressures. In the case of Resinox 10900 Natural at 150°C, the T_1 period lasted approximately 30 sec. due to the additional compression of cold preforms before start of extrusion. With more highly compressed preforms, T_1 would be expected to be reduced to no more than 10 sec.; the period of fluid flow T_2 lasted an additional 27 sec. after the start of extrusion, and T_3 including the period of rapid cross-linking, lasted a total of 57 sec., until the material became thermoset.

At the same extrusion speeds (1 in./min.), the experiments were repeated at both higher and lower temperatures. At 175°C. the material became thermoset before stable extrusion could be attained (i.e., during T_1). At 125°C. all of the material was extruded (total time 3 min.), without set-up being achieved (i.e., T_3 was never completed). However, in a second run made at 125°C. and at 0.2 in./min. crosshead speed, the T_3 thermoset condition was achieved in 15 min. "Tunneling-through" was noticeably absent at the slower rate of extrusion.

To transform the flow pressure data to practical application in transfer molding of phenolic, one would first convert the applied pressure to pounds per square inch. For a $^3/_8$ in. diameter piston of the type used in these experiments the area is approximately 0.11 in.^{2}. Thus the pressure in pounds per square inch would be approximately 9 times the force applied by the crosshead of the tensile machine. Since the total volume extruded was approximately 0.33 in.^{3} (total volume of the preforms), the rate of extrusion was approximately 0.33 cc. (or g.)/min. Inasmuch as the orifice used in these experiments was 0.083 in. in diameter and 0.315 in. long, one would conclude that a force of approximately 4500 psi is required to extrude Resinox 10900 through this orifice at a rate of 0.33 g./min.

An apparent viscosity can be calculated from these data, but it would be of doubtful accuracy in view of the rapidly changing character of the material during the test period.

It would be expected that similar pressures would be required in either transfer or compression molding of Resinox 10900 where the smallest orifice had approximately the same dimensions as the one used in these experiments. Regardless of the size of orifice used, the total time of plastic flow of Resinox 10900 at 125°C. would be 15 min., approximately 1 min. or less at 150°C., and less than 10 sec. at 175°C.

D. Peroxide Crosslinking of Ethylene–Vinyl Acetate (E/VA) Copolymer Rubber

In the two experiments reported here, the first was made with a Baldwin Mechanical Tate-Emery tensile testing machine, and the second using an

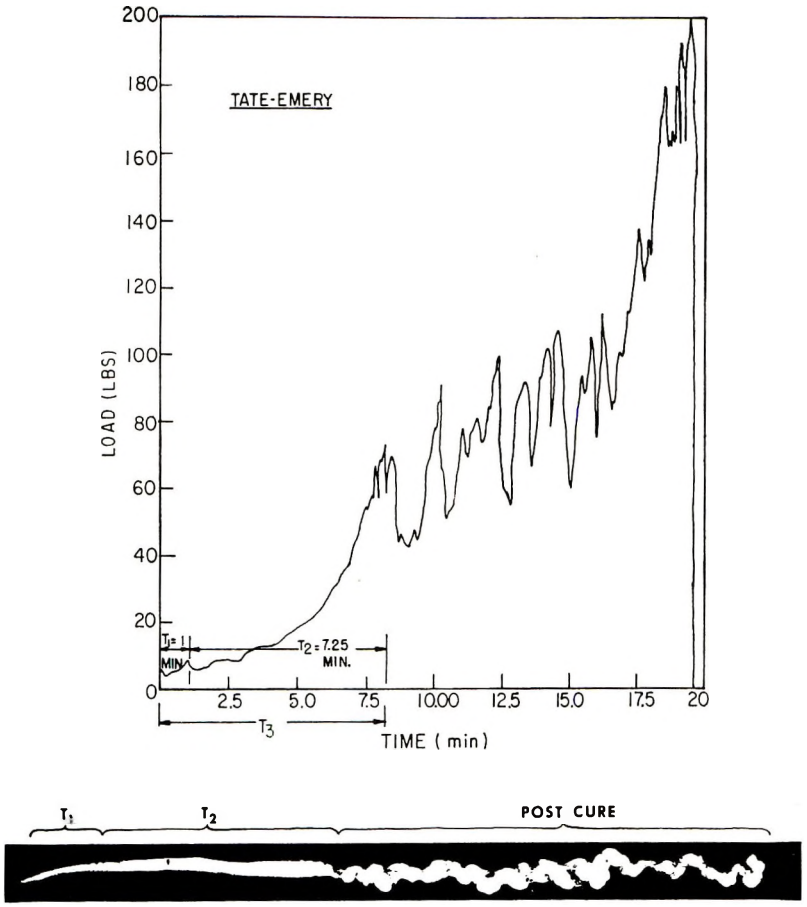

Fig. 18. Extrusion pressure vs. time of curing of E/VA (55/45) copolymer rubber.

Instron. The rheometer and orifice (0.083 × 0.315 in.) were the same in both runs.

In the first experiment, E/VA (55/45) copolymer rubber was compounded without fillers to contain 2.00 pph dicumyl peroxide (Di-Cup R), and cut into preforms of approximately $^3/_{16}$ in. to permit ready loading into the extruder cylinder. The rheometer temperature was set at 125°C. and the crosshead speed at 0.2 in./minute.

The preforms were quickly placed in the rheometer and extruded. Pressure was recorded continuously throughout the experiment. The pressure–time diagram, shown in Figure 18, is different from the diagram obtained with the thermosetting diallyl phthalate and phenol–formaldehyde molding materials. The flow–pressure diagram can, nonetheless, be conveniently divided into three distinct time sections of preheat (T_1), viscous flow (T_2), and the elapsed time until rapid crosslinking (T_3).

As noted in the photograph of the extruded strand placed immediately below the abscissa of the graph, a very significant increase in the size or

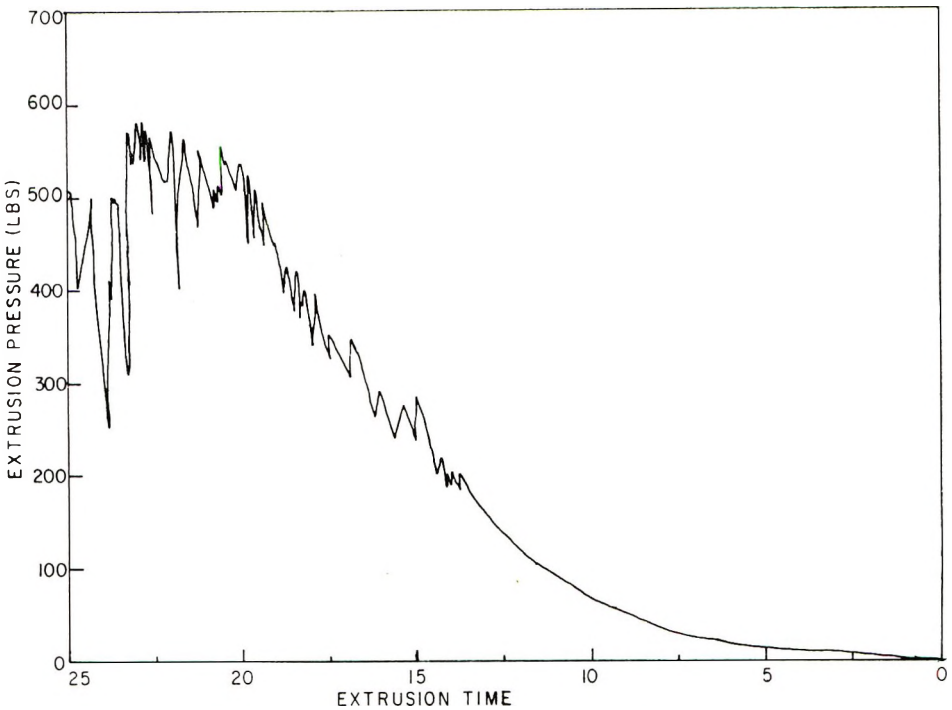

Fig. 19. Extrusion pressure vs. time of curing of E/VA (74/26) copolymer at 125°C.

"memory" of the extruded strand takes place during T_1 and T_2 time periods. Simultaneously the extrusion pressure increases progressively and smoothly. At the end of the T_2 period the strand begins to become wavy, and the extrusion pressure fluctuates. The polymer begins to flow through the orifice by rubbery deformation, the strand becomes very rough, and finally discontinuous.

The extruded strand shown in Figure 18 was sectioned at $^1/_4$ in. intervals along the time axis, and tested for solubility and specific viscosity. Up to the point where the strand began to become wavy (T_3), the polymer was completely soluble, and all samples had identical specific viscosities. Over a very short distance, less than $^1/_8$ in. of extruded strand, the extrudate became insoluble, although pronounced swelling was observed. The viscosity data were not unexpected, since the extensive branching preceding the formation of a complete network structure should not significantly increase the solution viscosity. However, a light-scattering molecular weight (M_w) taken along the length of the strand would undoubtedly have shown progressive and linear increases in average molecular weight.

In the second experiment the Instron tensile tester supplied the extrusion force at 125°C. and a crosshead speed of 0.2 in./min.; E/VA (74/26) copolymer, unfilled, and compounded to contain 6 pph of 50% active Varox [2,5-dimethyl-2,3-di(*tert*-butylperoxy)hexane] was used. This peroxide de-

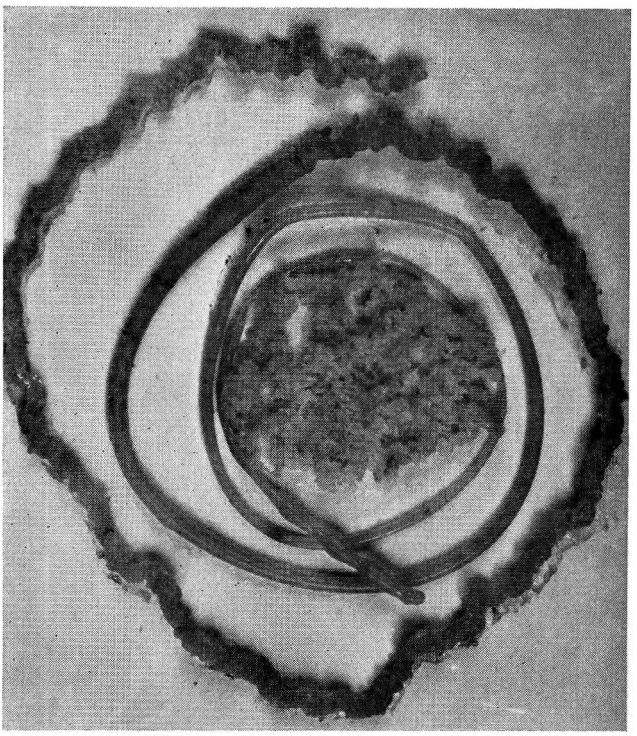

Fig. 20. Photograph of extruded strand of E/VA (74/26) copolymer rubber, showing increase in diameter of strand with time of cure.

composes at nearly the same time and temperature conditions as dicumyl peroxide, and accordingly comparable results were expected. Since the lower vinyl acetate content copolymers are generally less reactive than the 45% rubbers, the peroxide content, on an active basis, was increased from 2 to 3 pph.

The change in extrusion pressure with time of curing at 125°C. is shown in Figure 19. In this instance the data were replotted on the same basis as in the previous experiment. Again, the extrusion pressure and size (memory) of the extruded strand increased progressively with time of curing. A photograph and a plot of the memory data are shown in Figures 20 and 21. Increases in strand diameter to 150% of the orifice diameter are obtained in the time period up to the onset of waviness. It is believed that the memory increases may be used directly to estimate the degree of cross-linking of the rubber, although this has not yet been done.

E. Curing of Ethylene–Propylene Copolymer Rubber (EPR)

Five experiments were made using the rheometer in the Instron Tensile Tester and a crosshead speed of 0.2 in./min. EPR (Enjay 404) was compounded with and without fillers to contain 6.25 pph of 40% active dicumyl peroxide (Di-Cup 40C, Hercules Powder Company).

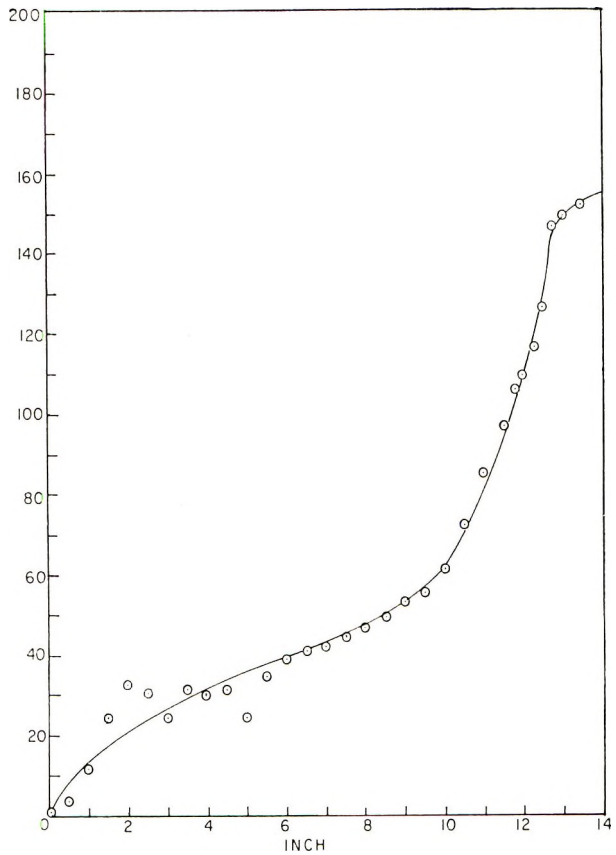

Fig. 21. Graph of strand diameter vs. time of cure of E/VA (74/26) copolymer rubber.

In the first experiment EPR rubber was extruded at 125°C. through the cylindrical orifice (0.083 × 0.315 in.) in the same manner described in the E/VA copolymer curing studies. At this temperature the entire extruder was emptied (ca. 30 min.) with little evidence of curing in terms of strand waviness, strand insolubility, or extrusion pressure increase (Fig. 22).

When the experiment was repeated at 150°C., wavy extrusion and insolubility were noted after about 14 min. of extrusion. The extrusion pressure increased progressively, and became high and erratic after the initial 15-min. period. The extruded strand also became progressively rougher, and finally discontinuous; it was extruded by melt shear through the orifice in small shreds. Figures 23 and 24 are photographs of the extruded strand and a plot of the time–pressure data. Unlike the E/VA copolymers, pronounced memory increase was not noted at 0.2 in./min. rate of extrusion. A higher rate of extrusion or a smaller orifice would probably have shown change in memory with curing. The curing at 150°C. (with EPR containing 3.2 pph of sulfur) was also studied, as shown in Figures 25 and 26. No pronounced difference in time or flow data was

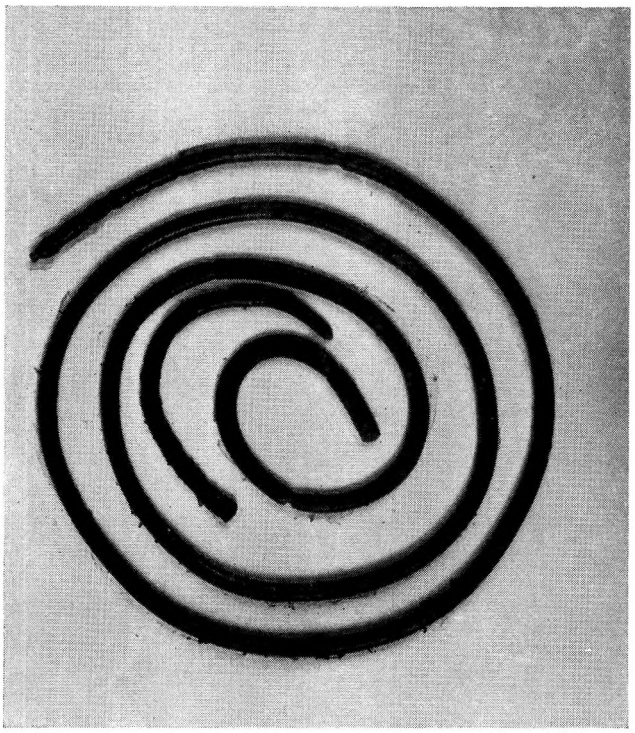

Fig. 22. Photograph of strand of EPR extruded at 125°C.

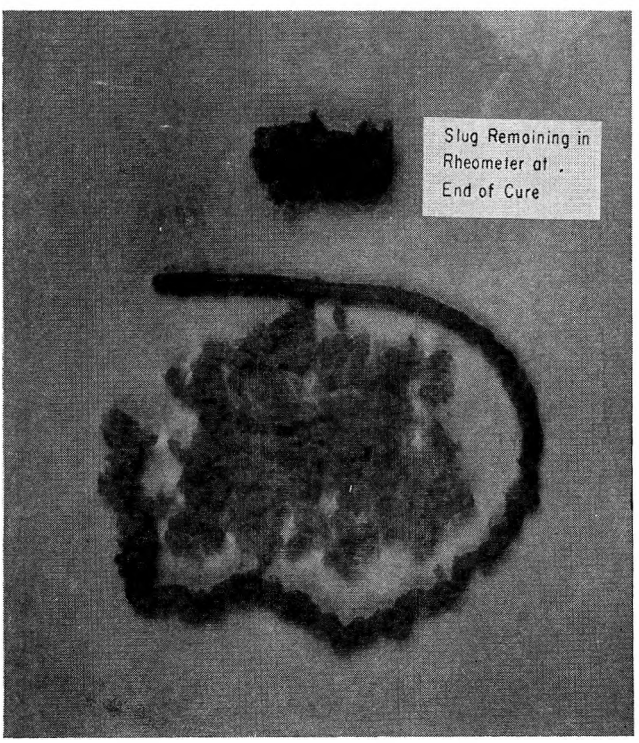

Fig. 23. Photograph of strand of EPR extruded at 150°C.

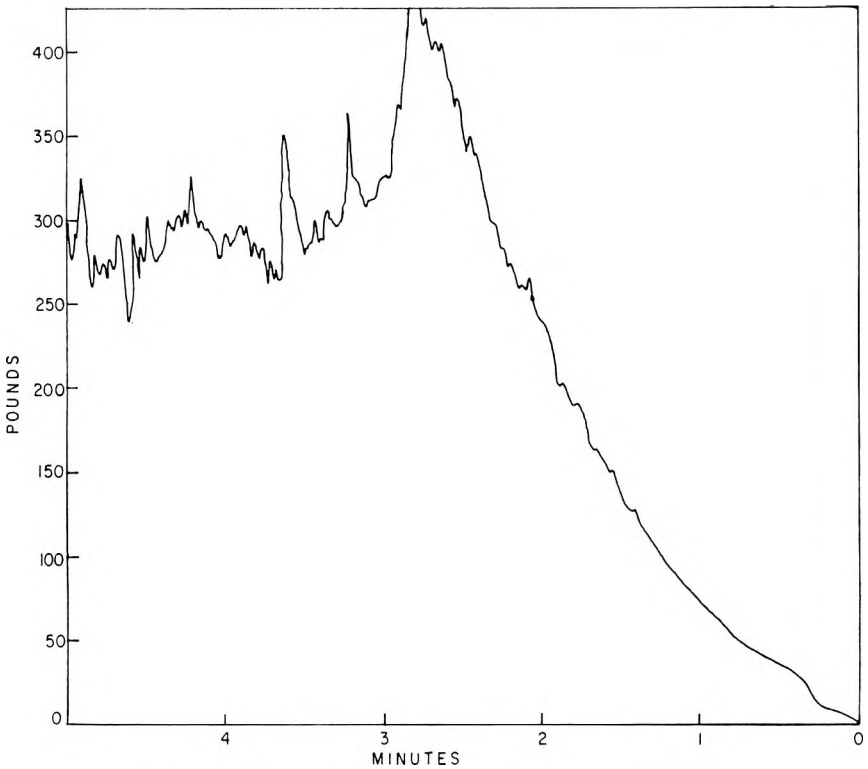

Fig. 24. Extrusion pressure vs. time of curing of EPR at 150°C.

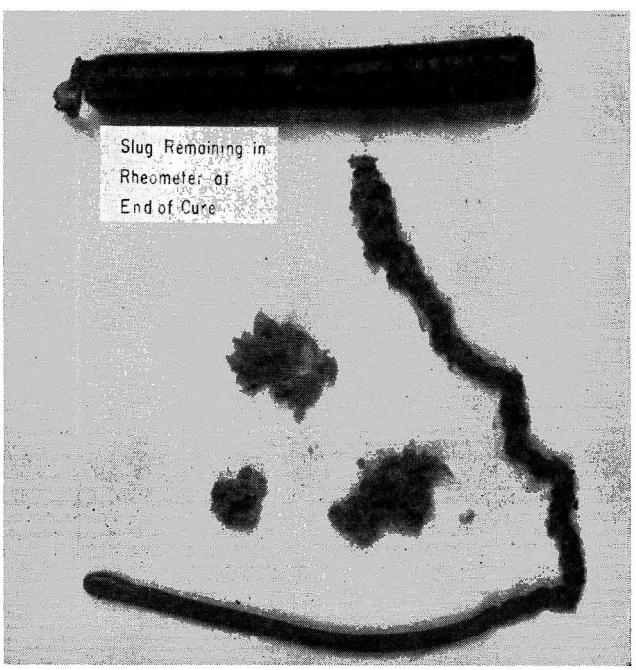

Fig. 25. Photograph of strand of EPR containing 3.2 pph of sulfur, extruded at 150°C.

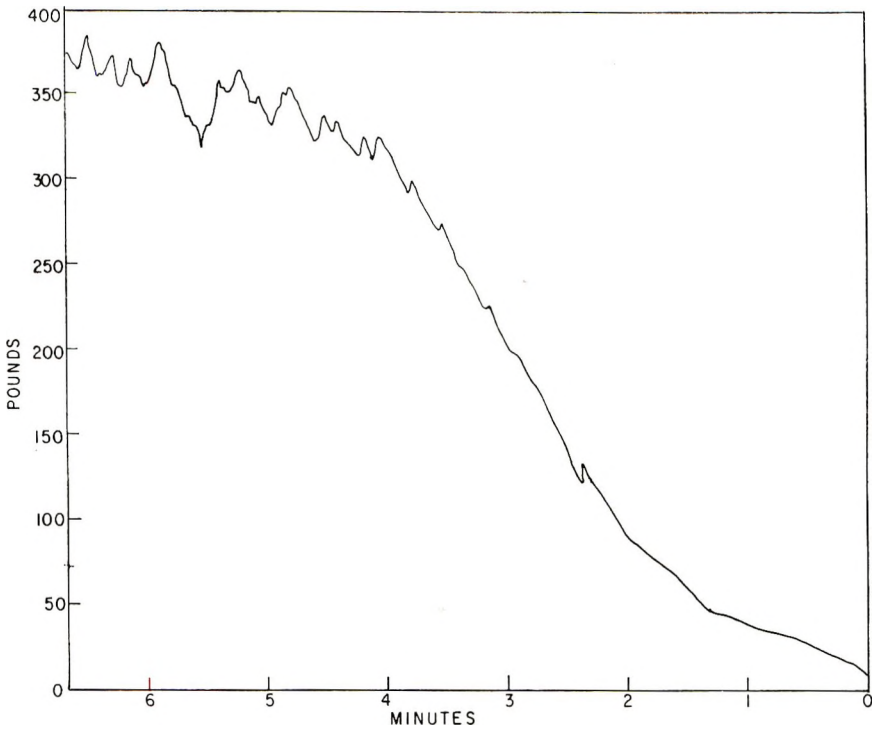

Fig. 26. Extrusion pressure vs. time of curing of EPR containing 3.2 pph of sulfur at 150° C.

noted. However, the plug remaining in the barrel of the extruder, after curing was completed, appeared to be better knitted together and more homogeneous than the sample cured with peroxide alone.

A fourth experiment was run at 150°C. on EPR containing 50 pph of Philblack A carbon black. As can be seen in Figures 27 and 28, the extrusion pressure curve was nearly double that of the unfilled material. Additionally, the time for curing appears to have been reduced significantly to less than 3 min. Thus, it appears that the inclusion of carbon black in the formulation reduces the time and/or temperature required for curing.

In our last experiment with EPR, the elastomer containing 50 pph of Philblack A was extruded at 140°C. to determine the time required to cure at this temperature. The 10°C. lower temperature reduced the time required for cure to about that found for the unfilled material at 150°C. (Figs. 29 and 30).

V. CONCLUSIONS

1. The capillary extrusion rheometer, with suitable temperature controls and operated in conjunction with an Instron or other comparable tensile testing machine, has been shown to be a valuable analytical tool for study-

ing and defining the curing characteristics of thermosetting plastics and rubbers.

2. The flow versus pressure data obtained on the extrusion rheometer can be correlated directly with the processing conditions required for these thermosetting plastics and/or rubbers via transfer molding, extrusion, etc.

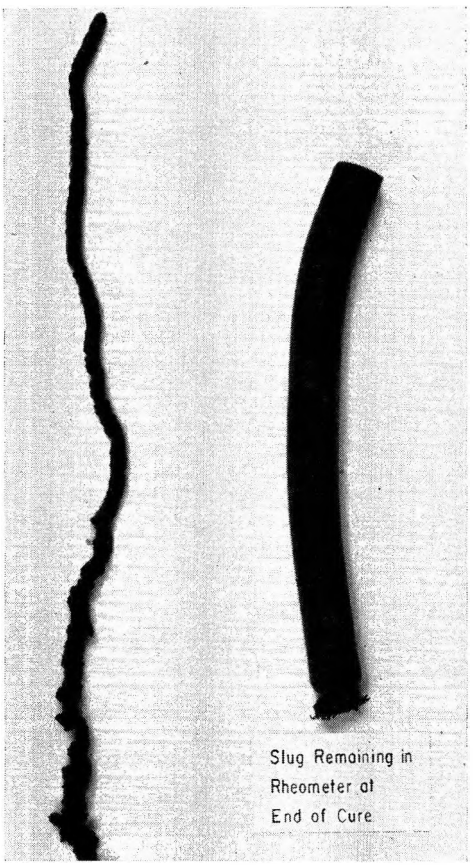

Fig. 27. Photograph of strand of EPR containing 50 pph of Philblack A carbon black extruded at 150°C.

3. A continuous and useful time history of the curing reaction in the plastics and rubbers is obtained in the extruded strands, which can be sectioned and analyzed to determine the degree of crosslinking at any time during the curing process.

4. Compared to the heated cure plate and the Mooney rheometer (used for thermosets and rubbers, respectively), the Monsanto capillary extrusion rheometer has important advantages, in that it supplies semiquantitative data which can be related directly to the processing of these materials and data from which "apparent viscosities" can be computed.

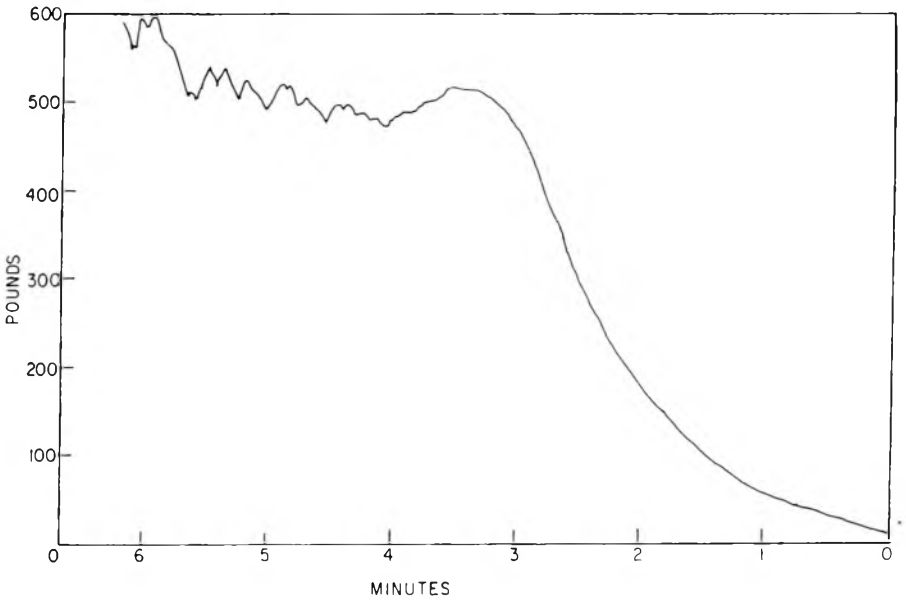

Fig. 28. Extrusion pressure vs. time of curing of EPR containing 50 pph of Philblack A carbon black at 150°C.

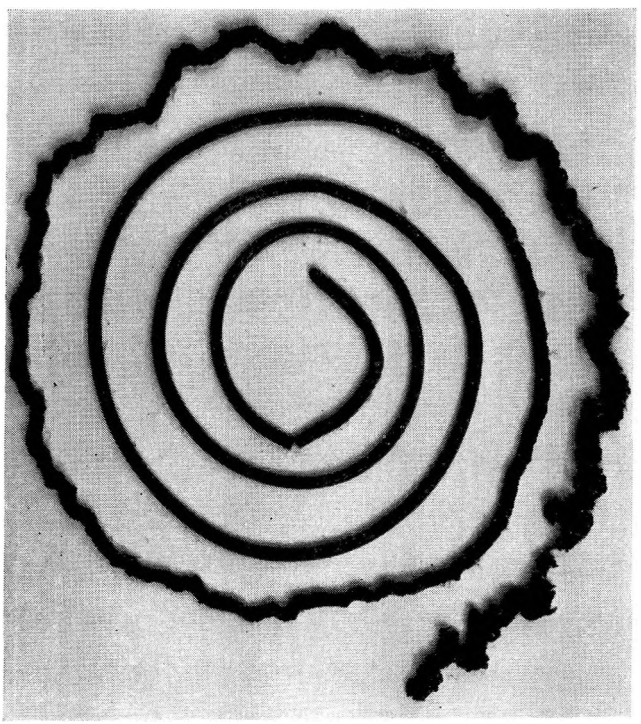

Fig. 29. Photograph of strand of EPR containing 50 pph of Philblack A carbon black extruded at 140°C.

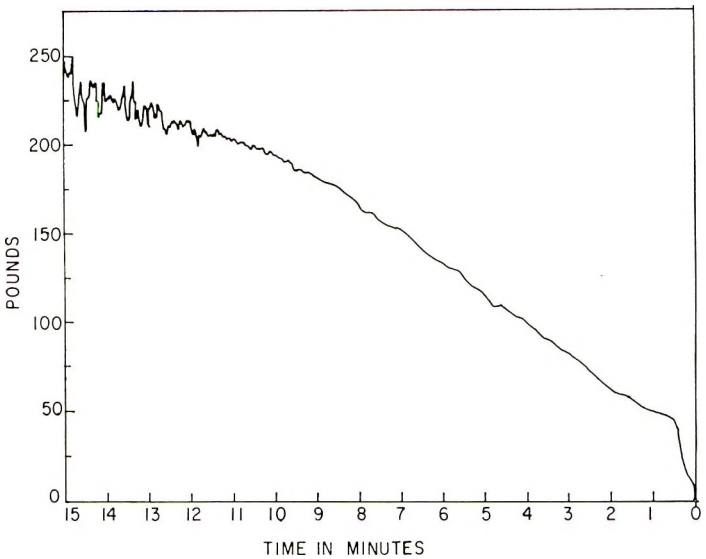

Fig. 30. Extrusion pressure vs. time of curing of EPR containing 50 pph of Philblack A carbon black at 140°C.

The authors gratefully acknowledge the aid of Mr. Carl Ruscetta, Jr., R. A. Fischbein, and E. G. Thomas of Mound Laboratory in the execution of much of the experimental work described in this paper.

We also wish to acknowledge the contributions of Mr. Anthony C. Schaefer of the Dayton Laboratory of Monsanto Research Corporation who performed many of the experiments on the curing of the rubbers listed in this report.

References

1. Salyer, I. O., private communication to R. E. Colwell, December 8, 1954.
2. Cox, W. P., and E. H. Merz, *J. Polymer Sci.*, **28,** 610 (1958).
3. Colwell, R. E., and E. H. Merz, *ASTM Bull.* ,**No. 232,** 63 (Sept. 1958).
4. Spur, R. A., B. M. Hanking, and J. W. Rowen, *J. Polymer Sci.*, **37,** 431 (1959).

Résumé

Grâce à un rhéomètre à extrusion capillaire, placé sur une machine d'essai Instron, on a étudié l'écoulement et la prise des matières plastiques thermodurcissables et des caoutchoucs. La plupart des expériences ont été faites en présence de phtalate de diallylle et on a mesuré la vitesse du traitement par la détermination par infra-rouge de l'insaturation résiduelle. On a aussi caractérisé le phénol–formaldéhyde. Enfin on a étudié le traitement par les peroxydes des caoutchoucs à base de copolymères d'éthylène et de propylène, et d'éthylène et d'acétate de vinyle. Cette étude a été faite en rapport avec le type de peroxyde utilisé. Les résultats obtenus par cette méthode (MCER) sont d'importance pratique quand il s'agit de prédire les relations pression–température pour la transformation des matières plastiques thermodurcissables et des caoutchoucs. De plus, l'histoire du traitement, que l'on obtient à partir du brin extrudé est également très importante théoriquement pour étudier la cinétique de la réaction et évaluer l'efficacité de divers traitements. On conclut en prédisant une utilisation importante de cette méthode (MCER) lors de l'étude du traitement des polymères thermodurcissables et des caoutchoucs.

Zusammenfassung

Mit einem modifiziertem Kapillarextrusionsrheometer kleiner Bohrung (MCER) zusammen mit einem Instron-Zugtestapparat wurden die Fliessund Verarbeitungseigenschaften von wärmehärtenden plastischen Massen und Kautschuken charakterisiert. Die Mehrzahl der Versuche wurde an Diallylphthalat durchgeführt, wo die Härtungsgeschwindigkeit auch durch Infrarotbestimmung des Verschwindens der Doppelbindungen bei fortschreitender Polymerisationshärtung verfolgt wurde. Weiters wurde Phenolformaldehyd charakterisiert. Schliesslich wurde die Vulkanisation von Äthylen–Propylenund Äthylen–Vinylacetatkopolymerkautschuken mit Peroxyd untersucht und eine Korrelation mit dem verwendeten Peroxydtyp aufgestellt. Es wird gezeigt, dass die MCER-Daten für die Voraussage der Zeit–Temperatur–Druckbeziehung bei der Verarbeitung wärmehärteder plastischer Massen und Kautschuke verwendet werden können. Ausserdem ist der Härtungsverlauf, wie er durch Analyse des kontinuierlich extrudierten Stranges erhalten wird, zur Untersuchung der Reaktionskinetik und zur Ermittlung der Wirksamkeit verschiedener Härtungssysteme von theoretischem Interesse. Eine weite Anwendung des MCER zur Untersuchung der Härtung wärmehärtender plastischer Massen und Kautschuke ist zu erwarten.

Received September 4, 1964
(Prod. No. 4539A)

JOURNAL OF POLYMER SCIENCE: PART A VOL. 3, PP. 1941–1948 (1965)

Concentration Dependence of the Reduced Viscosity of Dilute Aqueous Polyelectrolyte Solutions

R. L. DARSKUS, D. O. JORDAN, T. KURUCSEV, and M. L. MARTIN,
Department of Physical and Inorganic Chemistry, The University of Adelaide, Adelaide, South Australia

Synopsis

The concentration dependence of the reduced viscosity has been studied for several polyelectrolytes in conductivity water. It is shown that the viscosity maximum previously reported for polyelectrolyte solutions without added electrolyte can be explained either by the presence of ionic impurities in the solvent or by the contamination of the solutions. It is concluded that the folding chain theory of polyelectrolyte solutions requires amendment to account for the experimental results on counterion association. A suggested amendment to the theory implies that the application of the Huggins equation to the concentration dependence of polyelectrolyte solutions in the presence of added electrolyte may not lead to information concerning the interactions between the polyions in solution.

The ionization of a flexible, linear polyelectrolyte markedly increases the viscosity of its salt-free aqueous solution, often by several orders of magnitude. This increase in viscosity has been explained[1,2] in terms of an unfolding of the polymer coil due to the mutual repulsion between the increasing number of like charges attached to the coil as ionization proceeds. Similarly, the increase of the reduced viscosity on dilution of a salt-free polyelectrolyte solution has been attributed to the decreased screening of the fixed charges by the counterions and the consequent coil expansion.

The variation of the reduced viscosity with concentration of polyelectrolyte solutions containing a constant low concentration of added electrolyte shows a maximum in the reduced viscosity at low concentrations. The folding chain theory predicts this behavior, since after the polvions reach their maximum extensions with dilution, the concentration dependence should be determined solely by intermolecular interactions. Eirich was the first to point out[3] that, for the same reason, the variation of the reduced viscosity with concentration for salt-free polyelectrolyte solutions should also exhibit a maximum if the concentration is sufficiently low. This was confirmed by subsequent experimental studies involving viscosity measurements at very low concentrations[4–15] for almost all polyelectrolytes investigated. However, application of the Huggins equation[16] to the initial ascending portions of the reduced viscosity against concentration curves leads, in some cases, to anomalously high values of the interaction coefficients, thus casting considerable doubt on the validity of the above interaction explanation.

Since the concentration of the polyelectrolytes corresponding to the reduced viscosity maxima found with salt-free solutions is generally in the region of 5×10^{-5} g./ml., measurements show poor reproducibility. It has been suggested that this may be caused by the presence of ionic impurities[17] or by the absorption of atmospheric carbon dioxide.[18] In addition, the viscosity of biological macromolecules may be influenced by partial or complete denaturation.[19] In this communication an experimental re-examination of the viscosity of dilute aqueous solutions of some polyelectrolytes is presented, special emphasis being directed towards the possible existence of maxima in the variation of the reduced viscosity with concentration.

Experimental

Poly(4-vinyl-*N*-*n*-butylpyridinium bromide) (PVP-Br) sample E3-Q was prepared by quaternization of polyvinylpyridine (fraction E3, $[\eta]$ = 206 ml./g. in ethanol solution[20]) in nitromethane solution according to the method of Maclay and Fuoss.[21] The product obtained was a red powder. Analysis showed that 97% of the pyridine nitrogens in the sample were quaternized with *n*-butyl bromide, the remaining 3% with hydrogen bromide. Hydrodynamic measurements suggested that extensive degradation of the polymer had occurred during the quaternization reaction.

PVP-Br sample A1-Q was prepared by quaternization of a polymer fraction[22] ($[\eta]$ = 230 ml./g. in ethanol) in dimethylformamide solution at 50°C. for 12 hr. in the absence of atmospheric oxygen. The product was precipitated from aqueous solution by the addition of acetone, freeze-dried from a solution of *tert*-butanol, and dried in a vacuum. The product was an almost white powder. The degree of quaternization was found to be 1.00, and the absence of hydrogen bromide from the sample was confirmed by pH measurements on dilute aqueous solutions. The weight-average molecular weight of the sample determined by light scattering in 0.2*M* KBr solution was 1.65×10^6. No degradation of the polymer had occurred during the quaternization reaction.

Poly(vinylbenzyltrimethylammonium chloride) (PBTA-Cl) was obtained from the Dow Chemical Company, Midland, Michigan, U.S.A. Analysis confirmed that the polymer was completely amminated. Since the sample had been resin-treated to remove ionic impurities it was used as supplied without further purification. From light-scattering measurements in 0.2*M* KCl solutions the weight-average molecular weight was found to be 4.1×10^5.

Polyvinylimidazole (PVI) was obtained from the Badische Anilin-und Soda Fabrik A.G., Ludwigshafen, Germany. The material was dried to constant weight at 60°C. *in vacuo*.

Poly(styrenesulfonic acid) (PSSA) was obtained from the Dow Chemical Company as the sodium salt ($\bar{M}_w = 4 \times 10^5$). Aqueous solutions of the sample were freed from ionic impurities and the polyelectrolyte was

converted to the acid form by the use of ion exchange resins. The free acid was recovered by freeze-drying and stored in the dark over desiccants.

Poly(methacrylic acid) (PMA) was prepared from methacrylic acid in aqueous solution; benzoyl peroxide being used as initiator. The polymer was purified by reprecipitation and dried in a vacuum.

Distilled water had a specific conductance of 1–3 $\times$ 10^{-6} ohm^{-1}-$cm.^{-1}$.

Conductivity water of specific conductance 1.3–4 $\times$ 10^{-7} ohm^{-1}-$cm.^{-1}$ was prepared by distillation of distilled water from alkaline $KMnO_4$ in an all-glass still, passing it slowly through a mixed bed ion exchange resin column, and collecting either in a seasoned Pyrex glass flask or directly in the Ostwald viscometer.

The Ostwald viscometer used was of British Standards Specification design,[23] except for an additional bulb above the solution reservoir to allow dilutions to be made in the viscometer. The dimensions of the viscometer were such that the kinetic energy and end-effect corrections could be neglected for the purpose of the present investigation. The viscometer was suspended in a water bath at 25°C. controlled to $\pm$0.005°C. Measurements in an inert atmosphere were carried out by connecting the arms of the viscometer through a suitable combination of taps to a supply of nitrogen.

The Couette viscometer used has been described previously;[13] several minor modifications have been introduced to achieve greater stability. For measurements on salt-free solutions of polyelectrolytes, the stainless steel surfaces in contact with the solutions were coated with a poly(methyl methacrylate) film deposited from chloroform solution. The film was sufficiently thin to show interference colors. It was found that in the absence of this coating, the conductance of conductivity water increased rapidly on standing in the viscometer. Relative viscosities at mean velocity gradients 5–15 $sec.^{-1}$ were determined to a precision of $\pm$0.5% or better. Shear dependence (PVP-Br sample A1-Q) in this range was negligible.

Smooth reduced viscosity against concentration curves for the polyelectrolytes studied in the absence of added electrolyte could only be obtained if a single sample of conductivity water was used for a given series of concentrations. This was achieved by first filling the viscometer with pure water and adding small aliquots of a polyelectrolyte stock solution by means of an Agla micrometer syringe and after mixing well, removing by means of another micrometer syringe a volume equal to that added.

Results and Discussion

The results of viscosity measurements on the polyelectrolytes with conductivity water as solvent are summarized in Table I. The main features of the concentration dependence of the reduced viscosity for the various polyelectrolytes studied are illustrated by the results for poly(styrenesulfonic acid) shown in Figure 1, where the pronounced effect on the reduced viscosity of small amounts of impurity is demonstrated.

TABLE I
Viscosity Results on Polyelectrolytes Dissolved in Conductivity Water

Polyelectrolyte	Minimum Concentration studied, g./ml. × 10^6	Viscometer	Viscosity maxima
PBTA-Cl	2	Ostwald	Absent
PVI-40% HCl	10	Ostwald	Absent
PSSA	1	Ostwald	See Fig. 1
PVP-Br (E3-Q)	2	Ostwald	Absent
PVP-Br (A1-Q)	10	Ostwald	Present
	10	Couette	Absent
PMA-90% NaOH	4	Ostwald, Couette	Absent

The results on the high molecular weight ($\bar{M}_w = 1.65 \times 10^6$) sample of PVP-Br (A1-Q) require special mention. When studied in the capillary viscometer, the concentration dependence of the reduced viscosity was found to exhibit a maximum, even with the purest sample of conductivity water available. However, when studied in the Couette viscometer, at low rates of shear, no maximum was observed down to a concentration of 10^{-5} g./ml., thus indicating that shear effects may sometimes produce maxima. This is to be expected on the basis of the folding chain theory, since on expansion of the polyions the shear dependence of their solutions will increase, and, if measurements are made at high rates of shear, the observed reduced viscosity may decrease even though the extension of the polyions increases.

The results on PMA are not in agreement with previous work, which showed the presence of maxima in the concentration dependence of the

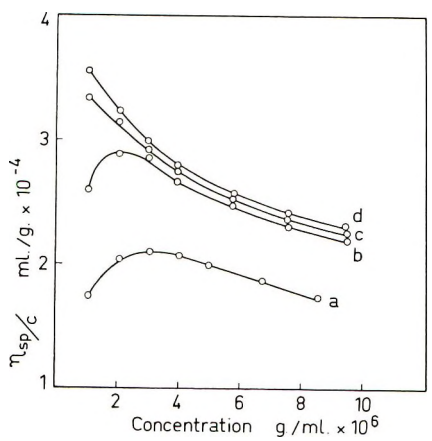

Fig. 1. Reduced viscosities of poly(styrenesulfonic acid) solutions as a function of concentration at various specific conductance of solvent: (*a*) 0.30 × 10^{-6} ohm^{-1} $cm.^{-1}$; (*b*) 0.20 × 10^{-6} ohm^{-1} $cm.^{-1}$; (*c*) 0.15 × 10^{-6} ohm^{-1} $cm.^{-1}$; (*d*) 0.13 × 10^{-6} ohm^{-1} $cm.^{-1}$

reduced viscosity for solutions of sodium polymethacrylate[5,9] and of sodium polyacrylate[4] at relatively high concentrations ($1\text{–}5 \times 10^{-4}$ g./ml.). This discrepancy could be due to the absorption of atmospheric carbon dioxide by the alkaline solutions of sodium polymethacrylate and polyacrylate in the case of the early work. We have found that at the lowest concentration of PMA studied, contact with air by the solutions caused a marked drop in the reduced viscosity compared with that measured in an inert atmosphere by as much as a factor of five.

In the presence of added electrolyte, the maximum in the curve relating the reduced viscosity with concentration occurs in general when the polyelectrolyte concentration c (expressed in equivalents per liter), is approximately the same as the concentration of the added electrolyte m. Conductivity water of specific conductance 2×10^{-7} ohm^{-1}-cm.$^{-1}$ contains about 2×10^{-6} eq./l. of ionic impurities, and with such water as solvent the maximum reduced viscosity occurs with PSSA solutions at a concentration of about 10^{-5} eq./l. (Fig. 1). Such curves should therefore be regarded as representing the variation of the reduced viscosity with polyelectrolyte concentration in the presence of a small constant amount of electrolyte rather than in salt-free solution. As the purity of the conductivity water is improved so the maximum occurs at lower polyelectrolyte concentrations (Fig. 1).

The interpretation of the concentration dependence of the reduced viscosity of polyelectrolytes is still controversial. According to the folding chain theory,[24,25] application of the Huggins equation[16]

$$\eta_{sp}/c = [\eta] + k'[\eta]^2c$$

to the initial ascending portion of curves relating the reduced viscosity and concentration at constant salt concentration may be used to ascertain the extent of the polyion interaction in solution. Similarly, the interaction coefficients k' may be calculated from plots involving an isoionic dilution technique[26,27] in which the sum $(m + rc)$ is kept constant with r empirically determined to give a linear dependence of the reduced viscosity on concentration. From such studies, the interaction coefficient k' is found to increase with m. The highest value reported so far has been $k' = 400$ at $m = 2 \times 10^{-5}$ eq./l. for solutions of sodium lignin sulfonate,[28] approximately a 1000-fold increase over the k' values generally observed for uncharged polymers. It has been suggested therefore that the viscosity behavior of polyelectrolytes should be explained by consideration of the changes in the interactions between the polyions rather than by changes in the polyion configuration.

An increase in the interactions between charged particles compared with their uncharged counterparts is expected from theoretical considerations and has been termed the secondary electroviscous effect.[29] The increase in viscosity is attributed to the energy dissipated when the particles passing each other are displaced perpendicularly to the stream lines due to the long-range repulsive forces between their double-layers. The magnitude

of the effect is expected to be highest for small particles at low ionic strengths.[29-31] Thus for silver iodide sols,[29] an over tenfold increase in the value of the first interaction coefficient was found as the concentration of added electrolyte was decreased from 3.9×10^{-1} to 3.5×10^{-5} eq./l.

Polyions, although having in many instances a local charge density comparable to that of the spherical silver iodide particles, would be expected to exhibit a much smaller secondary electroviscous effect on account of their large size. Consequently the very high interaction coefficients in polyelectrolyte solutions are difficult to justify on theoretical grounds and attemped explanations in general contain assumptions, such as the inclusion of the volume of the electrical double layer in the effective hydrodynamic volume of the polyions.[28] It would thus appear that the high values of k' obtained by applying the Huggins equation to the viscosity data for polyelectrolyte solutions do not necessarily represent true values of the interaction coefficients.

Recent studies have shown that the counterion binding by polyelectrolytes remains constant in the same range of concentration over which the characteristic increase of the reduced viscosity occurs with dilution.[32] Accordingly, the mechanism of configurational changes of the polyions with dilution in terms of a changing degree of counterion binding[24,25] must be amended by consideration of changes in counterion distribution rather than in counterion association. Consider an isolated polyion in an infinite volume of solvent containing a very low concentration m of a 1:1 electrolyte. The bulk counterion concentration is therefore m, but in the vicinity of the polyion the local counterion concentration m', will be much larger than m. At a low finite polyelectrolyte concentration, such that the bulk counterion concentration is still essentially m, each polyion now has only a finite volume from which to draw counterions, and m' therefore decreases. Since the degree of screening of the charges on the polyion is determined by the value of m' and not of m, the polyion expands. This expansion continues with increasing polyelectrolyte concentration until the concentration c of counterions supplied by the polyelectrolyte becomes an appreciable fraction of m, whereupon contraction occurs on further increase of c.

The high values of k' calculated from isoionic dilution curves of polyelectrolytes could, in a similar way, arise from a contraction of the polyions with dilution, since it is to be emphasized that a linear concentration dependence of the reduced viscosity cannot be taken as evidence for a constant polyion configuration.

We wish to thank Dr. S. D. Jones and Dr. J. Laddy, both of the Dow Chemical Company, for gifts of PBTA-Cl and PSSA, respectively, the Badische Anilin- und Soda Fabrik A.G. for the sample of PVI, and to acknowledge the award of a Commonwealth Postgraduate Scholarship to R.L.D.

References

1. Katchalsky, A., and D. Spitnik, *J. Polymer Sci.*, **2**, 432, 487 (1947).
2. Fuoss, R. M., and U. P. Strauss, *J. Polymer Sci.*, **3**, 602 (1948).
3. Eirich, F., *Discussions Faraday Soc.*, **11**, 153 (1951).
4. Alexander, P., and S. F. Hitch, *Biochim. Biophys. Acta*, **9**, 229 (1952).
5. Butler, J. A. V., and B. E. Conway, *Nature*, **172**, 153 (1953).
6. Eisenberg, H., and J. Pouyet, *J. Polymer Sci.*, **13**, 85 (1954).
7. Fujita, H., K. Mitsuhasi, and T. Homma, *J. Colloid Sci.*, **9**, 466 (1954).
8. Fujita, H., and T. Homma, *J. Colloid Sci.*, **9**, 591 (1954).
9. Conway, B. E., *J. Polymer Sci.*, **18**, 257 (1955).
10. Jordan, D. O., A. R. Mathieson, and M. R. Porter, *J. Polymer Sci.*, **21**, 463 (1956).
11. Butler, J. A. V., A. B. Robins, and K. V. Shooter, *Proc. Roy. Soc. (London)*, **A241**, 299 (1957).
12. van Duin, P. J., and J. J. Hermans, *J. Polymer Sci.*, **36**, 295 (1959).
13. Jordan, D. O., and T. Kurucsev, *Polymer*, **1**, 185 (1960).
14. Jordan, D. O., and T. Kurucsev, *Polymer*, **1**, 193 (1960).
15. Harrap, B. S., and E. F. Woods, *J. Polymer Sci.*, **49**, 353 (1961).
16. Huggins, M. L., *J. Am. Chem. Soc.*, **64**, 2716 (1942).
17. Flory, P. J., and J. E. Osterheld, *J. Phys. Chem.*, **58**, 653 (1954).
18. Alfrey, T., R. M. Fuoss, H. Morawetz, and H. Pinner, *J. Am. Chem. Soc.*, **74**, 438 (1952).
19. Kurucsev, T., *Arch. Biochem. Biophys.*, **102**, 120 (1963).
20. Jordan, D. O., A. R. Mathieson, and M. R. Porter, *J. Polymer Sci.*, **21**, 473 (1956).
21. Maclay, W. N., and R. M. Fuoss, *J. Polymer Sci.*, **6**, 511 (1951).
22. Darskus, R. L., D. O. Jordan, and T. Kurucsev, *Polymer*, in press.
23. British Standard Specification No. 188, "Determination of Viscosity in Absolute Units."
24. Fuoss, R. M., and U. P. Strauss, *Ann. N. Y. Acad. Sci.*, **51**, 836 (1949).
25. Markovitz, H., and G. E. Kimball, *J. Colloid Sci.*, **5**, 115 (1950).
26. Rosen, B., P. Kamath, and F. Eirich, *Discussions Faraday Soc.*, **11**, 135 (1951).
27. Pals, D. T. F., and J. J. Hermans, *J. Polymer Sci.*, **5**, 733 (1950).
28. Goring, D. A. I., and A. Rezanovich, *J. Colloid Sci.*, **15**, 472 (1960).
29. Harmsen, G. J., J. van Schooten, and J. T. G. Overbeek, *J. Colloid Sci.*, **8**, 64, (1953).
30. Dobry, A., *J. Chim. Phys.*, **52**, 809 (1955).
31. Harmsen, G. J., J. van Schooten, and J. T. G. Overbeek, *J. Colloid Sci.*, **10**, 315 (1955).
32. Botre, C., V. L. Crescenzi, A. M. Liquori, A. Mele, and F. Ascoli, *J. Polymer Sci.*, **40**, 169 (1959).

Résumé

On a étudié l'influence de la concentration sur la viscosité réduite de plusieurs polyélectrolytes dissous dans de l'eau de conductivité. On a montré que le maximum de viscosité antérieurement décrit pour des solutions de polyélectrolyte sans addition d'électrolyte peut être expliqué soit par la présence d'impuretés ioniques dans le solvant soit par la contamination des solutions. On tire la conclusion que la théorie de la chaîne repliée pour les solutions de polyélectrolyte exige des corrections pour tenir compte des résultats expérimentaux concernant l'association des contre-ions. On suggère une correction à la théorie qui mène à la conclusion que l'application de l'équation de Huggins relative à la dépendance, vis-à-vis de la concentration, de solutions de polyélectrolyte en présence d'électrolyte additionnel ne peut pas donner d'information concernant les interactions entre les polyions en solution.

Zusammenfassung

Die Konzentrationsabhängigkeit der reduzierten Viskosität wurde an einigen Polyelektrolyten in Leitfähigkeitswasser untersucht. Das früher in Polyelektrolytlösungen ohne Zusatzelektrolyten gefundene Viskositätsmaximum kann entweder durch die Anwesenheit von Ionenverunreinigungen im Lösungsmittel oder durch Verunreinigung der Lösung erklärt werden. Man kommt zu dem Schluss, dass die Kettenfaltungstheorie für Polyelektrolytlösungen einer Ergänzung zur Berücksichtigung der Versuchsergebnisse über Gegenionenassoziation bedarf. Es wird eine Ergänzung der Theorie vorgeschlagen, die dazu führt, dass die Anwendung der Huggins-Gleichung auf die Konzentrationsabhängigkeit von Polyelektrolytlösungen in Gegenwart eines Zusatzelektrolyten keine Information über die Wechselwirkung zwischen den Polyionen in der Lösung liefert.

Received October 7, 1964
(Prod. No. 4550A)

JOURNAL OF POLYMER SCIENCE: PART A VOL. 3, PP. 1949–1958 (1965)

Temperature Dependence of Dye Diffusion

SHLOMO ROSENBAUM,* *Research Department, The Dow Chemical Company, Williamsburg, Virginia*

Synopsis

The temperature dependence of the diffusion of cationic dyes in polyacrylonitrile fibers has been examined over a wide range of temperatures. The results were found to accord well with a free volume model of dye diffusion. Apparent activation energies increased with decreasing temperature above the glass transition temperature T_g, and became extremely high near T_g. The course of the dependence could be described by a relation of the form of the Williams, Landel, and Ferry equation.

Although the equilibrium uptake and diffusion behavior of water and other low molecular weight compounds from the vapor state have been used increasingly in recent years[1–6] for the study of polymer structure, the uptake of dyes from solution has received little attention for that purpose. This seems unfortunate, considering the easy experimental methods available and the relative simplicity of the diffusion behavior.[7] It may be due in part to an impression that the diffusion of dyes takes place in a manner different from that of other compounds so that the desired information cannot be obtained. It is commonly thought that dyes diffuse through water in canals or pores formed by swelling of the fiber on immersion in an aqueous bath and leading from the surface to the center of the fiber. The fiber merely provides irregular walls, in the nature of mechanical obstacles, which the dye has to avoid. Valkó early pointed out[8] inadequacies of this model for cellulose acetate. There have been a number of indications since[9–12] which show that the fibers play a more active role in the diffusion process, but the model persists both in qualitative thinking and in the foremost quantitative work. Recently, a free volume model of dye diffusion[13] was developed to give a relation[14] between diffusion coefficient of dye and relaxation time of polymer segments making up the fiber. Such segmental motion above the glass transition temperature T_g, measured by diverse physical methods, frequently conforms to a relation (WLF) due to Williams, Landel, and Ferry.[15] The present paper examines the temperature dependence of the diffusion of cationic dyes into polyacrylonitrile fibers with sulfonate sites and the applicability of the WLF equation to the description of such dye diffusion.

* Present address: The Dow Chemical Company, Walnut Creek, California.

Experimental

The experimental procedures for the dye sorption experiments have been described.[16] The dyes used were purified as in earlier papers.[7] Unless

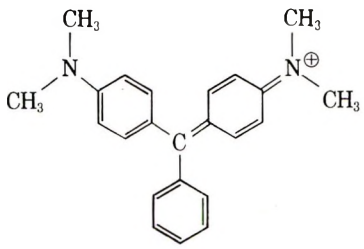

I

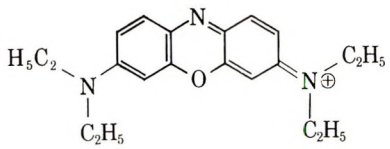

II

otherwise stated, the triphenylmethane dye Malachite Green (I) was used on a fiber (1) made from a copolymer of acrylonitrile with 5 mole-% methyl acrylate which was wet-spun from $ZnCl_2$ solution. The other experimental fibers (2 and 3) were prepared similarly from (almost) the same composition. The other dye (II) will be designated simply as the oxazine dye. All dyeing experiments were carried out in 0.05 M sodium acetate–acetic acid buffer at pH 4.0.

The measurement of linear axial thermal expansion is described elsewhere.[17]

Results and Discussion

It was suggested earlier[13,14] that the diffusion of dyes be treated by the methods used for diffusion in viscous liquids or rubbers rather than in porous solids. Apparently all dyeing processes are carried out above the glass transition temperature T_g, where enough free volume is available to allow appreciable motion of segments of the polymer molecules constituting the fiber. The process is readily visualized by an idealized lattice in which the free volume is present in the form of holes of the same size as a segment which can thus exchange places with the hole by jumping into it. An average polymer segment, about 20–30 chain atoms long,[18] will generally be larger than (but of the same order of magnitude as) most dye molecules. The movement of the free volume can thus explain the diffusion of the dye, since a dye molecule can also jump into a hole that has moved next to it, usually with greater ease than a polymer segment. While the dye may move faster, its motion is nonetheless governed by the movement of the holes, which in turn is determined by the time it takes the segments to make a jump. On this simplified model, different dyes will move faster than the average segment by a factor varying between 1 and z, where z is the coordination number.

The diffusion coefficient D of dye was shown[14] to be related to an average relaxation time τ of segments of polymer molecules of thickness δ oriented parallel to the fiber axis by

$$D = f(\delta^2/\tau)v_s \tag{1a}$$

if the volume fraction v_s of sites for the dye is smaller than 1. This simplifies to

$$D = f(\delta^2/\tau) \tag{1b}$$

when the dye can interact with a site at any position in the fiber. By the derivation of eqs. (1), f is determined by directional and jumping preferences. In the simplest case, where a segment can move into a hole it faces with the same ease as a dye molecule, it is given by $1/\pi$. It should be of the general order of magnitude of unity for most cases of interest.

Figure 1 shows the variation of the apparent diffusion coefficient D_a with reciprocal temperature for Malachite Green on an experimental fiber of T_g $\sim$57°C., determined[17] from the axial thermal expansion in water (Fig. 2). D_a was obtained from the slopes R of sorption–time curves (Fig. 3) and the relation[7]

$$D_a = (\pi/4)(R/A_w S)^2 \tag{2}$$

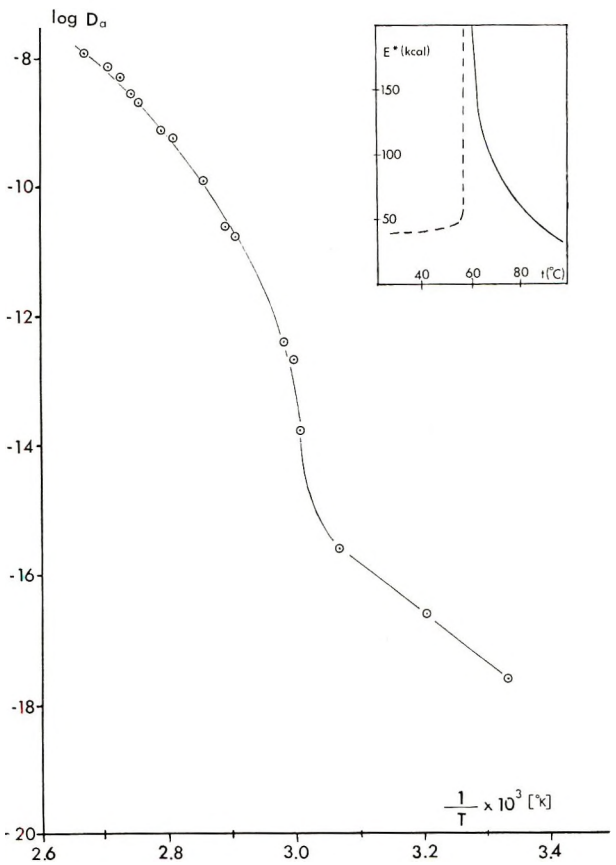

Fig. 1. Arrhenius plot of apparent diffusion coefficient D_a of Malachite Green in experimental polyacrylonitrile fiber. Inset plot shows variation with temperature of apparent activation energy.

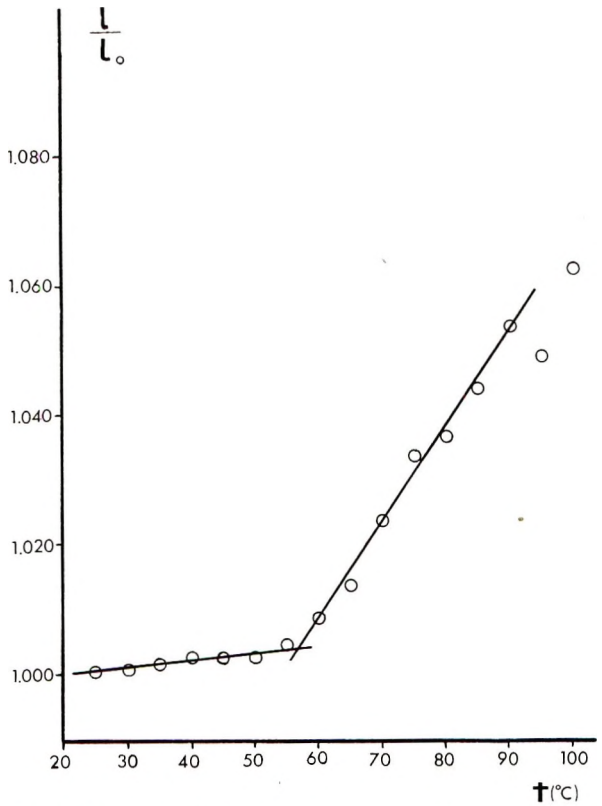

Fig. 2. Variation of fiber length in water with temperature.

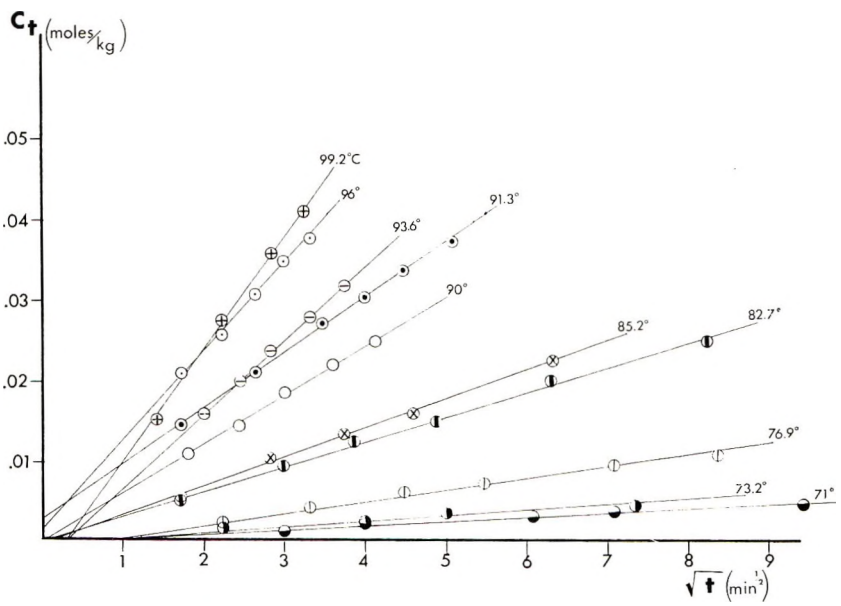

Fig. 3. Sorption–time curves at different temperatures. C_t is concentration of dye on fiber at time t.

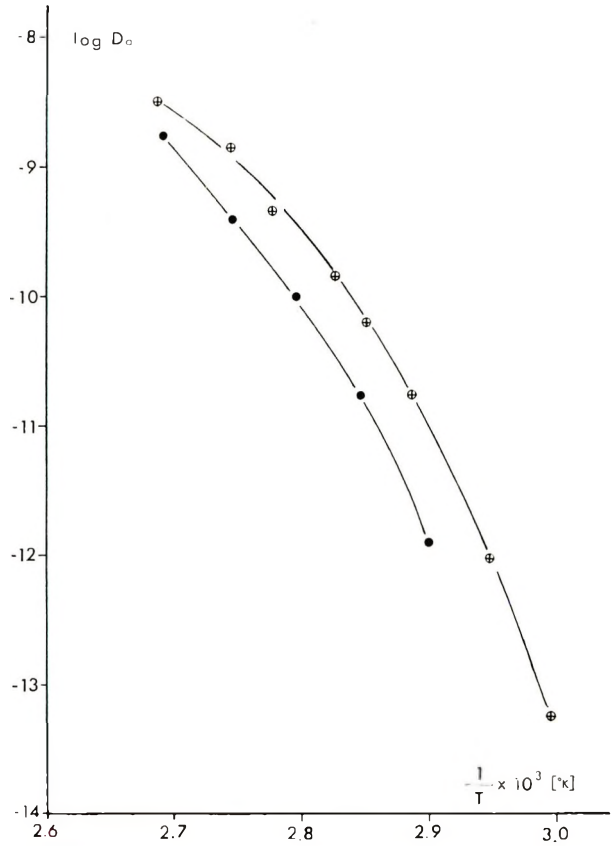

Fig. 4. Arrhenius plots on (⊕) system B (Table I); (●) system C.

where A_w is the outer fiber surface area of fiber of site concentration S and initially free of dye. Figure 4 shows data obtained on other experimental fibers. (D_a is expressed in square centimeters/minute in conformance with general practice for dye diffusion.)

The temperature dependence of diffusion coefficients is most often[3,19,20] represented by an Arrhenius equation

$$D = D_0 \exp \{-E^*/RT\} \tag{3}$$

where D_0 is the value extrapolated at infinite temperature and E^* is a constant activation energy. If the diffusion of the dye is governed by the movement of the free volume, we should expect a temperature dependence similar to that of other kinetic phenomena in polymers above the glass transition temperature. The apparent activation energy should then[2,15] decrease with increasing temperature above T_g. This is well confirmed by Figures 1 and 4, and more directly by the inset plot of Figure 1. Similar curvature in an Arrhenius plot has also been found by the less precise, but more direct, microscopic observation of the rate of radial dye penetration.[21]

TABLE I. Variation of Apparent Diffusion Coefficients with Temperature

System	Temperature t, °C.	Apparent diffusion coefficient D_a, cm.²/min.
A Malachite Green on experimental fiber 1	99.2	1.12×10^{-8}
	96.0	7.1×10^{-9}
	93.6	4.80×10^{-9}
	91.3	2.74×10^{-9}
	90.0	1.97×10^{-9}
	85.2	7.3×10^{-10}
	82.7	5.3×10^{-10}
	76.9	1.2×10^{-10}
	73.2	2.4×10^{-11}
	71.0	1.7×10^{-11}
	62.3	3.7×10^{-13}
	60.6	2.2×10^{-13}
	59.4	1.7×10^{-14}
	53.0	2.4×10^{-16}
	39.0	2.5×10^{-17}
	27.0	2.35×10^{-18}
B Oxazine dye on experimental fiber 2	98.9	3.03×10^{-9}
	91.4	1.29×10^{-9}
	87.1	4.33×10^{-10}
	80.8	1.50×10^{-10}
	77.4	7.3×10^{-11}
	73.5	1.82×10^{-11}
	66.0	9.8×10^{-13}
	60.8	5.6×10^{-14}
C Malachite Green on experimental fiber 3	99.0	1.75×10^{-9}
	91.3	4.32×10^{-10}
	84.6	9.85×10^{-11}
	78.6	1.65×10^{-11}
	71.3	1.26×10^{-12}

For a large number of amorphous polymers, the Williams, Landel, and Ferry (WLF) equation[15] has been shown to hold in its specific form

$$\log a_T = -[17.44\ (T - T_g)]/(51.6 + T - T_g) \tag{4}$$

where a_T is the ratio of the relaxation times τ (or observable quantities proportional to τ) at temperature T to that at T_g, in the present case D_{Tg}/D_T according to either form of eq. (1).

A $\log 1/D_a$ versus T plot of the data in Figure 1 could reasonably be fitted to a plot of $\log a_T$ versus $T - T_g$ only so as to give a T_g of ~40°C., which is 17–18°C. lower than that from other measurements, such as the thermal expansion shown earlier. The possibility that the changes detected near 60°C. in water (~35°C. higher in silicone oil) are due to another transition was regarded as remote. Where the required data have been obtained here or by other authors[22–25] they fulfil the qualitative criteria for T_g suggested

TABLE I (*continued*)

System	Temperature t, °C.	Apparent diffusion coefficient D_a, cm.²/min.
D Malachite Green on Orlon 42	97.6	2.14×10^{-10}
	95.2	1.5×10^{-10}
	90.1	4.8×10^{-11}
	85.4	1.15×10^{-12}
	83.2	2.9×10^{-13}
	79.7	3.6×10^{-14}
	74.0	2.5×10^{-15}
	70.4	1.7×10^{-15}
	64.5	6.4×10^{-16}
	55.0	4.6×10^{-16}
	45.2	9.9×10^{-15}
	45.0	1.9×10^{-15}
	25.0	3.6×10^{-16}
E Oxazine dye on Orlon 42	98.9	3.16×10^{-10}
	91.4	4.59×10^{-10}
	87.1	1.56×10^{-11}
	80.8	1.54×10^{-12}
	77.4	7.7×10^{-14}
	73.5	1.3×10^{-14}
	66.0	3.9×10^{-15}
	60.8	3.2×10^{-15}
	25.0	1.10×10^{-15}
F Malachite Green on Acrilan 16	99.0	4.16×10^{-10}
	91.3	1.36×10^{-10}
	84.6	2.69×10^{-11}
	78.6	9.7×10^{-12}
	71.3	3.0×10^{-14}

by Boyer.[26] More specifically, the dye uptake is negligible below but sets in with a high activation energy at this temperature, as seen in Figure 1 (or, more drastically, on a D_a versus T plot).

Tobolsky[27] and Ferry[5] have pointed out that the constants in eq. (4) do not appear to be universal. The more general relation (using Ferry's notation)

$$\log a_T = -[c_1^g (T - T_g)]/(c_2^g + T - T_g) \tag{5}$$

was suggested as of greater validity. From a plot of $(T - T_g)/\log a_T$ versus $T - T_g$, for the T_g values obtained from the linear thermal expansion (Fig. 2) and from the point of inflection in Figure 1, the values of 10.75 and 28.5 were obtained for the constants c_1^g and c_2^g, respectively. The curve in Figure 5 was then drawn according to the relation

$$\log a_T = -[10.75 (T - T_g)]/(28.5 + T - T_g) \tag{6}$$

The experimental points on which the curve is based are shown as dotted circles.

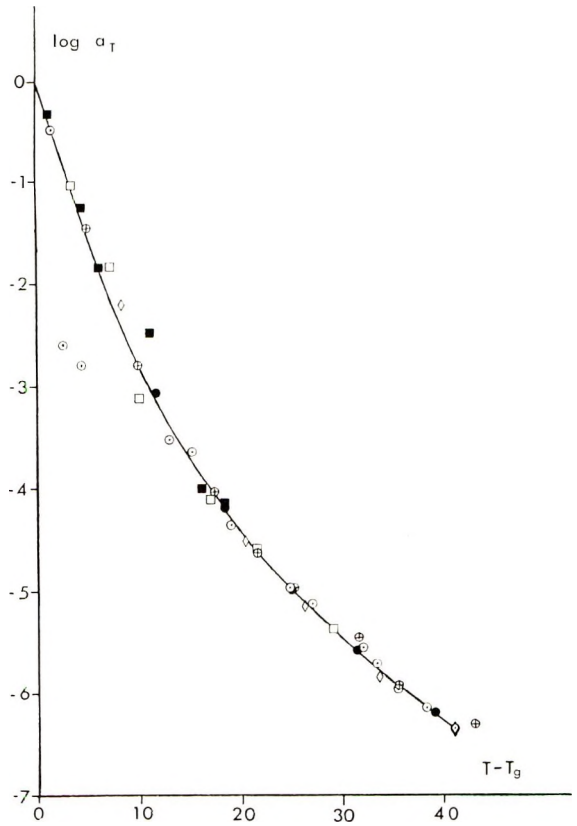

Fig. 5. Fit to eq. (6) of all data by horizontal and vertical shifts of log $1/D_a$ vs. T plots: (⊙) system A (Table I); (⊕) system B; (●) system C; (■) system D; (□) system E; (◇) system F.

Data for all fibers and dyes with which complete sorption curves were measured are listed in Table I. Plots of $1/D_a$ versus T for each were fitted to the same curve by horizontal and vertical shifts. The result (Fig. 5) is regarded as very satisfactory, including the agreement of glass transition temperatures obtained by extrapolation with those from direct, independent methods.[17] The relaxation times at the glass transition temperatures, from the vertical shift factor and eq. (1a), were not identical for all fibers, but they were in the vicinity (1–10 sec.) of those commonly found[6] by other methods.

The fit broke down below T_g, as it should. The extremely slow dye uptake there may be governed by motions released at a subtransition or possibly by pore diffusion. The wide experimental scatter makes any finding more doubtful than above T_g, but there was strong indication of differences between fibers. The details are of little importance for the discussion in this paper.

In one case (D), the fit to the specific WLF equation could also be regarded as satisfactory. This reflects not only the experimental scatter re-

maining, but also an insensitivity of the shape of the log a_T versus $(T - T_g)$ curve to the exact value of the constants in eq. 5. The departure of the constants in eq. (6) from those of the original WLF equation may be related to peculiarities in the glass transition of polyacrylonitrile.[17] The main point to be made, however, is that the results obeyed eq. (5). Conformance to a relation of the general form of the WLF equation at present appears to be[26] one of the most valid criteria for segmental motion released at a glass transition temperature. The dye diffusion treated here clearly fulfils the requirement. The free volume model of dye diffusion is now regarded as well established. It is, therefore, thought that future work can be concentrated on the development of a less simplified quantitative theory, specifically taking into account the effect on the probability of site encounters of the restraint exerted on a site by the rest of the polymer molecule[14] and the effect of free volume distribution on the dependence of the diffusion coefficient of a dye on its molecular size.

At the completion of this series of papers and of work in this laboratory, the author should like especially to express his appreciation to its director, W. J. Backer, for his constant encouragement. In addition, thanks are due again to A. Armen and T. Alfrey for helpful discussions.

References

1. Barrer, R. M., *J. Phys. Chem.*, **61**, 178 (1957).
2. Wilkens, J. B., and F. A. Long, *Trans. Faraday Soc.*, **53**, 1146 (1957).
3. Jeschke, D., and H. A. Stuart, *Z. Naturforsch.*, **16a**, 37 (1961).
4. Fujita, H., *Fortschr. Hochpolymer.-Forsch.*, **3**, 1 (1961).
5. Ferry, J. D., *Viscoelastic Properties of Polymers*, Wiley, New York, 1961.
6. Bueche, F., *Physical Properties of Polymers*, Interscience, New York, 1962.
7. Rosenbaum, S., and F. L. Goodwin, *J. Appl. Polymer Sci.*, **9**, 333 (1965).
8. Valkó, E. I., *Kolloidchemische Grundlagen der Textilveredlung*, Springer, Berlin, 1937.
9. Remington, W. R., and H. G. Schroeder, *Textile Res. J.*, **27**, 177 (1957).
10. Rosenbaum, S., Dissertation, Polytechnic Inst. of Brooklyn, New York, 1958.
11. Sprague, B. S., and R. W. Singleton, presented at Gordon Research Conference on Textiles, 1961.
12. Jones, F., *J. Soc. Dyers Colourists*, **77**, 57 (1961).
13. Rosenbaum, S., *J. Appl. Polymer Sci.*, **7**, 1225 (1963).
14. Rosenbaum, S., *Textile Res. J.*, **34**, 291 (1964).
15. Williams, M. L., R. F. Landel, and J. D. Ferry, *J. Am. Chem. Soc.*, **77**, 3701 (1955).
16. Rosenbaum, S., *Textile Res. J.*, **34**, 52 (1964).
17. Rosenbaum, S., *J. Appl. Polymer Sci.*, **9**, 2001 (1965).
18. Alfrey, T., *Mechanical Behavior of High Polymers*, Interscience, New York, 1948.
19. Vickerstaff, T., *The Physical Chemistry of Dyeing*, Interscience, New York, 1954.
20. Barrer, R. M., *Diffusion in and through Solids*, University Press, Cambridge, 1941.
21. Goodwin, F. L., and S. Rosenbaum, *Textile Res. J.*, in press.
22. Krigbaum, W. R., and N. Tokita, *J. Polymer Sci.*, **43**, 467 (1960).
23. Bohn, C. R., J. R. Schaefgen, and W. O. Statton, *J. Polymer Sci.*, **55**, 531 (1961).
24. Howard, W. H., *J. Appl. Polymer Sci.*, **5**, 303 (1961).
25. Beevers, R. B., and E. F. T. White, *Trans. Faraday Soc.*, **56**, 1529 (1960).
26. Boyer, R. F., *Rubber Chem. Technol.*, **36**, 1303 (1963).
27. Tobolsky, A. V., *Properties and Structure of Polymers*, Wiley, New York, 1960.

Résumé

La dépendance en fonction de la température de la diffusion des colorants cationiques dans les fibres de polyacrylonitrile, a été examinée dans un large domaine de températures. On a trouvé que les résultats correspondent bien avec le modèle du volume libre pour la diffusion des colorants. Les énergies apparentes d'activation augmentent avec une diminution de la température située au-dessus de la température de transition vitreuse T_g, et deviennent extrèmement élevées aux environs de T_g. L'évolution de cette dépendance peut être décrite par une relation de la forme de l'équation de Williams, Landel, et Ferry.

Zusammenfassung

Die Temperaturabhängigkeit der Diffusion kationischer Farbstoffe in Polyacrylnitrilfasern wurde in einem grossen Temperaturbereich untersucht. Die Ergebnisse stehen mit einem Modell des freien Volumens für die Farbstoffdiffusion in Übereinstimmung. Die scheinbaren Aktivierungsenergien nahmen oberhalb der Glasumwandlungstemperatur T_g mit fallender Temperatur zu und wurde in der Nähe von T_g extrem hoch. Der Verlauf der Abhängigkeit konnte durch eine Beziehung von der Form der Williams, Landel, Ferry Gleichung beschrieben werden.

Received September 29, 1964
Revised October 29, 1964
(Prod. No. 4557A)

JOURNAL OF POLYMER SCIENCE: PART A VOL. 3, PP. 1959–1967 (1965)

Kinetics of the Polymerization and Styrene Copolymerization of *m*- and *p*-Divinylbenzene

RICHARD H. WILEY and GIOVANNI DEVENUTO, *Department of Chemistry, College of Arts and Sciences, University of Louisville, Louisville, Kentucky*

Synopsis

The rate of polymerization and copolymerization with styrene of *m*-, 2:1/*m*:*p*-, commercial, and *p*-divinylbenzene in *tert*-butylbenzene decreases in the order listed at 65 and 80°C. The copolymerization of the *para* isomer at 80°C. accelerates more rapidly than does that of the other isomers. The overall activation energies increase from 14.9–20.8 kcal./mole to 23.5–26.9 kcal./mole in the polymerizations and from 9.0–12.1 to 13.0–17.6 kcal./mole in the copolymerizations over the time interval involved. The differences in rates and autocatalytic effects are attributed to differences in relative reactivities of the *m*- and *p*-vinylstyrene-derived radicals, the *m*- and *p*-alkyl styrene structures, and to the different distribution of divinyl units in the copolymers.

In previously described studies[1] of the kinetics of polymerization of pure divinylbenzene isomers in toluene, it was observed that there is a significant difference in the overall rates at which the *meta* and the *para* isomers polymerize in toluene. The *meta* isomer polymerizes more rapidly than the *para* isomer. The ratio of the rate constants at 60°C. was observed to be 1.56 and that at 80°C., 2.21. The conditions used were not suitable for direct determination of the activation energies for polymerization and copolymerization. Also, a complication was introduced by an apparent difference in chain transfer with the solvent (toluene). In order to obtain kinetic data suitable for determination of activation energies and to avoid the allylic hydrogen chain transfer complication, the present study of the kinetics in *tert*-butylbenzene was undertaken.

Experimental

Details of the preparation and purification of monomers have been given previously.[2] For this study the same samples of *m*- and 2:1/*m*:*p* described before[1] were used. The *para* isomer was a different sample prepared from phenylenediacrylic acid and purified by vapor-phase chromatography as described before, n_D^{35} 1.5857. Commericial divinylbenzene (55%, Koppers) was distilled before use, n_D^{25} 1.5620, and the amount used was based on its divinyl content with the ethylvinylbenzene content taken as styrene. The styrene (Distillation Products Co., n_D^{20} 1.5468) was

distilled before use. All monomers were redistilled shortly before use to remove inhibitor and traces of polymer, stored cold under nitrogen, and used under conditions demonstrated to involve no polymerization prior to the kinetic experiment. The *tert*-butylbenzene (Distillation Products Co.)

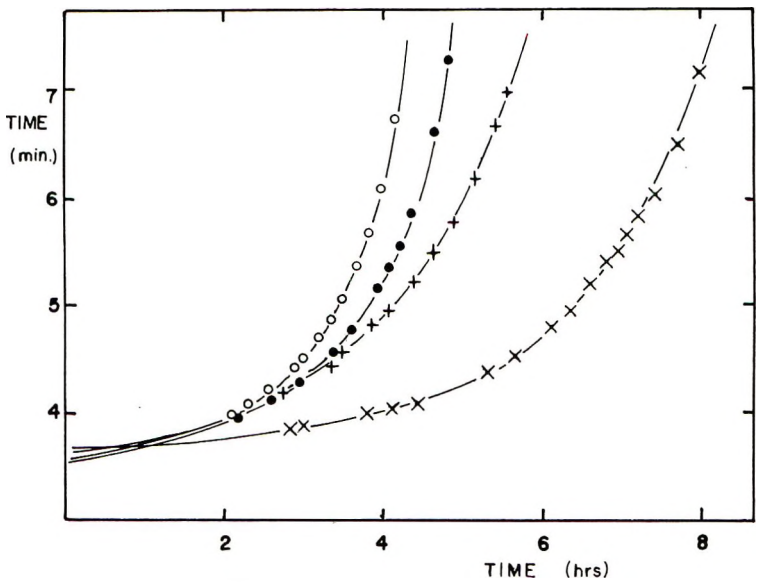

Fig. 1. Rate of polymerization of divinyl isomers in *tert*-butylbenzene at 65°C.: (O) *m*-divinylbenzene; (●) 2:1/*m*:*p*-divinylbenzene; (×) *p*-divinylbenzene; (+) commercial divinylbenzene. Abscissa, time of polymerization in hours; ordinate, efflux time in minutes.

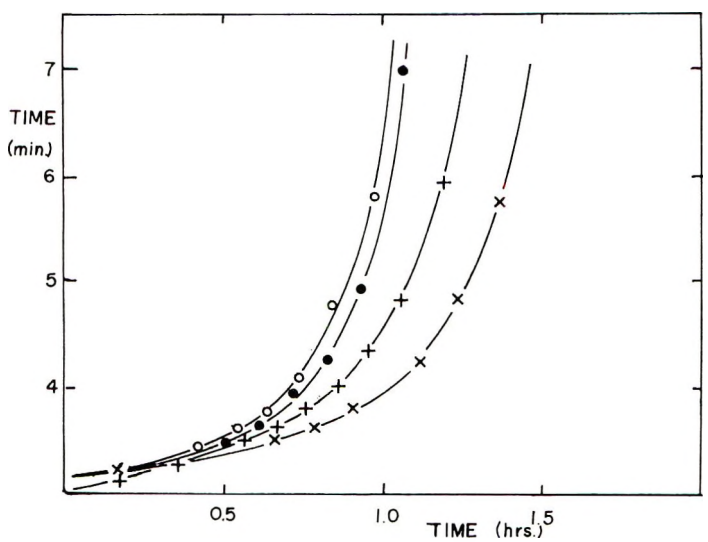

Fig. 2. Rate of polymerization of divinyl isomers in *tert*-butylbenzene at 80°C. Coordinates and symbols as in Figure 1.

was fractionated before use and stored under nitrogen; b.p. 60–61.5°C./18 mm., n_D^{20} 1.4928.

The kinetic experiments were run at 11.64% monomer concentration, viscometrically, under nitrogen, and in *tert*-butylbenzene as previously

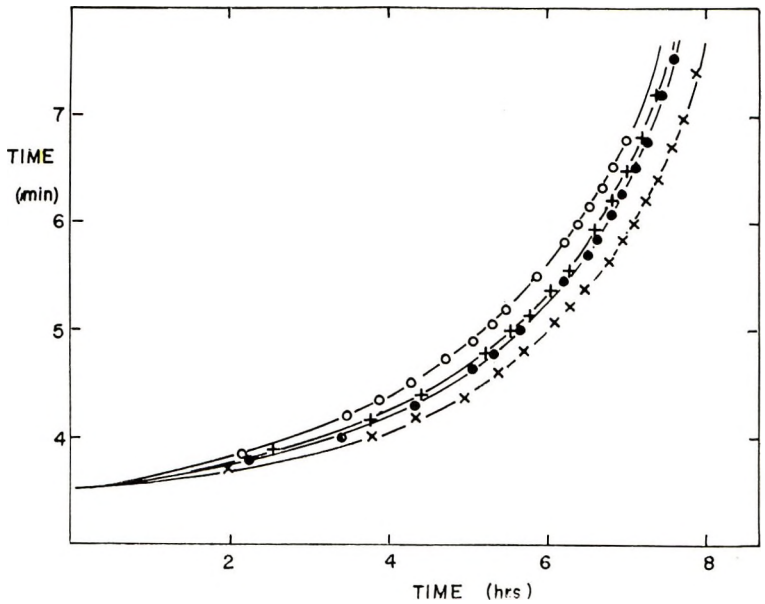

Fig. 3. Rate of copolymerization of divinyl isomers with styrene in *tert*-butylbenzene at 65°C.: (○) styrene–*m*-divinylbenzene copolymer; (●) styrene–2:1/*m*:*p*-divinylbenzene copolymers; (×) styrene–*p*-divinylbenzene copolymer; (+) styrene–commercial divinylbenzene copolymer. Coordinates as in Figure 1.

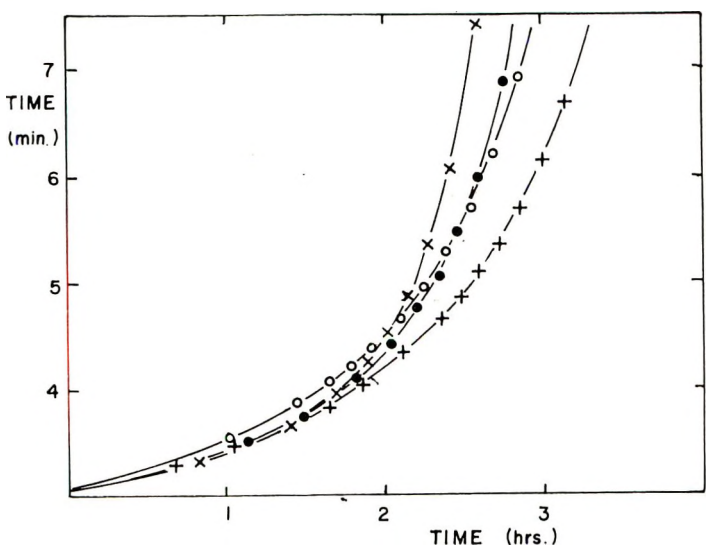

Fig. 4. Rate of copolymerization of divinylbenzene isomers with styrene in *tert*-butylbenzene at 80°C. Coordinates as in Figure 1; Symbols as in Figure 3.

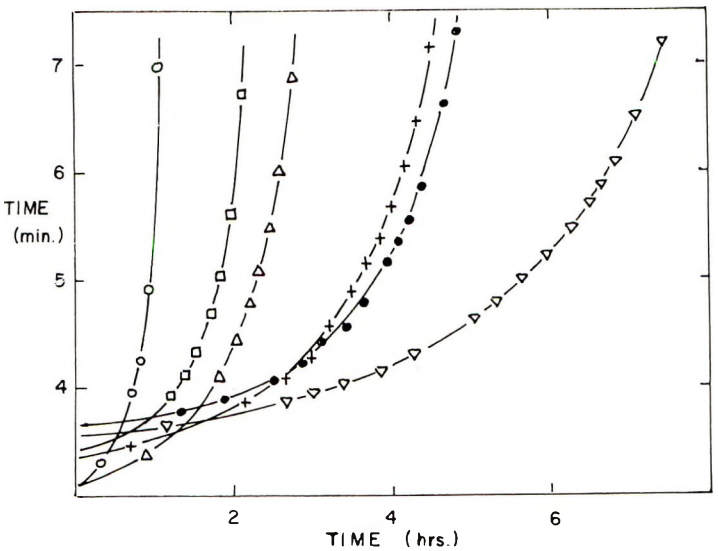

Fig. 5. Rate of polymerization and copolymerization with styrene of 2:1/*m*:*p*-divinylbenzene in *tert*-butylbenzene at 65, 72.5, and 80°C.: polymerization at (○) 80°C., (□) 72.5°C., and (●) 65°C.; copolymerization at (Δ) 80°C., (+) 72.5°C., and (∇) 65°C. Coordinates as in Figure 1.

described[1] for the toluene experiments. The initiator concentration used was 0.155 wt.-% in the polymerizations and 0.30% in the copolymerizations. The copolymerizations were all run with 0.5047 g. of a 3:1 by weight of a styrene–divinylbenzene mixture. This was added to 5 ml. of a solution of 14.51 mg. of dibenzoyl peroxide (0.30%) in 5 ml. of *tert*-butylbenzene to give a monomer concentration of 11.64%. Efflux times were recorded at 10-min. intervals during the last of the reaction time period. The elapsed time of polymerization was taken as the mid-time of the efflux determination. The data are recorded in Figures 1–4 for experiments at 65 and 80°C. for the various isomers and in Figure 5 for experiments at 65, 72.5, and 80°C. for the 2:1/*m*:*p* mixture of isomers. Duplicate determinations of efflux times gave values checking within ±2.5%.

Results and Discussion

The rate data confirm the previous observation that the overall rate of polymerization of the *m*- and *p*-divinylbenzene isomers decreases in the order: *meta;* 2:1/*m*:*p;* commercial; *para*-. This is true both in toluene and *tert*-butylbenzene and at 65 and 80°C. with the single exception of the reversal of the commercial-*para* order at 60°C. in toluene. That this reversal is related to allylic hydrogen chain transfer processes in toluene is suggested by its absence in *tert*-butylbenzene.

The rates of copolymerization with styrene at 65°C. are in the same decreasing order: *meta;* commercial ≅ 2:1/*m*:*p;* *para*. At 80°C. the copolymerization data show an anomalous behavior. The copolymeriza-

tion of the *para* isomer starts out most slowly, as at 65°C., but the rate increased more rapidly than it does for the other isomers with the result that it becomes the most rapidly copolymerizing system well before gelation time.

The activation energies, E_A, are calculated from the rate data at two temperatures and at reaction times corresponding to efflux times of 4, 5, 6, and 7 min. Additional data for the 2:1/*m*:*p* series have been obtained at 72.5°C. and used to calculate the activation energies for three temperature intervals. All of these are well within the range of experimental error and establish the reliability of the data for values calculated with one temperature interval. The data are summarized in Tables I–III. The time range

TABLE I
Ratios of Rate Constants and Activation Energies for Polymerization of Divinylbenzene (DVB) Isomers at 65 and 80°C.

Efflux time, min.	Commercial DVB[a] Rate ratio[b]	Commercial DVB[a] E_A, kcal./mole[c]	*m*-DVB Rate ratio[b]	*m*-DVB E_A, kcal./mole[c]	2:1/*m*:*p*-DVB Rate ratio[b]	2:1/*m*:*p*-DVB E_A, kcal./mole[c]	*p*-DVB Rate ratio[b]	*p*-DVB E_A, kcal./mole[c]
4	2.57	14.9	3.09	17.8	3.09	17.8	3.72	20.8
5	3.81	21.1	4.04	22.1	4.09	22.3	5.04	25.6
6	4.23	22.8	4.29	23.0	4.36	23.3	5.29	26.3
7	4.42	23.5	4.34	23.2	4.47	23.7	5.47	26.9
Limiting value[d]	4.52	23.8	4.35	23.3	4.48	23.7	5.54	27.1

[a] Commercial divinylbenzene (Koppers).
[b] Ratio of polymerization times $t_{65°}/t_{80°}$ at stated efflux time.
[c] Activation energy calculated as $E_A = [RT_1T_2/(T_2 - T_1)] \ln (t_1/t_2)$.
[d] Constant value that the ratios t_1/t_2 reach at gelation time, calculated by extrapolation.

TABLE II
Ratios of Rate Constants and Activation Energies for Copolymerization of Styrene–Divinylbenzene Isomers at 65 and 80°C.

Efflux time, min	Commercial DVB Rate ratio	Commercial DVB E_A, kcal./mole	*m*-DVB Rate ratio	*m*-DVB E_A, kcal./mole	2:1/*m*:*p*-DVB Rate ratio	2:1/*m*:*p*-DVB E_A, kcal./mole	*p*-DVB Rate ratio	*p*-DVB E_A, kcal./mole
4	1.77	9.0	2.57	14.9	1.91	10.2	2.15	12.1
5	2.16	12.2	2.58	15.0	2.45	14.2	2.75	16.0
6	2.23	12.7	2.58	15.0	2.61	15.2	2.96	17.1
7	2.27	13.0	2.59	15.0	2.67	15.5	3.05	17.6
Limiting value	2.27	13.0	2.60	15.1	2.68	15.6	3.07	17.7

TABLE III

Ratios of Rate Constants and Activation Energies for Polymerization of 2:1/*m*:*p*-Divinylbenzene and its Copolymerization with Styrene at 65, 72.5, and 80°C.

Efflux time, min.	Polymerization						Copolymerization					
	65°C./80°C.		72.5°C./80°C.		65°C./72.5°C.		65°C./80°C.		72.5°C./80°C.		65°C./72.5°C.	
	Rate ratio	E_A, kcal./mole	Rate ratio	E_A, kcal./mole	Rate ratio	E_A, kcal./mole	Rate ratio	E_A, kcal./mole	Rate ratio	E_A, kcal./mole	Rate ratio	E_A, kcal./mole
4	3.09	17.8	1.71	17.3	1.81	18.4	1.91	10.2	1.38	10.4	1.38	10.0
5	4.09	22.3	1.94	21.4	2.11	23.1	2.45	14.2	1.56	14.4	1.57	14.0
6	4.36	23.3	2.08	23.7	2.17	24.0	2.61	15.2	1.56	14.4	1.64	15.3
7	4.47	23.7	2.01	22.6	2.22	24.7	2.67	15.5	1.61	15.4	1.65	15.5
Limiting value	4.48	23.7	2.11	24.1	2.22	24.7	2.68	15.6	1.62	15.6	1.65	15.5

involved covers a period from which a significant amount of reaction has taken place (4 min.) to that of incipient gelation (7 min.). During this time there is an increase in the E_A values from 14.9–20.8 kcal./mole to 23.5–26.9 kcal./mole in the polymerizations and from 9.0–12.1 kcal./mole to 13.0–17.6 kcal./mole in the copolymerizations. The increase indicates that secondary (presumably branching, crosslinking, and transfer) reactions are involved within this time span. The magnitude of the E_A values is approximately the same as observed in the polymerization of styrene (20.5 kcal./mole).[3,4]

The structural and mechanistic interpretations of these data must take into consideration the inherent differences in rates of polymerization and copolymerization of the two isomers (*meta* and *para*), differences in chain transfer effects, and differences in autoacceleration effects. The last may result from formation of different molecular weight polymers or from inherent differences in the viscosities of the two types of branched and crosslinked structures. Not all of the data for model systems needed for complete understanding of the various factors involved are available but some comment can be made pending accumulation of such data.

The inherent differences in the rates are probably partially, at least, obscured by polymerizations of the second vinyl groups during the last of the reaction period. At the very beginning of the polymerization reaction, when the first vinyl group is predominantly involved, the *meta* isomer polymerizes and copolymerizes more rapidly with a lower activation energy. This indicates a more reactive, less resonance-stabilized character for the *m*-vinylstyryl derived radical. The E_A values (17.8 and 20.8 kcal./mole for *meta* and *para*, respectively) compared to that for styrene polymerization (20.5 kcal./mole) indicate that the *meta* isomer is more reactive than styrene and that the *para* isomer is of comparable reactivity. Comparisons of overall rates may, however, obscure compensating differences in the activation energies of propagation and termination reactions.

A comparison of the kinetic reactivities of the second vinyl groups is less easily made. One is a *meta* and the other a *para* alkyl-substituted styrene and, in copolymerizations, there are structural differences in the distribution of the divinyl isomer along the copolymer chain. From previous studies[5,6] of the monomer reactivity ratios of the two isomers, it is known that the *para* isomer enters the growing copolymer chain faster than does the *meta* isomer. The bunched *p*-divinylbenzene units will probably result in more unreacted units than are produced from the more uniformly distributed *meta* units. This would result in a less rapid accumulation of branches in the para derived structure and is consistent with a less pronounced viscosity increase dependent autocatalytic effect. The conclusion consistent with this analysis is that the second vinyl group of the *para*-derived structure is less reactive than that of the *meta*-derived structure. The unusually enhanced autoacceleration in the copolymerization of the *para* isomer at 80°C. indicates that this effect may have a different temperature dependency and thus be attributable to activation energy

differences as well as to more obviously involved frequency (or steric) factors. Differences in chain transfer processes and in viscosity characteristics of the differently shaped or sized molecules cannot be rigorously excluded at present.

Autoacceleration or gel effects producing kinetic data not unlike those observed in our present studies are commonly observed in polymerizing systems in which high viscosities are produced. The characteristics of such systems have been reviewed with reference to both styrene[7] polymerizations, in which it is not commonly observed, and in divinyl systems.[8,9] It is usually considered that gelation occurs after one, or at most but a few, crosslinkages are produced.[10] The acceleration is usually attributed to inhibition, via diffusion control, of the bimolecular termination in the high viscosity medium. The viscosity of a polymer solution varies among polymer types in terms of both molecular shape and size as well as solvent–polymer interaction phenomena. In the *m*- and *p*-divinylbenzene reactions all of these may be involved and may be so in different ways for the two isomers. Differences in chain transfer, producing shorter chains, differences in distribution of branching/crosslinking groups in the copolymers, and differences in solvent polymer behavior are all possible.

The authors wish to acknowledge with gratitude partial support of this study under contract AT-(40-1)-2055 between the University of Louisville and the Atomic Energy Commission. Samples of commercial DVB have been kindly supplied by the Koppers Company.

References

1. Wiley, R. H., and G. DeVenuto, *J. Polymer Sci.*, in press.
2. Wiley, R. H., and R. M. Dyer, *J. Polymer Sci.*, **A2**, 3153 (1964).
3. Rubens, L. C., and R. F. Boyer in *Styrene*, R. H. Boundy and R. F. Boyer, Eds., Reinhold, New York, 1952, p. 249.
4. Howard, R. N., and W. Simpson, *Trans. Faraday Soc.*, **47**, 212 (1951).
5. Wiley, R. H., and E. E. Sale, *J. Polymer Sci.*, **42**, 491 (1960).
6. Wiley, R. H., and B. Davis, *J. Polymer Sci.*, **B1**, 463 (1963).
7. Bamford, C. H., and M. J. Dewar, *Nature*, **157**, 845 (1946); *Proc. Roy. Soc. (London)*, **A192**, 309 (1947).
8. Bamford, C. H., W. G. Barb, A. D. Jenkins, and P. F. Onyon, *The Kinetics of Vinyl Polymerization by Radical Mechanism*, Academic Press, New York, 1958, p. 301.
9. Boundy, R. H., and R. F. Boyer, *Styrene*, Reinhold, New York, 1952, p. 724.
10. Walling, C., *J. Am. Chem. Soc.*, **67**, 441 (1945).

Résumé

La vitesse de polymérisation et de copolymérisation avec le styrène du *méta*-divinylbenzène, du mélange 2:1/*m*:*p*, du *p*-divinylbenzène commercial et du *ert*-butylbenène diminue dans l'ordre mentionné à 65 et 80°. La copolymérisation de l'isomère *para* est plus rapide à 80° que celle des autres isomères. Les énergies globales d'activation des polymérisations augmentent de 14.9–20.8 kcal/mole à 23.5–26.9 kcal/môle et celles des copolymérisations de 9.0–12.1 à 13.0–17.6 pendant l'intervalle de temps considéré. Les différences de vitesses et des effets autocatalytiques sont attribuées aux différences de réactivités relatives des radicaux dérivés du *méta*- et du *para*-vinyl-styrène, par les structures du *méta* et du *para*-alcoyl styrène, et par la distribution différente des unités divinyliques dans les copolymères.

Zusammenfassung

Die Polymerisations- und Copolymerisationsgeschwindigkeit mit Styrol nimmt für *meta*-, 2:1/*m*:*p*-, handelsübliches und *para*-Divinylbenzol in *t*-Butylbenzol in der angegebenen Reihenfolge bei 65 und 80° ab. Die Copolymerisation des *para*-Isomeren beschleunigt sich bei 80° mehr als die der anderen Isomeren. Die Bruttoaktivierungsenergie nimmt bei der Polymerisation von 14,8–20,8 kcal/Mol bis 23,5–26,9 kcal/Mol und bei der Copolymerisation von 9,0–12,1 bis 13,0–17,6 im verwendeten Zeitintervall zu. Die Unterschiede in der Geschwindigkeit und im autokatalytischen Effekt werden auf Unterschiede in der relativen Reaktivität der von *meta*- und *para*-Vinylstyrol abgeleiteten Radikale, auf die *meta*- und *para*-Alkylstyrolstruktur und auf die verschiedene Verteilung der Divinylbausteine in den Copolymeren zurückgeführt.

Received September 29, 1964
Revised November 3, 1964
(Prod. No. 4558A)

JOURNAL OF POLYMER SCIENCE: PART A VOL. 3, PP. 1969–1984 (1965)

Contribution à l'Etude de la Cinétique de Formation de Polymères Séquencés par Voie Radicalaire

JACQUES VUILLEMENOT, BERNARD BARBIER, GÉRARD RIESS, et ALBERT BANDERET, *Ecole Supérieure de Chimie de Mulhouse, Mulhouse (Haut-Rhin), France*

Synopsis

In order to study some aspects of radical polymerization initiated by a polymer, hexanediol sebacates in different degrees of polymerization were prepared. The endgroup was the *tert*-butyl perester which was used to polymerize the styrene. With such compounds, it is easy after the polymerization to take off the polyester backbone by hydrolysis. One can then study the mixture of polystyrene sequences and homopolystyrene made at the same time. It appears that if the speed of thermal decomposition of the *tert*-butyl perester group on the polyester is of the same order as that of the *tert*-butyl perbenzoate, the efficiency factor, i.e., the fraction of free radicals which effectively initiates the polymerization, is much smaller with a polymeric initiator. Moreover, the average degree of polymerization is much smaller in this case (even in the presence of a nonperoxidized polyester). It is believed that these two results can be explained by assuming each polyester backbone to act as a cage for the free radicals produced by its own perester group which aids their recombination and intramolecular transfer.

INTRODUCTION

Si actuellement l'on dispose bien de voies d'accès nombreuses et variées aux polymères "à séquences," on est beaucoup moins avancé en ce qui concerne la cinétique de ces réactions de greffage. Nous nous bornerons à évoquer les travaux de Smets[1] et de ses collaborateurs qui ont réussi à mettre en évidence l'influence de différents facteurs sur le rapport du polymère réellement fixé sur le tronc à l'homopolymère formé en même temps.

On peut en voir la raison dans le fait que la séparation du greffé et des homopolymères correspondants est difficile, sinon impossible, à réaliser quantitativement. Par ailleurs, si la caractérisation du greffé en taille et en composition est désormais possible, selon Benoit et Bushuk,[2] elle reste longue et délicate.

Nous avons abordé l'étude de la cinétique des réactions de greffage par une voie nouvelle qui a pour but d'apporter à l'oeuvre de Smets quelques données complémentaires originales.

Si, en effet, il est possible de détruire quantitativement le tronc porteur une fois le greffage réalisé, on perd sans doute du renseignement du fait que les charnières entre les séquences ont disparu définitivement, mais

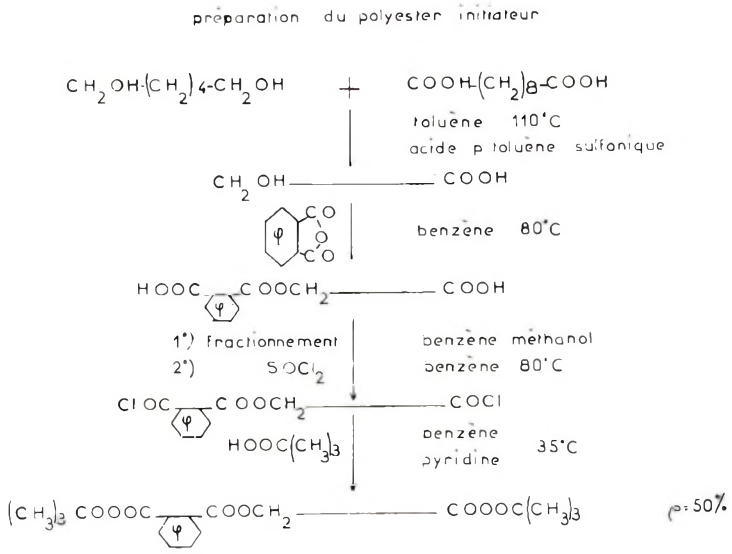

Fig. 1. Préparation du polyester initiateur.

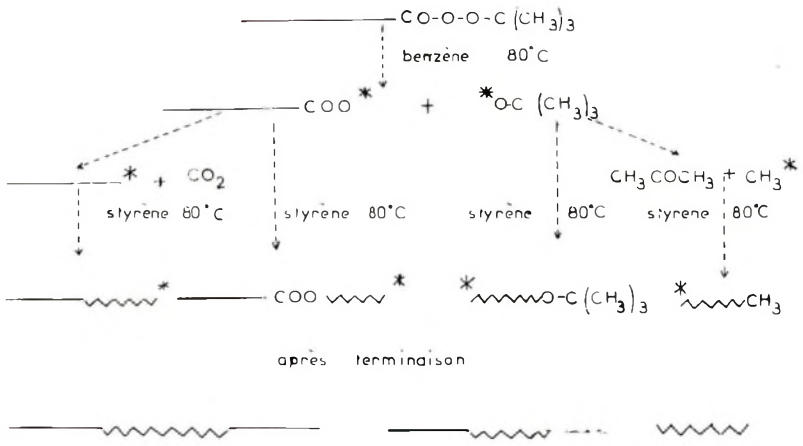

Fig. 2. Greffage.

on pourra connaître avec une bonne précision le degré de polymérisation moyen en nombre (DP_n) du mélange des séquences libérées et de l'homopolymère formé en même temps. En combinant cette valeur avec celle de la vitesse de polymérisation dm/dt nous montrerons que l'on obtient des renseignements relativement précis sur le facteur d'efficacité de l'initiation et sur les différents transferts que subit la nouvelle séquence au cours de sa croissance.

Nous avons donc préparé quelques polysébaçates d'hexanediol qui ont été muni en bout de chaine d'un groupe perester. Ce polyester perester a servi à promouvoir la polymérisation du styrène en solution benzénique

(Figs. 1 et 2) et la vitesse dm/dt de cette polymérisation a été mesurée. Le polymère brut recueilli a été hydrolysé et la fraction qui a résisté, constituée du mélange des greffons libérés et de l'homopolystyrène formé parallèlement, a été étudiée par les méthodes bien connues.

LES TECHNIQUES EXPERIMENTALES ET LES METHODES DE MESURE

Preparation et Caractérisation du Polyester Perester

Trois échantillons de polysébaçate d'hexanediol ont été préparés par une méthode déjà décrite par ailleurs.[3] Observons qu'en phtalant les groupes alcools terminaux éventuellement existants on obtient un produit contenant des groupes carboxy terminaux aliphatiques et aromatiques.

Ces produits ont été grossièrement fractionnés en précipitant au méthanol, d'une solution benzénique, d'abord une fraction de poids moléculaire élevé, puis une fraction principale qui seule a été utilisée.

La transformation en chlorure d'acide, puis en perester a été faite par les voies décrites.[3] Le taux de perester a été déterminé à l'aide d'une modification[4] de la méthode d'Ueberreiter et Sorge.[5] Elle consiste à doser par colorimétrie le bleu de méthylène formé par le peroxyde dans une solution du leucodérivé de ce colorant.

La masse moléculaire moyenne en nombre $\bar{M}_n$ a été évaluée par viscosimétrie selon Batzer.[6] Dans le benzène à 20°C,

$$[\eta] = 4{,}21 \times 10^{-2} \bar{M}_n^{0{,}69}$$

Le Tableau I résume les caractéristiques des polyesters peresters engagés.

TABLEAU I

$\bar{M}_n$	Nombre de groupes peresters par molécule
14,000	0,5
8,000	0,4
1,800	1,6

Technique du Greffage

Les polymérisations ont été faites dans des dilatomètres qui avaient été remplis en prenant toutes précautions pour éliminer au mieux l'oxygène.

Le réservoir du dilatomètre est garni d'une quantité connue d'une solution benzénique titrée de polyester perester. Le dilatomètre est connecté à une rampe à vide et on commence par éliminer le benzène par sublimation. A la rampe sont reliés des réservoirs contenant l'un du benzène prédistillé sur cuivre, puis sur sodium et l'autre du styrène débarrassé de son inhibiteur et séché sur CaH_2, avant d'être partiellement prépolymérisé thermiquement dans cette ampoule.

En congelant le contenu des tubes on peut abaisser la pression dans l'appareil à 10^{-2} mm Hg, puis introduire de l'azote bien débarrassé d'oxygène par passage sur le catalyseur B.T.S.*

Par fusion et recongélation répétées dans cette atmosphère, renouvelée par évacuation et introduction d'azote frais, on débarrasse aussi les réactifs de toute trace d'oxygène.

On distille alors une quantité exactement connue de benzène dans un tube jaugeur solidaire de la rampe. De là on fait distiller ce benzène dans le dilatomètre. On fait de même pour le styrène. Le dilatomètre ainsi garni est scellé et porté à 80°C. On relève en fonction du temps le niveau du liquide dans le capillaire du dilatomètre, et l'étalonnage de l'instrument permet de calculer la vitesse de polymérisation dm/dt connaissant la différence des volumes spécifiques du styrène et du polystyrène à 80°C: 0,2143 cm^3/g.[7] L'extrapolation à l'instant initial est facile et c'est cette vitesse initiale qui sera introduite dans nos calculs.

La polymérisation n'a jamais été poussée à des taux supérieurs à 10%. Le polymère est précipité au méthanol, pesé pour recouper la dilatométrie et hydrolysé en solution dioxanne/eau par l'acide sulfurique.

Etude des Polymères "à Séquences" Obtenus

Nous avons vérifié que ce traitement laisse le polystyrène inaltéré. Mais nous avons constaté que les constantes de Huggins de nos produits étaient d'autant plus élevées que $[\eta]$ est plus petit (Tableau II). Celà est dû au fait que les séquences polystyrène libérées par hydrolyse restent porteuses en bout de chaine de molécules d'hexanediol ou d'acide sébacique portant des groupes fonctionnels susceptibles d'associer (Fig. 3).

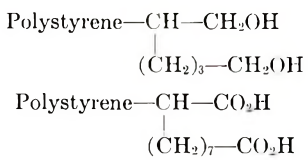

La présence de ces groupes CO_2H et OH qui associent fortement nous a fait renoncer à l'interprétation de courbes de distribution des M des polystyrènes débarrassés de polyesters. Ces distributions s'étendent sur un spectre de poids moléculaire beaucoup plus réduit que celle du polystyrène obtenu par initiation au perbenzoate de butyle tertiaire.

Comme ces polystyrènes détachés des polymères séquencés peuvent avoir une distribution de poids moléculaire particulière, il faut établir spécialement la relation empirique reliant le poids moléculaire moyen en nombre $\bar{M}_n$ et la viscosité intrinsèque dans l'intervalle où se trouvent nos produits.

Le Tableau III résume nos mesures osmotiques et viscosimétriques faites dans le benzène à 25°C.

* Catalyseur a base de cuivre, qui nous a été offert par la B.A.S.F. (Ludwigshafen) ce dont nous tenons à la remercier ici.

TABLEAU II

$[\eta]$ (benzene, 25°C), c.g.s.	$K' \times 10^2$	Promoteur
100	26	Perbenzoate de butyle tertiaire
86	22,5	
81	27	
61	20	
52	21	
45	23	
35	20	
112	26	Polyester perester, $\overline{M}_n$ = 1.800
106	24	
95	28	
72,4	29	
62,5	42	
33,5	44	
34	48	
28,4	42	
20	48	
13,5	68	
82	30	Polyester perester, $\overline{M}_n$ = 8.000
78	29	
62,5	34	
47	39	
102,5	27	Polyester perester, $\overline{M}_n$ = 14.000
72,5	28	
47	33	
27,5	58	

TABLEAU III

$[\eta]$ (benzene, 25°C,), c.g.s.	$\overline{M}_n$ (osmotique)
28,4	18.300 (13.000)[a]
35,2	33.800 (17.000)[a]
60,8	79.800
72,4	138.000
91,2	100.000
102,5	162.000

[a] Ces mesures ont été recoupées par le Dr. G. Müh du Deutsches Kuntstoff-Institut (Dir. Prof. K. H. Hellwege) Darmstadt. Nous tenons à les remercier très sincèrement.

Ces points peuvent être représentés par la relation

$$[\eta] = 2{,}35 \times 10^{-2}\overline{M}_n^{0,70}$$

assez voisine de celle de Bamford[8]

$$[\eta] = 3{,}40 \times 10^{-2}\overline{M}_n^{0,65}$$

et de Ewart et Tingey[9]

$$[\eta] = 0{,}75 \times 10^{-2}\overline{M}_n^{0,78}$$

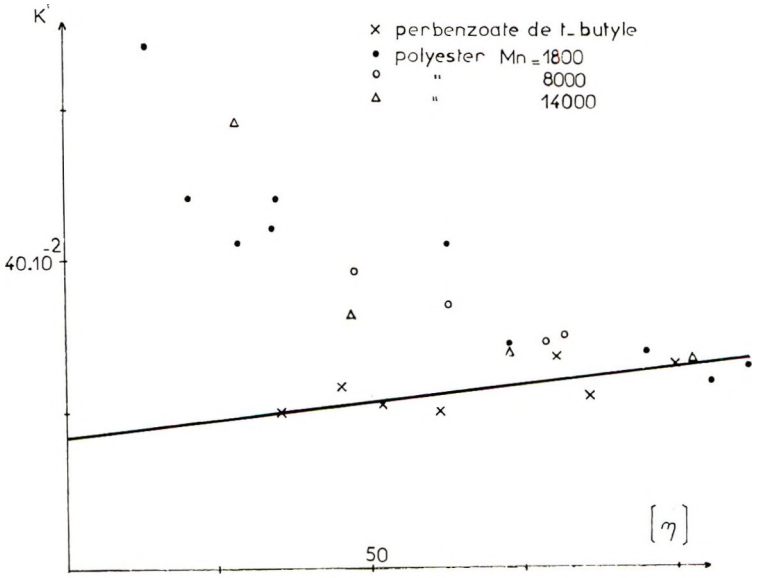

Figure 3.

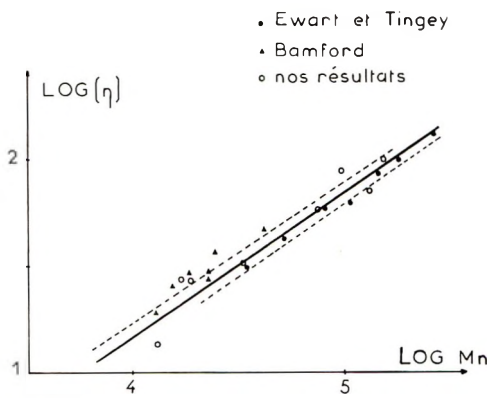

Figure 4.

obtenues sur des polystyrènes non fractionnés préparés par voie radicalaire (Fig. 4).

Cinétique de Décomposition des Polyesters Peresters

Enfin, nous avons étudié la vitesse de décomposition des groupes peroxydes non pas en solvant inerte, mais bien au sein d'une solution de styrène à 10% dans le benzène.

Opérant à 80°C, nous nous sommes donc placés dans les conditions exactes de nos essais de greffage. Les solutions de perester, macromoléculaire ou non, sont dégazées par congélation et refusion successives sous vide, puis maintenues en tube scellé à 80°C pendant des durées définies.

TABLEAU IV
Perbenzoate de Butyle tertiaire

Durée t, sec	Concentration, mole/l $\times 10^3$	
0	17	3
14.400	15,7	
15.000		2,79
28.000		2,38
29.700	14,9	
86.400		2,27
87.000	12,8	

Ensuite on dose le perester restant par la méthode décrite.[3] (Tableau IV). Précisons qu'en présence de styrène il faut, pour pourvoir appliquer la loi de Beer, engager des quantités très faibles (moins de 4×10^{-6} mole) de peroxyde dans les 50 cm³ de la solution prête à être colorimétrée. Si le perester est macromoléculaire et par conséquent non volatil, il vaut mieux éliminer le styrène par "freeze drying" avant de faire le dosage.

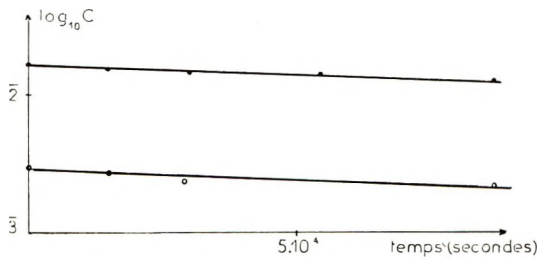

Figure 5.

La figure 5 montre que la réaction semble être du premir ordre:

$$k_d = 3 \times 10^{-6}$$

Cette valeur est nettement plus forte que les constantes de décomposition que l'on peut tirer par extrapolation à 80°C des données que Bloomquist et Ferris[10] ont obtenues entre 120 at 150°C: $0{,}4 \times 10^{-6}$.

Ces auteurs ont montré qu'à ces températures le perester subit une décomposition induite. Nos chiffres (Tableau V) ne nous permettent ni

TABLEAU V
Polyester Perester Macromoléculaire

Durée t, sec	Concentration, mole/l $\times 10^{-5}$	
0	21,8	6,6
28.800	16,9	
64.800	12,2	3,87
108.000	9,45	3,27
172.000	7,94	

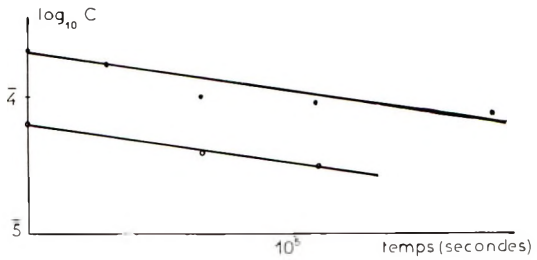

Figure 6.

d'infirmer ni de confirmer cette assertion; la décomposition induite si elle existe à 80°C étant tout juste perceptible sur nos courbes.

Les erreurs expérimentales assez importantes ne permettent pas de dire s'il y a décomposition induite ou non (Fig. 6) Il est surprenant de constater que

$$k_d = 7{,}2 \times 10^{-6}$$

est nettement plus élevée que la valeur trouvée pour le perester non macromoléculaire. Peut être est-ce dû au fait que les groupes carboxy sont partie aliphatiques partie aromatiques.

Dans le domaine de concentration de perester adapté à l'étude des réactions de greffage, on obtient des résultats suffisamment précis en considérant la réaction comme étant du premier ordre et en utilisant les valeurs indiquées.

ETUDE CINETIQUE

Promoteur Non Macromoléculaire

Pour vérifier que les techniques décrites avaient été appliquées de façon correcte, nous avons tout d'abord dépouillé, par les voies classiques, les résultats obtenus à l'aide de perbenzoate de butyle tertiaire comme promoteur.

On a pu constater que la vitesse de polymérisation dm/dt est bien proportionnelle à la racine de concentration C du promoteur (Fig. 7) et à une puissance tant soit peu inférieure à 1,5 de la concentration m en monomère (Fig. 8).

Etude des DP. Une première série de polymérisation de styrène en présence de polyester non peroxydé ($\bar{M}_n$ = 8.000) engagé à la concentration p (exprimée en nombre de fonctions ester par litre) amorcées au perbenzoate de *tert*-butyle, a permis de déterminer la constante de transfert sur polyester C_p. En effet, en tenant pour négligeable le transfert sur initiateur, on peut écrire:

$$\frac{1}{\mathrm{DP}_n} = \frac{k_t}{k_p^2}\left(\frac{dm/dt}{m^2}\right) + C_m + C_s\left(\frac{s}{m}\right) + C_p\left(\frac{p}{m}\right) \qquad (1)$$

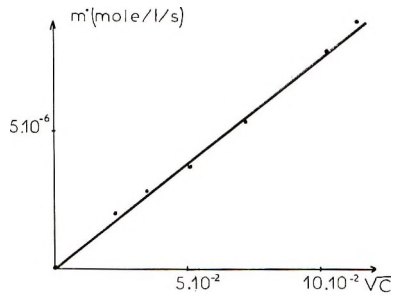

Figure 7.

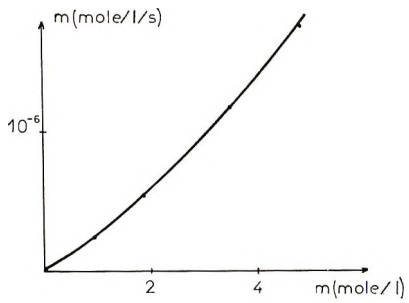

Figure 8.

où k_t est la constante de vitesse de la réaction de terminaison, k_p est la constante de vitesse de la réaction de propagation, m la concentration du monomère en mole/litre, s la concentration du solvant en mole/litre, C_m est la constante de transfert sur monomère soit 10^{-4},[11] C_s est la constante de transfert sur le solvant engagé à la concentration molaire s, soit 10^{-4},[12] et DP_n le degré de polymérisation moyen en nombre.

$$A = \frac{1}{DP_n} - C_m - C_s\left(\frac{s}{m}\right) = \frac{k_t}{k_p^2}\left(\frac{dm/dt}{m^2}\right) + C_p\left(\frac{p}{m}\right) \qquad (2)$$

TABLEAU VI[a]

p	DP_n	A	C_p
0	465	0	
0,407	374	$5,3 \times 10^{-4}$	13×10^{-4}
0,814	304	$11,4 \times 10^{-4}$	14×10^{-4}

[a] Concentration en perbenzoate de *tert*-butyle 3×10^{-2} mole/l, concentration en monomère m 0,86 mole/l.

Du Tableau VI on tire une valeur moyenne C_p calculée sur le nombre de fonctions ester par litre. Ramenée au nombre de groupes CH_2 $1,1 \times 10^{-4}$; cette valeur apparait nettement plus forte que celle du cyclohexane (1/6) $0,31 \times 10^{-4}$ à 100°C, (1/6) $0,024 \times 10^{-4}$ à 60°C,[12] ce qui prouve que la fonction ester facilite le transfert sur les CH_2 qui l'entourent.

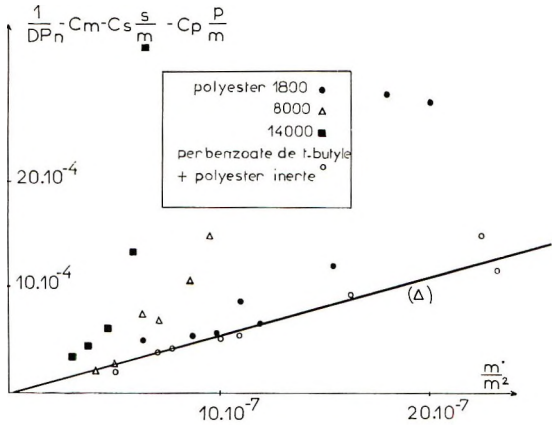

Figure 9.

Disposant ainsi d'une valeur C_p on peut écrire eq. (1) sous la forme

$$B = \frac{1}{\mathrm{DP}_n} - C_m - C_s\left(\frac{s}{m}\right) - C_p\left(\frac{p}{m}\right) = \frac{k_t}{k_p^2}\left(\frac{dm/dt}{m^2}\right) \qquad (3)$$

et porter B en fonction de $(dm/dt)(1/m^2)$ en se servant des valeurs prises dans le Tableau VII.

TABLEAU VII

m	$dm/dt \times 10^6$	$[\eta]$ benzene, 25°C, c.g.s.	$1/\mathrm{DP}_n \times 10^4$	p	$B \times 10^4$
0,95	2,4	44,9	21,3	0,407	14,1
1,83	5,4	62	13,4	0,407	9,4
3,46	11,9	90	7,8	0,407	5,2
4,80	17,6	96,2	7,4	0,407	5,3
1,85	3,7	85,4	8,3	0,203	5,5
1,85	7,9	50,9	18,5	0,814	11,7
2,0	2,8	90,2	7,9	0,407	3,9
2,0	2,0	112	6	0,407	2
0,95	3,6	35,5	29,6	4,407	22,6
2,0	9,0	49	18,9	0,407	14,9

On constate (Fig. 9) que les points représentatifs se placent assez bien autour d'une droite de pente $k_t/k_p^2 = 550$, valeur comparable à celles que l'on peut tirer des mesures de Bamford[8] (500), Matheson[10] (650), et Henrici et Olivè[13] (550) par extrapolation.

Etude du Facteur d'Efficacité *f*. On sait qu'une fraction f seulement du promoteur C décomposé déclanche effectivement la polymérisation. La formule

$$dm/dt = k_p m(fk_d/2k_t)^{1/2}C^{1/2} \qquad (4)$$

permet de calculer f puisque k_d a été mesuré.

Les valeurs expérimentales rassemblées au Tableau VIII montrent que f semble être indépendant de C mais croît nettement avec m.

TABLEAU VIII[a]

m	C	$dm/dt \times 10^6$	f	p
0,95	$5,2 \times 10^{-4}$	2,4	0,46	0,407
1,83	$5,2 \times 10^{-4}$	5,4	0,60	0,407
3,46	$5,2 \times 10^{-4}$	11,9	0,88	0,407
4,80	$5,2 \times 10^{-4}$	17,6	0,94	0,407
1,90	$5,2 \times 10^{-4}$	2,0	0,52	0,203
1,90	13×10^{-4}	2,8	0,56	0,407
1,90	26×10^{-4}	3,7	0,52	0,407
1,90	52×10^{-4}	5,4	0,66	0,407
1,90	104×10^{-4}	7,9	0,60	0,407

[a] $k_d = 3 \times 10^{-6}$ sec.$^{-1}$, $k_t/k_p^2 = 550$.

On observera que les valeurs de f sont comparables avec certaines données de la littérature[14,15] (Tableau IX).

TABLEAU IX

Promoteur	Température, T, °C	f	Référence
Peroxyde d'acetyle	65	0,83	14
Azobisisobutyronitrile	0	0,50	15
	25	0,48	
	60	0,43	
Dicumylperoxyde		1	15

Toutefois, nous observons une forte influence de m sur f, ce qui est contraire à ce que l'on a observé pour l'azobisisobutyronitrile.[15]

Promoteur Macromoleculaire

On peut comparer ces résultats absolument normaux, quand bien même ils ont été obtenus en présence de quantités importantes de polyester non peroxydé, à ceux que l'on obtient en utilisant un initiateur macromoléculaire. La seule différence entre les deux systèmes, c'est que dans le premier cas, la fonction perester est liée à un noyau benzénique, alors qu'elle est liée à une macromolécule dans le second.

Etude des DP. Tout d'abord observons qu'on a les mêmes relations entre dm/dt et C, et entre m et C que dans le cas précédent (Figs. 10 et 11).

A l'aide des résultats expérimentaux rassemblés dans le Tableau X on peut dresser la courbe représentant:

$$B = (1/\mathrm{DP}_n) - C_m - C_s\,(s/m) - C_p\,(p/m) \qquad (5)$$

en fonction de $(dm/dt)(1/m^2)$ que l'on compare à la droite obtenue avec un promoteur micromoléculaire (Fig. 9).

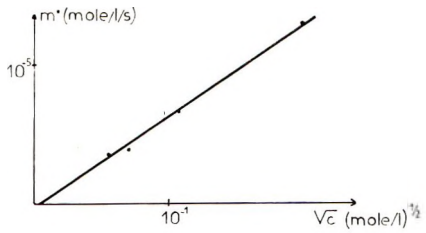

Figure 10.

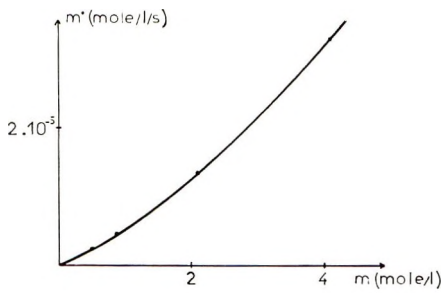

Figure 11.

TABLEAU X

m	$dm/dt \times 10^6$	$[\eta]$, c.g.s.	$1/DP_n \times 10^{-4}$	p	$B \times 10^{-4}$
Polyester de $\bar{M}_n$ = 1.800 à 1,6 groupes perester/mole					
4,06	32,6	35,2	30,7	0,407	28,4
2,08	13,2	28,4	41,5	"	37,9
0,86	4,38	19,7	69	"	60,9
0,51	2,40	13,1	125	"	111,5
2,09	6,75	60,8	13,7	0,111	12
3,62	8,25	107	6,26	0,049	5
2,01	3,9	99,6	6,90	"	5,5
1,09	1,3	71	11,4	"	8,6
0,504	0,454	33,9	32,8	"	28,2
Polyester de $\bar{M}_n$ = 8.000 à 0,4 groupes perester/mole					
0,502	0,255	39,6	26	0,325	14,9
0,785	0,525	50,1	18,2	"	10,7
1,27	1,13	67,2	12	"	6,9
2,52	3,14	120,5	5,2	"	2,8
3,62	5,32	147	3,9	"	2
0,775	0,38	70,5	11,2	0,0814	7,6
Polyester de $\bar{M}_n$ = 14.000 à 0,5 groupes perester/mole					
0,48	0,15	27	44,5	0,325	32,7
0,79	0,36	46,3	20,8	"	13,3
1,31	0,795	71,4	11,1	"	6,1
2,52	2,3	98,0	7,4	"	4,4
4,15	4,88	135	4,55	"	3,55

Il apparait que les points représentatifs ne sont situés sur la droite Δ que pour les petites valeurs de $(dm/dt)/m^2$.

Elles se placent au dessus de Δ pour des valeurs de $(dm/dt)/m^2$ d'autant plus faibles que le degré de polymérisation $\mathfrak{DP}$ du polyester perester est plus élevé (Fig. 9). Nous désignerons par δ la différence entre l'ordonnée de la droite Δ à la même abcisse.

On définit le degré de polymérisation $\mathfrak{DP}_n$ du polyester comme le nombre de fonctions esters moyen en nombre contenu dans une molécule.

Etude du Facteur d'Efficacité *f*. La méthode décrite, appliquée à l'ensemble des chiffres du Tableau XI permet de calculer f.

TABLEAU XI

m	$C \times 10^2$	$dm/dt \times 10^6$	f	p
	Polyester de $\bar{M}_n$ = 1 800 à 1,6 groupe perester/mole			
0,506	4,37	2,4	0,070	0,407
0,86	4,37	4,38	0,08	0,407
2,08	4,37	13,2	0,128	0,407
2,1	0,525	3,9	0,10	0,049
"	1,155	6,75	0,10	0,108
"	0,350	3,7	0,124	0,0325
4,06	4,37	32,6	0,20	0,407
	Polyestere de $\bar{M}_n$ = 8.000 à 0,4 groupe perester/mole			
0,520	0,3	0,255	0,015	0,326
0,785	"	0,525	0,02	"
1,27	"	1,135	0,037	"
2,52	"	3,14	0,072	"
3,62	"	5,32	0,10	"
	Polyester de $\bar{M}_n$ = 14.000 à 0,5 groupe perester/mole			
0,48	0,143	0,15	0,01	0,325
0,79	"	0,364	0,02	"
1,31	"	0,795	0,035	"
2,52	"	2,3	0,08	"
4,15	"	4,9	0,134	"

Il apparait que, quand le promoteur est macromoléculaire, la valeur de f tombe à une valeur comprise entre 2 et 25% de celle que donne un promoteur non macromoléculaire de même nature chimique.

DISCUSSION DES RESULTATS

Il semble que l'on puisse faire dériver les deux effets nouveaux décrits, c'est à dire les valeurs souvent très faibles de f et de DP_n, de la même cause.

Supposons que la pelote—dans le sens de Kuhn—constitue pour les deux radicaux libres issus de la scission thermique de son propre groupe perester une cage—dans le sens de Matheson[16]—particulièrement efficace.

A condition que les pelotes ne s'enchevêtrent pas trop, c'est à dire que le volume (V) offert à chaque macromolécule de polyester soit supérieur au volume propre V qu'elle occupe,* on peut penser que le micro et le macro radical jumeaux ont de grandes chances de se combiner au sein de cette cage efficace avant d'avoir pu amorcer une polymérisation notable; d'où la faible valeur de f.

Par ailleurs, si la polymérisation a pu s'amorcer, le radical polystyryle en croissance, fixé sur un tronc polyester a des facilités particulières de transfert sur son propre tronc porteur, ce qui se traduit par l'adjonction d'un nouveau terme, $C_p(p'/m)$, à l'éq. 1 où p' désigne la concentration de polyester au sein de la pelote.

$$\text{D'où} \quad \delta = C_p(p'/m)$$

Un calcul approché† montre que

$$\delta \simeq (C/\alpha)(1/m)(\mathfrak{D}\mathcal{P}^{1-\alpha}/\mathrm{DP})$$

où α est l'exposant de M de l'équation de Mark-Houwink, $\mathfrak{D}\mathcal{P}$ le degré de polymérisation du polyester engagé et DP celui du polystyrène formé. La Figure 12 montre dans quelle mesure nos expériences vérifient cette relation.

* Volume définit p.e., hydrodynamiquement selon Flory: $V = 1{,}5 \times 10^{-24} M\,[\eta] = 1{,}5 \times 4{,}21 \times 10^{-2} \times 10^{-24}\,M^{1{,}69}$ du polyester où $M = 14.000$, $V = 6{,}31 \times 10^{-19}$ cm^3, (V) = à la concentration maxima utilisée (50 g/l) $= 5{,}14 \times 10^{-19}$; $M = 8.000$, $V = 2{,}52 \times 10^{-19}$ cm^3, $(V) = 2{,}65 \times 10^{-19}$; $M = 1.800$, $V = 0{,}2 \times 10^{-19}$ cm^3, $(V) = 0.59 \times 10^{-19}$ cm.^{3}

† De

$$[\eta] = 0{,}025VN/M = KM^{\alpha}$$

où N = nombre d'Avogadro, on tire en toute généralité

$$V \simeq M^{1+\alpha} \simeq \mathrm{DP}^{1+\alpha}$$

en admettant

$$p' = \mathrm{DP}/\langle\bar{V}\rangle$$

$\langle\bar{V}\rangle$ désignant la valeur moyenne du volume hydrodynamique en cours de polymérisation. Ainsi

$$\delta \simeq (C_p/m)\,(\mathfrak{D}\mathcal{P}/\langle\bar{V}\rangle)$$

$$\simeq (C_p/m)\,[\mathfrak{D}\mathcal{P}/\langle(\mathfrak{D}\mathcal{P} + \mathfrak{D}\mathcal{P})^{1+\alpha}\rangle$$

avec

$$\frac{1}{\langle(\mathfrak{D}\mathcal{P} + \mathrm{DP})^{1+\alpha}\rangle} = \frac{\displaystyle\int_0^{\mathrm{DP}} \frac{d\mathrm{DP}}{(\mathfrak{D}\mathcal{P} + \mathrm{DP})^{1+\alpha}}}{\displaystyle\int_0^{\mathrm{DP}} d\mathrm{PD}} = \frac{1}{\alpha\mathrm{DP}}\left(\frac{1}{\mathfrak{D}\mathcal{P}^{\alpha}} - \frac{1}{(\mathfrak{D}\mathcal{P} + \mathrm{DP})^{\alpha}}\right)$$

$$\neq (1/\alpha\mathrm{DP})\,(1/\mathfrak{D}\mathcal{P}^{\alpha})$$

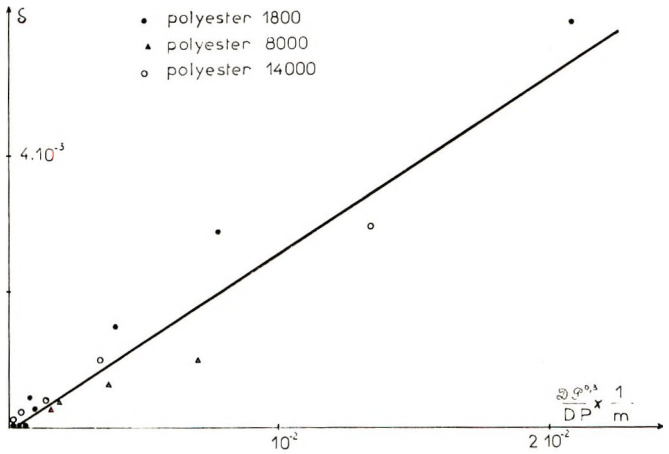

Figure 12.

CONCLUSION

En mesurant la vitesse de polymérisation et la vitesse de décomposition du promoteur au cours de la formation de greffons sur un tronc porteur, nous avons pu atteindre le facteur d'efficacité d'un promoteur macromoléculaire, et ce facteur est remarquablement faible.

D'autre part, l'étude du DP_n des greffons révèle l'existence d'un transfert intramoléculaire notable, caractérisé par une constante de transfert spécifique.

La connaissance de ces grandeurs qui sont accessibles expérimentalement dans le cas étudié, permet de calculer la taille moyenne et le nombre moyen de greffons portés par une molécule tronc, ainsi que la quantité d'homopolymère formé.

Les auteurs tiennent a remercier très vivement la Société d'Electro-Chimie d'Electro-Métallurgie et des Aciéries Electriques d'Ugine, qui a offert une bourse de thèse à deux d'entre eux (J. V. et B. B.) et a aimablement autorisé la publication de ces résultats.

References

1. Smets, G., A. Poot, et G. Duncan, *J. Polymer Sci.*, **54**, 65 (1961); M. Van Beylen et G. Smets, *Makromol. Chem.*, **69**, 140 (1963); G. Smets et W. Van Rillaer, *J. Polymer Sci.*, **A2**, 2417 (1964); W. Van Rillaer et G. Smets, *J. Polymer Sci.*, **A2**, 2423 (1964).
2. Benoit, H., et W. Bushuk, *Can. J. Chem.*, **36**, 1616 (1958); *Compt. Rend.*, **246**, 3167 (1958).
3. Vuillemenot, J., Thèse Strasbourg (1963); J. Vuillemenot, G. Riess, et A. Banderet, *Helv. Chim. Acta*, **44**, 888 (1961).
4. Banderet, A., G. Riess, et M. Brendle, *Bull. Soc. Chim. France*, sous presse.
5. Ueberreiter, K., et G. Sorge, *Angew. Chem.*, **68**, 352, 486 (1956).
6. Batzer, H., *Angew. Chem.*, **66**, 519 (1954).
7. Fox, T. G, et S. Loshack, *J. Polymer Sci.*, **15**, 371 (1955).
8. Bamford, C. H., et M. J. S. Dewar, *Proc. Roy. Soc. (London)*, **A192**, 309 (1948).
9. Ewart, R. H., et H. C. Tingey, *J. Am. Chem. Soc.*, **73**, 1961 (1951).
10. Bloomquist, A. T., et A. F. Ferris, *J. Am. Chem. Soc.*, **73**, 3408 (1951).

11. Matheson, M. S., E. E. Auer, E. B. Bevilacqua, et E. J. Hart, *J. Am. Chem. Soc.*, **73**, 1700 (1951).
12. Mayo, F. R., *J. Am. Chem. Soc.*, **65**, 2324 (1943).
13. Henrici, G., et S. Olive, *Makromol. Chem.*, **37**, 71 (1960).
14. Rembaum, A., et M. Szwarc, *J. Am. Chem. Soc.*, **77**, 3486 (1955).
15. Van Hook, J. P., et A. V. Tobolsky, *J. Polymer Sc.*, **33**, 429 (1958).
16. Matheson, M. S., *J. Chem. Phys.*, **13**, 584 (1945).

Résumé

Pour étudier certains aspects de la polymérisation radicalaire amorcée par un initiateur macromoléculaire, on a préparé des sébacates d'hexanediol de différents DP portant en bout de chaîne un groupe perester de *ter*-butyle, destinés à polymériser le styrène. Sur de tels produits il est facile, la polymérisation terminée, de'éliminer le tronc porteur de polyester par hydrolyse et d'étudier le mélange constitué de séquences de polystyrène libérées et d'homopolystyrène formé. On a trouvé que si la vitesse de décomposition thermique du groupe perester de *ter*-butyle porté par le polyester est comparable à celle du perbenzoate de *ter*-butyle, le facteur d'efficacité, c'est à dire la fraction des radicaux libres formés qui amorcent effectivement la polymérisation est beaucoup plus faible qu'avec un initiateur non macromoléculaire. Par ailleurs, le DP moyen du polystyrène formé est également bien inférieur à celui que donne un initiateur non macromoléculaire (même en présence de polyester non peroxydé). On croit pouvoir expliquer ces deux résultats en admettant que chaque tronc polyester constitue pour les deux radicaux libres issus de son propre groupe perester une "cage" particulièrement efficace qui favorise leur recombinaison ainsi que le transfert intramoléculaire.

Zusammenfassung

Um einige Aspekte der Polymerisation zu erforschen, die durch makromolekulare Radikale ausgelöst wird, wurden mit *tert*-Butylperesterendgrupepen verschene Polyhexandiolsebazate verschiedener Polymerisationsgrade hergestellt, die dann zur Polymerisation des Styrols eingesetzt wurden. Aus solchen Polymerisaten kann der Polyesterstamm leicht durch Hydrolyse entfernt und das zurückbleibende Gemisch aus Polystyrolpfropfstücken und Homopolystyrol genauer untersucht werden. Die thermische Zersetzungsgeschwindigkeit dieser makromolekularen Perester ist mit der des *tert*-Butylperbenzoats durchaus vergleichbar. Trotzdem ist für makromolekulare Initiatoren die relative Anzahl der gebildeten Radikale, die tatsächlich die Polymerisation auslösen, viel kleiner als für *tert*-Butylperbenzoat. Andrerseits erzeugt man mit ihnen Polystyrole wesentlich kleineren MG-s als mit einem nicht makromolekularen Initiator. Eine mögliche Erklärung besteht darin, dass man annimmt, dass die Makromoleküle für die beiden Radikale, die aus ihrer Perestergruppe stammen, einen sehr wirksamen Käfig bilden. Dadurch kommt es sowohl zu einer erhöhten polymerisationsunwirksamen Rekombination als auch zu einer innermolekularen Übertragungsreaktion.

Received November 5, 1964
(Prod. No. 4569A)

JOURNAL OF POLYMER SCIENCE: PART A VOL. 3, PP. 1985–1992 (1965)

Sugar Polythioacetals

ELIZABETH G. HORVATH, SHARON GARDLUND, SUBODH K. SEN, JAMES W. BERRY, and ARCHIE J. DEUTSCHMAN, JR.,
Department of Agricultural Biochemistry, The University of Arizona, Tucson, Arizona

Synopsis

Sugar polythioacetals have been prepared by polymerization of sugars with dithiols in dioxane solution with hydrogen fluoride catalyst. Polymerization was also carried out by using liquid hydrogen fluoride as solvent and catalyst. The polymers are colorless powders with inherent viscosities in the range of 0.03–0.24 and melting points of 81–160°C. The polythioacetals of the shorter-chain dithiols are soluble in polar solvents; those of the longer-chain dithiols are partially soluble.

INTRODUCTION

The first polythioacetals produced from a dithiol and an aldehyde or ketone were prepared by Fisher and Wiley[1] from tetrakis(mercaptomethyl)methane and 1,4-cyclohexanedione. Marvel et al.[2] investigated the formation of linear polymers from aliphatic and aromatic aldehydes with 1,6-hexanedithiol and 1,10-decanedithiol. These polymers had melting points of 40–135°C. and inherent viscosities of 0.14–0.45. Formaldehyde was also used with aliphatic dithiols[3] and hydrogen sulfide,[4] in bulk and in solvent. When the diethyl acetal of benzaldehyde was polymerized with 1,10-decanedithiol by Marvel and Farrar,[5] a polymer having an inherent viscosity of 0.21 was formed.

In our laboratories sugar polythioacetals were produced by the reaction of dithiols with a number of sugars in anhydrous dioxane-hydrogen fluoride solvent-catalyst system. This polymerization may be represented as shown in eq. (1).

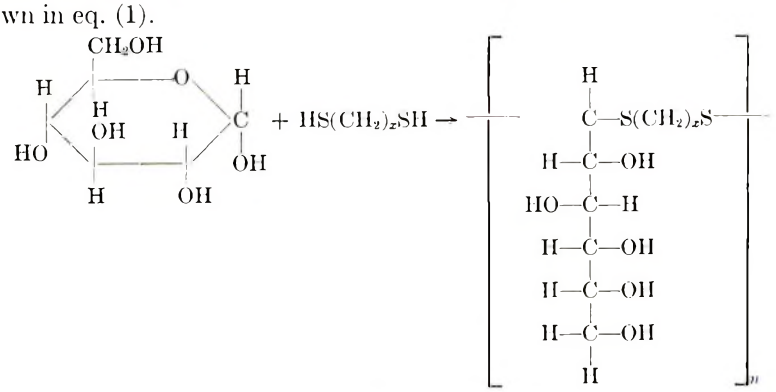

(1)

EXPERIMENTAL

Reagent grade anhydrous glucose and other sugars were used without further purification except for drying in an Abderhalden apparatus. The distilled dithiols were shown to be pure by vapor-phase chromatography.

A stock solution of about 50% anhydrous hydrogen fluoride in anhydrous peroxide-free dioxane was utilized; fresh stock solutions were prepared about every two weeks.

The extent of reaction or thiol conversion was ascertained by amperometric titration of the reaction mixture. Polymer melting points were determined with a Fisher-Johns hot stage apparatus. Solubility tests on the polymers were carried out according to the procedure of Brauer and Horowitz.[6] Inherent viscosity measurements were taken in *N*-methyl-2-pyrrolidone at 30°C. with the use of a Cannon-Fenske viscometer.

Preparation of Sugar Polythioacetals

Polymerization in Dioxane–Hydrogen fluoride solvent–catalyst system

Polymers of Glucose and 1,8-Octanedithiol, 1,9-Nonanedithiol, and 1,10-Decanedithiol. Powdered, dried sugar, or sugar derivative (0.0075 mole) was placed in a 2-oz. wide-mouthed polyethylene bottle together with 0.0075 mole of the dithiol, and an 8-ml. portion of a solution of 27% hydrogen fluoride in dioxane was introduced. The bottle was tightly capped and partially submerged in a constant temperature bath maintained at 13 ± 1°C. During the polymerization, stirring was maintained with a Teflon-coated magnetic bar.

When the reaction was over, the reaction mixture was diluted to 30 ml. with dioxane and stirred vigorously at room temperature. A 1-ml. aliquot of this solution was taken for thiol determination. Potassium carbonate solution (5%) was slowly poured into the remainder of the reaction mixture until the solution was basic to litmus.

The basic solution was filtered and washed with water; then the precipitated polymer was stirred in about 100 ml. of methanol for 15 min. The polymer, generally a finely dispersed solid in methanol, was filtered, washed with additional methanol, then ligroin, and finally vacuum-dried in an Abderhalden apparatus.

ANAL. Calcd. for polymer from 1,10-decanedithiol and glucose, $C_{16}H_{32}O_5S_2$: C, 52.14%; H, 8.75%; S, 17.40%. Found: C, 52.40%; H, 8.83%; S, 17.56%.

Polymers of Glucose and 1,6-Hexanedithiol and 1,5-Pentanedithiol. The procedure differed from the one described above in that the polymer was precipitated by dilution to 30 ml. with methanol stirring and cooling, rather than by neutralization with potassium carbonate solution.

Polymers of Glucose and α,α-Dimercapto-*p*-xylene, Ethyl Cyclohexyl Dimercaptan, and Other Cases Involving an Oil Rather Than a Solid Product. The procedure differed from the general procedure in that after the reaction mixture was made basic, an oil was dispersed throughout the

solution. It was separated and dried to a resinous mass in a vacuum desiccator.

Polymerization in liquid hydrogen fluoride solvent–catalyst system

Powdered, dried glucose (1.35 g., 0.0075 mole) was placed in a 2–4-oz. polyethylene bottle and 1.65 ml. (0.0075 mole) 1,10-decanedithiol was added. The desired volume of liquid hydrogen fluoride was transferred to the bottle, and the capped bottle was partially submerged in a low temperature bath maintained at the desired temperature. (The desired amount of hydrogen fluoride gas was liquified in a polyethylene graduated cylinder immersed in a cold bath at −20 to −30°C.)

The reactions were allowed to proceed for various lengths of time. After the reaction was completed, the bottle was uncapped while in the low temperature bath. Ethyl ether was slowly added dropwise with vigorous stirring. (Care must be taken to prevent a temperature increase while precipitating the polymer, as overheating at this point gave rise to colored, insoluble products). After about 30 ml. was added, the contents of the reaction bottle were neutralized with 5% potassium carbonate solution. The product, which was generally a gum at this point (approximately 2 g.) was added to about 75 ml. of methanol. (This treatment probably removes monomer, and low molecular weight polymer.) The solid which resulted from this washing was filtered, washed with water, methanol, and ligroin and dried *in vacuo*. Measurements of thiol conversion were not attempted because of the difficulty involved in obtaining a representative aliquot.

The results of some exploratory reactions are summarized in Table I.

TABLE I
Exploratory Polymerization of Glucose with 1,10-Decanedithiol in 100% Hydrogen Fluoride[a]

Amount HF, ml.	Time, hr.	Temp., °C.	Melting point, °C.	Inherent viscosity
10	5	−32	78–95	0.16
15	17	−32	82–92	0.13
20	15	−33	90–105	0.14
10	54	−37	Decomp.[b]	0.24
15	6	−31	100–113	0.20
[c]	88	−26	Decomp.	Insol.

[a] 0.0075 mole of monomer was used.

[b] The polymer became rubbery and started to decompose around 180°C.; it was glassy and semiliquid below this point.

[c] Catalyst was 13 ml. of 70% hydrogen fluoride in dioxane.

Preparation of D-Glucose Di-*n*-decyl Dithioacetal

A mixture of 1.8 g. (0.01 mole) of glucose, 3.46 g. (4.12 ml., 0.02 mole) of 1-decanethiol, and 10 ml. of 27% hydrogen fluoride–dioxane solution in a

2-oz. polyethylene bottle was stirred (with a magnetic stirrer) for 28 hr. in a bath at 13 ± 1°C.

The reaction mixture was slowly neutralized with 100 ml. of a 5% potassium carbonate solution. The product was filtered, washed with water, and dried *in vacuo* to give a crude yield of 3.38 g. or 64%. The dithioacetal was recrystallized three times from 95% ethanol and melted sharply at 98–99°C.

ANAL. Calcd. for $C_{26}H_{54}O_5S_2$: C, 61.13%; H, 10.67%; S, 12.55%. Found: C, 61.20%; H, 10.50%; S, 12.79%.

Thiol Conversion by Amperometric Titration

The method of Kolthoff and Harris[7] was utilized.

The 1-ml. aliquot of the diluted reaction mixture (sugar–thiol in dioxane–HF described above) was made up to 100 ml. volume with methanol. A 5-ml. aliquot of this solution, 10 ml. of dilute ammonium hydroxide solution and 1 ml. of 1*M* ammonium nitrate solution were added to a 100 ml. volumetric flask, and this solution was made up to volume with additional methanol. This solution was then titrated against 0.005*M* silver nitrate solution. A standard consisting of dithiol (diluted in the same manner) was also titrated, and the ratio indicated the extent of thiol conversion.

Paper Chromatography

Paper chromatography was performed on the reaction mixtures before they were diluted to 30 ml. volume (where possible). Spots of increasing strength were placed on Whatman #1 chromatography paper. After they dried, the spots were made alkaline with a spot of concentrated ammonium hydroxide solution. The paper was run for 3–4 hr. with the use of the solvent system ethyl acetate–pyridine–water (8:2:1). Silver nitrate solution was used as an indicator.[8]

RESULTS AND DISCUSSION

After screening various solvent catalyst–systems, it was found that in general, strong acid catalysts (at room temperature and above) gave colored intractable products; at lower temperatures, however, soluble colorless, polymeric material was produced. Hydrochloric and perchloric acid catalysts had only limited applicability, i.e., a narrow temperature and concentration range. Hydrogen fluoride proved to be the most versatile as well as efficient catalyst. It had a wider temperature range activity; it improved the solubility of the sugars in dioxane; it could be employed alone or in conjunction with other strong acids. Experiments with liquid hydrogen fluoride demonstrated that at −30°C. (or below) polymers were formed.

To ascertain optimum reaction conditions, a systematic study was initiated concerning time, temperature, catalyst concentration, and solvent–catalyst–monomer ratio effects. Table II furnishes information on the scope of these experiments. Preliminary experiments with hydrogen

TABLE II
Polymerization of Glucose with 1,10-Decanedithiol in Dioxane with Hydrogen Fluoride Catalyst[a]

HF concn., %	HF–dioxane volume, ml.	Time, hr.	Temp., °C.	Thiol conversion, %	Melting point, °C.	Inherent viscosity
22	33	26	12	40	70–81	0.07
25	24	15	6	62	80–110	0.09
25	24	37	6	85	99–114	0.12
25	24	15	18	81	110–135	0.09
25	24	37	18	82	133–150	0.12
25	42	15	6	41	81–98	0.12
25	42	37	6	72	104–123	0.11
25	42	15	18	71	94–102	0.10
25	42	37	18	75	129–152	0.13
28	15	26	12	81	119–132	0.12
28	33	26	0	84	112–130	0.09
28	33	4	12	58	98–120	0.08
28	35	26	12	82	136–147	0.11
28	33	26	12	81	110–122	0.09
28	33	26	12	82	117–148	0.12
28	33	26	12	81	127–144	0.09
28	33	26	12	84	111–130	0.10
28	33	26	12	79	140–155	0.10
28	33	48	12	74	122–137	0.09
28	33	26	24	68	93–102	0.14
28	51	26	12	75	132–157	0.09
31	24	15	6	84	116–132	0.17
31	24	37	6	94	127–137	0.16
31	24	15	18	74	102–115	0.16
31	24	37	18	73	92–101	0.12
31	42	15	6	81	118–134	0.14
31	42	37	6	68	130–143	0.15
31	42	15	18	62	93–102	0.14
31	42	37	18	64	95–103	0.14
34	33	26	12	71	96–104	0.18

[a] 0.0075 mole of each monomer was used.

fluoride–dioxane catalyst–solvent system indicated that catalyst concentrations in the range of 14–50% at 0–24°C. gave the most desirable product.

Statistical treatment of the data (the approach successfully used for starch vinylation studies[9]) of thirty experiments (Table II) revealed that neither a maximum nor a minimum value for the data existed. Consequently, no extrapolation of the data would yield what might be designated as the "optimum" polymer. Moreover, it was found that high-melting polymers did not necessarily exhibit high inherent viscosity, nor was a higher extent of thiol conversion accompanied by a subsequently higher viscosity. Nevertheless, the statistical analysis of the experiments furnished sufficient information to predict reaction conditions giving a high-melting product, a product yielding high thiol conversion ratio, and one

TABLE III
Polymerization of Glucose with 1,10-Decanedithiol at Optimum Predicted Statistical Conditions Based on Thiol Conversion, Melting Point, and Inherent Viscosity[a]

Characteristic being maximized	Conditions for maxima				Results of polymerization		
	Catalyst concn., %	HF–dioxane volume, ml.	Time, hr.	Temp., °C.	Thiol conversion, %	Melting point, °C.	Inherent viscosity
Thiol conversion	36	36	12	2	83	116–139	0.09
Melting point, °C.	32	48	13	7	66	137–160	0.08
Inherent viscosity	27	8	28	13	84	104–113	0.18

[a] The polymerization was carried out in dioxane–hydrogen fluoride solution with 0.0075 mole of each monomer.

exhibiting the highest inherent viscosity to date in the system employing 1,10-decanedithiol and glucose with hydrogen fluoride–dioxane. Table III summarizes the results of these findings.

The infrared spectrum of the polymer of glucose and 1,10-decanedithiol was taken in potassium bromide and was compared to the spectrum of D-glucose di-*n*-decyl dithioacetal. The CH frequencies in the region of 1465 cm.$^{-1}$ were less intense in the polymer than in the monomeric acetal.

The maximum inherent viscosity was of main interest, and in the 1,10-decanedithiol–glucose system this was realized with 8 ml. of 27% hydrogen fluoride–dioxane catalyst–solvent system at 13°C. for 28 hr. reaction time. Thus, a number of sugars and sugar derivatives were reacted with 1,10-decanedithiol and a number of dithiols were reacted with glucose under these conditions. Experimental results are given in Tables IV and V.

In all cases, paper chromatography on the polymer and residual solution

TABLE IV
Characteristics of the Polymerization Products of Various Dithiols Reacted with Glucose[a]

Dithiol	Thiol conversion, %	Melting point, °C.	Inherent viscosity
1,5-Pentanedithiol	94	80–126	0.10
1,6-Hexanedithiol	93	83–133	0.12
1,8-Octanedithiol	97	105–130	0.12
1,9-Nonanedithiol	92	110–133	0.13
1,10-Decanedithiol	84	102–110	0.19
α,α'-Dimercapto-*p*-xylene	81	93–124	0.03
Ethyl cyclohexyl dimercaptan	82	98–122	0.10

[a] The polymerization was carried out with 0.0075 mole of each monomer at 13 ± 1°C. for 28 hr. with a catalyst–solvent system of 8 ml. of 27% hydrogen fluoride–dioxane.

indicated polymeric material to be present. Single spots were found only where the sugar monomers would be expected.

Equivalent weight determination by amperometric titration[7] led to erratic results and was abandoned.

TABLE V
Characteristics of the Polymerization Products of Various Sugars and Sugar Derivatives Reacted with 1,10-Decanedithiol[a]

Sugar or derivative	Thiol conversion, %	Melting point, °C.	Inherent viscosity
Glucose	84	102–110	0.19
Mannose	96	145–149	0.16
Galactose[b]	85	110–136	0.10
Xylose	96	82–107	0.16
2,3,4,6-Tetra-*O*-methyl-D-glucoside	92	Oil	0.05
Fructose	88	63–81	0.24

[a] The polymerization was carried out with 0.0075 mole of each monomer at 13 ± 1°C. for 28 hr. with a catalyst–solvent system of 8 ml. of 27% hydrogen fluoride–dioxane.

[b] The procedure differed from that previously described in that galactose was allowed to dissolve in hydrogen fluoride–dioxane for about 1 hr. before the 1,10-decanedithiol was added.

The polymers were more soluble in polar than nonpolar solvents. The polymer prepared from glucose and 1,10-decanedithiol was soluble completely in dimethyl sulfoxide and hexamethyl phosphoramide and partially with swelling in dimethylacetamide, dimethylformamide, pyridine, and *N*-methyl-2-pyrrolidone.

This is a report of work done under contract with the U.S. Department of Agriculture and authorized by the Research and Marketing Act. The contract was supervised by the Northern Utilization Research and Development Division of the Agricultural Research Service.

References

1. Fisher, N. G., and R. H. Wiley (to E. I. du Pont de Nemours and Co.), U.S. Pat. 2,389,662 (1945).

2. Marvel, C. S., H. H. E. Shen, and R. R. Chambers, *J. Am. Chem. Soc.*, **72**, 2106 (1950).

3. May, G. B., E. W. Wheatley, and J. W. Fisher (to British Celanese Ltd.), Brit. Pat. 694,441 (1953).

4. P. Bapseres and J. Signouret (to Societe National des Petroles d'Aquitaine), Fr. Pat. 1,330,819 (1963).

5. Marvel, C. S., and R. C. Farrar, Jr., *J. Am. Chem. Soc.*, **79**, 986 (1957).

6. Brauer, G. M., and E. Horowitz, in *Analytical Chemistry of Polymers*, Part III, G. Kline, Ed., Interscience, New York, 1962, p. 101.

7. Kolthoff, I. M., and W. E. Harris, *Ind. Eng. Chem., Anal. Ed.*, **18**, 161 (1946).

8. Whistler, R. L., and M. L. Wolfrom, *Methods in Carbohydrate Chemistry*, Vol. I, Academic Press, New York, 1962, p. 28.

9. Berry, J. W., H. Tucker, and A. J. Deutschman, Jr., *Ind. Eng. Chem.*, **2**, 318 (1963).

Résumé

Des polythioacétals de sucre ont été préparés par polymérisation de sucres avec des dithiols en solution dans le dioxanne en présence d'acide fluorhydrique comme catalyseur. La polymérisation a également été effectuée au moyen d'acide fluorhydrique liquide comme solvant et comme catalyseur. Les polymères sont des poudres blanches possédant des viscosités inhérentes se situant entre 0.03 et 0.24 et des points de fusion allant de 81 à 160°C. Les polythioacétals provenant des dithiols à chaîne plus courte sont solubles dans les solvants polaires; ceux provenant de dithiols à chaîne plus longue sont partiellement solubles.

Zusammenfassung

Zuckerpolythioacetale wurden durch Polymerisation von Zuckern mit Dithiolen in Dioxanlösung mit Fluorwasserstoff als Katalysator dargestellt. Die Polymerisation wurde auch in flüssigem Fluorwasserstoff als Lösungsmittel und Katalysator ausgeführt. Die Polymeren bilden farblose Pulver mit Viskositätszahlen von 0,03 bis 0,24 und Schmelzpunkten von 81 bis 160°C. Die Polythioacetale der kürzerkettigen Dithiole sind in polaren Lösungsmitteln löslich, diejenigen der längerkettigen Dithiole sind zum Teil löslich.

Received September 11, 1964
Received December 21, 1964
(Prod. No. 4596A)

JOURNAL OF POLYMER SCIENCE: PART A VOL. 3, PP. 1993–2008 (1965)

Deformation Mechanism of Polyethylene Spherulite*

TAKASHI ODA, SHUNJI NOMURA, and HIROMICHI KAWAI,
Department of Polymer Chemistry, Faculty of Engineering,
Kyoto University, Kyoto, Japan

Synopsis

A deformation mechanism for polyethylene spherulites has been proposed which is based on the affine transformation method. Individual crystal lamellae are taken as the orientation units within the spherulites and are allowed to rotate around the *a*- and *b*-axes of the crystal. Deductions based on this model and on previous models are compared with experimental results obtained with four kinds of polyethylene film. These results agree fairly well with the predictions of the present model and suggest that the plastic deformation of crystal lamellae by gliding along the (110) plane predominates over the untwisting of crystal lamellae at the initial stage of deformation.

INTRODUCTION

To clarify the mechanical properties of crystalline polymers which are still obscure in contrast to those of amorphous polymers, it is necessary to understand the mechanical behavior in terms of the response of the crystalline phase, composed of crystallites and their aggregates, as well as the noncrystalline phase.

In a previous study of this series,[1] the mechanical behavior of a low-density polyethylene was investigated by means of simultaneous measurements of x-ray diffraction and birefringence, and the elasticity of the polymer was interpreted in terms of the orientation recovery of the crystallites and the polymer chains in the noncrystalline phase. The orientation of the crystallites during stretching of the polymer was further interpreted in terms of the deformation mechanism of a spherulite by using an affine transformation method proposed by Sasaguri et al.[2]

In this paper, the orientation behavior of crystallites during stretching of the bulk polymers is discussed in more detail for high-density as well as low-density polyethylenes by modifying the affine transformation method.

TEST SPECIMEN AND EXPERIMENTAL PROCEDURE

Two types of polyethylene, Yukalon K-3202 (Mitzubishi Yuka Co., Japan) and Marlex 50 (Phillips Chemical Corp., U. S. A.) having different degrees of branching and other indices as listed in Table I, were used as test polymers.

* Part of M.S. thesis of T. Oda presented to the Department of Polymer Chemistry, Kyoto University on March 11, 1964.

TABLE I
Physical Indices of Polyethylenes Used

	Melt index[a]	Intrinsic viscosity, dl./g.[b]	Huggins constant* k'[b]	Degree of branching[c]
Marlex 50	5.0	1.429	0.25_7	0.0
Yukalon K-3202	3.5	(0.958)	(0.44_1)	2.0

[a] ASTM D-1238-57T.
[b] Xylene solution at 75°C.
[c] Number of CH_3/100 carbon atoms, determined from infrared spectroscopy at 1376 and 1368 cm.$^{-1}$ at melt.

TABLE II
Casting Conditions, Density, and Degree of Crystallinity of the Polyethylene Films Tested

	Casting	Annealing	Density, g./cc.[a]	Degree of crystallinity, %[b]
Marlex 50 quenched	Melted at 180°C. for 10 min., cooled to 125°C., and quenched into ice water	None	0.954	78.6
Marlex 50 annealed	Melted at 180°C. for 10 min., cooled to 125°C., held at 125°C. for 1 hr., and cooled gradually to room temperature	at 125°C. for 2 hr.	0.970	90.5
Yukalon K-3202 quenched	Melted at 140°C. for 10 min., cooled to 105°C. and quenched into ice water	None	0.904	50.1
Yukalon K-3202 annealed	Melted at 140°C., for 10 min., cooled to 105°C., held at 105°C. for 1 hr., and cooled gradually to room temperature	At 105°C. for 2 hr.	0.909	55.1

[a] Measured by flotation method in mixture of benzene and carbon tetrachloride at 30°C.
[b] Calculated from density at 30°C.

The polymers were cast into thin films, about 0.3 mm. thick, by using a laboratory press and spacers under the conditions given in Table II. The quenched samples of the polymers were prepared by being dropped into ice water from the melt, while to obtain the annealed samples the polymers were gradually cooled on the press to room temperature, annealed, and then gradually cooled again to room temperature. The crystallites were randomly oriented, showing no preferential orientation of any crystallographic axis under x-ray diffraction examination. Some physical prop-

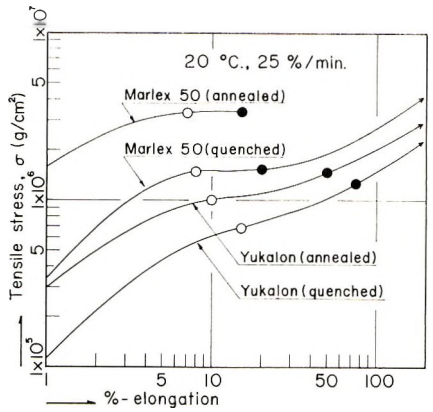

Fig. 1. Tensile stress vs. strain relation of four kinds of polyethylene film at 20°C. under a constant rate of elongation of 25%/min.

erties, such as density and degree of crystallinity of the polymer films, are also listed in Table II.

The tensile stress versus strain relation under a constant rate of elongation of 25%/min. at 20°C. is shown in Figure 1. The higher the degree of crystallinity of the sample film, the lower the strain for the yield point and for the beginning of necking, as indicated by open and closed circles, respectively in Figure 1. The microscopic examination shows that the spherulite can deform without destruction up to the necking point of each sample film, i.e., up to about 50–70% elongations for low-density polyethylene and about 15–20% elongations for high-density polyethylene.

The experimental procedure for evaluating the average orientation of the crystallographic axes of crystallites from x-ray diffraction was the same as described in the previous paper.[1] The degree of orientation of a specific crystallographic axis was represented by the orientation factor, defined as

$$F_\delta = (1/2)(3\,\overline{\cos^2\delta} - 1)$$

where δ is the angle between the specific crystallographic axis and the stretching direction about which the crystallites orient in cylindrical symmetry, i.e., uniaxial orientation.

EXPERIMENTAL RESULTS

The changes of orientation factor of the three crystallographic axes, *a*-, *b*-, and *c*-axis, with stretching of the sample film under a constant rate of elongation of 25%/min. at 20°C. are shown in Figure 2. The crystal *c*-axis shows positive orientation, while the *a*- and *b*-axes show negative orientation except for slight positive orientation of the *b*-axis at relatively low elongations; i.e., the *c*-axis tends to orient parallel, while the *a*- and *b*-axes are perpendicular to the stretching direction. It is seen that the

lower the density of the sample film, the more easily the orientation proceeds, being probably affected by the difference of crystal size, crystal perfection, and the rigidity of crystal superstructure between the samples. On comparing the orientation behavior of the *a*-axis with that of the

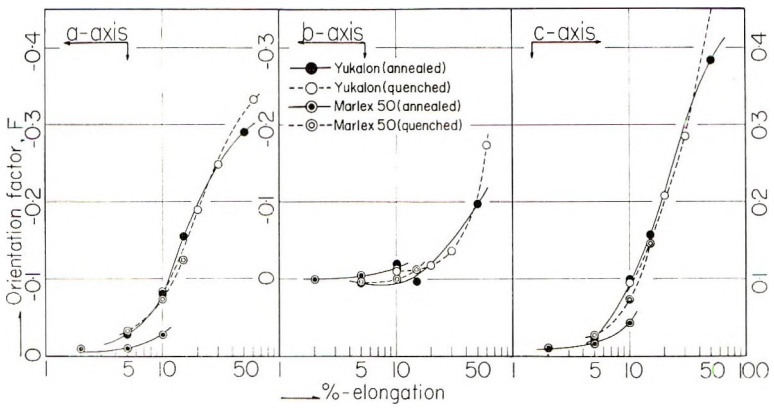

Fig. 2. Orientation behavior of three crystallographic axes of polyethylene with stretching of the bulk polymers at 20°C. under a constant rate of elongation of 25%/min.

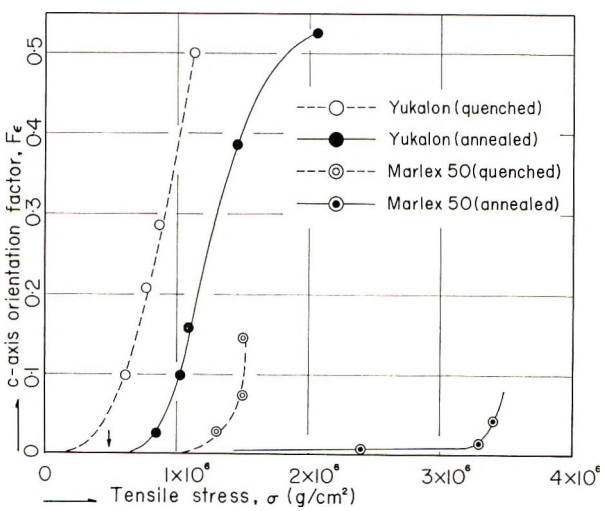

Fig. 3. Tensile stress vs. *c*-axis orientation factor. Arrow shows a minimum stress level for the crystal transformation from the folded-chain type to the fringed-micellar type crystal.

b-axis, it is also seen that the *a*-axis can be oriented more easily than the *b*-axis, which may be ascribed to the anisotropism of polyethylene crystal, the difference of physical properties between the directions along the principal crystallographic axis, or to a preferential deformation mechanism of polyethylene spherulites.

Figure 3 shows the relationship between the c-axis orientation factor and tensile stress, which are replotted from Figures 1 and 2. The tensile stress value is apparent; not the actual value after stress relaxation under a given per cent elongation when x-ray diffraction was taken, but a maximum value when the sample film was stretched at the given elongation. The arrow along the stress axis indicates the stress level at which the folded chain molecule in the crystal is pulled out normally against the folded plane; i.e., the minimum yield stress for crystal transition from the folded-chain type to the fringed-micellar type crystal.*

DISCUSSION

The orientation behavior of crystallites during stretching of the bulk polymer may be greatly affected by the deformation mechanism of a spherulite, the superstructure of aggregated crystallites.

Recently, two types of spherulite deformation model have been proposed by Wilchinsky[4] and Sasaguri et al.,[2] respectively, who used the affine transformation methods which had been also used by Kuhn and Grun[5] in their calculation of the birefringence of a rubber network as follows:

$$N(\Omega,\omega) = \frac{N(\lambda_1\lambda_2\lambda_3)^2}{4\pi[\lambda_1^2\lambda_2^2\cos^2\Omega + \lambda_3^2\sin^2\Omega(\lambda_2^2\cos^2\omega + \lambda_1^2\sin^2\omega)]^{1/2}} \quad (1)$$

where N is the total number of oriented units within the spherulite, and $N(\Omega,\omega)$ is the number per unit of the solid angle in the deformed state.

Wilchinsky discussed not only the uniaxial orientation in the stretching direction (OZ direction) while keeping the volume of spherulite constant: ($\lambda_1 = \lambda^{-1/2}$, $\lambda_2 = \lambda^{-1/2}$, and $\lambda_3 = \lambda$), but also a special case of the deformation such as ($\lambda_1 = \lambda^{-1}$, $\lambda_2 = 1$, and $\lambda_3 = \lambda$), where λ is the elongation ratio along the stretching direction. He also discussed a special case of deformation where the spherulite composed of multiple concentric cells is deformed while keeping the thickness of these cells constant.

He took the c-axis as the orientation unit within the sperulite on the basis that the crystallites are connected by tie molecules along this axis. Hence, the crystallites would tend to orient in the direction of spherulite elongation.

This model may be valid for a crystalline system of low degree of crystallinity in which the crystallites are randomly embedded in an amorphous matrix and have no crystal isotropism nor definite superstructure. However, in the case of polyethylene, the model may be too simple, differing from the actual structure of a spherulite and being unable to describe the difference of orientation behavior between the a- and b-axis during stretching as mentioned above.

* Calculated from Lennard-John type interaction between molecules of 100 A. length and 5.4 A. distance.[3]

Sasaguri-Hoshino-Stein's Model Taking into Account the Crystal Transition

Sasaguri et al.[2] have taken the radial fiber (crystal lamella grown radially) as the oriented unit within the spherulite and discussed the uniaxial orientation in the OZ direction while keeping the volume of the spherulite constant. Equation (1) for the number of radial fibers per unit of the solid angle in the deformed state can be simplified as follows:

$$N(\Omega,\omega) = \frac{N}{4\pi(\lambda^{-2}\cos^2\Omega + \lambda\sin^2\Omega)^{3/2}} \tag{2}$$

where $\lambda_3 = \lambda$.

The number of radial fibers between Ω and $\Omega + d\Omega$ is

$$N(\Omega)\sin\Omega d\Omega = \int_{\omega=0}^{2\pi} N(\Omega,\omega)\sin\Omega d\,\Omega d\omega$$

$$= \frac{N\sin\Omega}{2(\lambda^{-2}\cos^2\Omega + \lambda\sin^2\Omega)^{3/2}}\,d\Omega \tag{3}$$

The average square cosine of the radial fiber direction with respect to the OZ axis is given by

$$\overline{\cos^2\Omega} = \frac{1}{N}\int_{\Omega=0}^{\pi} N(\Omega)\cos^2\Omega\sin\Omega\,d\Omega$$

$$= \frac{\lambda^3}{\lambda^5 - 1}\left[1 - \frac{\tan^{-1}(\lambda^3 - 1)^{1/2}}{(\lambda^3 - 1)^{1/2}}\right] \tag{4}$$

Recent investigation of the structure of polyethylene spherulites revealed that the radial fibers grow in such a way that the crystal b-axis is parallel to the fiber axis and the c- and a-axes are perpendicular to this fiber axis and rotate periodically around the fiber axis.[6,7] If the spherulite deforms without any crystal transition nor reorientation within the radial fibers, the affine transformation model given by eq. (4) would predict a strong positive orientation of the crystal b axis and negative orientation of the a- and c-axes with respect to the stretching direction OZ, which have not been observed experimentally.

Sasaguri et al. have modified the affine transformation by taking account of the crystal transition, as shown in Figure 4, from the b-axis parallel to the c-axis parallel to the fiber axis when the radial fiber is elongated. Namely, the change of length of radial fiber, whose initial length is R_0, may be given, as function of λ and Ω, as follows:

$$R = R_0\lambda^{1/2}/(\lambda^{-1}\cos^2\Omega + \lambda^2\sin^2\Omega)^{1/2} \tag{5}$$

They have proposed one of the simplest representations for the crystal transition as follows:

$$\begin{aligned} X_{c,c} &= X_{c,c,0} & R &< R_0 \\ X_{c,c} &= X_{c,c,0} + \gamma(R/R_0 - 1) & R &\geqq R_0 \end{aligned} \tag{6}$$

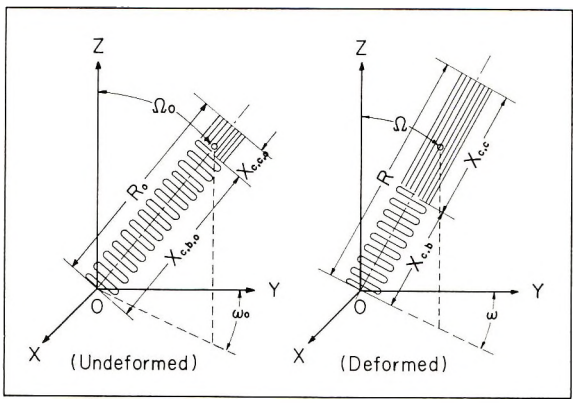

Fig. 4. Spherulite deformation model proposed by S-H-S, taking into account the crystal transformation from the folded-chain type to the fringed-micellar type crystal within the crystal lamella.

where $X_{c,c}$ is the fraction of c-axis-parallel crystals, and γ is a parameter of the ease of the crystal transition.

Usually, polyethylene has an orthorhombic crystal cell with the crystal a-axis perpendicular to the crystal b- and c-axis. Therefore, the a-axis is always perpendicular to the radial fiber axis, being independent on the crystal transition within the radial fiber during the deformation of spherulite.

The orientation factor of the crystal a-axis with respect to the stretching direction OZ, F_α, can be defined by

$$F_\alpha = (3\,\overline{\cos^2 \alpha} - 1)/2$$

where α is the angle between the crystal a-axis and the OZ direction. The crystal a-axis is always perpendicular to the fiber axis and gives the following relation as:

$$\cos \alpha = \sin \Omega \cos \kappa \tag{7}$$

where κ is the angle between the crystal a-axis and the plane which contains OZ and the fiber axis. When one assumes that the a-axis rotates randomly around the fiber axis and κ is independent of Ω, then

$$\overline{\cos^2 \alpha} = \overline{\sin^2 \Omega} \cdot \overline{\cos^2 \kappa}$$

and

$$\overline{\cos^2 \kappa} = \int_0^{2\pi} M(\kappa) \cos^2 \kappa \, d\kappa = {}^1/_2$$

where $M(\kappa)$ is a distribution function of κ.

Consequently, $\overline{\cos^2 \alpha}$ may be given by

$$\overline{\cos^2 \alpha} = (1/N) \int_{\Omega=0}^{\pi} ({}^1/_2) \sin^2 \Omega \, N(\Omega) \sin \Omega \, d\Omega \tag{8}$$

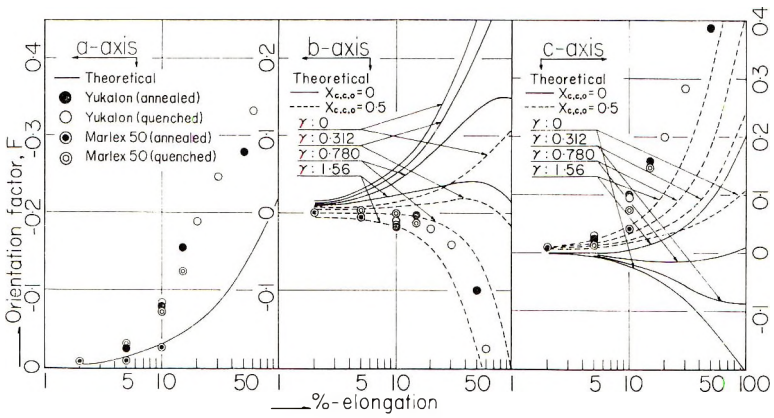

Fig. 5. Comparison of experimental results with the theoretical values from the model proposed by S-H-S.

To evaluate the orientation factor of the crystal b-axis, F_β, on the other hand, it is necessary to take account of the crystal transition, and $\overline{\cos^2 \beta}$ may be given by

$$\overline{\cos^2 \beta} = \frac{1}{N}\left[\int_{\Omega=0}^{\pi} (1 - X_{c,c}) \cos^2 \Omega\, N(\Omega) \sin \Omega\, d\Omega + \int_{\Omega=0}^{\pi} X_{c,c}\, (^1/_2) \sin^2 \Omega\, N(\Omega) \sin \Omega\, d\Omega\right] \quad (9)$$

where β is the angle between the crystal b-axis and the OZ direction. The first term in the right-hand side of eq. (9) is attributed to b-axis-parallel crystals and the second term is that of c-axis-parallel crystals in which the crystal b-axis is assumed to rotate randomly around the fiber axis.

Further concrete calculation of the orientation factors as a function of λ can be performed by substituting eq. (3) into eq. (8) for F_α and eqs. (3), (5), and (6) into eq. (9) for F_β. The results of numerical calculation given by Stein and Sasaguri[8] up to 100% elongation for F_α and F_β are shown in Figure 5, together with our experimental results, where $X_{c,c,0}$ is taken for the two extreme values of 0 and 0.5, γ is varied from 0 to 1.56, and the elongation ratio of the spherulite, λ, is assumed to be identical to the per cent elongation of bulk polymer.

As seen in Figure 5, the results for Marlex 50 (annealed), a sample of extremely high degree of crystallinity, at relatively low elongations agree well with the theory, providing that $X_{c,c,0}$ and γ are taken as considerably large values. This means that the spherulite has considerable amounts of c-axis-parallel crystals, even in the undeformed state, and that the b-axis-parallel crystals, which have been accepted as radially grown crystal lamella of the folded-chain type, are easily transformed to c-axis-parallel crystals, probably due to micronecking of the lamella. The possibility of the crystal transition may be understood from the tensile stress level during stretching

which is much higher, as shown in Figure 3, than the minimum yield stress for the transition. However, the existence of c-axis-parallel crystals in the undeformed state, whether in interlamellae or interspherulites, is uncertain.

In general, however, the theoretical results for a axis orientation behavior, which is independent of the crystal transition, deviate considerably from the experimental results, demanding strongly some modifications of the theory so as to enhance the a-axis orientation.

Oda-Nomura-Kawai Model Taking into Account the Crystal Rotations around the Crystal a- and b Axes

In order to modify the Sasaguri-Hoshino-Stein (S-H-S) model, it may be necessary, as discussed above, to enhance the a-axis orientation by taking into account some other deformation mechanisms.

One way might be to take account of the orientation of the isolated crystallites within the matrix surrounding the spherulites, whose fraction may not be negligible, especially for low-density polyethylene. However, at the present time, one cannot estimate what fraction of crystalline phase is embedded within the matrix as isolated crystallites and how such crystallites are embedded. When one accepts the fringed-micellar structure for the matrix, preferential c-axis orientation may be discussed by using a model as Wilchinsky's, which, however, is nothing more than the concept of c-axis-parallel crystals within the radial fiber in the S-H-S model and does not allow for predominating a-axis orientation.

Another possibility may be to take other deformation mechanisms in the radial fibers, especially in the lateral zone of the spherulite, into account. Indeed, as given by eq. (6), any consideration for the deformation, except for the orientation, of the radial fibers at the lateral zone of the spherulite has not been taken into account.

Crystal lamellae within the spherulite may be bound to each other by tie chains, which run through from one lamella to another along the crystal c axis.[10] When the spherulite is deformed, as shown in Figure 6, the lamellae in the longitudinal zone may be squeezed out, and the lamellae in the lateral zone may be splayed apart from each other. Thereby, the lamellae in the longitudinal zone may be deformed so that the crystal c-axis tends to orient parallel and the crystal b-axis perpendicular to the radial fiber axis, being accompanied by c-axis orientation parallel towards the plane which includes OZ and the radial fiber axis, i.e., the crystals within the lamella rotate around the a-axis, being accompanied by untwisting of the lamella. On the other hand, the lamellae in the lateral zone may be so deformed that the crystal c-axis tends to orient parallel and the a axis perpendicular to the plane including OZ and the fiber axis, i.e., the crystals within the lamella rotate around the b-axis so as to untwist the lamella. The former deformation may be irreversible in nature, probably due to plastic deformation of the crystal along a glide plane such

as the (110) plane of polyethylene crystal, while the latter may be of a reversible nature.

When one assumes that the degree of the crystal rotations within the lamella is related to the ratio of the vertical angles of a circular cone before and after the spherulite deformation, θ/θ_0 and that the volume of the circular cone is kept constant, the degree of the crystal rotations $f(\lambda,\theta)$ may be given by

$$f(\lambda,\theta) = (\theta/\theta_0)^2 = (R_0/R)^3 \tag{10}$$

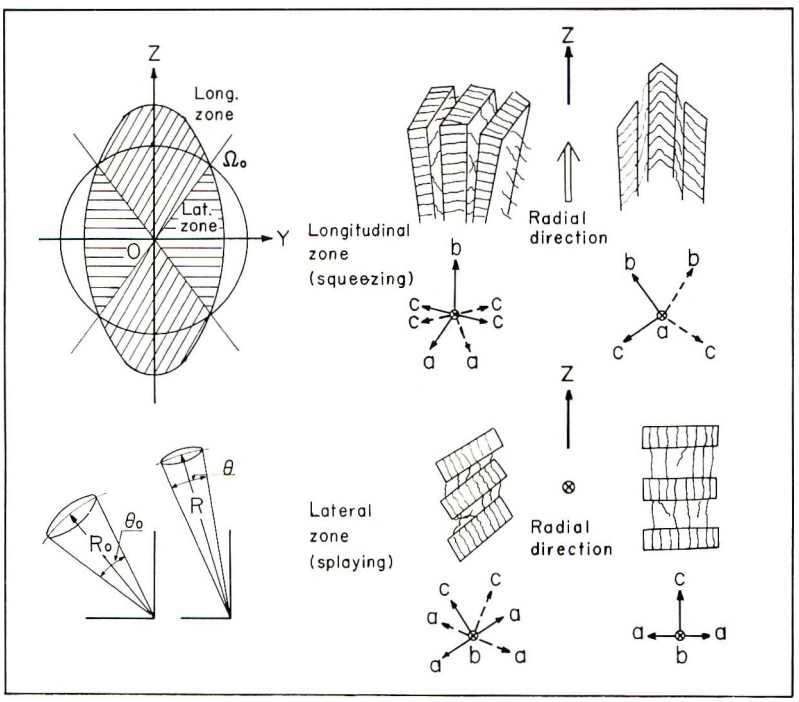

Fig. 6. Spherulite deformation model by O-N-K, taking into account crystal rotations around the crystal a and b axes within the crystal lamella.

The crystal rotations may be affected by other factors, such as crystal unisotropism, perfection of crystal lamella or their superstructure, and the degree of the crystal rotation; f may be modified as f^m and f^n, where m and n are parameters of the ease of the crystal rotations around the crystal a- and b-axes, respectively.

When one assumes that the radial fiber consists only of the b-axis-parallel crystals at undeformed state; i.e., $X_{c,c,0} = 0$, then the changes of orientation of the crystal a- and b-axes during the deformation of spherulite given by eq. (4) may be modified as follows:

$$\overline{\cos^2 \alpha} = \frac{1}{N/2} \left\{ \int_{\Omega=0}^{\Omega_0} N(\Omega) \sin^3 \Omega \left[\int_{\kappa=0}^{2\pi} M_\Omega(\kappa) \cos^2 \kappa \, d\kappa \right] d\Omega \right.$$

$$\left. + \int_{\Omega=\Omega_0}^{\pi/2} N(\Omega) \sin^3 \Omega \left[\int_{K=0}^{2\pi} M'_\Omega(\kappa) \cos^2 \kappa d\kappa \right] d\Omega \right\}$$

$$= \frac{1}{N/2} \left[\int_{\Omega=0}^{\Omega_0} N(\Omega) \sin^3 \Omega \, (\overline{\cos^2 \kappa})_\Omega \, d\Omega \right.$$

$$\left. + \int_{\Omega=\Omega_0}^{\pi/2} N(\Omega) \sin^3 \Omega \, (\overline{\cos^2 \kappa})'_\Omega d\Omega \right]$$

$$= \frac{1}{N/2} \left[\int_{\Omega=0}^{\Omega_0} N(\Omega) \sin^3 \Omega (^1/_2) \, f_\Omega^{\,n} \, d\Omega \right.$$

$$\left. + \int_{\Omega=\Omega_0}^{\pi/2} N(\Omega) \sin^3 \Omega (^1/_2) \, f_\Omega^{\,-n} \, d\Omega \right] \quad (11)$$

and

$$\overline{\cos^2 \beta} = \int N'(\beta) \cos^2 \beta \, d\beta$$

$$= \int_0^{\pi/2} \int_0^{\pi/2} \int_0^{2\pi} N'(\Omega,k,\kappa) \, q(\Omega,k,\kappa) d\kappa dk d\Omega$$

where k is the angle between a radial fiber and the crystal b-axis, κ is the angle between the crystal a-axis and the plane which includes the radial fiber and OZ axis, and $N'(\Omega,k,\kappa) = N(\Omega)M_\Omega(k,\kappa)$.

$q(\Omega,k,\kappa)$ cannot be given by a simple functional form* and one assumes that

$$q(\Omega,k,\kappa) = \cos^2 \Omega q_\Omega(k,\kappa)$$

between $\Omega = 0$ and $\Omega = \Omega_0$, then

$$\overline{\cos^2 \beta} = \frac{1}{N/2} \left\{ \int_{\Omega=0}^{\Omega_0} N(\Omega) \sin \Omega \cos^2 \Omega \left[\int_0^{\pi/2} \int_0^{2\pi} M_\Omega(k,\kappa) q_\Omega(k,\kappa) d\kappa \, dk \right] \right.$$

$$\left. \times d\Omega + \int_{\Omega=\Omega_0}^{\pi/2} N(\Omega) \cos^2 \Omega \sin \Omega d\Omega \right\}$$

$$= \frac{1}{N/2} \left\{ \int_{\Omega=0}^{\Omega_0} N(\Omega) \sin \Omega \cos^2 \Omega \, [\overline{q_\Omega(k,\kappa)}]_\Omega \, d\Omega \right.$$

$$\left. + \int_{\Omega=\Omega_0}^{\pi/2} N(\Omega) \sin \Omega \cos^2 \Omega \, d\Omega \right\}$$

$$= \frac{1}{N/2} \left[\int_{\Omega=0}^{\Omega_0} N(\Omega) \sin \Omega \cos^2 \Omega \, f_\Omega^{(m+n)} \, d\Omega \right.$$

$$\left. + \int_{\Omega=\Omega_0}^{\pi/2} N(\Omega) \sin \Omega \cos^2 \Omega \, d\Omega \right] \quad (12)$$

* The concrete functional form of $q(\Omega, k, K)$ may be given by $q = \cos^2 \beta = (\cos k \cos \Omega + \sin k \sin K \sin \omega)^2$.

where the angle Ω_0 can be given, as a function of the elongation ratio λ, as follows:

$$\Omega_0 = \cos^{-1}[(\lambda^3 - \lambda^2)/(\lambda^3 - 1)]^{1/2} \tag{13}$$

The changes of orientation of the crystal a and b axes as a function of the elongation ratio of spherulite can be calculated by substituting eqs. (10), (5), and (3) into eqs. (11) and (12), respectively. Some results are shown in Figure 7 for n and $m + n$ varied from 0 to 5/6.

As seen from Figure 7, the theory gives a fairly good prediction of the experimental results, suggesting that n changes from 0 to unity and $m + n$ changes from 0.5 to unity; i.e., m changes from 0.5 to 0 with elongation. This means that crystal rotation around the a-axis predominates over lamella untwisting (crystal rotation around the b-axis) at the initial stage

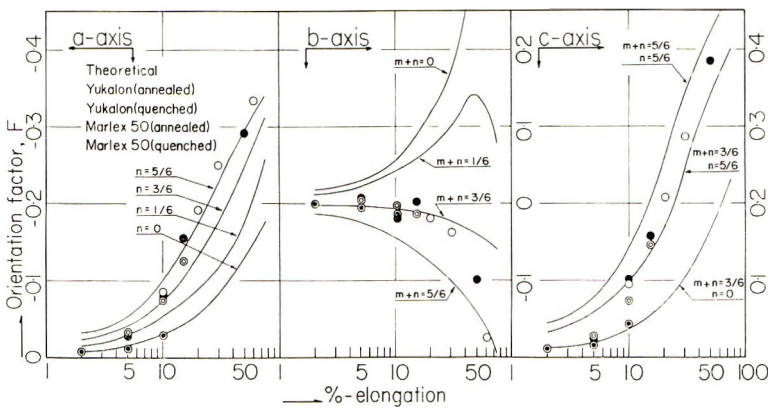

Fig. 7. Comparison of experimental results with the theoretical values from the model proposed by O-N-K.

of spherulite deformation and that the situation changes inversely with the elongation of the spherulite. The b-axis orientation due to the orientation of a radial fiber, which should give a positive orientation with respect to the OZ axis, may be compensated by the predominant crystal rotation around the a axis within the radial fiber and results in a less negative orientation of the crystal b-axis than the crystal a-axis at the initial stage of elongation.

Quite recently, Sasaguri, Yamada, and Stein have further modified their model by adding the untwisting of lamellae to their crystal transition model on almost the same concept as mentioned above and formulated the λ dependence of birefringence for the special case of a two-dimensional, disk-shaped spherulite.[9] Their formulation may be easily extended to calculating the λ dependence of a uniaxial orientation of crystals during the deformation of a three-dimensional spherulite.

For the orientation of the crystal c-axis in the folded-chain type crystals, which is always perpendicular to the radial fiber axis, the average square of the direction cosine is given by

$$\overline{\cos^2 \epsilon} = \int_0^{\pi} N'(\epsilon) \cos^2 \epsilon d\epsilon = \int_{\Omega=0}^{\pi} \int_{K'=0}^{2\pi} N'(\Omega,\kappa') \sin^2 \Omega \cos^2 \kappa' d\kappa' d\Omega$$

$$= \int_0^{\pi} N_1(\Omega) \sin^3 \Omega \left\{ \int_0^{2\pi} M_\Omega(\kappa') \cos^2 \kappa' d\kappa' \right\} d\Omega$$

$$= \int_0^{\pi} N_1(\Omega) \sin^3 \Omega (\overline{\cos^2 \kappa'})_\Omega \, d\Omega \tag{14}$$

where ϵ is the angle between the crystal c-axis and OZ axis and κ' is the rotational angle of the crystal c-axis with respect to the plane including the radial fiber and OZ axis and is usually random-distributed around the fiber axis, which gives the value of $\overline{\cos^2 \kappa'}$ as $^1/_2$.

When one defines a factor g for the preferential orientation of the c-axis around the fiber axis due to the untwisting of the crystal lamella as

$$g = 2\,\overline{\cos^2 \kappa'} - 1 \tag{15}$$

then eq. (14) can be rewritten as

$$\overline{\cos^2 \epsilon} = \int_0^{\pi} N_1(\Omega)(^1/_2)(g + 1)_\Omega \sin^3 \Omega d\Omega \tag{16}$$

Taking account of the orientation of the crystal c-axis in the transformed crystals, which is always parallel to the radial fiber axis, the total orientation of crystal c-axis can be given by

$$\overline{\cos^2 \epsilon} = (1/N) \left[\int_0^{\pi} (1 - X_{c,c}) N(\Omega) \sin^3 \Omega (^1/_2)(g + 1)_\Omega \, d\Omega + \int_0^{\pi} X_{c,c} N(\Omega) \cos^2 \Omega \sin \Omega d\Omega \right] \tag{17}$$

For the orientation of the crystal b-axis, which is independent on the untwisting of crystal lamella for the portion of $(1 - X_{c,c})$ and may be of random around the radial fiber axis for the portion of $X_{c,c}$, $\overline{\cos^2 \beta}$ is still given by eq. (9).

Sasaguri, Yamada, and Stein have represented the factor g, as functions of λ and Ω, as follows:

$$g = \eta(\lambda - 1) \sin^2 \Omega \tag{18}$$

where η is a parameter of the ease of the untwisting of the crystal lamella, and eqs. (15) and (18) result in a limitation for the value of η as follows:

$$-1 \leqq \eta(\lambda - 1) \sin^2 \Omega \leqq 1 \tag{19}$$

The results of calculations from eqs. (17) and (9) for crystal c- and b-axis orientation as a function of λ are shown in Figure 8 together with the experimental results, where γ and η are varied from 0 to 1.56 and from 0 to 2, respectively, and $X_{c,c,0}$ is taken as 0.5.

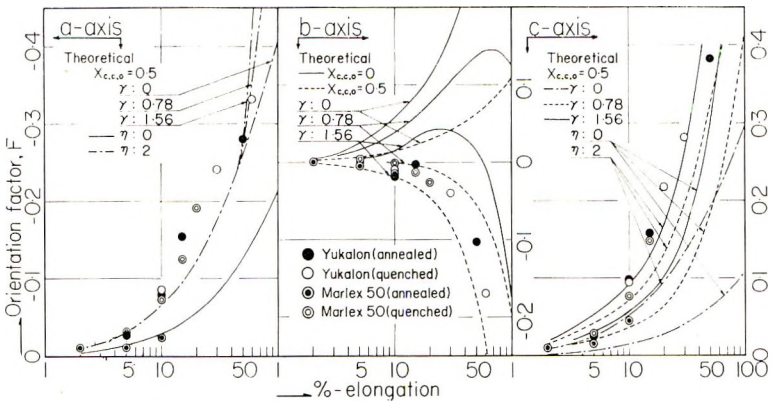

Fig. 8. Comparison of experimental results with the theoretical values from the model proposed by S-Y-S.

As seen from the results, γ and η should be near zero at the initial stage of spherulite deformation and increase with the increase of the elongation ratio, which suggests that the crystal orientation is mainly attributable to the orientation of radial fibers at the initial stage of spherulite deformation and attributable thereafter increasingly to the crystal transition and the untwisting of the crystal lamella.

CONCLUSIONS

Four types of models for the deformation mechanism of polyethylene spherulite, as given by Wilchinsky; Sasaguri, Hoshino, and Stein; Oda, Nomura, and Kawai; and Sasaguri, Yamada, and Stein have been discussed in relationship to the experimental results on the changes of orientation for three crystallographic axes of polyethylene crystallites with stretching of four kinds of polyethylene films.

Wilchinsky's model, which takes the crystal *c* axis as the orientation unit within the spherulite, seems to be too simple, reflecting the actual structure of spherulite and being unable to describe the difference of orientation behavior between crystal *a* and *b* axes.

The Sasaguri-Hoshino-Stein (S-H-S) model, which takes the crystal lamella grown radially as the orientation unit within the spherulite and allows the crystal transition from *b*-axis parallel (folded-chain type crystal) to *c*-axis parallel (fringed-micellar type crystal) to the radial direction within the crystal lamella, agrees qualitatively with the experimental results, providing that one can assume a considerable fraction of a *c*-axis-parallel crystals at an undeformed state and ease of the crystal transition.

The Oda-Nomura-Kawai (O-N-K) model, which also takes the crystal lamella as an orientation unit within the spherulite and allows crystal rotations around the crystal *a*- and *b*-axes within the lamella, agrees fairly well with the experimental results, suggesting that the plastic deformation of crystal lamella probably due to gliding along the (110) plane predomi-

nates over the lamella untwisting at the initial stage of spherulite deformation. This mechanism can explain the *a*-axis orientation behavior which predominates over the *b*-axis orientation with the stretching of the bulk polymer.

The Sasaguri-Yamada-Stein (S-Y-S) model, which modifies the S-H-S model by adding the lamella untwisting to the crystal transition, also agrees fairly well with the experimental results, providing that a considerable fraction of c-axis-parallel crystals be assumed at the undeformed stage of a spherulite.

The latter two models (O-N-K and S-Y-S), which are essentially similar to each other and result in somewhat different deformation mechanism in detail, still give some discrepancies from the experimental results. One of the possible reasons for this may be the invalidity of the affine transformation assumption, especially for the lateral zone of the spherulite where the deformation may be more complicated and more serious than that predicted by the theories.

The authors are indebted to Prof. Richard S. Stein, Polymer Research Institute, University of Massachusetts, Amherst, Mass., U.S.A. and Prof. Keinosuke Kobayashi, Institute for Chemical Research, Kyoto University, Kyoto, Japan, for their valuable suggestions and discussions on this paper.

Thanks are also due to the financial support by the grant from the scientific research funds (Kagaku Kenkyu-hi) of the Ministry of Education, Japan, and the grant from the Mitzubishi Yuka Co., Tokyo, Japan.

References

1. Fujino, K., H. Kawai, T. Oda, and H. Maeda, paper presented before the 4th International Congress on Rheology, Providence, R. I., August 1963; *Trans. Soc. Rheol.*, **8**, in press.
2. Sasaguri, K., S. Hoshino, and R. S. Stein, *J. Appl. Phys.*, **35**, 47 (1964).
3. Kobayashi, K., Y. Taniguchi, I. Kimura, and S. Kimura, paper presented before the 15th Annual Meeting of the Japan Chemical Society, Kyoto, Japan, April 1962.
4. Wilchinsky, Z. W., *Polymer*, **5**, 271 (1964).
5. Kuhn, W., and F. Grun, *Kolloid-Z.*, **101**, 248 (1942).
6. Price, F. P., *J. Polymer Sci.*, **37**, 71 (1959); *ibid.*, **39**, 139 (1959).
7. Fujiwara, Y., *J. Appl. Polymer Sci.*, **4**, 10 (1960).
8. Stein, R. S., and K. Sasaguri, ONR Technical Report No. 54, Contract NONR 3357(01), University of Massachusetts, Amherst, Mass., 1963.
9. Sasaguri, K., R. Yamada, and R. S. Stein, *J. Appl. Phys.*, **35**, 47 (1964).
10. Takayanagi, M., *Mem. Fac. Eng. Kyushu Univ.*, **23**, 48 (1963).

Résumé

On a proposé un mécanisme de déformation des sphérulites de polyéthylène basé sur la méthode de transformation par affinage. Des lamelles individuelles de cristal, prises comme unités d'orientation à l'intérieur des sphérulites, peuvent se mouvoir autour des axes *a* at *b* du cristal. Des déductions basées sur ce modèle ainsi que sur d'autres modèles antérieurs sont comparées aux résultats expérimentaux obtenus avec quatre sortes de films de polyéthylène. Ces résultats s'accordent remarquablement bien avec les prévisions du présent modèle et suggèrent que la déformation plastique des lamelles de cristal par glissement le long du plan (110) l'emporte sur la distorsion des lamelles de cristal au stade initial de la déformation.

Zusammenfassung

Ein Deformationmechanismus für Polyäthylensphärolithe wurde auf Grundlage der Methode der affinen Transformationen aufgestellt. Individuelle Kristallamellen werden als Orientierungseinheiten innerhalb der Sphärolithe angenommen und ihre Rotation um die kristallographische a- und b-Achse zugelassen. Aus diesem und anderen, früheren Modellen abgelieitete Folgerungen werden mit den an vier verschiedenen Polyäthylenfilmtypen erhaltenen Versuchsergebnissen verglichen. Diese Ergebnisse stimmen recht gut mit dem heir gewählten Mödell überein und zeigen, dass die plastische Deformation von Kristallamellen durch Gleitung längs der (110)-Ebene von grösserer Bedeutung als die Entdrillung der Kristallamellen im Anfangsstadium der Deformation ist.

Received September 14, 1964
Revised November 10, 1964
(Prod. No. 4574A)

JOURNAL OF POLYMER SCIENCE: PART A VOL. 3, PP. 2009-2018 (1965)

Copolymerization of 2,6-Dimethyl-4-bromophenol with 2-Methyl-4-bromo-6-allylphenol and Other *p*-Bromophenols*

K. C. TSOU,† H. E. HOYT, and B. D. HALPERN, *Central Research Laboratory, Borden Chemical Company, Philadelphia, Pennsylvania*

Synopsis

A series of poly(phenylene oxide) copolymers was prepared from 2,6-dimethyl-4-bromophenol and 2-methyl-4-bromo-6-allylphenol by the Price method of interfacial oxidative coupling. The physical and chemical properties of the copolymers were correlated with the molar proportions of the bromophenols. The thermosetting rates were proportional to the concentration of the allyl function and were of interest in the development of high-temperature thermosetting resins and adhesives. The preparation and copolymerization of 2-methyl-6-(α-methallyl)-4-bromophenol were also investigated. Homopolymerization of 2-methyl-4-bromophenol or 2,2′-methylenebis-(4-bromo-6-methylphenol) under the same conditions did not occur to any significant degree. When these bromophenols were used in attempted copolymerizations with 2,6-dimethyl-4-bromophenol, only low molecular weight homopolymers of the latter were obtained. The effect of these nonpolymerizing bromophenols as chain stoppers is discussed in connection with the mechanism for this type of polymerization.

Among the new types of high temperature polymers, poly(2,6-substituted 1,4-phenylene oxide)[1-3] is potentially one of the most useful because of the unusual thermal stability of the polymer backbone, monomer availability and ease of polymerization. Copolymerization of 2,6-dimethyl-4-bromophenol and 2-methyl-4-bromo-6-allylphenol was, therefore, of interest because the pendant allyl group in the copolymer should provide a curing site to impart a thermoset structure by free radical crosslinking or by conversion to the epoxide. While Kurian and Price had reported the preparation of the homopolymer of 2-methyl-4-bromo-6-allylphenol, no work has been reported on the copolymerization of these or any two phenols. This paper presents our experience in such copolymerization study and may provide useful data for other new copolymers of similar type.

* This work was done under Army Contract No. DA-36-034-ORD-3501-RD, Picatinny Arsenal, Dover, New Jersey.

† Present address: Harrison Dept. of Surgical Research, School of Medicine, University of Pennsylvania, Philadelphia, Pa.

EXPERIMENTAL

Monomers

2,6-Dimethyl-4-bromophenol, m.p. 74–75°C., was prepared from bromination of pure 2,6-dimethylphenol as described by Staffin and Price.[1]

2-Methyl-6-allyl-4-bromophenol was prepared by the Claisen rearrangement of pure 2-methyl-4-bromophenyl allyl ether[4] at 210°C. As the purity of the phenol is essential to obtain copolymers of reasonably good molecular weight, a somewhat detailed procedure is given. A 500-g. portion of pure 2-methyl-4-bromophenyl allyl ether was heated at 210°C. for 2 hr. In order to control this highly exothermic reaction and to minimize exposure to air, it was carried out in the presence of sufficient hexane under reflux to maintain the temperature. This was conveniently regulated by the use of a Dean-Stark trap and by adding or removing hexane distillate as needed. The product of the rearrangement was transferred to a 2-liter separatory funnel. Three volumes of hexane were added as solvent, after which a small amount of insoluble tarry material was separated. The hexane solution was now cooled to 10°C. and extracted with 280 ml. of precooled (10°C.) Claisens alkali (350 g. KOH, 250 g. H_2O, 1000 ml. methanol). The extraction procedure was repeated with 180 ml. Claisens alkali, and the solution was acidified with 350 ml. cooled dilute 6*N* HCl. The acidified material was extracted with 200 ml. carbon tetrachloride, and the resulting organic layer was washed four times with 50 ml. water. The carbon tetrachloride was removed by flash distillation under vacuum, and the product was vacuum distilled at 0.4 mm. The weight of crude phenol was 288 g. (57.8% conversion). This crude phenol was found by vapor-phase chromatography to have four constituents: about 80% of the desired phenol; 17% of a more volatile phenol identified later as 2-methyl-4-bromophenol (I); 2.2% of another low-boiling unidentified material; and about 1% of a low-boiling substance tentatively identified as diallyl. The product was carefully fractionated at 0.4 mm. Hg pressure at 10/1 reflux ratio under a 3-ft. Vigreaux column. The first fraction of 50 g. (10% yield) (maintaining heat on the condenser) was largely crystalline 2-methyl-4-bromophenol and boiled at 97–102°C./0.4 mm. A 207-g. portion of product (41.4% yield) was collected in the range 102–107°C.; n_D^{25} = 1.5736, d_4^{25} = 1.5207, molar refraction = 54.0 (calcd. 53.6). Vapor-phase chromatography showed a single peak with suggestion of a slight shoulder. This analysis was used as the best criterion of purity. When more than a single peak was found, the product was refractionated.

The residue from the Claisens extraction was washed with water and distilled; 187.5 g. (37.4%) of the starting material which showed only one peak by gas chromatography and was pure enough to be reused in the rearrangement.

2-Methyl-6-(α-methallyl)-4-bromophenol was prepared by the same steps. 2-Methyl-4-bromophenol was converted to the crotyl ether by

treatment with crotyl bromide in the presence of potassium carbonate,[2] and the purified ether (b.p. 120–121°C./3 mm. Hg, n_D^{22} = 1.5512, bromine 33.18%, calcd. 33.12%) was rearranged by controlled heating to the α-methallyl phenol. This rearrangement, which took place at the surprisingly low temperature of 170°C., likewise gave rise to byproducts (including 2-methyl-4-bromophenol). The α-methallyl phenol was isolated by careful fractional distillation; yield 33.6%; boiling point 92–95°C./0.3 mm. Hg, n_D^{25} = 1.5671.

ANAL. Calc.: C, 55.3%; H, 5.40%; Br, 33.17%. Found: C, 55.6%; H, 5.34%; Br, 33.48%.

Polymerization Procedures

The procedure used is essentially that used by Price for the preparation of the homopolymer, with necessary modifications to insure higher molecular weight polymers. In small-scale polymerizations, a Morton flask was used to promote agitation. For larger-size preparations, an equivalent effective agitation was achieved by inserting a baffle with the stirrer.

Our work confirmed the observation of Price[3] that when potassium ferricyanide was used as the oxidizing agent, the polymerization was essentially complete within a few minutes. Stirring was prolonged for 3 hr. to insure reproducibility and provide basis for comparison. Preparation of a 50:50 copolymer of 2,6-dimethyl-4-bromophenol and 2-methyl-6-allyl-4-bromophenol is shown to illustrate the general procedure used in the preparation of these polymers.

4-Bromo-2,6-dimethylphenol (50.2 g., 0.50 mole) and 2-methyl-6-allyl-4-bromophenol 56.7 g. (0.50 mole) were dissolved in 500 ml. 10% sodium hydroxide (1.38 mole). One liter benzene was added, and the mixture was cooled to 5°C. After the flask was well purged with purified oxygen-free nitrogen, a solution of potassium ferricyanide (1.65 g., 0.05 mole, in 100 ml. water and precooled to 5°C.) was added at once at the nitrogen outlet. The temperature of the liquids rose within 1 min. to 10°C. (exotherm), where it was held by control of the bath temperature for 1 hr. Stirring was continued for an additional 2 hr. at room temperature.

The benzene layer was separated, and the aqueous layer was thrice extracted with 300 ml. benzene. The benzene solution was washed first with dilute HCl, followed several times with water, and then evaporated on a steam bath to about 500 ml. This extracted solution was added slowly to 2 liters of methanol with good stirring and cooling. The precipitated polymer was collected, washed well with methanol, and dried to give 60 g. of the copolymer (theory 91%), $[\eta]$ = 0.29. No polymer was obtained when benzene was omitted.

Polymerization of 2-Methyl-6-(α-methallyl)-4-bromophenol was carried out under similar conditions. Only very low molecular weight ([] η = 0.085) polymer was obtained. Copolymer was prepared when admixed with 50 mole-% of 2,6-dimethyl-4-bromophenol in a similar manner. The intrinsic viscosity was found to be 0.121.

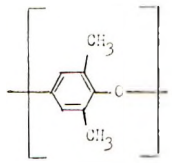

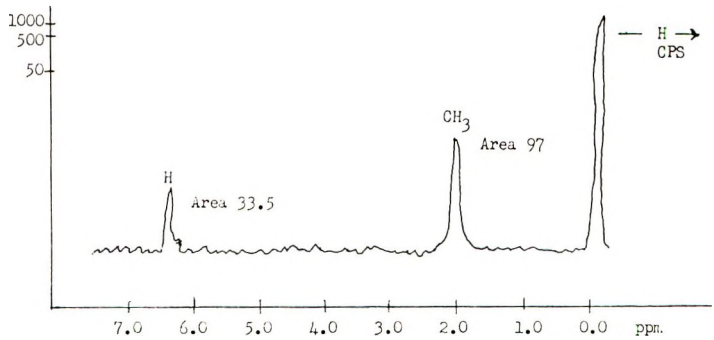

Fig. 1. NMR spectrum (60 Mcycle) on poly(2,6-dimethyl-phenylene oxide) (Price method). Solvent, CCl_4; filter band width, .2; RF field, 0.2; sweep time, 250; sweep width, 500; sweep offset, 80.

Chromatographic fractionation of the copolymer was carried out by absorption on an alumina packed column, followed by elution with benzene, then benzene–ethanol. It was noted that the initial fractions gave higher intrinsic viscosities, an interesting result observed by us also on the homopolymer of 2,6-dimethyl-4-bromophenol. It is thought that the relatively greater content of bromine in the lower molecular weight fragments results in a more polar fraction, more strongly absorbed. The fractions were examined for their infrared spectra. From the allyl bands at 6.1 and 11.0 μ, it was concluded that there was true copolymer distribution, as the intensity of the bands of each fraction was the same.

RESULTS AND DISCUSSION

Mechanism of Price Polymerization

The mechanism of copolymerization is likely to be the same as that of homopolymerization of 2,6-dimethyl-4-bromophenol which has been discussed by Price[1,3] and Hay.[5] Recently, a series of papers appeared in which Hay and co-workers[6,7] further elaborated on the mechanism and synthesis of analogous polymer. Since we have independently corroborated many of their findings, it would be superfluous to discuss the mechanism in detail except to point out that we are convinced that the novelty of the Price method lies in its interfacial oxidative coupling nature. We have also measured the ratio of CH_3—H and Ar—H (Fig. 1) by NMR, and found very little branching in the polymer.

The linearity of polymer can be explained by assuming that the bromine end of the 2,6-dimethyl-4-bromophenol dipole is closer to the interface than the methyl groups. This is also consistent with the fact that very little OH group has been found in the termination step, in spite of the well-known efficiency of the CH_3 group in the aromatic nucleus. If the abstraction of hydrogen from water were to take place to form the polymeric phenol, the presence of excess alkali in the water phase would immediately convert it to the phenoxide anion which would then take part in the same oxidative coupling process; thus it seems to us that in this mechanism the main termination step should be only a coupling of the two polyphenoxy radicals. Moreover, if a monomeric phenoxy radical were in the vicinity of such a polyphenoxy radical, a similar coupling reaction could take place. Evidence for the latter may be found in our experimental work in attempted copolymerization of 2,6-dimethyl-4-bromophenol with other bromophenols (see Table II).

There remains the question of the mode of linking the coupling process. Price[3] has recently suggested the formation of an α-phenoxy-ketone linkage as shown in eq. (1).

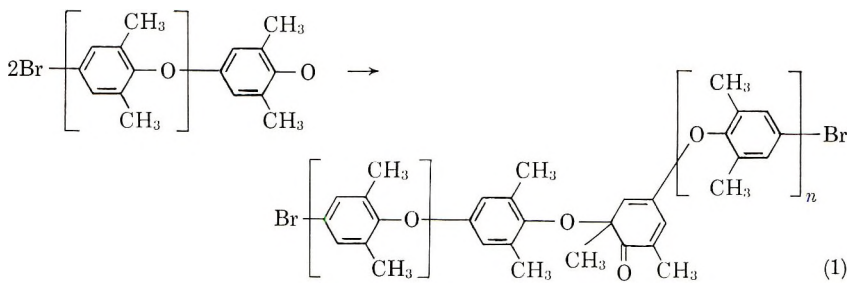

(1)

This possibility can be supported by our findings in chromatographic separation of this polymer, where it was found that the weak 5.85 μ band does seem to increase in intensity in the lower molecular weight fractions. The other possible mode is that of a peroxide formation as shown in eq. (2).

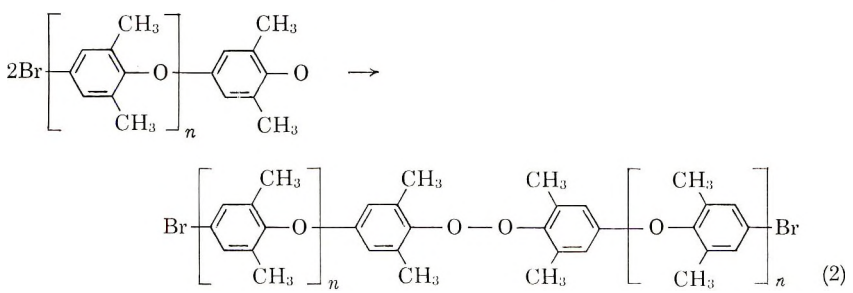

(2)

This possibility was suggested indirectly by the observation that poly(2,6-dimethyl-1,4-phenylene oxide) becomes slowly insoluble in benzene after molding on the hot plate, even at a temperature as low as 500°F. This behavior was independent of molecular weight of fractions and was ac-

celerated by exposure to higher temperature and also took place under nitrogen. Mild hydrogenation of the polymer was, therefore, carried out in benzene in order to cleave the suspected peroxide linkage. However, this treatment did not result in appreciable reduction of the viscosity of the polymer. We therefore conclude that the peroxide group is not present in these polymers and that the α-phenoxyketone linkage proposed by Price and Chu[3] is the probable mode of termination.

Copolymerization

The preparation of the copolymer follows essentially the same procedure as that used in the preparation of the homopolymer. The different copolymer ratios are determined only by the ratio of the corresponding phenols. Copolymer structure was subsequently confirmed by the bromine addition analysis[9] for the allyl function and the intensity of the allyl bands (6.10 and 11.0 μ) in the infrared spectra. High yields and low recoveries of material in the benzene–methanol filtrate and in the caustic layer assure substantially complete conversion of the phenols to polymer. Tentative structure proof of the copolymer was further reinforced by the fact that the infrared spectra on chromatographically separated fractions were remarkably similar throughout the molecular weight range (24,000–13,600),

TABLE I
Homopolymers and Copolymers from 2,6-Dimethyl-4-bromophenol (I) and 2-Methyl-6-allyl-4-bromophenol (II)

Prepn. No.	II in prepn., mole-%	Designation	Intrinsic viscosity $[\eta]^a$	Molecular wt. from $[\eta]^b$	Min. molding temp., °F.[c]	Cure time at 500°F., sec.[d]	Bromine in polymer, %	Conversion, %
1	0	Homopolymer I	0.540	35,000	550	3600+	0.90	90.2
2	100	Homopolymer II	0.352	25,500	300	3	2.49	80.2
3	70	Copolymer 70	0.318	23,800	400	20	—	83.1
4	50	Copolymer 50	0.287	22,000	400	39	1.83	93.5
5	20	Copolymer 20	0.330	24,200	450	80	2.55	92.8
6	10	Copolymer 10	0.387	27,600	450	187	2.30	88.7

[a] At 30°C. in benzene.

[b] $[\eta] = 1.50 \times 10^{-7} M_n^{1.44}$ determined on fractionated samples of poly (2,6-dimethylphenylene oxide) by relating intrinsic viscosity to osmotic molecular weight.

[c] The minimum surface temperature at which the polymer could be spread on a hot plate.

[d] Time required to lose Newtonian flow at 500°F., determined by a method similar to that of stroke cure for phenolics by D'Alelio.[10]

each fraction showing allyl bands at 6.1 and 11 μ. The properties of the copolymers and homopolymer thus prepared are summarized in Table I.

Copolymerization of 2,6-Dimethyl-4-bromophenol with Other Bromophenols

As mentioned earlier, in the Claisen rearrangement of 2-methyl-4-bromophenyl allyl ether to 2-methyl-4-bromo-6-allylphenol, up to 10% conversion to 2-methyl-4-bromophenol occurred. This contamination was not easily recognizable, since the refractive index value was not affected significantly by this impurity. In our initial attempts at homopolymerization and copolymerization with the use of impure preparations, conversions to polymer were generally below 50%, and the polymers were of low viscosity ($[\eta]$ = 0.06–0.16 for the homopolymeric 2-methyl-6-allylphenylene oxide). After more rigorous purification of the monomer, the yield of polymerization was high, and the intrinsic viscosity of the product increased to around 0.35. This improvement suggested to us that the impurity, 2-methyl-4-bromophenol acted as a chain stopper in the polymerization.

TABLE II
Polymerization of 2,6-Dimethyl-4-bromophenol (I) in the Presence of Nonpolymerizing Phenols: 2-Methyl-4-bromophenol (II) and 2,2′-Methylenebis-(4-bromo-6-methylphenol) (III)

System	Conversion, %[a] Based on both monomers	Based on I only	Br in polymer, wt.-%	$[\eta]$	Min. molding temp., °F.	Molecular wt[b]	Infrared spectra
I only[c]	—	90.2	0.9	0.54	550	35,000	All spectra very similar and typical of the homopolymer, poly-(2-6-dimethyl phenylene oxide)
I + 2 mole-% II[d]	76.9	78.2	1.60	0.43	500	29,500	
I + 50 mole-% II[d]	45.1	85.3	5.60	0.12	500	11,000	
I + 12 mole-% III[e]	35.0	44.0	7.94	0.26	400	20,500	

[a] Theory weight of polymer calculated conventionally for infinite polymerization, that is, weight of bromophenol minus HBr equivalent. Since all polymers are finite and contain bromine this is an approximate value.
[b] Based on our equation: $[\eta] = 1.50 \times 10^{-7} M_n^{1.44}$.
[c] Prepared according to Staffin and Price.[1]
[d] Prepared according to Claus.[4]
[e] Prepared according to Beaver.[8]

That 2-methyl-4-bromophenol (II) itself does not polymerize effectively in the Price method had been shown earlier by us in our attempt to form "ladder" polymers from this phenol. Similar attempts were made with 2,2′-methylenebis-(4-bromo-6-methyphenol) (III).

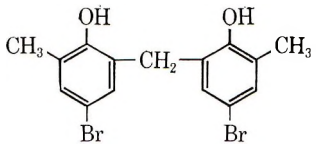

III

Conversions of these phenols to polymers were only 1% for II and negligible for III, except for a small dimer fraction. In both cases we were able to recover the starting phenol at better than 80% of the input.

In order to study the effect of these nonpropagating phenols on the Price polymerization, they were added to polymerizations of pure 2,6-dimethyl-4-bromophenol, with the results shown in Table II.

From the lowered viscosities and conversions, the increased bromine values, and the identity of the infrared spectra, one may infer that this polymerization is readily terminated by reactive but nonpropagating phenols. In terms of the termination mechanism this would appear to be by the coupling of the phenoxy radical of such a phenol with a poly-2,6-dimethylphenoxy radical.

Stability on Storage of Allyl Polymers

Kurian and Price[2] reported that after standing two or three weeks in air, polymers containing allyl substituents showed no tendency to melt at 570°F. and became insoluble. Even though we did notice on long standing (one year) a slight loss in solubility, there was no appreciable loss in moldability in the case of two homopolymers, nor any changes in the case of a copolymer, as shown in Table III.

TABLE III
Storage of Copolymer 50($[\eta]$ = 0.290)

Storage time, days	$[\eta]$	Min. molding temp., °F.	Benzene solubility
3	0.288	400	Complete
34	0.293	400	Complete
178	0.291	400	Complete

Molding Experiments for Copolymer of 2,6-Dimethyl-4-bromophenol and 2-Methyl-4-bromophenol (Copolymer 50)

As the copolymer appears to thermoset with time when molded on a temperature-controlled hot plate, an attempt was made to measure the physical change in terms of hardness of disks molded from copolymer 50 at increasing periods, as shown in Table IV. The disks, $1^1/_8$ in. in diameter and $^3/_{32}$ in. thick, were molded at 200–210°C. at 10,000 psi.

TABLE IV
Hardness of Copolymer 50 as Molded Disks

Molding time, min.	Rockwell hardness E	Deviation
2	98.2	2.0
5	99.4	0.9
15	101.2	0.9

Rockwell hardness was considerably higher than that found on poly(2, 6-dimethylphenylene oxide) disks which gave values of M78. The hardness was also higher than most commercial plastics including phenolics (also on the M scale).

References

1. Staffin, G. D., and C. C. Price, *J. Am. Chem. Soc.*, **82**, 363 (1960).
2. Kurian, C. J., and C. C. Price, *J. Polymer Sci.*, **49**, 267 (1961).
3. Price, C. C., and N. C. Chu, *J. Polymer Sci.*, **61**, 135 (1962).
4. Claus, A., *J. Prakt. Chem.* (2), **38**, 324 (1888).
5. Hay, A. S., *J. Polymer Sci.*, **58**, 581 (1962).
6. Endres, G. F., and J. Kwiatek, *J. Polymer Sci.*, **58**, 893 (1962).
7. Blanchard, H. S., H. L. Finkbeiner, and G. A. Russell, *J. Polymer Sci.*, **58**, 467 (1962).
8. Beaver, D. J., *J. Am. Chem. Soc.*, **74**, 3410 (1952).
9. Snell, F. D., and F. M. Biffen, *Commercial Methods of Analysis*, McGraw-Hill, New York, 1944, p. 346.
10. D'Alelio, G. F., *Experimental Plastics*, Wiley, New York, 1946, p. 165.

Résumé

On a préparé une série de copolymères d'oxyde de polyphénylène à partir de 2,6-diméthyl-4-bromophénol et de 2-méthyl-4-bromo-6-allylphénol par la méthode de Price de couplage oxidant interfacial. Les propriétés physiques et chimiques des copolymères ont été mis en corrélation avec les proportions molaires des bromophénols. Les vitesses de thermodurcissement sont proportionnelles à la concentration en fonction allyle et sont intéressantes dans la fabrication dés résines et adhésifs thermodurcissables à haute température. On a aussi étudié la préparation et la copolymérisation du 2-méthyle-6-(α-méthallyl)-4-bromophénol. L'homopolymérisation du 2-méthyl-4-bromophénol ou du 2,2′-méthylènebis(4-bromo-6-méthylphénol) dans les mêmes conditions, n'a pas eu lieu avec autant de succès. Quand ces bromophénols sont utilisés dans des copolymérisations avec le 2,6-diméthyl-4-bromophénol, on obtient seulement des homopolymères de faibles poids moléculaires. On discute de l'influence de ces bromophénols non-polymèrisables bloquant la chaîne en relation avec la mécanisme de ce type de polymérisation.

Zusammenfassung

Eine Reihe von Polyphenylenoxyd-Copolymeren wurde nach der Methode der oxydativen Grenzflächenkupplung von Price aus 2,6-Dimethyl-4-bromphenol und 2-Methyl-4-brom-6-allylphenol dargestellt. Die physikalischen und chemischen Eigenschaften der Copolymeren wurden zum Molverhältnis der Bromphenole in Korrelation gesetzt. Die Geschwindigkeit der Wärmehärtung war zur Allylgruppenkonzentration proportional, was für die Entwicklung von hochtemperaturwärmehärtenden Harzen und Klebern von Interesse war. Weiters wurde die Darstellung und Copolymerisation von 2-Methyl-6-

(α-methallyl)-4-bromophenol untersucht. Die Homopolymerisation von 2-Methyl-4-bromphenol oder 2,2′-Methylenbis-(4-brom-6-methylphenol) trat unter den gleichen Bedingungen nicht in wesentlichem Ausmass auf. Bei Einsatz dieser Bromphenole zur Copolymerisation mit 2,6-Dimethyl-4-bromphenol wurden nur niedermolekulare Homopolymere des letzteren erhalten. Die Wirksamkeit dieser nichtpolymerisierenden Bromphenole im Kettenabbruch wird im Zusammenhang mit dem Mechanismus dieser Polymerisationsart diskutiert.

Received August 2, 1963
Revised July 27, 1964
(Prod. No. 4515A)

JOURNAL OF POLYMER SCIENCE: PART A VOL. 3, PP. 2019-2026 (1965)

Dissolution and Crystallization Temperatures of High Polymers. II. New Method of Characterization of Polyacrylonitrile

R. CHIANG, *Chemstrand Research Center, Inc., Durham, North Carolina*

Synopsis

Polyacrylonitriles prepared under different conditions have similar infrared spectra, x-ray diffraction patterns, and densities, but they show marked differences in dissolution and crystallization behavior. On the basis of the dissolution and crystallization behavior, a characterization method, sensitive enough to show a small difference in chain regularity in the polymer, yet independent of the physical state and previous history of the sample, has been developed. With this method, polyacrylonitriles with different chain regularities can be conveniently differentiated.

Introduction

Acrylonitrile reacts readily with both free-radical and anionic initiators to form crystalline polymers. A number of initiators have been reviewed by Thomas.[1]

Inspired by the discovery of stereoregular and crystalline polymers synthesized by means of Ziegler-Natta or modified Ziegler-Natta catalysts in recent years, different laboratories, in an attempt to prepare polymers with improved crystallinity and stereoregularity, studied the effects of polymerization conditions on the properties of polyacrylonitrile.

However, because the molecular configuration and crystal structure of polyacrylonitrile is not definitely known, characterization of the polymer is exceedingly difficult. General methods such as x-ray diffraction, measurement of density and mechanical properties, infrared and nuclear magnetic resonance spectroscopy applicable to characterization of semicrystalline polymers fail to detect any differences in chain regularity in polyacrylonitrile;[2,3] nor is the method of melting point measurement applicable because polyacrylonitrile decomposes before it melts.

In this paper, a new method is described which is developed on the basis of the dissolution and crystallization behavior of polyacrylonitrile.[4] This method is sensitive enough to show even small differences in crystallizability of the polymer and in stability of the crystals formed. With this method, polyacrylonitriles with different chain regularities can be differentiated.

Crystallization of Polyacrylonitrile from Dilute Solution

Polyacrylonitrile crystallizes from dilute propylene carbonate solution in the form of platelets,[5] which redissolve in the same solvent at a temperature about 30°C. above the crystallization temperature, T_c. The rate of crystallization decreases as the temperature of crystallization increases. The temperature above which the crystallization becomes prohibitively slow is referred to as the highest practical crystallization temperature, whereas the temperature at which the crystal redissolves, as indicated by loss of opacity, is referred to as the dissolution temperature T_s.

According to recent experiments and current theory,[6-10] the thickness of a polymer crystal depends directly on the crystallization temperature. The theoretical relation between the melting temperature of a crystal of finite thickness or stepheight and the thickness of the crystal is given by the equation:

$$\Delta T = (T_m)_\infty - (T_m)_\xi = 2\sigma_e(T_m)_\infty/\xi\Delta H_u \tag{1}$$

where $(T_m)_\xi$ is the melting temperature of a crystal of stepheight ξ, $(T_m)_\infty$ is that of a crystal of infinite stepheight, σ_e is the interfacial energy per unit area of the platelets, and ΔH_u is the enthalpy of fusion.

Jackson, Flory, and Chiang[11] indicate a relation between the melting temperature and the dissolution temperature such that $(T_m)_\xi = T_s$ and $(T_m)_\infty$ relates to the dissolution temperature of an infinitely thick crystal in solution. Consequently, the dissolution temperature is also influenced by the thickness of the crystal, and the depression of the dissolution temperature ΔT serves as a converse measure of the stability of the crystal in solution.

Dependence of the Dissolution Temperature on Crystallization Temperature

In principle, $(T_m)_\infty$ can be determined, according to eq. (1), by plotting $(T_m)_\xi$ or T_s against $1/\xi$ and extrapolating to $\xi = \infty$. However, because it is difficult to determine ξ, this method is not used here. Instead we employed the method of extrapolation proposed by Hoffman[6] and by Mandelkern.[10] For polymers crystallized in bulk, they showed, on the basis of nucleation theory, that the observed melting point $T_{m,\text{obs}}$ is the arithmetic mean of the equilibrium melting point, T_m^0, and the crystallization temperature, T_c; that is,

$$T_{m,\text{obs}} = {}^1/_2(T_m^0 + T_c)$$

or

$$(T_m^0 - T_{m,\text{obs}}) = {}^1/_2(T_m^0 - T_c) \tag{2}$$

While the proportionality constant $^1/_2$ may vary somewhat, the linear relationship between the observed melting point and the crystallization temperature generally proves to be valid. In the present work, eq. (2) is

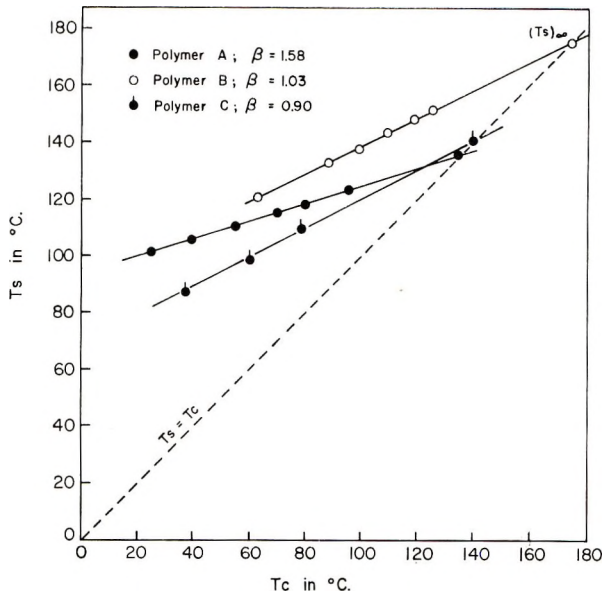

Fig. 1. Dissolution temperature vs. crystallization temperature for polymers of acrylonitrile isothermally crystallized from propylene carbonate.

applied to the crystallization of high polymers from dilute solution with T_m replaced by T_s. Figure 1 is a plot illustrating the linear relationship of T_s and T_c. In this figure, lines representing the experimental relation between T_s and T_c interesect the $T_s = T_c$ line. On this line, $\Delta T = 0$; therefore, at the intersection point, $T_s = T_c = (T_s)_\infty$ according to eq. (1). The value of $(T_s)_\infty$ thus obtained is a characteristic constant of the sample and reflects only the chain regularity of the polymer. Variation in the value of $(T_s)_\infty$ among the polymers is attributed to variation in structural regularity among them.[12,13]

This method relates essentially to conventional solubility measurements which have been used to characterize crystalline or stereoregular polymers. The conventional solubility tests suffer, however, from the disadvantage that the results obtained without standardization of the conditions of determination are often affected by the physical state and thermal history of the sample. The present method eliminates these uncertainties by controlling the conditions of crystallization. The dissolution temperatures obtained on carefully crystallized samples can be reproduced to ± 1 °C.

Experimental Results

The procedure for measuring the dissolution and crystallization temperatures has been described previously.[4] A small amount (ca. 0.2 cc.) of the hot, concentrated solution was introduced into about 10 cc. of propylene carbonate maintained at constant temperature. A rapid temperature equilibrium was achieved upon mixing. The solution was al-

lowed to crystallize. The crystallization was observed visually by onset of cloudiness in the liquid. After crystallization, the dissolution temperature was determined by introducing the crystallized sample, without drying, into a large excess of propylene carbonate, the temperature of which had been set previously. By several trials, a precise value of the dissolution temperature was obtained.

Samples prepared under different conditions were used in this investigation: polymer A was a sample prepared with a redox catalyst, while polymers B, C, and D were prepared with an organometallic coordination catalyst developed in this laboratory. Samples A and B have been shown by electron microscopy to crystallize from propylene carbonate solutions in the form of platelets.[4,5]

The dissolution temperatures of polymers A, B, and C are given in Table I and plotted against T_c in Figure 1. Straight lines are obtained in all cases. The values of $(T_s)_\infty$ for polymers A, B, and C are 134, 175, and 140°C., respectively. The highest crystallization temperature for polymers A, B, and C are 95, 125, and 77°C., respectively. Regardless of differences in dissolution and crystallization behavior, these polymers showed no differences in x-ray diffraction patterns, infrared spectra, or densities.

As further illustration of the utility of the crystallization-dissolution temperature method, one-point dissolution temperatures determined on various samples of polyacrylonitrile prepared with free-radical, anionic,

TABLE I
Dissolution and Crystallization Temperatures of Polyacrylonitrile in Propylene Carbonate

Polymer	T_s, °C.	T_c, °C.
A	102.0	25.0
	106.0	40.0
	111.0	55.0
	115.0	70.0
	117.0	80.0
	122.0	95.0[a]
	(135)[b]	(135)[b]
B	121.2	61.5
	133.5	87.4
	138.0	98.0
	143.5	108.5
	148.0	118.0
	152.0	125.0[a]
	(175)[b]	(175)[b]
C	86.5	40.0
	97.5	61.5
	107.0	77.0[a]
	(140)[b]	(140)[b]

[a] The highest practical crystallization temperature.
[b] Extrapolated dissolution temperature $(T_s)_\infty$.

and organometallic initiators are included in Table II. For these one-point dissolution temperature measurements, finely divided powders were obtained by crystallization at 25°C. by precipitation in methanol. All of these polymers again showed no differences in x-ray diffraction, infrared spectrum, or density, in agreement with the work reported by Bohn, Schaefgen, and Statton.[2] However, they displayed marked differences in their dissolution temperatures.

TABLE II
Some Properties of Polymers of Acrylonitrile Prepared with Various Catalysts

Polymer	Initiator	Polymer density (25°C.), g./cc.	T_c, °C.[a]	T_s, °C.	$(T_s)_\infty$, °C.
A	Persulfate–SO_2	1.175	95	125	134
B	Organometallic coordinate complex in DMF at −78°C.	1.172	125	152	175
C	Same catalyst in DMF at −30°C.	—	77	107	140
D	Same catalyst in DMF at 0°C.	1.175		65–115	
E	*n*-BuLi in toluene at −78° C.[14]	1.17		80–100	
F	NaSR in DMF at −78°C.[b]	—		125	
G	NaCN in DMF at −78°C.[b]	—		60–95	
H	BuLi complexed with oxygenated compound	—		100–105	
I	BEt_3 and pyridine activated with an organic peroxide[c]	1.172			
J	1:2 $AlEt_3$–acetylacetone in DMF at 75°C.	1.179		120–126 110–115	
K	143 $AlEt_3$–acetylacetone in DMF at 25°C.	1.175		110–130	
L	AIBN in benzene at 60°C.	1.17		<125	

[a] The crystallization temperature for all samples except those for Polymers A, B, and C was 25°C. The finely divided powders were obtained by precipitation of the polymer from dilute DMF solution in a large excess of methanol, followed by washing and drying. DMF = dimethylformamide; AIBN = azobisisobutyronitrile.

[b] Data of Evans.[15]

[c] Data of Mottus and Fields.[16]

Discussion

From the dissolution and crystallization temperatures, one can derive values of $(T_s)_\infty$, the dissolution temperature of crystals of infinite step-height, and σ_e, the surface energy required for the formation of the crystals.[4] Since both quantities are affected by the degree of perfection of the crystals as influenced by the molecular regularity of the polymer, determination of the dissolution and crystallization temperatures actually gives a measure of

molecular regularity. This method, of course, yields no further information regarding the nature of the various kinds of structural regularities, or the absolute concentration of the individual irregularities present. Furthermore, the dissolution temperature observed is that of the most perfect crystal and may not be representative of the whole sample. This is especially true when we deal with stereoblock polymers or copolymers with block character.

In polyacrylonitrile, many irregularities have been observed and reported, such as branching,[17] crosslinking, head-to-head placements,[18] naphthylenic condensed rings,[19] cyanoethyl groups,[1] etc. Therefore, one cannot say with assurance whether the differences observed in the melting points are associated with stereoregularity or with other forms of molecular regularity. Qualitatively speaking, the differences in dissolution temperatures among all the polymers reported here are too great to be attributed to a small amount of structural irregularity. Therefore, it appears more likely to be due to stereoregularity.

The possibility of polyacrylonitriles having different degrees of stereoregularity is not inconsistent with views expressed in the literature. Arcus and Bose[20] stated that polyacrylonitrile prepared by Bacon's reduction-activation procedure[21] is atactic. It exhibits an x-ray diffraction pattern characteristic of the amorphous polymer. Liang and Krimm,[22] on the basis of infrared spectra, found no evidence of syndiotactic structure in polyacrylonitrile and concluded that it is more or less atactic with the nitrile groups being randomly placed along the chain.

Despite its lack of stereoregularity, polyacrylonitrile is capable of crystallizing.[4] The ability of polyacrylonitrile to crystallize can perhaps be attributed in part to the small size of the nitrile group and in part to strong intermolecular dipole–dipole interactions.[23] Inasmuch as the true crystal structure is still uncertain, the possibility that the small nitrile groups, whether isotactic or syndiotactic, can be incorporated in the crystalline lattic without destroying the crystallinity cannot be excluded.

The difference in slope of the T_s–T_c plot for polymer A and that of polymers B and C is not clear at the present. According to Hoffman, the stepheight of the platelets is normally limited to a narrow range, its value being determined by the thickness of the primary nuclei, ζ_p^*. However, in any actual case, some crystals are thinner then ζ_p^* and some are thicker; the observed stepheight is somewhat higher than ζ_p^* by a factor β introduced arbitrarily, such that $\zeta = \beta\,\zeta_p^*$. As a result, the expression

$$T_s(\text{obs}) = [(T_s)_\infty + T_c]/2$$

is replaced by a more general formula:

$$T_s(\text{obs}) = (T_s)_\infty(1 - {}^1/_2\beta) + T_c/2\,\beta$$

The fact that β is considerably higher than 1 for polymer A indicates that there is a significant number of crystals with stepheight higher than ζ_p^* in polymer A, which may arise from recrystallization or thickening during

measurements or may reflect the chain mobility in the crystal. The values of β for polymer B and C are all shown in Figure 1.

Conclusion

The solution and crystallization measurements described here yield strong evidence that among various polyacrylonitrile samples, the crystals must vary in perfection and hence in stability even though they show no difference in infrared and x-ray diffraction spectra. The difference in perfection and stability, as reflected by the different crystallization and melting behavior, is attributed to the stereoregularity of the polymer.

However, the final proof of the stereoregularity in polyacrylonitrile and its quantitative measurements must await the refinement of such other independent determinations as nuclear magnetic resonance. If the degree of tacticity and the melting point can be correlated, this method of dissolution and crystallization temperature measurement can be developed into a sensitive technique for determining the tacticity in the polymer.

The extension of this method to other crystalline or stereoregular polymers is currently under investigation.

The author is indebted to Dr. R. Buchdahl for valuable discussions during the course of this work and to Dr. H. N. Friedlander for reading and criticizing the manuscript.

References

1. Thomas, W. M., *Fortschr. Hochpolymer.-Forsch.*, **2,** 401 (1961).
2. Bohn, C. R., J. R. Schaefgen, and W. O. Statton, *J. Polymer Sci.*, **55,** 531 (1961).
3. Chiang, R., *J. Polymer Sci.*, **A1,** 2765 (1963).
4. Chiang, R., J. H. Rhodes, and V. F. Holland, *J. Polymer Sci.*, **A3,** 479 (1965).
5. Holland, V. F., S. B. Mitchell, W. L. Hunter, and P. H. Lindenmeyer, *J. Polymer Sci.*, **62,** 145 (1962).
6. Hoffman, J. D., and J. I. Lauritzen, *J. Res. Natl. Bur. Std.*, **64A,** 73 (1960); J. D. Hoffman, and J. J. Weeks, *ibid.*, **66A,** 13 (1962).
7. Price, F. P., *J. Polymer Sci.*, **42,** 49 (1960); *J. Chem. Phys.*, **35,** 1884 (1961).
8. Frank. F. C., and M. Tosi, *Proc. Roy. Soc. (London)*, **A263,** 323 (1961).
9. Flory, P. J., *J. Am. Chem. Soc.*, **84,** 2857 (1962).
10. Mandelkern, L., *Crystallization of Polymers*, McGraw-Hill, New York, 1964, Chap. 9.
11. Jackson, J. B., P. J. Flory, and R. Chiang, *Trans. Faraday Soc.*, **59,** 1906 (1963).
12. Flory, P. J., *Trans. Faraday Soc.*, **51,** 848 (1955).
13. Miller, R. L., *SPE Trans.*, **3,** 123 (1963).
14. Miller, M. L., *J. Polymer Sci.*, **56,** 203 (1962).
15. Evans, E. F. (to du Pont Company), U. S. Pat. 3,006,894, October 31, 1961.
16. Mottus, E. H., and J. E. Fields, paper presented before the Division of Polymer Chemistry, 144th Meeting, American Chemical Society, Los Angeles, April 1963.
17. Miller, M. L., P. A. Button, R. F. Stamm, L. Rapoport, and E. H. Gleason, paper presented at 129th Meeting, American Chemical Society, New York, March 1956; results are quoted by Thomas in ref. 1.
18. Mark, H. F. (to International Polaroid Corporation), German Pat. 1,098,205, January 26, 1961.
19. Grassie, N., and J. N. Hay, *J. Polymer Sci.*, **56,** 189 (1962).
20. Arcus, C. L., and A. Bose, *Chem. Ind. (London)*, **1959,** 456.
21. Bacon, R. G. R., *Trans. Faraday Soc.*, **42,** 14 (1946).

22. Liang, C. Y., and S. Krimm, *J. Polymer Sci.*, **31**, 513 (1958).
23. Flory, P. J., *Principles of Polymer Chemistry*, Cornell Univ. Press, Ithaca, N. Y., 1953, p. 56.

Résumé

Des polyacrylonitriles préparés sous différentes conditions, ont des spectres infrarouges, des diagrammes de diffraction aux rayons-X et des densités semblables, mais ils montrent des différences importantes dans leur comportement de dissolution et de cristallisation. En se basant sur ces différences de comportement, on a développé une méthode de caractérisation assez sensible pour montrer un petite différence dans la régularité de la chaîne de polymère. Cette méthode est indépendante de l'état physique et de l'historique de l'échantillon. Avec cette méthode, on peut différencier commodément des polyacrylonitriles ayant des régularités de chaîne différentes.

Zusammenfassung

Unter verschiedenen Bedingungen dargestellte Polyacrylnitrile besitzen ähnliche IR-Spektren, Röntgenbeugungsdiagramme und Dichten, zeigen aber merkliche Unterschiede im Lösungs- und Kristallisationsverhalten. Auf der Grundlage des Lösungs- und Kristallisationsverhaltens wurde eine Charakterisierungsmethode entwickelt, welche empfindlich genug ist, um einen kleinen Unterschied in der Kettenregelmässigkeit des Polymeren erkennen zu lassen, aber doch unabhängig vom physikalischen Zustand und der Vorgeschichte der Probe ist. Mit dieser Methode können Polyacrylnitrile mit verschiedener Kettenregelmässigkeit unterschieden werden.

Received September 25, 1964
Revised November 13, 1964
(Prod. No. 4575A)

JOURNAL OF POLYMER SCIENCE: PART A VOL. 3, PP. 2027-2031 (1965)

Fracture Processes in Polymeric Materials. VII. The Nature of Local Inelastic Processes in Glassy Polymers

J. P. BERRY, *Rubber and Plastics Research Association of Great Britain, Shawbury, Shrewsbury, Shropshire, England*

Synopsis

The nature of the response to the local stress in the vicinity of a flaw in a glassy polymer is considered in the light of recent work on the nature and structure of craze marks. It is concluded that the response is similar to that which gives rise to a craze mark and that the structure of the layer at the fracture plane responsible for optical effects is likewise similar to that of a craze mark. This hypothesis resolves some of the inconsistencies in the earlier concept of the layer structure as a domain of oriented molecules.

It is generally accepted that the tensile strength of materials which fail in a brittle manner is limited by the presence of flaws, and a considerable body of theory has been derived from this assumption. Prominent in this field is the theory due to Griffith,[1] and the consequences of applying this theory, and its extension by Orowan,[2] to the glassy polymers poly(methyl methacrylate) and polystyrene have been explored.[3-6] From the results of these investigations it was concluded that two factors are primarily responsible for determining the brittle fracture strength of these materials. The first is the energy dissipated in the vicinity of the flaw as it begins to increase in size (the fracture surface energy)[3] and the second is the propensity of the material to generate structural defects (craze marks) under the influence of the imposed stress.[4] This crazing behavior determines the size of the inherent flaw (which corresponds to the Griffith flaw) in the material. Since the importance of these factors was first appreciated, developments in a number of fields have indicated that the details of the original interpretation of the underlying molecular mechanisms require some modification.

It is believed that the effective flaws in a sample of glassy polymer immediately before rupture in a tensile test are associated with the craze marks that are generated by the stress.[4] The phenomenon of crazing is still only imperfectly understood, but a fairly comprehensive conception of the nature of the marks themselves is beginning to emerge.[7-11] It has been shown that they are regions of local yielding, and it is the structural, and hence optical, change resulting from this process that renders them visible.[7] The yielding results in orientation of the polymer molecules within the

craze mark normal to its plane, i.e., in the direction of the imposed stress. In many cases the material within the yielded region is not homogeneous, but contains voids which occupy about 50% of the volume.[8-10] The spatial and size distribution of these voids has been studied by a silver infiltration technique, which reveals that they are distributed randomly throughout the craze mark, with a wide range of sizes, down to the limit of resolution of the electron microscope.[9] This work indicates that the structure of the craze mark results from two types of local response to imposed stress: (*1*) the extension and orientation of polymer molecules and (*2*) the formation of voids. It appears that the first response is analogous in some respects to that which a ductile sample demonstrates on a macroscopic scale in cold drawing.

It has been noted that interference color effects are discernable on the fracture surfaces of poly(methyl methacrylate)[13] and this observation, together with the discrepancy between the observed and theoretical values of the fracture surface energy, led to the suggestion that an energy dissipating inelastic process associated with the moving crack front resulted in an ordering of the molecules in the vicinity so that they were oriented preferentially normal to the fracture plane.[3] In view of the above considerations and in particular with regard to the postulated structure of the craze marks, it would seem that this hypothesis is inadequate, and that it is necessary to consider the possibility that the surface layer consists of oriented molecules interspersed with voids. There are a number of experimental observations that are more consistent with this structure than that involving only oriented molecules suggested earlier.[13]

The brilliance of the observed colors indicates that there is a marked difference in refractive index between the layer and the substrate, and a sharp interface separating them. The first would require a high degree of orientation and ordering if the effect were due to this cause alone, but no significant amount of order can be detected by x-ray or electron diffraction techniques. If the formation of the surface structure involved only molecular orientation, the interface would be expected to correspond to the shoulder region in a cold-drawn specimen. The interface is there quite different from that observed at a craze mark. In particular, it does not show the high reflectance characteristic of the latter, which closely resembles the reflectivity of a fracture surface. The refractive index of the interference layer at a poly(methyl methacrylate) fracture surface has recently been shown to be the same as that of a craze mark in the material, which provides more direct evidence for their similarity of structure.[11]

As noted above, the change in refractive index necessary to explain the observed optical effects would demand a considerable extent of molecular orientation if this alone were responsible. Such a degree of molecular orientation demands, in turn, a large local elongation of the sample and a considerable reduction in cross-sectional area. However, the thickness of the region in which this effect is observed at the fracture plane is very small compared with the sample cross section. Because the thin layer is con-

strained by the substrate, effectively no reduction in cross-sectional area is possible, and the material is therefore in a state of hydrostatic tension. Void formation is thus a natural consequence of the stress system. Similar considerations apply to the structure of craze marks.[9]

The optical effects associated with the structure of the fracture surface layer and the concomitant discrepancy in the fracture surface energies are observed at ambient temperatures at which molecular translational motion is greatly retarded.[5] It would be expected that the energy required for void formation by separation of molecular segments would be less than that required for moving chains of such segments past one another. Hence void formation may be possible under conditions where chain orientation is prohibited.

The suggestion has been made that the local temperature at the crack tip may be much higher than the ambient because of the local energy dissipation, and that for this reason molecular translational motion may be possible under apparently unfavorable conditions.[14] However, if the formation of the surface layer involved only molecular orientation, it would be necessary for this orientation to persist after the crack front had passed at the relatively high temperature. The crack velocity is so high that there is little possiblity of heat conduction away from the newly formed structure sufficiently quickly to prevent disorientation.

It has been reported that the fracture surface colors in poly(methyl methacrylate) are sensitive to high vacuum[15] and to inert liquids such as water and silicone oil.[16] While the effect of such agents is difficult to understand on terms of the orientation hypothesis, the presence of voids in the surface layer provides an explanation for the effects observed.

On the assumption that it is the energy dissipated in local molecular orientation that is responsible for the observed discrepancy between the experimental and calculated fracture surface energies, if a fracturing crack is propagated in a direction normal to that along which the molecules have been preferentially orientated by a prior thermal treatment, the observed fracture surface energy should be reduced. In fact, the fracture surface energy is increased under these conditions, and reduced when the crack travels in the direction of molecular orientation.[17]

In view of the above considerations it is to be expected that the experimental fracture surface energy will include contributions from the energy to create voids, and from that to cause molecular translation. The relative contributions from these two mechanisms will depend on the specific details of the system and the conditions under which fracture is induced, and are difficult to establish *a priori*. Furthermore, the optical properties of the surface layer (if such is formed) will also depend on the contributions from the two types of response to the local stress, and such contributions will not necessarily be the same as those involved in determining the fracture surface energy. It is these factors which preclude, in most cases, an uniquivocal interpretation of the effect of the experimental variables on the fracture surface energy and on the optical properties of fracture surfaces.

If the proposed structure of the craze mark is accepted, the relation of the phenomenon of crazing to fracture becomes clearer. As the imposed stress on the sample is increased from zero, a point is reached when the visible craze marks appear. As the stress is further increased, the craze marks grow in size, and it is reasonable to assume that the voids therein will begin to coalesce until a true (Griffith) crack is formed. This hypothesis is supported by the observed dependence of the detailed structure of the silver-infiltrated craze marks on size.[9] This crack is then activated by the stress to cause failure. Because the rate of growth of craze marks is determined by the stress level,[12] some dependence of the tensile strength on the rate of stressing is to be expected from this cause and this has in fact been observed.[4] Once the initial crack begins to increase in size, the stress conditions at its tip are unlikely to undergo any dramatic change, and hence it would be expected that the structure associated with the travelling crack tip, and which is apparent at the fracture surface, would resemble that of its logical precursor, the craze mark.

The above considerations indicate that there is probably a close relationship between the structure of the craze marks and that of the interference layer at the fracture surface of a glassy polymer; the first is essentially the precursor of the second. This relationship is important in consideration of the tensile strength of glassy polymers and in particular to the two factors which are important in determining the strength, i.e., the fracture surface energy and the inherent flaw size. These factors cannot be considered completely independent, since they both depend on the same kind of local response of the material to the stress. It is probably this factor that is responsible for the relatively small range of tensile strength values for glassy polymers. According to the Griffith-Orowan theory, the tensile strength is related directly to the fracture surface energy and inversely to the inherent flaw size. A high value of the former would be associated with the ability to deform inelastically at the tip of a flaw and to dissipate energy by this process. Since the same basic response is involved in the formation of a craze mark, then the inherent flaw size should also be large under these conditions. The tensile strength is determined by the ratio of these factors, and it is probable, for the reasons discussed above, that this ratio is relatively insensitive to changes in the material constitution or the test conditions.

References

1. Griffith, A. A., *Phil. Trans. Roy. Soc.*, **A221**, 163 (1921).
2. Orowan, E., Proceedings of the Symposium on *Fatigue and Fracture of Metals*, Wiley, New York, 1950, p. 139.
3. Berry, J. P., *J. Polymer Sci.*, **50**, 107 (1961).
4. Berry, J. P., *J. Polymer Sci.*, **50**, 313 (1961).
5. Berry, J. P., *J. Polymer Sci.*, **A1**, 993 (1963).
6. Berry, J. P., *J. Polymer Sci.*, **A2**, 4069 (1964).
7. Spurr, O. K., and W. D. Niegisch, *J. Appl. Polymer Sci.*, **6**, 585 (1962).
8. Kambour, R. P., *Nature*, **195**, 1299 (1962).

9. Kambour, R. P., *Polymer*, **5**, 107 (1964).
10. Kambour, R. P., General Electric Report No. 63-RL-(3407C); *J. Polymer Sci.*, **A2**, 4159 (1964).
11. Kambour, R. P., General Electric Report No. 63-RL-(3492C); *J. Polymer Sci.*, **A2**, 4165 (1964).
12. Sauer, J. A., and C. C. Hsaio, *Trans. ASME*, **75**, 895 (1953).
13. Berry, J. P., *Nature*, **185**, 91 (1960).
14. Higuchi, M., *J. Japan. Soc. Test. Mat.*, **9**, 79 (1960).
15. Newman, S. B., and I. Wolock, *Adhesion and Cohesion*, Elsevier, New York, 1962, p. 218.
16. Benbow, J. J., *Proc. Phys. Soc. (London)*, **78**, 970 (1961).
17. Broutman, L. J., Dept. of Civil Eng. Res. Rept. R 63-35, M.I.T., 1963.

Résumé

La nature de la réponse à une tension locale dans la proximité d'une fissure dans un polymère vitreux est considérée du point de vue des travaux récents sur la nature et la structure des craquelures. On tire la conclusion que la réponse est semblable à celle qui donne lieu à une craquelure et que la structure de la couche au plan de brisure, responsable des effets optiques, est également semblable à celle d'une craquelure. Cet hypothèse résout quelques unes des contradictions dans les conceptions antérieures, qui considéraient la structure de la couche comme un domaine de molécules orientées.

Zusammenfassung

Die Natur des Verhaltens unter lokalen Spannungen in der Nähe einer Fehlstelle in einem glasigen Polymeren wird im Lichte der neueren Arbeiten über die Natur und Struktur von Rissspuren betrachtet. Man kommt zu dem Schluss, dass das Verhalten demjenigen ähnlich ist, das zu einer Rissspur führt und dass die Struktur der für die optischen Effekte verantwortlichen Schicht an der Bruchfläche in gleicher Weise derjenigen einer Rissspur ähnlich ist. Diese Annahme beseitigt einige der Unstimmigkeiten in dem früheren Konzept der Schichtstruktur als eines Bereichs orientierter Moleküle.

Received October 12, 1964
(Prod. No. 4577A)

JOURNAL OF POLYMER SCIENCE: PART A VOL. 3, PP. 2033-2045 (1965)

Thermochemiluminescence of Polycarbonate and Polypropylene

R. E. BARKER, JR., J. H. DAANE, and P. M. RENTZEPIS,* *General Electric Research Laboratory, Schenectady, New York*

Synopsis

Experimental techniques for observing total and spectral thermochemiluminescence (TCL) are discussed in general along with some data for the systems polycarbonate–O_2, polycarbonate–CO, and polypropylene–O_2. Since TCL is the process whereby heated materials undergo thermally activated reactions and emit light in excess of the amount prescribed by the blackbody radiation law, its study may be expected to yield information about the structure and degradation of the materials. It has been observed that TCL spectra are both time- and temperature-dependent. A simple mathematical model for analyzing TCL data under conditions of a linear heating rate is discussed. The result also should be of use in thermogravimetric analysis.

INTRODUCTION

Many organic materials, including most polymers, emit small quantities of light when heated to moderate temperatures in the presence of O_2. Ashby,[1] Vassil'ev et al.,[2] and Stauff et al.[3] have described experiments and hypotheses which deal with this phenomenon. Recently Schard and Russell[4,5] have used total "oxyluminescence" in the study of polymer degradation. The purpose of this paper is to discuss some experiments involving total and spectral thermochemiluminescence (TCL) of Lexan poly(bisphenol A carbonate) (General Electric Company trademark) resin (PC) and polypropylene (PP).

EXPERIMENTAL

One of our experimental arrangements is shown in Figure 1. Stopcocks were manipulated with a black rubber glove through the side of a light-tight container. Samples (usually in the form of powder) were heated in a Pyrex cell with a quartz window, which could be evacuated and to which various gases could be admitted. (Some experiments were conducted by use of a Fisher-Johns melting point apparatus covered with aluminum foil in open air.) Relative pressure was monitored with a thermocouple gauge and gaseous products were later analyzed with a Consolidated 21-620 mass spectrometer. Condensation and extractable products were examined

* Present address: Bell Telephone Laboratories, Murray Hill, New Jersey.

with an F and M Model 500 vapor-phase chromatograph. Experiments have been carried out by (*1*) heating the polymer and gas environment together, (*2*) heating the polymer to a given temperature *in vacuo* and then admitting the gas, or (*3*) repeatedly reheating the same sample in its gaseous environment. The gases used were O_2, CO_2, and CO.

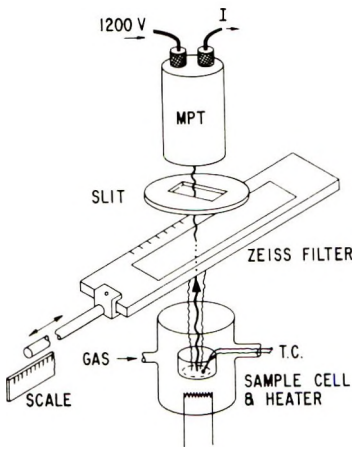

Fig. 1. Schematic view of apparatus used to obtain TCL spectra. It consists of a Pyrex cell with a heater, thermocouple, and vacuum connections, separated from a Dumont 6467 multiplying phototube by a monochromatizing device (Zeiss graded interference filter or glass filters and a shutter). Signals vs. time and temperature were displayed on a meter, usually on a Varian G-10 recorder or Textronix 545A oscilloscope.

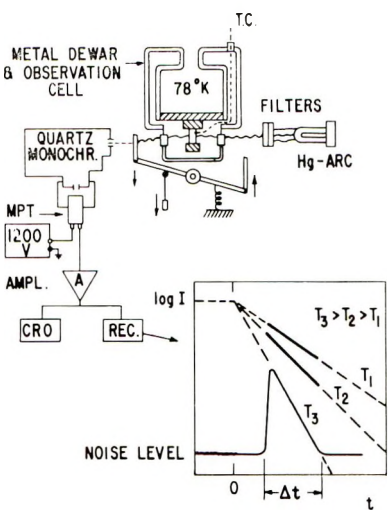

Fig. 2. Arrangement for measuring phosphorescence spectra. Exciting radiation from a Hg arc was passed through appropriate filters onto a sample in an evacuated cell at low temperature. A mechanical shutter cut off the exciting radiation and allowed the phosphorescence to enter a Gaertner L234-150 monochromator which was coupled to the MPT and recording system. If decay is exponential then log(current) vs. time is linear. Observed signals, as schematically illustrated here, have a saw-tooth shape due to the finite times required for shutter operation.

For Lexan resin and PP at about 250°C. in air, TCL may be seen with a totally dark-adapted eye. In addition to the photomultiplier–Zeiss filter system indicated in Figure 1, attempts were made to obtain TCL emission spectra by using a series of glass filters and also by using a Gaertner L234-150 monochromator with Polaroid 3200 film and a slit width of 25 μ. The photographic method produced no spectrum after exposures of up to 8 hr.

For comparison with its TCL spectrum, the ultraviolet-induced phosphorescence spectrum of PC at $\approx 80°$K. was obtained with the arrangement depicted in Figure 2.

The Dumont 6467 multiplying phototube (MPT) was calibrated with a Perkin-Elmer Model 98 monochromator and a radiation thermocouple standardized against an NBS source. The Zeiss filter, in the geometry used, and with a slit width of 8 mm., had a band width of 210 A. It is estimated that about twenty times as much light is available at the MPT as with the quartz monochromator of $f/4.5$ aperture and 25 μ slit width.

Total TCL of PP

Although some of the results are of a preliminary nature and related experiments are still in progress, certain aspects may be of fairly general

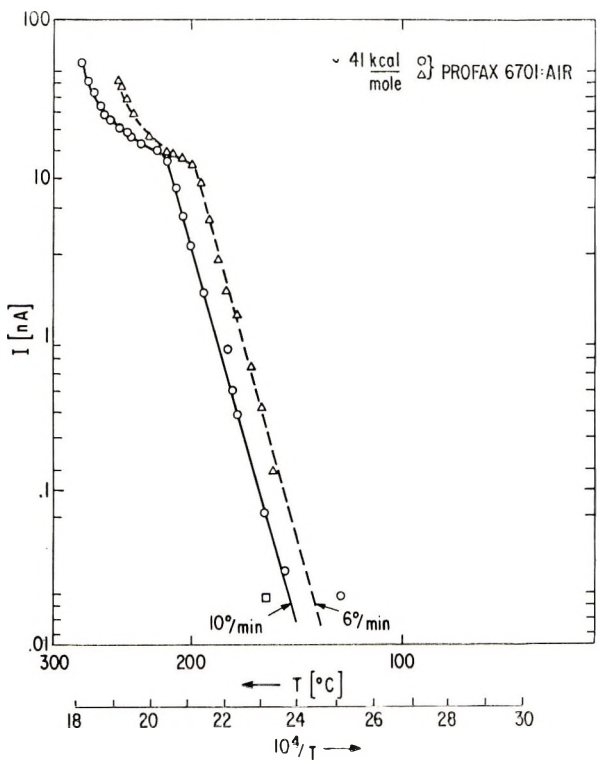

Fig. 3. MPT response to total TCL as a function of $1/T$. The curves are for unstabilized PP powder in air. The slope is about 40 kcal./mole for both heating rates.

interest. As observed by Schard and Russell,[4,5] TCL is an activated process (log I versus $1/T$ is linear over appreciable ranges). Some typical results are shown in Figure 3. When Ashby's[1] data for PP in O_2–N_2 mixtures are analyzed this way, the apparent activation energies E_a of Table I result.

TABLE I
Apparent Activation Energies for PP From Ashby's Data

$[O_2]/[O_2 + N_2]$	E_a, kcal./mole
1.00	17.6
0.21	15.8
0.11	10.0
0.064	7.2
0.026	5.6

We have found that TCL measurements in a stagnant system tend to yield low values for E_a, and thus that flow or replacement of the boundary layer gases is important. Results such as those of Figure 3 for unstabilized PP powder (Profax 6701) gave $E_a \approx 41$ kcal./mole. Results obtained by other techniques are compared in Table II. Our larger value may be due

TABLE II
Comparison of Apparent Activation Energies for PP Oxidation

Method	Sample	E_a, kcal./mole
O_2 absorption[a]	Isotactic (0.2 g.)	29
Infrared spectroscopy[b]	Isotactic (2.5 mil film)	31[c]
TGA in vacuum[d]	Linear	58
TCL (oxyluminescence)[e]	Compression-molded[a] (15 mil)[f]	23.3
TCL[g]	Isotactic, powder	37

[a] Data of Rysavy et al.[6]
[b] Data of Stivala et al.[7]
[c] The initial value is 31 kcal./mole; a long-term effect showed $E_a = 22 \pm 1$ kcal./mole.
[d] Data of Madorsky.[14]
[e] Data of Schard and Russell.[5]
[f] Highly crystalline.

to the fact that powder samples were used. To further investigate this and related matters, experiments are being devised which will utilize a series of molecular flow capillaries in conjunction with a high conductance vacuum exhaust system and an X-Y recorder to obtain a rapid direct display of I versus λ at a series of temperatures.

Total TCL of PC

A typical Arrhenius plot for PC is shown in Figure 4. Lee[8] used thermogravimetric analysis (TGA) and found $E_a \approx 15$–35 kcal./mole for the initial stage of oxidative degradation. In the range 450–500°C., $E_a \approx$

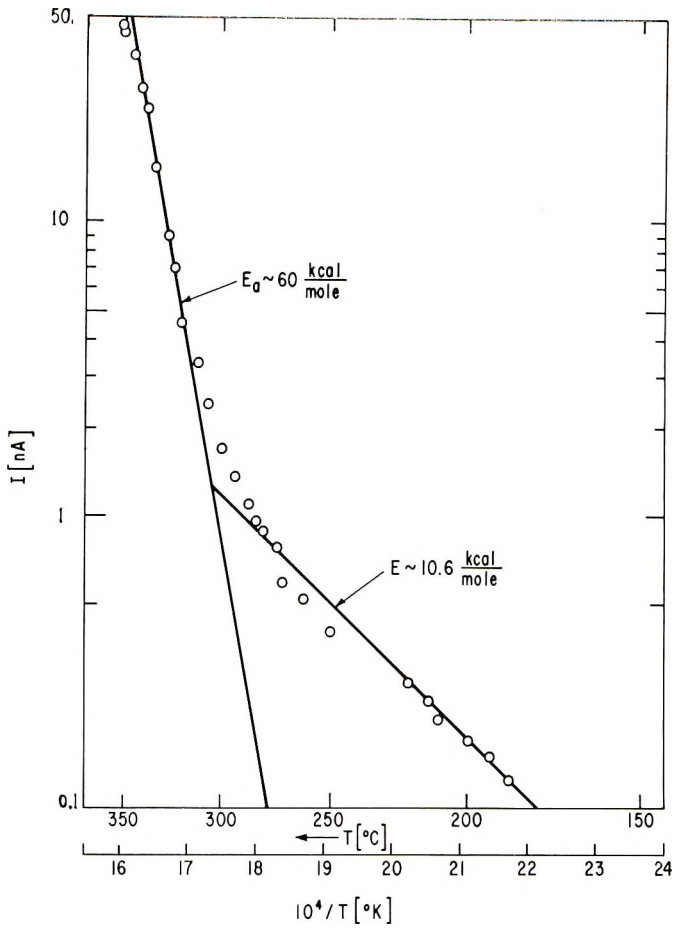

Fig. 4. Total TCL for Lexan powder in air. There appears to be an intermediate segment with an apparent activation energy $E_a \approx 35$ kcal./mole. The displacement of points in the vicinity of 250°C. is probably due to melting.

33 kcal./mole, whereas above 500°C. Lee obtained 55 kcal./mole. These values are in reasonable agreement with unpublished TGA results of Goldblum,[9] who obtained 18–31 kcal./mole in the 300–400°C. range for weight loss in air and 52 kcal./mole for the corresponding value in N_2. In the temperature range of our experiments, H_2O, CO, and CO_2 were the main gaseous products of PC oxidation, and phenol was the main condensation product. At the considerably higher temperatures considered by Lee,[8] there are a variety of products, and he has proposed a number of reaction schemes.

Cycling experiments indicate that log I_n, is approximately a decreasing linear function of the number of cycles n of heating and cooling the same samples (equal times, temperature ranges, etc.). Experiments in CO gave TCL signals with E_a of about the same magnitude as for O_2. Check runs

in CO_2 and *in vacuo*, with careful shielding of hot spots on the heat source and a cooled MPT, indicated no detectible signal up to over 300°C.

The increase of MPT dark current and changes in sensitivity due to heating can be a very serious complication; thus it is desirable to use a cooled MPT.

Williams-Eyring Method

Even though graphs of log I versus $1/T$ exhibit long linear sections, there is the important question of the meaning and uniqueness of the calculated activation energy since the TCL experiments are not carried out isothermally. Similar difficulties are encountered in the study of thermoluminescence (TL) and in TGA. We shall use a model which is analogous to one developed by Williams and Eyring[10] for TL arising from recombination of electrons and traps in various solids; however a somewhat simpler mathematical expression than the one discussed by Goldblum[9] and by Woodberry, Eyring, and Gabrysh[11] will be given.

Three simplifying assumptions are made: (*1*) TCL intensity I is due to a single type of reaction and

$$I = -\alpha dN/dt \tag{1}$$

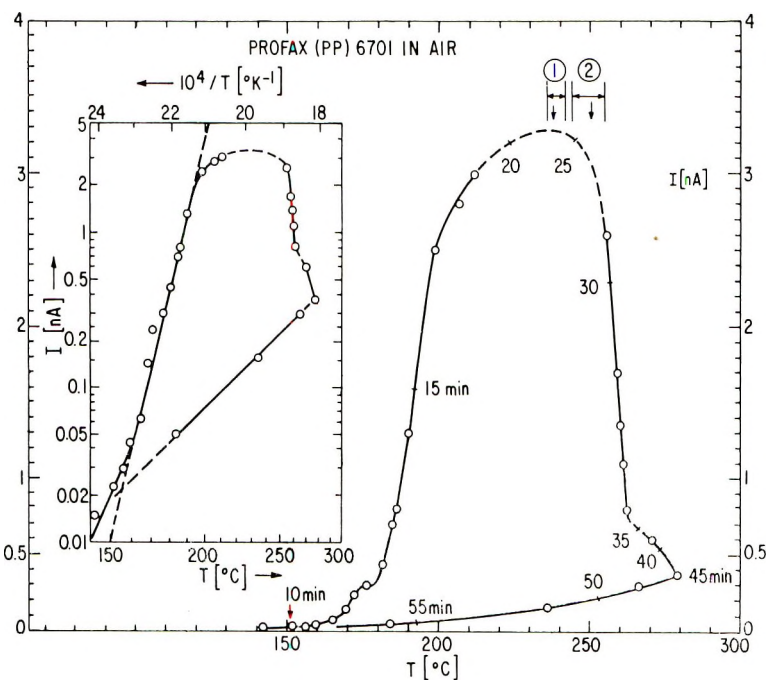

Fig. 5. Typical heating cycle for an unstabilized PP powder sample. The main curve is total photocurrent vs. T and the insert on the left is the same data on reciprocal temperature and logarithmic scales.

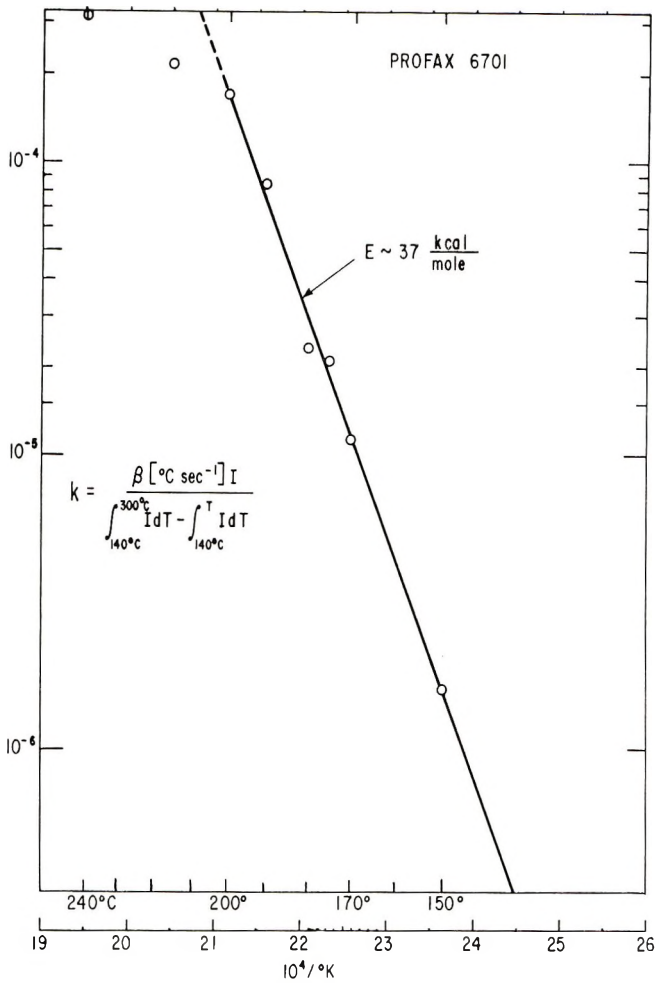

Fig. 6. Reaction coefficient k for TCL of unstabilized PP. Calculations are based on a modified Eyring-Williams metastable state model. Compare the activation energy with the apparent values of Figures 3 and 5.

where α is a constant and N is the number of unreacted TCL centers remaining; (*2*) the reaction is first-order,

$$dN/dt = kN \tag{2}$$

and (*3*) a constant heating rate $\beta = dT/dt$ is maintained until the reaction is completed. Thus $I = -\alpha\beta(dN/dT)$ so that

$$\int_{T_0}^{T} I dT = \alpha\beta(N_0 - N) \tag{3}$$

and

$$\int_{T_0}^{\infty} I dT = \alpha\beta N_0$$

Thus

$$(N_0 - N)/N_0 = \int_{T_0}^{T} I dT / \int_{T_0}^{\infty} I dT = 1 - (N/N_0) \tag{4}$$

It follows from eqs. (2) and (4) that

$$dN/dT = -N_0 I / \int_{T_0}^{\infty} I dT \tag{5}$$

and

$$k = -(\beta/N)\,(dN/dT) = \beta I/(N/N_0) \int_{T_0}^{\infty} I dT$$

$$= \beta I \Big/ \left(\int_{T_0}^{\infty} I dT - \int_{T_0}^{T} I dT \right) = \beta I \Big/ \int_{T}^{\infty} I dT \tag{6}$$

Even when none of the simplifying assumptions are exact, this approach may provide qualitative insight into TCL mechanisms.

The data for PP which are presented in Figure 5 were analyzed by using eq. (6), and the results are shown in Figure 6. Relative values of the quantity $\int_{T_0}^{\infty} I dT - \int_{T_0}^{T} I dT$ were determined by weighing cardboard sections of an I versus T plot. The total "area" is about 2.3×10^3 nA. °K., and, since $\beta \approx 0.1$°K./sec., the rate k in the vicinity of 190°C. (or the 15 min. mark, Fig. 5) is $\approx 7.6 \times 10^{-5}$ sec.$^{-1}$ or $k \approx 1.7 \times 10^{-6}$ sec.$^{-1}$ at 150°C. These values have comparable magnitudes to the rates for the formation of degradation products of PP given by Rysavy et al.[6] (their Fig. 5).

At present only a very crude approximation can be given for the photon yield per reaction $y = n/N = \dot{n}/\dot{N}$. In eq. (1), $\alpha \propto gy$, where g is a light collection efficiency that we estimate to be $\approx 1\%$. The MPT has an average sensitivity $\bar{S}_\lambda \approx 2 \times 10^4$ nA./nW. between 0.36 and 0.53 μ, so that on assuming an average photon energy $h\bar{\nu} \approx 4.5 \times 10^{-19}$J., we obtain an average flux rate into the MPT, $\dot{n}_p \approx I/\bar{S}_\lambda h\bar{\nu} \approx 10^4$ photons/sec., or $\dot{n} \approx g^{-1}\dot{n}_p \approx 10^6$ photons/sec. when $I \approx 1$ nA. For PP at 190°C. (Fig. 5) we assume an active mass of 0.1 g. so that $\dot{N} \approx kN \approx 7 \times 10^{-5}$ sec.$^{-1} \times 1.4 \times 10^{21}$ reaction sites $\approx 10^{17}$ reactions/sec. Finally $y = \dot{n}/\dot{N} \approx 10^{-11}$ photon/reaction. Another way to estimate y is to take the ratio of total charge transferred $\int_0^{\infty} I dt$ to the charge $\bar{S}_\lambda g h\bar{\nu} N$ that would pass if a photon accompanied each reaction, i.e.,

$$y \approx \int_0^{\infty} I dt / (\bar{S}_\lambda g h\bar{\nu} N) \tag{7}$$

From the temporal data of Figure 5 the integral is about 3 μA.-sec. and $\bar{S}_\lambda g h\bar{\nu} \approx 10^{-16}$ coul./photon. For 0.1 g., $N \approx 1.4 \times 10^{21}$ sites, we obtain $y \approx 2 \times 10^{-11}$ photon/reaction, in order of magnitude agreement with the first estimate. The value $y \approx 10^{-11}$ is probably a lower limit, since both g and N may be smaller than the values assumed.

TCL Spectra and Discussion

It is an attractive hypothesis to suppose that the chemical reaction is the site of an intense "hot spot" which is capable of exciting an adjacent molecular group to a higher electronic state from which luminescent decay may occur. Figure 7 shows some preliminary results (subject to improve-

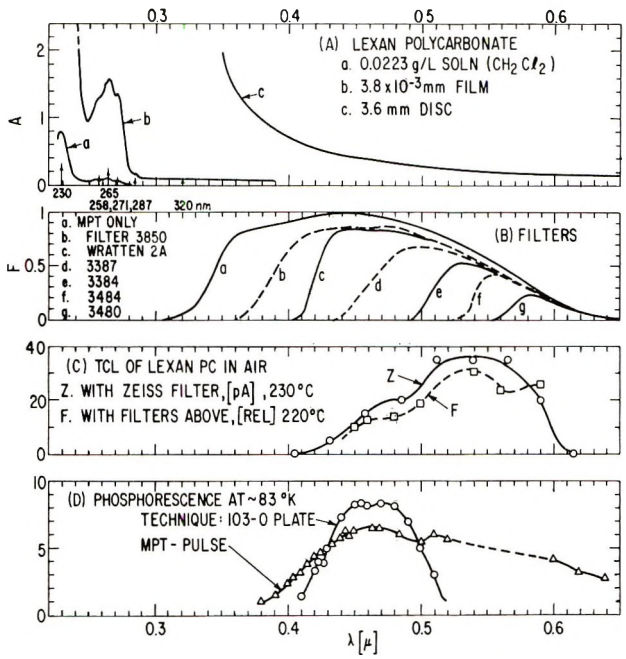

Fig. 7. Summary of optical data for Lexan resin. (*A*) absorption spectra for widely different numbers of molecules in the spectrophotometer's path; concentrations are in the ratio 1:20:20,000. The peak near 0.23 μ may be the ^1L_a band of the substituted benzene ring, which occurs at 0.203 μ in benzene itself. The structure near 0.265 μ is probably the ^1L_b band, near 0.25 μ in benzene. A very weak absorption at 0.287 μ is probably due to the C=O group. Damage by high energy irradiations, including ultraviolet light, produces new absorption bands which are dependent on time, temperature and environment and which may continue to change for a long time after cessation of irradiation. (*B*) Relative MPT sensitivity when used with various filters to estimate the relative TCL spectrum F in (*C*). (*C*) Curve Z is the TCL spectrum obtained with the Zeiss filter without sensitivity corrections. (*D*) Phosphorescence as measured by the "pulse technique" (described in connection with Fig. 2) and also by using a 103-0 spectroscopic plate. Plate sensitivity is low beyond 0.51 μ so that no radiation was observed at longer wavelengths.

ments in future experiments) which have been obtained with the goal of elucidating the TCL for Lexan resin in oxygen in the range 100–300°C. and checking the hypothesis mentioned above. The absorption spectra (Fig. 7*A*) were obtained with a Cary 14 spectrophotometer.

The relative overall response of the phototube and a set of filters, designated by F_i ($i = a, b, c, \ldots, g$), are shown in Figure 7*B*. Assuming linearity of the tube, the signal should be

$$I_i = K\int_0^\infty F_i W_\lambda d\lambda$$

where W_λ is the radiant power density of the TCL and K is a proportionality factor which depends on sensor area and geometry. The "areas"

$$A_i = \int_0^\infty F_i d\lambda$$

were determined graphically (Fig. 7*B*), and the TCL spectrum W_λ was estimated by application of the mean value theorem in the form:

$$\text{Relative TCL signal} \approx \mathrm{K} < \mathrm{W}_\lambda >_{\mathrm{av}} = I_i/A_i$$

This estimate and the spectrum obtained by use of the Zeiss filter are in reasonable agreement considering the wide band pass of the Corning filters.

The two remaining curves in Figure 7*D* are phosphorescent spectra of PC. One was obtained by using the Gaertner quartz monochromator and a Kodak 103-0 spectroscopic plate. It is the result of about 20 exposures of 10 sec. each to a sample at 80°K. which was excited by 30-sec. pulses (mainly 3650 A.) from a mercury arc. The MPT–pulse curve was obtained by placing the MPT at the exit slit of the monochromator and measuring the peak heights of phosphorescence decay at a series of wavelengths while the evacuated sample was at 80°K. Figure 2 depicts the experimental arrangement used. Unfortunately, the present resolutions of phosphorescence and TCL (Figs. 7*C*, 7*D*) do not enable us to decide whether the "local hot spot" hypothesis is valid. It is to be hoped that future improvements in these spectra and examination of the fluorescence will increase our understanding of the mechanism.[12] There is a fair chance that TCL in polymers may be due to energy transfer from excited reaction products P′ to very small traces of fluorescent impurities (acceptors A). Whether due to impurities or to intrinsic luminescent groups, a scheme which has been developed by Vassil'ev[12] to explain chemiluminescence in hydrocarbon solutions admixed with substituted anthracenes may have some validity in "solid" amorphous polymers [eqs. (8)].

$$\text{Hydrocarbon} + \text{oxidizing agent} \rightarrow {}^3\mathrm{P}' + \text{other products} \tag{8a}$$

$${}^3\mathrm{P}' + {}^1\mathrm{A} \xrightarrow{k_{\mathrm{PA}}} {}^1\mathrm{P} + {}^1\mathrm{A}' \tag{8b}$$

$${}^1\mathrm{A}' \xrightarrow{k_{1,1}} {}^1\mathrm{A} + h\nu_f \tag{8c}$$

$$\xrightarrow{k_{1,3}} {}^3\mathrm{A}', \xrightarrow{k_{3,1}} {}^1\mathrm{A} + h\nu_p \tag{8d}$$

The presuperscripts 1 and 3 denote singlet and triplet states, respectively, and the primes denote electronic excitation. Thus, within the framework of this model, the observed TCL should be due to the fluorescence ν_f

and/or phosphorescence ν_p of acceptor materials. According to Vassil'ev, spin orbit coupling is the mechanism leading to a measurable intermolecular energy transfer rate k_{PA}. He expressed the problem in the language of quantum mechanics and predicted that k_{PA} should be a monotonic increasing function of the number and mass of substituent halogens since such substituents strengthen the spin orbit interaction and increase the triplet character. His prediction is borne out for a number of substituted anthracenes and k_{PA}(9,10-dibromoanthracene) $\approx 10^3 \times k_{PA}$(9,10-diphenylanthracene).

Since this study was carried out we have become aware of the studies of Chandross and Sonntag[13] which pertain to chemiluminescence reactions in solutions and presumably involve only the abstraction of electrons from negative aromatic radical ions by suitable oxidizing agents (O.A.). Most of their reported work pertains to reactions which evolve the fluorescence of 9,10-diphenylanthracene ($A\phi_2$) although they also have mentioned some other emitters. In highly condensed form, their observations and interpretations may be expressed as in eqs. (9)–(11)

$$A\phi_2 + \text{potassium} + \text{THF} \xrightarrow{\text{Boil}} K^+A\phi_2^- + \ldots \tag{9}$$

$$A\phi_2Cl_2 + 2A\phi_2^- \rightarrow 2A\phi_2 + A\phi_2^* + 2Cl^- \tag{10a}$$

$$A\phi_2^* \rightarrow A\phi_2 + h\nu_f \tag{10b}$$

$$\text{O.A.} + A\phi_2^- \xrightarrow{\text{Dioxane}} {}^1(A\phi_2)^* \rightarrow {}^1(A\phi_2) + h\nu_f \tag{11}$$

where O.A. represents benzoyl peroxide, oxalyl chloride, mercuric chloride, aluminum chloride, and Cl_2. Equation (10) may be considered a special case of eq. (11). The emission spectrum was judged to be the same in each case. It appears from a comparison of eq. (8) with eqs. (10) and (11) that the fundamental processes are really not the same although they are related. [Note that the A of eq. (8) may be equivalent to ACl_2, $A\phi_2$, etc. of eqs. (9)–(11).] In the experiments of Chandross and Sonntag,[13] the

TABLE III
Phosphorescence Pulse Height versus Temperature for PC[a]

Temperature T, °K.	I/I_0
80	~1
100	0.99
120	0.97
140	0.87
160	0.67
180	0.42
200	0.33
220	0.24
240	0.12
260	0.08

[a] Pulse height denotes the height of the "saw tooth" of Figure 2.

negative ions of the luminescent molecules are directly involved in the activating reaction, whereas in Vassil'ev's observations the energy of the oxidation reaction first excites a hydrocarbon intermediary from which energy transfer to unionized ACl_2, $A\phi_2$, etc. must occur. It may be that neither type of these processes is involved in our observations, but the Vassil'ev[12] model seems the most promising.

Table III gives data for pulse height at λ-452 nm. versus temperature. The observed decrease in I/I_0 is thought to be due mainly to a decrease in lifetime $\tau = t/\ln (I_0/I)$ as may be inferred from the schematic data of Figure 2. At 80°K., $\tau \approx 1.8$ sec., and there appears to be a dependence on λ. TCL spectra of PP are shown in Figure 8. These curves should be compared with Figure 5. The variation in spectral shape with increasing temperature may indicate the presence of two competing TCL reactions, or it may merely reflect the changing surface character of the polymer as it oxidizes. We favor the idea of two reactions, however, as Schard and Russell[4] show small differences in PP can affect the luminous process.

In summary, methods for obtaining and analyzing TCL data have been discussed. The fact that TCL spectra as shown in Figures 5 and 8 appear to be time- and temperature-dependent leads to the possibility that the method may eventually become a tool of utility comparable with TGA.

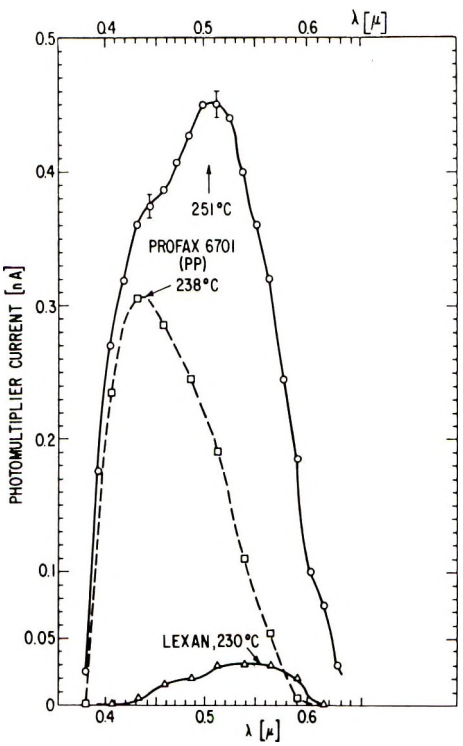

Fig. 8. TCL spectra taken with the use of Zeiss filter. The two upper curves correspond to points (*1*) and (*2*) on Figure 5. An 8-mm. salt was used, corresponding to a band width of 210 A.

The authors wish to acknowledge helpful discussions with Dr. E. E. Bostick, Dr. F. F. Holub, Mr. E. J. Lawton, Dr. D. T. F. Marple, Mr. R. H. Savage, and Dr. A. G. Tweet, and to thank Miss D. V. McClung for obtaining the absorption spectra.

References

1. Ashby, G. E., *J. Polymer Sci.*, **50,** 99 (1961).
2. Vassil'ev, R. F., and A. A. Vichutinskiĭ, *Nature*, **194,** 1276 (1962); F. R. Vassil'ev, *Nature*, **196,** 668 (1962).
3. Stauff, J., H. Schmidkunz, and G. Hartmann, *Nature*, **198,** 281 (1963).
4. Schard, M. P., and C. A. Russell, *J. Appl. Polymer Sci.*, **8,** 985 (1964).
5. Schard, M. P., and C. A. Russell, *J. Appl. Polymer Sci.*, **8,** 996 (1964).
6. Rysavy, D., L. Balaban, V. Slavik, and J. Ruza, *Polymer Sci. U.S.S.R.*, **3,** 855 (1963).
7. Stivala, S. S., L. Reich, and P. G. Kelleher, *Makromol. Chem.*, **59,** 28 (1963).
8. Lee, L. H., *J. Polymer Sci.*, **A2,** 2856 (1964).
9. Goldblum, K. B., Chemical Materials Dept., General Electric Co., private communication.
10. Williams, F. E., and H. Eyring, *J. Chem. Phys.*, **15,** 289 (1947).
11. Woodberry, H. A., H. Eyring, and A. F. Gabrysh, *J. Phys. Chem.*, **66,** 551 (1963).
12. Vassil'ev, R. F., *Nature*, **200,** 773 (1963).
13. Chandross, E. A., and F. I. Sonntag, *J. Am. Chem. Soc.*, **86,** 3179 (1964).
14. Madorsky, S. L., *J. Res. Natl. Bur. Std.*, **62,** 219 (1959); S. D. Bruck, *Polymer*, **5,** 435 (1964).

Résumé

On discute d'une façon générale des techniques expérimentales employées pour observer la thermochimiluminescence totale et spectrale (TCL) ainsi que de certaine résultats obtenus avec les systèmes polycarbonate–O_2, PC–CO, et polypropylène–O_2. Puisque la TCl est le processus par lequel des matériaux chauffés subissent des réactions activées thermiquement et émettent de la lumière en excès suivant la quantité prévue par la loi de radiation des corps noirs, on peut s'attendre à ce que l'étude de la thermochimiluminescence fournisse des informations au sujet de la structure et de la dégradation des matériaux étudiés. On a observé que les spectres de TCL dépendent du temps et de la température. On discute d'un modèle mathématique simple pour analyser les résultats obtenus lors d'une vitesse de chauffage linéaire. Le résultat obtenu peut également être employé pour l'analyse thermogravimétrique.

Zusammenfassung

Versuchsmethoden zur Beobachtung der totalen und spektralen Thermochemiluminiszenz (TCL) werden im allgemeinen an Hand einiger Daten für die Systeme Polycarbonate–O_2, PC–CO und Polypropylen–O_2 diskutiert. Da TCL der Vorgang ist, durch welchen erhitzte Stoffe thermisch aktivierte Reaktionen eingehen und Licht im Überschuss über die durch die durch das Gesetz des schwarzen Strahles vorgeschriebene Mente emittieren, kann man erwarten, dass ihre Untersuchung Informationen über die Struktur und den Abbau der Stoffe liefert. Es wurde beobachtet, dass TCL-Spektren sowohl zeit- als auch temperaturabhängig sind. Ein einfaches mathematisches Modell zur Analyse von TCL-Daten unter linearen Erhitzungsbedingungen wird diskutiert. Das Ergebnis sollte auch bei thermogravimetrischer Analyse verwendbar sein.

Received August 20, 1964
Revised December 7, 1964
(Prod. No. 4591A)

JOURNAL OF POLYMER SCIENCE: PART A VOL. 3, PP. 2047–2054 (1965)

Ethylene–Propylene Copolymers. I. Monomer Reactivity Ratios

R. D. BUSHICK, *Research and Development Division, Sun Oil Company, Marcus Hook, Pennsylvania*

Synopsis

The copolymerization of ethylene and propylene with diisobutylaluminum chloride and various vanadium-containing compounds gave a series of reactivity ratio values for ethylene which decreased in the order: $VO(O\text{-}n\text{-}Bu)_3 > VOCl(OEt)_2 > VOCl_2OEt > VO(OEt)_3 \simeq VOCl_3$. All of the catalyst systems were extremely sensitive to changes in the ethylene feed concentration. The reactivity ratio product suggested a random arrangement of monomer units with each catalyst system except $VOCl_3$.

INTRODUCTION

The copolymerization of two monomers such as ethylene and propylene has received a great deal of attention during the past several years, especially after the development of homogeneous coordination catalyst systems. Much of the interest in such elastomeric copolymers was stimulated by their chemical and physical properties.

Several types of soluble catalyst systems are described in the literature. One of the first consisted of a trialkylaluminum or an alkylaluminum halide with vanadium oxytrichloride or vanadium tetrachloride.[1–5] Amorphous copolymers of ethylene and propylene containing 30–60% ethylene were reported to have been obtained by use of these systems. Another consists of dialkylaluminum halides with esters or halogenated esters of orthovanadic acid[6,7] and with vanadium acetylacetonate.[8] These systems likewise are reported to produce amorphous copolymers of ethylene and propylene with an ethylene content as high as 70–80%. Phillips and Carrick[9] prepared crystalline copolymers of low propylene content from a catalyst system composed of tetraphenyltin, aluminum bromide, vanadium tetrachloride, and small amounts of oxygen. The latter author has also polymerized ethylene[10] using an alkyl aluminum halide and vanadium pentoxide which was made hydrocarbon-soluble by adding a small amount of an aluminum halide. The above type of vanadium coordination catalysts used for ethylene–propylene copolymerization are less stereospecific than those used for polyethylene or isotactic polypropylene and often may lack stereospecific character completely.

The present work was undertaken to obtain a better understanding of the behavior of ethylene and propylene in the presence of various soluble

catalyst systems. Only the vanadium component was changed, and the resulting copolymers were analyzed to determine the effect of changes in the catalyst system on polymer composition. The polymerization was accomplished in the laboratory by copolymerizing a number of monomer mixtures over a large mole fraction range and evaluating the data by means of the well known copolymer composition equation.

EXPERIMENTAL

Materials

The *n*-heptane (Phillips, 99% min.) was distilled from sodium metal and stored under nitrogen pressure in quart crown cap bottles fitted with a rubber puncture disk. The water content was 4 ppm or less.

The vanadium compounds were purchased from Anderson Chemical Company and were used as dilute solutions after first being purified by vacuum distillation.

Diisobutylaluminum chloride was purchased from Texas Alkyls, Inc. and was used as a dilute solution (25% by volume) without further purification.

The ethylene and propylene were polymerization-grade materials obtained from Sun Olin and Sun Oil Co., respectively. The ethylene was 99.9% pure with a typical analysis of 8 ppm oxygen, 3 ppm nitrogen, <5 ppm each for carbon monoxide, carbon dioxide, methane, and ethane, 3 ppm nitrogen, and 3–4 ppm hydrogen. The propylene contained <1 ppm methane, <20 ppm ethane, <1 ppm COS, and 10 ppm water.

Polymerization

The feed mix was prepared by premixing ethylene and propylene in the desired proportions in LPG cylinders. The composition was determined by gas chromatography after the mixture was allowed to equilibrate for at least twelve hours. Any residual contamination by oxygen or water was removed by bubbling the ethylene–propylene feed through a scrubber, which contained 250 g. of triisobutylaluminum and 1700 ml. of mineral oil.

All glassware was scrupulously cleaned and dried in an electric furnace before use. The apparatus was assembled and allowed to cool to room temperature under a nitrogen atmosphere. Transfer of the solvent from crown cap storage bottles was accomplished by means of a stainless steel tube ($^1/_4$ in. diameter) fitted with a hypodermic needle on each end and a Hoke valve in the center. The solvent was pressured into the flask and purged with nitrogen, while stirring was continued. The nitrogen flow was replaced with the appropriate ethylene–propylene feed, the solvent was saturated, and a sample was removed by means of a hypodermic syringe and analyzed at room temperature by gas chromatography. A

6-ft. column with 15% SF-96 on Chromosorb W was used. A plot of the mole ratio of propylene to ethylene in the liquid phase versus the mole ratio of propylene to ethylene in the gas phase served as a check on the analytical data and was used to compute new values where necessary for the composition of the liquid phase. The solubility data for ethylene and propylene in heptane are also available in the literature.[11]

The apparatus used for all the polymerization reactions consisted of a one-liter, three-necked Morton flask with a serum fitting, high-speed stirrer, thermometer, gas inlet, and gas outlet tube. The flask was suspended in a mineral oil bath which was maintained at 30°C. by means of a Roto-stat thermoregulator and a Fisher transistor control unit. An open-flask polymerization technique was employed whereby the feed gas was introduced under the solvent at a very high space velocity. This is necessary to maintain steady-state conditions throughout the polymerization reaction; otherwise, the supply of the more reactive monomer in the vapor space would be decreased substantially during the polymerization reaction, and the end result would be a drift in the copolymer composition. The excess feed was passed from the reaction vessel through a mercury bubbler into a 500-ml. flask that served both as a gas reservoir and to prevent air from being drawn back into the system during the onset of the polymerization reaction. The reservoir, in turn, was vented to the atmosphere.

The catalyst was added to the reaction flask by way of hypodermic syringes through a rubber serum cap, and the concentration of the reducing agent was always tenfold greater than that of the transition metal component. The catalyst components were handled as dilute solutions. A small exotherm resulted when the polymerization reaction was initiated. This peak temperature (33°C.) could be easily maintained throughout the duration of the polymerization reaction, since the polymerization time was short and the conversion low, usually 10% or less.

The polymerization was terminated by adding two milliliters of an isopropanol–citric acid solution to the reaction flask. The copolymer formed was completely soluble in the solvent; the only exception being a small amount of gel (usually $<<0.1$ g.) which resulted when the feed gas contained a very high concentration of ethylene. The solution was filtered through cheesecloth into 2 liters of a 60/40 acetone–methanol mixture. The coagulated polymer was further washed with acetone, cut into small pieces, and dried in a vacuum oven at 80°C. for 60–90 min.

Infrared Analysis

The methyl to methylene ratio was determined by measuring the 2950 and 2853 cm.$^{-1}$ absorption bands with a Perkin-Elmer Model 221 spectrometer. Samples were made by pressing, between salt plates, a thin film of the copolymer which was previously swelled with carbon tetrachloride. Polyethylene and atactic polypropylene were used as reference materials for calibrating the system.

RESULTS AND DISCUSSION

The copolymerization of two monomers can be adequately described by four propagation steps which constitute the basis for the development of the well known copolymer composition equation.[12] The Fineman and Ross[13] modification, expressed as eq. (1), was used to evaluate all of the copolymerization

$$F/f(f - 1) = r_1 F^2/f - r_2 \quad (1)$$

data obtained in this investigation (Table I). A plot with F^2/f as the abscissa and $F/f(f - 1)$ as the ordinate gave a linear correlation for each catalyst system examined, with a slope of r_2 and an intercept of $-r_1$, as illustrated in Figure 1. A common type of plot (Fig. 2) of the mole fraction M_2 of M_2 in the feed versus the mole fraction m_2 of M_2 in the copolymer gives a set of curves showing how each of the catalyst systems differ in activity. All of the curves are characteristic of ionic copolymerization systems. The reactivity ratio value for ethylene was found to decrease in the order: $VO(O\text{-}n\text{-}Bu)_3 > VOCl(OEt)_2 > VOCl_2(OEt) > VO(OEt)_3 \simeq VOCl_3$. Although the ethylene content of the copolymer prepared from a catalyst system in which a trialkyl vanadate was the vanadium component was higher than with other systems, the rate of the polymerization was definitely lower. Vanadium compounds containing halogen(s) were more active by a factor of two in the polymerization systems used.[7]

The reactivity ratio products for the systems examined are shown in Table II together with results that have appeared in the literature. This study is thought to be the first published systematic investigation of the vanadium systems mentioned with diisobutylaluminum chloride. Like

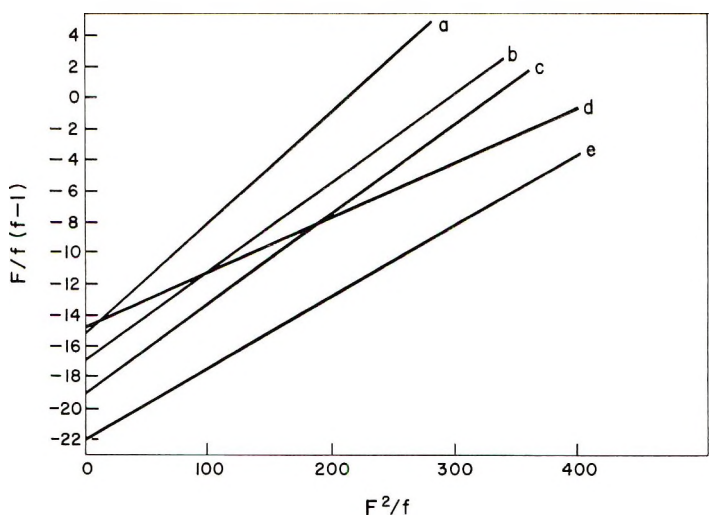

Fig. 1. Fineman-Ross treatment of data for diisobutylaluminum chloride and (*a*) $VO(OEt)_3$, (*b*) $VOCl(OEt)_2$, (*c*) $VOCl_2(OEt)$, (*d*) $VOCl_3$, and (*e*) $VO(O\text{-}n\text{-}Bu)_3$.

TABLE I
Copolymerization of Ethylene and Propylene with Various Catalyst Systems

Catalyst system	Run no.	Feed $M_{C_2H_4}$	Co-polymer $m_{C_2H_4}$	F	f
$VO(O\text{-}n\text{-}Bu)_3$–$Al(i\text{-}C_4H_9)_2Cl$	1	0.053	0.51	21.20	0.962
	2	0.060	0.58	15.80	0.725
	3	0.065	0.60	14.25	0.666
	4	0.089	0.67	10.21	0.493
	5	0.095	0.69	9.53	0.450
	6	0.104	0.72	8.66	0.389
	7	0.105	0.72	8.52	0.389
	8	0.125	0.76	7.00	0.316
	9	0.151	0.80	5.62	0.250
	10	0.198	0.85	4.05	0.176
$VOCl(OEt)_2$–$Al(i\text{-}C_4H_9)_2Cl$	1	0.061	0.52	15.50	0.923
	2	0.072	0.58	12.89	0.724
	3	0.091	0.66	10.00	0.515
	4	0.094	0.67	9.65	0.491
	5	0.099	0.68	9.10	0.470
	6	0.110	0.67	8.10	0.491
	7	0.111	0.70	8.00	0.429
	8	0.116	0.71	7.62	0.408
	9	0.166	0.78	5.04	0.282
	10	0.213	0.85	3.70	0.177
	11	0.221	0.84	3.63	0.191
$VOCl_2(OEt)$–$Al(i\text{-}C_4H_9)_2Cl$	1	0.069	0.55	13.50	0.818
	2	0.091	0.63	9.95	0.587
	3	0.099	0.65	9.10	0.538
	4	0.103	0.67	8.75	0.492
	5	0.158	0.76	5.33	0.282
	6	0.151	0.78	5.65	0.316
	7	0.176	0.80	4.68	0.250
	8	0.189	0.79	4.30	0.266
$VO(OEt)_3$–$Al(i\text{-}C_4H_9)_2Cl$	1	0.076	0.54	12.23	0.852
	2	0.089	0.60	10.14	0.666
	3	0.104	0.63	8.60	0.586
	4	0.108	0.62	8.26	0.613
	5	0.137	0.705	6.30	0.418
	6	0.154	0.72	5.50	0.389
	7	0.192	0.83	4.20	0.205
	8	0.212	0.80	3.72	0.250
	9	0.215	0.81	3.65	0.235
$VOCl_3$–$Al(i\text{-}C_4H_9)_2Cl$	1	0.032	0.42	30.25	1.380
	2	0.032	0.41	30.20	1.440
	3	0.051	0.50	18.60	1.000
	4	0.068	0.55	13.70	0.820
	5	0.079	0.60	11.67	0.666
	6	0.070	0.59	13.08	0.660
	7	0.070	0.69	13.32	0.450
	8	0.115	0.70	7.70	0.429
	9	0.125	0.71	7.00	0.408
	10	0.127	0.71	6.87	0.409
	11	0.121	0.70	7.26	0.430
	12	0.134	0.72	6.46	0.389

most of the other systems investigated during the last few years, those covered in this work (with the exception of vanadium oxytrichloride) have reactivity ratio products near unity, suggestive of a random arrangement of monomer units in the polymer chain. The value of 0.55 for the $VOCl_3$ system indicates that the alternating tendency is slightly greater than for a perfectly random copolymerization. The fact that one can indeed obtain a random arrangement even though the reactivity ratio product is less than unity implies that the reactivity ratios themselves may be in error. The above value is close to that obtained for both the VCl_4–$Al(C_6H_{13})_3$ and

TABLE II
Reactivity Ratio Values for Copolymers of Ethylene and Propylene Prepared with Soluble Catalyst Systems

System	$r_{C_2H_4}$	$r_{C_3H_6}$	$r_{C_2H_4}r_{C_3H_6}$
$VO(O\text{-}n\text{-}Bu)_3$–$Al(i\text{-}C_4H_9)_2Cl$[a]	22.00	0.046	1.01
$VOCl(OEt)_2$–$Al(i\text{-}C_4H_9)_2Cl$[a]	18.90	0.056	1.06
$VOCl_2OEt$–$Al(i\text{-}C_4H_9)_2Cl$[a]	16.80	0.055	0.93
$VO(OEt)_3$–$Al(i\text{-}C_4H_9)_2Cl$[a]	15.00	0.070	1.04
$VOCl_3$–$Al(i\text{-}C_4H_9)_2Cl$[a]	14.80	0.037	0.55
VCl_4–$Al(n\text{-}C_6H_{13})_3$[b]	7.08	0.088	0.68
$VOCl_3$–AlR_3, AlR_2Cl[c,d]	26.00	0.040	1.04
$VOCl_3$–$Al(i\text{-}C_4H_9)_3$[c]	28.00	—	—
$VOCl_3$–$Al(n\text{-}C_6H_{13})_3$[f]	17.95	0.065	1.15
$VOCl_2OR$–$Al(C_2H_5)Cl_2$[g]	17.50	0.050	0.88
$VO(OR)_3$–$Al(C_2H_5)Cl_2$[h,d]	26.00	0.040	1.04
VAc_3–$Al(C_2H_5)Cl_2$[i]	15.00	0.040	0.60

[a] Present work.
[b] Data of Mazzanti et al.[2]
[c] Data of Lukach et al.[3]
[d] Systems determined by converting gas-phase data through solubility parameters to obtain reactivity ratio values in the liquid phase.
[e] Calculated value from data of Karol and Carrick.[14]
[f] Data of Mazzanti et al.[1]
[g] Data of Bier.[15]
[h] Data of Lukach et al.[7]
[i] Data of Natta et al.[8]

VAc_3–$Al(C_2H_5)_2Cl$ systems (Table II). Although their respective reactivity ratio products are less than unity, the polymers formed are believed to be of the random type.[16] An infrared study of the structure of copolymers of ethylene and propylene supports the above view.[17–19]

Errors[20] for the first and fifth catalyst systems shown in Table II were of the order of ± 0.60 and ± 0.006 for $r_{C_2S_4}$ and $r_{C_3H_6}$, respectively, as determined from an r_1 versus r_2 plot. We can assume that the magnitude of the errors involved with the other catalyst systems will be of the same order. A comparison between the copolymer composition calculated from the copolymer composition equation and that determined by infrared is in good agreement and is a reflection of the accuracy of the experimental work.

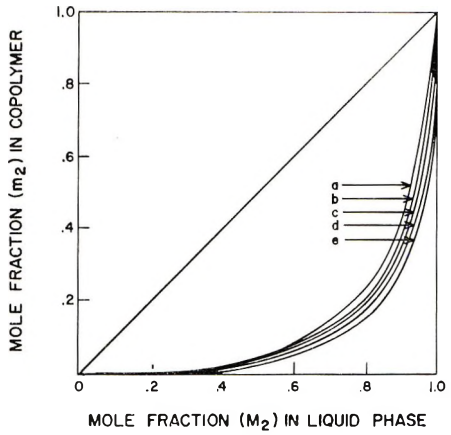

Fig. 2. Mole fraction plot for diisobutylaluminum chloride with (*a*) $VOCl_3$, (*b*) $VO(OEt)_3$, (*c*) $VOCl_2OEt$, (*d*) $VOCl(OEt)_2$, and (*e*) $VO(O\text{-}n\text{-}Bu)_3$.

The composition of the copolymers changed noticeably with that of the gaseous feed and all catalyst systems studied were found to be extremely sensitive to changes in the ethylene concentration. This is the result of actually working along the steep portion of the mole fraction curves in Figure 2.

A comparison of the monomer sequence distribution for the catalyst systems mentioned in this work will be the subject of a later publication.

The author wishes to thank Mrs. A. Donnell and Mr. R. W. King and those in their respective groups for the analysis of copolymer samples. He is also grateful to Sun Oil Company for permission to publish this work.

References

1. Mazzanti, G., A. Valvassori, and G. Pajaro, *Chim. Ind. (Milan)*, **39**, 743 (1957).
2. Mazzanti, G., A. Valvassori, and G. Pajaro, *Chim. Ind. (Milan)*, **39**, 825 (1957).
3. Lukach, C. A., H. M. Spurlin, and S. G. Olsen (to Hercules Powder Co.), Belg. Pat. 583,040 (1959).
4. Kelly, R. J., H. K. Garner, H. E. Haxo, and W. R. Bingham, *Ind. Eng. Chem. Prod. Res. Develop.*, **1**, 210 (1962).
5. Junghanns, E., A. Gumboldt, and G. Bier, *Makromol. Chem.*, **58**, 18 (1962).
6. Belg. Pat. 588,764 (to Farbewerke Hoechst) 1959.
7. Lukach, C. A., S. G. Olsen, and H. M. Spurlin (to Hercules Powder Co.), Belg. Pat. 583,039 (1959).
8. Natta, G., B. Mazzanti, A. Valvassori, G. Sartori, and D. Fiumani, *J. Polymer Sci.*, **51**, 411 (1961).
9. Phillips, G. W., and W. L. Carrick, *J. Am. Chem. Soc.*, **84**, 920 (1962).
10. Kluiber, R. W., and W. L. Carrick (to Union Carbide Corp.), U. S. Pat. 3,073,209 (1963).
11. Sherwood, T. K., and R. L. Pigford, *Absorption and Extraction*, McGraw-Hill, New York, 1952.
12. Alfrey, T., J. J. Bohrer, and H. Mark, *Copolymerization*, Vol. VIII of High Polymer Series, Interscience, New York, 1952.
13. Fineman, M., and S. D. Ross, *J. Polymer Sci.*, **5**, 269 (1950).

14. Karol, F. J., and W. L. Carrick, *J. Am. Chem. Soc.*, **83**, 2654 (1961).
15. Bier, G., *Angew. Chem.*, **73**, 186 (1961).
16. Natta, G., G. Mazzanti, A. Valvassori, G. Sartori, and D. Moreno, *Chim. Ind. (Milan)*, **42**, 125 (1960).
17. Veerkamp, T. A., and A. Veermans, *Makromol. Chem.*, **50**, 147 (1961).
18. van Schooten, J., E. W. Duck, and R. Berkenbosck, *Polymer*, **4**, 135 (1963).
19. van Schooten, J., E. W. Duck, and R. Berkenbosck, *Polymer*, **2**, 357 (1961).
20. Mayo, F. R., and C. Walling, *Chem. Rev.*, **46**, 191 (1950).

Résumé

La copolymérisation de l'éthylène et du propylène à l'aide de chlorure de diisobutylaluminium et de différents composés contenant du vanadium, donne pour l'éthylène, une série de valeurs du rapport de réactivité, qui diminue dans l'ordre: $VO\text{-}n\text{-}Bu)_3 > VOCl(OEt)_2 > VOCl_2OEt > VO(OEt)_3 \simeq VOCl_3$. Tous les systèmes catalytiques sont extrèmement sensibles aux changements de concentration en éthylène monomère. Le produit du rapport des réactivités suggère un arrangement statistique des unités monomériques avec chaque système catalytique, à l'exception de $VOCl_3$.

Zusammenfassung

Die Copolymerisation von Äthylen und Propylen mit Diisobutylaluminiumchlorid und verschiedenen vanadiumhaltigen Verbindungen lieferte eine Reihe von Reaktivitätsverhältnissen für Äthylen, welche in der Reihenfolge $VO(O\text{-}n\text{-}Bu)_3 > VOCl(OEt)_2 > VOCl_2 > VO(OEt)_3 \simeq VOCl_3$ abnahmen. Alle Katalysatorsysteme waren gegen Anderungen der Äthylenkoz entration im Polymerisationsansatz extrem empfindlich. Das Produkt der Reaktivitätsverhältnisse sprach bei jedem Katalysatorsystem mit Ausnahme von $VOCl_3$ für eine statistische Anordnung der Monomerbausteine.

Received August 20, 1964
Revised November 25, 1964
(Prod. No. 4580A)

JOURNAL OF POLYMER SCIENCE: PART A VOL. 3, PP. 2055–2061 (1965)

Synthesis of Vinylphosphonium Compounds

ROBERT RABINOWITZ, ARTHUR C. HENRY, and RUTH MARCUS,
Chemical Department, Central Research Division, American Cyanamid Company, Stamford, Connecticut

Synopsis

Tributylvinylphosphonium bromide has been prepared by sodium carbonate dehydrobromination of the 2-bromoethyl salt resultant from the reaction of tributylphosphine and dibromoethane. Tributylvinylphosphonium chloride was prepared from the bromide by ion exchange. Triethylvinylphosphonium bromide, tricyclohexylvinylphosphonium bromide, and dimethylphenylvinylphosphonium bromide were prepared by sodium carbonate treatment of the acetate resulting from acetic anhydride acetylation of the salt formed from the reaction of ethylenebromohydrin and the corresponding phosphine. An attempt to prepare a vinylphosphonium salt directly by heating vinyl bromide and tributylphosphine at 160°C. in an autoclave gave no isolable product; however, infrared evidence indicated the possible presence of the expected vinylphosphonium salt.

INTRODUCTION

The discovery that tributylvinylphosphonium bromide (TBVPB) is converted to a high molecular weight polymer upon irradiation of its aqueous solutions[1] was quite unexpected. Although vinylphosphonium salts have been known for more than a century,[2] no preparative work has been reported since this initial study. It was the purpose of this investigation to devise a convenient route to TBVPB as well as to prepare several other vinylphosphonium salts so that the scope of the discovery could be measured.

EXPERIMENTAL

Materials

Tributylphosphine was obtained from the Food Machinery Corp. (no longer available). It was distilled prior to use to insure the absence of the oxide. Phenyldichlorophosphine was obtained from the Victor Chemical Co. and was distilled prior to use. Methyl iodide, ethyl bromide, 1,2-dibromoethane, cyclohexyl bromide and chloride, ethylene bromohydrin, and dioxane were Eastman White Label grade. The chlorobenzene, carbon disulfide, acetic anhydride, sodium carbonate, acetonitrile, and phosphorus trichloride were reagent grade. Vinyl bromide was obtained from Columbia Organic Chemicals Co., Inc.

Preparation of Tributylvinylphosphonium Bromide

2-Bromoethyltributylphosphonium Bromide. To 300 ml. (650 g., 2.95 moles) of 1,2-dibromoethane in a three-necked flask equipped with a condenser ($CaCl_2$ trap), thermometer, nitrogen inlet, and mechanical stirrer was added 33 g. (0.164 mole) of tributylphosphine during a 1-hr. period at 55°C. The excess 1,2-dibromoethane was removed *in vacuo*, and the 63.7 g. residue was treated with 200 ml. of boiling chlorobenzene. (Addition of boiling chlorobenzene to the residue rather than addition of cold chlorobenzene and heating of the mixture to boiling is imperative.) The residue flask was washed immediately with several small portions of boiling chlorobenzene until quantitative transfer was made. The resultant solution was refluxed for 1 min. in the presence of a small amount of anhydrous magnesium sulfate and filtered. The filtrate, upon cooling, deposited a voluminous amount of crystals. These were collected under nitrogen and washed with ether; a yield of 45.5 g. (71.6%), m.p. ~75°C. was obtained.

ANAL. Calculated for $C_{10}H_{22}PBr_2$: C, 43.15%; H, 7.44%; P, 7.92%; Br, 40.9%. Found: C, 43.1%; H, 7.95%; P, 7.92%; Br, 40.9%.

Tributylvinylphosphonium Bromide. A solution of 45.5 g. (0.112 mole) of 2-bromoethyltributylphosphonium bromide in 450 ml. of fresh (EWL) dioxane containing 49.2 g. (0.42 mole) of sodium carbonate was heated at reflux for 4 hr. under nitrogen. A mechanical stirrer was in operation throughout. The hot solution was filtered to separate the inorganic salts. Upon cooling crystallization occurred. The crystals were collected and washed with 150 ml. of boiling dioxane. Another crop was obtained upon concentration of the mother liquor. The combined crops were dried in a vacuum oven at room temperature for 1 hr. The total yield was 29.2 g. (102%), m.p. 150–152°C.

A successful scale-up of the above procedure to convert tributylphosphine to TBVPB was carried out. The reaction was run at sevenfold the level described and an overall yield of 55% was obtained.

Attempted Preparation of TBVPB by Reacting Tributylphosphine with Vinyl Bromide

Tributylphosphine (10 g.) in 50 ml. of acetonitrile was reacted with 110 g. of vinyl bromide in an autoclave at 150°C. for 6 hr. All attempts to isolate any TBVPB from the reddish-brown liquid reaction mixture were unsuccessful, although the infrared spectrum of the reaction mixture after removal of the volatiles indicated the possibility of the presence of some TBVPB.

Preparation of Tributylvinylphosphonium Chloride

Direct Exchange between TBVPB and Excess NaCl. To a solution of 106 g. (1.82 mole) of sodium chloride in 106 g. of water was added 3.2 g. (0.012 mole) of TBVPB. The water was evaporated *in vacuo* and the

crystalline residue heated in 125 ml. of boiling acetonitrile. The acetonitrile was stripped off leaving a white solid, 2.2 g., m.p. 147–149°C.

ANAL. Calculated for $C_{14}H_{30}PCl$: C, 63.8%; H, 11.4%; P, 11.75%; Cl, 13.4%. Found: C, 59.32, 58.82%; H, 10.01, 9.95%; P, 11.68, 11.21%; Cl, 10.02%; Br, 6.30%.

Exchange between TBVPB and Dowex-1 Anion-Exchange Resin. Approximately 1.5 lb. of Dowex-1 anion-exchange resin was conditioned as follows: 3.5 l. of 1*M* HCl was passed through followed by water washing until neutral to Hydrion paper, 3.5 l. of 1*M* NaOH was passed through followed by water washing until neutral to Hydrion, 7.0 l. of 1*M* HCl was passed through, followed by water to neutral, then 3 l. of acetone was passed through, and finally the column was re-equilibrated with water. A solution of 20 g. of TBVPB in 100 ml. of water was put on the column and the rate of flow adjusted to 2 ml./min. Periodically the effluent was tested with silver nitrate for chloride ion. The solution was collected at the first sign of cloudiness and continued until the effluent gave only a cloudiness (rather than a curdy precipitate) with silver nitrate. A total of 1.5 l. was collected. This was evaporated, leaving 16.6 g. of crystalline product, m.p. 158–164°C., containing 0.5% Br. The column was reactivated by passing through 7.0 l. of 1*M* HCl followed by water washing until neutral. The entire 16.6 g. was passed through as before and the effluent evaporated leaving a 15 g. residue. This was recrystallized four times from boiling dioxane (80–100 ml.), and finally colorless crystals were obtained, 8.6 g. (50%), m.p. 164–166°C.

ANAL. Calculated for $C_{14}H_{30}PCl$: C, 63.8%; H, 11.4%; P, 11.75%; Cl, 13.4%. Found: C, 63.53%; H, 11.70%; P, 11.82%; Cl, 13.68%; Br, 0.10%.

Preparation of Triethylvinylphosphonium Bromide

Ethylmagnesium Bromide. A solution of 327 g. (3.0 mole) of ethyl bromide in 1.2 l. of ether was slowly added to 72.9 g. (3.0 g.-atom) of magnesium at such a rate so as to maintain a gentle reflux. External cooling was necessary initially, and stirring was continued until only a small amount of magnesium remained. This solution was used directly in the next step.

Triethylphosphine. Into the Grignard solution was added dropwise 137.4 g. (1.01 mole) of phosphorus trichloride in 255 ml. of ether while maintaining the temperature at 5°C. The addition required 2 hr. After completion of addition the mixture was allowed to warm to room temperature and the stirring continued for 3 hr. The greyish slurry was hydrolyzed by adding a solution of 120 g. of ammonium chloride in 720 ml. of water dropwise at 5–10°C. until no further heat was evolved, and then rapidly adding the remainder of the solution. Vigorous stirring was maintained until the material caked on the walls was removed. An emulsion mainly in the ether layer was present at this point. The mixture was put in a separatory funnel, the water drawn off, and the ether layer washed with

~3 l. of ether in small portions, leaving the emulsion behind in each case (the washings were continued until the carbon disulfide–phosphine test showed only a light pink color). The water layer was washed once with 400 ml. of ether and this extract combined with the main material. This was dried over sodium sulfate, concentrated, and distilled in a nitrogen atmosphere; 39.6 g. (24.5%) of triethylphosphine was obtained, b.p. 125°C.

Triethyl-2-hydroxyethylphosphonium Bromide. To a solution of 49 g. (0.39 mole) of ethylene bromohydrin in 76 ml. of dimethoxyethane (glyme) at 80–90°C. was added 41.3 g. (0.35 mole) of triethylphosphine. A nitrogen atmosphere was maintained throughout. During the addition a solid material started to separate. The mixture was stirred for 2 hr. at 85–90°C. and was then filtered; 81.2 g. (94%) of a white crystalline hydroscopic solid was obtained.

2-Acetoxyethyltriethylphosphonium Bromide. The 81.2 g. from the previous step was mixed with 115 ml. of acetic anhydride and refluxed for 3 hr. The solid dissolved during this period. The reaction mixture was evaporated to constant weight *in vacuo;* 103.4 g. of a yellowish oil was obtained.

Triethylvinylphosphonium Bromide. The 103.4 g. from the last step was mixed with 125 ml. of dioxane and 57.5 g. of sodium carbonate and heated at reflux while stirring for 4 hr. The solution was allowed to cool and the mixture extracted with acetonitrile. The extract was evaporated and a 54 g. residue was obtained. This was recrystallized from boiling dry dioxane containing a minimum of dry acetonitrile; 43.1 g. was obtained (55% based on the 2-hydroxyethyl compound), m.p. 253–256°C. The product was very hydroscopic and required dessicating.

ANAL. Calculated for $C_8H_{18}PBr$: C, 42.6%; H, 7.99%; P, 13.8%; Br, 35.5%. Found: C, 42.27%; H, 8.05%; P, 13.58%; Br, 35.48%.

Preparation of Tricyclohexylvinylphosphonium Bromide

The synthesis of this material parallels in many respects the synthesis of the triethyl compound and therefore will be described in general terms. Specific details will be given where necessary.

The Grignard reagent was prepared from either cyclohexyl chloride or bromide. When the former was used a trace of iodine or methyl iodide was required to start the reaction. In a typical case, 20.8 g. (0.86 g.-atom) of magnesium was allowed to react with 100 g. (0.84 mole) of cyclohexyl chloride. The Grignard reagent was subsequently treated with 36 g. (0.26 mole) of phosphorus trichloride. The emulsion which resulted from the hydrolysis was broken with aluminum sulfate. After drying the ether layer and concentrating to 200 ml., 17 ml. of carbon disulfide was added, and 32.5 g. of a red solid was isolated. The red solid was put into 150 ml. of absolute ethanol and the solution was boiled until all the red color disappeared. Upon cooling 20.5 g. (27.2% based on cyclohexyl chloride) of a white crystalline precipitate was isolated. The entire product was treated with 11.7 g. of ethylene bromohydrin in glyme. A total of 18.4 g. (69%)

of the 2-hydroxyethyl compound was obtained, m.p. 220–221°C. This was treated with acetic anhydride. After devolatilizing the reaction mixture, the product was isolated by trituration and washing with ether, 19.4 g. (96%). This was put into 15 ml. of pure dioxane containing 6.85 g. of sodium carbonate and refluxed for 4 hr. The hot solution was filtered and the product recovered by treating with filter cake with boiling acetonitrile until no more material was extracted. Upon cooling, white crystals formed in the acetonitrile. They were collected and recrystallized from dioxane–acetonitrile; m.p. >350°C.

ANAL. Calculated for $C_{20}H_{36}PBr$: C, 62.0%; H, 9.3%; P, 8.02%; Br, 20.65%. Found: C, 62.05%; H, 9.74%; P, 7.80%; Br, 20.66%.

Preparation of Dimethylphenylvinylphosphonium Bromide

Methylmagnesium bromide (3 mole) was prepared by a standard method.[3] To this was added dropwise 248.2 g. (1.39 mole) of phenyldichlorophosphine while maintaining the temperature at 10–15°C. After the addition was complete the reaction mixture was stirred for 1 hour without any external heating or cooling. The reaction mixture was cooled to 0°C., and a solution of 150 g. of ammonium chloride in 900 ml. of water was added very slowly while the temperature was maintained below 15°C. After about one-third of the ammonium chloride solution had been added the mixture caked up. Then 0.1 g. of diphenylamine was added, the solids broken up, and the remainder of the salt solution gradually added. The ether layer was separated, the water layer washed with ether, and the ether extracts combined and dried over sodium sulfate. The ether was stripped off and the yellow liquid residue distilled under nitrogen with the use of a silvered 1-ft., vacuum-jacketed Vigreaux column and a full reflux-partial take-off head; 88.1 g. (68%), b.p. 116°C./42 mm., was obtained.

ANAL. Calculated for $C_8H_{11}P$: C, 69.5%; H, 7.91%; P, 22.0%. Found: C, 69.2%; H, 7.91%; P, 22.5%.

The 2-hydroxyethyl compound was prepared as before by using 128.0 g. (0.93 mole) of the phosphine and 124 g. (0.99 mole) of ethylene bromohydrin in 190 ml. of glyme. A yield of 240 g. (98%) of product was obtained as a viscous colorless liquid which slowly crystallized. This was converted to the 2-acetoxyethyl compound by heating 235.3 g. (0.9 mole) of it with 275.4 g. (2.7 mole) of acetic anhydride at 115°C. for 4 hr. After vacuum stripping, 270.6 g. (99%) product was obtained. This entire amount was dissolved in 300 ml. of dioxane, and to the solution at 85°C. was slowly added 142 g. (1.33 mole) of sodium carbonate. The solution was heated at reflux for 5.5 hr. Then 500 ml. of acetonitrile was added at 82°C., the solution filtered, and upon cooling 109.7 g. of the product was isolated. Further work-up of the mother liquor resulted in a total yield of 190 g. (87%) of the dimethylphenylvinylphosphonium bromide. This was recrystallized by dissolving in dry acetonitrile, decolorizing with charcoal, drying over alumina, filtering, and adding hot hexane at the boiling point

until just cloudy. Upon cooling the purified product was isolated, m.p. 167–168°C.

ANAL. Calculated for $C_{10}H_{14}PBr$: C, 49.0%; H, 5.7%; P, 12.62%; Br, 32.5%. Found: C, 49.05%; H, 5.69%; P, 12.08%; Br, 32.33%.

RESULTS AND DISCUSSION

Five vinylphosphonium salts were prepared and characterized. The procedure used to prepare the tricyclohexyl-, triethyl-, and dimethylphenylvinylphosphonium salts were modifications of a route used in this laboratory to prepare tributylvinylphosphonium bromide:[4,5]

$$R_3P + BrCH_2CH_2OH \rightarrow [R_3\overset{+}{P}CH_2CH_2OH]Br^-$$

$$[R_3\overset{+}{P}CH_2CH_2OH]Br^- + \left(CH_3\overset{O}{\overset{\|}{C}}\right)_2O \rightarrow [R_3\overset{+}{P}CH_2CH_2O\overset{O}{\overset{\|}{C}}CH_3]Br^-$$

$$[R_3\overset{+}{P}CH_2CH_2O\overset{O}{\overset{\|}{C}}CH_3]Br^- \xrightarrow{Na_2CO_3} [R_3\overset{+}{P}CH{=}CH_2]Br^-$$

This procedure worked quite satisfactorily and undoubtedly could be adapted to the synthesis of a large variety of vinylphosphonium salts.

The preparation of tributylvinylphosphonium bromide was accomplished in 55–72% yield (based on tributylphosphine) by a very simple route:

$$Bu_3P + \text{excess } BrCH_2CH_2Br \rightarrow [Bu_3\overset{+}{P}CH_2CH_2Br]Br^-$$

$$[Bu_3\overset{+}{P}CH_2CH_2Br]Br^- \xrightarrow{Na_2CO_3} [Bu_3\overset{+}{P}CH{=}CH_2]Br^-$$

A very large excess of 1,2-dibromoethane is required to reduce to a minimum the formation of the ethylenebis(tributylphosphonium salt) (I), since

$$\underset{(II)}{Bu_3P + [Bu_3\overset{+}{P}CH_2CH_2Br]Br^-} \rightarrow \underset{(I)}{[Bu_3\overset{+}{P}CH_2CH_2\overset{+}{P}Bu_3]2Br^-}$$

bromide ion is probably more readily displaced from the 2-bromoethyltributylphosphonium bromide (II) than from 1,2-dibromoethane by the nucleophilic tributylphosphine. The satisfactory operation of this route was based on the separation of II from the initial reaction mixture in a reasonably pure form. When the initial reaction mixture, after removal of the excess 1,2-dibromoethane, was treated directly with Na_2CO_3, the tribuylvinylphosphonium bromide that was isolated was impure. It is likely that this procedure could be used for the preparation of other vinylphosphonium salts,* but no exploratory work along these lines was attempted because of the relative difficulty in preparing the purified phosphines.

Tributylvinylphosphonium chloride was prepared by passing the bromide through a Dowex-1 anion-exchange resin column in the chloride form. A

* Hoffmann[2] prepared triethylvinylphosphonium bromide by thermally dehydrobrominating the corresponding 2-bromoethyl compound.

much simpler procedure, mixing the bromide in a 150-fold excess of sodium chloride in aqueous solution, devolatilizing, and extracting the resultant crystalline material with boiling acetonitrile, failed. A much greater than statistical amount of phosphonium bromide appeared in the extract, probably as a result of a lower solubility of the bromide than the chloride in water.

The most direct route to a vinylphosphonium salt is the reaction of a vinyl halide with a tertiary phosphine. The low reactivity of vinyl halides towards nucleophilic displacement is well documented. Nevertheless it was felt that under suitable conditions a reaction should occur. Tributylphosphine was reacted with vinyl bromide at 150°C. in acetonitrile solution in an autoclave. Although no tributylvinylphosphonium bromide could be isolated from the reaction mixture, the infrared spectrum of the devolatilized reaction mixture indicated the possibility of its presence.

References

1. Pellon, J., and K. J. Valan, *Chem. Ind. (London)*, 1963, 1358.
2. Hoffmann, A. W., *Ann. (Suppl.)*, **1**, 145, 275 (1861).
3. *Organic Syntheses*, Vol. 28, Wiley, New York, 1948, p. 6.
4. Keough, P. T., and M. Grayson, *J. Org. Chem.*, **29**, 631 (1964), footnote 8.
5. Valan, K. J., Central Research Division, American Cyanamid Co., Stamford, Connecticut, unpublished results.

Résumé

On prépare le bromure de tributylvinylphosphonium par déshydrobromation au carbonate de sodium du sel de 2-bromoéthyle qui résulte de la réaction entre la tributylphosphine et le dibromoéthane. On prépare le chlorure de tributylvinylphosphonium au départ du bromure par échange d'ion. On prépare le bromure de diméthylphénylvinylphosphonium par traitement au carbonate de sodium de l'acétate formé par acétylation à l'anhydride acétique du sel formé au cours de la réaction entre la bromhydrine éthylique et la phosphine correspondante. Les essais de préparation du sel de vinylphosphonium par chauffage direct du bromure de vinyle et de tributylphosphine à 160°C en autoclave, ne donne aucun produit décelable; cependant l'analyse infra-rouge indique la présence possible du sel de vinylphosphonium désiré.

Zusammenfassung

Tributylvinylphosphoniumbromid wurde durch Natriumkarbonat-Dehydrobromierung des 2-Bromäthylsalzes aus der Reaktion von Tributylphosphin mit Dibromäthan dargestellt. Tributylvinylphosphoniumchlorid wurde aus dem Bromid durch Ionenaustausch gewonnen. Triäthylvinylphosphoniumbromid, Tricyclohexylvinylphosphoniumbromid und Dimethylphenylvinylphosphoniumbromid wurden durch Natriumbehandlung des Acetats aus der Essigsäureacetylierung des in der Reaktion zwischen Äthylenbromhydrin und dem entsprechenden Phosphin gebildeten Salzes dargestellt. Ein Versuch zur Darstellung eines Vinylphosphinsalzes durch direkte Erhitzung von Vinylbromid und Tributylphosphin in einem Autoklaven auf 160°C lieferte kein isolierbares Produkt, das Infrarotspektrum sprach jedoch für die Gegenwart des erwarteten Vinylphosphoniumsalzes.

Received August 17, 1964
Revised November 30, 1964
(Prod. No. 4588A)

JOURNAL OF POLYMER SCIENCE: PART A VOL. 3, PP. 2063–2074 (1965)

Polymerization of Vinylphosphonium Compounds

ROBERT RABINOWITZ and RUTH MARCUS, *Chemical Department, Central Research Division, American Cyanamid Company, Stamford, Connecticut*

Synopsis

The mechanism of the ionizing radiation-initiated polymerization of aqueous solutions of tributylvinylphosphonium bromide (TBVPB) to high molecular weight polymers was established to be free radical. Similar polymerization was observed in acetone, acetonitrile, and acetic acid. The failure of even high radiation doses to induce the polymerization of TBVPB when in chlorobenzene solution was explained on the basis of the interaction of chlorine atoms with bromide ions. Triethylvinylphosphonium bromide, tricyclohexylvinylphosphonium bromide, and dimethylphenylvinylphosphonium bromide gave little or no polymer using conditions which polymerized TBVPB almost completely. Conventional oxidizing peroxidic free radical catalysts failed to initiate the polymerization of TBVPB. Nonoxidizing materials like di-*tert*-butyl peroxide and azo compounds did catalyze the polymerization to give high molecular weight polymers. Apparently the oxidizing peroxides are quickly reduced by the bromide ion before any homolytic cleavage can occur. Tributylvinylphosphonium chloride was polymerized in aqueous solution using potassium persulfate, the homolytic cleavage of persulfate competing favorably with redox processes involving the chloride ion. Copolymerization of TBVPB with a series of common monomers resulted in copolymers containing varying amounts of phosphorus in the expected order.

INTRODUCTION

Attempts to convert vinyl phosphorus compounds to high molecular weight polymers have been in progress for some time.[1] Except for an isolated[2] result reported by Tsetlin and co-workers concerning the polymerization of diethyl- and diphenylvinylphosphine oxide to polymers of molecular weights of 30,000 by ionizing radiation, all efforts have been fruitless, in that low molecular weight oligomers have resulted. (Similar work in this laboratory[3] has resulted in polymers of molecular weight 10,000 or less.) These attempts have involved exclusively free radical initiation; however, Allcock has extended this in the case of diphenylvinylphosphine oxide to anionic initiation.[4] The maximum molecular weights obtained in his work were in the 10,000 (DP $\sim$50) region. In view of all this it was quite surprising and unexpected that tributylvinylphosphonium bromide (TBVPB) was polymerized to a very high molecular weight polymer in aqueous solution[5] and in the crystalline state[6] by use of ionizing radiation. The purpose of this work was to elucidate the mechanism of the radiation-initiated polymerization of TBVPB to high molecular weight and to study the polymerization behavior of other vinylphosphonium salts[7] to measure the scope of the discovery.

TABLE I
Survey Radiation Homopolymerization of TBVPB

Run	Dose rate, Mrad/hr.	Dose, Mrad	Solvent	Concn., %	Temp., °C.	Wt. monomer, g.	Polymer, %[a]	[η] (30°C., 0.3*M* LiBr), dl./g.	Molecular weight
1	0.5	1	H_2O	30	R.T.	1.95	33	0.27	
2	0.5	2	H_2O	30	R.T.	1.95	40	0.32	
3	0.5	3	H_2O	30	R.T.	1.95	77	0.26	
4	0.5	4	H_2O	30	R.T.	1.95	70	0.26	
5	0.5	2	H_2O	30	R.T.	1.95	46	0.21	
6	0.5	2	H_2O	30	60	1.95	94	0.46	
7	0.5	2	H_2O	30	100–110	1.95	92	0.78	676,000
8	1.5	1.5	H_2O	30	R.T.	1.95	57	0.30	
9	0.13	1.04	H_2O	30	R.T.	1.95	87	0.48	143,000
10	0.5	2	H_2O	5	R.T.	0.60	92	0.38	
11	0.5	2	H_2O	10	R.T.	1.20	95	0.42	
12	0.5	2	H_2O	15	R.T.	1.80	90	0.42	

13	3.5	3.5	H_2O	33	0	2.0	32	0.10	
14	0.75	1.9	H_2O	33	R.T.	2.0	95	0.36	83,000
15	3.5	3.5	1:1MeOH–H_2O	33	−40	2.0	0	—	
16	0.75	1.9	1:1MeOH–H_2O	33	R.T.	2.0	0	—	
17	0.5	2	MeOH	33	R.T.	2.0	0	—	
18	0.5	2	Acetone	33	R.T.	2.0	12	0.094 (20°C.)	
19	0.5	2	CH_3CN	33	R.T.	2.0	16	0.11	
20	0.5	2	CH_3COOH	33	R.T.	2.0	54	0.22	
21	0.5	2	C_6H_5Cl	8	R.T.	0.65	0	—	
22	0.5	2	C_6H_5Cl	8	R.T.	0.65	Then sample irradiated at 100–110°C. as below		
	0.5	2			100–110		0	—	
23	0.5	3	C_6H_5Cl	8	R.T.	0.65	Then sample irradiated at 60°C. as below		
	0.5	2			60		0	—	
24[b]	1.5	9	C_6H_5Cl	6.5	R.T.	0.65	0	—	
25[b]	0.5	2	C_6H_5Cl	6.5	R.T.	0.65	0	—	

[a] Where per cent polymer is low or zero, this was confirmed by monomer isolation.

[b] Purified (distillation of reagent material) was used in these experiments. In 157-12 the degassing was carried out at 0°C./10 mm., the conditions used for the aqueous systems.

EXPERIMENTAL

Homopolymerization of TBVPB by Using Ionizing Radiation and by Conventional Free Radical Techniques

In almost all cases polymerizations were carried out in sealed tubes which had previously been degassed three times at −78°C. (0°C. with water solutions). The radiation source was a 3 M.e.v. Van de Graaff accelerator, 5 in. scan, 10 cm. from the center of the target to the plate on which the sample rested. The dose rates reported are based on a previous calibration of the various points on the plate at various currents.

The polymerization mixtures were worked up in a number of similar ways. In one, the solvents were removed and the residue taken up in boiling dioxane (a solvent for TBVPB). This was repeatd several times until the cooled dioxane extract was free of TBVPB. Then the residue was dissolved in water and this solution put in Fisher dialyzing tubing and dialyzed for 24–72 hr. The dialyzed solution was evaporated and the residue dried under high vacuum. In a second isolation procedure the polymerization mixture was evaporated as before, however, it was then dialyzed directly (if the initial solvent was water the evaporation was, of course, omitted). The intrinsic viscosity was determined in 0.3*M* LiBr at 30°C. In selected samples, molecular weights were measured by light scattering. The data are summarized in Tables I and II.

Attempted Radiation Polymerization of Tricyclohexylvinylphosphonium Bromide, Triethylvinylphosphonium Bromide, and Dimethylphenylvinylphosphonium Bromide

Samples (2 g.) of each of the phosphonium compounds were put into 6 ml. of water. Since the cyclohexyl compound did not dissolve, 3 ml. of acetonitrile was added, which brought most of the compound into solution. These tubes were degassed three times at 0°C. and sealed. They were then irradiated with a dose rate of 0.5 Mrad/hr. for 4 hr. at room temperature.

Cyclohexylvinylphosphonium Bromide. The solid that did not go into solution was scraped from the side of the opened tube after the solution had been poured off. Analysis of this (0.14 g.) by NMR revealed it to be 94.5% starting monomer. The solution was heated to drive off the acetonitrile thus precipitating more material, 1.17 g., infrared spectrum identical to that of monomer, 87% monomer by NMR. The mother liquor was stripped, and an additional 0.56 g. of material obtained. This, too, had an infrared spectrum identical to that of monomer, except that a small absorption was noted in the OH region which could not be removed by overnight drying or by 6 hr. in the vacuum oven. The NMR spectrum revealed it to be 77% of starting monomer.

Triethylvinylphosphonium Bromide. The water was evaporated, leaving 1.82 g. of a solid residue, m.p. 235–255°C. (m.p. of pure monomer is 255–256°C.). The infrared spectrum was identical to that of pure monomer. Recrystallization from acetonitrile–dioxane gave 1.72 g., m.p. 250–255°C.

Dimethylphenylvinylphosphonium Bromide. The water solution was evaporated, leaving 1.84 g. of a solid residue. This was recrystallized from dioxane–acetonitrile, a total of 1.69 g. being recovered, m.p. 165–167.5°C.

TABLE II
Free Radical Homopolymerization of TBVPB

Run	Wt. monomer, g.	Solvent, ml.	Initiator, mole-%[a]	Temp., °C.	Time, hr.	Polymer, %	[η] (30°C., 0.3*M* LiBr), dl./g.	Molecular weight	Recovered monomer, %
26	1.00	C_6H_5Cl, 3	DTBP, 1.0	130	124.5	50			—
27	1.00	C_6H_5Cl, 3	DTBP, 0.1	130	124.5	8			—
28	1.00	C_6H_5Cl, 3	Bz_2O_2, 1.0	80	121	—			91
29	1.00	C_6H_5Cl, 3	*t*-BPB, 1.0	100	142	—			100
30	2.0	H_2O, 6	H_2O_2, 2.0	80	97	—			86
31	2.0	H_2O, 6	$K_2S_2O_8$, 2.0	80	97	—			85
32	2.0	C_6H_5Cl, 8	ABCN, 3.5	95	24	68	0.24		
33	2.0	C_6H_5Cl, 6	ABCN, 1.0	95	168	79	0.26	106,000	
34	2.0	C_6H_5Cl, 6	ABCN, 0.2	95	168	15	0.18		
35	2.0	C_6H_5Cl, 6	ABCN, 0.04	95	168	17			
36	2.0	C_6H_5Cl, 6	AIBN, 1.0	60	168	92	0.23	109,500	
37	2.0	C_6H_5Cl, 6	AIBN, 0.2	60	168	58	0.22		
38	2.0	C_6H_5Cl, 6	AIBN, 0.04	60	168	7	0.11		
39	2.0	C_6H_5Cl, 6	AIBN, 2	42.5	72	91	0.20		
40	2.0	C_6H_5Cl, 6	AIBN, 1	42.5	210	89	0.22		
41	2.0	Acetone, 6	AIBN, 3.5	60	68	79	0.12	25,000	
42	2.0	CH_3CN, 6	AIBN, 3.5	60	68	79	0.17	33,000	
43	2.0	C_6H_5Cl, 6	AIBN, 3.5	60	66	88	0.20	80,000	

[a] DTBP, di-*tert*-butyl peroxide; Bz_2O_2, benzoyl peroxide; *t*-BPB, *tert*-butyl perbenzoate; ABCN, azobiscyclohexanenitrile; AIBN, azobis-isobutyronitrile.

Attempted Radiation Copolymerization of Triethylvinylphosphonium Bromide and TBVPB

A solution of 2.0 g. of the triethyl compound in 6 ml. of water and another solution of 0.4 g. of TBVPB and 1.6 g. of the triethyl compound in 6 ml. of water were irradiated for 5 hr. at a dose rate of 0.75 Mrad/hr. No polymer was isolated from either on work-up. On the other hand, a solution of 2 g. of TBVPB in 6 ml. of water which was irradiated at the same dose rate for only 2.5 hours gave a 90% yield of polymer, $[\eta](30°C., 0.3M$ LiBr) = 0.36 dl./g., molecular weight 83,000.

Attempted Polymerization of Tributylvinylphosphonium Chloride

Heating solutions of tributylvinylphosphonium chloride in water with a catalytic amount of succinic acid peroxide at 60°C., and in chlorobenzene with a catalytic amount of benzoyl peroxide at 80°C. did not result in the formation of any polymer.

Successful Polymerization of Tributylvinylphosphonium Chloride

A solution containing 0.5 g. of the chloride and 10 mg. of potassium persulfate in 3 ml. of water was purged with nitrogen for 5 min. and heated at 80°C. After 24 hr. a noticeable increase in viscosity had occurred. The water was evaporated, and the residue extracted twice with 10 ml. portions of boiling dioxane. The residue was again evaporated (3 hr., 1.0 mm.). The resultant polymeric product was extremely hygroscopic, 0.5 g. (100%), $[\eta](30°C., 0.3M$ LiBr) = 0.75 dl./g.

Reactions of $S_2O_8^=$ and Succinic Acid Peroxide with I^-, Br^-, and Cl^-

To aqueous solutions of potassium persulfate and succinic acid peroxide was added a dilute solution of potassium iodide. Both solutions colored immediately but qualitatively the persulfate solution was slower.

To solutions of 1.0 g. of potassium persulfate and 1.0 g. of succinic acid peroxide in 25 ml. of water were added equal volumes of a dilute aqueous solution of potassium bromide. The succinic acid peroxide solution became orange immediately and had an odor of bromine whereas the persulfate solution remained colorless. On standing it developed a yellow color. Heating the persulfate solution at 80°C. greatly hastened the bromine formation.

A solution of sodium chloride was mixed with one of succinic acid peroxide. Although no color developed, the odor of chlorine was unmistakable.

Copolymerization of TBVPB

All copolymerizations were carried out by mixing the components into a constricted heavy-walled test tube, degassing three times at −78°C., sealing, and then heating at 60°C. All initial compositions contained 2.320 g. of TBVPB, 70 mole-% of the comonomer, 3 ml. of acetonitrile, and 1 mole-% of AIBN (0.0411 g.).

Methyl Methacrylate. The mixture was heated for 4 hr. The resultant viscous solution was diluted and precipitated into methanol; 1.16

g. of polymer was obtained. This was dissolved in acetone and reprecipitated into hexane; 1.10 g. of polymer was obtained containing 0.23% P.

Styrene. The mixture was heated for 18.5 hr. It did not precipitate in methanol or acetone. Then 0.041 g. of hydroquinone was added and the solvent evaporated using very little heat. The residue, still having a styrene odor, was dialyzed in acetone for 24 hr. The diazylate was stripped, leaving 2.74 g. of material still having a styrene odor. The polymer was dissolved in acetone and precipitated into water. This was repeated and 1.62 g. was obtained. The first filtrate, upon evaporation, gave TBVPB. Finally the polymer was dissolved in acetone and precipitated into hexane; 0.6 g. of polymer resulted containing 2.87% P.

Acrylonitrile. The mixture was heated for 7 hr., at which point the viscous yellow solution was added into excess methanol; 0.86 g. of polymer was obtained. This was dissolved in DMF and precipitated into methanol; 0.48 g. of polymer was obtained, which on analysis showed C, 57.1%; H, 6.15%; N, 10.45%; Br, 6.98%; P, 2.44%.

Vinyl Acetate. The mixture was heated for 11 hr. Since the final solution gave no precipitate when added to methanol, acetone, or dioxane, the solvent was evaporated and the residue taken up in water and dialyzed for 24 hr. A yield of 1.83 g. of polymer was obtained containing 7.74% P.

Methyl Acrylate. The mixture was heated for 3 hr. The resultant solution gave no precipitate when added to methanol, higher alcohols, acetone, chlorobenzene, or dioxane, and the polymer was therefore precipitated and reprecipitated into water. The second precipitation gave a gum which was dried by heating in vacuo. No weight of the polymer was obtained; it contained 1.40% P.

Acrylamide. Acrylamide polymerizes very rapidly under the specified conditions; however, when the catalyst concentration was decreased to 0.1 mole-% a slower polymerization occurred. The solution after 8 hr. appeared to contain a gel. The entire mixture was transferred into water, everything dissolving including the gel. This solution was dialyzed for 24 hr. and 0.27 g. of polymer, 4.51% P, was obtained upon removal of the water.

RESULTS AND DISCUSSION

Radiation Polymerization of TBVPB in Water

The result of Pellon and Valan was confirmed;[5] ionizing radiation will convert TBVPB into a high molecular weight polymeric substance. Doses as low as 1 Mrad were used to convert 2 g. samples of monomer into high polymer in over 87% yield.

The mechanism of the radiation-induced polymerization was studied in some detail by the conventional techniques: variation of concentrations, dose rates, doses, temperature, and solvents. Since the phosphonium group is a strong electron-withdrawing species, the possibility of an anionic chain process existed. However, the successful polymerization of TBVPB in acetic acid solution ruled out any anionic mechanism, leaving the free radical process as the only possible alternative. Despite

the high conversions in many cases, the results could be interpreted as being consistent with this mechanistic course.

Thus, in an experiment where identical aqueous solutions were exposed to similar total doses at a dose rate difference of a factor of 12 (runs 8 and 9), the more slowly initiated sample gave a higher molecular weight and a higher yield. This follows from the conventional bimolecularly terminated free radical polymerization mechanism, where when the steady-state radical concentration is lower, a chain can grow to a greater length before termination occurs by interaction with another growing chain. Inherent in this result is that chain transfer with solvent or monomer is relatively unimportant. The increase of molecular weight with increasing temperature under constant dose and dose rate conditions (runs 5, 6, 7) was expected, since in a conventional free radical process the activation energy for propagation is considerably higher than that for termination.

Radiation Polymerization of TBVPB in Nonaqueous Solvents

Since TBVPB is a salt, it was expected that in solvents other than water, where hydration of the phosphonium ion could play an important role in its reactivity, that major differences in polymerization characteristics might be noted. The solvents chosen were those having g values of the same or similar magnitude, methanol (6.3), acetonitrile (7), chlorobenzene (5–10), and acetone (11.8).* Water has a g value of 8.

Acetone, Acetonitrile, and Methanol. Polymerizations carried out in acetone and acetonitrile (runs 18 and 19) resulted in the formation of polymer. However, the yields and molecular weights were considerably lower than those obtained when the process is carried out under aqueous conditions. With methanol as solvent no polymer at all was observed; even when 1:1 methanol–water was used as a solvent no polymer formation was noted. Since only a few experiments were carried out with these solvents it is not worthwhile to speculate on the differences between these and the aqueous experiments. The lack of any polymerization in methanol is undoubtedly due to the competing rapid addition of methanol across the vinylphosphonium double bond.[9]

Chlorobenzene. No polymer was observed when solutions of TBVPB in chlorobenzene were irradiated with doses up to 9 Mrad and at temperatures as high as 110°C. This was rather surprising, since the g value for chlorobenzene is about the same as that for water, and aqueous solutions under these conditions polymerized to over 90% of completion. Initially this lack of polymerizability was considered a reflection of differences in solvation abilities of chlorobenzene and water. This, coupled with the fact that benzoyl peroxide (80°C.) and *tert*-butyl perbenzoate (100°C.) failed to initiate the polymerization of TBVPB in chlorobenzene and only di-*tert*-butyl peroxide (130°C.) was effective, seemed like a reasonable explanation (Table II). However, as it will soon be discussed, azo catalysts at temperatures as low as 42.5°C. effected the polymerization in chlorobenzene and therefore another explanation was required. Al-

* These g values are the number of radicals which can be trapped by diphenylpicrylhydrazyl, etc./100 e.v.[8]

though no proof will be presented, it is possible to account for the lack of polymerizability of TBVPB in chlorobenzene in the presence of ionizing radiation by assuming that the radicals first formed are reduced by the bromide ion and are therefore unavailable for starting chains. The generated bromine can then act as inhibitor:

$$Cl\cdot + Br^- \rightarrow Cl^- + Br\cdot$$

$$Br\cdot + Br\cdot \rightarrow Br_2$$

$$R'\cdot + CH_2{=}CH\overset{+}{P}R_3 \rightarrow R'CH_2{-}\dot{C}H\overset{+}{P}R_3$$

$$R'CH_2{=}\dot{C}H\overset{+}{P}R_3 + Br_2 \rightarrow Br\cdot + R'CH_2{-}CHBr\overset{+}{P}R_3$$

Attempted Radiation Initiation of Other Vinylphosphonium Compounds

Attempt to polymerize triethylvinylphosphonium bromide, dimethylphenylvinylphosphonium bromide, and tricyclohexylvinylphosphonium bromide in aqueous solution led to the recovery of almost pure monomer. Only in the latter case was any indication of polymerization obtained and this was by NMR analysis, monitoring the vinyl/aliphatic C—H ratio, rather than by chemical isolation. These attempts were made under conditions which led to high conversion of TBVPB to polymer. Although an exhaustive study was not made and therefore these structural effects are not readily understood, the results suggest that satisfactory homopolymerization characteristics for vinylphosphonium compounds may be the exception rather than the rule.

Conventional Free Radical Initiation of TBVPB

Di-*tert*-butyl peroxide was effective in converting TBVPB in chlorobenzene to polymer at concentrations of 1.0 and 0.10 mole-%, the yield in the latter case being only 8%. However, attempts to polymerize TBVPB by using benzoyl peroxide (chlorobenzene, 80°C.), *tert*-butyl perbenzoate (chlorobenzene, 100°C.), hydrogen peroxide, and potassium persulfate (water, 80°C.) all failed, in that no polymer was detected. Initially it was concluded that TBVPB was following the pattern of the other vinyl phosphorus monomers that have been studied[1] in this and other laboratories; that is polymerization occurred if at all, only at high temperatures. However, this was difficult to reconcile with the high molecular weight polymers obtained by using ionizing radiation at room temperature, particularly after the mechanism was shown to be free radical.

In the mixing of the peroxidic material with the TBVPB and solvent, a yellow coloration was noted to occur immediately (except with DTBP) which faded during the heating period. No explanation was available for these observations until it was considered probable and demonstrated experimentally that the peroxides were being reduced very rapidly by the bromide ion and hence were unavailable for the formation of free radicals and naturally no polymer could be expected. It also was understandable why DTBP functioned as an effective initiator since it is not an oxidizing peroxide. Consequently two other nonoxidizing free radical initiators

were studied, AIBN and azobiscyclohexanenitrile (ABCN). Polymers were obtained over the range of temperature of 42.5–95°C. in high yields and high molecular weights. All these polymerizations were carried out in chlorobenzene.

The effect of other solvents was investigated briefly. Thus in acetone and acetonitrile, with 3.5 mole-% of AIBN, 79% and 72% of polymer was obtained under conditions which gave a 88% yield in chlorobenzene. These differences are not considered significant. The molecular weights of the polymers obtained in acetone, acetonitrile, and chlorobenzene were 25,000, 33,000, and 80,000, respectively. These differences may merely reflect differences in chain transfer properties of the solvents.

Free Radical Polymerization of Tributylvinylphosphonium Chloride

Since the ease of oxidation of halide ions decreases in the order $I^- > Br^- > Cl^- > F^-$, it was considered worthwhile to convert TBVPB to the corresponding chloride and to attempt to polymerize this with peroxidic initiators which failed to work with the bromide. The chloride was prepared by ion exchange techniques[7] and a material containing only 0.1% Br was obtained. It was determined separately that chloride ion reacted rapidly with succinic acid peroxide, and therefore it was not surprising that this peroxide did not initiate the desired polymerization. Benzoyl peroxide also failed as an initiator. Since it had been observed that bromide ion reacted very much more slowly with persulfate than with succinic acid peroxide, it was considered likely that the free radical breakdown of persulfate at 80°C. might compete favorably with any redox processes involving the more difficultly oxidized chloride ion. Thus, when a catalytic amount of potassium persulfate was added to an aqueous solution of the phosphonium chloride and this heated for 24 hr. at 80°C., a 100% conversion to polymer of intrinsic viscosity 0.75 dl./g. (30°C., 0.3*M* LiBr) occurred. This successful polymerization gave further support to the explanation that the failure of oxidizing peroxidic materials to initiate the polymerization of TBVPB was because the peroxides were reduced by the bromide ion.

Copolymerization of TBVPB with Other Vinyl Monomers

A cursory examination of the copolymerization of a series of vinyl monomers with TBVPB was carried out. The following comonomers were examined: methyl methacrylate, styrene, acrylonitrile, vinyl acetate, methyl acrylate, and acrylamide. In every case the copolymer contained phosphorus, although the reactivity of TBVPB appeared to vary considerably, being at a low with MMA and a high with vinyl acetate, which was the anticipated order.

Relationship of Intrinsic Viscosity and Molecular Weight for Radiation- and Conventional Radical-Initiated TBVPB Polymer

The intrinsic viscosities of all the vinylphosphonium polymers prepared in this study were measured in 0.3*M* LiBr at 30°C. The light-scattering

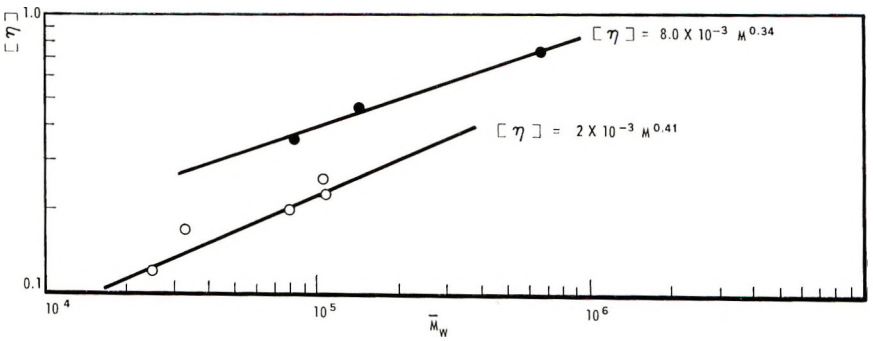

Fig. 1. Relationship of the molecular weight and intrinsic viscosity (30°C., 0.3*M* LiBr) of poly-TBVPB.

molecular weights of several representative homopolymers were determined, and these data appear in Tables I and II. By plotting the logarithm of the intrinsic viscosities versus the logarithm of the molecular weights (Fig. 1) an interesting relationship was observed. Two straight lines could be drawn, one including only the conventional free radical points and the other only the radiation points. The following relationship between intrinsic viscosity and $\bar{M}_w$ was derived from this plot by least-squares calculation.

For conventional free radical:

$$[\eta] = 2 \times 10^{-3} M^{0.41}$$

For radiation:

$$[\eta] = 8.0 \times 10^{-} M^{30.34}$$

It is readily apparent that these relationships are quite different. For a given molecular weight, a conventional free radical-initiated polymer has a much lower intrinsic viscosity than one prepared by ionizing radiation. The usual conclusion for such an observation is that those polymers prepared by conventional free radical methods are more highly branched. This is, of course, contrary to what one would expect and may be an erroneous conclusion in the case of this highly ionic polymer. The refractive index increments, $\Delta n/\Delta c$, were different for the two preparations, confirming that basic differences exist between them. No effort shall be made to try to specify the exact nature of this difference or differences.

We wish to thank Mr. C. Spiers who performed by Van de Graaff irradiations and Mr. R. J. Roach and Dr. A. T. Guertin who determined the intrinsic viscosities and light-scattering molecular weights.

References

1. Rabinowitz, R., R. Marcus, and J. Pellon, *J. Polymer Sci.*, **A2**, 1233 (1964).
2. Tsetlin, B. L., T. Ya. Medved, Yu O. Chikishev, Ye. M. Polykorpov, S. R. Rafikov, and M. I. Kabachnik, *Vysokomol. Soedin.*, **3**, 1117 (1961).
3. Allcock, H. R., *J. Polymer Sci.*, **A2**, 4087 (1964).
4. Allcock, H. R., and R. L. Kugel, *J. Polymer Sci.*, **A1**, 3627 (1963).
5. Pellon, J., and K. J. Valan, *Chem. Ind. (London)*, **1963**, 1358.

6. Chen, C. S. H., and D. G. Grabar, *J. Polymer Sci.*, **C4**, 849 (1963).
7. Rabinowitz, R., A. C. Henry, and R. Marcus, *J. Polymer Sci.*, **A3**, 2055 (1965).
8. Webb, R. L., Central Research Division, American Cyanamid Co., private communication.
9. Keough, P. T., and M. Grayson, *J. Org. Chem.*, **29**, 631 (1964).

Résumé

La polymérisation d'une solution aqueuse de bromure de tributylvinylphosphonium (TBVPB), initiée par une radiation ionisante donne un polymère de haut poids moléculaire par un mécanisme radicalaire. La même polymérisation est observée dans l'acétone, l'acétonitrile, et l'acide acétique. L'impossibilité de polymériser le TBVPB dans le chlorobenzène, même avec des fortes doses de radiation est expliquée par l'interaction des atomes de chlore avec les ions bromure. Le bromure de triéthylvinylphosphonium, le bromure de tricyclohexylvinylphosphonium et le bromure de diméthylphénylvinylphosphonium ne donnent pratiquement pas de polymères dans les conditions où le TBVPB est polymérisé complètement. Les catalyseurs oxydants radicalaires conventionnels, dérivés des peroxydes oxydants, n'initient pas la polymérisation du TBVPB. Des produits non-oxydants comme le peroxyde de di-*ti*-butyle et les produits azoïques catalysent la polymérisation pour donner des polymères de haut poids moléculaire. Les peroxydes oxydants sont probablement vite réduits par les ions bromure avant l'addition homolytique. En polymérisant le chlorure de tributylphosphonium en solution aqueuse avec du persulfate de potassium, la rupture homolytique du persulfate est en compétition favorable avec les processus d'oxydoréduction, impliquant les ions chlorure. La copolymérisation de TBVPB avec une série de monomères courants donne des copolymères, contenant des quantités variables de phosphore dans l'ordre prévu.

Zusammenfassung

Für die durch ionisierende Strahlung initiierte Polymerisation wässiger Lösungen von Tributylvinylphosphoniumbromid (TBVPB) zu hochmolekularen Polymeren wurde ein radikalischer Mechanismus nachgewiesen. Eine ähnliche Polymerisation wurde in Aceton, Acetonitril, und Essigsäure beobachtet. Die Unmöglichkeit, auch mit hohen Strahlungsdosen die Polymerisation von TBVPB in Chlorbenzollösung anzuregen, wurde durch eine Wechselwirkung der Chloratome mit Bromidionen erklärt. Triäthylvinylphosphoniumbromid, Tricyclohexylvinylphosphoniumbromid und Dimethylphenylvinylphosphoniumbromid lieferten unter Bedingungen, bei welchen TBVPB fast vollständig polymerisierte, wenig oder kein Polymeres. Die konventionellen, oxydierenden, peroxydischen Radikalkatalysatoren konnten die Polymerisation von TBVPB nicht starten. Nicht oxydierende Stoffe wie Di-*t*-butylperoxyd und Azoverbindungen katalysierten die Polymerisation und lieferten hochmolekulare Polymere. Offenbar werden die oxydierenden Peroxyde durch das Bromidion rasch reduziert, bevor noch eine homolytische Spaltung auftreten kann. Tributylvinylphosphoniumchlorid wurde in wässriger Lösung mit Kaliumpersulfat polymerisiert. Die homolytische Spaltung des Persulfats konkurriert offenbar erfolgreich mit Redoxprozessen unter Beteiligung des Chloridions. Kopolymerisation von TBVPB mit einer Reihe der üblichen Monomeren führte zu Kopolymeren mit wechselndem, in der erwarteten Reihenfolge liegenden Phosphorgehalt.

Received August 17, 1964
Revised November 30, 1964
(Prod. No. 4587A)

BOOK REVIEW

New Perspectives in Biology. MICHAEL SELA, Editor, Elsevier, Amsterdam, 1964. xviii + 285 pp., $14.50.

This volume contains a collection of lectures presented on the occasion of the inauguration of an Institute of Life Sciences at the Weizmann Institute of Science in Rehovoth, Israel, in June 1963. The roster of speakers was an unusually distinguished one, including five holders of the Nobel prize and a number of others who would have qualified for it equally well, or may yet receive it in the future.

The lectures are divided into groups characterized as "New Perspectives in Protein Research" (Edsall, Kendrew, Neurath, Anfinsen, Katchalski, Lipmann); "Structure and Function of Nucleic Acids" (Chargaff, Elson, Gierer, Ochoa); "Organization and Function of Enzyme Systems and Subcellular Units" (Lynen, Theorell, Weber, Nachmansohn); "New Antibiotics" (Chain); "Chemical Approaches to Immunology" (Heidelberger, Sela); and "Cellular, Subcellular and Molecular Aspects of Differentiation" (Kellenberger, Sachs, Klein, Feldman). In spite of the wide range of subjects covered, the style is generally such as to make the treatise accessible not only to the specialist but also to the nonspecialist, who maintains a more or less superficial interest in biological chemistry.

As Kendrew says in his concluding remarks, the glamour of the spectacular achievements in molecular biology is such that there may be a tendency to hold rather too many meetings in this field. Nevertheless, the symposium covered in this volume was assembled in an unusually imaginative manner and even those who are familiar with the details of work in one area, should find the reading of the entire volume eminently worthwhile and enjoyable. The historical perspective of Edsall's remarks and the iconoclastic tone of Chargaff's lecture enliven greatly the presented material. It is inevitable that the rapidity of progress in the field which was being reviewed should produce a situation where some of the discussions should appear incomplete at the time the book was published. It is to the great credit of the authors that they project such future developments, so that the gap does not appear serious. For instance, the value of Neurath's discussion of proteolytic enzymes is hardly diminished by the fact that the lecture preceded the determination of the complete aminoacid sequence of trypsin and chymotrypsin.

It is this reviewer's conviction that every polymer chemist should become familiar with such concepts of the physical chemistry of natural macromolecules as the specific conformation of globular proteins, the specificity of enzyme–substrate and antigen–antibody interactions, or the genetic code. While the present volume can hardly serve as an introductory text, it is most stimulating for those who want to maintain a feeling for the important trends in this general area.

Polytechnic Institute of Brooklyn
Brooklyn, New York

Herbert Morawetz

POLYMER NEWS

On May 27 and 28, 1965, Dr. Herman F. Mark will be honored on his 70th birthday by a symposium to be held at the Polytechnic Institute of Brooklyn. This two-day event, to be known as the Herman F. Mark Symposium, will be published at a later date in the *Journal of Polymer Science, Part C*, Polymer Symposia series.

THURSDAY, MAY 27, 1965, Morning Session

Welcome:	Ernst Weber, President Polytechnic Institute of Brooklyn
	Charles G. Overberger, Director Polymer Research Institute
Chairman:	Linus Pauling Center for the Study of Democratic Institutions Santa Barbara, California
Honorary Chairman:	Masao Horio Kyoto University Kyoto, Japan
Speakers:	"Theory of Polyelectrolytes" Bruno Zimm University of California La Jolla, California
	"The Role of van der Waals Interactions on the Conformational Stability of Helical Macromolecules" Alfonso Liquori University of Naples Naples, Italy
	"Translations of the Genetic Code" Paul M. Doty Harvard University Cambridge, Massachusetts
Discussion Leaders:	Aharon Katchalsky-Katzir Weizmann Institute Rehovoth, Israel
	Paul J. Flory Stanford University Stanford, California
	Otto Wichterle Czechoslovak Academy of Science Praha, Czechoslovakia

THURSDAY, MAY 27, 1965, Afternoon Session

Chairman: W. Kern
Organisch-Chemisches Institut der Universitat Mainz
Mainz, Germany

Honorary Chairman: C. S. Marvel
University of Arizona
Tucson, Arizona

Speakers: "Non-Fickean Diffusion and Swelling Stresses in Glassy Polymers"
Turner Alfrey, Jr.
Dow Chemical Company
Midland, Michigan

"Conjugates of Biologically Active Molecules with Synthetic Polymers"
Ephraim Katchalski
Weizmann Institute
Rehovoth, Israel

"Radiation Induced Radicals in Polyethylene and Polypropylene"
Bengt Ranby
Royal Institute of Technology
Stockholm, Sweden

Discussion Leaders: Charles C. Price
University of Pennsylvania
Philadelphia, Pennsylvania

H. Hopff
Swiss Federal Institute of Technology
Zurich, Switzerland

Georges Smets
Universite de Louvain
Louvain, Belgium

FRIDAY, MAY 28, 1965, Morning Session

Chairman: Peter Debye
Cornell University
Ithaca, New York

Honorary Chairman: Anton Peterlin
Research Triangle Institute
Durham, North Carolina

Speakers: "Equation of State Properties of Chain Liquids and Glasses"
Robert Simha
University of Southern California
Los Angeles, California

"Transport in Polymers"
Harry L. Frisch
Bell Telephone Laboratories
Murray Hill, New Jersey

"Some Aspects of The Optical Activity Problem in Polymers"
Robert Ullman
Ford Motor Company
Dearborn, Michigan

Discussion Leaders:

Walter H. Stockmayer
Dartmouth College
Hanover, New Hampshire

Karl A. Wolf
Heidelberg, Germany

C. E. H. Bawn
University of Liverpool
Liverpool, England

FRIDAY, MAY 28, 1965, Afternoon Session

Chairman:

V. A. Kargin
Academy of Science
Moscow, U.S.S.R.

Honorary Chairman:

I. Sakurada
Kyoto University
Kyoto, Japan

Speakers:

"Viscoelasticity of Polymers"
Arthur V. Tobolsky
Princeton University
Princeton, New Jersey

"The Use of Generating Functions in the Calculation of M.W. Distributions from Rate Equations"
J. J. Hermans
Chemstrand Research Center, Inc.
Durham, North Carolina

"Some Problems in Ammonia Synthesis"
Rudolf Brill
Fritz-Haber-Institut Der Max-Planck-Gesellschaft, Berlin, Germany

Discussion Leaders:

A. J. Staverman
Central Laboratory, T.N.O.
Delft, The Netherlands

C. H. Bamford
The University of Liverpool
Liverpool, England

George Goldfinger
Naugatuck Chemical—U.S. Rubber
Naugatuck, Connecticut